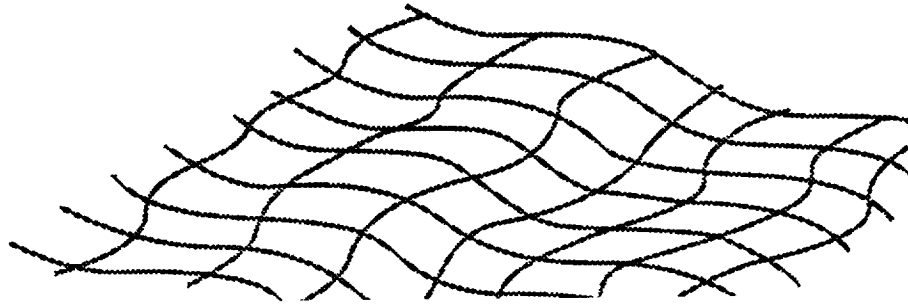


FIBER-TEX 1992

*The Sixth Conference on Advanced
Engineering Fibers and Textile
Structures for Composites*



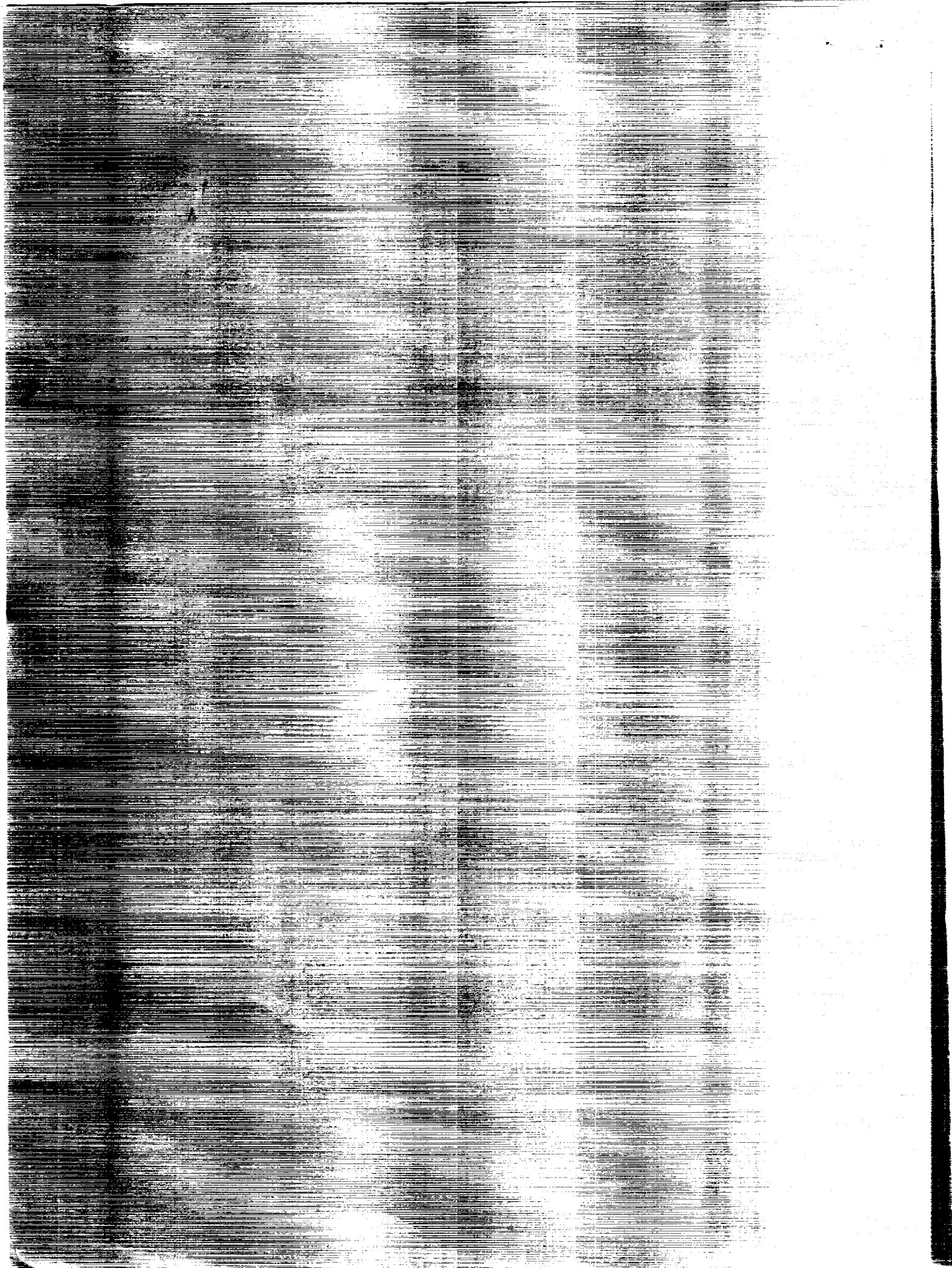
(NASA-CP-3211) FIBER-TEX 1992: THE
SIXTH CONFERENCE ON ADVANCED
ENGINEERING FIBERS AND TEXTILE
STRUCTURES FOR COMPOSITES (NASA)
357 p

N94-16845
--THRU--
N94-16865
Unclas

H1/24 0179710

~~XXXXXXXXXX~~

372P



NASA Conference Publication 3211

FIBER-TEX 1992

*The Sixth Conference on Advanced
Engineering Fibers and Textile
Structures for Composites*

Edited by
John D. Buckley
NASA Langley Research Center
Hampton, Virginia

Proceedings of a conference sponsored by the National
Aeronautics and Space Administration, Washington, D.C.,
the Department of Defense, Washington, D.C.,
Drexel University, Philadelphia, Pennsylvania,
Clemson University, Clemson, South Carolina, and
North Carolina State University, Raleigh, North Carolina,
and held in Philadelphia, Pennsylvania
October 27-29, 1992

NASA

National Aeronautics and
Space Administration

Office of Management

Scientific and Technical
Information Program

1993



PREFACE

The *FIBER-TEX 1992* proceedings contain the papers jointly sponsored by the National Aeronautics and Space Administration, Drexel University, the Department of Defense, the Center for Advanced Engineering Fibers at Clemson University, and the North Carolina State University. The conference was held at the Grand Hall, Creese Student Center at Drexel University in Philadelphia, Pennsylvania on October 27-29, 1992 to create a forum to encourage an interrelationship of the various disciplines involved in the fabrication of materials, the types of equipment, and the processes used in the production of advanced composite structures. Topics discussed were Advanced Engineering Fibers, Textile Processes and Structures, Structural Fabric Production, Mechanics and Characteristics of Woven Composites, and the latest requirements for the use of textiles in the production of composite materials and structures as related to global activities focused on textile structural composites.

Certain materials and processes are identified in this publication in order to adequately specify procedures. In no case does such identification imply recommendation or endorsement by the government, nor does it imply that the materials or processes are the only or best ones available for the purpose.

John D. Buckley
NASA Langley Research Center



CONTENTS

PREFACE	iii
AN OVERVIEW OF THE NASA TEXTILE COMPOSITES PROGRAM H. Benson Dexter	1
TECHNO-ECONOMIC REQUIREMENTS FOR AUTOMOTIVE COMPOSITES Scot Arnold	33
RESEARCH IN TEXTILE COMPOSITES AT K.U. LEUVEN Ignaas Verpoest, Jan Ivens, Aart Willem van Vuure, and Vassilios Efstratiou	49 -3
DESIGN AND COST DRIVERS IN 2-D BRAIDING Alberto Morales	69 -4
WEAVING MULTI-LAYER FABRICS FOR REINFORCEMENT OF ENGINEERING COMPONENTS B. J. Hill, R. McIlhagger, and P. McLaughlin	79 -5
EFFECT OF TOW ALIGNMENT ON THE MECHANICAL PERFORMANCE OF 3D WOVEN TEXTILE COMPOSITES Timothy L. Norman, Patti Allison, Jack W. Baldwin, Brian K. Gracias, and Dave Seesdorf	97 -6
AN ENGINEERING APPROACH FOR THE APPLICATION OF TEXTILE COMPOSITES TO A STRUCTURAL COMPONENT Jack W. Baldwin, Brian K. Gracias, and Steven R. Clarke	115 -7
NEW TEXTILE COMPOSITE MATERIALS DEVELOPMENT, PRODUCTION, APPLICATION Petr Y. Mikhailov	125 -8
PRODUCTION AND APPLICATION OF CHEMICAL FIBERS WITH SPECIAL PROPERTIES FOR MANUFACTURING COMPOSITE MATERIALS AND GOODS OF DIFFERENT USAGE R. Levit	139 -9
FIBERS AND MATERIALS OF MEDICAL APPLICATION L. I. Fridman	147 -10
TEXTILE COMPOSITE PROCESSING SCIENCE Alfred C. Loos, Vincent H. Hammond, David E. Kranbuehl, and Gregory H. Hasko	151 -11
INFLUENCE OF FIBER PACKING STRUCTURE ON PERMEABILITY Zhong Cai and Alexander L. Berdichevsky	167 -12
CHARACTERIZATION OF VOIDS FORMED DURING LIQUID IMPREGNATION OF NONWOVEN MULTIFILAMENT GLASS NETWORKS AS RELATED TO COMPOSITE PROCESSING Anant D. Mahale, Robert K. Prud'homme, and Ludwig Rebenfeld	183 -13

10

DEVELOPMENT OF BRAIDED FIBER SEALS FOR ENGINE APPLICATIONS	203	-14
Zhong Cai, Rajakkannu Mutharasan, Frank K. Ko, Guang-Wu Du, and Bruce M. Steinetz		
QUANTIFICATION OF PROCESSING ARTIFACTS IN TEXTILE COMPOSITES	215	-15
Christopher M. Pastore		
STOCHASTIC DAMAGE EVOLUTION IN TEXTILE LAMINATES	235	-16
Yuris A. Dzenis, Alexander E. Bogdanovich, and Christopher M. Pastore		
DEVELOPMENT OF TEST METHODS FOR TEXTILE COMPOSITES	249	-17
John E. Masters, Peter G. Ifju, and Mark J. Fedro		
THREE-DIMENSIONAL ANALYSIS OF ANISOTROPIC SPATIALLY REINFORCED STRUCTURES	271	-18
Alexander E. Bogdanovich		
TECHNO-ECONOMIC REQUIREMENTS FOR COMPOSITE AIRCRAFT COMPONENTS	305	-19
Ray Palmer		
AEROELASTIC AIRFOIL SMART SPAR	343	-20
Skott Greenhalgh, Christopher Pastore, and Moishe Garfinkle		
ATTENDEES	353	

1 994012373

N 9 4 - 1 6 8 4 6

AN OVERVIEW OF THE NASA TEXTILE COMPOSITES PROGRAM

H. Benson Dexter
NASA Langley Research Center
Hampton, Virginia

INTRODUCTION

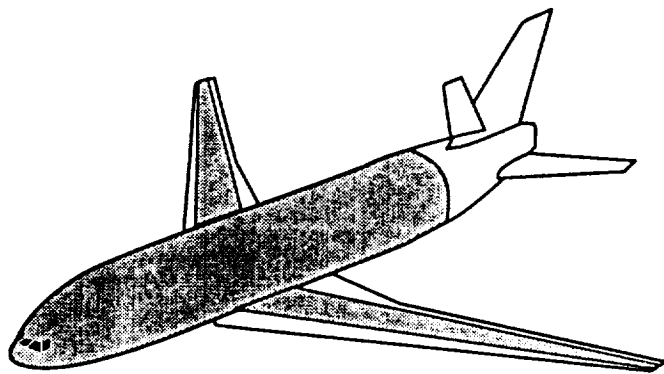
The NASA Langley Research Center is conducting and sponsoring research to explore the benefits of textile reinforced composites for civil transport aircraft primary structures. The objective of this program is to develop and demonstrate the potential of affordable textile reinforced composite materials to meet design properties and damage tolerance requirements of advanced aircraft structures. In addition to in-house research, the program includes major participation by the aircraft industry and aerospace textile companies. The major program elements include development of textile preforms, processing science, mechanics of materials, experimental characterization of materials, and development and evaluation of textile reinforced composite structural elements and subcomponents. The NASA Langley in-house research is focused on science-based understanding of resin transfer molding (RTM), development of powder-coated towpreg processes, analysis methodology, and development of a performance database on textile reinforced composites. The focus of the textile industry participation is on development of multidirectional, damage-tolerant preforms, and the aircraft industry participation is in the areas of innovative design concepts, cost-effective fabrication, and testing of textile reinforced composite structural elements and subcomponents.

Textile processes such as 3-D weaving, 2-D and 3-D braiding, and knitting/stitching are being compared with conventional laminated tape processes for improved damage tolerance. Through-the-thickness reinforcements offer significant damage tolerance improvements. However, these gains must be weighed against potential loss in in-plane properties such as strength and stiffness. Analytical trade studies are underway to establish design guidelines for the application of textile material forms to meet specific loading requirements. Fabrication and testing of large structural components are required to establish the full potential of textile reinforced composite materials. The goals of the NASA Langley-sponsored research program are to demonstrate technology readiness with subscale composite components by 1995 and to verify the performance of full-scale composite primary aircraft structural components by 1997. The status of textile reinforced composite structural elements under development by Boeing, Douglas, Lockheed, and Grumman are presented. Included are braided frames and woven/stitched wing and fuselage panels.



CURRENT STATE OF COMPOSITES TECHNOLOGY FOR TRANSPORTS

The goals of the NASA ACT program include extensive application of advanced composite materials to primary wing and fuselage structures, reduction of the structural weight by 30 to 50 percent, and development of cost-effective fabrication methods. In general, advanced composite materials have been limited to secondary structures. A 25-percent weight saving has been achieved, but the use of brittle materials dictated low-strain designs. In addition, development of automated fabrication processes has been slow. Some of the barriers to expanded application of composites in primary wing and fuselage structures are indicated in figure 1.



Goals

- Extensive application to wing and fuselage structures
- 30 to 50% weight reduction
- Cost effective fabrication

Status

- Limited to secondary structures
- 25% weight reduction achieved
- Brittle materials dictate low-strain designs
- High fabrication costs

Barriers

- Low damage tolerance of laminated constructions
- Expensive prepreg materials
- Labor intensive manufacturing
- Insufficient data base
- Inadequate analytical tools

Figure 1

TEXTILE REINFORCED COMPOSITES

The NASA Langley Research Center has assembled a multidisciplinary team to conduct research on textile reinforced composites. The current team includes NASA Langley in-house personnel, numerous universities, textile fabricators, and major aerospace contractors. The team will expand to meet program needs as required. Figure 2 indicates the scope of the research effort that is currently underway. Recent program emphasis has been on development of aircraft quality textile preforms, development of science-based processes, development of mechanics methodologies, and experimental characterization of textile reinforced composite materials. These technologies are maturing and future emphasis will shift to design, analysis, fabrication, inspection, and test of structural elements and subcomponents. Douglas, Lockheed, Boeing, and Grumman have provided a much needed focus on realistic airframe structures.

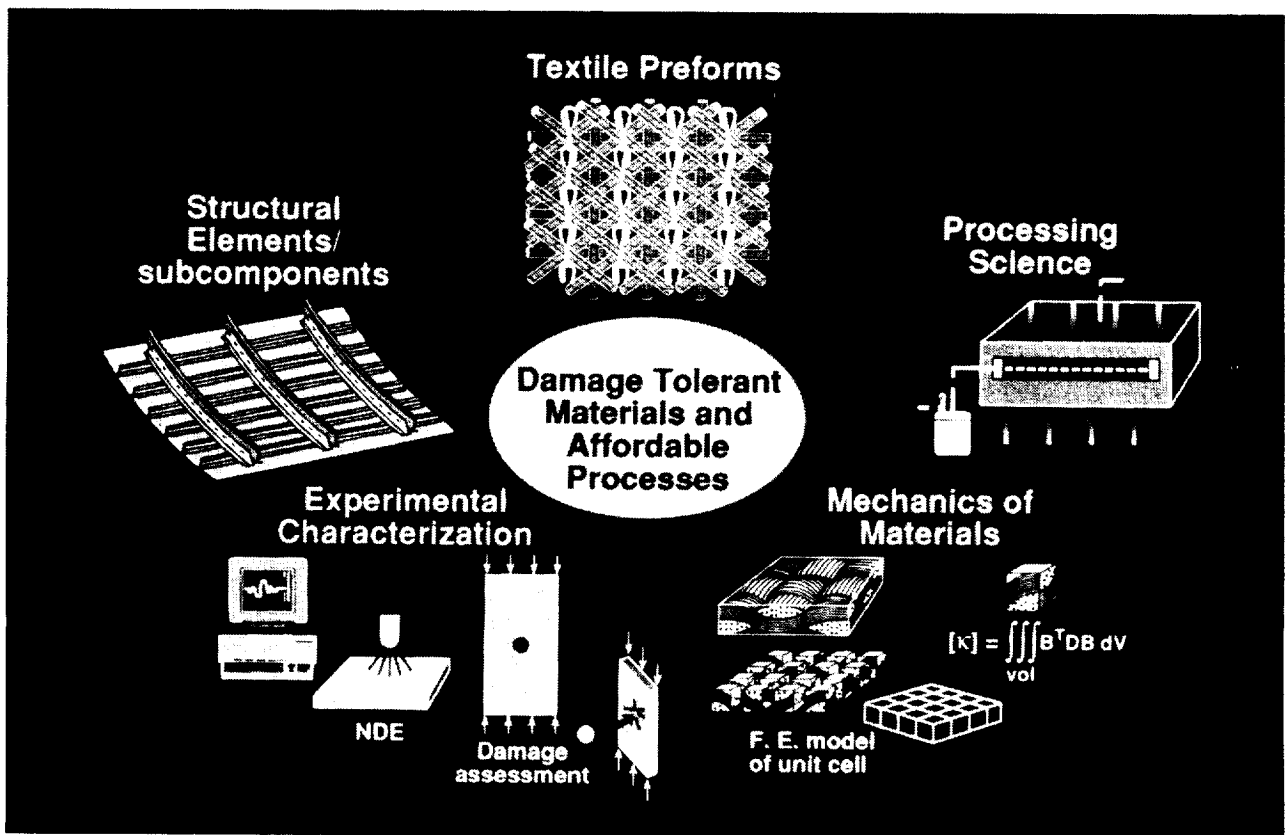


Figure 2

TEXTILE MATERIAL FORMS OF INTEREST

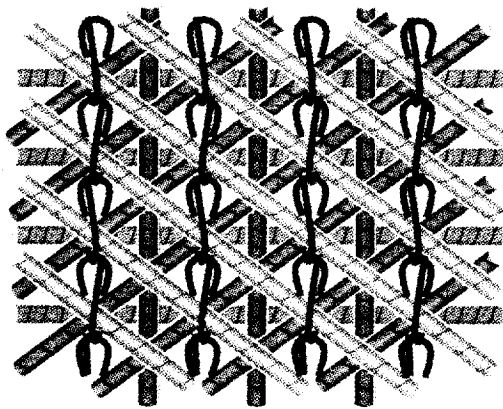
Textile material forms that have the most potential for primary aircraft structural applications are indicated in figure 3. The ultimate goal is to minimize the number of individual plies required to build-up part thickness. Integral weaving and braiding will result in near-net structural shapes that require only minimal machining and fastening. Multilayer-multiaxial knitted fabrics are being investigated as a cost-effective replacement for biaxial woven broadgoods. The knitted fabrics can be postformed to achieve selected structural shapes. If high concentrations of 0-degree reinforcements are required, low crimp uniweave fabric can be added to woven, knitted, or braided material forms. Through-the-thickness stitching has been used to provide improved out-of-plane strength, damage tolerance, and delamination resistance. It is expected that continued developments in automation of textile processes will result in significant cost savings in fabricating textile preforms for aircraft structures.

- **Low crimp uniweave fabric**
- **Integrally woven fabric shapes (2-D, 3-D)**
- **Multiaxial knitted fabric (0, 90, $\pm\theta$)**
- **Braided preforms (2-D, 3-D, interlock)**
- **Stitched combinations of woven, knitted and braided preforms**

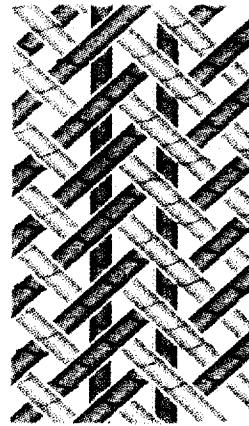
Figure 3

TEXTILE MATERIALS BEING EVALUATED

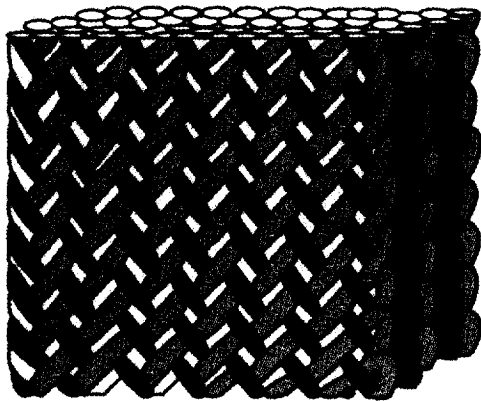
The textile materials that are currently being investigated in the NASA Langley program are shown in figure 4. Quasi-isotropic (+45, 0, -45, 90) multiaxial warp knit fabrics have been produced by Hexcel and Milliken. Tests have been completed to assess performance differences between 3, 6, and 12K tows. Kevlar and polyester knitting yarns and Kevlar and carbon stitching yarns are being investigated. Triaxial (0 ± 30) braids produced by Fiber Innovations have been evaluated. Both stitched and unstitched materials have been tested. Atlantic Research has produced 3-D braids for improved impact resistance and tests have been conducted. Test results have been compared to results for stitched triaxially braided materials. A new braiding process called layer-to-layer interlock has been developed by Albany International and tests are underway. Several different 3-D interlock weave configurations have been produced by Textile Technologies, Inc. All of these materials are being tested to assess mechanical properties and impact damage tolerance. Stitched uniweave fabric is being evaluated extensively by Douglas for damage tolerant wing structures.



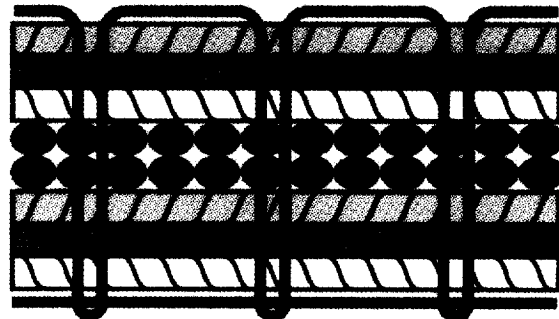
**Multiaxial warp knit
(stitched & unstitched)**



**2-D triaxial braid
(stitched & unstitched)**



3-D braid



Uniweave/stitched

Figure 4

NET-SHAPED TEXTILE PREFORMS

Some of the textile preforms that are being considered for structural applications are shown in figure 5. Weaving is well-suited for production of stiffened panels. However, automated weaving processes are currently limited to (0/90) fiber orientations in the skin and stiffening elements. Off-axis reinforcement, if required, must be bonded or stitched onto the surfaces of the (0/90) preform. Two-dimensional multilayer braiding is being used to produce complex curved shapes such as fuselage frames. The braiding process provides multidirectional fiber continuity throughout the preform structural shape. Both 2-D and 3-D braiding processes can produce structural shapes that are difficult or inefficient to achieve by other processes.

The knitted sine wave beam shown in figure 5 was produced by postforming knitted fabric to a specified shape. Epoxy powder tackifiers or stitching can be used to tack layers together. The integrally woven Y-spar shown in figure 5 can be produced in continuous lengths. As with the hat-stiffened panel, off-axis reinforcement must be added to the spar as a secondary operation.

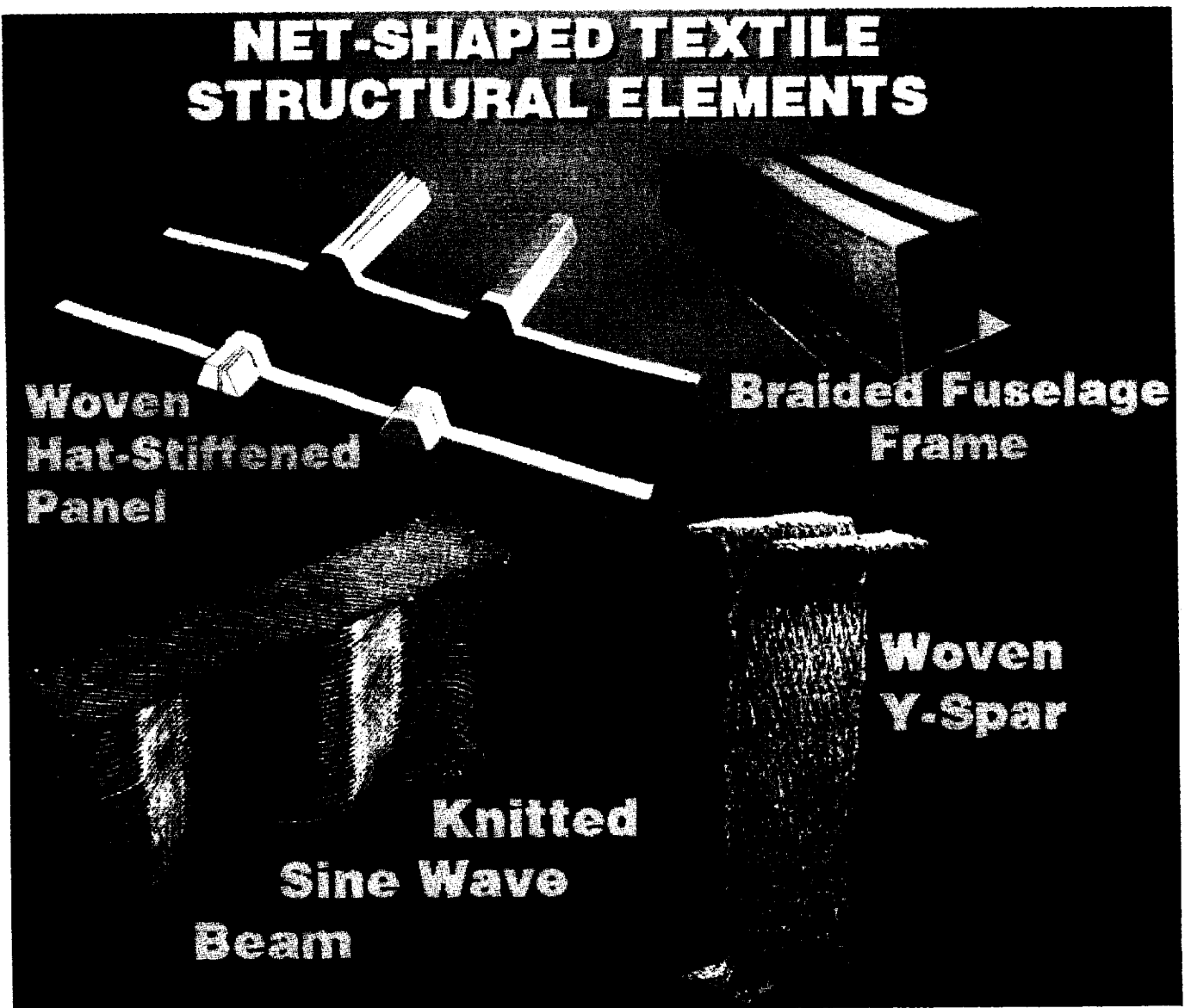


Figure 5

COST-EFFECTIVE PROCESSES AND FABRICATION METHODS

Cost-effective processes and fabrication methods must be developed to produce cost-competitive aircraft-quality composite structures from the preforms discussed previously. The objectives and program elements for this research are shown in figure 6. Two major areas of research focus are resin transfer molding (RTM) and powder-coated towpreg. RTM is one of the most promising processes to achieve cost-effective structures because it uses resins and fibers in their lowest cost form. RTM has been used for many years but previous applications did not have stringent performance requirements. New resins with enhanced flow properties, higher strength, and improved toughness are currently under development. Appropriate tooling concepts must be developed to make cost-effective use of RTM. Analytical models are being developed to understand the RTM process and to eliminate trial-and-error procedures that are commonly used.

Powdered resins are a potential alternative to RTM. Powder-coated tows, if properly prepared, can be used in textile processes such as weaving and braiding. Hence, pumping of resin into the preform, as with RTM, can be eliminated. The powder coating process is in its infancy and significant research is required before aircraft-quality composite structures can be produced. The research program elements shown in figure 6 are currently being pursued by NASA Langley, aerospace contractors, and universities.

- **Objectives**
 - **Develop innovative processes and tooling concepts for RTM**
 - **Optimize powder coating techniques, demonstrate weaving and braiding characteristics, and develop fabrication processes**
- **Program elements**
 - RTM**
 - **Improved RTM resins with high modulus, strength and toughness**
 - **Analytical processing science models for liquid, semi-solid and paste resins**
 - **Innovative compaction and tooling concepts for structural elements**
 - Powdered resins**
 - **Optimized powder coating techniques**
 - **Weaving and braiding trials**
 - **Fiber wet-out and preform consolidation studies**
 - **Tooling concepts for complex structural shapes**
 - **Technology demonstration through structural element fabrication**

Figure 6

PROCESSING SCIENCE OF TEXTILE REINFORCED COMPOSITES

Science-based processing studies are underway for textile reinforced composites. Analytical and experimental studies are being conducted to characterize preform and resin behavior for RTM. Major program elements are shown in figure 7. To model the RTM process, preform properties such as permeability and compaction, and resin viscosity as a function of temperature and time, must be known. Experimental studies are underway to determine preform permeability and compaction coefficients as a function of preform architecture. Resin infiltration studies are underway to predict how various resins flow through porous fiber preforms. Infiltration is affected by preform porosity, resin viscosity, flow direction, and applied pressure. Once the preforms are infiltrated, a cure kinetics analysis is performed to predict the degree of cure. A finite element analysis that utilizes preform and resin characteristic data has been employed to predict initial resin mass required, resin front position and time required for preform infiltration, resin viscosity and degree of cure, and final part thickness and fiber volume fraction.

Dielectric sensors are being used to track resin behavior as a function of time and to verify the RTM simulation model discussed above. The sensors can monitor infiltration position, resin viscosity, and degree of resin cure. The in-situ sensors can be used for real-time feedback control so that processing parameters can be modified if required. Flow visualization studies are being conducted to verify flow front position and to substantiate sensor output.

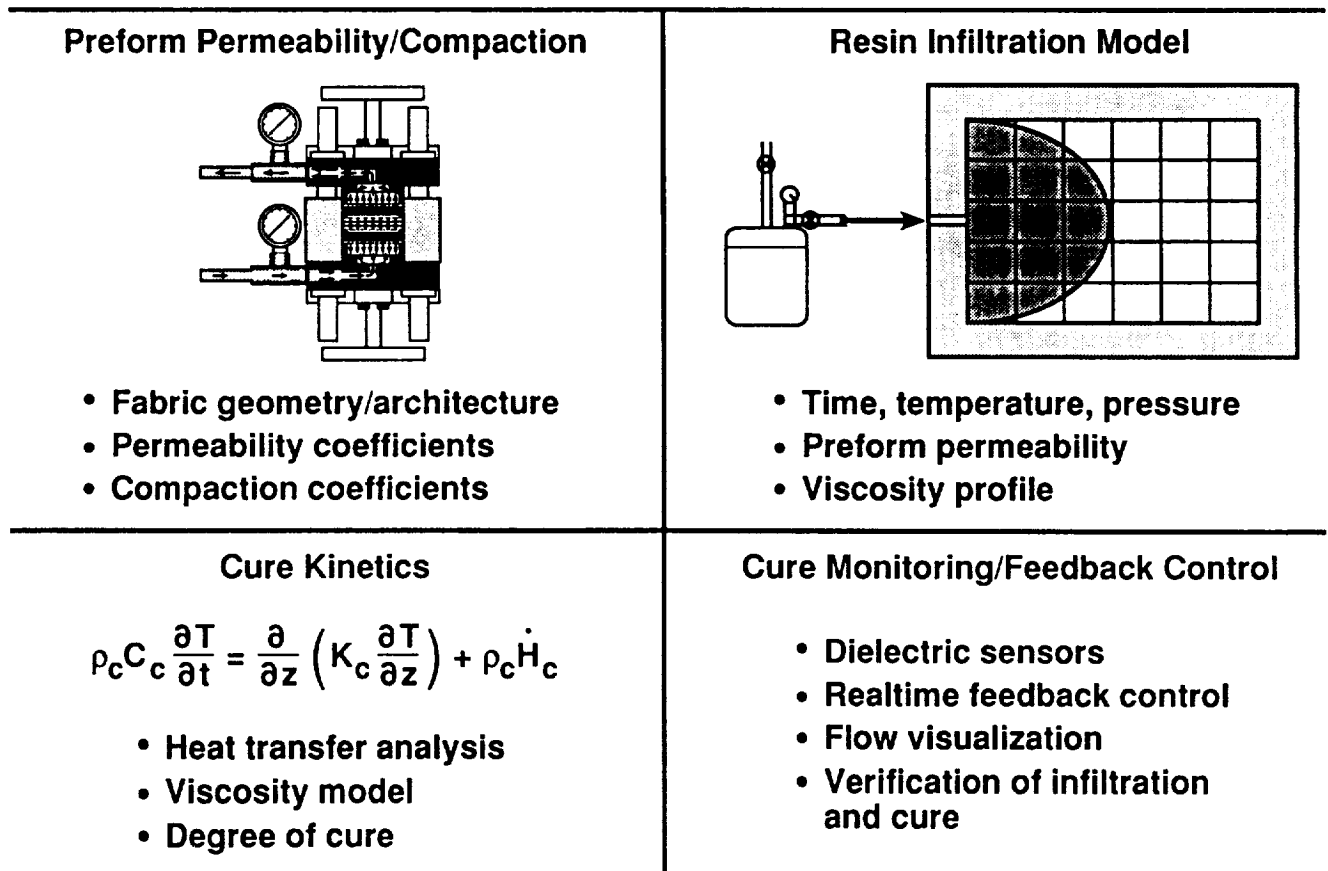


Figure 7

COMPACTION AND PERMEABILITY CHARACTERISTICS OF HEXCEL KNITTED FABRIC

An important part of resin transfer molding textile material forms is understanding the compaction and permeability characteristics of the material. Compaction and permeability coefficients can be used to predict fiber volume fraction and ease of resin infiltration. As shown in figure 8, fiber volume fraction and fabric thickness are nonlinear functions of compaction pressure. The Hexcel knitted fabric had a nominal uncompact fiber volume fraction of approximately 37 percent and a thickness of approximately 0.39-inch. To achieve a fiber volume fraction of 60 percent and a final thickness of 0.250-inch, a compaction pressure of approximately 35 psig is required.

Also shown in figure 8 is the effect of fiber volume fraction on permeability. Permeability is a function of fabric architecture, compaction, porosity, and fluid flow direction. Permeability along a fiber bundle can be an order of magnitude greater than transverse to the fiber bundle. Permeability for the Hexcel knitted fabric is approximately $5 \times 10^{-10} \text{ in}^2$ for a fiber volume fraction of 60 percent. At a fiber volume fraction of 50 percent, the fabric would be much easier to infiltrate at a permeability of $14 \times 10^{-10} \text{ in}^2$.

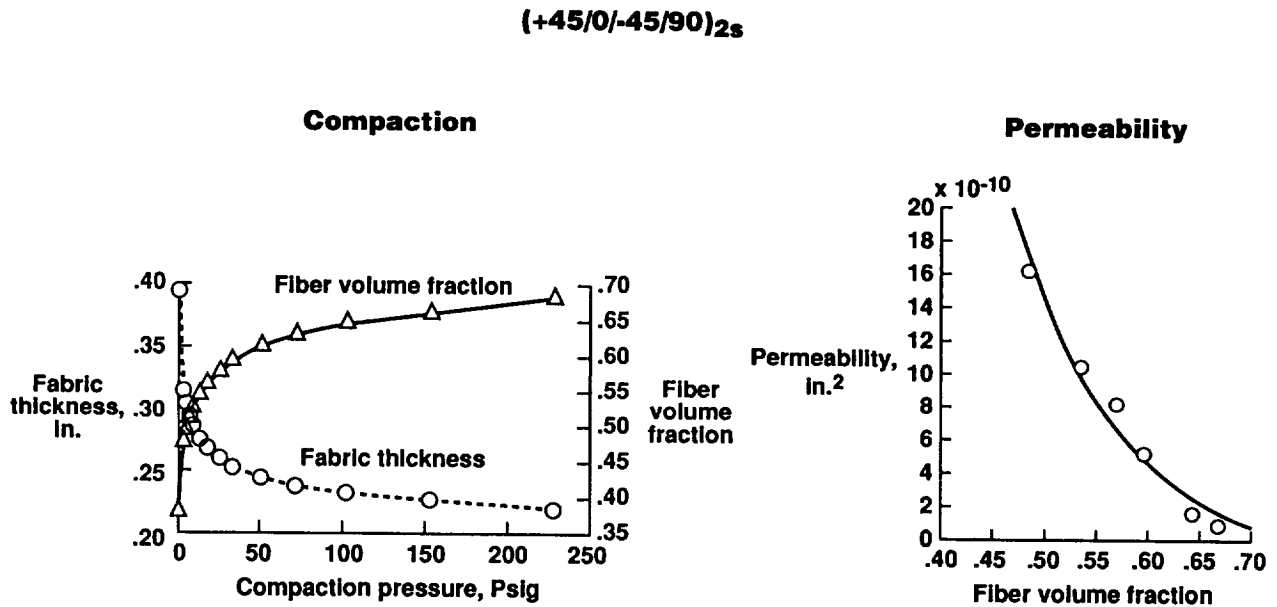


Figure 8

FLOW VISUALIZATION APPARATUS

Flow visualization experiments were conducted to vary analytical predictions of flow front position as a function of time. The experimental apparatus is shown in figure 9. Major components in the experimental set-up included an injection mold with a poly (methyl methacrylate) top plate, a video camera and high resolution tape recorder, and an air pressurized resin pot. In addition, a total of nine Frequency Dependent Electromagnetic Sensors (FDEMS) were mounted in the aluminum bottom plate of the mold. The output leads from the sensors were connected to a multiplexer which was used to analyze the signals from the sensors. Resin can be injected into the mold through a center injection port or side ports. Once the resin comes in contact with a particular sensor, a definitive change in the sensor output is recorded and the time required for sensor wet-out is compared with analytical predictions.

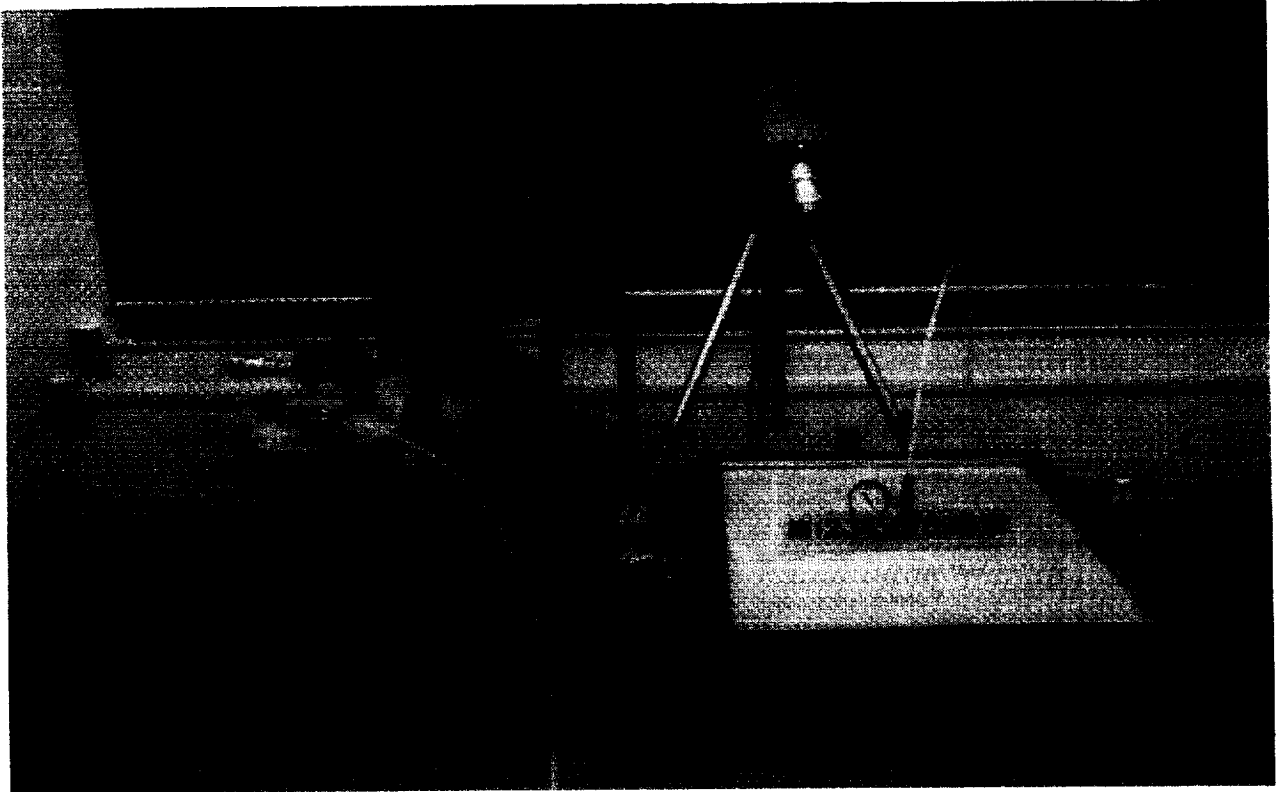


Figure 9

VERIFICATION OF RTM MODEL AND FDEMS SENSOR

Flow visualization experiments were conducted to compare predicted resin flow fronts with measured flow fronts. To enhance visualization, a fiberglass fabric with corn oil and red dye were used in the initial experiments. The viscosity of the oil and dye mixture was measured to be 40 cp. Test results are shown in figure 10 for a center port injection at an injection time of 30 seconds. An overlay of the predicted flow front and the sensor locations are also shown in the figure. Test results indicate that sensor number 4 wet-out at 27 seconds which is in close agreement with the flow front prediction. Additional experiments are underway to verify analytical predictions for aerospace grade RTM resins.

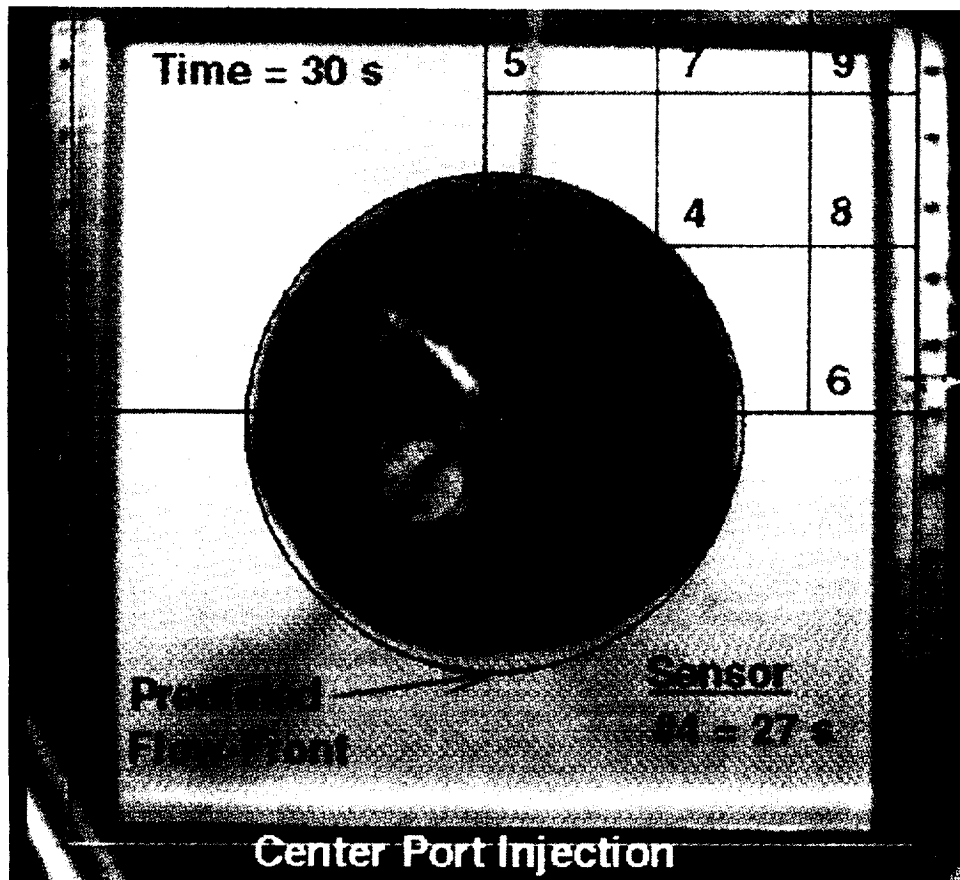


Figure 10

POWDER-COATED TOWPREG TECHNOLOGY FOR TEXTILE REINFORCED COMPOSITES

NASA Langley is conducting in-house research and is sponsoring grant and contract research to advance powder-coated towpreg technology. The objective of this research is to develop powder-coated towpreg technology as a viable alternate to RTM for fabrication of textile reinforced composites. The approach outlined in figure 11 includes optimization of the process, verifying the capability to weave and braid complex preforms, understanding compaction (bulk factor) and consolidation issues, and fabrication high quality structural elements. BASF and Lockheed Aeronautical Systems Company are key participants in an effort to scale-up the process for production applications. Three-dimensional woven panels and braided frames are being fabricated to assess the viability of the powder-coated towpreg process.

- **Objective:**

- **Develop powder-coated towpreg technology as a viable alternate to RTM for fabrication of textile reinforced composites**

- **Approach:**

- **Optimize coating processes**
- **Verify capability to weave and braid preforms**
- **Conduct compaction/consolidation studies**
- **Fabricate panels and frames and evaluate structural performance**

Figure 11

POLYMER POWDER RESEARCH

Some of the powders and product forms that are being investigated in the NASA LaRC program are listed in figure 12. Four different epoxy powders and two polyarylene ether powders are being investigated for subsonic commercial transport applications. Several polyimide and bismaleimide powders are being considered for application to future high-speed civil transport aircraft. The uniformity of powder deposition is indicated in the photograph of powder prepreg. Eight harness satin fabric that was woven with powder-coated towpreg is shown in the lower left of figure 12. Processing/consolidation studies are underway with this fabric. Mechanical properties will be compared with properties obtained with conventional prepreg fabric.

Some of the powder-coated product forms that are being investigated include uniweave prepreg tape, woven broadgoods, 2-D/3-D woven and braided textile preforms, and towpreg ribbon for use in advanced tow placement machines.

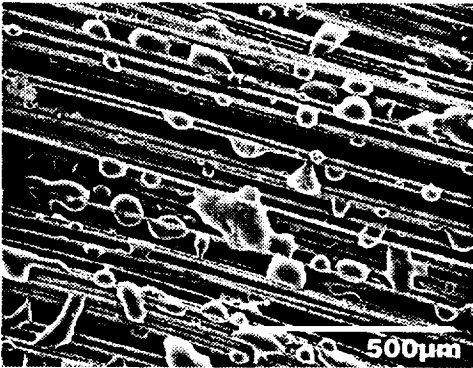
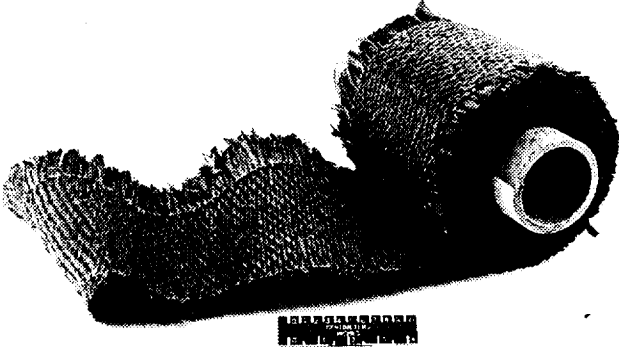
Powder Resins	Powder Prepreg
<p>Epoxies:</p> <ul style="list-style-type: none">CET-3 (Dow)PR-500 (3M)High Tg (3M)RSS1952 (Shell) <p>Polyarylene ethers:</p> <ul style="list-style-type: none">PEEK (ICI)PEKK (DuPont) <p>Polyimides:</p> <ul style="list-style-type: none">LaRC-TPI (MTC)PMR-15 & Mods (LaRC)New-TPI (MTC) <p>Bismaleimides:</p> <ul style="list-style-type: none">Compimide (Shell)	
Woven Powder Towpreg	Product Forms
	<ul style="list-style-type: none">• Uniweave prepreg tape• Woven broadgoods• 2-D/3-D woven and braided textile preforms• Towpreg ribbon for advanced tow placement

Figure 12

MECHANICS OF MATERIALS MODELS FOR TEXTILE COMPOSITES

NASA Langley has assembled a team of mechanics experts to develop methodologies and models to predict performance of textile reinforced composites. The major program elements are outlined in figure 13. An accurate description of the fiber architecture is required to adequately predict mechanical response. Mathematical formulations are being developed to describe yarn path and geometry of repeating unit cells. Stress-strain relationships will be developed from the homogeneous or continuum mechanics viewpoint. The upper right schematic in figure 13 illustrates a strategy that is mathematically similar to the finite element discretization method. Master subcells that reflect the essence of the repeating geometry are arranged in the pattern necessary to model the unit cell. The stiffness matrix for the unit cell is computed by standard matrix manipulations of the stiffness matrices of the master subcells. This type of model may be used to directly define the A, B, D coefficients or to calculate effective elastic moduli by imposing the correct boundary conditions on the unit cell.

Continuum level strength models will be developed in conjunction with the stress-strain models. This will allow a first approximation of load carrying capacity to be obtained from the average stresses computed by a global structural analysis using the homogenized stiffness properties. The average stresses will then be evaluated in a tensor polynomial failure criterion, for example, using phenomenological strength parameters determined from simple coupon tests.

A methodology will be developed to predict damage progression and residual strength using global/local analysis strategies to address damage tolerance requirements. Initial emphasis will be on modeling impact damage. Fatigue behavior will be experimentally characterized and then treated analytically. Fatigue life prediction methodologies will be developed for in-plane tension and compression loads and for out-of-plane loads.

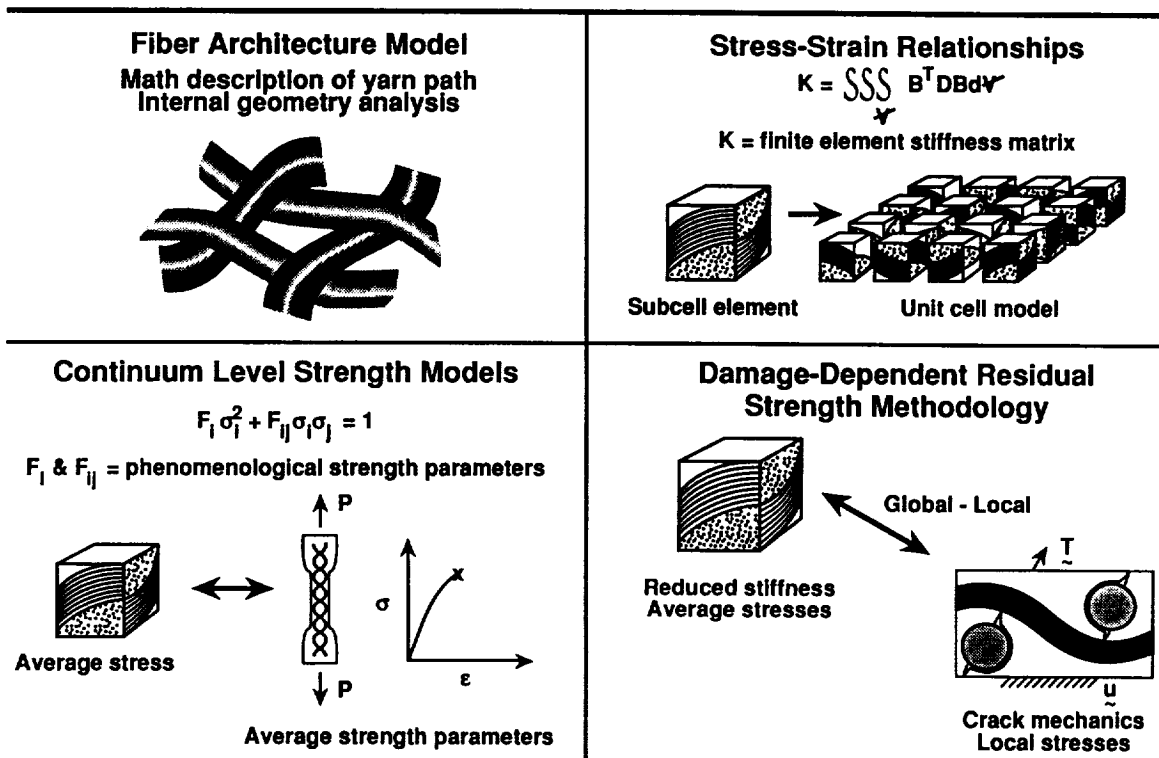


Figure 13

EXPERIMENTAL CHARACTERIZATION AND PRELIMINARY DESIGN PROPERTIES

An experimental characterization program is underway at NASA Langley to develop mechanical properties, damage tolerance, and preliminary design properties for textile reinforced composites. The objectives and program elements are shown in figure 14. Materials being characterized include woven, braided, knitted, and stitched fiber architectures. Most of the tests conducted to date have focused on in-plane mechanical properties and impact damage tolerance. A limited amount of fatigue tests have been conducted under compression-compression constant amplitude loading. Additional fatigue tests that include tension-tension and tension-compression cyclic loading are being conducted. Bearing and out-of-plane strength tests are also being conducted to assess material performance. Structural element level tests such as crippling, stiffener pull-off, and panel buckling will be expanded in the near future. Special fixtures and load introduction techniques will be developed as necessary. These tests will provide preliminary design properties and a database for comparison with analytical models.

- **Objectives**
 - **Develop experimental data base to characterize the mechanical behavior and damage tolerance of selected textile architectures**
 - **Develop preliminary design properties to support design of selected structural elements and subcomponents**
- **Program elements**
 - **In-plane mechanical properties data base for woven, braided and knitted/stitched composites**
 - **Out-of-plane strength and delamination resistance**
 - **Impact damage tolerance and notch effects**
 - **Bearing/mechanical fasteners**
 - **Tension and compression fatigue response**
 - **Preliminary design properties for specific structural elements and subcomponents**

Figure 14

TEST SPECIMENS

The test specimens that are currently being used in the NASA Langley in-house test program are shown in figure 15. The specimens have a nominal thickness of 0.250 inch with length and width as indicated in the sketches. Test results obtained to date indicate that strain gages must be selected to match particular fiber architectures. Factors such as tow size, tow spacing, and textile unit cell dimensions must be accounted for in making strain measurements. For example, a material braided with 3K tows will have a smaller unit cell than a material braided with 12K tows. The local strain response of these materials may be different, and different size strain gages may be required to accurately measure material response. Strain gages that are located directly over a through-the-thickness stitch could be affected by local material response. The size and location of resin pockets could also affect local material response. Additional research on development of standard test methods for textiles will be discussed in a subsequent figure.

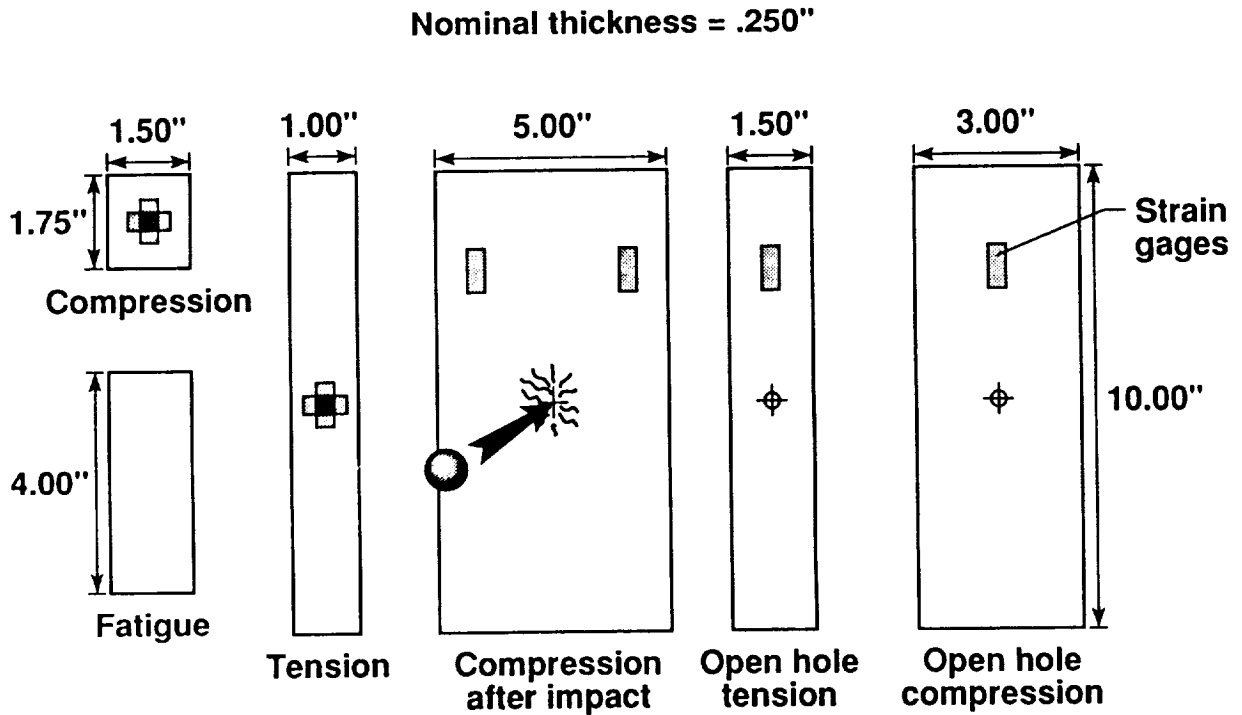


Figure 15

MULTIAXIAL WARP KNITTING CONCEPTS

Several multiaxial warp knitting concepts are being investigated at NASA Langley. Two concepts for aerospace grade carbon fabrics are shown in figure 16. Equipment is available at Milliken and Hexcel to produce the fabric concepts indicated in the figure. The Milliken fabric is knitted on a Mayer multiaxial warp knitting machine that spaces the carbon fiber tows leaving gaps that allow the knitting needles to pass through the fabric without damaging the carbon tows. As indicated in the figure, a chain knit is used.

Hexcel fabrics were knitted with both chain and tricot knit styles, as shown in the figure. The tricot knit is required to hold 0-degree tows on the surface of the fabric. The Hexcel fabric is knitted on a Liba multiaxial warp knitting machine that does not provide gaps for the knitting needles to pass through the fabric. As a result, the knitting needles impale and damage the carbon fiber tows as they pass through the fabric. Fiber misalignment is caused by the needle penetration and lack of tension on the carbon tows. The tradeoff in the two knitting methods is between fiber damage and misalignment and fiber volume fraction. The Mayer machine produces a fabric with less fiber damage but has a lower as-fabricated fiber volume fraction. Fiber volume fractions of over 60 percent have been achieved with the Milliken fabric but a consolidation pressure of well over 100 psi is required to spread the fibers and close the gaps between the carbon tows. Another knitting company, Saerbeck, that can produce high quality knitted carbon fabrics, utilizes a second generation Liba machine. Saerbeck has developed improved procedures to control tension on the carbon fibers during the knitting process.

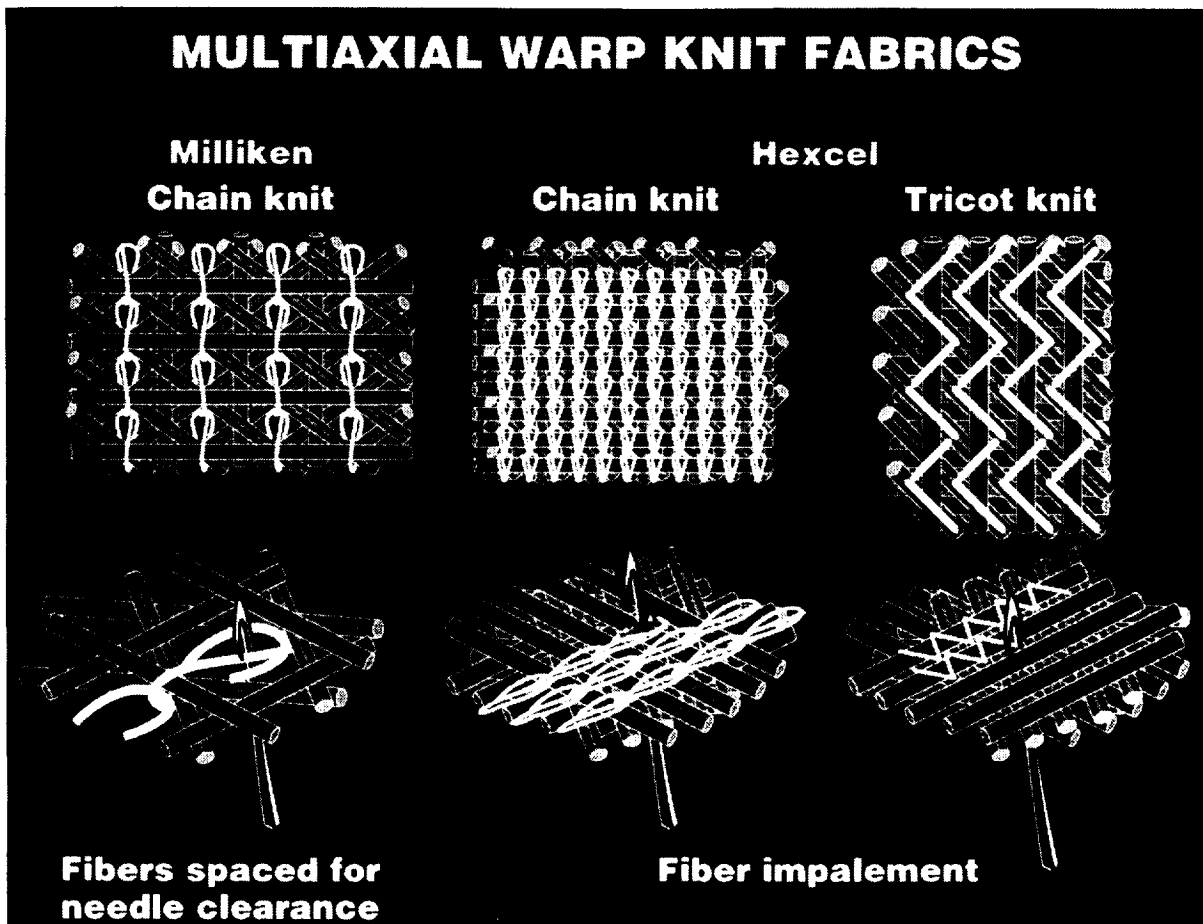


Figure 16

PHOTOGRAPHS OF KNITTED FABRICS

Photographs of the Hexcel, Milliken, and Saerbeck knitted fabrics are shown in figure 17. The Hexcel (+45, 0, -45, 90) chain knitted fabric shown in the upper left of the figure indicates significant gaps and fiber misalignment in the surface tows. Also, some fiber damage can be seen where the knitting yarns penetrate through the fabric. The Milliken (-45, +45, 0, 90) chain knitted fabric shown in the upper right of the figure indicates uniform gaps and minimal misalignment.

The Hexcel (0, -45, 90, +45) tricot knitted fabric has significant gaps between the 0-degree surface tows, whereas the Saerbeck (0, +45, 90, -45) fabric photograph indicates only small gaps between the 0-degree surface tows. However, some slight fiber waviness is evident in the Saerbeck fabric. The gaps in all the fabrics are potential sites for resin pockets to form during the resin transfer molding process. These resin pockets can contribute to the formation of microcracks in the cured composite.

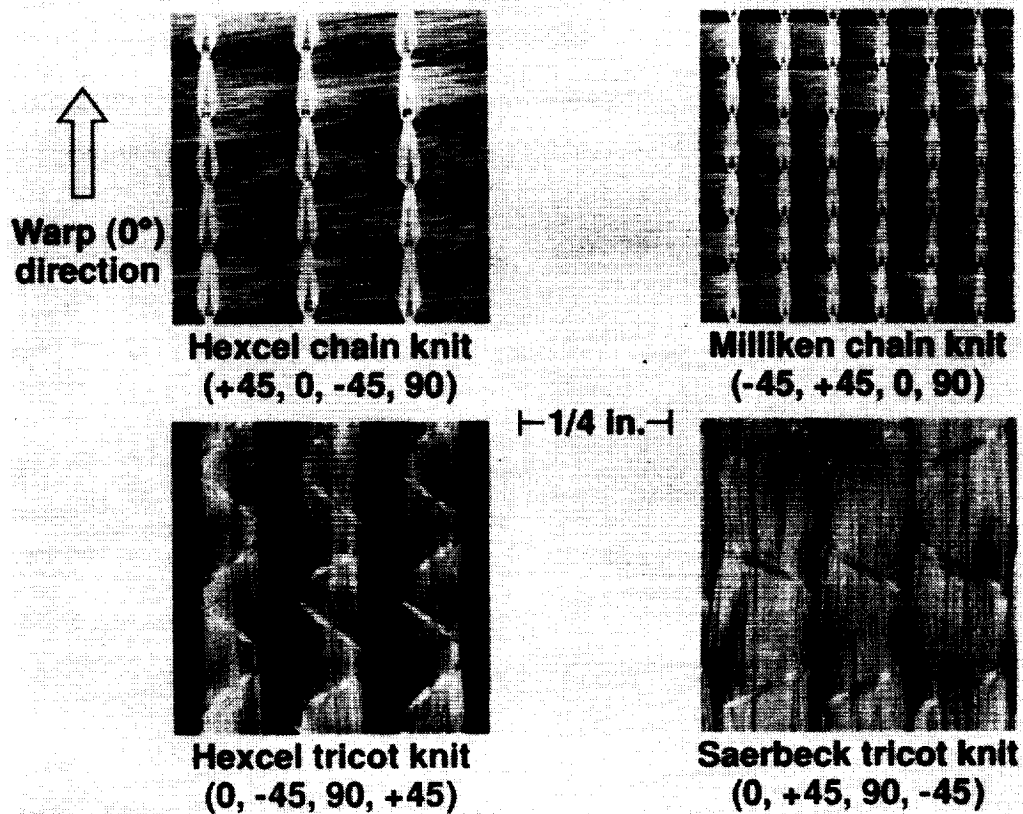


Figure 17

COMPRESSION STRENGTH OF KNITTED FABRIC COMPOSITES

The compression strengths of the Hexcel and Milliken knitted fabric laminates are compared with the strength of prepreg tape laminates in figure 18. Results indicate that the average compression strength for the Hexcel knitted fabric laminates is about 25 percent lower than the strength for the prepreg tape laminates. The Milliken knitted fabric laminates indicate a 20 percent reduction in compression strength compared to the prepreg tape laminates. These reductions in strength are partially attributed to fiber waviness caused by gaps in the knitted fabrics. No significant differences in compression strength were indicated between 3, 6, or 12K tows for the Hexcel knitted fabric laminates, or between the two resin systems used in either knitted laminates. These results indicate that significant cost savings can be achieved by using the larger tow sizes since fewer layers are required for thickness build-up and the larger tow sizes cost less per pound compared to the smaller tows.

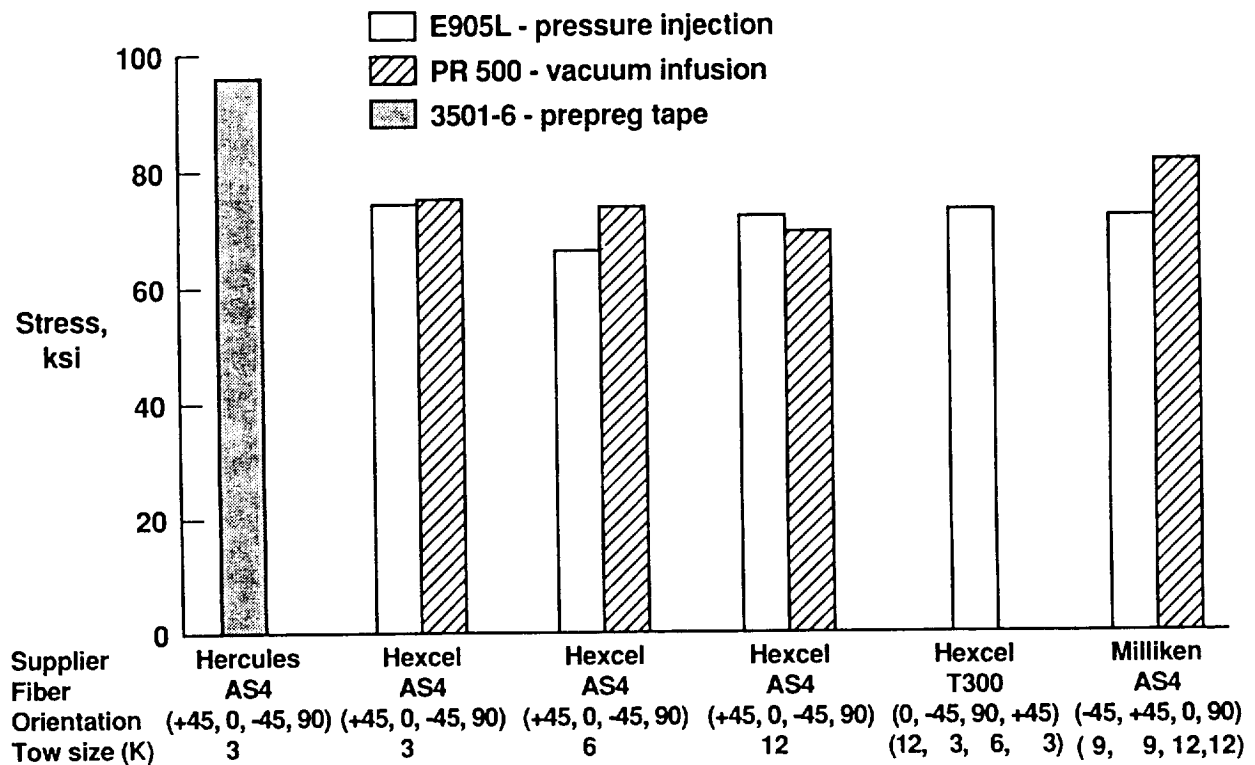


Figure 18

COMPRESSION AFTER IMPACT STRENGTH OF KNITTED FABRIC COMPOSITES

Compression after impact (CAI) strength tests were conducted to compare the damage tolerance of knitted fabric laminates with conventional prepreg tape laminates. The 1/4-inch thick laminates were impacted with 1/2-inch diameter aluminum spheres at an impact energy of 30 ft-lbs with the NASA Langley air gun. The test results shown in figure 19 indicate that the knitted fabric laminates that were resin transfer molded with the toughened PR 500 resin had CAI strengths up to 50 percent higher than the brittle 3501-6 prepreg tape laminates. The knitted fabric laminates with E905L resin had CAI strengths that were up to 30 percent higher than the prepreg tape laminates. These results indicate significant improvements in damage tolerance for the knitted fabric laminates. However, they still fall well below the target of 40 ksi, desirable for airframe structural applications. Additional through-the-thickness reinforcement such as heavy density stitching is required to achieve the target value.

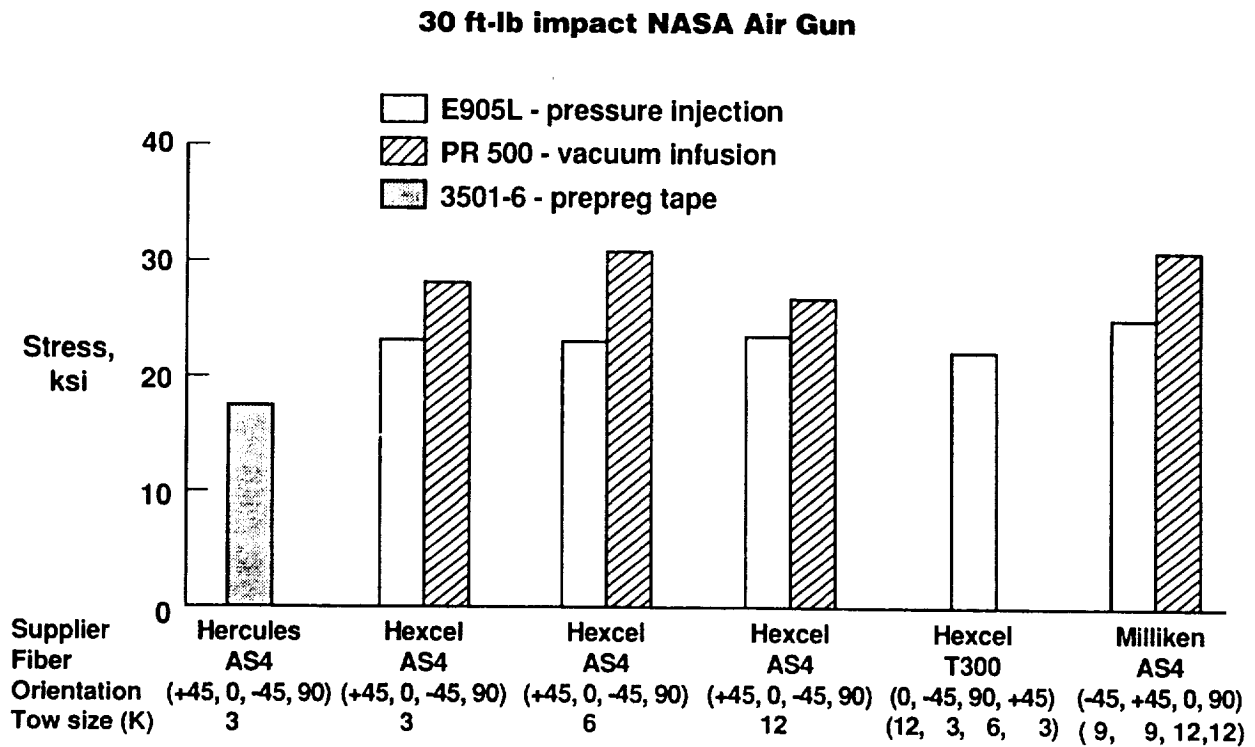


Figure 19

COMPRESSION AFTER IMPACT STRENGTH OF KNITTED/STITCHED FABRIC COMPOSITES

Compression after impact strength tests were also conducted to determine the effect of stitching on the strength of knitted fabric laminates, figure 20. The Hexcel preforms that were knitted with 3K and 12K tows were stitched by Ketema with a modified lock stitch. The preforms were stitched in the 0-degree direction in columns 0.33-inch apart with a stitch pitch of 1/8 inch. The Milliken preforms were stitched by Puritan Industries with a chain stitch. The panels were chain stitched in the 0-degree and 90-degree directions with rows and columns 1/4-inch apart with a stitch pitch of 1/8 inch. All the preforms were stitched with a 1500 denier Kevlar thread.

The panels were impacted at an energy level of 30 ft-lbs with the same procedure described earlier. The Milliken knitted/stitched fabric laminates with the PR 500 resin system achieved the target of 40 ksi CAI strength. The Hexcel knitted/stitched laminates fell below the target. The toughened PR 500 resin system exhibited consistently higher CAI strengths than the E905L, as was noted in the unstitched results. Results of a previous stitching study, reference 1, indicated strengths over 45 ksi with stitched uniweave fabric laminates when a stitch spacing of 3/16 inch was used. Based on those findings, it is expected that the Hexcel fabric laminates would achieve the target value if the stitch spacing was reduced to no more than 3/16 inch. Additional details on test results for knitted fabrics are reported in reference 2.

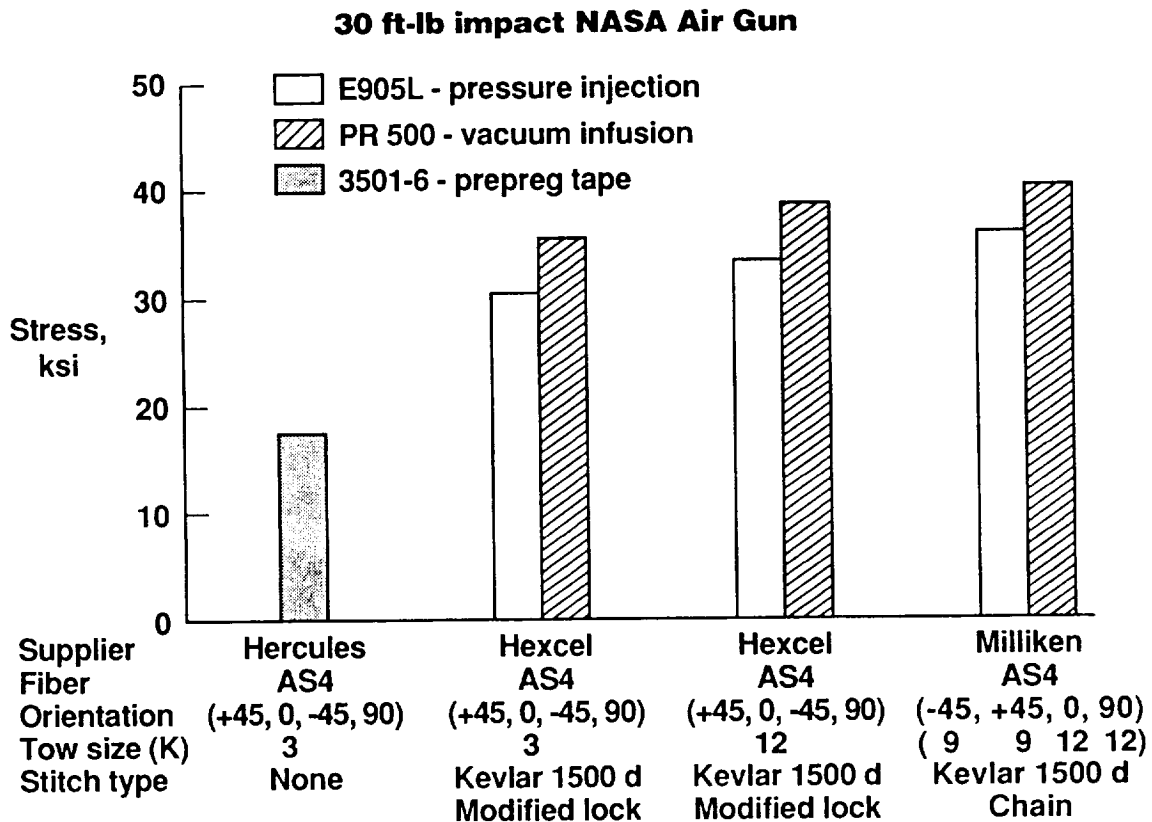


Figure 20

PERFORMANCE COMPARISON OF AS4/PR500 SAERBECK KNITTED AND UNIWEAVE FABRIC COMPOSITES

Douglas Aircraft Company and NASA Langley have been developing a data base on uniweave fabrics for application to wing structural components. The Douglas design for the wing skin material consists of 54 plies of uniweave fabric with 44 percent of the fibers in the 0-degree direction, 44 percent of the fibers in the ± 45 -degree directions, and 12 percent of the fibers in the 90-degree direction. Concerns for stability and the ability to handle large pieces of the uniweave fabric led Douglas to investigate other fabric options. A knitted fabric produced by Saerbeck in Germany was selected. A description of the fabric was discussed earlier. The test results presented in figure 21 were developed at NASA Langley in a cooperative effort with Douglas. It should be noted that the test results are preliminary and additional tests are planned to expand the data base.

Tension, compression, open hole tension, open hole compression, and CAI tests were conducted to compare the performance of the knitted and uniweave fabric laminates. All of the fabrics were resin transfer molded with the 3M PR 500 resin except the stitched uniweave CAI panel which was fabricated with Hercules 3501-6 resin. Also, the uniweave panel was stitched with S-2 glass whereas the Saerbeck panel was stitched with Kevlar. The stitched uniweave panel was impacted at an energy level of 40 ft-lbs with a drop weight apparatus. The other panels were impacted at an energy level of 30 ft-lbs with the air gun previously described. Test results shown in figure 21 indicate comparable performance between the two fabrics. Both fabrics meet the design requirements for the Douglas wing skin. It should be noted that the Saerbeck knitted fabric consisted of six 4-ply stacks whereas the uniweave fabric consisted of 54 plies to build up the required thickness of 0.30 inch. This difference has important cost implications in terms of labor savings.

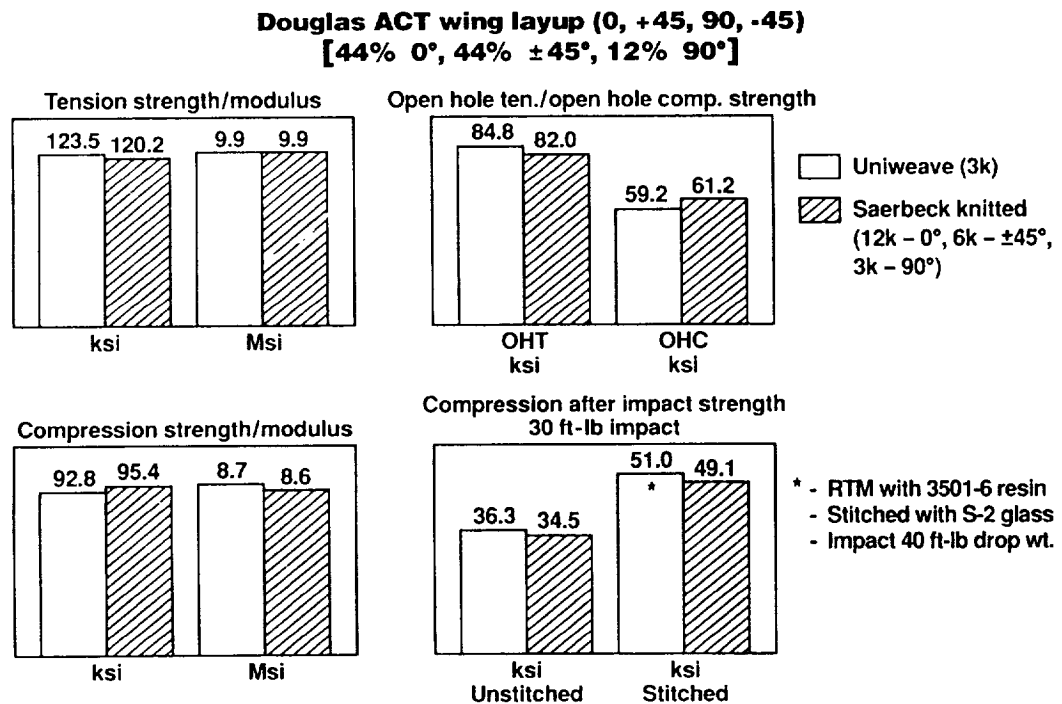


Figure 21

COMPRESSION AND COMPRESSION-AFTER-IMPACT STRENGTH OF BRAIDED COMPOSITE PANELS TESTED IN THE 0° DIRECTION

Compression and compression-after-impact (CAI) strengths of 2-D braided, 2-D braided/stitched, and 3-D braided composites are compared in figure 22. The braided preforms were fabricated with AS4 carbon fibers with a ($\pm 30/0$) fiber architecture. The preforms were infiltrated with British Petroleum E905L epoxy resin. An impact energy of 30 ft.-lbs was used to impact the panels, which had nominal thicknesses of 0.24 inch.

Test results indicate that the 3-D braided panels had the highest undamaged strength, over 60 ksi, whereas the 2-D braided/stitched panels had the highest CAI strength, over 40 ksi. It is somewhat surprising that the CAI strength for the 3-D braided panels was only slightly better than the CAI strength for the 2-D braided panels which have no through-the-thickness reinforcement. Additional testing is underway to further understand the behavior of braided materials. Additional details on braided test results are reported in reference 3.

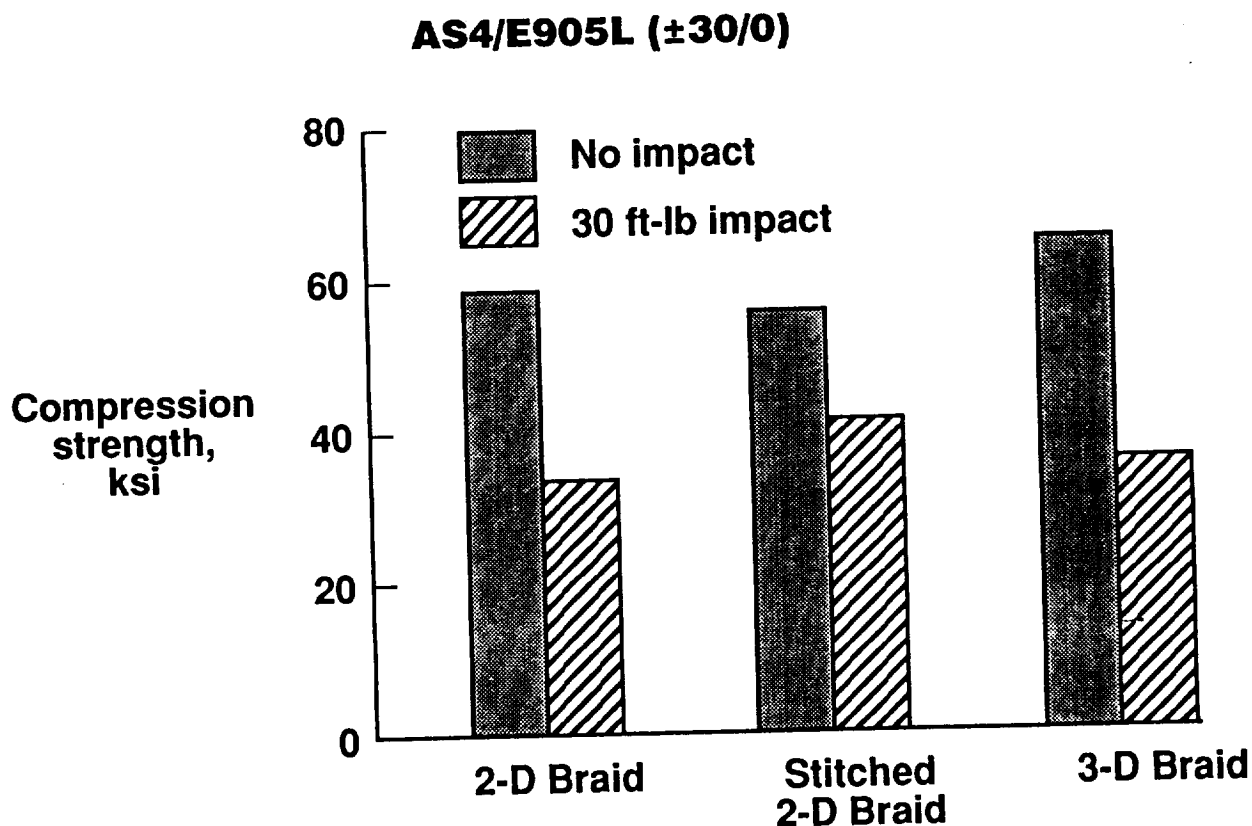


Figure 22

STANDARD TEST METHODS FOR TEXTILE REINFORCED COMPOSITES

New test techniques will be required to characterize some of the unique properties of textile reinforced composites. The sketches shown in figure 23 indicate some of the types of tests that must be conducted to explore the benefits of textile material forms. Some of the currently used in-plane test methods may be adequate for textile materials. However, modification of specimen dimensions and strain measurement techniques may be required for some textile architectures. The effect of textile unit cell dimensions on mechanical behavior must be characterized. Since textile materials with through-the-thickness reinforcement offer significant improvement in out-of-plane load capability, adequate test methods must be developed to assess performance improvements. Subelement level tests such as stiffener pull-off must also be developed. Analytical studies, in conjunction with experiments, must be performed to assure that stress states are understood and that local effects are representative of global material response. Available standard test methods in the composites industry will be investigated and used where appropriate.

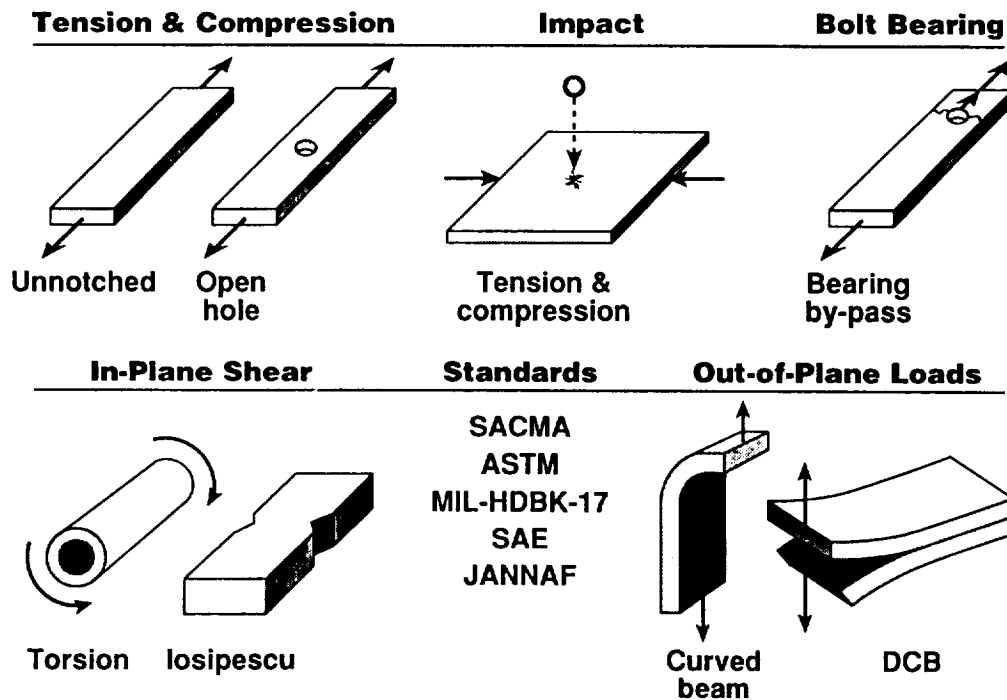


Figure 23

TEXTILE REINFORCED COMPOSITE FUSELAGE SUBCOMPONENTS

As part of the ACT program, specific fuselage subcomponents were selected as candidates for application of textile material forms. Based on discussions between NASA Langley, Lockheed, Grumman, and Boeing, the four subcomponents shown in figure 24 were selected. These structural subcomponents were selected to exploit damage tolerance and through-the-thickness strength capability of textile materials. Structural tests will be conducted on each structural subcomponent to verify the performance of textile architectures. Analytical predictions will be performed and results will be correlated with experimental behavior.

Particular design issues associated with each subcomponent are indicated in figure 24. Several textile processes such as integral weaving, braiding, knitting, and stitching are being used to produce near net-shaped structural subcomponents. Some obvious candidates include continuously braided circumferential frames, integrally woven stiffened panels, and stitched reinforcement around window openings. An integrated design-build-team effort is being conducted by Boeing, Lockheed, and Grumman. This is necessary since some of the subcomponents will be delivered to Boeing for test in their fixtures. Additional test articles will be delivered to NASA Langley for testing in new combined load machines/fixtures that are under development.

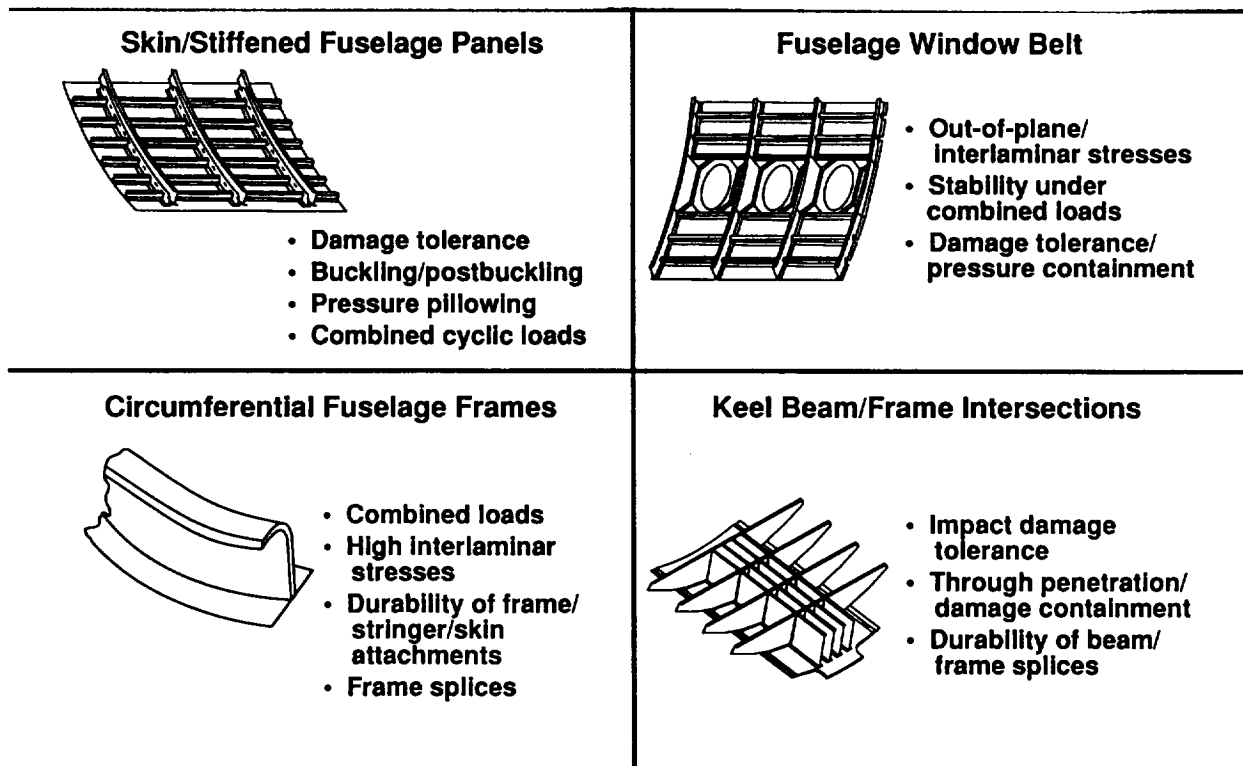


Figure 24

WOVEN/STITCHED WINDOW BELT PREFORM

As discussed previously, Grumman is conducting research on textile preforms for applications to fuselage structures. The fuselage window belt is an area of the fuselage that has complex loading states and is a good candidate for textile reinforced composites with through-the-thickness reinforcement. The window belt preform shown in figure 25 was designed by Grumman and fabricated by ICI Fiberite. The cross-stiffening elements were integrally woven in one piece with IM7 carbon fibers. The 0-degree fibers along the webs of the stiffening elements are continuous through the intersections. To achieve the necessary shear stiffness for the stiffeners, ± 45 -degree woven fabric was laid up over the stiffener elements and subsequently stitched onto the skin through the stiffener flanges with Kevlar thread. The window belt preform will be resin transfer molded by R-Cubed Composites. The window cut-outs will be machined away prior to shear testing by Grumman.

A second preform is being fabricated by Textile Technologies, Inc. and Fiber Innovations, Inc. This preform will be fabricated with 2-D braiding in the stiffening elements and 2-D weaving in the skin. The preform will be fabricated with AS4 carbon fibers and Kevlar stitching.

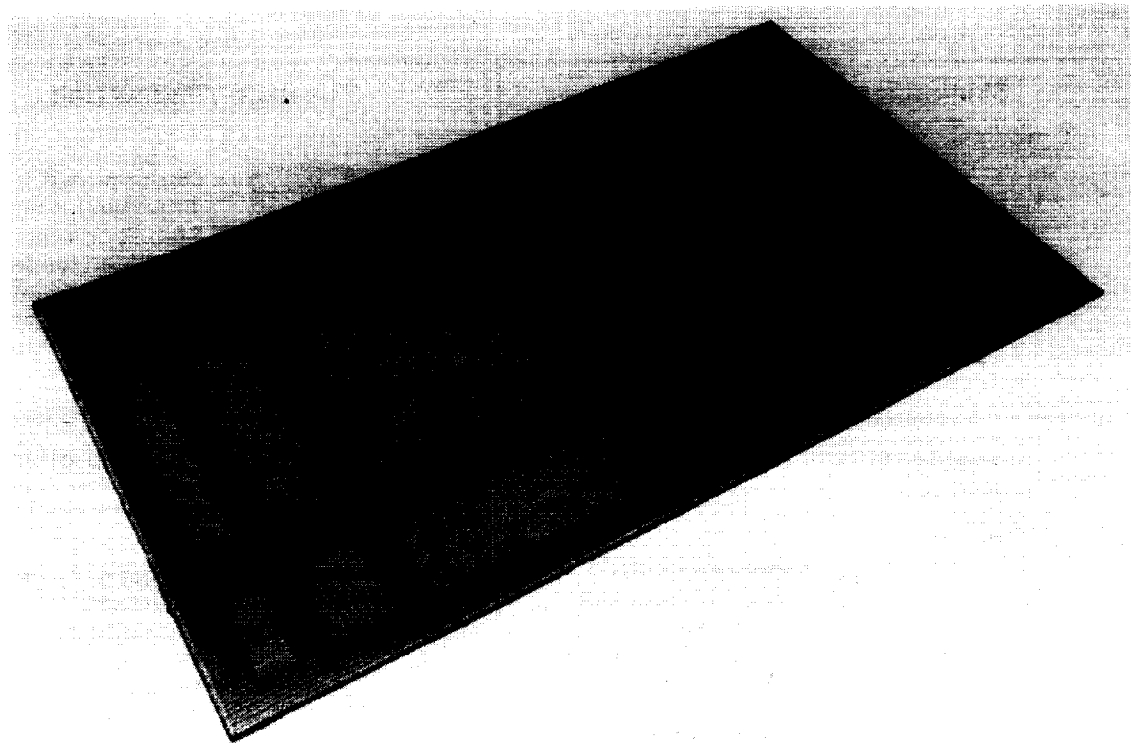


Figure 25

3-D BRAIDED F-FRAME

Previous studies have demonstrated that braiding is an excellent textile process to develop preforms for complex structural shapes. As part of the NASA ACT program, Lockheed Aeronautical Systems company is conducting research on textile reinforced composites for aircraft fuselage structural applications. The braided F-frame shown in figure 26 was designed by Lockheed and Atlantic Research Corporation. The design included some innovative bifurcation concepts that allowed the preform to be split open to achieve the F-configuration. The frame was braided by Atlantic Research on an automated 3-D braiding machine. The major advantage of the 3-D braiding process is that one-piece, near net-section preforms with through-the-thickness fibers can be fabricated. The preform shown in figure 26 was braided in a rectangular box which was subsequently split to achieve two preforms. The preform was resin transfer molded by Lockheed with a resin injection pump and a fixed cavity mold.

Preform and RTM Composite

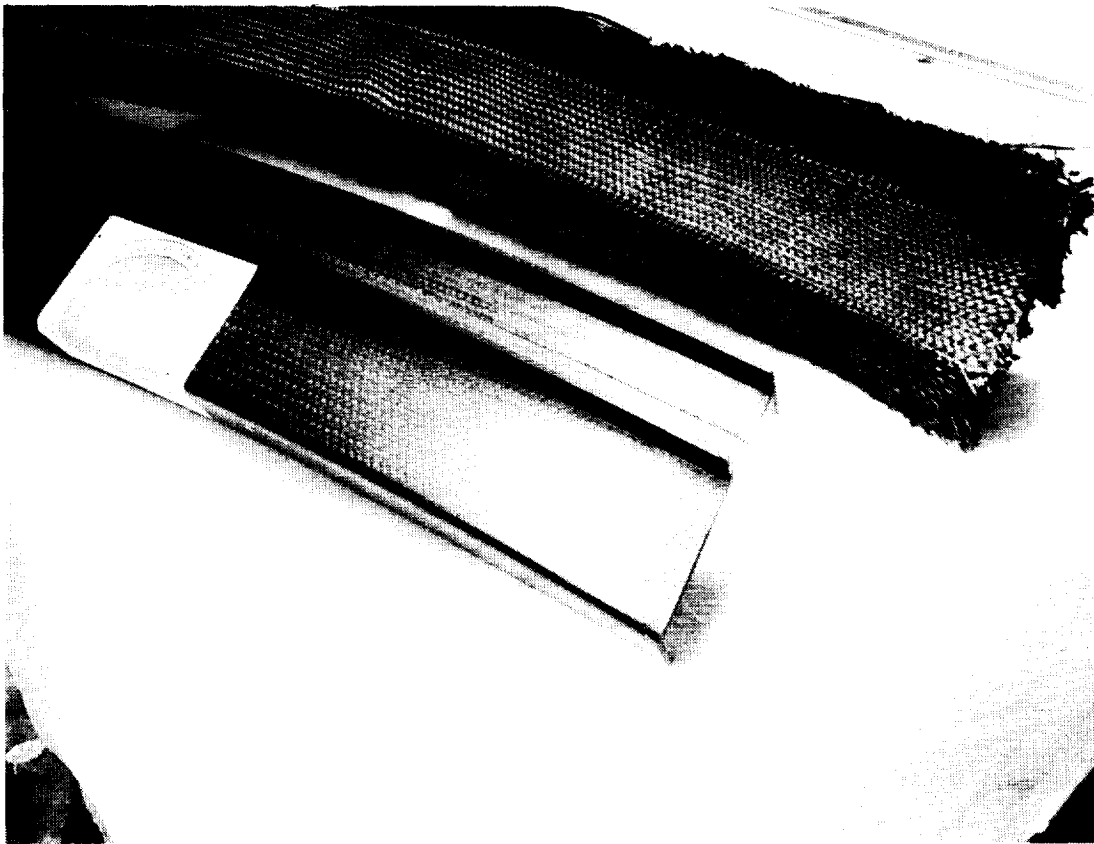


Figure 26

WINGBOX CRITICAL TECHNOLOGY ISSUES

Critical technology issues that must be solved to achieve widespread application of textile reinforced composites in transport wing components are indicated in figure 27. As part of the NASA ACT program, Douglas Aircraft Company is conducting research to address these critical issues. The major focus is on development of damage tolerant structural concepts and cost-effective fabrication processes. Program emphasis is on stitched preforms and resin infusion processes. Material level coupons and test panels have been fabricated and tested to demonstrate the damage tolerance characteristics of stitched composites. Through-the-thickness resin infusion processes have been developed as a cost-effective method to infiltrate resin into the structural preforms. Stiffened panel tests are underway to demonstrate the structural performance of woven/stitched composite materials. Larger wingbox components will be fabricated in the next phase of the program to address some of the scale-up issues associated with fabrication of woven/stitched composites.

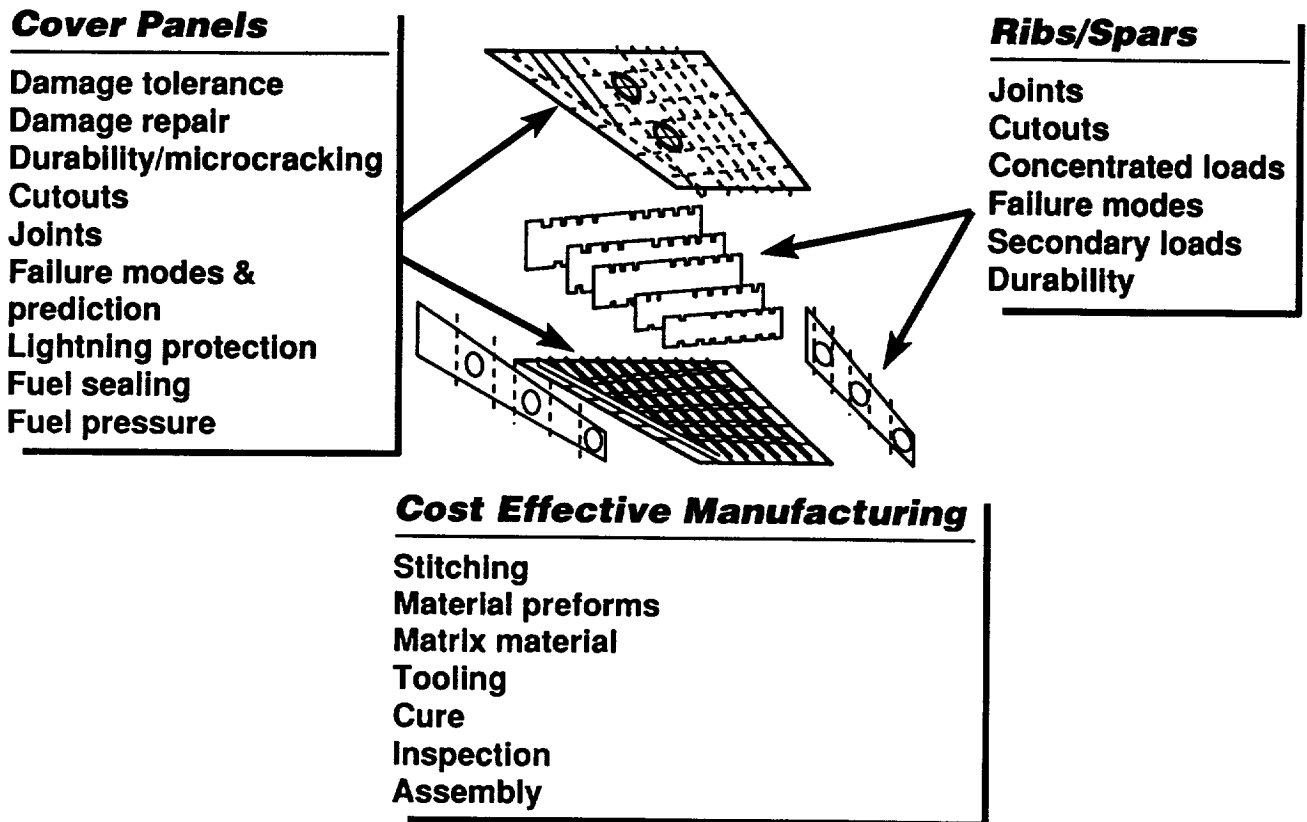


Figure 27

UNIWEAVE/STITCHED WING PANEL

A four-stringer woven/stitched wing panel that was fabricated by Douglas Aircraft Company is shown in figure 28. The AS4/3501-6 panel also has two integral rib attachments that are stitched onto the skin. This panel was fabricated by stacking layers of unidirectional woven fabric (uniweave) to the desired thickness and stitching the layers together. The stiffeners and rib attachments were laid up in a similar manner and subsequently stitched to the skin. The preform was placed in a tool, resin was infused into the preform, and the panel was cured in an autoclave. Panels of this type are being fabricated by Douglas to demonstrate fabrication technology and to develop a data base on structural response of woven/stitched composite materials.

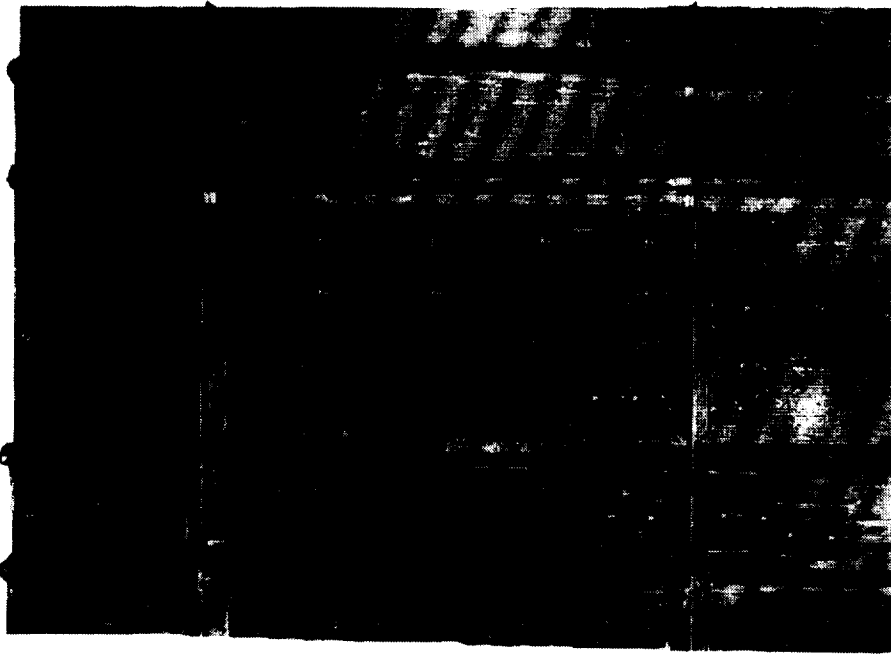


Figure 28

CONCLUDING REMARKS

Redirection of some of the NASA ACT contracts on textile reinforced composites has provided an aircraft structures focus to the NASA Langley textile composites program. Textiles are being applied to specific structural elements where textiles offer a clear advantage over more conventional material forms. The NASA Langley textile reinforced composites program is addressing some of the key technology issues associated with the use of these relatively new material forms. Engineering design guidelines and performance requirements for application of textiles to aircraft structures will be established. Analytical models will be developed to predict material behavior and structural performance.

New NDE-based process/quality control methods must be developed for textile preforms and composites. Real-time feedback controls must be developed to assess quality during the fabrication process to eliminate undue scrap. Processing and fabrication studies that focus on science-based understanding of processing parameters and tooling concepts will be accelerated. Trial-and-error processing studies that have been conducted in the past are too costly and must be minimized. New test methods are required to establish an accurate assessment of textile material performance. Design property databases for applicable textile material forms must be generated so that designers can conduct accurate trade studies.

Structural elements and subcomponents that exploit the full potential of textile material forms will be designed, fabricated, and tested. An integrated team that includes textile preformers, structural designers, analysts, process engineers, and tool designers has been established to work together for cost-effective structural application of textile materials.

REFERENCES

1. Palmer, Raymond J.; Dow, Marvin B.; and Smith, Donald J.: Development of Stitching Reinforcement for Transport Wing Panels. Presented at First NASA Advanced Composites Technology Conference held in Seattle, Washington, October 29-November 1, 1990. NASA CP-3104, Part 2, pp. 621-646. January 1991.
2. Dexter, H. Benson; and Hasko, Gregory H.: Performance of Resin Transfer Molded Multiaxial Warp Knit Composites. Presented at Third NASA Advanced Composites Technology Conference held in Long Beach, California, June 8-11, 1992. NASA CP-3178, Part 1, pp. 231-261, January 1993.
3. Deaton, Jerry W.; Kullerd, Susan M.; and Portanova, Mark A.: Mechanical Characterization of 2-D, 2-D Stitched and 3-D Braided/RTM Materials. Presented at Third NASA Advanced Composites Technology Conference held in Long Beach, California, June 8-11, 1992. NASA CP-3178, Part 1, pp. 209-230. January 1993.



1994012374

**TECHNO-ECONOMIC REQUIREMENTS
FOR AUTOMOTIVE COMPOSITES**

N 9 4 - 1 6 8 4 7

**Scot Arnold
Materials Science Department
Ford Motor Company**

New technology generally serves two main goals of the automotive industry: one is to enable vehicles to comply with various governmental regulations and the other is to provide a competitive edge in the market. The latter goal can either be served through improved manufacturing and design capabilities, such as computer aided design and computer aided manufacturing, or through improved product performance, such as anti-lock braking (ABS).

Although safety features are sometimes customer driven, such as the increasing use of airbags and ABS, most are determined by regulations as outlined by the Federal Motor Vehicle Safety Standards (FMVSS). Other standards, set by the Environmental Protection Agency, determine acceptable levels of emissions and fuel consumption. State governments, such as in California, are also setting precedent standards, such as requiring manufacturers to offer zero-emission vehicles as a certain fraction of their sales in the state.

The Role of New Technology in the Automotive Industry

- **A capability to satisfy future regulatory constraints on fuel consumption, safety, and emissions**

Customer driven

Government regulations

- **Strengthen the ability for world class competition**

The drive to apply new materials in the automobile stems from the need to reduce weight and improve fuel efficiency. While fuel efficiency is partly driven by the market, the main “customer” is the EPA and its CAFE ratings. Primary weight savings are achieved through direct replacement of the current material, steel for example, with a lower density material. Primary savings create opportunities for secondary reductions through resizing other components of the vehicle which are sensitive to weight, such as the powertrain and suspension. Lighter body structure, through primary savings, leads to smaller engine and chassis structure. Secondary savings, however, are usually not realized in practice until the entire vehicle is redesigned--usually a product generation after the primary savings are made.

Light weight materials create opportunities to add new customer driven features while maintaining the weight class of the vehicle. Additional devices for compliance with safety, emissions, and other regulations require weight to be eliminated to maintain fuel economy ratings. Direct replacement of structures with lightweight materials offers one of the most effective means to reduce vehicle weight without having to invest in redesigning the structure and powertrain. However, if the investment in design and engineering is available, lightweight materials can offer significant performance advantages in dynamic applications, such as connecting rods and pistons, where lower inertial loads lead to overall powertrain downsizing. Other benefits include better noise, vibration, and harshness (NVH) due to the better damping capabilities of some composite materials.

New Lightweight Materials: A Critical Element of Future Automotive Technology

- **Drastically improved fuel economy**
- **Provide substantial secondary weight savings through total systems downsizing**
- **Higher “payload” weight fraction**
 - Customer features
 - Regulatory compliance features
- **Improved “NVH” and Quality**
 - Better damping
 - Low dynamic masses

The automotive industry remains one of the largest users of steel. Most automotive basic manufacturing technology centers around the forming and assembly of steel structures. However the scope of materials used in the automobile can be divided roughly into sheet, bar, and bulk applications. Sheet applications are divided into sheet metal (steel and aluminum) and plastics. The majority of automotive structure today is composed of sheet steel. There are limited applications where aluminum is being processed on the same manufacturing infrastructure as steel. Plastic sheet materials are divided into thermoplastics and thermosets which can each be divided into composites and NEAT materials. SMC is a thermoset composite which is becoming increasingly common in non-structural applications. Thermoplastic composites, such as glass filled polypropylene (e.g. Azdel or Taffen) are used in applications where impact resistance is important such as bumper beams and load floors.

Bar applications cover those parts which serve as heavily loaded structure such as moving engine components, chassis parts, brake rotors, etc. Most of these applications are suited for metals except in some cases where structural fiber reinforced plastics are acceptable. Currently many applications using steel are being replaced with either forged or cast aluminum. Intake manifolds are an example where iron was replaced by aluminum which is now starting to be replaced by engineering plastics.

The bulk applications include housings and interior systems such as the instrument panel. These types of components can easily take advantage of the low manufacturing cost and lightweight of die cast aluminum, magnesium (in the future), and injection molded thermoplastics

Types of Automotive Materials

- **Sheet Applications**

Sheet Metal: Aluminum and Steel

Plastics: SMC, GTP (Azdel), TPs

- **Bar Applications**

Castings: Aluminum, Iron, Magnesium, and Zinc

Extrusions: Aluminum

Forgings: Aluminum and Steel

Plastics: FRP

- **Bulk Applications**

Castings: Aluminum, Iron, Magnesium, and Zinc

Moldings: FRP and TP

Composite materials are being used by the automotive industry at an increasing rate mainly in non-structural body closures such as hoods and decklids. They offer reduced weight and, in some cases, lower investment cost. However, continued acceptance of these materials has slowed as the applications have become more integral to the body structure and critical to crash energy management. There are many barriers to using a new material which include both design limitations as well as manufacturing incompatibility. Design limitations are centered on the difficulties using a single material system for large scale parts integration. This prevents cost-effective materials substitution since the vehicle design has been optimized with steel. The vehicle needs to be re-designed and optimized with the new material to achieve the same cost-effectiveness as with steel.

The limitations to designing reliable crash energy management structures are closely coupled to the difficulties associated with producing composites with predictable properties. The automotive industry is largely devoted to metal forming and assembly. These basic manufacturing processes are very different from the processes used to produce most fiber reinforced plastics. Compression molded SMC and BMC are somewhat similar to automotive mass production, yet they do not produce materials which are capable of efficient use in highly loaded structural applications. Aerospace composite materials, on the other hand, have enough control placed on the alignment and wet-out of the fibers to achieve high structural reliability. Aerospace manufacturing control is far too costly for application in mass production. Thus the challenge is to develop processes with optimal control and cost for mass production of structural composites.

Automotive Composite Applications

- **Potential candidates for lightweight body applications**

- **Initial acceptance barriers:**

Design	}	Effect Product Cost
Manufacturing		

- **Exterior Applications**

Structural

Non-structural

- **Interior Applications**

The body-in-white (BIW) has the greatest potential for application of fiber reinforced plastics. However, the BIW is highly integrated and requires extensive re-design in order to substitute new materials for steel. Many chassis components, on the other hand, are bolted on to the frame or underbody and offer simpler materials substitution opportunities. For example, crossmembers, which are bolted on to the frame rails, are low risk candidates for composite materials. Little or no change to the assembly line is required and the carry-over steel component can be used as a back up if the composite development program fails. When part of the BIW is replaced with a different material, so many changes in the design and manufacturing process are required that the expense and risk may outweigh the benefits. The best strategy for offsetting the risk and cost against the benefits of new technology is to apply it where the current technology remains an acceptable alternative. This way, if the new technology is unsuccessful, the entire program is not jeopardized.

The Role for Composite Materials in Automotive Applications

- **Structural Applications**

 - Body-in-White, e.g. Floor-pan

 - Chassis and Powertrain, e.g. Crossmember and Drive Shaft

 - Engine, e.g. Block

- **Non-Structural Applications**

 - Exterior Body Panels, e.g. Hood

 - Interior, e.g. Load Floor

 - Bumper Fascia

Composite materials have very high specific properties which make them very attractive alternatives to ferrous metals in weight sensitive structural applications. These weight efficiencies are attainable at relatively low cost since most polymer-based composites are priced the same or lower than lightweight metals. In structural applications conventionally held by stamped and welded sheet steel, polymer composites offer lower investment cost since they can be processed in fewer steps requiring expensive tooling. Composite molding processes are capable of producing large structures which integrate many of the equivalent components in the steel application. Combined with fewer operations, polymer composites have significant low investment advantages not common in sheet metal forming.

There are other physical performance merits composites possess such as damage tolerance and energy absorption. However, the difficulty of achieving reliable performance in crash is complicated by process and design limitations. It is currently very difficult to produce low cost composite parts with high structural reliability in crash-worthy applications.

Composite Materials: Advantages

- **High specific mechanical properties**
- **Relatively low materials costs (relative to Aluminum and Magnesium)**
- **Potential for low investment**
- **High capability for developing integrated structures**
- **Improved damage tolerance and energy absorption**

The disadvantages of automotive composites arise mainly in the comparison with sheet steel. Much of the automotive industries' basic manufacturing capacity, world-wide, is in forming and assembling steel sheet. Composites have significantly higher materials cost relative to steel even when adjusted for the lower density. The cycle times of most molding operations are significantly longer than steel stamping operations even though the latter requires several steps. One of the most efficient means to low cost composites is to reduce part count from the equivalent steel assembly. Consolidation with composites reduces both recurring and nonrecurring (tooling) costs.

Since steel is the traditional material used in automotive structure, there remains significant resistance to using new materials, such as composites. This resistance is primarily rooted in limitations to understanding how to effectively design with composites. Further limitations are due to the existing manufacturing capability. Since automotive companies are capitalized to process steel they look to suppliers to produce non-ferrous components. It is likely that capital could be replaced by machinery to process new materials. However, the rate and timing of this process is still undetermined.

Composite Materials: Disadvantages

- **High materials cost (relative to Steel)**
- **High recurring manufacturing cost (relative to metal processes)**
- **Limited existing design tools and experience**
- **Limited compatibility with existing structures and manufacturing operations**

The economics of competing materials systems must be assessed on two levels: the material and the processing cost. For sheet type systems such as sheet metal or plastic films, aluminum is one of the highest priced and steel is the lowest priced. Plastic sheet materials fall into a spectrum of prices depending on the performance criteria. Thermoplastics tend to be priced higher than thermoset materials. For profile sections (moldings, castings, and extrusions), NEAT and reinforced polymers tend to cost more than metal castings and extrusions.

Processing costs can be broken up into fixed and variable costs which are also referred to as nonrecurring and recurring costs. Tooling and direct equipment costs are driven by the process and tend to be lower for plastics and composites than metals processing, especially for sheet materials. This relationship is due to the fewer operations to make plastic parts when compared with the steps or conditions necessary to process metals. Labor cost is driven by the cycle times of the individual steps in the production process. Plastics and composites usually have long cycle times, although few steps, when compared to metals processing. When comparing plastics and composites to metals, the high variable and low fixed costs of the former are combined to give low production volume advantages. At higher production volumes, however, metals usually yield lower unit costs.

Material Substitution Economics: Overview

- **Material Cost:**

Sheet: Al>TP>FRP>Fe

Profiles: FRP>Al>Fe

- **Processing Cost**

Tooling: Al>Fe>FRP

Equipment: Al,Fe>>FRP

Labor: FRP>Al,Fe

Recurring: FRP>Al,Fe

To further illustrate the role of lightweight materials in the automotive industry, consider their role in the aerospace market. The customer of aerospace systems demands low weight since it directly impacts the economics of the mission. The military needs to reduce weight in air vehicles to increase the payload, while the commercial airline industry wants to minimize fuel costs and maximize passenger capacity. At current fuel prices, the automobile buyer is usually not basing purchasing decisions on the fuel economy of the vehicle. It is the EPA who demands a certain fuel efficiency through CAFE standards. The automotive producers must determine the optimum weight reduction premiums based on product mix, profit objectives, and vehicle weight class constraints.

Like the automotive industry, the aerospace industry has focused its manufacturing capability around a single class of materials. For the most part, aircraft are constructed from aluminum bar, plate, and sheet. Military aircraft often contain a considerable amount of titanium. Unlike automotive applications however, aerospace production volume tends to be very low. The service reliability of aircraft has to be very high since the performance objectives of the structure are very high. Thus aerospace production methods rely heavily on using very high quality and cost materials with extensive testing and inspection of finished products. The low production rate with extensive inspection steps, of normal manual operations, enables composite materials to integrate into aerospace structure without creating havoc in the process. Automotive production requires reliability to be maintained through process control which trades material performance for speed to achieve an optimum mix.

Another critical difference between automotive and aerospace materials is the customer. Buyers of aircraft are very sensitive to the operations and support cost of the system and can be more easily persuaded to see the benefits of new materials in reducing the use-cost of the vehicle. Automotive buyers are removed from the design and engineering of the vehicle and are currently not perceived to be interested in the materials content of the vehicle unless there is a great deal of other value-added benefit.

Economic Perspective: Automotive vs. Aerospace

- **Lightweight Premium**

 - AS: Customer will pay high premium to achieve mission goals - weight driver

 - AM: Customer indifferent to weight, CAFE is weight driver

 - AM: Weight premium is based on constrained optimization of product mix objective, profit, position in weight class

- **Manufacturing**

 - AS: Low production volume -low tooling and facilities cost

 - AS: Minimum process control - maximum material control

 - AM: Trade material control for maximum process control

 - AM: Inspection traded for Total Quality Control

- **Aerospace customer pays R&D, manufacture, and O&S**

 - More long-range view - mission objectives drive weight premium

- **Customer more sensitive to initial cost than O&S cost**

 - Minimize costs to satisfy regulations

The cost effective use of new materials is closely coupled to the production volume of interest. Fortunately, new materials use favors low production volumes which is the current trend in the automotive industry. Traditionally auto-makers have favored mass production and long product lifetimes. The current trend is to produce fewer copies of a larger proliferation of products for a shorter lifetime and hence capture a larger share of the overall market. However, the low volume objective of low capital investment and quick lead-time come in direct conflict with the high engineering risks associated with new materials. It is also difficult to mobilize the automotive industry away from its current orientation, high production rate and low manufacturing flexibility, towards higher flexibility and lower production rate.

Production Economics

- **Production Volume**

Range: 10,000 to 1,000,000 /yr

Trend: 10,000 to 100,000 /yr

- **Low Volume Objectives**

Fast product response - short lead time

Low tooling and facilities investment

Low engineering cost - low technical risk

- **Current technology oriented towards high volume**

High production rate

Low flexibility

Structural composites offer potential tooling investment reductions when compared to a functionally equivalent steel structure. This reduction comes from both the lower number of forming steps and the potential to form highly integrated structures from a single molding. However, the long cycle times of most composites processes, which scale with the size of the part, require optimizing the level of integration. As the level of integration increases, the size and complexity of the part may increase the cycle time such that the tooling investment, required to meet production volume, eliminates the cost benefits over steel weldments.

Currently, however, the high engineering cost of implementing composite materials in high production volume automotive applications, more than offsets the design and tooling savings. New technology, such as composites, are best implemented in small incremental steps. Low production volume vehicles, where premiums are often paid for improved performance and the production risks are lower, are excellent platforms for introducing new technology. On higher production volume systems, “bolt-on” applications which can be made transparent to the assembly line are low risk avenues for new technology as well. However, on high production volume platforms, the performance premiums paid are much lower than specialty niche vehicles. Low risk applications for new materials systems are the only way automotive producers can gain manufacturing and engineering design experience necessary for wide spread acceptance.

Composite Materials Production Economics

- **Lower tooling cost options compare to metal processes**

 - One-step process

 - Opportunities for parts integration

- **New technology requires high engineering investment**

 - Small incremental steps

 - Very low production volume

 - Small, low-risk components - “bolt-ons”

 - No manufacturing or engineering experience base

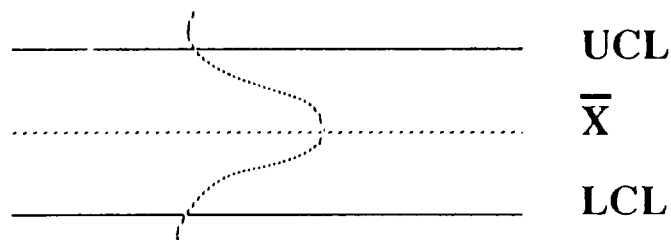
In high volume production, reliable high quality output is achieved through process control. The process needs to be “in control” such that the majority of the product variation is due to random non-controllable events which lie well within the tolerance limits of the design. The variations in material properties which occur in composites must not affect the reliability of the product. In the aerospace industry this is insured by diligent inspection steps and by using expensive high quality materials. In the automotive industry low cost materials are used in high speed, highly controlled processes with enough “over-design” to make up for variations in material properties.

For example, aerospace composites are typically made through the hand layup of pre-impregnated fiber tapes. These tapes are carefully made and characterized so that the fiber alignment and wet-out are well controlled. Unfortunately the high cost of the materials and the lack of control over the manual layup process result in very high product cost. Many of these companies are interested in resin transfer molding, RTM, due to its faster cycle times and lower materials costs. However, there is not enough control over the fiber orientation and fiber wet-out to insure high quality. Thus the research and development effort is aimed at improving the control in RTM.

On the other hand, the automotive industry does not need to derive the highest level of material properties; rather it needs to achieve reliable control over the process for predictable properties. Thus the thrust of automotive structural composites research and development is to achieve higher production rates and control with acceptable material performance. The automotive industry needs to be able to get the same manufacturing performance from RTM as obtained with SMC only with a significant improvement in materials properties.

Production Economics

- Manufacturing control is the critical objective - $C_{pk} > 1.33$



- Material properties controlled by over-design

Sacrifice weight reduction for control

- For example with liquid composite molding (LCM) vs. other FRP processes

Aerospace applications - Design LCM to same control as hand lay-up at faster rates.

Automotive applications - Design LCM to same control as SMC at lower rates

In order to illustrate the process by which new materials are introduced into the automobile, consider the substitution of steel with fiber reinforced plastic. For example, consider a steel hood being replaced by a compression molded SMC hood. The basis for the material change is most likely to reduce vehicle weight. The manager of the vehicle program will pay a penalty for eliminating weight. The penalty is estimated by assessing the need to remain in a given weight class against production volume and profitability constraints. CAFE regulations limit the number of vehicles which may be sold in a given weight class which often adversely affects profitability. Reducing the vehicle weight will enable the producer to increase the number of vehicles in desired weight classes.

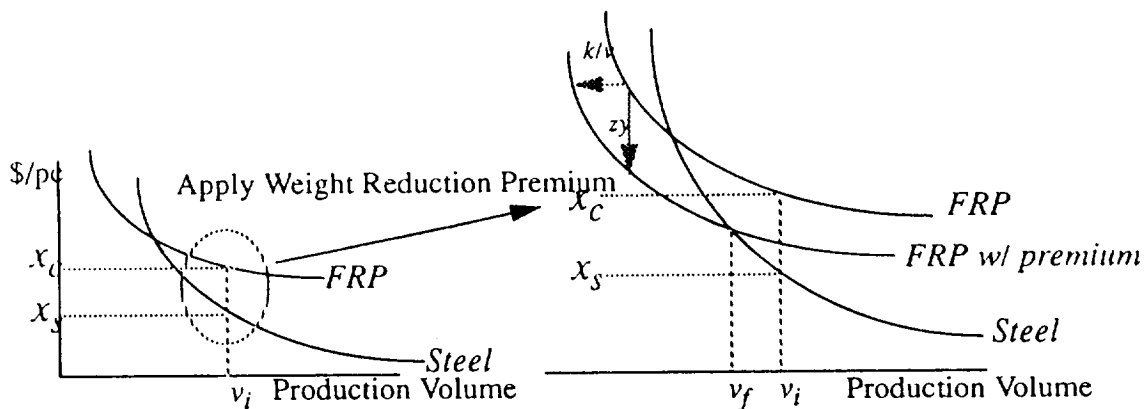
Example: Steel vs. FRP

- Structural application needing lower weight

Steel part costs x_s and weighs w_s

FRP part costs x_c and weighs y less than the steel part

Program will spend z \$/lb saved for lower weight and or invest k



There are two main strategies behind the implementation of new technology in automotive products. In the past, compliance with regulatory constraints has been one of the most significant driving forces behind the development and implementation of new automotive technology. This type of driver will, however, limit the “enthusiasm” for the development of the technology. Since the producer is satisfying a standard, their preference for performance is binary; they will only pay to satisfy the standard not to exceed it. This means that the most conservative route will be taken to achieve the goal. The timing of the development process is usually set by the regulators and thus must be met. To minimize the risks of meeting the timing plan, new inventions must be limited to as few as possible.

One of the most effective means of developing the new technology at minimum risk is to buy it from a supplier. Unfortunately this often means that competitors are able to purchase the technology as well. The other driver for implementing new technology is to use it for achieving world class products. This is a situation where the producer is potentially willing to pay for superior performance if it is perceived that value is directly added to the product yielding higher profits.

Attitudes Towards Enabling Technology

- **Helps future products satisfy expected CAFE standards and other regulations**

 - Achieve goals at minimum investment

 - Zero risk of achieving goals - minimize number of inventions

 - Buy technology from supplier

 - Timing set by regulation - Can drive initial premiums higher than long term goal

- **Helps products achieve world class status**

 - Attempt to develop technology in-house or with supplier partnership

 - Risk reducing pilot programs

There are numerous examples in the past where new materials technologies have been implemented in products to achieve both better performance and regulatory compliance. High strength steels have been incorporated into the vehicle structure to achieve approximately 10% weight savings over mild steel. However, initially many obstacles had to be overcome as body and assembly operations learned how to form and weld these “newer” materials. Galvanized steel was introduced in order to reduce body corrosion and improve durability. This enabled U.S. made vehicles to compete better with Japanese vehicles whose superior paint technology provided improved corrosion protection.

Ford has started manufacturing aluminum block engines both for their improved fuel efficiency, weight savings, and for the market appeal. Casting aluminum blocks presents many technical challenges for a company who has traditionally used iron blocks. The challenges are both in adopting a whole new casting technology as well as learning to machine dissimilar metals.

Forged connecting rods are being replaced by powder metal, PM, rods on a regular basis. There are many advantages to the PM rods. They are delivered to the machining and assembly line in a closer net shape than the forged rods. There is better control over the mass variation leading to easier balancing. The cap is easily “cracked” from the rod blank providing a perfect mating surface and eliminating several machining and grinding operations on mating faces. The pin-end aperture is formed into the blank eliminating a drilling operation. All of these cases represent new technology which was essentially compatible with the basic manufacturing infrastructure, at some level of the overall process, of the automotive producer. The last two required the participation of a supplier since the basic forming processes, PM and aluminum block casting, were not traditionally used by the automotive industry.

Past Examples

- **High Strength Steel**

Weight Reduction

- **Galvanized Steel**

Corrosion Resistance

- **Aluminum Engine Block**

Weight Reduction

High Tech Image

- **Powder Metal Connection Rod**

Reduced Machining Investment

Successful implementation of new materials requires that they meet both technical and economic standards set by the specific industry. They must at least meet the performance level of the existing material. Surpassing the basic criteria is only desirable if there is value added to the product which the customer will pay a premium for. It is also very difficult for industries to rapidly shift to a new manufacturing technology successfully. Changing manufacturing technology requires intense capitalization both in equipment and in human resources. New materials which are compatible with the current manufacturing capacity are likely to be adopted quicker.

New materials must also show that they can be processed to give repeatable properties without severely affecting the productivity of the operations. Usually new technology has a higher unit cost, possibly a transient due to learning or volume effects, which must be offset by budgeted premiums. These premiums are usually paid to enable new technologies to be used with low risks. The risk of implementing new technology has to be low so that the development of the entire system is not jeopardized. One of the best strategies for developing new technology for production is to gain experience with low risk incremental applications such as pilots or easily substituted components. The most sought after technology will be that which enables producers to maintain or, even better, attain a competitive position in the marketplace.

Conclusions

- **Technical requirements for new materials**

 - Maintain or surpass required performance standards

 - Compatible with existing manufacturing technology

 - Repeatable properties

- **Economic requirements of new materials**

 - Higher cost offset by premium for enabling technology

 - Low technical risk

 - Affordable and low risk incremental applications

 - Critical technology to maintaining competitive standing

1994012375

RESEARCH IN TEXTILE COMPOSITES AT K.U. LEUVEN

Ignas Verpoest, Jan Ivens, Aart Willem van Vuure, Vassilios Efstratiou

Department of Metallurgy and Materials Engineering
Katholieke Universiteit Leuven
de Croylaan 2, 3001 Leuven (Belgium)

N 94-16848

11
P. 50

ABSTRACT

An overview is presented of the research on textile composites at K.U. Leuven. Investigated are three dimensionally woven sandwich fabric preforms for delamination resistant sandwich structures, velvet woven 2.5 dimensional fabrics for delamination resistant laminates and knitted fabrics with good drapability for laminates of complex shape.

INTRODUCTION

Textiles for composites have been around since cotton fabrics were impregnated with resins to protect the fragile mummies in Ancient Egypt. Also, soon after the introduction of glass fibres in the thirties, woven glass fabrics were used to reinforce thermoset resins. The same happened with carbon fibres in the sixties.

For decades however, the type of textile used as composite reinforcement was limited to plain or satin weaves. After initial (mainly military) developments for very specific applications, it is only since the early eighties that new textiles are especially designed for composite applications. This brought along a fundamental communication problem: the world of deniers, decitexes, warps and wefts had to be connected to the world of MPa's, ksi's, quasi-isotropic laminates and CAI. Textile people had to listen to the specific requirements of an engineering material, and composites engineers had to get acquainted with the possibilities and limitations of the textile technology.

In the United States and Japan as well as in Europe, a small number of universities have played a key role in bridging this originally wide gap between the worlds of textile and composites. Some of these university research groups had a background in textile engineering, but it might be surprising that the majority had no connections at all with textiles. They discovered the textiles world while looking for more efficient fibre preforms - more efficient in mechanical properties as well as in processing.

At the Katholieke Universiteit Leuven (Belgium), no background in textiles was present when an occasional contact with a Belgian weaving company revealed the possibilities of using the velvet weaving technique for specific composites applications. We suggested to the weaving company not to cut the pile threads when the fabric leaves the loom, like is done in classic velvet weaving (see figure 1). In this way, a double layer fabric, in which both layers are connected, was obtained, and it was found that this 3D-fabric was the ideal preform for sandwich structures [1-2]. Moreover, the velvet type fabric was seen as a potential material to solve the longstanding problem of the low interlaminar fracture toughness of composites: the short fibres, sticking out of the 2D-fabric could act as crack deviators, hence increasing the energy dissipation during crack growth. Because the fibres sticking out of the 2D-fabric were in fact cut, we jokingly called them 2.5D-fabrics, a name which has since then been taken over seriously by other authors.

Preliminary experiments showed that our hypotheses were valid: delamination resistant laminates were manufactured using the 2.5D-fabrics [1-3], and light, stiff and impact resistant sandwich beams were made out of the 3D-fabrics. To investigate more in depth the advantages and potential applications of the 3D-fabrics, a European wide project, supported by the European Community in the framework of the BRITE-EURAM program, was started. Belgian, Dutch, German, Italian and Spanish companies and universities are now collaborating in order to further optimise the fabric geometry and the processing of the 3D-fabrics.

Once our interest was raised for advanced textiles, we actively looked for other existing, well established textiles technologies, which could be introduced into the composites community. To our surprise, almost no reports could be found on the use of knitted fabrics in composites, although the potential advantage of superior drapability was obvious. Cooperation was started with a Belgian knitting company, and soon it was found that knitted fabrics indeed represent an interesting compromise between acceptable mechanical properties and superior drapability [4], moreover, excellent impact resistance as was recently discovered.

In the following paper, a general overview is presented of five years of research in textiles for composites. The paper is really meant as an overview; more detailed information on processing and on mechanical properties can be found in the papers mentioned in the reference list.

3D SANDWICH FABRICS

The sandwich fabric is produced by a variant of the classic velvet weaving technique (see fig. 1), which is used for the production of corduroy textiles. In the case of velvet production, the resulting distance fabric is cut in two, leading to two soft surfaces of pile fibre ends. By skipping this last action, the sandwich structure is retained. In figure 2 the structure of the

fabric is shown and a picture is included of the view of the fabric in warp direction. In the standard fabrics glass fibres are used.

The main advantage of the use of this material in sandwich composites is the fact that the pile fibres in the core (which determine the 3D character) bind the skins of the material together, thus hindering the delamination between skin and core. Compared with more traditional sandwich structures with a honeycomb or foam core, the structure has a much higher delamination resistance. Honeycomb structures only have a small contact surface to which the skins adhere; foam cores do delaminate fairly easy in the zone just below the adhesive layer.

Production methods

The sandwich fabric can be impregnated with resin rather easily, with the same equipment that is being used for 2 dimensional textiles. Until now primarily thermoset resins like polyester, epoxy and phenolic resin have been used, depending on the application. The production of the final, cured structure can be done in various ways (see fig. 3).

Especially for applications in the polyester industry, where the material is primarily used as core material in laminated products, the material is cured without further treatment. It can be laminated in the same way as normally used glass mats or fabrics. As only limited core thicknesses (up to 6 mm) are used and the pile fibres are quite resilient, the pile fibres will almost completely stretch themselves after impregnation. A useful sandwich structure is obtained in this way. Additional layers of 2 dimensional fabrics or glass mats are used to obtain thicker skins with a higher flexural stiffness. Also to obtain a smooth outer surface it may be necessary to add an additional layer.

For higher pile lengths (above 15 mm) it is necessary to do a stretching operation to counteract the buckling of the pile fibres under the weight of the upper skin. The Italian company Metalleido, member of the Aficoss-team, has developed a mechanical stretching process to realize fully stretched and perpendicularly aligned pile fibres. The same result can be obtained by injecting an expanding foam in the core, which stretches the pile fibres.

The use of foam in the core is optional. Until now polyurethane and phenolic foams have been used. Next to the potential use to stretch the pile fibres, the foam is also applied for structural reasons (reinforcement of the core), for its contribution to energy absorption during impact or for other reasons as the watertight sealing of the core or for isolation purposes.

Applications

Applications of the material are found on a large scale in the polyester composite industry. Examples are sidespoilers for trucks, panels for train compartments and a tankwall through which leaking fluids can be drained.

When introducing a new type of material, the properties and price have to be compared with existing materials and other materials in development. Our material has interesting opportunities in areas where there are no extreme demands for mechanical properties and especially for mechanical properties by weight, that is mainly outside of the aerospace industry. In the polyester industry high resin weight percentages of around 60% can be used to support the pile fibres at their 'feet' and still light structures do result. The same does account for applications which are presently being studied, using epoxy and phenolic resin.

Properties

To produce panels with a high flexural stiffness, sandwich fabrics with a larger core thickness have to be chosen. Once more it is stated that to counteract collapse of the fabrics under their own weight, innovative production techniques have to be used. The mechanical properties can be further improved by injecting a stiff foam in the core. For fabrics with a thickness above 15 mm the use of a foam is even indispensable. The foam does increase the weight but still very light panels are obtained. In figure 4 the 4 point bending stiffness of 10 and 20 mm thick panels is compared, impregnated with epoxy resin and partly foamed up with polyurethane. The densities of the materials are about 230 kg/m^3 for the 10 mm thick panels (core density 45 kg/m^3) and around 130 kg/m^3 for the 20 mm panels (core density 40 kg/m^3), without foam.

The shear resistance of the material is a weak spot. The shear resistance is especially of importance when short spans are used during flexural loading. For short spans the greater part of the deflection is caused by shear in the core. In the pictures in figure 5 clearly the shearing of the 20 mm thick structure can be seen, while the material, having part of the pile fibres woven under an angle of 45 degrees, shows much more true bending behaviour. At larger spans the stiffness of the skins will be of increasing importance for the flexural resistance. The data in figure 4 for the 4 point bending stiffness have been obtained for a relatively short span of 200 mm. The total deflection has been attributed to true bending. The low shear stiffness is thus contributing heavily to the values. In this way the values are conservative guesses for the flexural stiffness of larger panels. It is not possible to relate the flexural stiffness of the material directly to the one of honeycomb structures, as the stiffness of the honeycomb depends on the type of adhered skin. The comparison thus has to be made on the basis of the compressive and shear properties.

For certain applications the material could replace honeycomb structures, because of the mentioned strong improvement of the delamination resistance between skin and core and the high cost of honeycomb structures. In figure 6b the measured skin peel strength is shown, which can be used to compare the resistance against delamination [5]. The fact that skin peel strength values up to four times as high as those for honeycomb structures have been found (for high pile density material with 50 piles/cm²) can be attributed to the fact that the skins are connected to each other by the pile fibres. The fibres have to be broken before skin separation occurs.

For the compressive strength comparable values are obtained as for commonly used aramid fibre paper phenolic resin honeycombs (Nomex), of comparable density [6]. In figure 6a the compressive strengths of various materials are shown. When comparing with honeycombs the properties have to be related to the density of the material. In this case the proper comparison is made by relating to the core density. The specific compressive strengths of the various 3D materials are comparable to the reference honeycomb material.

The shear strength of the 3D sandwich material of 10 mm thickness in standard configuration with perpendicular pile fibres is only one fourth of the shear strength of a comparable aramid fibre paper phenolic resin honeycomb. By weaving part of the pile fibres under an angle of 45 degrees this difference can be halved.

Modelling work

Because the mechanical properties of the sandwich structure are highly dependent on the constitution, especially on the fabric geometry, it is useful to develop models to depict the influence of the various parameters. This is one of the major goals of the research at KU Leuven. The work is carried out in cooperation with the University of Zaragoza (Spain) and Drexel University (USA).

In the first place the parameters are studied which determine the behaviour of the core, as there are the pile fibre length, density, angles, geometry, the possible support by resin at the pile feet and contact points of the pile fibres, and the reinforcement of the core by a foam. The core is divided in subcells which contain one pile bundle. The bundle is segmented. To calculate the stiffness matrix, the stiffness matrices of the elements are combined by assuming either constant stress or constant strain, depending on the loading situation. Also the foam support can be included.

Further, the stiffness of the used fabrics in the skins is modelled. Again, the structure is divided in subcells with their characteristic contribution to the stiffness matrix.

The global composite stiffness is calculated using the "fabric geometry model". First results of this model calculation are presented in [7].

2.5 DIMENSIONAL FABRICS

As is well known, the out of plane properties of laminates are much lower than the in plane properties, by the lack of reinforcement in the third direction. Delaminations between layers, for instance after impact loading, are a major problem. Various solutions have been suggested, but they very often have a drawback on other mechanical properties. For instance, the use of a tough interlayer does improve the delamination resistance, but leads to a decrease of the shear modulus.

The growth of delaminations can be hampered by diverting the crack front and by inducing pull out of fibres in the delaminating zone. This is what is done by using 2.5 D fabrics.

Production

The 2.5 D fabric is produced with the same velvet weaving technique as is being used for the 3D sandwich fabric (fig.1). At the end of the weaving process the pile fibres are cut and two hairy, plain weavings result, which have the pile bundles sticking in the third dimension (fig. 7). As for the 3D fabric, pile fibre length and density can be varied.

The fabrics can be impregnated with resin, laminated and cured by conventional production methods. It appears that the in plane properties of the laminates do not decrease by the addition of the pile fibres. For certain properties, like the tensile strength, even a slight increase is observed.

Various fibre types can be used; in the research conducted at KU Leuven, use was made of carbon and glass fibres as fabric material and glass and aramid fibres as pile material.

Properties

The delamination resistance of a material is tested by means of fracture toughness tests, based on an analysis of fracture mechanics. In this approach the energy is calculated for delamination growth over a certain area, expressed as the material parameter G_C , the fracture toughness. Three modes of fracture propagation are considered: mode I, which is a crack opening mode under tensile loading, and modes II and III, which are two types of shear mode.

In our research mode I tests (DCB tests; see fig. 8) and mode II tests were performed. The results have been reported in reference 3. The 2.5 D laminates were compared with similar fabrics without pile fibres.

The results of mode I tests on pure glass fabrics are shown in figure 9. The sharp increase in fracture toughness in the presence of pile fibres is evident. In the case of carbon fabrics similar results are obtained (fig. 10). The increase in fracture toughness is caused by the fact that the propagating crack, which runs through the matrix when using plain weave fabrics, is now hindered on its way by the pile fibres. This means that the bond between pile fibres and resin has to be broken and that pile bundles have to be pulled out of the resin. The dissipated friction energy can be modelled and is given by the following formula:

$$G_C = G_{C,p}(\text{plain}) + \frac{n \cdot 2 \pi \cdot r \cdot l \cdot G_{C,int}}{100}$$

The second term describes the extra energy absorption by the presence of the pile fibres (r is the fibre bundle radius, l the pile fibre length, n the number of pile bundles per cm² and G_{C,int} the fracture toughness of the fibre matrix interface).

Besides the fracture toughness also the impact behaviour of 2.5 D laminates has been studied. Here especially the residual compressive strength after impact is of interest. Figure 11 shows that the normalised compressive strength after impact for most 2.5D laminates is higher than the value for plain weaves. Furthermore, the absolute strength values do not decrease in case the impact energy is doubled.

Conclusion

Our results show that the use of 2.5 D fabrics leads to an improvement of the delamination resistance. Both fracture toughness tests and compression after impact tests do show this. The improvement is obtained without affecting other material properties and without a change in production method. This imposes major advantages over plain weave fabrics in applications where delamination resistance and impact resistance are of interest: in the aerospace industry, but also in e.g. ship building.

KNITTED FABRICS

The fundamental difference between woven fabrics and knitted fabrics is found in the way the fibres are interconnected. Woven fabrics feature straight yarns in plane and only show out of

plane curvature at places where the yarns cross. Knitted fabrics however, feature the interconnection of yarns by loops, leading to strong curvature in the plane of knitting.

This fact would suggest that the mechanical properties of composite materials reinforced with knitted fabrics will differ largely from the properties of woven fabric composites. Both stiffness and strength would be negatively influenced by the curvature of the fibres. On the other hand, one could expect that by stretching the loops, the materials would be very flexible in shaping. These two hypotheses were the basis of our research.

Production

Starting point was a knitted glass knit fabric, with a surface density of 455 g/m^3 . The material was developed by the NV Saturn, a daughter company of the NV Wydooghe, Izegem Belgium. The structure is such that the yarns have a preferential orientation in warp and weft direction (although these weaving terms are strictly not being used for knitted textiles).

The knits were impregnated at KU Leuven with epoxy resin and cured to B-stage. These prepregs were laminated to lay-ups of 1,3,6 and 10 layers and cured in an autoclave at 140° C under a pressure of 7 atmosphere. To evaluate the mechanical properties, tensile tests were performed parallel to, perpendicular to and under an angle of 45 degrees with the direction of knitting.

Properties

The stiffness shows a remarkable isotropy: in the three tested loading directions the Youngs modulus is about equal (fig. 12). This is a distinct advantage over fabrics, which show a decrease in stiffness in the diagonal direction up to 40%, compared with warp and weft direction. The degree of anisotropy of knitted fabrics can be controlled by adjusting the knitted structure.

In figure 12 it can be seen that the number of layers in the laminate has a significant influence on the stiffness. This is also shown in figure 13a; the same effect is also found for the strength (fig. 13b). There are two reasons for this effect. In the first place, the fibre volume fraction will increase with the number of layers. Knits are fairly open structures and in a composite of only one layer the holes between the yarns have to be filled with resin. By using more layers the yarns of adjacent layers will fill each others holes, leading to a higher fibre volume fraction. The second reason also has to do with this effect: the filling of holes in adjacent layers leads to a mechanical interlocking of yarns and thus to an improvement of stiffness and strength.

In figure 13 also a comparison is made with woven fabric composites and with glass mat reinforced composites. Above three layers of knitted textiles, stiffness and strength approach

the values of fabric composites and are double as high as the values for mats. This shows that knits are an attractive compromise: they combine the freedom of shaping of discontinuous fibre composites with the good mechanical properties of woven fabrics. Put differently: by using knits one can circumvent the poor mechanical properties of mats and the limited drapability of fabrics.

The good drapability of knitted textiles had an additional positive effect. In a simulated experiment knits were stretched for 30% and subsequently cured. In the loading direction an increase of stiffness and strength of 45% was found, while the properties perpendicular to the stretching direction hardly changed (fig. 14). This shows that draping can only improve the mechanical properties. Furthermore, the degree of stretching poses an additional possibility to control the anisotropy in mechanical properties, next to the adjustment of the knitted structure.

CONCLUSION

In this review paper, developments in textiles for composites, achieved in the Department of Metallurgy and Materials Engineering of the K.U. Leuven have been presented.

A new type of sandwich structure has been developed, based on double layer fabrics. The structures show good and tunable flexural stiffness and compression strength, and excellent skin peel strength. In this way, they can compete with honeycomb and foam core sandwich structures, certainly in those applications where cost is the key factor in materials selection.

A solution was presented for the long-lasting problem of the poor delamination resistance of composite laminates. It was shown that composites based on 2.5D-fabrics have a higher interlaminar fracture toughness and superior compression-after-impact values.

Finally, it was proved experimentally that the belief that knitted fabrics are useless for composites is based on an unfortunate prejudice. Both stiffness and strength of knitted fabric composites are in between the values for woven fabric and random mat composites, but the major advantage is their superior drapability compared to both these materials.

It is believed that creative thinking will find more ways to use "old" textiles in the "new" world of composites.

ACKNOWLEDGEMENTS:

The authors wish to thank the companies involved in the research presented in this paper: Schlegel and Parabeam for the 2.5D and 3D fabrics and Saturn for the knitted fabrics. Also all the students who contributed to this work (C. McGoldrick, K. Verbrugge, J. Dendauw, Y. Bonte, J. Morel, P. Debaere, M. De Vleeschauwer, T. Chalermsowan, P. Vandeurzen, J. Swaelen, J. Van Zegbroek, E. Weyers, J. Teuwen, L. Saliën, P. Scheldeman and A. Cosaert) and those who helped guide their work (P. De Meester and M. Wevers from K.U. Leuven, P. Robinson from Imperial College, H. Bonte from K.I.H. Oostende and G. Ceulemans from Groep T, Leuven).

REFERENCES

- [1] Verpoest I., Bonte Y., Wevers M., De Meester P., Declercq P., in New Generation Materials and Processes. Proc. SAMPE Milano, 1988, pp 13 - 21.
- [2] Verpoest I., Wevers M., De Meester P., Declercq P. in SAMPE J., Vol. 25, 1989, pp 51 - 56.
- [3] Ivens J., Debaere P., McGoldrick C., Verpoest I., Van Der Vleuten P. in Composites, (submitted)
- [4] Dendauw J., Verpoest I. in Proc. ECCM-5 Bordeaux, 1992, pp 927-932.
- [5] Ivens J., Verpoest I., Van der Vleuten P. in Proc. ECCM-5 Bordeaux, 1992, pp 941-947.
- [6] Ivens J., Verbrugge K., Verpoest I., Van Der Vleuten P. in Proc. SAMPE Conf. Maastricht, 1991, pp 417-425.
- [7] Du G.W., Ko F.K., Vandeurzen P., Verpoest I. in Proc. Fiber-Tex 1992 Philadelphia (PA), 1992.

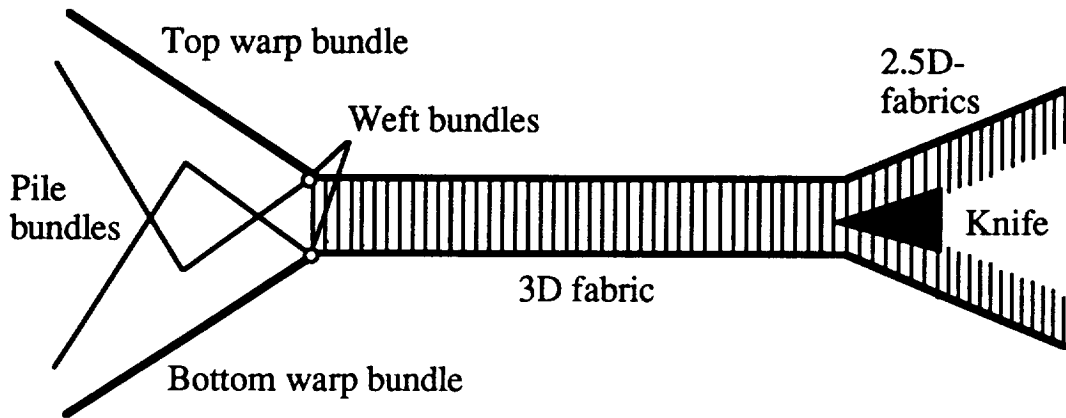
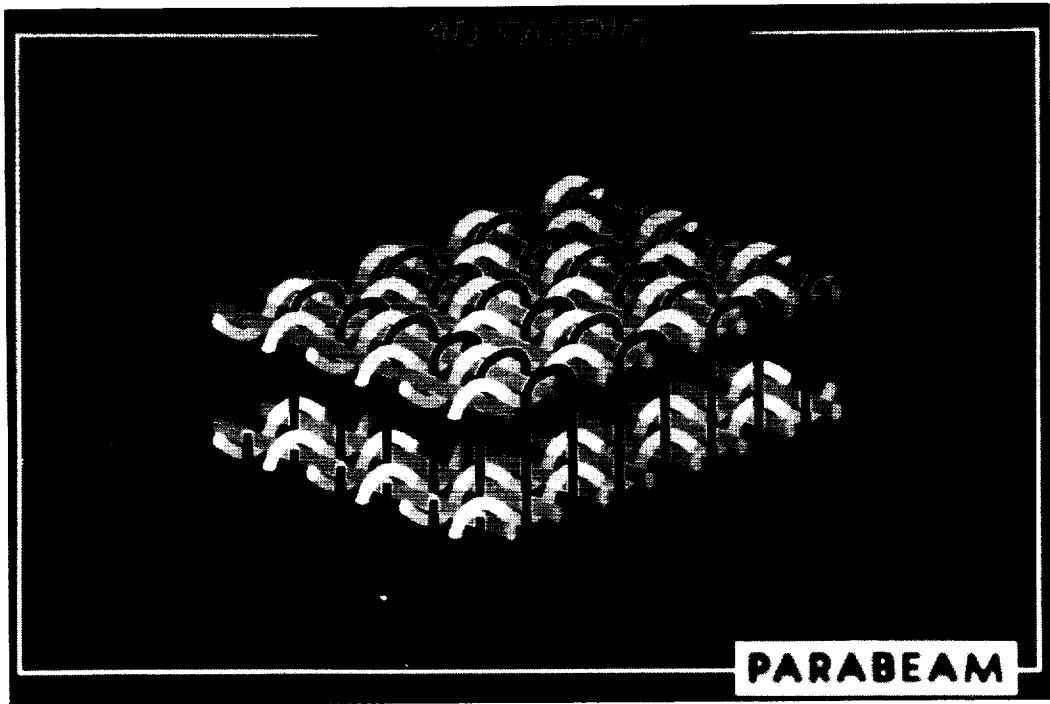
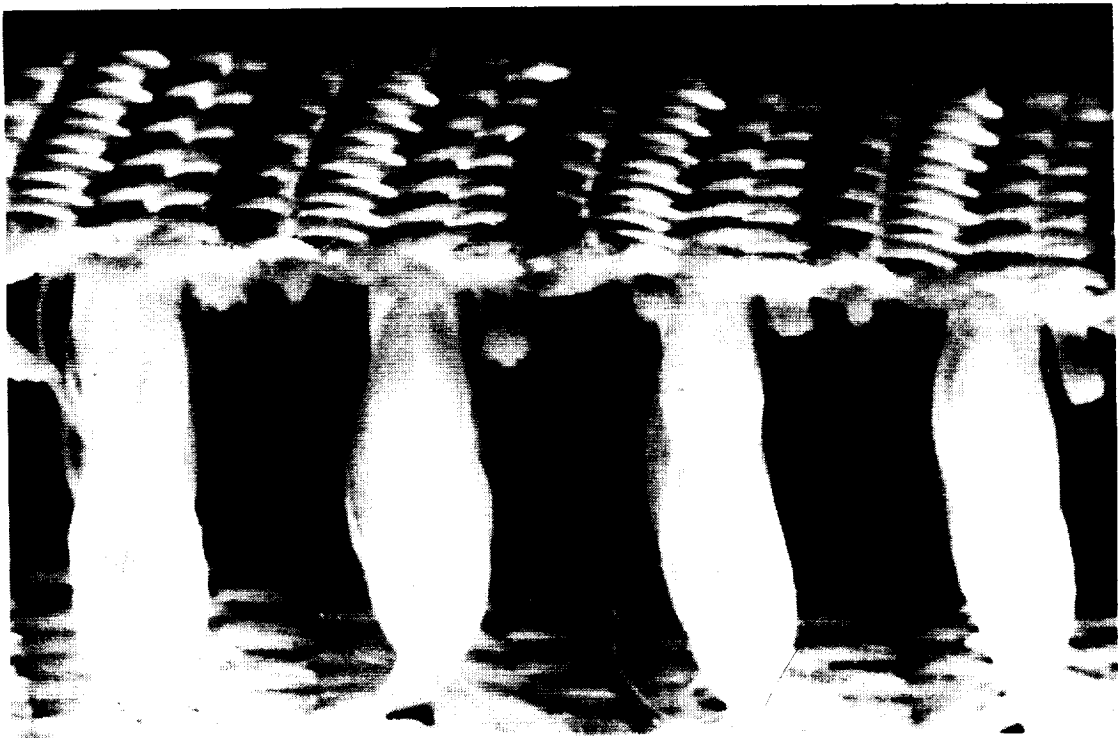


Figure 1: Production process of a 2.5- and a 3-dimensional fabric.



2a



2b

Figure 2(a & b): Schematic representation and photograph of a three-dimensional fabric.

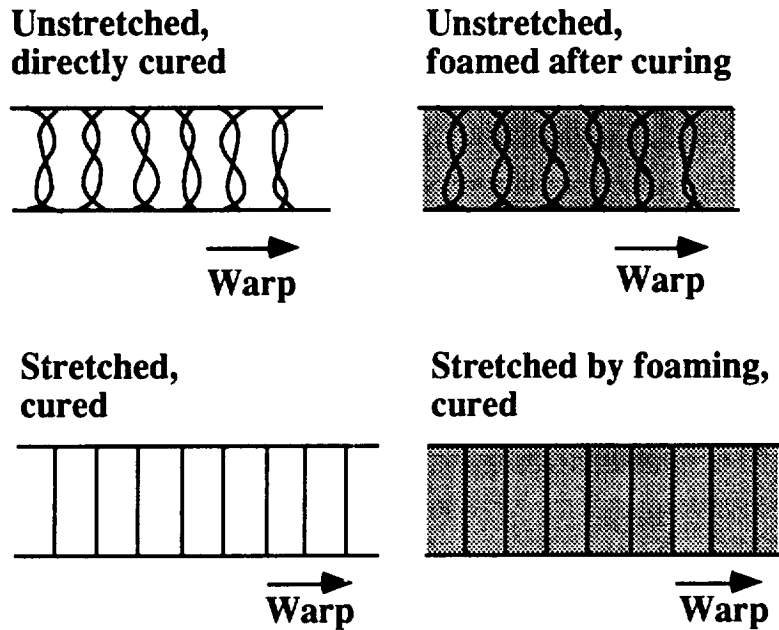


Figure 3: The end shape of the panel can be different (unstretched without foam, stretched without foam, unstretched with foam, stretched with foam).

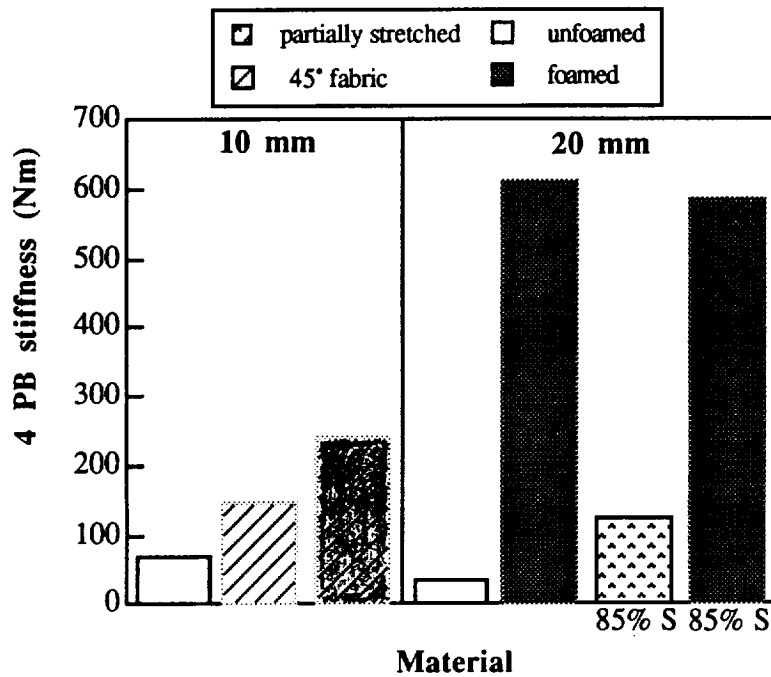
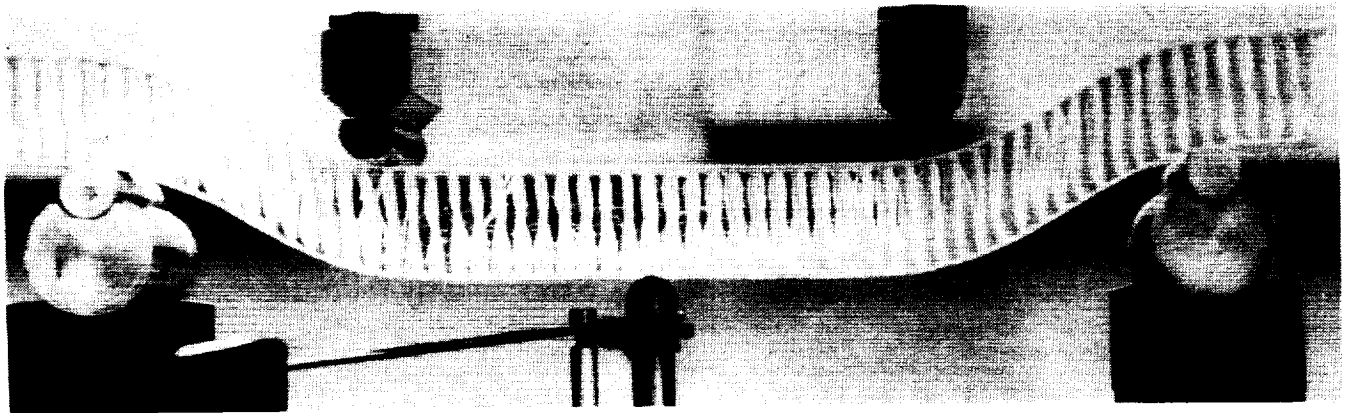
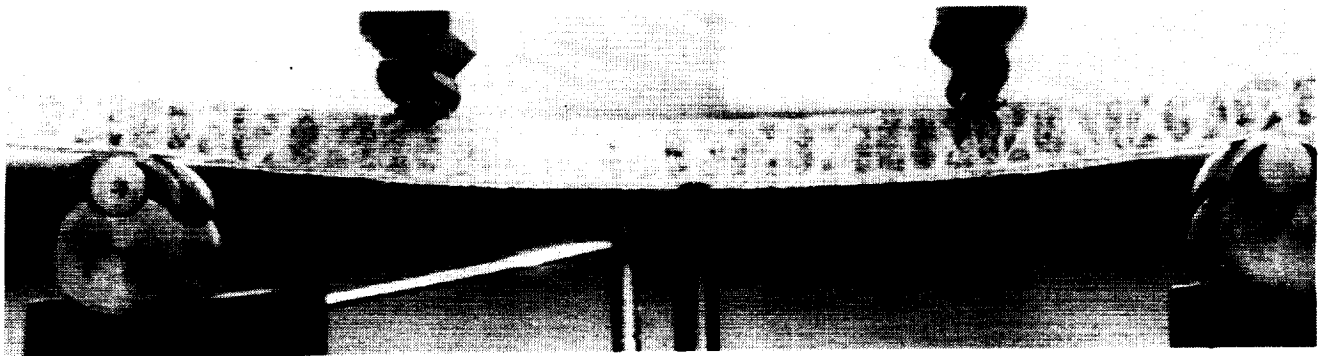


Figure 4: 4 point bending stiffness (span length 200 mm) for two different pile lengths (10 and 20 mm) and pile density 25 piles/cm². The results are normalised to the width. The specimens were tested in the warp direction (resin content 55% by weight; foam density 60 kg/m³).



5a



5b

Figure 5(a & b): Photographs of the deformation of an unfoamed specimen and a foamed specimen with 45° pile fibres: the deformation of the first sample is mainly caused by shear deformation. The specimen with the 45° pile fibres has only a low amount of shear deformation.

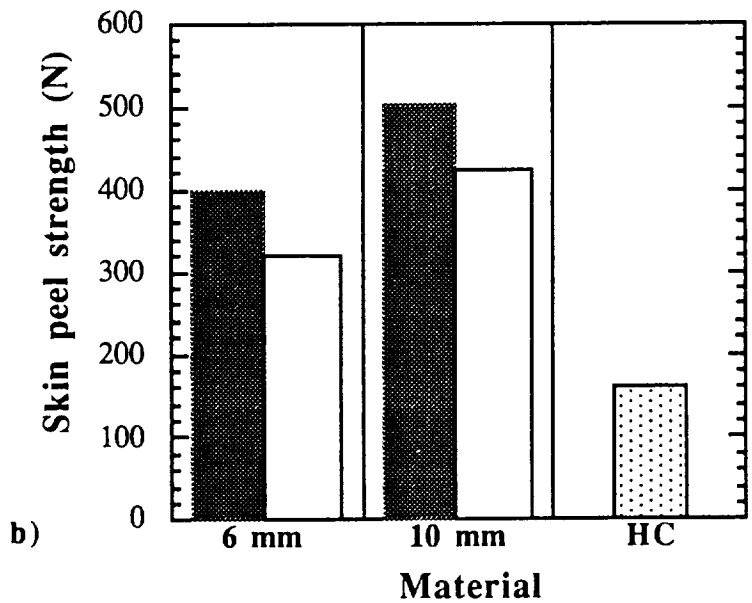
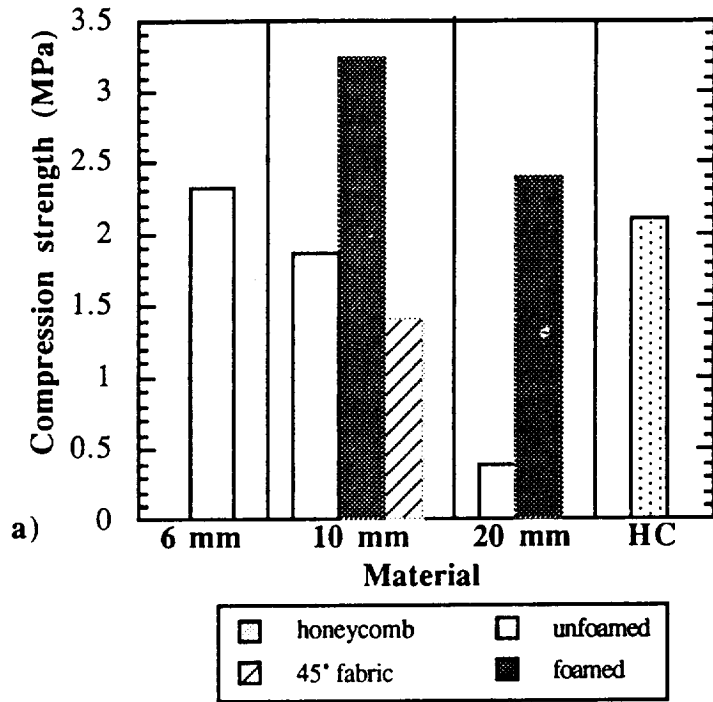


Figure 6: Flat compression strength (a) and skin peel strength (b) of different 3D sandwich panels with different pile lengths (6, 10 and 20 mm). As a comparison the values for a honeycomb structure (Nomex®) were also included.

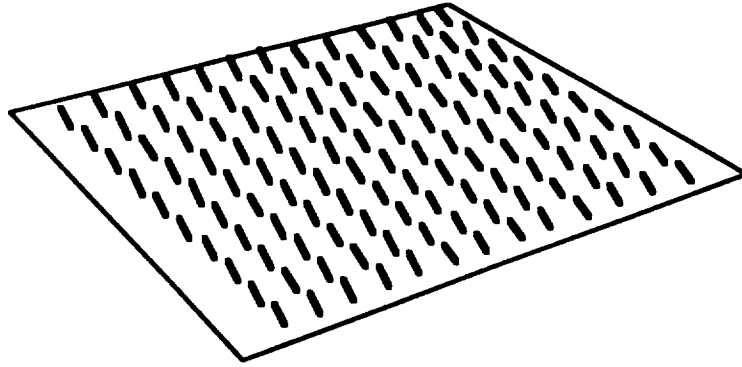


Figure 7: Schematic view of a 2.5D fabric. The pile bundles are not standing up, but are lying down.

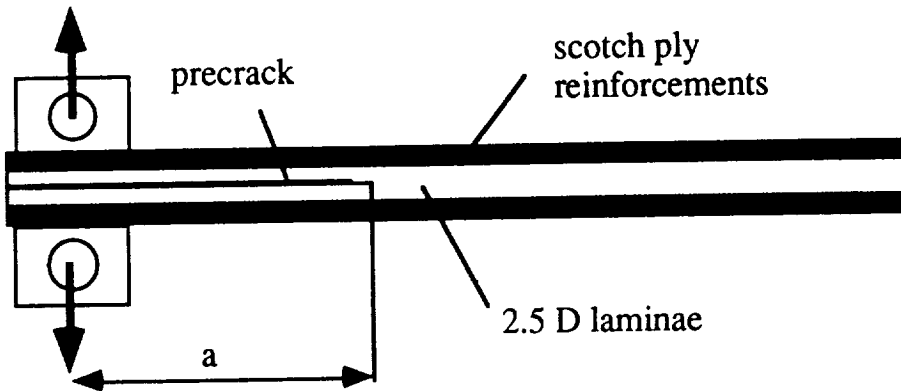


Figure 8: Double Cantilever Beam Specimen (mode I type of loading).

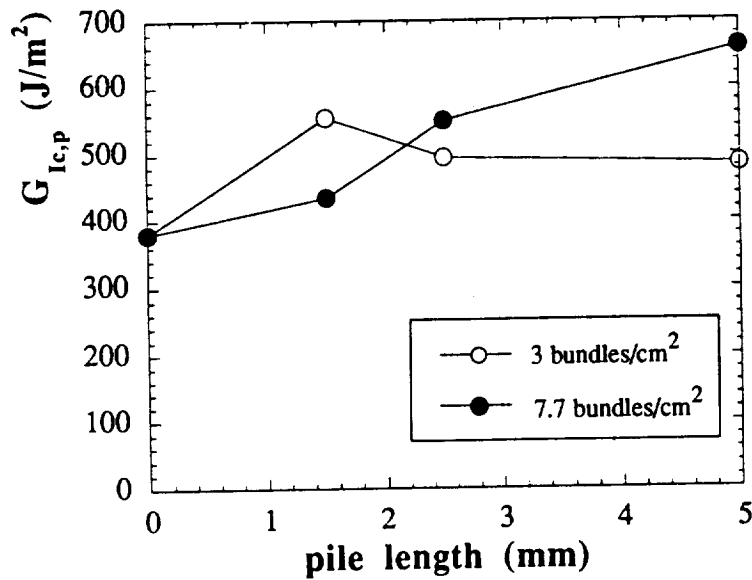


Figure 9: Mode I fracture toughness of 2.5D glass fabric laminates as a function of the pile length and pile density (in number of bundles per cm²).

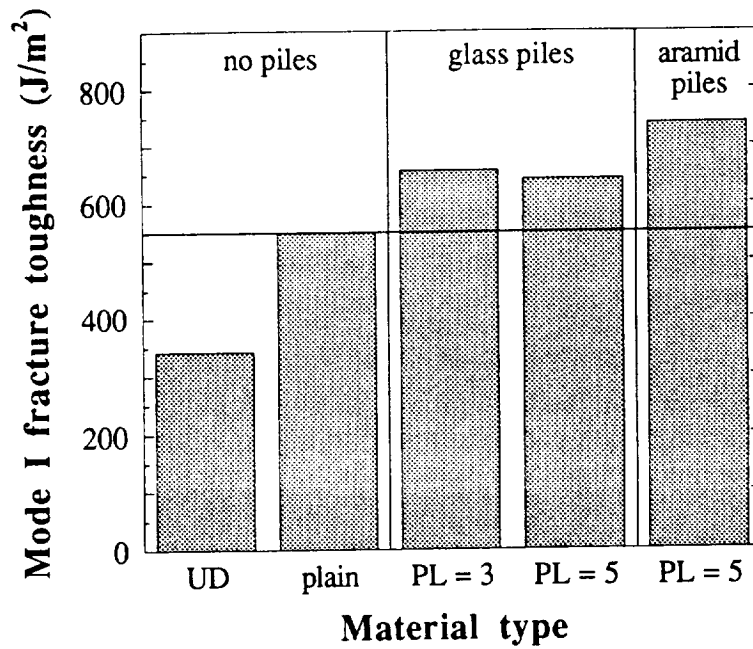


Figure 10: The mode I fracture toughness of 2.5D carbon fabric laminates with glass and aramid pile fibres, respectively, as a function of the pile length (PL). As a comparison, the fracture toughness of a unidirectional composite is added.

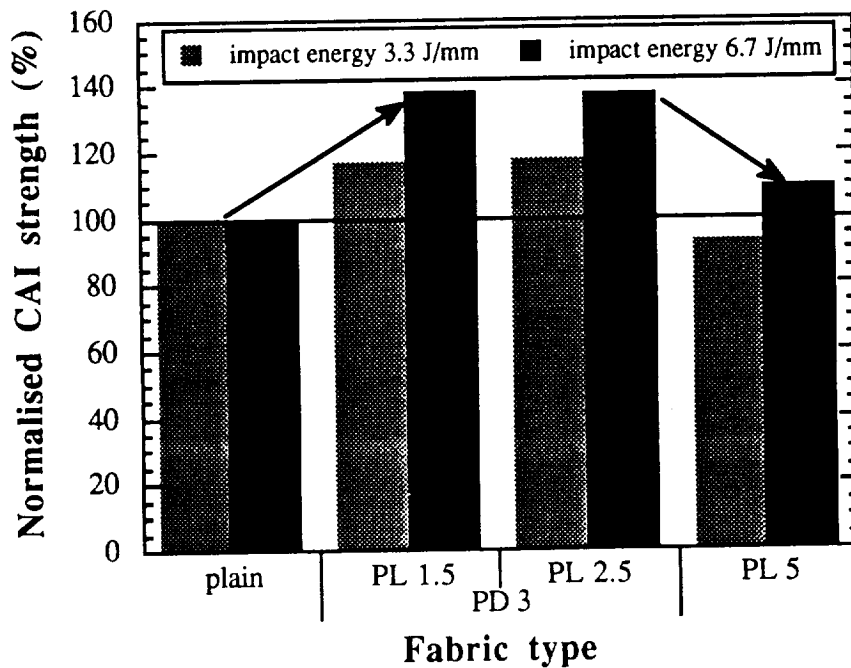


Figure 11: Compression strength after impact for different materials with two different impact energies (PL is the pile length in mm, PD is the pile density in number per cm²). The tests were performed on pure glass fabrics.

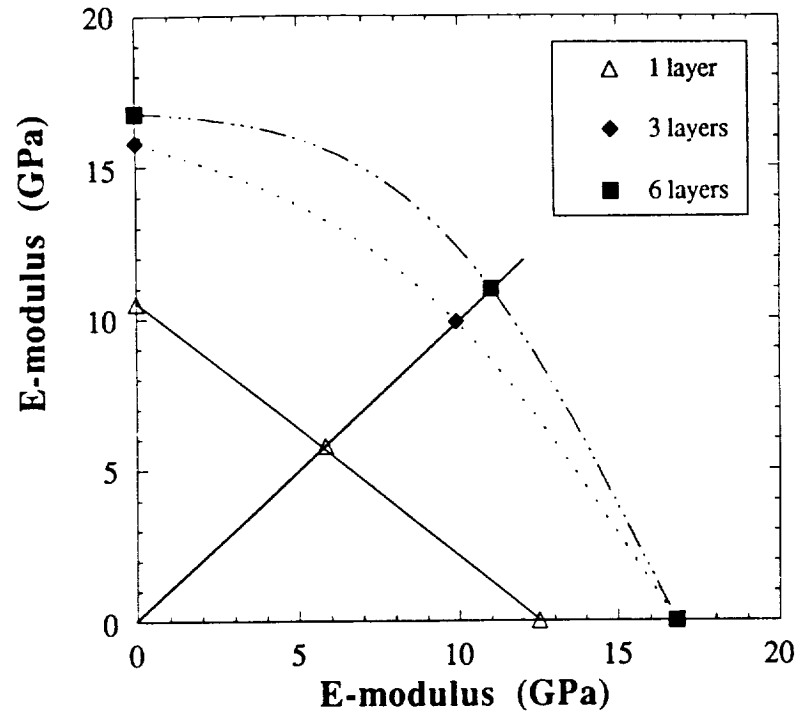


Figure 12: Stiffness of a knitted fabric composite in different directions.

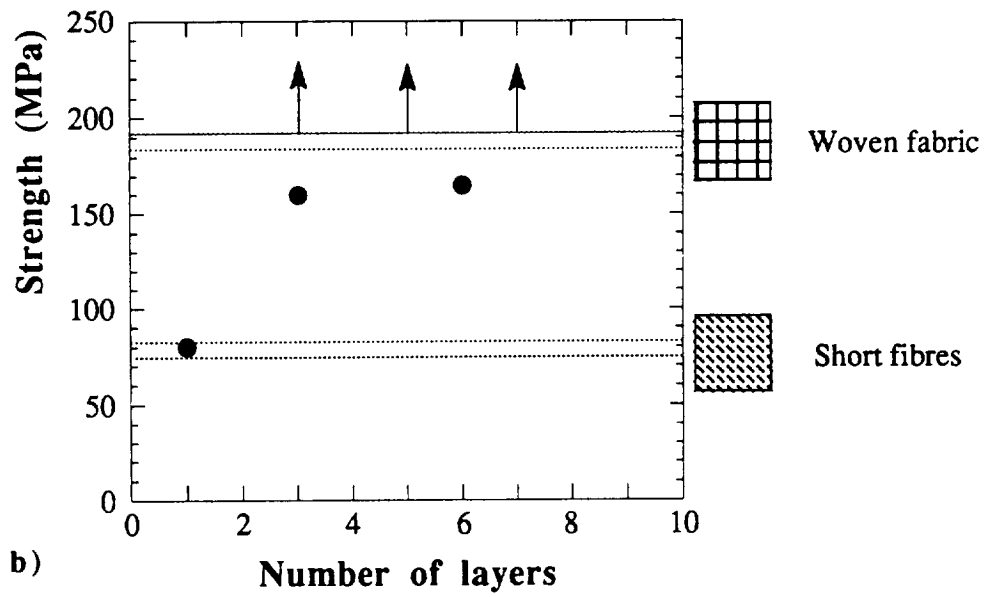
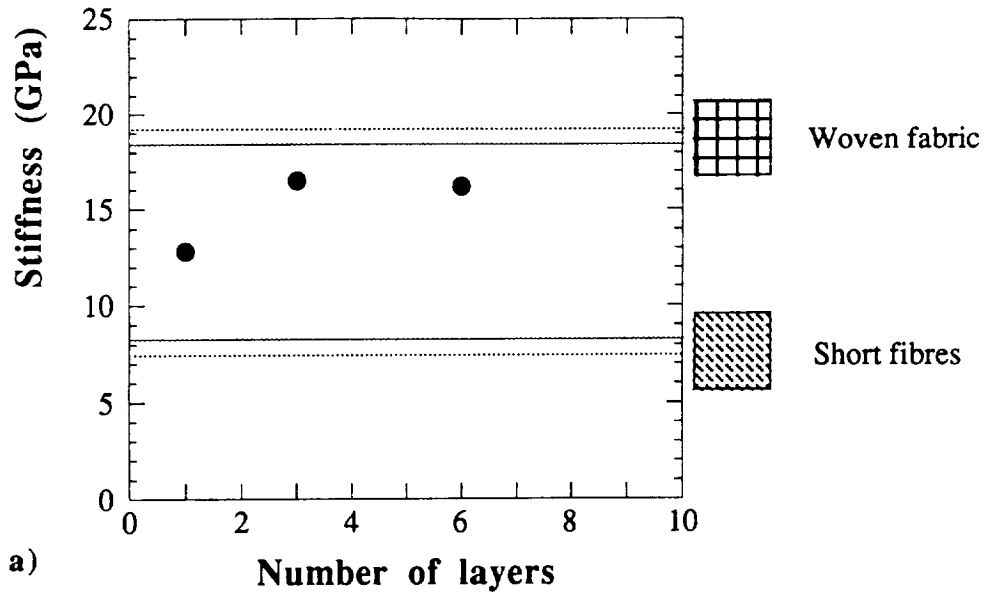


Figure 13: Stiffness (a) and strength (b) of knitted fabric composites in comparison with woven fabric and short fibre composites.

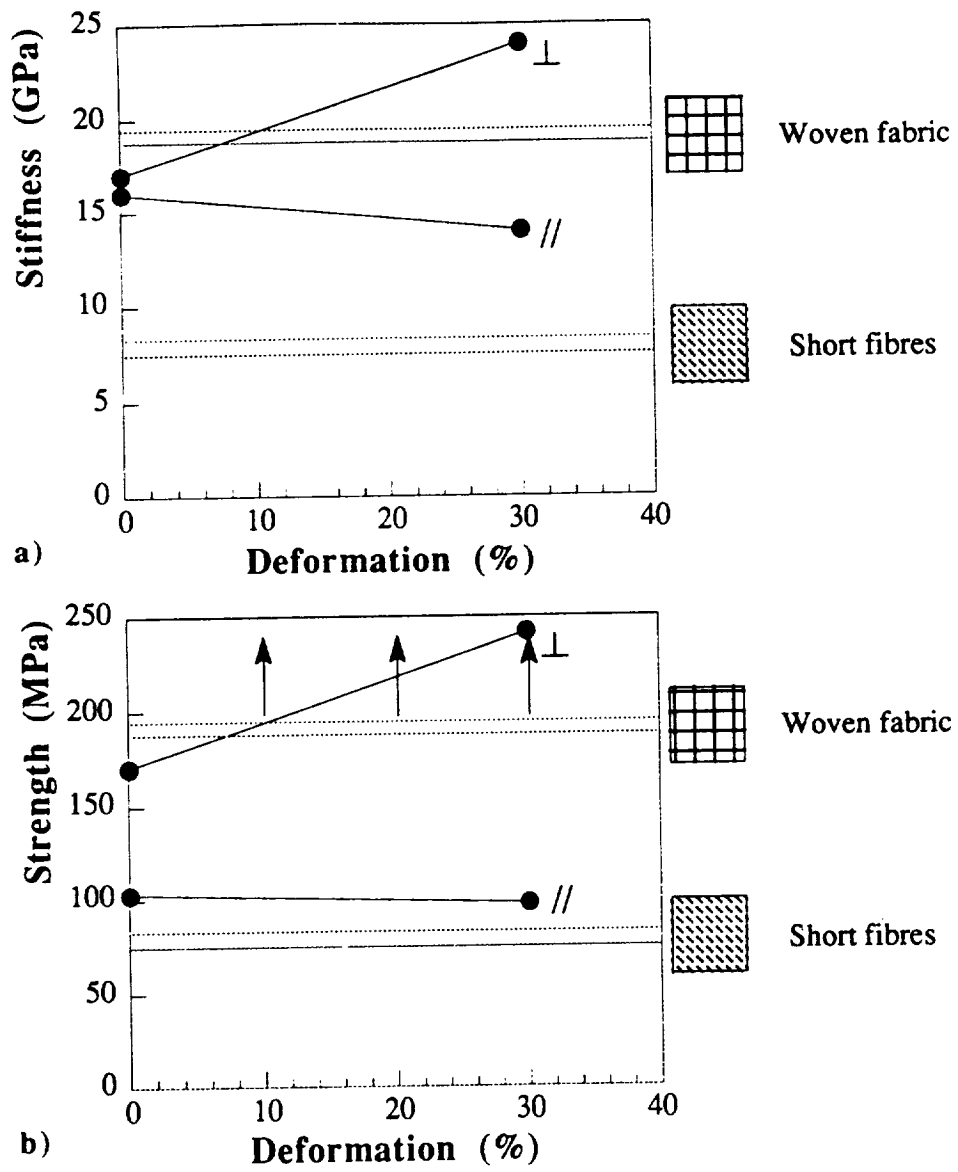


Figure 14: Influence of the deformation on the stiffness (a) and strength (b) of knitted fabric composites.

1994012376

Design and Cost Drivers in 2-D Braiding

59-24
N94-16849

Alberto Morales
ICI Fiberite
Greenville, Texas

ABSTRACT

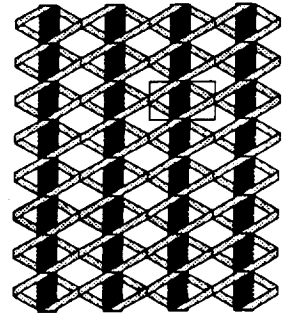
Fundamentally, the braiding process is a highly efficient, low cost method for combining single yarns into circumferential shapes, as evidenced by the number of applications for continuous sleeving. However, this braiding approach cannot fully demonstrate that it can drastically reduce the cost of complex shape structural preforms.

In this paper factors such as part geometry, machine design and configuration, materials used, and operating parameters are described as key cost drivers and what is needed to minimize their effect on elevating the cost of structural braided preforms.

Introduction

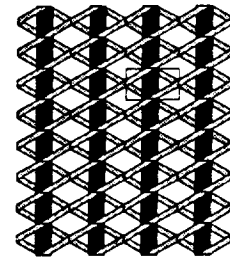
- **2-D Braiding is viewed as a highly efficient, low cost method for combining single yarns into circumferential shapes. i.e. continuous sleeving.**
- **This cost effectiveness prompted the use of braiding beyond continuous sleeving into complex shape structural preforms.**
- **However, the braiding approach cannot fully demonstrate that it can drastically reduce the cost of complex shape structural preforms.**
- **There are several factors why the cost effectiveness of 2-D braiding is not fully seen in structural preforms.**
- **Among these factors there are:**
 - **Low production quantities of preforms**
 - **Stiff, brittle fiber materials that are hard to braid**
 - **Stringent quality control requirements**
 - ***Fiber Architecture***
- **The first three factors are specific to each application and usually there is very little that can be done to minimize their effect on cost.**
- **Fiber architecture is a cost driver that is often overlooked.**

What is fiber architecture?



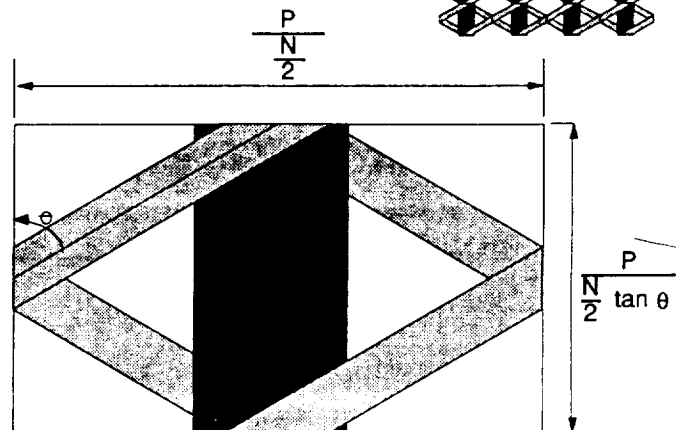
- **Fiber architecture is a graphical and numerical means by which a textile structure is described.**
- **This description must have sufficient elements to satisfy the needs of composite designers and textile engineers.**

Braid Architecture



The braid architecture is defined by five elements:

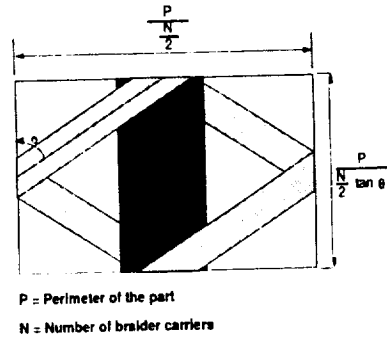
- 1) **Number of Carriers - N**
- 2) **Perimeter of the Part - P**
- 3) **Braid Angle - θ**
- 4) **Braid Yarn Yield**
- 5) **0° Yarn Yield**



P = Perimeter of the part

N = Number of braider carriers

Braid Architecture



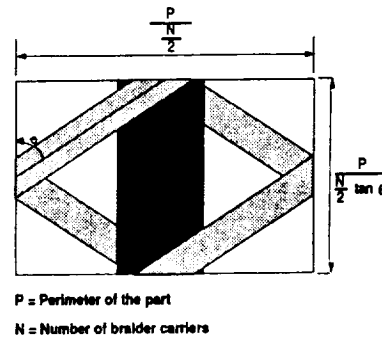
Number of Carriers - N

- The number of carriers will influence the size of the braid unit cell.
- The more carriers used, the smaller the unit cell.
- A small unit cell translates into a more uniform fabric with greater coverage.

Braid Angle

- The braid angle affects the size of the unit cell.
- The larger the braid angle the smaller the unit cell.
- A small unit cell means greater coverage and uniformity.

Braid Architecture



Perimeter of the Part

- 2-D braiding is unique in that braid unit cell is intimately linked to the perimeter of the part.
- A larger perimeter means a larger unit cell with less coverage.

Axial Yarn Yield and Braid Yarn Yield

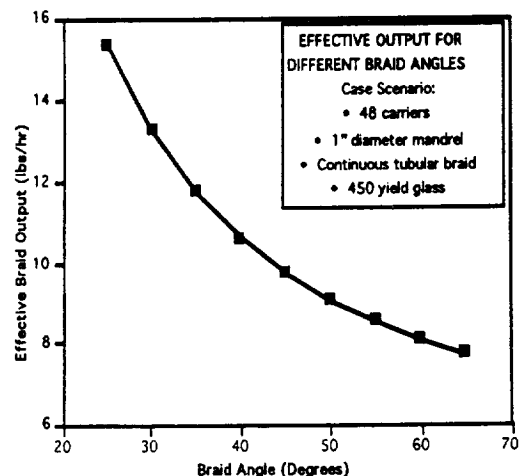
- The size of the yarns will not influence the size of the unit cell, but how well the unit cell is covered.
- Using fine yarns will leave a more open area than if using larger size tows.

Effect of Braid Architecture on Cost

- Each component that defines the braid architecture has a direct effect on the time that it takes to braid the part.
- Depending on what parameter is changed
 - the braiding time varies or
 - the number of times the machine needs to be re-spooled changes.

Effect of Braid Angle

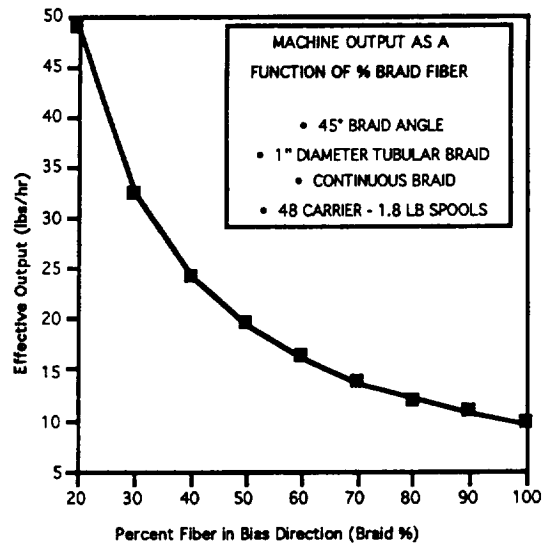
- The braid angle will determine the ratio of braider RPM and take-up speed.
- For a specific length of the part, a braiding machine takes longer to braid a large braid angle than a smaller one.
- The output in effective lbs/hr will be greater on a small braid angle.



Note: Effective braid output takes into account the time that the machine is down for re-spooling.

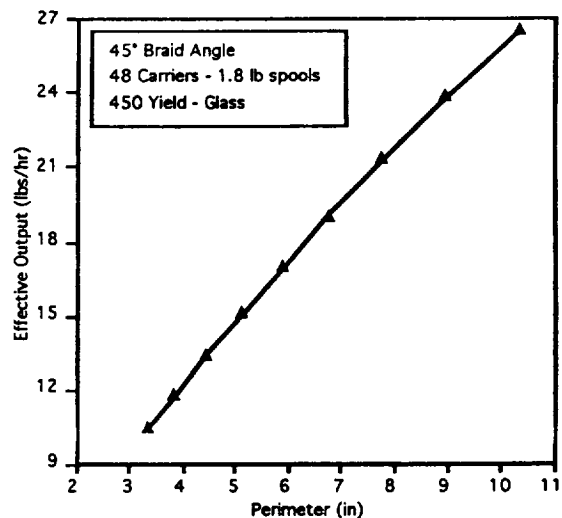
Effect of Yarn Yield

- The 0° fiber is introduced into the braid from a stationary creel; therefore, very large spool packages (5 lbs) can be used in the 0° creel.
- The braider spools can only carry 0.25 - 1 lb of material.
- A higher percentage of fiber in the 0° axis will exhibit a higher output in lbs/hr, since the machine will yield more lbs of material before it needs to be stopped for re-spooling.



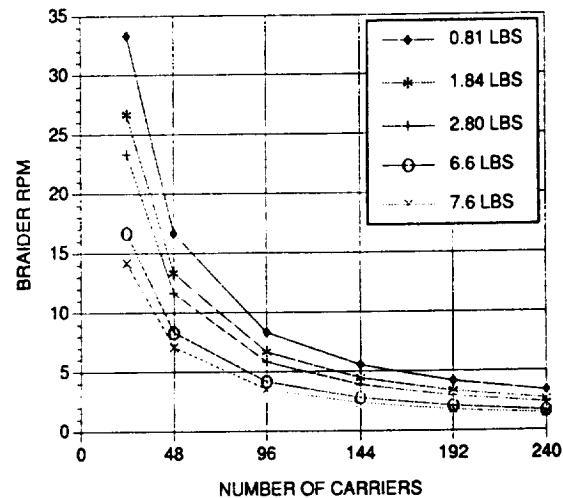
Effect of Part Perimeter

- A smaller perimeter part will take longer to braid than a larger one.
- The braider has to make more revolutions to cover the same length.
- The coverage of the part has to be taken into account since a larger perimeter part will have less coverage.



Effect of Number and Size of Carriers

- Intuitively, one would like to use a braider with the highest number of carriers capable of carrying the most material.
- This intuition is erroneous since the braider RPM is not taken into account.
- When the number of carriers increases so that the distance they have to travel to complete a revolution.
- The size of the carriers will also affect the RPM of the braider; larger carriers will slow down the machine.



Summary

1. **Effect of Braid Angle** - A larger braid angle takes longer to braid than a smaller one.
 2. **Effect of Yarn Yield** - Having a higher percentage of 0° yarns will yield higher lbs/hr.
 3. **Effect of Part Perimeter** - A smaller perimeter takes longer to braid than a larger one.
 4. **Effect of Number and Size of Carriers** - Larger number of braiders and larger carriers will slow down the braiding machine.
- **ALWAYS** estimate the coverage of the part in order to establish how uniform a part you will have, or if the braid architecture is realistic (no jamming of tows).

Conclusions

- **There are several factors that affect the cost of braided preforms.**
- **Most of the factors are inherent to their load bearing, structural applications.**
- **However, fiber architecture is a factor that we control during the design of the part.**
- **It is essential to understand each element of the braid architecture both from a performance and cost point of view in order to maximize the cost effectiveness of braiding.**



1994012377

WEAVING MULTI-LAYER FABRICS FOR REINFORCEMENT OF
ENGINEERING COMPONENTS

B J HILL, R McILHAGGER, P McLAUGHLIN

N94-16850

UNIVERSITY OF ULSTER
Engineering Composites Research Centre

SUMMARY

P 18

This paper assesses the performance of interlinked, multi-layer fabrics and near net shape preforms for engineering applications, woven on a 48 shaft dobby loom using glass, aramid and carbon continuous filament yarns. The interlinking was formed using the warp yarns.

Two basic types of structure have been used. The first used a single warp beam and hence each of the warp yarns followed a similar path to form four layer interlinked reinforcements and preforms. In the second two warp beams were used, one for the interlinking yarns which pass from the top to the bottom layer through-the-thickness of the fabric and vice versa, and the other to provide "straight" yarns in the body of the structure to carry the axial loading. Fabrics up to 15mm in thickness have been constructed with varying amounts of through-the-thickness reinforcement. Tapered T and I sections have also been woven, with the shaping produced by progressive removal of ends during construction.

These fabrics and preforms have been impregnated with resin and cured to form composite samples for testing.

Using these two basic types of construction, the influence of reinforcement construction and the proportion and type of interlinking yarn on the performance of the composite has been assessed.

Preliminary conclusions drawn from this work include:

- * it is possible to weave such preforms on standard dobby looms
- * there is an optimum proportion of interlinking yarn
- * after resin impregnation improved engineering properties have been achieved
- * the process has significant economic advantages over conventional prepreg lay-up procedures
- * significant reductions in waste can be achieved
- * hybrid structures can be produced incorporating a range of generic yarn types

INTRODUCTION

Composite technology has grown considerably since man ascertained that bricks were stronger when straw was included in the clay mixture. Now composite materials are extensively used in the aerospace, automotive, construction and medical industries. Their high strength to weight ratios, ease of processing and the capability of in-building strength in the principal stress directions have given composites an advantage over their metallic counterparts.

Traditional composites are manufactured by superimposing layers of resin impregnated material into a mould prior to curing. The lay-up procedure is carefully controlled to provide the required properties and eliminate spring-back in the finished product. These layered structures are prone to delamination, particularly in bending, leading to catastrophic failure.(1) Research has shown that delamination can be restricted by linking the layers together to give improved through-the-thickness properties.(2,3) Researchers have demonstrated that improved mechanical properties can be achieved by sewing the layers together and that these improvements may be due to the through-the-thickness yarns acting as "crack stoppers".(4,5,6,7) Other researchers have established that three-dimensional flat fabrics offering similar properties can be woven on a conventional loom.(8,9,10,11,12)

It has been demonstrated that composites manufactured from 3-D woven fabrics give improved damage tolerance (13,14, 15) and in addition Hirokawa et al have established that 3-D orthogonal woven composites had better compressive strength and flexural fatigue strength than 2-D composites (16). A further development by McGoldrick et al (17) has shown that velvet structures can be utilised to produce, what they term, 2.5D fabrics to overcome the problem of delamination in composites and Mohamed et al (18) have developed a computerised machine for weaving 3-D orthogonal net shapes. These developments indicate the amount of research being undertaken to develop interlinked woven structures for composites.

At the University of Ulster a 48 shaft computerised dobby loom has been used to weave multi-layered, interlinked fabrics and near net shape components for engineering applications using glass, carbon and aramid yarns.

REINFORCEMENT PRODUCTION

Yarn Selection and Properties

Four types of yarn have been used for this research:

glass (texturised)
glass (continuous filament)
carbon (continuous filament)
aramid (continuous filament)

The tensile strength of these yarns was measured as a straight tensile test and as a loop strength using a Textechno Statimat M instrument. Typical results for the four types of yarn are given in Table 1.

The tensile strength of the continuous filament glass yarn was approximately twice that of the texturised glass yarn and in terms of tenacity about 2.5 times stronger. The tenacity of the continuous filament glass yarn was in turn about half that of the carbon yarn which was about half that of the aramid yarn.

Since the interlinking yarns in the proposed 3-D reinforcements used in this work not only act as "crack stoppers" but are also the strength component holding the layers together, it was considered that a loop test may be a more relevant method of testing the yarn strength than the straight tensile test.

For the texturised glass yarn the loop strength and the straight tensile strength are approximately equal. However, the loop strengths of the other three yarns differ considerably from the straight tensile strength indicating the very poor transverse strength of these highly structured fibres. The loop strengths of the continuous filament glass yarn and the carbon yarn were approximately half that of the respective tensile strengths, whereas the loop strength of the aramid yarn was 67% higher than the tensile strength. This array of tensile and loop strength behaviour gave a range of properties from which it may be possible to draw conclusions about the influence of yarn properties on reinforcement and composite behaviour and performance.

Three-Dimensional Weaving

A series of reinforcements was woven in plain weave constructions using the 1460 tex texturised glass yarn. These were 4-layer interlinked structures with all the warp yarns being used to form the through-the-thickness (Z) element. The structures all weighed about 3500 g/sqm and were approximately 4.5 mm in thickness. They were woven with Z-direction reinforcement in the range 6.9% and 18.5%. Difficulties were encountered in testing the tensile strength of some of these reinforcements because of breakage at the clamps. (19,20)

The data gained from these trials was used for the production of two sets of T-section preforms, one from the

texturised glass yarn and one from a straight continuous filament yarn. The T-sections were woven with a four-layer stem or web and with a two-layer flange. As in the case of the interlinked fabrics the basic structure for each layer was a plain weave with each warp end within the reinforcement structure being involved equally in the interlinking or "stitching" together of the layers. The interlinking in the 4 layer segment was formed by transferring warp ends from layer 1 to layer 3 and from layer 2 to layer 4 for one pick before returning them to their original position. Similarly ends in layers 3 and 4 were transferred to layers 1 and 2 respectively and back. This is illustrated in Fig 1 with one end interlinking from layer 1 to layer 3. The formation of a warp link over one pick has been found to give the optimum results as far as performance properties of structural components are concerned. All the warp ends did not form the interlink at the same pick but were staggered so as to avoid possible lines of weakness. The type of construction used creates symmetry about the mid-plane. In this way it was hoped to reduce any tendency for the composite component to spring back after impregnation with resin and curing.

T-section preforms were woven with the Z proportion ranging from 3.2% to 18.5% (Fig 2). In order to assess the effectiveness and the optimum amount of the through-the-thickness element, a strength test was devised for these T-section preforms whereby the ends of the flanges were clamped in a tensile testing machine and the force to pull the web apart through its centre plane was measured. This force was termed the interplane strength, and was measured by clamping the full width (50mm) of the samples in the jaws of the tensile machine and as a grab test where the centre 25mm was held. Results indicated that there was an approximate linear relationship between percentage Z element and interplane strength up to 10% to 12% after which the increase tailed off. The most important feature of these tests was a visualisation of the mode of breakdown. This implied that the effects of the through-the-thickness element on the interplane strength are complex and that the construction of the T-section at the juncture where the construction changes from a pair of double interlinked layers to four interlinked layers is critical.

After impregnation and curing of these T-sections, a similar strength test was undertaken. Results from this indicated that the Z element does not have a significant effect on the initial failure of the composite component but considerably improved the energy absorbing properties of the composite in interplane strength. (Fig 3) The visualisation of the mode of breakdown indicated that the resin impregnated component broke down in a significantly different manner to the fabric reinforcement, with the

latter being able to deform in the area between the clamps whereas the resin prevents the component from taking up this configuration. This behavioural difference in testing between the reinforcement and composite has forced us to question the validity of using fabric strength results to measure the effectiveness of the through-the-thickness yarn.

The interlinking and construction of these fabrics and preforms has been accomplished by using plain weave structures. This introduced crimp into the yarns in the structure, especially in the warp direction which may also be the direction of the principal stress. From an engineering standpoint the yarns should be preferably in as straight a line as possible, ideally with no crimp. In order to optimise the fibre properties a further series of reinforcements was woven using T300 carbon (12k) yarn. In this series the fabrics were woven with layers of straight warp yarns interspaced with straight weft yarns with no interweaving, the structure was held together by using two further layers of warp yarns one on the top of the reinforcement and the other on the bottom. These interlinking warp layers bound the reinforcement together by being woven from the top face to the bottom face and vice versa. As in the previous structures this interlinking was over one pick before returning to the original face.(Fig 4)

Different face weave patterns and different interlinking yarn counts were chosen to give a range of through-the-thickness proportions from 2% to 18%. The reinforcements were woven on a shuttle loom and so further binding was achieved by the selvedge. This is an important factor in the transfer of the preform from the loom to the resin impregnation process. Depending on the number of layers structures from 3.5mm to 15mm were woven. These have not yet been impregnated but it is envisaged, based on previous research, that the composites will be 2.7 to 12mm thick with a 55 to 60 per cent fibre volume fraction. The analysis of the woven structures is given in Table 2.

One of the problems encountered during weaving was filamentation of the filaments against the outside edges of the headles holding the warp yarns lying in the same vertical plane.(Fig 5) This problem can be overcome by modifying the headles, but this may limit the types of construction which can be produced. The seriousness of this limitation has not been fully investigated yet.

Aramid yarns were used to construct a similar series of reinforcements to those woven from the T300 carbon yarns. For these fabrics five layers of straight warp were interspaced with seven layers of weft, none of these layers was interwoven. A coherent structure was formed by linking

two further layers of warp yarns from the top and bottom faces, in a analogous manner to the carbon samples. The fabrics ranged in thickness from 4.0mm to 10.4mm and with a weight range of approximately 4000g/sqm to 7500g/sqm. The problem of filamentation found with the carbon yarns did not occur with the aramid yarns. Details are given in Table 3.

Preform Production

One of the issues of conventional composites made by the lay-up route is the production of trimming waste; this would be a major problem in the mass production industries eg automotive industry. In an attempt to overcome this it was concluded that tests should be made to create near-net shape components on the loom. The T-section preforms, previously discussed, were the first attempt, since this configuration is a much used load bearing component in the engineering industry. As was stated earlier, these interlinked T-section composites while exhibiting better energy absorbing properties than their laid-up counterparts were still not ideal in their construction. In the area where the structure changed from 4-layers to 2 layers a cleavage zone was created where the structure was opened out to form the T-section shape, giving a resin rich seam. The cleavage was formed because the yarn paths in all four layers of the interlinked structure were identical.(Fig 6) Trials are being conducted to try to overcome this problem by using different weave structures in each of the layers or modifying the structure at the juncture of the interlinking layers, so that when the preform is folded to form the T-piece, a gap is not formed at the line of separation between the 4-layer and 2-layer structures.

However, this research has shown that near net shape preforms can be woven on a conventional loom and that there is the potential for significantly reducing waste.

While there are significant advantages in producing uniform cross-section near net shape components on the loom there would be an even greater advantage if tapered and other sections could be produced. The initial research at the University of Ulster has examined the feasibility of weaving these shaped preforms using cotton yarns of different colours in each of the layers so that the yarn paths could be followed.(21) Shaped I-sections were woven with the shaping produced by dropping out selected warp yarns until the required shape was produced. The samples were woven with 4 and 6 interlinked layers as the centre web of the section with this dividing into 2 and 3 interlinked layers to form the flange.(Fig 7)

Further trials have been conducted on the weaving of 4 layer open ended box shapes with tapered ends. These multi-layer shapes are seamless and can be designed to be a precision fit product that can be placed over a mould. (Fig 8)

Components have been woven with localised reinforcement in either the warp or weft direction. These areas of localised reinforcement can be rectangular or tapered. The base fabric was woven with three interlinked layers with the localised reinforcement either six or ten layers in thickness. (Fig 9, Fig 10)

These trials have indicated that the loom is a very versatile machine for preform production and that it is possible to manufacture a great many of the shapes required by the engineering and medical industries. However, a number of problems still exist, for example yarn path length which could be overcome by examining weave structures. The shaping of preforms was performed by leaving out selected yarns; this produced waste which could make the process uneconomic. Reductions in the amount of waste could be achieved by utilising these "free" yarns in other structures in a manner similar to nesting in engineering or lay planning in the clothing industry. Nevertheless, if shaping is to be achieved then some waste is inevitable. Research on these problems continues.

The weaving process lends itself easily to the production of hybrid structures where yarns of a different composition to the base reinforcement are introduced. These yarns can be inserted in either the warp or weft direction and in any position in the three dimensional structure. This versatility makes the loom a very powerful tool in the manufacture of composite reinforcements. It should be noted that weaving is not the only method used to manufacture composite reinforcements and that for certain end uses one or more of the other methods may be more suited.

Economics

A theoretical assessment of the economic feasibility of weaving three-dimension interlinked fabrics was undertaken. A comparison was made of the cost of producing a component by the convention lay-up technique against the cost of manufacture using a woven three-dimensional fabric.

A number of assumptions were made:

- * Yarn costs were the same for both processes,
- * Weaving costs were based on the rate of pick insertion,
- * The same total weight of both types of fabric,
- * Cutting waste was the same for both processes,
- * Actual labour costs in hand lay-up were used,

- * After lay-up the cost of both processes was the same,
- * No major capital was required for the 3-D weaving,
- * No account of overheads or depreciation were taken into account.

Taking account of a longer time to set up the loom to weave the three dimensional fabric, and this only has marginal influence on the final cost, it was concluded that at weaving speeds of 40 to 50 picks per minute the cost of the component made from the 3-D fabric would be cheaper than the conventional lay-up component.

However, a number of disadvantages must be considered: In the lay-up method plies can be oriented in any direction; this is not the case with 3D fabrics where only the two mutually perpendicular directions can be achieved. Using the lay-up method, components of any thickness and profile can be manufactured. 3-D weaving is restricted, at present, to a relatively small number of plies, thereafter, the product is laid up in the conventional manner. Profiling is not yet readily achieved on a conventional loom without significant waste implications.

Nevertheless, this limited economic assessment of the process together with a visualisation of its potential and an understanding of the needs of industry has led the researchers at the University of Ulster to conclude that the operation has considerable potential.

CONCLUSIONS

This paper has shown that it is possible to weave three dimensional multi-layer interlinked fabrics on a dobby loom. Shaped preforms can also be woven with uniform and tapered cross-sections provided care is taken with the choice of structure. It is probable that improvements to these structures are possible with slight modification to the loom, especially the headles.

Three-dimensional fabrics give improved engineering properties over conventional composites made by the lay-up method.

The economics of the process, in theory, give possible benefits over the traditional method, with considerable potential for reduction in the production of waste.

REFERENCES

- 1 M LUGER
"Fibre Substrates in Fabric Composites"

- 2 J S BROOKS, B J HILL, R McILHAGGER, P McLAUGHLIN
"Controlled Failure in Composite Materials"
Proceedings of the 4th Conference of Irish Durability
and Fracture Committee, Queens University Belfast,
(1986), 101-109
- 3 R McILHAGGER, B J HILL, P McLAUGHLIN
"Flexural Properties of Sewn Carbon Fibre Composites"
Journal of the Textile Institute (in print)
- 4 J W SAWYER
"Effect of Stitching on the Strength of Bonded
Composite Single Lap Joints"
AIAA Journal, 23, 11, (1985), 1749
- 5 A MAYADAS, C PASTORE, F K KO
"Tensile and Stress Properties of Composites by Various
Reinforcement Concepts"
30th National SAMPE Symposium. 30, (1985), 1284
- 6 L A MIGNERY, T M TAN, C T SUN
"The Uses of Stitching to Suppress Delamination in
Bonded Composites"
ASTM STP876, Delamination and Debonding, (1985), 371
- 7 P McLAUGHLIN, M GOKSOY, J S BROOKS, B J HILL,
R McILHAGGER
"A Fail Safe Technique for Polymeric Composite
Materials - Consolidation by Sewing"
Advances in Manufacturing Technology Conference, Queens
University Belfast, (1988), 554-564
- 8 Aerospace America
"Materials - Aerospace Highlights"
Dec 1984 p27
- 9 P G ROLINCK jnr
"A Unique Automated 3-D Weaving Technology"
32nd International SAMPE Symposium, (1987), 195-207
- 10 G F FERNANDO, M P ANSELL, C GEORGALLIDES, A NEWTON
"Design, Fabrication and Properties of Composites with
Multi-layered and 3-D Glass Fabric Reinforcement"
TEQC 87, Testing, Evaluation and Quality of Composites,
Conference Proceedings, Butterworth (1987), 96-104
- 11 W L LACHMAN, J A CRAWFORD, L E McALLISTER
"Multi-directional Reinforced Carbon/Carbon Composites"
Proceedings of the 2nd International Conference on
Composite Materials, ICCM2, Toronto, Ontario, (1978),
1302-1319

- 12 G PING, K GREENWOOD
 "The Scope for Fabric Engineering by Means of the Weave"
 J Text. Inst., (1986), No2, pp88-103
- 13 F J ARENDTS, K DRECHSLER, J BRANDT
 "The Application of Three-Dimensional Reinforced Fiber-Preforms to Improve the Properties of Composites"
 34th international SAMPE Symposium, Proceedings May 8-11 1989, 2118 - 2128
- 14 M CHOLAKARA, B Z JANG, C Z WANG
 "Mechanical Properties of 3-D Composites"
 ANTEC '89, 1549 - 1551
- 15 J BRANDT, K DRECHSLER, H RICHTER
 "The Application of 2-D and 3-D Woven Thermoplastic Fibre Preforms for Aerospace Components"
 36th International SAMPE Symposium, Proceedings April 15 -18 1991, 92 -101
- 16 T HIROKAWA, J YASUDA, Y IWASAKI
 "The Characteristics of 3-D Orthogonal Woven Fabric Reinforced Composites"
 36th International SAMPE Symposium, Proceedings April 15 -18 1991, 151 -160
- 17 C MCGOLDRICK, J MOREL, M WEVERS, I VERPOEST
 "2.5D Fabrics for Delamination Resistant Composite Structures"
 Composites,3, May-June 1991, 284 - 290
- 18 M M MOHAMED, Z ZHANG, L DICKSON
 "3-D Weaving of Net Shapes"
 Proc 1st Japan International SAMPE Symposium, Proceedings Nov 28 - Dec 1 1989, 1488 - 1493
- 19 C M HARPER, B J HILL, R McILHAGGER
 "The Effects of Varying the Z-Directioned Fibre Proportion on the Through-the-Thickness Properties of Woven Glass Fibre Preforms"
 Proc of the 8th Conference of the Irish Manufacturing Committee - Advances in Manufacture, 1991, 77 -87
- 20 C M HARPER, B J HILL, R McILHAGGER
 "Manufacturing and Testing Engineering Preforms: The Influence of Frequency and Positioning of Through-the-Thickness Fibre"
 Proc of the 9th Conference of the Irish Manufacturing Committee - Technology in Manufacturing for Europe, 1992 488 - 501

21 P McLAUGHLIN

"Design and Manufacture of Multi-Layer and Three-Dimensional Woven Reinforcements for Composite Materials" M.Phil Thesis 1992

TABLES

Table 1 Yarn Strength Properties

	Tensile Strength			
	Yarn Count tex	Strength N	Extension at Break %	Tenacity cN/tex
Texturised Glass	1460	191	2.50	13.1
Continuous Filament Glass	1200	381	2.90	31.8
Carbon	814	501	1.72	61.6
Aramid	836	1096	4.03	131.2
	Loop strength			
Texturised Glass	1460	195.6	2.45	13.4
Continuous Filament Glass	1200	199.2	1.71	16.6
Carbon	814	289.0	0.89	35.5
Kevlar 49	836	1839.2	4.17	220.0

Table 2 Analysis of Carbon Typical Structures

Straight Warp Layers	Straight Weft Layers	Interlinking Yarn	Thickness mm	Weight g/sqm
3x12k	4x12k	2x3k	3.5	2896
5x12k(2)	6x12k(2)	2x12k(2)	5.4	4227
5x12k(2)	6x12k(2)	2x12k(2)	8.3	5125
19x12k(2)	21x12k(2)	2x12k(2)	15.0	12690

Table 3 Analysis of Aramid Typical Structures

Straight Warp Layers	Straight Weft Layers	Interlinking Yarn	Thickness mm	Weight g/sqm
5x7900d'tex	7x7900d'tex	2x7900d'tex	4.0	3750
5x7900d'tex	7x7900d'tex	2x7900d'tex	7.3	7420
5x7900d'tex	7x7900d'tex	2x7900d'tex	10.4	7720

FIGURES

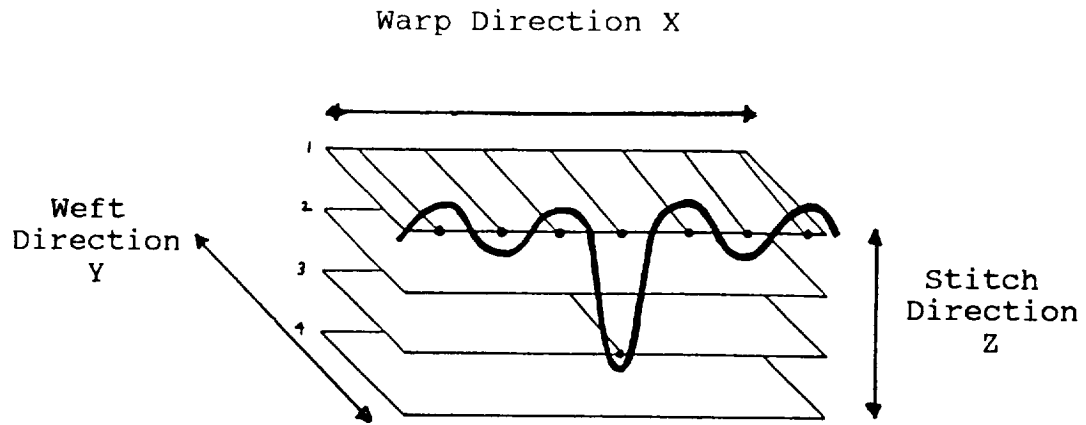


Fig 1 Warp Stitching

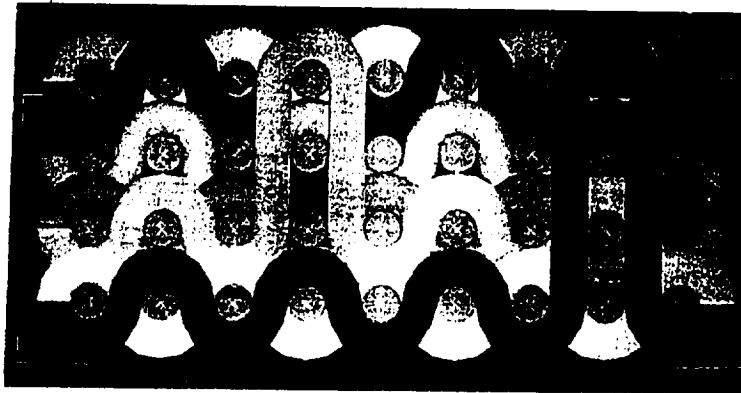


Fig 2 Weave Structure of Plain Weave T-Section

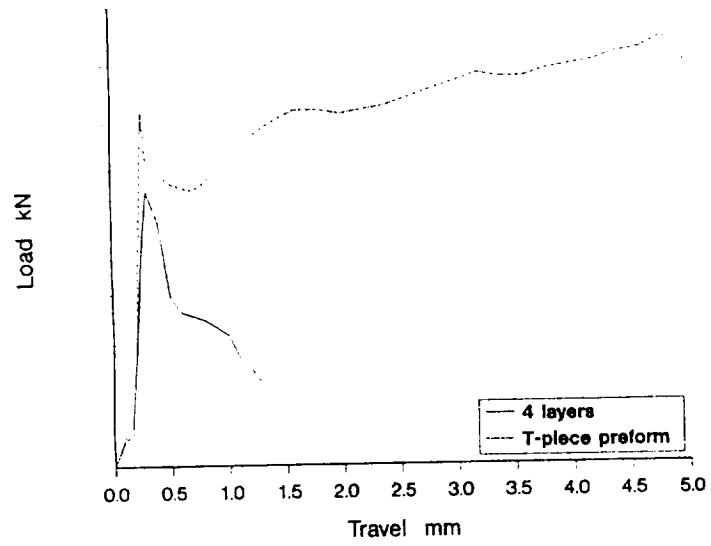


Fig 3 Graph of Load Against Travel

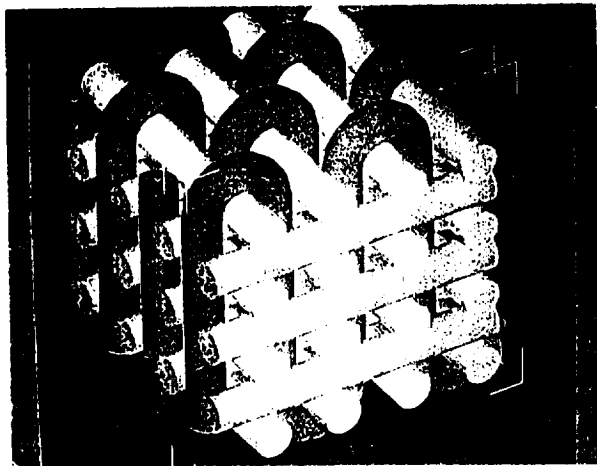


Fig 4 Weave Structure of Interlinked Fabric



Fig 5 Yarn and Headle Position in Conventional Shafts

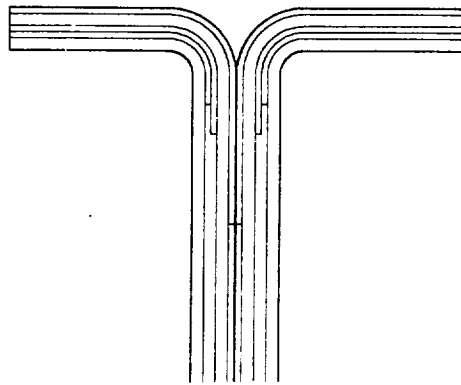
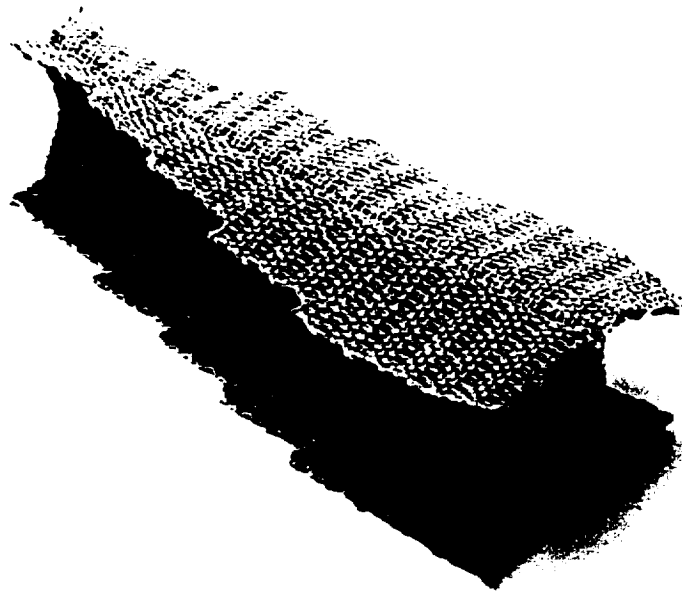
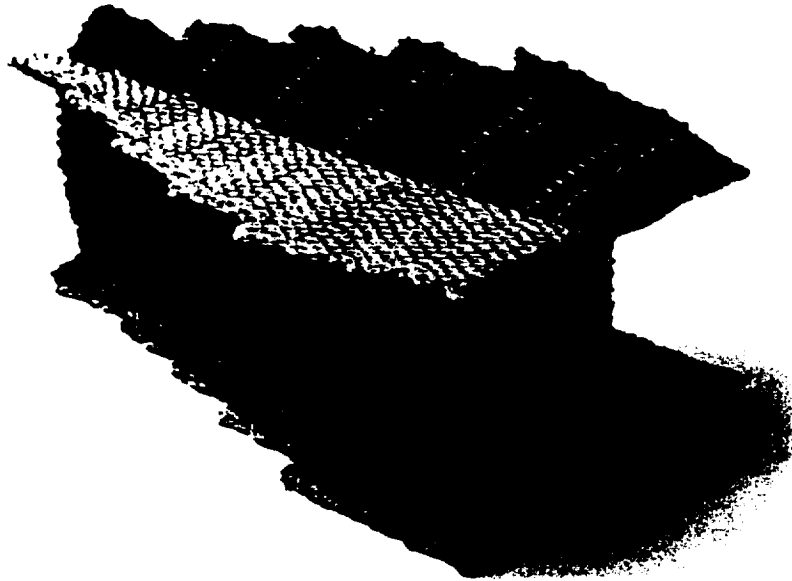


Fig 6 T-Section Illustrating "Cleavage"



(a)



(b)

Fig 7 Shaped I-Beam (a) 4 Layer Stem with 2 Layer Flange
(b) 6 Layer Stem with 3 Layer Flange

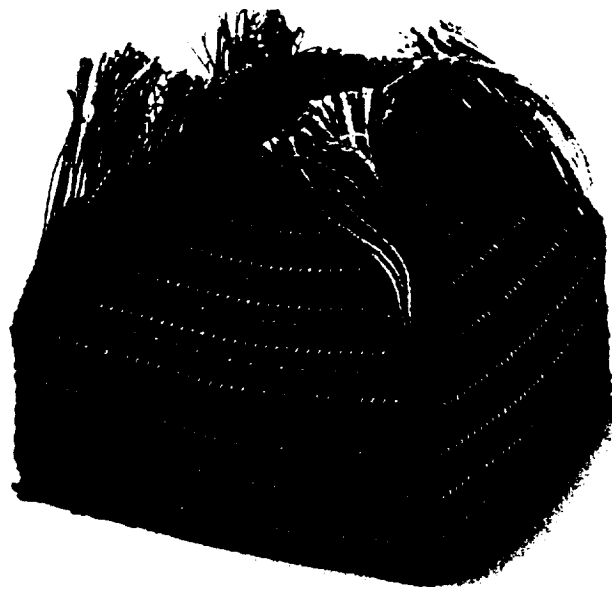


Fig 8 Two Layer Open Ended Shaped Box



Fig 9 Localised Reinforcement (Warpwise)

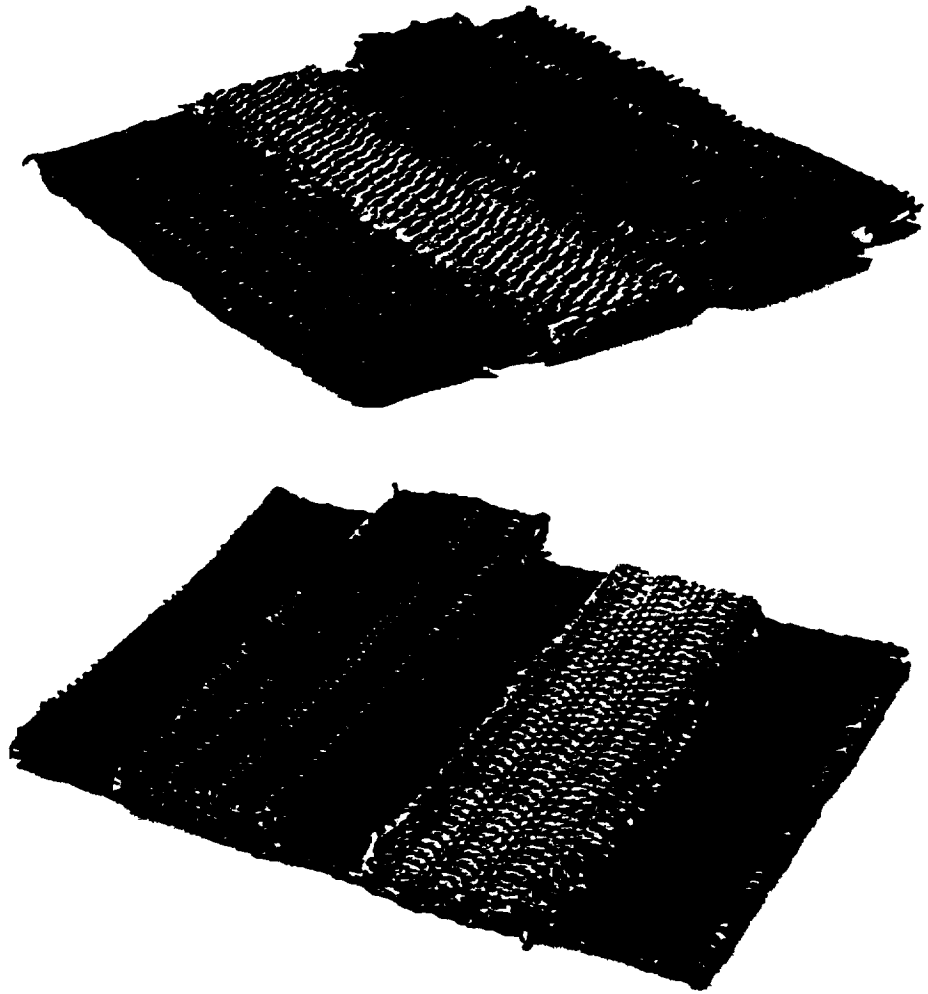


Fig 10 Localised Reinforcement (Weftwise)

1994012378

56-24

17770
N 9 4 - 1 6 8 5 1

EFFECT OF TOW ALIGNMENT ON THE MECHANICAL PERFORMANCE OF 3D WOVEN TEXTILE COMPOSITES

Timothy L. Norman
Department of Mechanical and Aerospace Engineering,
West Virginia University, Morgantown, WV 26506

Patti Allison , Jack W. Baldwin , Brian K. Gracias
General Electric Aircraft Engines, Cincinnati, OH

Dave Seesdorf
Westinghouse, Pittsburgh, PA

ABSTRACT

Three-dimensional (3D) woven preforms are currently being considered for use as primary structural components. Lack of technology to properly manufacture, characterize and predict mechanical properties and predict damage mechanisms leading to failure are problems facing designers of textile composite materials. In this study, two material systems with identical specifications but different manufacturing approaches are investigated. One manufacturing approach resulted in an irregular (nonuniform) preform geometry. The other approach yielded the expected preform geometry (uniform). The objectives of this study are to compare the mechanical properties of the uniform and nonuniform angle interlock 3D weave constructions. The effect of adding layers of laminated tape to the outer surfaces of the textile preform is also examined. Damage mechanisms are investigated and test methods are evaluated.

INTRODUCTION

Multidimensional textile composites are widely becoming an increasingly popular alternative to traditional laminated composite materials in that they may offer distinct advantages in strength, cost, manufacturability, and damage resistance. These materials, however, are relatively new and possess a number of fiber, resin, and angular orientation possibilities. For these reasons, there is a great need to characterize their behavior. 3D composites pose a viable alternative to more conventional materials such as titanium and aluminum for lightweight, high strength designs with a requirement for a high resistance to impact damage.

Few investigations have been conducted to determine damage mechanisms in 3D woven textile composites, although recent studies have been conducted on damage of braided textile

composite materials (currently not published). Reference 1 investigated damage development and manufacturing of braided composites. Their study investigated mechanics of materials and manufacturing of 2D, 2D triaxial and 3D braid patterns. The structural performance was evaluated through an extensive mechanical test program. Of particular interest was the characterization of the mechanical response and possible failure mechanisms of braided composite material systems, and the effect of different fiber architectures on mechanical behavior. Open hole tension, unnotched tension and compression, compression after impact, in-plane shear, transverse shear, transverse tension and bearing tests were conducted. The effect of unit cell size on strain gage strain was also investigated. The failure mechanism of the fully braided composite loaded in tension was described as shear-out which occurred along tow boundaries in the following repeating sequence: 1) braided tow failure, 2) cracks forming at the broken tow boundary and propagating until a braided cross-over point, 3) failure of an intersecting tow at the cross-over point, 4) cracks forming at the intersection broken tow boundary and propagation until the next braided cross-over point. Failure of triaxially braided composites was observed as starting as longitudinal tow failure, followed by load redistribution into the braided tows, followed by the shear-out failure described above.

Many interesting findings were presented by reference 2 after testing the impact properties of 3D braided graphite/epoxy composites. 3D braided composites show excellent impact insensitivity as compared to laminated composites. After low velocity impact testing, 3D braided composites exhibited "surface matrix cracking in resin pockets, separation of fiber tows, fiber tow breaking, and debonding of matrix and fiber filament within broken fiber tow." In tests of reference 2, most of the broken fiber bundles were found in "fiber crimp areas" (areas where the weaving of the yarns made bends into or away from an interface). From these observations, it was hypothesized that the existence of small fiber-to-fiber interfaces in 3D braids would cause "inter-fiber-tow stresses" to develop. In this instance, fiber tow breakage was considered to be much more detrimental than fiber tow separation.

The diversity of the woven preform makes the composite unique in that there is no real layer of lamination as in traditional laminated composites. It is the 45° fibers that actually resist the interlaminar shear forces that normally cause parallel planes to separate within a material (ref. 3). Advantages of woven textile composites are an increase in impact properties due to the weave's ability to resist delamination and shear cracking (ref. 4) and the overall composite's increased energy absorption characteristics (ref. 5). As a consequence of these properties, there is a gain in the composite's residual tensile and compressive strength (ref. 4) with a loss in in-plane strength and stiffness.

In this study, two material systems with identical specifications but different manufacturing approaches are investigated. One manufacturing approach resulted in an irregular (nonuniform) preform geometry. The other approach yielded the expected preform geometry (uniform). The objectives of this study are to compare the mechanical properties of the uniform and nonuniform angle interlock 3D weave constructions. The effect of adding layers of laminated tape to the outer surfaces of the textile preform is also examined. Damage mechanisms are investigated and test methods are evaluated.

MATERIAL ARCHITECTURE

Four different material architectures are used in this study and are identified as: uniform, uniform with tape, nonuniform, nonuniform with tape. Cross-sectional views of the uniform and nonuniform preforms are shown in figures 1 and 2, respectively.

The 3D woven preform was designed to provide exceptional strength in the length direction and to enhance through the thickness resistance to delamination normally present in laminated composites. To provide that strength, the preform was designed to have 50% fibers in the X direction (called 0°), 30% fibers in the Y direction (called 90°), and 20% fibers in the out-of-plane Z direction (called $\pm 45^\circ$). Calculations showed actual fiber percentages in a random 0 tensile specimen section from the uniform preform were found to be 35% 0° fibers, 35% 90° fibers, and 14% $\pm 45^\circ$ fibers, by using a weave consisting of 0° and 90° fibers, with $\pm 45^\circ$ fibers forming an "angle interlock weave configuration" (ref. 6) acting to stitch the preform together. No information is available to date for actual fiber percentages for nonuniform preform.

Since this architecture is 3-D with many interlocking weaves of tows, the structure is difficult to visualize. As a result, determining damage mechanisms and damage progression of the composite requires careful evaluation of many planes of view. By nature, the 3-D weave configuration of the preform causes there to be a continuously varying cross-section. This contradicts the typical convention of laminated composites where there is a constant material cross-section, making material sectioning a matter of personal preference. The complexity of this 3-D textile structure necessitates a well planned method of evaluation. The material evaluation technique/protocol created was based on the idealized planes of view shown in figures 1b and 2b.

EXPERIMENTAL PROCEDURE

Specimens were machined from four graphite/epoxy panels, two 12" x 10" x 0.50" and two 12" x 10" by 0.75". The two 0.75" thick panels contained a co-cured tape layup on both outer surfaces of the panel. The specimens were machined for the following tests: knight compression, 0° interlaminar shear, 90° interlaminar shear, flatwise tension, 0° tension, 90° tension and 0° flexural. Flexural tests were not conducted for specimens with tape. Testing was conducted by Delsen Testing Laboratories, Inc. (Glendale, CA 91201-3011).

Knight compression tests were conducted according to ASTM D 695-89. The specimens were tested such that the load was applied in the Z (out-of-plane) direction. Modulus was determined from the initial linear portion of the load-strain curve. Interlaminar shear strength specimens were tested in accordance with the procedures outlined in ASTM D 2344-89. Specimens were machined to a span to a depth ratio of 4:1. Flatwise tension specimens were tested in accordance with the procedures outlined in ASTM C 297-66(88). Strain was measured using micromeritics strain gage CEA-06-125-UW-350. Specimens were tested at a rate of 0.005 inches/minute. Ultimate strength, modulus and strain to failure were recorded. Modulus was determined from the initial portion of the load-strain curve. Tensile properties for 0° and 90° specimens were tested in accordance with procedures outlined in ASTM 639-89, using a

type II tensile specimen configuration and a Micro-Measurements CEA-06-125UW-350 strain gage. Ultimate strength, modulus and strain to failure were recorded. Flexural tests were conducted according to ASTM D 790-86 method II, procedure A. A span of 7.5 inches was used to conduct the test. Modulus was determined from the initial linear portion of the load deflection curve. Recent studies have shown that unit cell size should be considered when selecting strain gage size. Unit cell size was not a consideration in the present study.

After testing, macro- and micro-scopic inspections were conducted. In the macroscopic examination stage, inspection and photographs of the tested specimens were performed under low power of a dissecting microscope. Following macroscopic inspections, specimens were sectioned and polished for microscopic inspection. An Olympus SZH research dissecting microscope was used to obtain photomicrographs of the polished cross-sections.

RESULTS

Pretest Conditions

Specimens of uniform construction with tape were used to investigate pre-test characteristics. Tows appeared to be well bonded to matrix but were present with microcracks (figure 3). These microcracks were also found lying in resin pockets. Microcracks are not clearly observed in the photo because of the epoxy used when making the mold of the specimen. This emphasizes the importance of using a radioluscent filler in the epoxy for materials with voids and cracks in resin filled areas. Cracking was not restricted to a single fiber direction or plane of view. A small resin rich layer between coincident fiber bundles within the same tow can also be recognized in the figure.

The exact cause of these pre-existing cracks or their effect on material strength and damage resistance is unknown, but stress fractures in fibers during the weaving process and shrinkage during cure are viable explanations for their origination. This problem was corrected in subsequent material preforms.

Strength and Stiffness

Tension

Figures 4 and 5 show tensile strength and stiffness, respectively, for 0° and 90° uniform, uniform with tape and nonuniform specimens. The data shown in the figures has been normalized to the 0° tensile properties. Both 0° and 90° specimens of figure 4 show reductions in strength for the nonuniform preform. Uniform specimens with tape resulted in further reductions in strength. Testing of nonuniform preform with tape was discontinued due to the applied gripping force necessary to prevent slippage of the specimen. This high grip force caused out-of-plane compression failure, which may have resulted in strength reductions. Stiffness reductions for nonuniform specimens are also observed in 90° specimens. Nonuniform specimens, however, exhibited a small increase in stiffness of approximately 5%. Stress-strain curves for 0 and 90 degree uniform specimens are shown in figures 6 and 7, respectively. Uniform and nonuniform specimens exhibited similar behavior: a region of linear elastic behavior followed by a region of nonlinear behavior. Average 0° uniform strain at failure was higher than nonuniform; however, average 90° uniform strain at failure was higher than nonuniform strain at failure.

Flatwise Tension

Figure 8 shows a comparison of strength and stiffness for flatwise tension uniform and nonuniform specimens with and without tape. Results of this figure show that through thickness strength and stiffness is higher for nonuniform specimens than for uniform specimens: out-of-plane strength was only slightly higher but stiffness was significantly higher. Strength and stiffness decrease when tape is added to uniform specimens. Tape decreased stiffness of uniform specimens but increased strength of nonuniform specimens.

Interlaminar Shear and 0° Flexure

Results from interlaminar shear strength tests are shown in figure 9. These results show that interlaminar shear strength and stiffness of 0° and 90° uniform specimens was higher than that of nonuniform specimens. No significant differences were found between nonuniform specimens with or without tape. Notable decreases were observed for uniform specimens with tape. 0° flexure test results (fig. 10) show that stiffness and strength was significantly higher for uniform than for nonuniform specimens.

Knight Block Compression

Knight block compression strength and stiffness of uniform specimens was higher than nonuniform specimens (fig. 11). Strength and stiffness of uniform specimens with tape increased but decreased for nonuniform specimens with tape.

Damage Mechanisms

Tension

A pronounced "arrowhead" failure pattern became characteristic of the through thickness damage in the 0° tensile specimens (fig. 12). Tow separation occurred between adjacent 90° tows along the shear plane that runs along the 0 direction created by the interlocking geometry of the $\pm 45^\circ$ architecture. The direction of the fracture reverses at the midplane of the composite where the $\pm 45^\circ$ tows cross. The 90° specimens failed nearly perpendicular to the loading direction (fig. 13). All specimens exhibited matrix cracking, tow rupture and tow pullout at the fracture site. Intra-tow fracture occurred in tows perpendicular to the loading direction. Widespread matrix cracking is present at the fracture site and at locations remote from the fracture site. Figure 14 shows a photomicrograph of a 90° specimen after loading that exhibits matrix cracking, fiber breakage and intra-tow failure. Figure 15 shows a crack propagating through 0° and 90° fibers and fiber debonding.

Flatwise tension

Top ply failure and bond failure between the test specimen and the end tape were commonly observed for specimens without tape. For specimens with tape, top ply failure in the composite and delamination failure between the tape and the textile composite were commonly observed. Delamination of the top ply occurred by crack bridging with bridging traction supplied by the through thickness weave profile at the interface. Cracking was also observed through the thickness in the resin along the transverse and longitudinal tows.

Interlaminar Shear and Flexural Test

Delamination at the resin interface between the tape and textile was commonly observed in uniform and nonuniform specimens with tape. Cracking is observed in 0° uniform and nonuniform flexural test specimens (fig. 16) propagating from load application point and spreading through the thickness following the $\pm 45^\circ$ tow by crack bridging with the bridging traction supplied by the through thickness yarns. The transverse shear cracks in 90° specimens are oriented radially from the load application point, and propagate in a staircase fashion similar to damage observed in laminated composites subjected to transverse impact loading.

Knight Block Compression

Compression failure occurred with extensive delaminations between tows and matrix. A 45° shear failure on the 90° cross-section was also observed. Damage was confined primarily to the textile material; little damage occurred in the composite laminate tape. Uniform specimens broke into two pieces at failure whereas nonuniform specimens remained intact. Decreased compliance of the nonuniform specimens may have caused these failure differences.

SUMMARY

Strength and Stiffness

In general, strength and stiffness decreased with nonuniformity. There were three exceptions:

- o Flatwise tension strength and stiffness increased
- o Small increase in 0° tensile modulus
- o No significant effect on out-of-plane strength

Tensile stress-strain curves of both materials showed a linear portion followed by nonlinear region until failure. 0° uniform specimens exhibited higher strain to failure than nonuniform. 90° nonuniform exhibited higher strain to failure than uniform.

Effect of Tape

In-Plane and Shear Loading

- o Tape reduced strength
- o Small effect on stiffness (In-plane only)

Out-of-Plane Loading

- o Tape increased nonuniform strength (T&C)
- o Tape reduced uniform strength (C)
- o Tape reduced uniform and nonuniform stiffness (T)

Damage Mechanisms

Pretest Conditions

- o Cracks in neat resin pockets
- o Intra-tow resin line (consolidation)
- o Cracks in tows

General Failure Mechanisms

In-plane loading - matrix cracking, tow rupture and tow pullout.

Flatwise tension - top ply delamination, transverse and longitudinal tow/matrix interface cracking, end tap debonding, tape debonding.

Interlaminar Shear - transverse cracking along through thickness weave emanating from load application point, tape separation at interface

Knight Block Compression - 45° shear failure in 90° section, uniform specimens broke into pieces whereas nonuniform remained intact.

Evaluation of Test Methods

Some tests developed for isotropic materials do not properly evaluate material performance. High grip pressure required in tensile tests caused delamination and fracture. Out-of-plane tests resulted in end tab failure and delamination of the tape. The single most complicating factor of all tests is the lack of understanding as to what constitutes failure. Most textile composites continue to carry load after "fracture". Textile composites are more difficult to test and draw conclusions from to evaluate the quality of the composite.

Damage Progression

It is likely that matrix cracking in a resin pocket on fiber matrix interface is the first form of damage found in the textile composite. Continued loading causes crack to propagate to neighboring tows, which causes high stress concentrations at the interface. With increased loading, tow rupture occurs. The crack continues to propagate along tow/resin interface, causing the crack formation to follow a pattern created by the geometry of the 3-D architecture, i.e. weave angle.

RECOMMENDATIONS

Most test methodology used on textile composite materials was developed for isotropic materials. Test results developed for isotropic materials may not necessarily provide an accurate assessment of 3D textile preforms. Therefore, there is a great need to develop new test methodology that can truly evaluate the performance of the textile composite.

A second recommendation would be to establish what constitutes failure in textile composite materials. Clearly, there are different levels of failure. For isotropic materials, failure is easily identified, usually resulting in catastrophic fracture, leaving the specimen virtually incapable of carrying load. Laminated composites are able to carry load even after significant delaminations and transverse shear cracking, but load carrying capability quickly diminishes with fiber breaks. Textile composites continue to carry load after noticeable fracture. Significant deformation can develop without catastrophic failure. Despite this quality, textile

composites are often evaluated with the same criteria as isotropic or laminated composite criteria. This interpretation of test data will undoubtedly present a false picture of textile composites. Failure criteria for textile composite materials needs to be established.

A third recommendation is to investigate the effects of architecture on damage patterns. Crack movement might possibly be anticipated with a preform being woven so as to inhibit a continual snowballing energy buildup in the crack front along the tow. Increasing the resistance to crack growth (fracture toughness) of the matrix might prolong crack initiation. Additionally, decreasing the size and number of the neat resin pockets might delay or eliminate the onset of crack initiation. As evidenced by the variation in damage in the 0° and 90° tensile test specimens, architecture does have a direct effect on the way in which the textile composite fails. Design for failure might play an important role in the use of textile composites.

ACKNOWLEDGEMENT

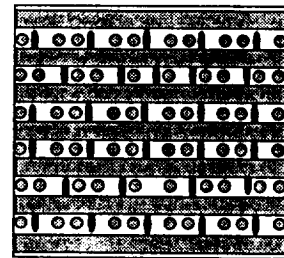
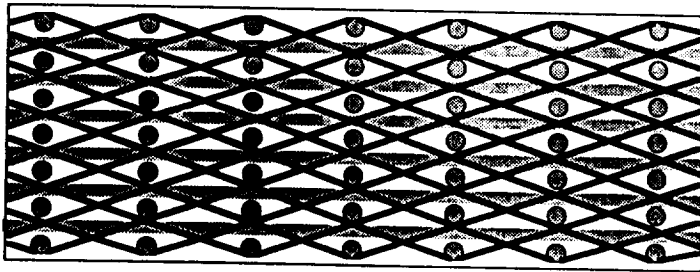
This work was supported by General Electric Aircraft Engines.

REFERENCES

1. Fedro, Mark J. and Wilden, Kurtis: Characterization and Manufacture of Braided Composites for Large Commercial Aircraft Structures. Ninth DOD/NASA/FAA Conference on Fibrous Composites in Structural Design, November 4-7, Lake Tahoe, NV, 1991.
2. Gong, J.C. and Sankar, B.V.: Impact Properties of Three Dimensional Braided Graphite/Epoxy Composite. *Journal of Composite Materials*, Vol. 25, June, 1991.
3. Mohamed, Mansour H.: Three-Dimensional Textiles. *American Scientist*, Vol. 78, November-December, 1990, p. 530.
4. Bishop, Sarah M. : Strength and Failure of Woven Carbon-Fiber Reinforced Plastics for High Performance Applications. *Textile Structural Composites*, Composite Materials Series, 3, 1989, pp. 173-207.
5. Naik, N.K., Shembekar, P.S., and Verma, M.K. : On the Influence of Stacking Sequence on Notch Sensitivity of Fabric Laminates. *Journal of Composite Materials*, Vol. 24, August, 1990, p. 838.
6. Zawislak, S.P. and Maiden, J.R.: Advanced Weaving Concepts for Complex Structural Preforms. Fiber-Tex, NASA Conference Publication 3038, 1988, p. 91.



(a)

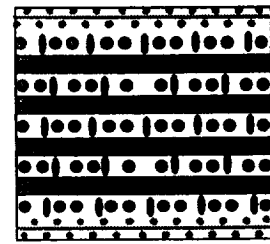
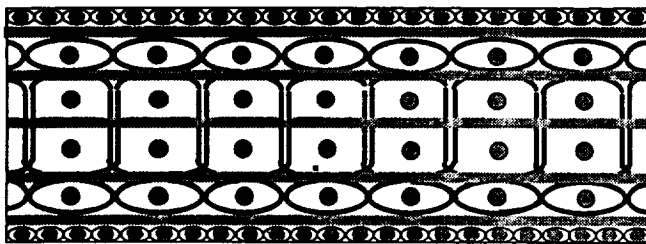


(b)

Figure 1. Cross-sectional view of the uniform construction shown as a) photomicrograph of 90° view, and b) computer drawing of 90° and 0° views.



(a)



(b)

Figure 2. Cross-sectional view of the nonuniform construction shown as a) photomicrograph of 90° view, and b) computer drawing of 90° and 0° views.



Figure 3. Photomicrograph of 90° cross-sectional view of a uniform construction showing cracking in tows found in pretest specimens.

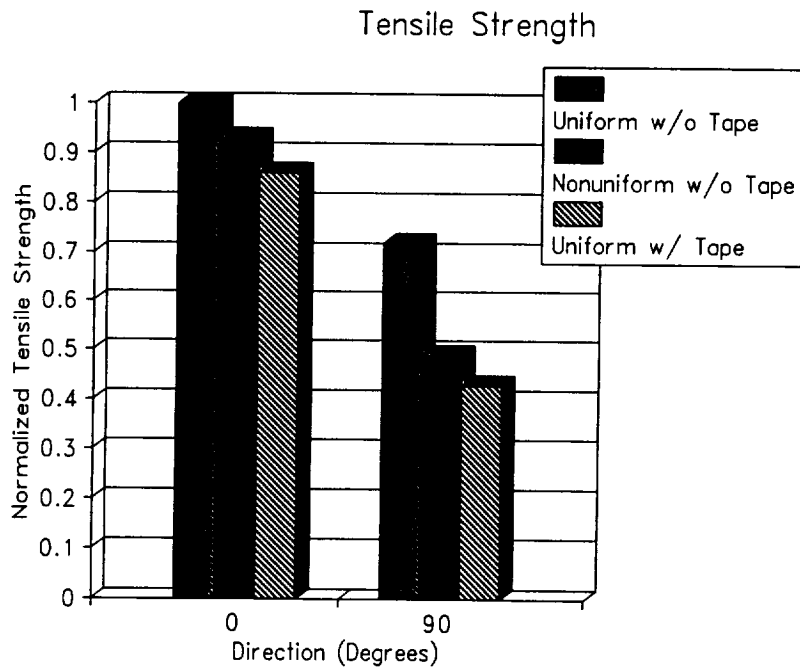


Figure 4. Tensile strength of uniform and nonuniform specimens.

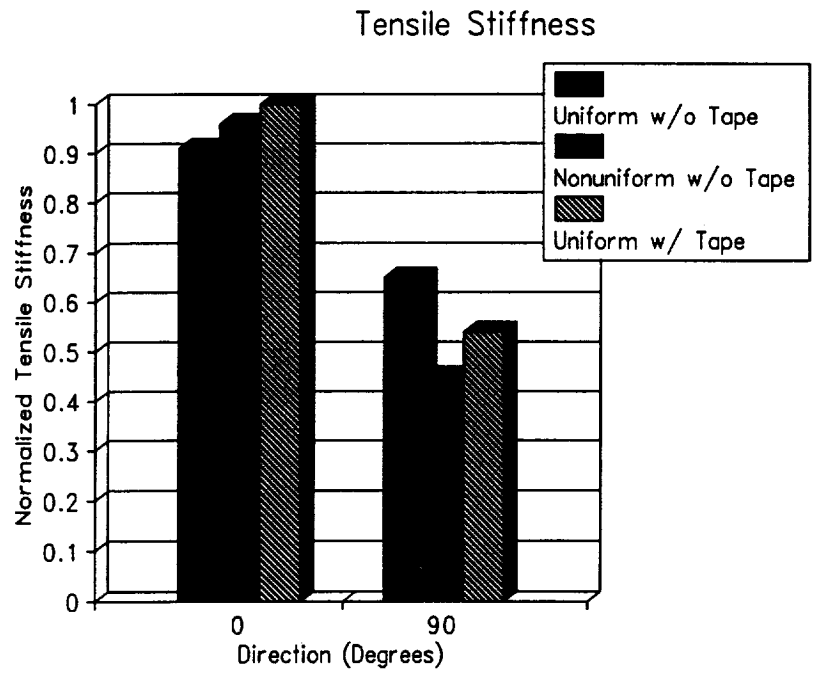


Figure 5. Tensile stiffness of uniform and nonuniform specimens.

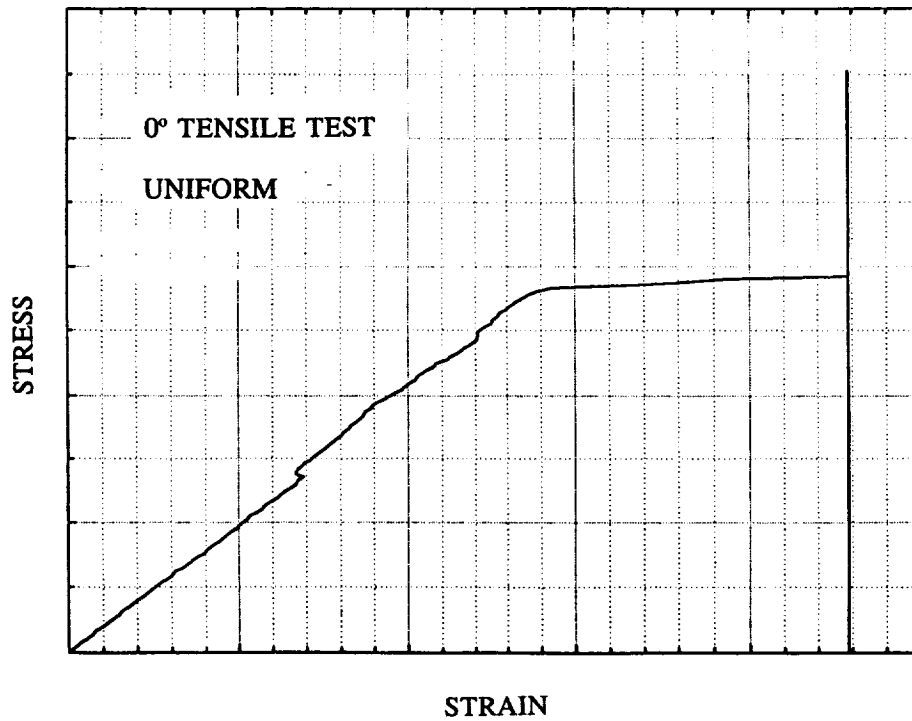


Figure 6. Stress-strain curve of 0° uniform specimen under tensile loading.

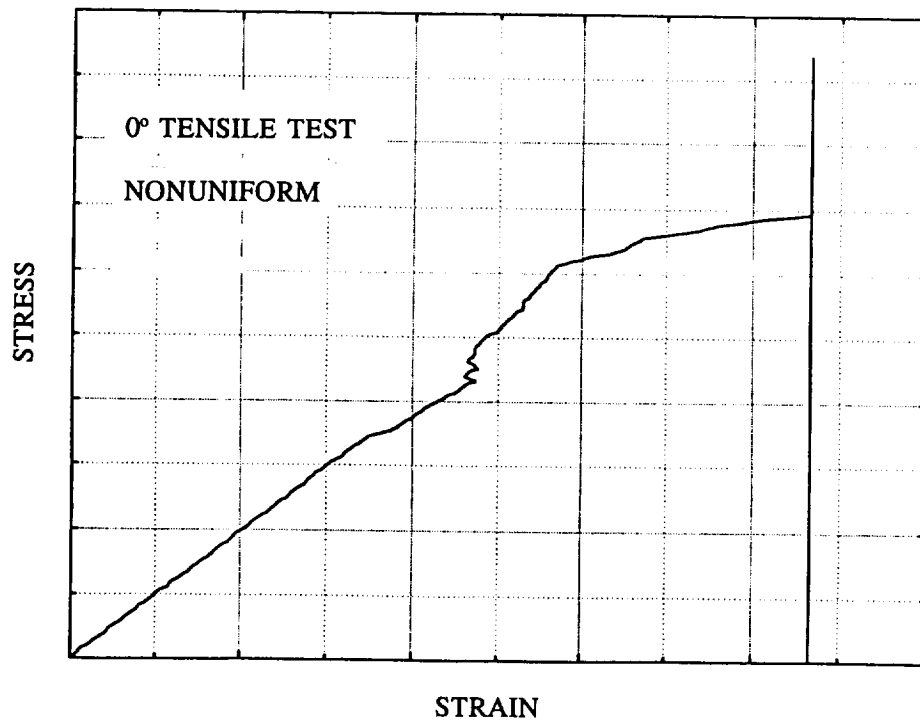


Figure 7. Stress-strain curve of 0° nonuniform specimen under tensile loading.

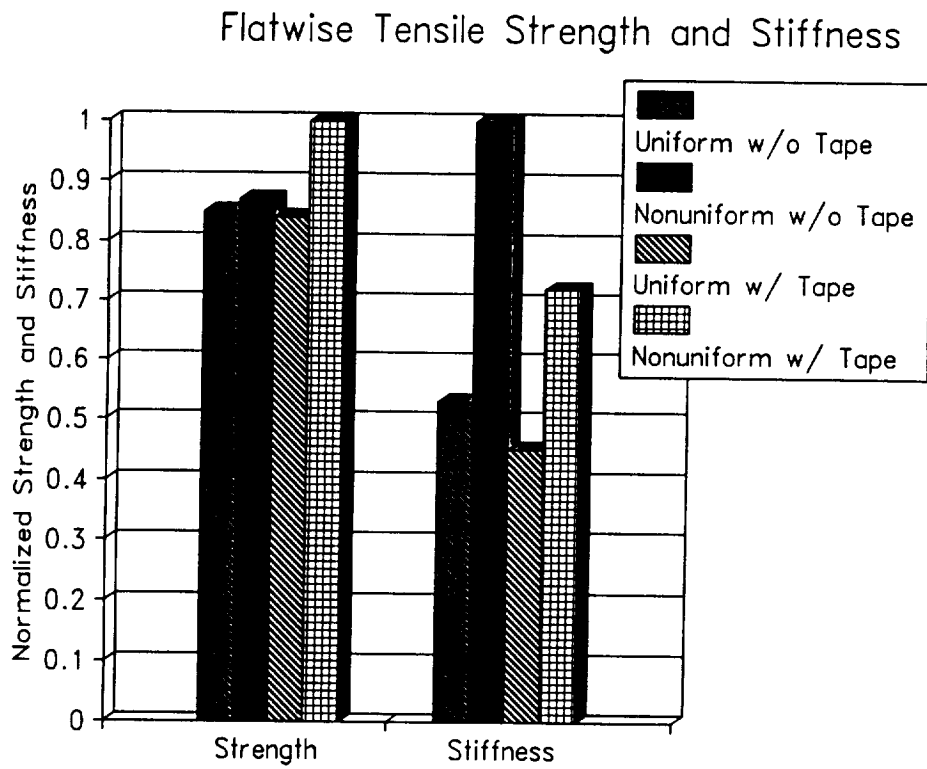


Figure 8. Strength and stiffness of uniform and nonuniform flatwise tension specimens.

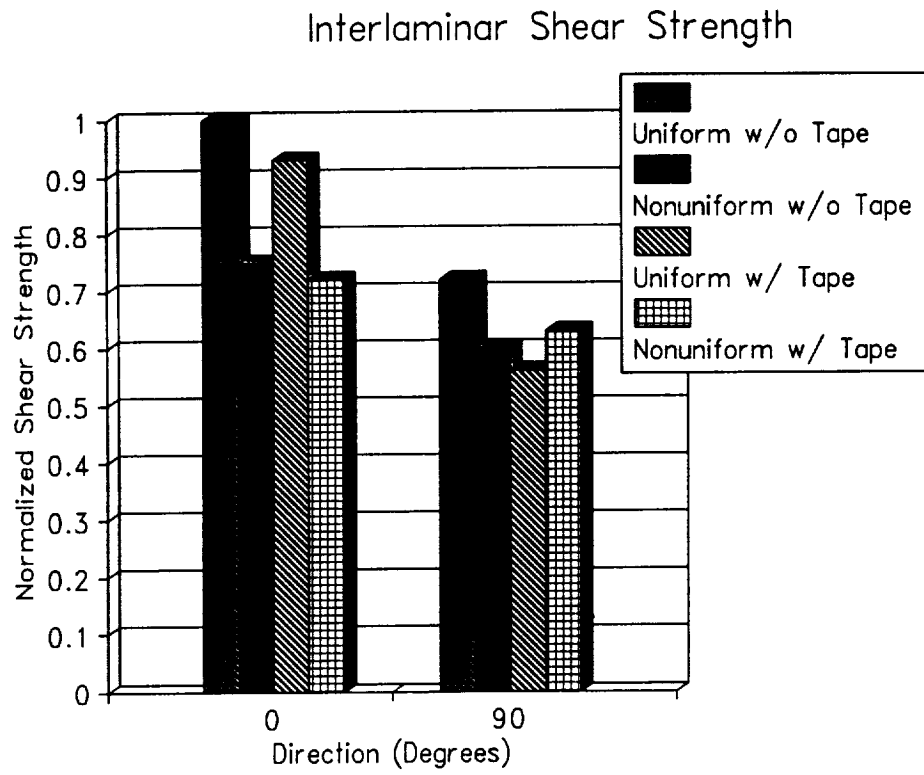


Figure 9. Interlaminar shear strength for uniform and nonuniform specimens.

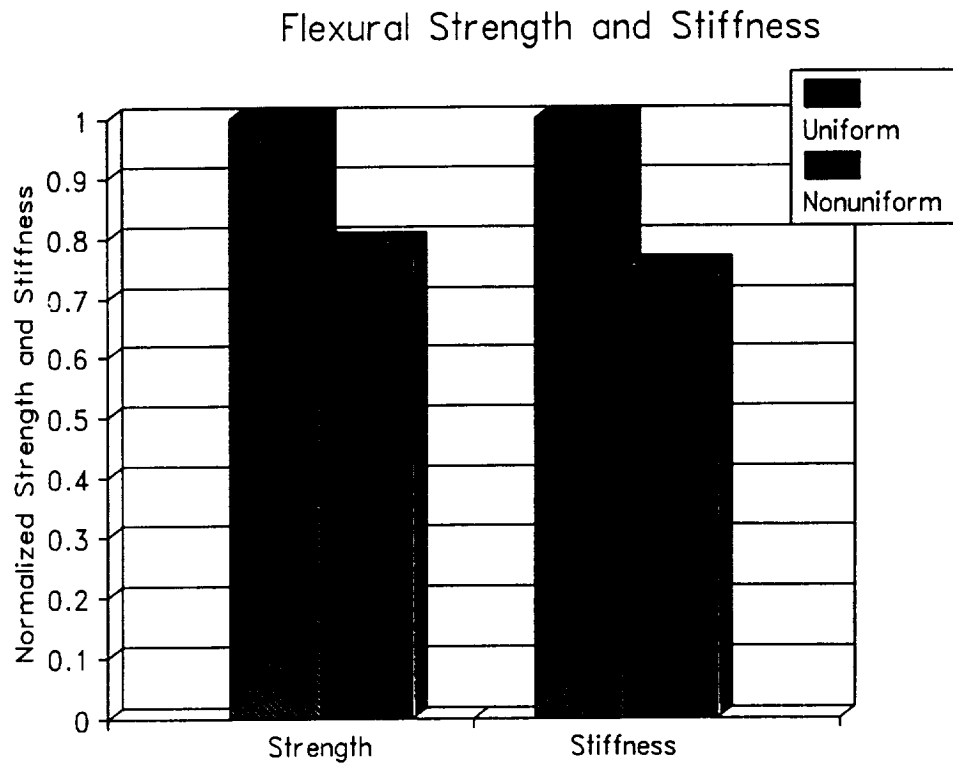


Figure 10. Flexural strength and stiffness for uniform and nonuniform specimens.

Knight Block Strength and Stiffness

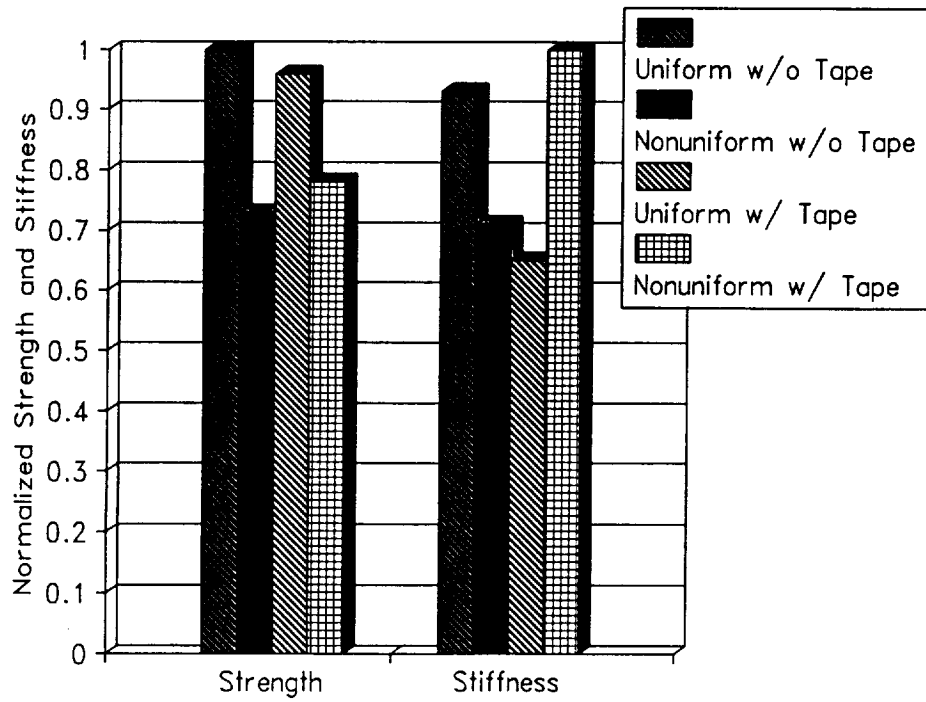


Figure 11. Knight block strength and stiffness for uniform and nonuniform specimens.



Figure 12. 90° cross-sectional view of a 0° uniform failed specimen. Failure progresses along the 45 degree through thickness tows.

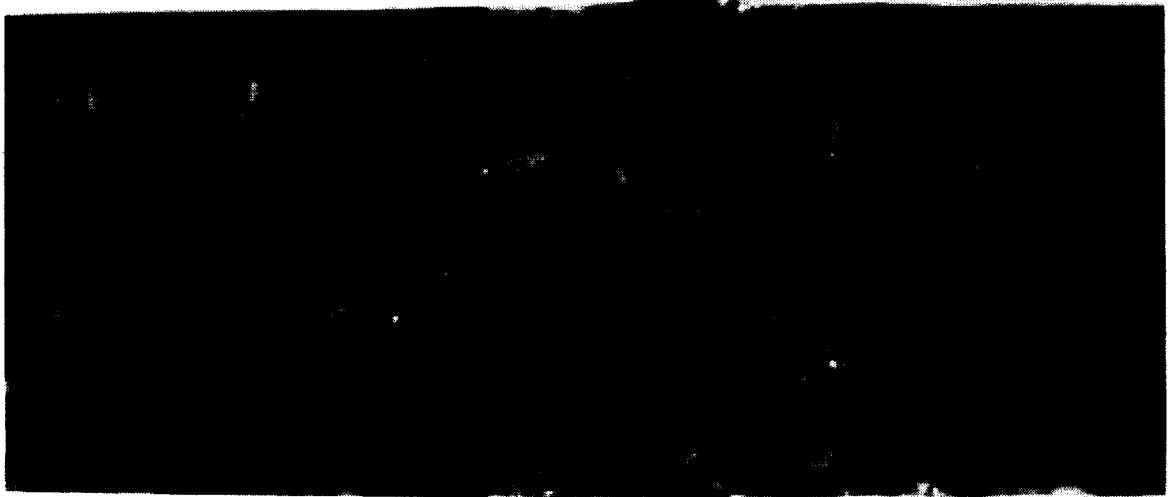


Figure 13. 0° cross-sectional view of a 90° nonuniform failed specimen. Failure progresses through the thickness perpendicular to the load.

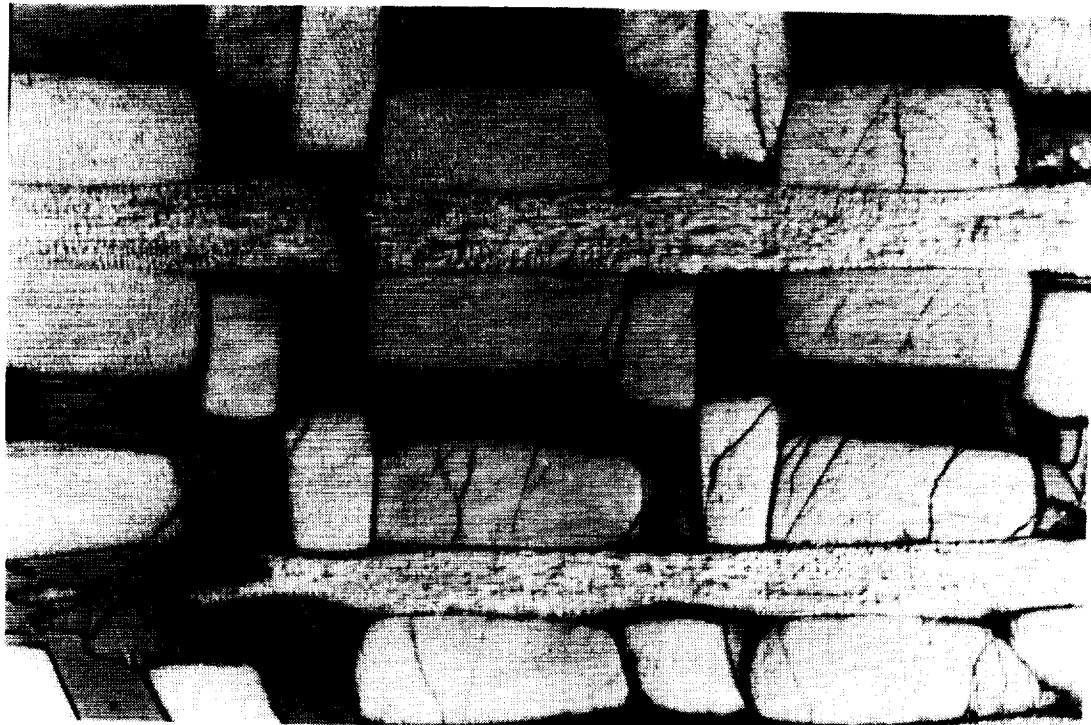


Figure 14. 0° cross-sectional view of a 90° tensile specimen. The photograph shows significant matrix cracking, fiber-matrix debonding and intra-tow cracking.

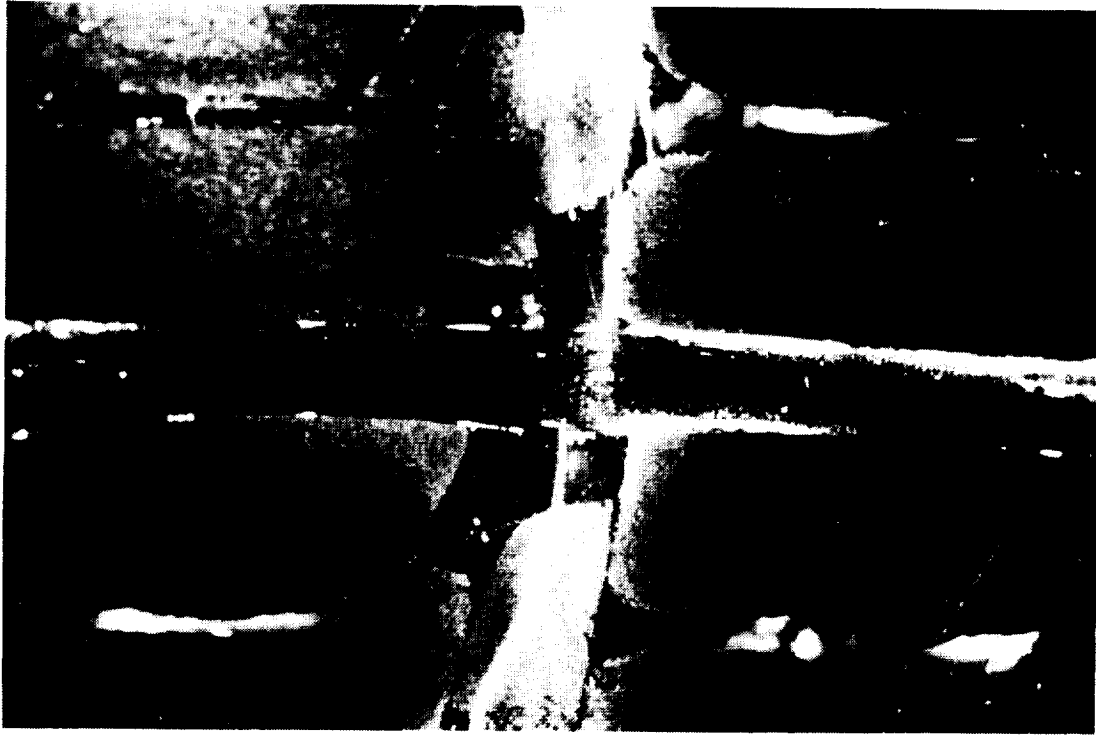


Figure 15. Photomicrograph showing a matrix crack propagating through 90° and 45° tows. The photograph also shows fiber debonding.



Figure 16. Cracking in a 0° flexure test specimen. Cracks are seen propagating from the load application point and along the fiber/matrix interface.



1994 012379

**AN ENGINEERING APPROACH FOR THE
APPLICATION OF TEXTILE COMPOSITES
TO A STRUCTURAL COMPONENT**

51-24

17-11

p 10

N94-16852

**Jack W. Baldwin
Brian K. Gracias
GE/Aircraft Engines**

**Steven R. Clarke
ICI/Fiberite**

PRECEDING PAGE BLANK NOT FILMED

114

THE DEFINING OBJECTIVE: Improve impact resistance of composite fan blades by using some form of 3D reinforcement

BLADE DESIGN REQUIREMENTS:

- Correct aerodynamic shape
- Maximum life
- Aeroelastically stable
- Resistance to FOD (foreign object damage)

CONSTRAINTS:

- Budget
- Time
- Manpower

OUR MISSION STATEMENT:

Develop a cost effective, damage tolerant blade which satisfies all blade design criteria.

GOALS - TECHNICAL:

- 1) TEXTILE ARCHITECTURE
- 2) RESIN
- 3) PROCESSING
- 4) TEST METHODOLOGY
- 5) ANALYSIS

GOALS - NON-TECHNICAL:

- **QUALITY:** Build quality into the mfg. process and end product from day one.
- **FOCUS:** Identify key program needs and then stay focused.
- **SYSTEMS APPROACH:** Coordinate resources and interact frequently to provide insight and solutions to potential problems.
- **TEAMWORK:** Utilize all team members to their fullest extent. Know when to modify team as program evolves.
- **COMMITMENT:** Sustain a high level of commitment and sense of urgency.
- **CHALLENGE CONVENTIONAL WISDOM:** Use a "clean sheet of paper" approach within the team , and amnesty to constantly challenge both technical and non-technical paradigms alike.

CREATING THE PROJECT TEAM:

1) GE first identified their areas of expertise as well as their shortcomings.

2) GE then sought team members with the following characteristics:

- Technical expertise (in textiles, tooling, RTM, etc)
- Track record of systems approach to problem solving
- Resources and commitment of same to support the program
- Shared sense of urgency
- Open minds and a "can do" attitude

TEAM MEMBER SELECTION PROCESS

- Established basic goals and process outline
- Contacted potential suppliers
- Assessment of supplier:
 - Design
 - Manufacturing
 - Quality Issues
 - Non-technical Issues
 - Business Issues
- Final Selection
- The team identified and prioritized technical issues

GROUND RULES OF TEAM PARTICIPATION

- Fixed goals but flexible approach to getting there.
- Timing and task assignment remained flexible.
- Weekly status meetings involved all team members.
- Direct communication between specific team members encouraged.
- Technical approach was constantly challenged by all team members.
- Flexible team - technical experts were "borrowed" to solve very specific problems, then "returned".

THE TEAM WENT TO WORK...

TEXTILE

GOALS & CHALLENGES

- Fiber volume: 55 - 60 %
- High thickness: ~3 in
- Through thickness reinforcement
- Fibers straight with no crimp
- Continuously changing geometry
- Net shape
- Electronic transfer of data
- Inspection of preform

FIBERITE and 3D-Weaving

TECHNICAL ISSUES

- Translation of geometry to woven preform
- Fiber architecture design
- Ability to weave thick sections
- How to handle large number of yarns
- Adaptation of conventional loom design
- Certification of woven preform

RESIN

GOALS & CHALLENGES

- How to determine the best resin
- Toughness
- High tensile modulus, strength
- High strain-to-failure
- No microcracking, low shrinkage
- Low viscosity
- Long pot life
- Compatibility with fiber types
- Compatibility with prepreg resins
- Readily available

DOW CHEMICAL

TECHNICAL ISSUES

- How to determine wetout
- Injection equipment compatibility
- Process & tool design
- Cure cycle

PROCESSING

GOALS & CHALLENGES

- Electronic transfer of part shape data
- Uniform resin flow in mold
- Large resin injection pressures
- Equipment compatibility with resin
- No part porosity
- Inspection of injected part

GE/CORPORATE RESEARCH & DEVELOPMENT
ADVANCED TECHNOLOGY & RESEARCH
FIBERCRAFT/DESCON

TECHNICAL ISSUES

- Preform permeability
- Resin pressures
- Resin viscosity
- Cure cycle
- Tool gating for RTM mold
- Pumping equipment
- Vacuum capability
- Injection time
- Part removal

TEST METHODOLOGY

GOALS & CHALLENGES

- Provide data for design use
- Assess improvement in interlaminar properties
- Assess response to high energy impact

GEAE MATERIALS BEHAVIOR
WEST VIRGINIA UNIVERSITY
ICI/FIBERITE

TECHNICAL ISSUES

- How to measure basic mechanical properties; in particular, shear
- How to measure impact toughness
- Determine failure modes
- Correlate measurements to actual impact test results

ANALYSIS

GOALS & CHALLENGES

- Stiffness and strength models
- Failure models
- Compatibility with finite element analysis

GE/CORPORATE RESEARCH & DEVELOPMENT
NORTH CAROLINA STATE UNIVERSITY

TECHNICAL ISSUES

- Part geometry and "unit cells"
- Application of models within blade analytical methodology
- Level of detail required
- Verification of models

RESULTS - TECHNICAL:

- 1) **TEXTILE ARCHITECTURE:** Fiberite demonstrated the ability to:
 - 3D-weave thick, high fiber volume preforms to net shape;
 - handle complex part geometry;
 - adapt quickly to changing part design.
- 2) **RESIN:** Dow's resin is tough, easy to RTM, and does not microcrack.
- 3) **PROCESSING:** ATR demonstrated the ability to cleanly inject thick, high fiber volume preforms with no porosity;
GE/CRD accurately predicted resin flow within the tool cavity.
- 4) **TEST METHODOLOGY:** Demonstrated 'ductile' behavior, interlaminar strength confirmed - very difficult to shear. Methodology requires further refinement.
- 5) **ANALYSIS:** Preliminary design tool available within GE, need further effort to achieve all goals. GE/CRD currently exploring these issues.

RESULTS - TECHNICAL: (cont)

IMPACT TESTS

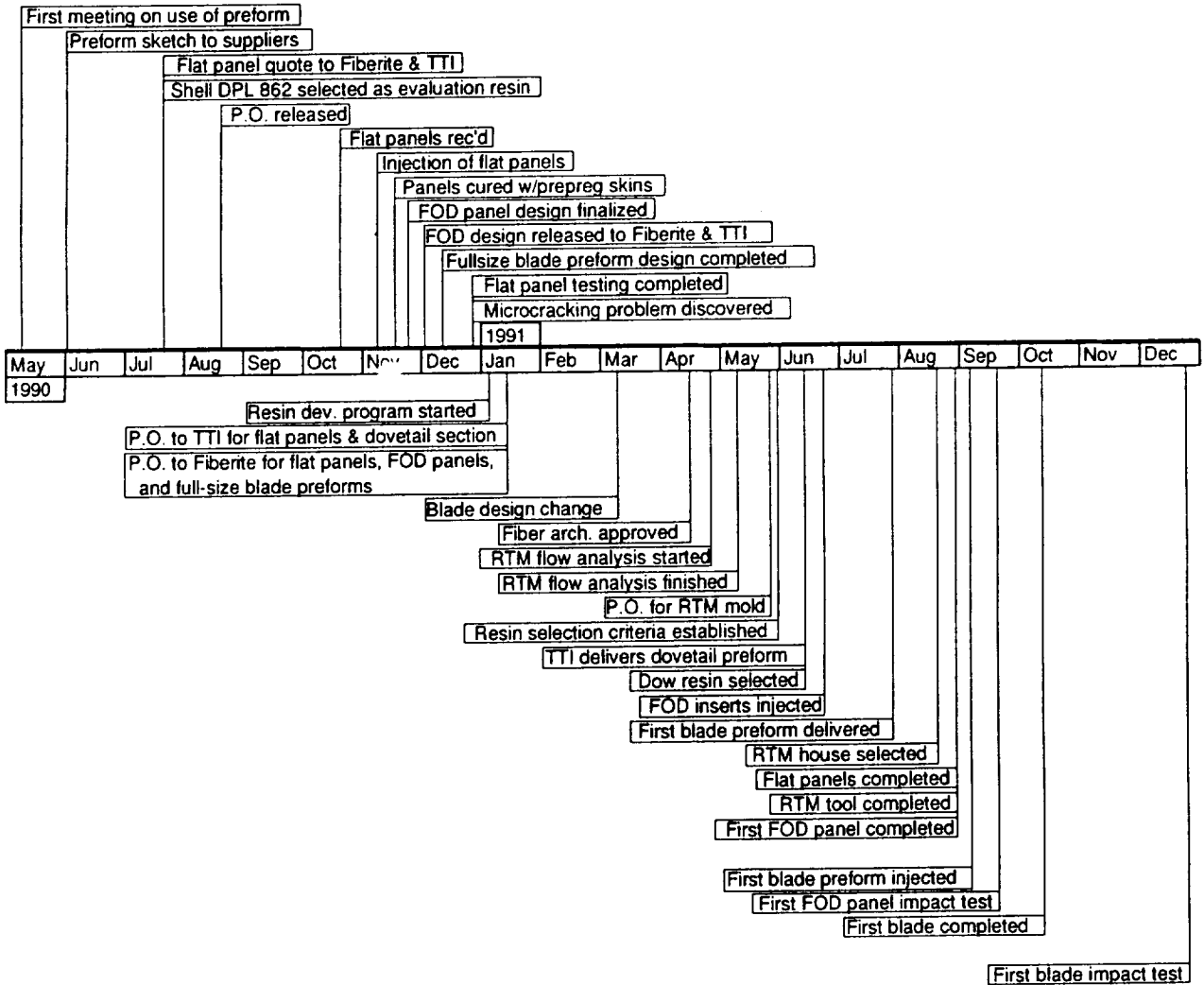
- **Static panel tests showed very promising results for the weave-resin combination; comparable to the standard all-prepreg panel tests**
- **Whirligig blade static impact tests - two blades manufactured and tested:**
 - **impacted by a 2.5 lb. simulated bird**
 - **impacted blades cycled on a shake table to 1,000,000 cycles (high amplitude in first two fundamental modes) - no damage propagation**

MATERIALS AND PROCESS ARE PROVEN!

RESULTS - NON-TECHNICAL:

- **The team completed the project on time and within budget.**
- **Technology base can be applied to other engine components.**
- **Improved resins can find their way further into the engine (i.e. higher Tg for components in the hotter sections).**
- **Success of this program has expanded GEAE interest from composite prepreg laminates to also include textiles and RTM.**
- **Real production potential has increased resin manufacturers' interest in expanding development of truly tough RTM resins.**

PROGRAM TIMELINE



CONCLUSIONS - TECHNICAL:

- **3D-woven preforms increase damage tolerance.**
- **Thick, complex shapes can be mass produced economically.**
- **Preform technology and tooling technology can be combined to provide high quality, net shape parts.**
- **Tough, microcrack-resistant RTM resins are available.**

TEXTILE PREFORMS COMBINED WITH RTM CAN PRODUCE HIGH PERFORMANCE, COST EFFECTIVE COMPOSITE STRUCTURES WHICH MEET OR EXCEED AEROSPACE QUALITY STANDARDS.

CONCLUSIONS - NON-TECHNICAL

- **Teamwork works!**
- **Teamwork is not always easy.**
- **Timeframes and budgets don't have to be limits to success.**
- **Open interaction between Design, Manufacturing, Quality, and Sourcing is essential.**
- **Technical constraints were identified and eliminated by having the entire team all working together and constantly challenging conventional wisdom.**

1994012380

NEW TEXTILE COMPOSITE MATERIALS DEVELOPMENT,
PRODUCTION, APPLICATION

53.24
N 94-16853
1.14

Petr Y. Mikhailov, Ph.D., Corresponding Member of International and Russian Engineering Academies, Academician of the Engineering Academy in St. Petersburg, General Director of the Research Institute of Chemical Fibers and Composite Materials Works, *Khimvolokno* RI, St. Petersburg, 195030, Russia.

The history of the Research Institute and Chemical Fibers/Composite Materials Works, *Khimvolokno* RI in St. Petersburg, goes back to the eighteenth century. In 1717, by Peter the Great's edict, the "Gunpowder Manufactory" was erected on the Okhta River on the outskirts of St. Petersburg, and later it became a huge gunpowder works closed down soon after World War I.

In 1930 the chemical (viscose) fibers works, the first in Russia, was erected on the territory of the former gunpowder works.

The branch of the Artificial Fibers Institute was established in 1948, and in 1968 the works was reconstructed into a pilot industrial enterprise intended to produce new fibers.

In 1985 the organization achieved a new status and became independent: the "Research Institute and Chemical Fibers/Composite Materials Works" (*Khimvolokno* RI) in St. Petersburg.

At present the Institute and Works constitute a unified complex engaged in the creation of new types of chemical fibers, textile and composite materials:

- laboratory research in synthesis of new polymers and production of fibers based on them
- creation of pilot plants which enable development of new fibers technologies
- pilot industrial production of the developed fibers
- manufacture of textile materials and products based on new fibers
- manufacture of polymer-polymer composites and some types of products based on such composites
- reclaiming of chemicals, gas emission cleaning, and sewage treatment
- twisting of fiber structure and properties, textile and composite materials
- economy, economic trends, and marketing in the field of the developed materials and products

In Russia, the *Khimvolokno* RI is the leader in the development and manufacture of fibrous and composite materials having special properties, including the types of materials (1-4) that follow:

- high-strength and high-modulus fibers made of poly-para-aramides and poly-para-arylates (para-polyesters)
- heat-resistant fibers made of polyimides, polybenzimidazoles

- fluorocarbon polymer fibers
- carbon fibers based on viscose and polyacrylonitrile precursors
- various types of polyvinyl alcohol fibers
- porous and reinforced films for ultrafiltration
- single-component and multicomponent (combined) textile fabrics of all types based on the above-mentioned and other fibers: braids, ribbons, fabrics, knitted fabric, nonwoven fabrics, cords, ropes, etc.
- polymer-polymer composites and products: constructional, heat-shielding, chemoresistant, antifriction, electrical and radio engineering products, etc.

New types of fibers, filaments, and combined textile and composite materials based on them have been adequately described in the literature (3–12). Many developments by *Khimvolokno* RI in St. Petersburg are basically new and original both for Russian and world-wide practice.

In what follows, the main data are presented for some types of fibers, textile structures and composite materials manufactured on their basis. Developments in carbon fibers and fibrous carbon materials for engineering and medical applications are also discussed by Prof. R. M. Levit and Prof. L. I. Fridman in their papers.

SUPER-HIGH-STRENGTH, SUPER-HIGH-MODULUS FIBERS, FILAMENTS, AND MATERIALS MANUFACTURED ON THEIR BASIS

New types of super-high-strength and super-high-modulus organic fibers and filaments, and textile and composite materials based on them are available in a wide range of products. They play an important role in the manufacture of products for engineering, sports, medical and other applications: ropes, cables, ribbons, reinforced fabrics, nonwovens, fabricated rubber products, composites, etc.

The main types of fibers and filaments for such applications are as follows (3–5, 9–11):

- polyvinyl alcohol types for MVM and MVP vinol
- para-aramid types for SVM and terlon

Although the fibers and filaments are available in a wide range of linear densities, the main filaments of 29.4 tex and 58.8 tex have the following properties:

Characteristics	MVM vinol	SVM	Terlon
Strength, GPa	1.2–1.6	4.2–4.5	3–3.3
Modulus of elasticity, GPa	25–35	120–130	125–140
Elongation, %	5–6	3–3.5	2–3

Should the need arise, the thinner filaments of 14.2 tex are manufactured and the braids with linear density 1000 tex are produced by splicing filaments of 58.8 tex.

Since the above-mentioned filaments feature high rigidity, the corresponding conditions have been developed for processing them, allowing the maintenance of their structure and properties to remain almost unchanged, i.e., to ensure efficient use of 90% or more of their rated strength (1–4, 13–15).

The super-high-strength ropes are manufactured from the terlon and SVM filaments and braids on cord-braiding machines. The rope core is composed of parallel super-high-strength filaments and is braided with polyfen, vinol, arimid and SVM filaments. Those may be illustrated by referring to the properties of the 6 mm and 10 mm diameter ropes.

rope dia, mm	6	10
rope mass, g/m	22	66
breaking load, GPa	17–30	70–95
elongation, %	4–5	4–5

The strength of SVM ropes is 2–5 times that of polyamide and polyester ropes. The annual loss of rope strength due to sea water or oil products does not exceed 25–35%.

Nonwoven fabrics are manufactured from SVM fibers having the above properties as well as from all types of fibrous waste after being cut. Nonwoven fabrics are manufactured on the plants including the 4–11-Ш card machine, the ПШ carding converter, and the VM -1800 M needle-punching machine or the БП -180 sew-knit machine. The two types of nonwoven fabrics designed and produced are as follows:

- needle-punch MIP
- sew-knit MVP

The principal consumer characteristics of the fabrics are as follows:

Characteristics	MIP	MVP
Surface density, g/m ² ,		150–200
Punching density, 1/cm ²	1	–
Knitting density per 100 mm (horizontal-vertical)		40/36 knitted fabric

Because of fibrillation of fibers in carding, the resulting web is well formed and production of nonwoven fabrics presents no problem.

When epoxide and epoxyphenol binders are used, both types of nonwoven fabrics allow production of constructional fabric-based laminates possessing high mechanical properties.

Fiber content, %	50–75
Density, g/cm ³	1.25–1.3
Strength, MPa:	450–480
Tensile strength	450–480
Bending strength	470–520
Shear strength	110–120

Super-high-modulus filament-based fabrics play an important role in the manufacture of constructional composite materials. High rigidity of the filaments calls for development of special conditions to prepare them for weaving as well as for development of the weaving process itself. In this case, the following factors are important: reduction of an excessive bend radius of filament-guiding parts, reduction of filament friction, reduction of filament tension, and a change in the loom set-up scheme to reduce dynamic forces in the filaments. Weaving is performed on shuttle and shuttleless looms at reduced speeds. The fabrics produced have the characteristics shown in Table 1.

Braids, fabrics and nonwoven materials of super-high-modulus fibers and filaments form the basis for production of various types of composite materials, where epoxide and epoxy-phenol binders are used, by employing molding methods. The properties of these materials are given in Table 2 for illustration only.

HEAT-RESISTANT AND NONFLAMMABLE FIBERS, FILAMENTS AND TEXTILE FABRICS

Among the high-heat-resistant and nonflammable fibers and filaments designed and produced by *Khimvolokno* RI in St. Petersburg, there are two main types:

- polyamide: Arimid, Arimid T
- polyamidobenzimidazole: Togilen

Their principal characteristics are as follows:

Characteristics	Arimid, filament,	Togilen, filament,	Togilen, fiber,
Linear density, tex	11-100	11-200	0.12-0.44
Strength, cN/tex	40-60	40-60	30-50
Elongation, %	6-12	10-15	20-25
Strength retention at 300°C	55-65	60-70	60-70
Strength retention after heating at 300°C, 100 h, %	60-80	80-95	80-95
Oxygen index	42-45	43-46	43-46
Moisture content (at 65% relative humidity), %	2-3	13-15	13-15

Fibers and filaments, arimid and togilen, are classed as heat-resistant and nonflammable materials. It should be noted that arimid has low hygroscopicity and high dielectric properties, whereas togilen is the most hygroscopic material of all the filaments of a similar class (1, 2, 4, 9, 11).

Woven Fabrics Based on Arimid and Arimid T. Filaments.

These filaments are readily processed into knitted fabrics using standard facilities. In most cases, textile fabrics consist only of arimid filaments, though occasionally these are combined with polyphenylene filaments. The characteristics of two types of fabric are given in Table 3 for illustration only.

The applications are largely governed by thermal characteristics, nonflammability, low hygroscopicity and high dielectric properties. These are

- high-temperature electrical insulation (filaments, ribbons, fabrics)
- protective clothing for firemen, welders, etc.
- decorative finishing material, curtains, fabrics for aircrafts, ships, automobile and railway transport, and welfare rooms.

It should be noted that intensive yellow colouring places definite restrictions on their application as decorative finishing materials.

Table 1. Characteristics of Reinforcing Fabrics Based on High-Modulus Filaments

Filament	Weaver	Linear density of filaments, tex	Number of filaments per 10 cm	Thickness, mm	Surface density g/m ²	Strength of strip 25 mm wide, N	Elongation, %
MVM vinol	Basket 2/2	93.5/93.5	140/155	0.65	300	1450/1650	9/10
SVM	Linen	29.4/29.4	150/160	0.30	110	1600/1800	14/12
	Basket 2/2	29.4/29.4	300/250	0.35	180	2700/2400	11/9
	Sateen 8/3	29.4/29.4	255/235	0.40	160	2100/2600	12/9
Terlon	Linen	58.8/58.8	178/142	0.42	130	2500/2100	—

Table 2. Characteristics of Composites Based on Textile Fabrics Made From High-Modulus Filaments

Reinforcing Filler	Density g/cm ³	Strength, MPa		Modulus in tension GPa	Elongation at rupture
		tensile	bending		
Unidirectional braid, SVM	1.3–1.32	1500–2500	280–300	80–84	1.7–2.1
SVM fabric	1.28–1.32	500–750	—	32–40	2.5–4.0
Nonwoven fabric, SVM	1.27–1.30	210–300	—	14–17.5	—
Unidirectional braid, Terlon	1.30–1.32	1300–2000	280–300	90–100	1.5–2.0
Terlon fabric	1.28–1.32	400–600	—	35–42	2.0–3.0

Table 3. Characteristics of Fabrics Based on Heat-Resistant, Nonflammable Arimid Filaments

Characteristics	Types of fabric	
	linen	crêpe
Weave	linen	crêpe
Linear density	29.4/29.4	29.4/29.4
Number of filaments (stitches) per 10 cm	230/240	248/275
Thickness, mm	0.25	0.32
Surface density, g/m ²	130	157
Strength of strip 25 mm wide, N	—	1500–1900
Elongation, %	—	15/13

Textile fabrics based on togilen fibers and filaments are readily manufactured using standard textile facilities. When combined with woolen or chemical fibers, the fibers are also readily processed. The assortment comprises various structures of knitted and nonwoven fabrics. The characteristics of (knitted) fabrics are given in Table 4 for illustration only. Their applications are largely governed by high thermal properties, nonflammability, and high hygroscopicity. These are

- protective clothing for firemen, metal-makers, welders, drivers, pilot, pilots, etc.
- decorative finishing materials, mats for aircraft, ships, automobile and railway transport, public buildings and rooms
- high-temperature filtering media
- thermal insulation, and some other products

It should be noted that in mass and as ready-made material, togilen can be coloured in bright hues.

Togilen fibers and filaments are distinguished for their unique properties among other types of heat-resistant and nonflammable fibers and materials based on them that are produced in other countries.

Table 4. Characteristics of (Knitted) Fabrics Based On Heat-Resistant, Nonflammable Togilen Filaments

Characteristics	Togilen	
	Fabric	Knitted fabric
Weave	twill 2/2	satin-stitch
Linear density	58.8/58.8	29.4
Number of filaments (stitches) per 10 cm	200/220	120/90
Thickness, mm	0.40	0.55
Surface density, g/m ²	240	—

FIBERS AND TEXTILE FABRICS BASED ON FLUOROCARBON POLYMERS

In Russia the *Khimvolokno* RI (St. Petersburg) is the leader in the development and manufacture of fibers and filaments based on fluorocarbon polymers. The two main types of fibers and filaments manufactured are as follows:

- polyfen (manufactured from polytetrafluoroethylene)
- ftorin (manufactured from a copolymer of tetrafluoroethylene with hexafluoropropylene)

Table 5. Characteristics of Fabrics and Filaments Based on Fluorocarbon Polymers

Characteristics	Polyfen Complex filament	Ftorin		4MB Staple fiber
		Monofilament	Complex filament	
Linear density, tex	13-44	10-70 (0.13-0.5 mm)	4-20	3-5
Density, g/cm ³	2.2-2	2.15-2.16	2.15-2.16	2.15-2.16
Strength, MPa	250-820	150-180	170-210	130-180
Elongation at rupture, %	15-30	15-30	15-35	20-50
Permissible operating temperature, °C	up to +225	up to +200	up to +200	up to +200

The main characteristics are given in Table 5 for illustration only. Fibers and filaments of polyfen and ftorin types have unique properties: absolute chemical resistance, nonflammability, biological inertness, low friction coefficient, high dielectric characteristics, absolute nonhygroscopicity and nonwettability (1, 2, 4, 9, 11, 16, 17).

Antifriction Textile Fabrics Based on Polyfen Filaments.

Antifriction polymer materials based on fluoroplastic, polyamides and some other polymers and extensively used in engineering, are essentially bonded in their application by the magnitude of unit pressure, friction wear and other indicators. Woven fabrics based on polyfen filaments made it possible to avoid these disadvantages. The designed fabrics, such as naftlen, aftlen, daclen, vsetal, etc., have an original structure with such an arrangement of mutually related filament systems that only polyfen filaments appear on the right side, thereby forming an antifriction layer. The inside of the fabrics is composed of the filaments of vinol, cotton yarn and other materials having a high friction coefficient. This side of the fabric can be bonded to any hard surface as may be required. The structure and surface of naftlen and aftlen fabrics are smooth, and those of daclen fabric are corrugated. The characteristics of these fabrics are given in Table 6.

Special features of the fabrics are high strength and low creep. They can be used in the friction units of machinery, lubricated and unlubricated, and can operate at moderate speeds and under high unit loads.

The above-mentioned fabrics offer the possibility of carrying large-sized cargoes and structures, whose mass amounts to hundreds and thousands of tons, such as bridge bays and structures, a large-sized apparatus, ships on building berths, etc.

Table 6. Characteristics of Antifriction Fabrics

Characteristics	Fabrics				
	Naftlen	Aftlen	Daclen	Vsetal	Ancotex
Weave	Combined two-layer			Combined multi-layer	
Right side and inside layers	Polyfen vinol	Polyfen cotton	Polyfen arimid	Polyfen vinol	Polyfen lavsan
Thickness, mm	2.5	0.5	1.0	1.4	5
Surface density g/m ²	1500	500 and lower	600 and lower	1300	2800
Surface	smooth	smooth	corrugated	corrugated	corrugated
Maximum unit load, MPa	600	600	600	1800	900
Friction coefficient	0.016	0.016	0.016	0.08-	0.012-
For steel	0.032	0.032	0.028	0.016	0.022

The composite antifriction material, atalen, is produced by combining naftlen, daclen and other fabrics with the plates made of metal (aluminium alloys), glass-reinforced and organic plastics that are bonded together. This material is manufactured in the form of sheets and offers the possibility of carrying heavy large-sized structures and cargoes up to 100–150 thousand tons.

All of the above materials have no match among the antifriction materials used in various fields of engineering where high unit loads and average speed of movement are employed.

Chemoresistant textile fabrics based on polyfen and ftorin fibers and filaments include a variety of filtering, protective and nonwoven fabrics designed for filtering corrosive liquids and gases. Unique chemoresistance allows these fully fluorinated fibers and filaments to be used in the manufacture of nitric, phosphoric and sulphuric acids, chemical agents, fertilizers, etc.

Fabrics are largely used to filter corrosive liquids, while nonwoven materials are preferred in filtration of gases. Gauzes and nonwoven materials based on ftorin monofilaments are most efficiently used to form the layers for trapping splashes of concentrated process gases.

Another important application of polyfen filament-based fabrics is reinforcement of fluorocarbon polymer films employed as ion-exchange membrances for electrolysis (of sodium chloride solutions in the manufacture of caustic soda and chlorine) and reinforced ultrafiltration films (described below).

The fabrics manufactured from polyfen and ftorin filaments may not be wetted with molten metal and are used in the manufacture of working clothes and protective means for nuclear reactors and similar plants where liquid metal heat-transfer agents are employed.

Polyfen and ftorin fibers and filaments are also used in the manufacture of packing cords and glands for rotary shafts in chemical equipment (reactors, pumps), and gaskets for various devices such as gate valves, etc. In these cases, braided cords of square, rectangular and round cross sections are manufactured by combining fluorine filaments with carbon, asbestos and other filaments. High chemoresistance, heat resistance and a low friction coefficient ensure long service life for them.

DEVELOPMENTS OF NEW TYPES OF TEXTILE COMBINED AND COMPOSITE MATERIALS

Based on a wide range of new types of fibers, pilot and industrial plants and shops for the manufacture of textile combined and composite materials are available at the institute; it develops new types of fibers to order for organizations and firms both in Russia and other countries (1–4, 18, 19).

Yarn and woven fabrics based on para-aramid high-modulus fibers.

In some types of industrial woven fabrics, the employment of the yarn based on para-aramid fibers, both in pure form and in combination with other fibers, such as wool, is an absolute necessity. The SVM fibers used for this purpose have the following characteristics:

linear density, tex	3.5–4.2
modulus of elasticity, GPa	100–120
elongation, %	3–33
cutting length, mm	65
oil content, %	1–2

The yarn is manufactured by a spinning apparatus system that is similar to the one employed to produce woolen yarn and comprises the main equipment that follows: *Befama* two-web machine, ПБ-114-Ш ring-spinning machine.

A special feature of SVM fibers is their partial fibrillation in combing, which ensures the adequate binding of the web and roving.

The 100% SVM fibers yarn has the following characteristics:

Linear density, tex	150–170
Coefficient of variation for Linear density, %	6–6.5
Number of twists per 1 m	230–250
Relative strength, cN/tex	28–35
Elongation, %	3–3.2

At the same time, the institute has designed woolen yarn containing 10% of SVM fibers.

The yarn enables production of the fabrics and knitted goods used to manufacture protective means for people engaged in some forms of mechanical and chemical production. Moreover, the SVM yarn fabrics are used in the manufacture of composite materials and articles having substantially curved surfaces where the low-tonnage fabrics based on super-high-strength para-aramid filaments cannot be used. The terlon fiber-based yarn, whose properties are nearly the same as the SVM yarn, is used for the same purposes.

Carbon Filament-Based Fabrics.

The traditional method of producing carbon fibrous materials such as fabrics, nonwoven materials, ribbons, and knitted goods is to manufacture them from fibers and filaments of precursors (viscose or polyacrylonitrile) subsequently carbonized and graphitized. This method, however, has its own limitations:

- impossibility of obtaining dense structures because of an abrupt reduction in the size across the fibers carbonized, which results in an increase of through porosity

- impossibility of producing the combined woven fabrics which include, along with carbon fibers and filaments, some other types

In order to create new types of composite materials, the institute has designed the fabrics based on carbon fibrous filaments having the following properties:

Characteristics	Ural H	Types of filament		YKH-5000
		YKH-2500		
Linear density, tex		225		450
Fiber strength, GPa	1.3–1.5	2.5	–	2.7
Modulus of elasticity, GPa	150–170	200	–	240

In processing carbon filaments, a serious problem was presented by their brittleness, which made it necessary to development special conditions for the process of preparing them for weaving as well as for the weaving itself.

In forming packages and warp beams, the filaments were gently laid without excessive kinks, the threads were treated with oil, and the speed and tension of filaments were half and one-third as much as the traditional ones. The weaving was accomplished on CТБ-type shuttleless looms with modernized filament-guiding devices at reduced speeds.

The institute has designed the fabrics in which either warp filaments or weft filaments are of carbon type, and the second system filaments consists of any specified types of ordinary chemical fibers. Their special feature is the choice of such weaving conditions that the carbon filaments are laid without bending as if they are braided with ordinary chemical filaments.

When tested for bending, compression and tension, the structural composites based on the above-mentioned fabrics had indices 15–20% higher than those of the materials based on fabrics where ordinary webs of the same filaments were employed.

Hybrid woven fabrics and reinforcing semifinished items based on high-strength and high-modulus para-aramid and carbon filaments are produced by the methods of weaving and by placing one over another the layers of filaments or fabrics composed of alternate components. In this manner the fabrics are produced for the manufacture of reinforced structural thermosetting plastics with controlled mechanical properties, in particular, rigidity.

Reinforced ultrafiltration film membranes have been developed and are available in two main types:

- the type based on aliphatic polyimides and reinforced by polyimide filament gauze (FAM-PA):
- the type based on fluorocarbon polymers and reinforced by fluorocarbon fiber or fabrics.

The above two types of ultrafiltration materials are designed for fine treatment of liquids in the electronic industry, biotechnology, the medical equipment industry, and in the treatment of fuel and chemical agents, etc. The FAM-PA material is used to filter low-corrosive media.

The FKM-PTFE material is used to filter solutions of acids, alkalies, organic solvents and other highly corrosive media. The principal characteristics of these materials are given in Table 7.

Table 7. Principal Characteristics of Reinforced Ultrafiltration Film Membranes

Characteristics	FAM-PA	FKM-PTFE		
		0.2 type	0.5 type	1.0 type
Minimum size of retain particles, μm	3.0	0.2	0.5	1.0
Rate of water flow (at a pressure drop of 0.05 MPa), $\text{cm}^3/\text{cm}^2\cdot\text{s}$	2.0	0.1	0.25	0.6
First bubble pressure, MPa	0.02	0.09	0.05	0.02

In conclusion, it should be noted that the *Khimvolokno* Research Institute in St. Petersburg attaches great importance to integration with institutes, works, and firms in Russia and other countries (CSFR, USA, Poland, Japan, Germany, Finland) that is accomplished by establishing two-sided contacts and with the assistance rendered by the Russian concern *Khimvolokno* and its organizations and International and Russian academies.

In St. Petersburg especially close relations were established within the scope of the Engineering Academy, the Institute of Light, and the Textile Industry (research developments in new types of fibers and woven fabrics), Machine-Building Production Association (development), and the Integrated Fine and Industrial Fabrics Works (production of woven fabrics).

REFERENCES

1. Mikhailov P. Y., Nachinkin O. I., Perepelkin K. E.: *Chemical Fibers*, 1990, no. 6, pp. 3–10.
2. *Khimvolokno* RI, Booklet, Leningrad, Nauka, 1991.
3. *Production and Application of Fibers Having Specific Properties. Collected Works* ed. by Perepelkin K. E. Mitishchy, VNIV. Proyekt, 1980, pp. 110
4. *Chemical Fibers, Fibrous and Composite Materials for Industrial Applications. Collected works* ed. by Nachinkin O. I. and Kuznetsova G. B. Leningrad, *Khimvolokno* RI, 1990, pp. 292 .
5. Perepelkin K. E.: *Structure and Properties of Fibers*, Moscow: Khimiya, 1985, pp. 208.
6. *Reference Book of Composites*, ed. by G. Lubin. Russian translation, ed. by B. E. Gebler, Moscow, *Machinostroyenie*, 1988. V.1, pp. 448, V.2, pp. 584.
7. Yang H. H.: *Aromatic High-Strength Fibers*, New York, Wiley Intersci. Publ., 1989, pp. 874.
8. Jambrich M., Pikler A., Diavik I.: *Fizika Vlanien*, Bratislava, Alfa, 1987, pp. 542.
9. Perepelkin K. E.: *Zbornik Fibrichem '89. Sekcia A.*, Bratislava, CSVTS, 1989, pp. 11–26.
10. Budnitsky G.A.: *Chemical Fibers*, 1990, no. 2, pp. 5–13
11. Perepelkin K.E.: *Chemical Fibers*, 1991, no. 4, pp. 27–32.
12. *Textile Structural Composites*, ed. by Tsu-Wei Chon and Frank K. KO., Amster., Russian transl. ed. by Y. M. Tamopolsky and V. D. Protasova, Moscow, Mir., 1991, pp. 432.
13. Andreyev A. A., Mikhailov P. Y., Ovchinnikova M. V., Rumyantseva I. A.: *Third International Symposium on Chemical Fibers, Preprints. Kalinin, VNIISV*, 1981, V.6, pp. 101–112.
14. Mikhailov P. Y., Perepelkin K. E., Andreyev A. A., Rumyantseva I. A.: *Chemical Fibers*, 1983, no. 5, pp. 41–43.
15. Andreyev A. A. Mikhailov P. Y., Pershikov V. N., Andriyenko A. Y.: *Chemical Fibers*, 1986, no. 2, pp. 36–38.
16. Kovalev A. D., Mikhailov P. Y.: *Antifriction Fibrous Materials*, Leningrad, LDNTP, 1983, pp. 16.
17. Kovalev A. D., Mikhailov P. Y., Kotomkina R. V.: *New Home Self-Oiling Materials Manufactured from Chemical Fibers*, Moscow, NIITEKHIM. 1986, pp. 46.
18. Kazakov M. Y., Volkova N. S., Bunareva Z. S.: *Chemical Fibers*, 1991, no. 4, pp. 4–6.
19. Mikhailov P. Y., Andreyev A. A., Krasina N. L.: *Chemical Fibers*, 1991, no. 4, pp. 6–7.

199402/381

**PRODUCTION AND APPLICATION OF CHEMICAL
FIBERS WITH SPECIAL PROPERTIES FOR
MANUFACTURING COMPOSITE MATERIALS
AND GOODS OF DIFFERENT USAGE**

№ 94-16854

R. Levit, Dr. of T. S., Professor

Scientific Research Institute of Chemical Fibers
and Composite Materials
NII "Chimvolokno"
St. Petersburg, Russia

The development of modern technologies demands the creation of new nonmetallic, fibrous materials with specific properties. In Fig. 1 you can see the selection of fibers and materials developed by NII "Chimvolokno", St. Petersburg, which we can conventionally divide into two groups:

Heat-resistant fibers	Refractory fibers
Fire-resistant fibers	Chemoresistant and antifriction fibers
Thermotropic fibers	Fibers on the basis of polyvinyl alcohol
Fibers for medical application	Microfiltering films
Textile structures	Paperlike and nonwoven materials
Composite materials	

Figure 1. Fibers and materials developed by St. Petersburg NII "Chimvolokno" in cooperation with allied companies.

In cooperation with NPO "Chimvolokno" MYTITSHI we developed and started producing heat-resistant high-strength fibers on the base of polyhetarearilin and aromatic polyimides (SVM and terlon); heat-resistant fibers on the base of polyemede (aramid); fire-retardant fibers (togilen); chemoresistant and antifriction fibers on the basis of homo and copolymers of polytetrafluoroethylene (polyfen and ftorin); water soluble, acetylated and high-modulus fibers from polyvinyl alcohol (vylen). Separate reports will deal with textile structures and thermotropic fibers, as well as with medical fibers. The author of this report will discuss in detail one of the groups of refractory fibers—carbon fibers (CF) and about the corresponding paperlike nonwoven materials. Also, composite materials (CM) and their base, which is the subject of the author's research since 1968, will be discussed.

Due to certain circumstances and the economic situation in Russia, the major part of CF is produced on the base of fibers from polyacrylonitrile and hydrocellulose fibers (viscose). CF from pitch are produced on an experimental scale. The concept of carbon fibers (CF) is very broad. This large group of materials can be divided into several subgroups, such as:

1. Fibers for construction application
2. Heat-resistant
3. Materials with controlled electrophysical properties
4. Materials with controlled physical/chemical properties (i.e., sorbents, accelerators, filters, antifriction materials, etc.)

According to the level of physical and mechanical characteristics, (strength and Young's Modulus), CF are very often subdivided into high-modular, high-strength, medium-modular and soft/low modular CF. The latter, if they are produced using modern technology, cannot be considered as low-quality fibers because CF are characterized by complex properties, not by one or two characteristics. An attempt to receive CF with maximum Young's Modulus (E) and strength, which is clear from the point of view of structural materials, resulted in the worsening of other characteristics, such as increase of crispness, decrease of flexibility, and reduction of relative elongation. This gives a negative effect when CF are applied, for example, as electroconductive fillers of plastic materials, rubbers, papers, films, artificial leather, etc. In Fig. 2 you can see the graphical dependence $lge = f(E)$ for CF produced in different countries. As follows from Fig. 2, value \mathcal{E} decreases almost linearly with the increase of value " E "; down to $E = 400\text{--}500$. Any attempt to select some special property and, on this base, to rate CF as "better" or "worse" fibers will suffer a setback because the change of one property is connected with the alteration of several others.

Depending on the practical problem, the type of CM or any other material which found it necessary to use CF, we should decide on which class of CF to use. Economics is very important here. High-modular and high-strength CF (HCF) are 6–7 times more expensive than soft CF with controlled electrophysical properties. At the same time, costs of soft CF with branched pore structure, i.e., fibrous adsorbers, are as high as HCF. The cost of medium-modular CF and HCF, used for thermal protection, development of antifriction materials and others, has intermediate value.

From the chemical composition point of view, all of the industrial CF can be subdivided into carbon and graphite-like fibers. Carbon polymer is the base of the first CF which can receive thermal treatment up to 800–900°C, where, as graphitolile polymer, is the base of the second fibers received in the process of thermal treatment within the range of the temperature 1500–2500°C.

During the last 25 years, scores of CF and HCF of all the above mentioned types were developed in Russia by the Institute NII "Chimvolokno", NII "Graphite" and NPO "Chimvolokno." Table 1 gives the main CF, which are used for reinforcement of CM. Here we can also see the properties of CM received on their base. If the strength of industrially produced HCF is at the level of 350–400 kg/mm², then at the pilot installations where we receive HCF, the strength is 50% higher. At NII "Chimvolokno" we developed the assortment of medium-molecular (MMCF) and soft (SCF) carbon fibers on the base of the industrial fiber "Nitron", from the copolymerization of acrylonitrile with methylacrylate, itaconic acid and industrial viscose fibers produced in two. We also received carbon staple fibers with the length of 50–60 mm on cutting machines. The properties of these fibers are listed in Table 2.

The research work which preceded the development of the technology of middle-modulus and soft CF with controlled electrophysical and physical properties enabled us to draw a deep

analogy between CF, coals, and cokes, taking into account specific characters of the oriented structure of original polymeric fibers—the raw material for CF synthesis. Namely, this analogy explains practically the equal level of electrical characteristics for one and the same temperature-time conditions of treatment. At the same time, the specific character of oriented structure of source, (raw and CF), provides physical and mechanical characteristics which are by an order of 1–2 times greater than corresponding characteristics of cokes. Depending on the thermal treatment temperature (TTT) there is a basic difference between the changes of mechanical and electrical properties of carbonized source fibers (polymers). This is because the mechanical properties are greatly affected, with the other conditions being equal, by supermolecular structure of the substance, while the electrical properties depend on chemical structural changes. Thus while using CF and SCF as electroconductive CM filler, it is not necessary to increase the cost of the technological process using high-oriented fibers or to subject the processed fiber to high elongation or mechanical tension both at the stage of its prior treatment and during carbonization or graphitization.

Middle (MMF) and soft (SMF) fibers are carbon fibers of wide application, and they are used in numerous technological fields with great economic effect (Fig. 3). Machine-cut CF are widely used as an effective antistatic additive to synthetic materials (i.e., papers, plastic material, artificial leather, rubber, etc.). In contrast to the majority of organic and nonorganic antistatics, these agents are not washed out by liquids, they do not migrate to the surface, nor do they attenuate materials; but in certain cases they reinforce and give constant antistatic properties to synthetic materials.

Adding 1.5% Uglen fiber, 5 mm cut, to PVC composition while manufacturing artificial leather decreases its electrical resistance R_0 from 10^{10} to 10^4 – 10^6 ohm. In this case CF used as electroconductive filler are much more effective than carbon black and graphite, because similar to the last, they have electronic hole conductivity (different CF types spread over a large area from semiconductors to conductors) and already, in case of a small filling, create a semiconductive or conductive network. This is because soft CF with their relatively high flexibility and slight brittleness are hardly affected when they are injected into CM by means of mixing with the other ingredients.

For the same reason, SCF having CF with specified properties are considered to be excellent conductive fillers for manufacturing electroconductive papers and paper-like composite materials (Fig. 4). They substitute for black carbon graphite and other active fillers. Carbon fibrous papers are used for electromodelling, shielding of underground electrical cables and transformer inputs, and most of all for obtaining heat-producing layers of low-temperature nonmetallic composite electrical heating elements (HE). At present, industry produces electroconductive carbon-fibrous papers with $R_0 = 8 + 10^4$ ohm, similar to CF-cellulose and CF synthetic fibers. On the base of carbon-fibrous papers, non-metallic, electrical, rigid, and flexible composite heating elements are produced for voltages of 6–220v and operating temperatures up to 80–200°C. Rigid sheet HE of the laminated plastic type (sleterm) or the glass-textolite type (glasterm), are flexible on a carbon-fibrous paper base, duplicated by film or rubber layers and used for heating of different areas; especially for travelling covered vans and houses, the operator cabins of road-building machines, tower cranes, green-houses, farms, the thermostating of equipment, etc.

Carbon and graphitized braids and laces were developed as HE, providing temperatures up to 250°C. Original and high productive equipment was used for their manufacture, for example, ovens used for the direct treatment of CF by high-temperature currents.

The above-mentioned fibers and the developed nonwoven materials (thick felts of lycron type) are used with great economic effect as electrodes or components of composite electrodes for

- electrochemical extraction of gold and other precious metals from diluted solutions
- adjustment of the moisture content of soil in agriculture
- electrothermic production of carbide, calcium and white phosphor
- medical purposes
- electrochemical deactivation of metallic surfaces from radioisotopes

On SCF and MCF base with controlled electrophysical properties, a large assortment of radiotechnical CM was received: screening CM absorbing waves with increased acoustic characteristics for loudspeakers, CM for "locating" stormclouds, and others.

Highly effective composite antifriction materials were developed for sliding bearings and stuffing box sealings on MCF and SCF base combined with thermoplastic and reactoplastic.

We have developed a number of heat insulating CM on the same base of CF. In fact, the strength of these materials is not worse, but in certain cases even better than the strength of CM, including the more expensive HMCF. In relation to this research, work was conducted on obtaining construction sheet CM on the base of combinations of high modular and soft CF, in particular, ribbon LU-P and thin carbon felt lycron. Positive results were obtained in the case of combined carbon plastic when the bending stress limit per active layer is considerably higher.

It is rather promising to use binders containing SCF and HMCF in the process of developing composite carbon plastics.

Table 1. Carbon Fibers (CF) Carbon Fibrous Materials (CFM) Composite Materials (CM).

Assortment	Make of material	Filament diameter d μ	WI./Unit Length tex	Density g/cm^3	CF and CFM Properties			CM Properties							
					σ GPa	E GPa	ϵ %	σ_x^+ GPa	E_x^+ GPa	σ_x^- GPa	σ_{bend} GPa	E_{bend} GPa	τ_{shear} MPa		
Yarn, Roving Fiber	VMN-3	7		1.6	1.2-1.5	200-250	0.6-0.8								
	VMN-4	6		1.7	2.0-2.2	200-270	0.6-0.8								
	VMN-RK	6		1.6	2.0-2.5	300-350	0.6-0.8								
	VMN-S	6		1.9	1.5-	400	0.6-0.8								
	Liral-N			1.6	1.5	70	1.5								
	Granit-P		410	1.8	3.5-4.0	320-400		1.4	110	1.0					
	VEN-210	10		1.9	1.5	340	0.6-0.8								
	UKN-5000		400	1.75	3.0-3.5	180-220	1.5	1.5	130						
	UKN-P5000		400	1.75	3.5	210-230	1.5	1.7			1.2	2.0	140	80	
	UKN-5000M		400	1.75	4.0-4.5	240									
	UKN-300		450	1.75	3.0	200-220	0.8-1.0								
	UKN-400		125-410	1.75	4.0-4.5	220-250		1.9	140	1.3					
	Kulon-M			1.95	3.0	600									
	Kulon-N24			1.75	2.5-3.0	380-400	0.6-0.8								
	Uglen-9	9	12000	1.6	0.5	20-25	1.8-2.5	0.2		0.3	0.3				30
Evlon	13	32000	1.7	1.5-2.0	80-100	1.5-2.0	0.5		0.3	0.5				27	
FFE	12	30000	1.8	1.1-1.5	120-180	1.3-1.6									
Band (Ribbons)	LU-3	Thickness mm	Width mm												
	LU-4	0.1-0.2	90-250	1.75	2.5-3.0	250-300	0.8								
	LU-P	0.1-0.2	90-250	1.75	3.0-3.5	300-350	0.8								
	LU-24P	0.1-0.2	250	1.75	2.9-3.0	265	0.8-1.0	0.8	140	0.6	1.25	125	60		
	Eluz-P	0.17	250	1.8	2.5-3.0	320-350	0.8	1.3	240	1.0					
	Kulon	0.2-2.2	250	1.75	3.0-3.2	235		1.0	130	1.0	1.3	110	70		
	Kulon-P	0.2	90-250	1.95	2.5	450-500	0.5-0.6								
	UOL-300K	0.2	90	2.0	2.5-3.0	450-550		1.2	265	1.0					
	UralTz 3/2		300		3.0-3.5	180-220	1.5	1.5	130	1.2					
	Ural-15	1.7	200		1.0-1.2	30-50		0.15	35						
	Ural-25			1.6	1.5-1.7	70-80	1.5-2.0								
Ural-LO	0.3		1.75	1.7-2.0	150-200	1.0									
Cloth	UUT-2	0.5-0.6	600	1.6	0.8-1.2	20-25	1.2-2.4								
	UTM-8	0.5-0.9	600	1.6	0.5-0.8	50-60									
	TMP-4	0.6	600	1.6	0.6-0.8	5-10									
	PTU-3/2	2.0-2.2	600	1.6	1.2	5-10									
	UT-900	2.5	900		3.0-5.0	180-220	1.5	0.7	65						
	Ural-T	0.5	500		1.0-1.3	30-50	0.9-1.1	0.2	50						
	Ural-TM/4	1.8	500		1.3			0.15	35						

Table 2. Properties of widely used CF

CF	d , μ	σ , GPa	E GPa	ϵ %	$\delta v 10^4$, $\Omega \cdot m$	TCR $1/gr:10^3$	d $\mu/grad$
Uglen	7-10	0.4-0.6	19.5-24.5	1.8-2.5	4.3	-2.0	22.1
Gralen	6-9	0.3-0.5	29-39	1.3-1.7	1.9	-0.6	26.1
Evlon	12-14	1.5-2.0	78-98	1.5-2.0	2.1	-0.9	-
FFE	11-13	1.0-1.5	118-147	1.3-1.6	1.0	-0.4	-

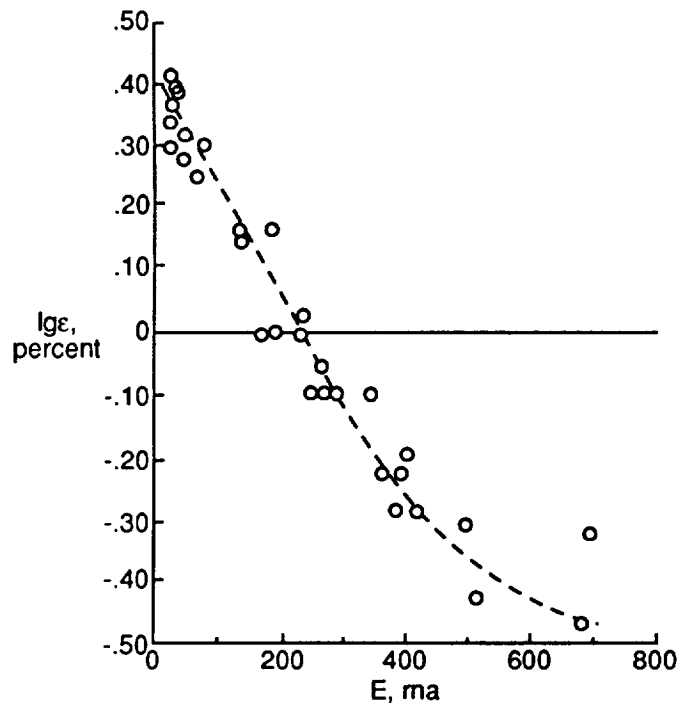


Figure 2. Dependence of the value of relative elongation (\mathcal{E}) of carbon fibers on the modulus of elasticity (E).

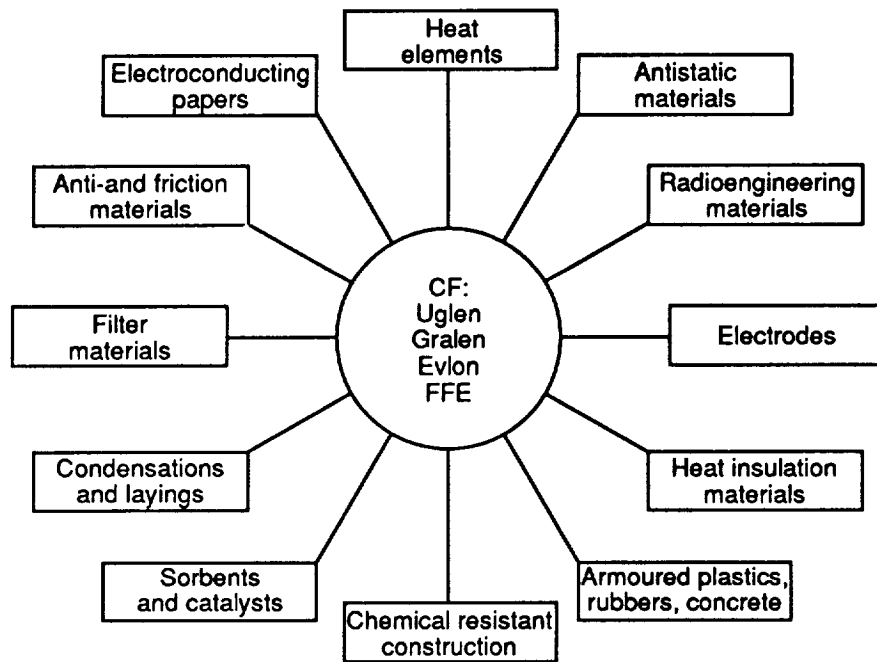


Figure 3. Field of application of soft and middle-modular CF.

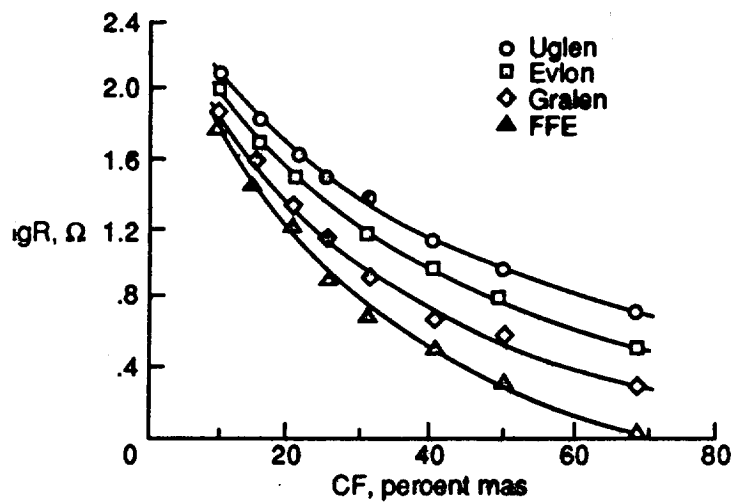


Figure 4. Variation of electrical conductivity of carbon fibrous paper (CF-cellulose) in relation to CF contents. 1-uglen; 2-evlon; 3-gralen; 4-FFE.



1994012382

FIBERS AND MATERIALS OF MEDICAL APPLICATION

L. I. Fridman, Dr of Sciences, Professor
St. Petersburg, RussiaS/10-24
N 94-16855

P. 4

1. CARBON FIBROUS ADSORBENTS

It was Hippocrates's idea that medicine is plus and minus: we take away everything that is extra and add what is missing, and the person who is doing that in the best possible way is the best doctor. Efferent sorption methods of organism detoxication (by medical trend) are presented today.

The application of carbon in medicine goes back to the time when ancient Egyptians and the doctors of Hippocrates's school recommended it for powdering of wounds. In 1830 French pharmacist Turey demonstrated an effective experiment at the meeting of the Academy of Sciences; he had taken a lethal dose of strychnine and successfully neutralized the toxic effect with charcoal. The American Hort was evidently the first doctor who used active carbon with the therapeutic aim of saving the patient poisoned by a corrosive sublimate.

Recently, specialists have shown their keen interest in the problem of treating exogenous and endogenous intoxications. This has been stipulated by the growing production and accumulation of chemical products for industrial, agricultural and domestic needs. We should take into account the growing production of various drugs and peoples' contact with them; consequently, it is imperative to improve the method of accelerated clearance of the organism from toxic products.

To solve this problem the industrial production of carbon fibrous adsorbents was developed and implemented at NII *Chimvolokno* in St. Petersburg. As a source of raw material we used cellulose fibers which were heat treated from 500 up to 900°C and subsequently activated by steam, carbon dioxide or their mixture at the temperature of 900-1000°C to burn out (degree of activation) 30-60% of the mass. Application of carbon fibers as the source of raw material on a base of pitch and polyacrylonitrile resulted in obtaining sorbents with stimulating and carcinogenic properties. Carbon fibrous adsorbents on a cellulose base are not toxic and carcinogenic and do not possess irritant and allergic effects.

By changing the heat treatment temperature of cellulose fibers and by also using a type of activating agent (as well as conditions of activation/time and temperature), it is possible within a wide range to vary the porous structure and chemical state of the resulting adsorbents.

Table 1. Dependence of Physical Parameters of Carbon Fibrous Adsorbent Structure on the Type of Activating Agent and Degree of Activation

	Degree of activation	Volume of pores, sm^3			Characteristic break of micropores X, nm	Specific surface of mesopores m^2/gr	density gr/cm^3
		micro	meso	macro			
Activating Agent	17	0.28	0.04	0.00	0.58	41	1.78
	20	0.31	0.07	0.00	0.62	48	1.79
	25	0.34	0.09	0.01	0.71	43	1.81
	30	0.39	0.19	0.02	0.73	83	1.84
	39	0.44	0.16	0.04	0.76	109	1.92
	46	0.62	0.06	0.06	0.95	189	1.98
	22	0.13	0.09	0.02	0.57	34	1.96
	38	0.25	0.15	0.04	0.62	73	2.01
	56	0.37	0.23	0.07	0.64	90	2.06
	64	0.51	0.25	0.09	0.69	105	2.09

Application of small size materials (the diameter of a single fiber is 6–15 mkm) and shape promote easier gas extraction. Fibrous shapes: threads, tow, fabrics, nonwoven materials) provide uniform (in section) development of destructive processes: thermal decomposition of cellulose and subsequent burning out of charcoal during the activation. This in its turn results in the formation of a uniform microporous structure of adsorbents displaying high velocities and specific sorbtion processes. We have conducted sorbtion research by marking substances to determine the spectrum of those substances which are absorbed by carbon-fibrous sorbents with the aim of applying them. For comparison we investigated the absorption of the same substances by grained active carbon SKH-4M and Adsorba-3000C.

Table 2. Absorbing Ability of Adsorbents /mg/l/ with Respect to Low Molecular Substances

Sorbent	Original concentration mg, 5%	ADSORBA 300C SKN-4M						Carbonfibrous adsorbent, degree of activation-50%		
		Time of activation, min								
		5	30	60	5	30	60	5	30	60
Medinol	20	1.50	9.45	18.30	14.42	25.45	25.65	29.60	29.80	29.92
Creazinin	15	5.40	11.25	14.73	13.51	18.30	19.55	21.50	22.42	22.45
Uric acid	50	9.75	20.85	40.95	41.85	69.32	73.25	74.72	44.93	74.95

The results of laboratory tests on animals and comprehensive laboratory investigations enabled us to implement carbon fibrous adsorbents into clinical practice (in a wide range) as hemosorbents/lymphoplasmosorption/mecvosorbents, enterosorbents, and sorbents in application therapy.

Table 3. Absorbing Ability of Adsorbents /mg/gr/ with Respect to Medium Molecular Substances

Sorbate	Initial concentration	ADSORBA-3000 SKN-4M						Carbonfibrous adsorbent		
		Duration of Contact, min								
		5	10	60	5	30	60	5	30	60
Vitamin B-12	33 mkg/ml	0.12	0.70	0.79	1.37	3.95	4.53	4.54	4.88	4.95
Insulin	7.5 mg/ml	0.04	0.05	0.05	0.90	3.50	5.35	7.50	7.50	7.50
Ribonucleasa "Sigmo"	30mkg/ml	-	-	-	-	-	-	4.49	4.50	4.50

Effectiveness of Carbonfibrous enterosorbents is shown in Table 4.

Table 4. Variation of LD₅₀ When Grained Charcoal "Carbolen" and Fibrous Carbon are Used as Enterosorbent

LD₅₀ is a lethal dose of exogenous poison causing the death of 50% of the experimental animals in our experiment with rats (quantity of poison in mg on 1 kg of animal weight).

Toxic substances	LD ₅₀ , mg/kg		
	Control without sorbent	Carbolen	Carbonfibrous sorbent
Carbontetrachloride	22215	2901	3425
1,2 dichlorethane	640*	829	1042
barbamyl	276	388	519
carbophos	0.875	1.132	1.500
strychnine	7	21.6	30.2

Experimental data demonstrate promising results of entorhinal application of fibrous sorbent in cases of poisoning danger. A striking clinical effect using derivatives of phenothiazine in the application of fibrous enterosorbents was obtained with patients suffering from alcohol poisoning. It was successfully used in the treatment of hepatitis A and B; in the case of leptospirosis the death rate was reduced from 25% to 7-8%; in the case of acute gastro-intestinal disturbance a prescription of fibrous sorbent resulted in quick cupping of intoxication and diarrhea syndrome; in the case of resorptive fever enterosorption provides cupping of gastroenteropathy and decreases the general level of endogenous intoxication. With the same aim enterosorption was successfully applied to patients having complications from drug-and-radiotherapy cancer treatments. Positive effects were also obtained with patients suffering from food and drug allergy, and also from diabetes mellitus.

The application of carbon-fibrous sorbents in the case of hemosorption demonstrated that their effect on the contoured blood elements does not exceed analogical indexes of spherical carbon hemosorbents. Hemosorption on a carbonfibrous sorbent base was employed in the case of leptospirosis, rheumatoid arthritis, critical forms of myasthenia, psoriasis, asthma, and exotoxicoses. On the basis of such studies it was assumed that fibrous sorbents are highly effective hemosorbents in therapeutic endo-4 exogenno intoxications. The high rate of sorption determines the advantages of their application at the departments of intensive therapy/revivification.

The problem of effective removal of toxic products from wound surfaces is one of the vital problems of purulent surgery. Sorbing dressing consisted of a carbon-fibrous adsorbent layer between two layers of gauze. Dressings with fibrous carbon are comfortable; they are easily adapted to the wound surface for any relief not causing traumatosis of the wound. It was noted as decreasing intoxication, diminishing edema, preventing secondary necroses development, limiting fibrinous films, strengthening of epithelization of the wound surface, stimulating granulation growth, and shortening the period of preparation of wounds for epidermatoplasty. The subjective state of patients was improved; temperature dropped within 1-3 days of starting the application of dressings and drains with carbonfibrous sorbent.

Patients with a lightning form of anaerobic infection were under supervision also. In the process of cytologic examination of wounds it was found that after the first dressing the total number of freely lying microbic bodies decreased by an order of 1-3, and a considerable number of connective elements appeared. Positive dynamics of perpheric blood indexes and decreasing toxemia within the stages of leukocyte destruction were noted. During the treatment of burned patients a trauma from the dressings was noted. Dressings were successfully applied in the case of patients with post injection abscesses of soft tissues, in the complex therapy of nonformed intestinal fistula, in the course of complex

*Not able to verify with the author.

treatment of first and second degree peritonitis. Tampons with carboniferous sorbents were tested for treatment of postnatal ruptures of the perineum of a woman in labor. Due to the application of sorbing dressings it was possible to escape dangerous septic consequences in patients suffering from puerperal endometriosis.

The obtained results enable us to consider the application of sorption with carbonfibrous sorbents to be very promising, especially in cases of mass arrivals of wounded people, when the application of dressings with fibrous carbon allows extension of the prehospital period.

Sorbent application can be used not only for wound and burn treatments, but also for protection of surfaces injured by chemical and biochemical toxic substances.

Finalizing the research results of applying carbon sorbents in medicine, we can conclude that in cases of acute poisoning it is desirable to apply, simultaneously, hemo and enterosorption. When treating wounds and burns accompanied by exogenous intoxication, it is possible to apply a complex sorption method of treatment, including hemo, enterosorption and application therapy.

COMPRESSION-DISTRACTION APPARATUS OF ACADEMICIAN B. KALNBERZ

The apparatus is designed for setting fractured bones. The construction base of Kalnberz's apparatus consists of hexahedral rings and clamps to provide a special rigid truss structure.

Application of modern composite materials (CFM) for manufacturing apparatus elements enabled us to improve its parameters considerably. In particular, we decreased the apparatus weight, preserved its strength, and improved the deformative characteristics and operational-hygienic properties.

CFM were used in the construction of rings and rods with a directed arrangement of reinforced fibers of different types. The necessary level of elasto-strength properties of directed-reinforced material was obtained by reinforcement hybridization. The surface modification of the apparatus elements was carried out by applying a special protective polymer layer to provide the apparatus elements with the necessary surface medical-biological properties, namely: nontoxicity, possibility of sterilization by any known methods without surface damage, prevention of injury to the doctor's hands and the patient's body. Medical-biological tests and the clinical ones of the Kalnberz apparatus were conducted using modern CFM. The results of the tests are given below.

Reinforcing filler	Mass gr	Inner diameter, mm	Breaking load	Destruction deformation, mm	Mass of serial elements, gr
	62	150	3200	16	72
Glass roving	71	170	3050	19	-
Glass roving + 5% SVM	78	200	2550	29	172
Glass roving = 10% SVM	91	240	2100	36	217
Glass roving + carbofiller	78	240	2400	-	-

1994021383

511-24

N94-16856
1.16

TEXTILE COMPOSITE PROCESSING SCIENCE*

Alfred C. Loos and Vincent H. Hammond
Department of Engineering Science and Mechanics
Virginia Polytechnic Institute and State University
Blacksburg, VA 24061-0219

David E. Kranbuehl
Chemistry Department
College of William and Mary
Williamsburg, VA 23185

Gregory H. Hasko
Lockheed Engineering and Sciences Co.
NASA Langley Research Center
Hampton, VA 23681-0001

ABSTRACT

A multi-dimensional model of the Resin Transfer Molding (RTM) process was developed for the prediction of the infiltration behavior of a resin into an anisotropic fiber preform. Frequency dependent electromagnetic sensing (FDEMS) has been developed for in-situ monitoring of the RTM process. Flow visualization and mold filling experiments were conducted to verify sensor measurements and model predictions. Test results indicated good agreement between model predictions, sensor readings, and experimental data.

* This work was made possible through the support of the National Aeronautics and Space Administration-Langley Research Center grant number NAG1-343 with Virginia Tech and grant number NAG1-237 with the College of William and Mary.

INTRODUCTION

Resin Transfer Molding (RTM) is of interest to the aircraft industry as a cost-effective method for the production of near-net shape primary aircraft structures. The RTM process also lends itself to the use of textile preforms manufactured through a variety of automated textile processes. Often, these preforms have through-the-thickness stitching for improved damage tolerance and delamination resistance. The challenge presently facing RTM for use in the aircraft industry is to refine the process to insure complete infiltration and cure of a geometrically complex shape preform with the high fiber volume fraction needed in the industry.

Towards this goal, a joint research program between NASA Langley Research Center, Virginia Polytechnic Institute and State University, and the College of William and Mary is designed to develop a science based understanding of RTM for aircraft composites. A necessary part of this project is to characterize the emerging resins and preforms used in the RTM process. Elements of the program include:

- Analytical modeling of the RTM process
- In-situ sensing of resin flow during the RTM process
- Mold filling and flow visualization experiments
- Preform and resin characterization
- Sensor/model intelligent process control

This paper will discuss the theoretical basis of the RTM process model and the characterization of the preforms used in the process. The use of Frequency Dependent Electromagnetic Sensing (FDEMS) for monitoring resin front position and cure will also be addressed. Results of two dimensional flow visualization and mold filling experiments performed to verify the process model will be presented.

RESIN PROCESS SIMULATION

The model, which is based on the finite element/control volume technique, was developed to predict the resin flow front position and pressure distribution inside the preform as a function of time. The following assumptions are made in the analysis: 1) the preform is a porous medium, 2) the preform permeability is heterogeneous and anisotropic, 3) the resin is incompressible and low Reynolds number flow is present, and 4) the injection is performed under isothermal conditions.

User defined variables such as the time/temperature/pressure profile along with the preform layup sequence and tooling assembly are input into the model. A flow diagram for the simulation model is given in Figure 1. The compaction and permeability behavior of the preform coupled with resin viscosity behavior are used by

the model to predict the resin front position as a function of time. Once the preform is completely infiltrated, the degree of cure and total cure time are calculated by the model. The model outputs this data along with temperature as a function of time for later analysis. Panel thickness and the resulting final fiber volume fraction are also determined by the model.

PREFORM CHARACTERIZATION

In order for the model to correctly evaluate the infiltration behavior of the resin into the dry preform, it is necessary to characterize the porosity and permeability behavior of the preform. The porosity behavior is determined by measuring the compaction pressure necessary to achieve the desired level of fiber volume fraction. The fiber volume fraction is then related to the porosity and the preform thickness by the following equations:

$$\phi = (1 - v_f) = \left(1 - \frac{\xi}{t\rho_f}\right) \quad (1)$$

where ϕ is the porosity, v_f is the fiber volume fraction, t is the preform thickness, ρ_f is the fabric density, and ξ is the areal weight. This relationship is illustrated in Figure 2. The areal weight is the weight of the sample per unit area.

The steady state permeability behavior is determined by passing a fluid of known viscosity and volumetric flow rate through the preform and recording the pressure drop that occurs as the fluid passes through the fabric. Then, through the use of Darcy's Law,

$$Q = \frac{KA}{\mu} \frac{\Delta P}{\Delta x} \quad (2)$$

the permeability can be determined for each fiber volume fraction. The permeability is denoted as K , A is the flow area, the volumetric flow rate is Q , and μ is the viscosity of the fluid. The pressure difference is written as ΔP and the change in length is denoted as Δx . A diagram of the steady state permeability fixture is given in Figure 3.

EXPERIMENTAL

The set up for the flow visualization experiments conducted at Virginia Tech consisted of a 2 ft x 2 ft aluminum frame with a 1.5 inch thick poly (methyl methacrylate) top plate. The preform was composed of eleven (11) layers of Style 162 E-glass at a nominal fiber volume fraction of 43%. A dyed corn oil with a viscosity of 39.6 cps was injected into the mold at a constant pressure of 5.7 psi. The infiltration pattern was recorded through the use of a video camera. Frequency Dependent Electromagnetic Sensing (FDEMS) was used to determine the time at which the flow front passed a pre-selected point in the mold.

Two tests were conducted at NASA Langley Research Center to verify the simulation model. For these tests, a 1 ft x 1 ft stainless steel mold was used. The preform, composed of TTI IM7/8HS compressed to a fiber volume fraction of 60%, was injected at a constant flow rate of 10 cc/min with an epoxy resin. In one case, the viscosity of the epoxy was 58 cps while, in the second case, the viscosity was 165 cps. FDEMS were used to monitor the advancement of the flow front inside the closed mold. The total time required to fill the mold was also recorded.

The objectives of these tests were threefold:

- 1) To verify the flow-front and infiltration-time predictions of the RTM process simulation model
- 2) To verify permeability versus compaction measurements obtained from the preform characterization experiments
- 3) To demonstrate the ability of FDEMS sensing to detect the position of the flow front.

RESULTS

Preform Characterization

The compaction behavior for the TTI IM7/8HS preform is given in Figure 4. That of the Style 162 E-glass is shown in Figure 5. In both cases, the pressure needed to compress the preform is initially non-linear but then flattens out at the higher fiber volume fractions. The pressure required to compact the TTI IM7/8HS preform to an identical fiber volume fraction is less than that needed for the Style 162 E-glass preform.

The permeability behavior of the TTI preform is given in Figure 6 while that of the glass preform is provided in Figure 7. Experiments have shown that the permeability of both preforms decreases as the fiber volume fraction increases. This

results from the available pore space in the preform being closed off at the higher fiber volume fractions, thereby restricting fluid flow.

Flow Visualization - Single Side Port Injection

The details for the flow visualization test are shown in Figure 8. The corn oil enters the mold through the single side port and flows around the preform in a quarter inch channel until the entire channel is filled. The corn oil then enters the preform from each side, fully saturates the preform, and exits through a centrally located port.

It was noticed that the pressure failed to remain constant at the early stages of injection. The pressure fell from the set injection pressure to almost zero as the channel was filling. Only after the preform was initially infiltrated did the pressure return to the pre-set position. Therefore, pressure was monitored as a function of time and this resulting curve was input into the model.

A comparison between experimental and model-predicted flow fronts are given in Figures 9-11. At each time, there is good correlation between the predicted and experimental flow fronts. The irregularly shaped experimental flow fronts were attributed to the wavy nature of the plexiglass lid which allowed for spatial variations in permeability not accounted for in the model predicted flow fronts.

A grid showing the FDEMS locations in the baseplate has been overlaid on Figures 9 and 11. The time at which some sensors wetted out has also been provided. Through these times, a comparison can be made between model predicted, experimental, and sensor measured flow front positions as a function of time. The sensor measured times were usually within a few seconds of both the experimental and model predicted values. The accuracy of the sensors can be improved by increasing the scanning rate used during the data acquisition.

Mold Filling Experiments - Single Side Port Injection

A schematic diagram for the RTM mold filling experiments is shown in Figure 12. The resin is transferred from the constant injection rate cylinder to the mold through plastic tubing. A shim is placed on top of the preform to insure that the desired fiber volume fraction is reached. A steel plate with a venting port is then placed on top of the shim. A vacuum is then applied to assist in the removal of air from the preform.

As mentioned earlier, the preform has a nominal fiber volume fraction of 60%

while an epoxy/diluent mixture was used to achieve different viscosity resins. The resin is injected at 10 cc/min into the single side port and proceeds to fill a 0.25" high by 0.25" wide channel. Then resin then infiltrates the preform until saturation is achieved. The resin then exits through the venting port.

FDEMS were used to measure the position of the flow front inside the mold cavity. Six (6) sensors were used: three (3) were placed on the edge of the preform, one (1) in the center of the preform. The remaining two (2) were placed approximately three inches from the center. Their locations are illustrated in Figure 13.

A comparison between model predicted and sensor measured flow front positions is given in Figure 14. The sensors located along the edge of the channel filled much faster than predicted. The two sensors located near the center of the mold agree fairly well with the model predicted times. This indicates that the permeability of the preform governs the infiltration behavior once the channel is completely filled.

The most important thing to note from Figure 14 is that the flow front passed the exit port (located above the center sensor) prior to complete infiltration of the preform. This is not desirable as this may result in a large region of entrapped air or many small voids. Both of these will result in a noticeable decrease in mechanical properties for the composite. Based on this observation, the model was used to simulate a dual port injection. The result of this simulation is shown in Figure 15. This figure shows the two resin fronts meeting at the center of the preform.

SUMMARY AND CONCLUSIONS

A multi-dimensional RTM process simulation model has been developed which can describe the infiltration of a resin into a dry textile preform along with the cure of the resulting saturated preform. This model is useful in predicting the total infiltration time needed along with the selection of optimal port locations in the mold. The model can also be used in determining the optimal cure cycle for a particular resin system. Frequency Dependent Electromagnetic Sensing (FDEMS) has been developed for use in the in-situ monitoring of the RTM process. These sensors were able to detect the resin front position as a function of time during the infiltration process. The sensors are also able to monitor the resin properties during the subsequent cure cycle.

A series of flow visualization and mold filling tests have been performed to verify the predictive capability of the model along with the ability of the sensors to monitor resin front position. Results from these tests indicated that the sensors were able to accurately monitor the front position during infiltration and that model predicted flow front positions agreed well with the experimental front positions.

Future work will concentrate on verifying the heat transfer analysis aspect of the model. Also, the sensor's ability to monitor resin properties during cure will be evaluated. The production of actual panels will be modeled and monitored with the sensors. The panels will be evaluated to determine possible manufacturing defects along with their mechanical properties.

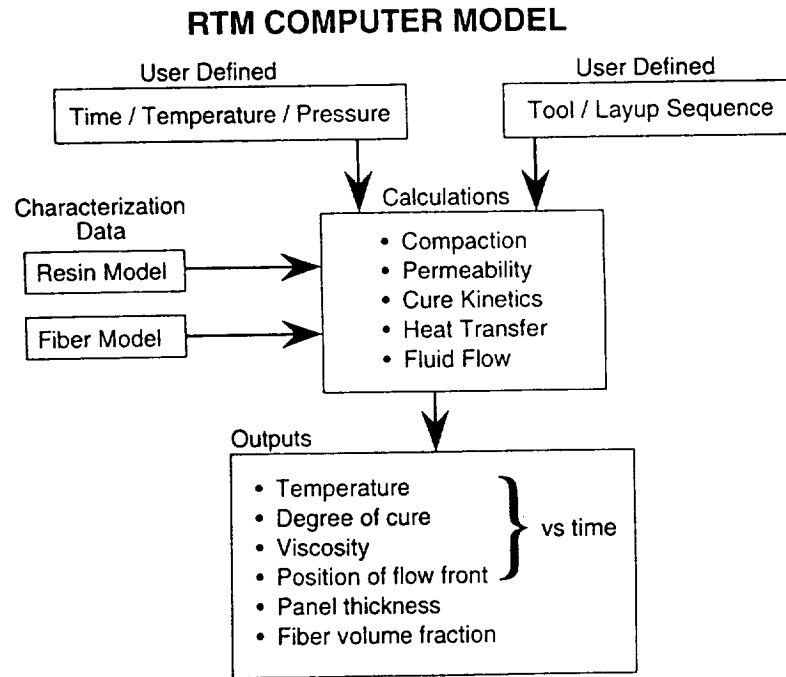


Figure 1: Flow chart of RTM simulation model.

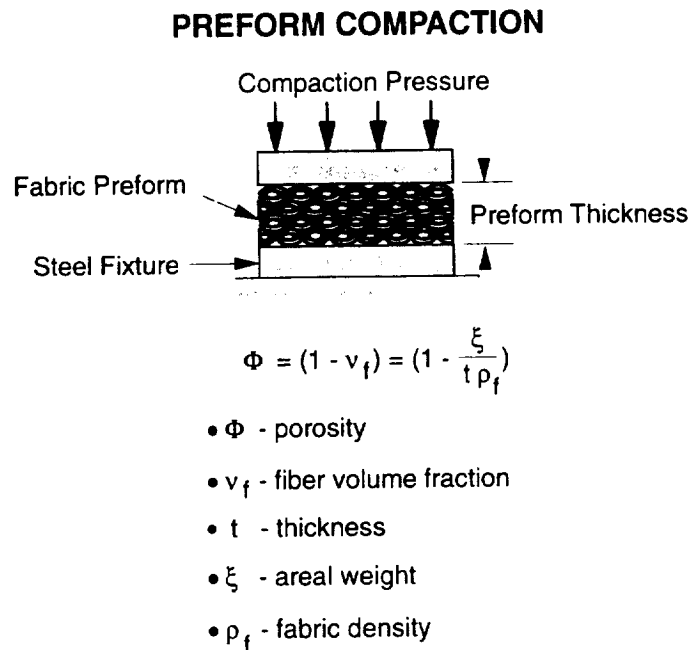
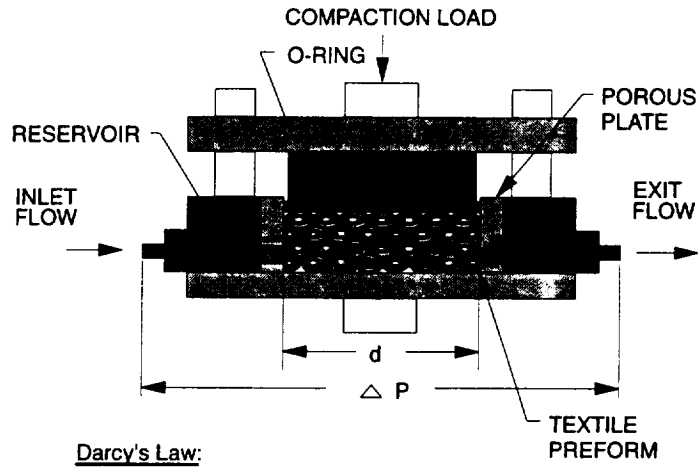


Figure 2: Schematic diagram relating preform thickness to porosity.



Darcy's Law:

$$Q = A \frac{K \Delta P}{\mu d}$$

WHERE:

- Q = VOLUMETRIC FLOW RATE
- K = PERMEABILITY CONSTANT
- μ = VISCOSITY OF FLUID
- $\Delta P/d$ = PRESSURE GRADIENT
- A = AREA NORMAL TO FLOW

Figure 3: Diagram of steady state permeability fixture.

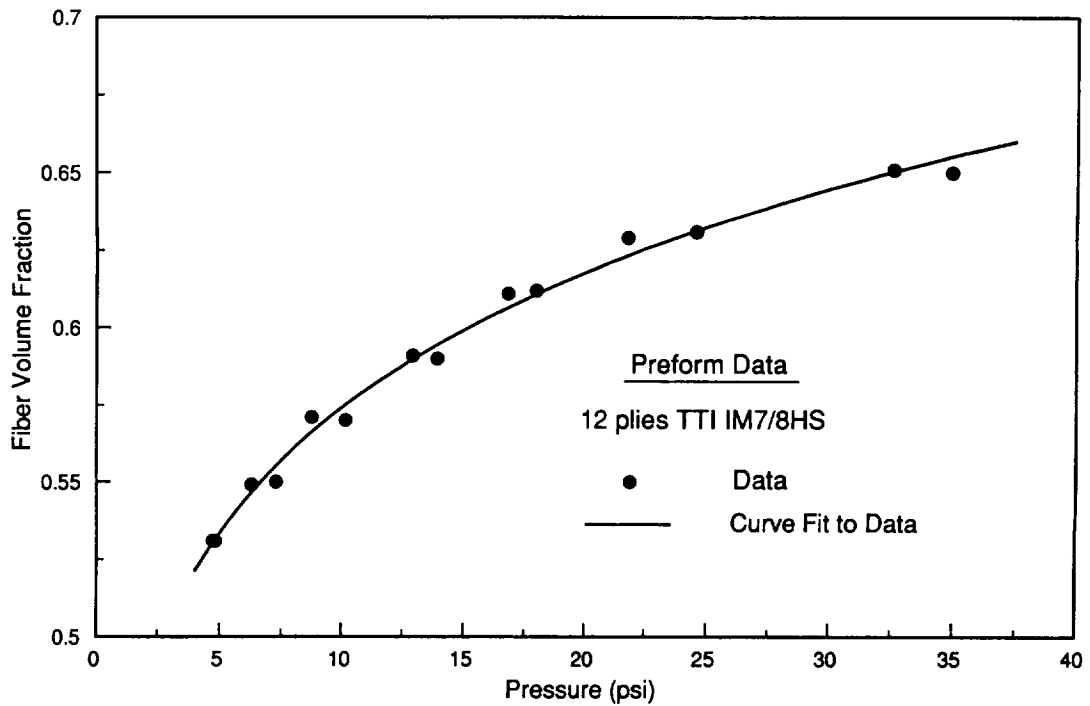


Figure 4: Compaction Behavior for the TTI IM7/8HS preform.

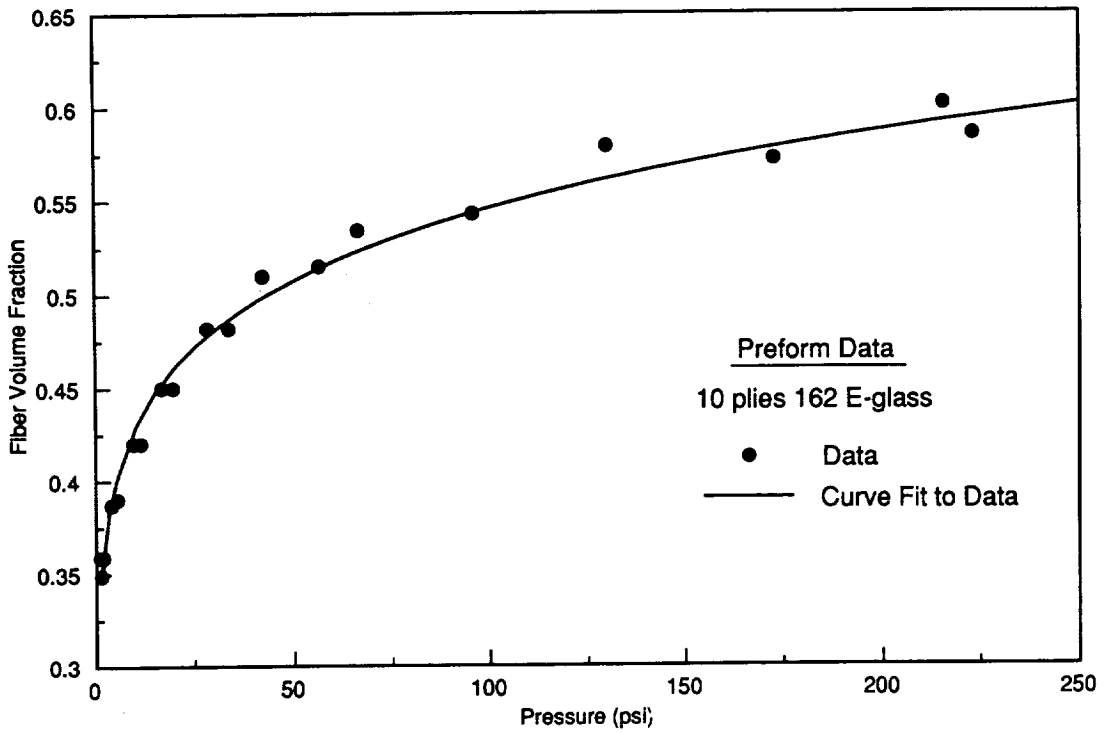


Figure 5: Compaction Behavior for the Style 162 E-glass preform.

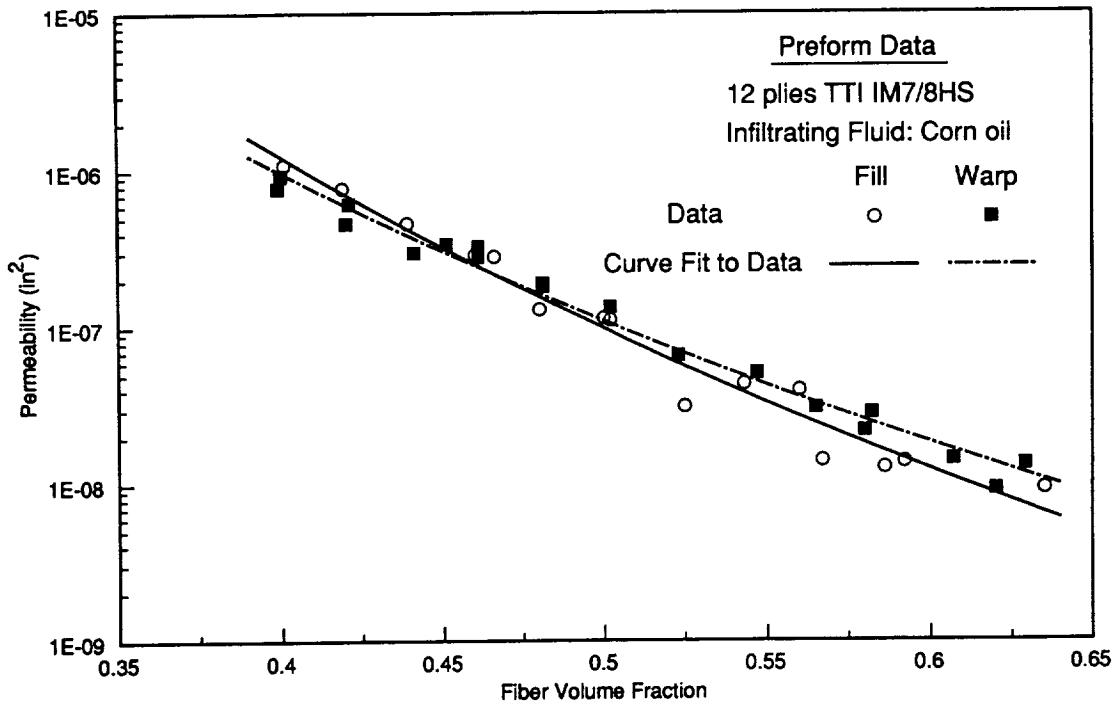


Figure 6: In plane permeability behavior for the TTI IM7/8HS preform.

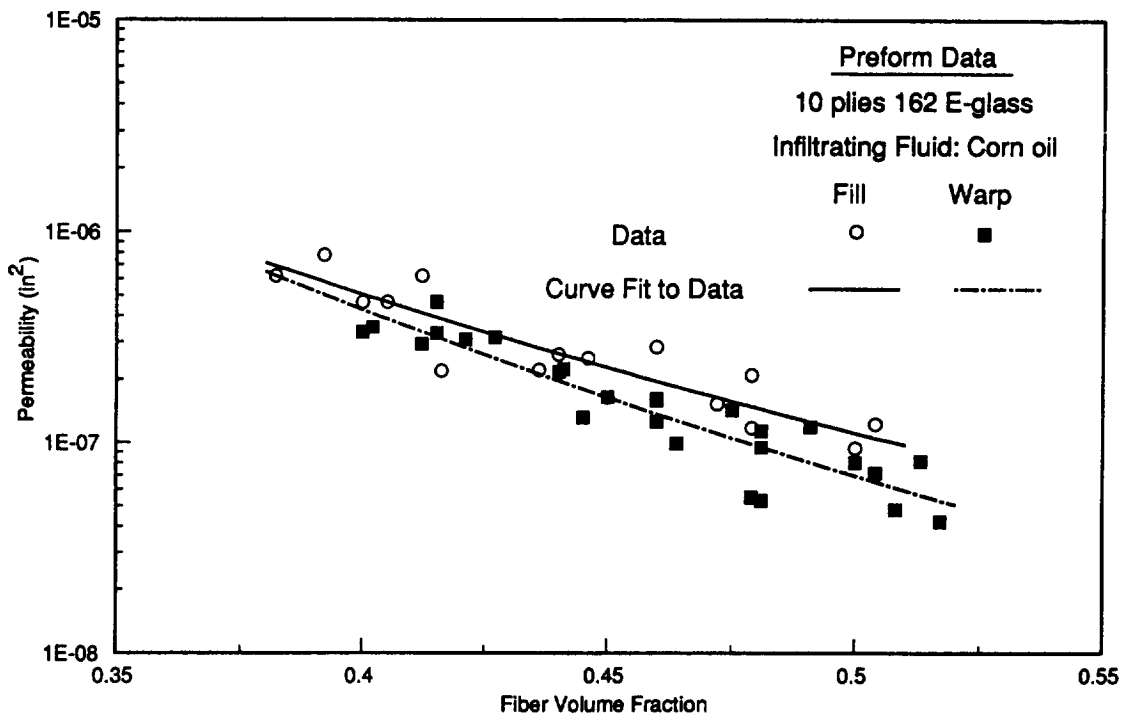


Figure 7: In plane permeability behavior for the 162 E-glass preform.

FLOW VISUALIZATION TEST SINGLE SIDE PORT INJECTION

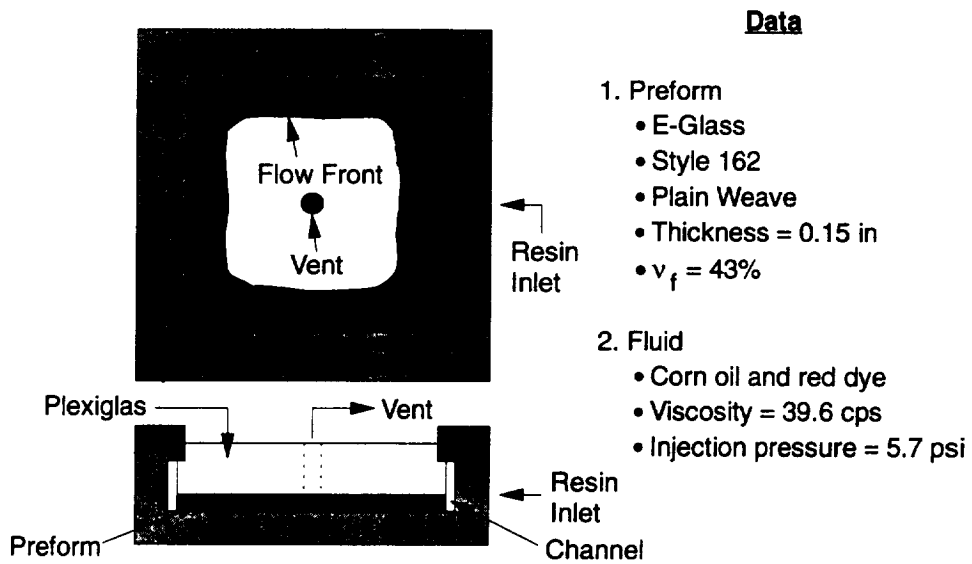


Figure 8: Details of single side port injection flow visualization test.

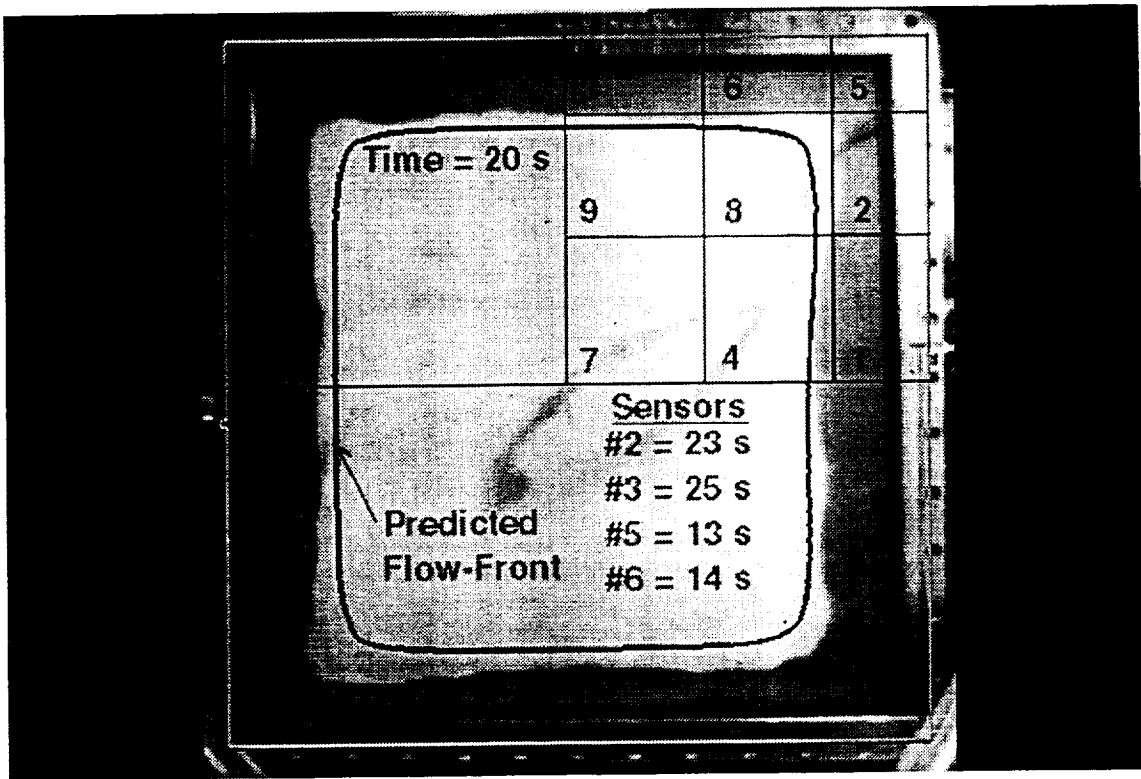


Figure 9: Comparison between model predicted and recorded flow fronts at an infiltration time of 20 seconds.

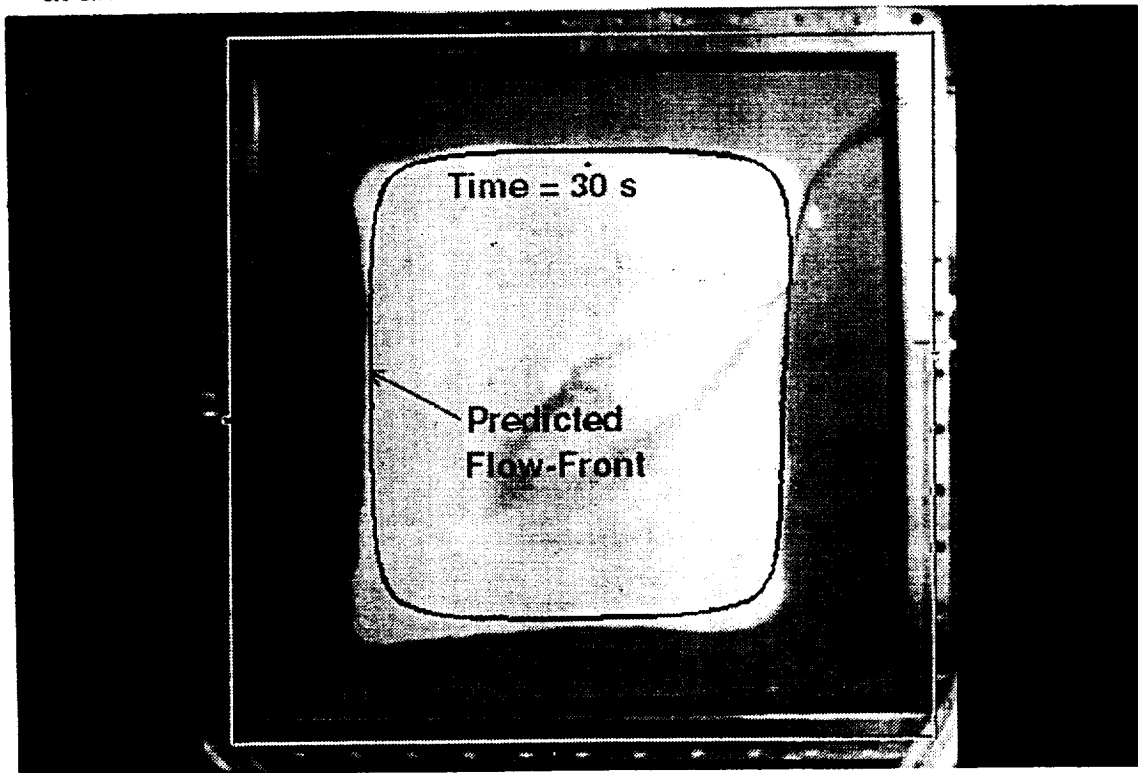


Figure 10: Comparison between model predicted and recorded flow fronts at an infiltration time of 30 seconds.

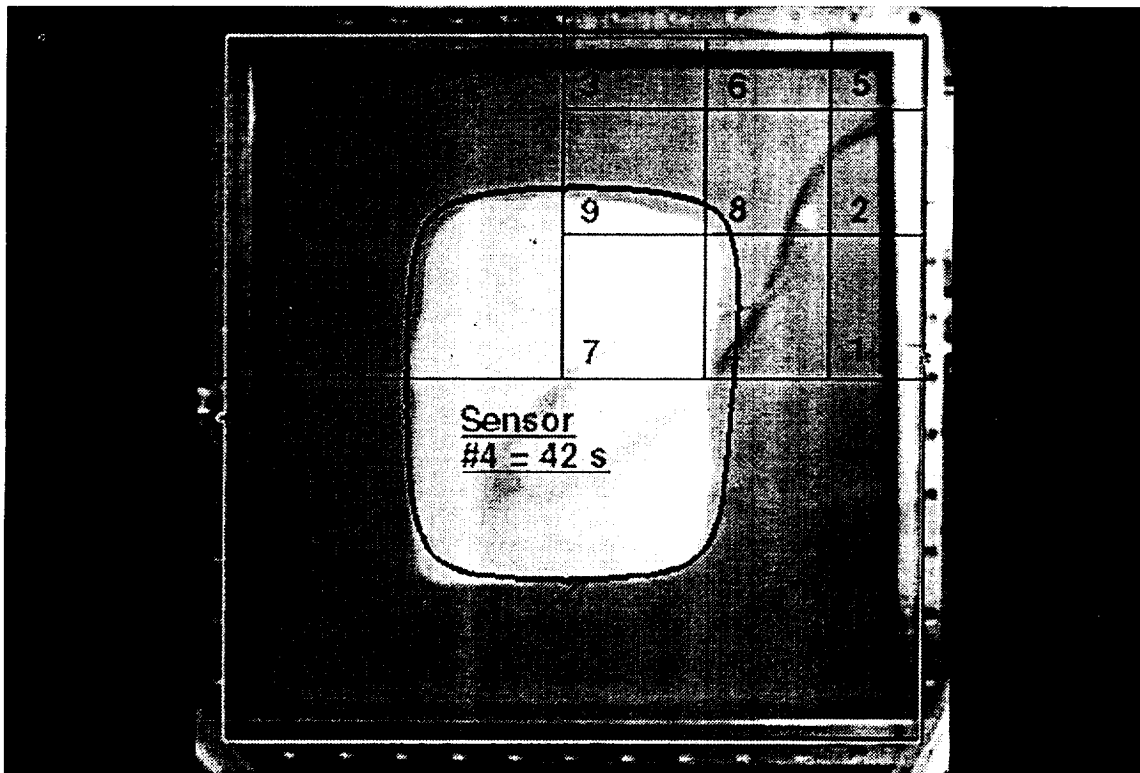


Figure 11: Comparison between model predicted and recorded flow fronts at an infiltration time of 45 seconds.

MOLD FILLING EXPERIMENTS SINGLE SIDE PORT INJECTION

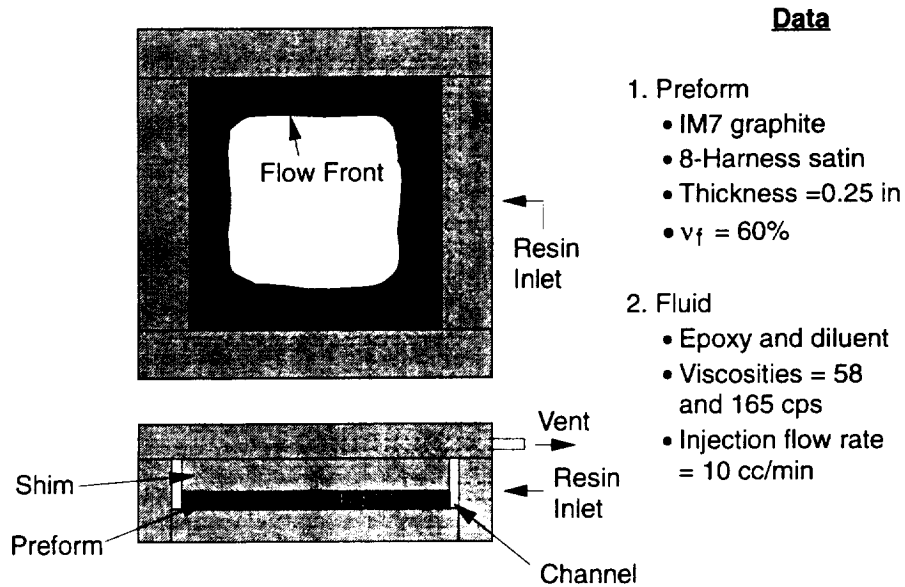


Figure 12: Details of single side port injection mold filling experiment.

Bottom Plate of RTM Mold

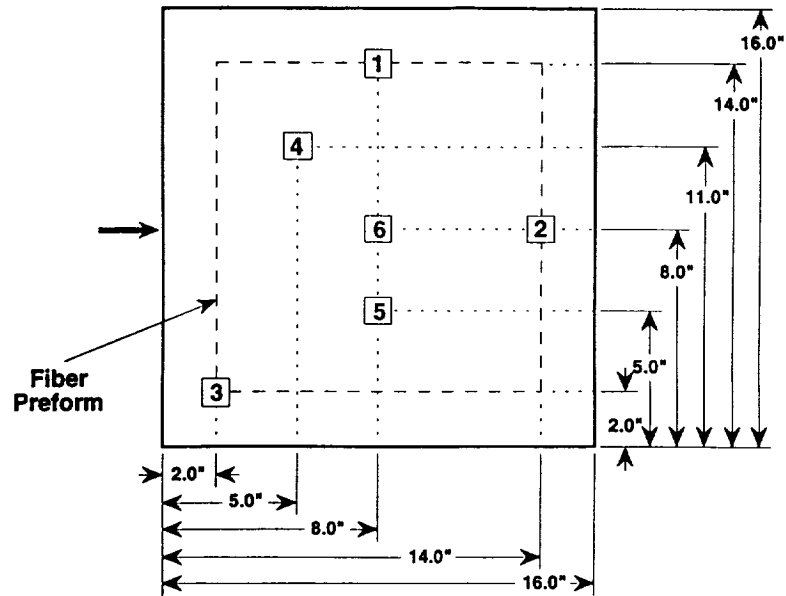


Figure 13: Location of FDEMS Sensor Array.

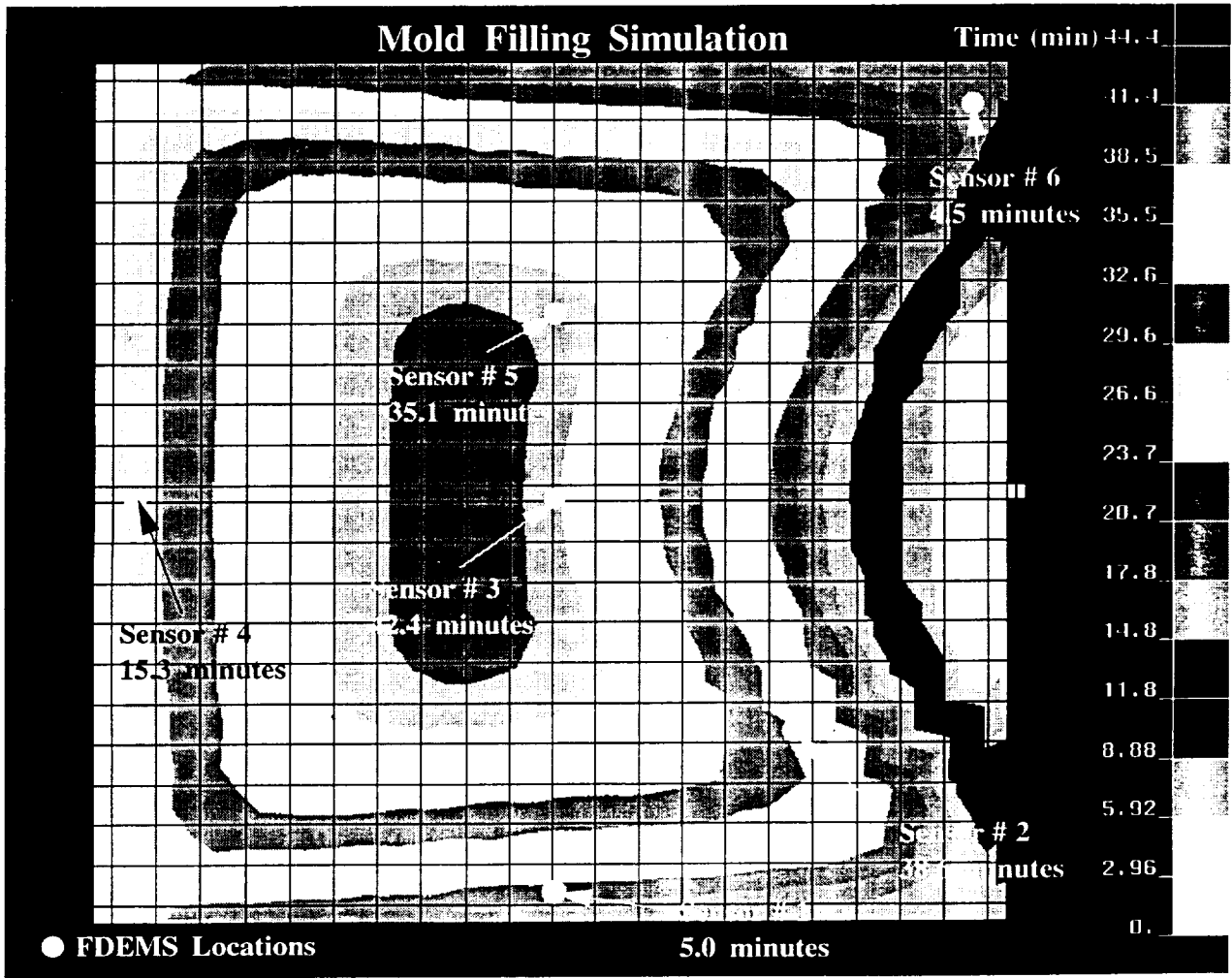


Figure 14: Comparison between model predicted and recorded flow fronts.

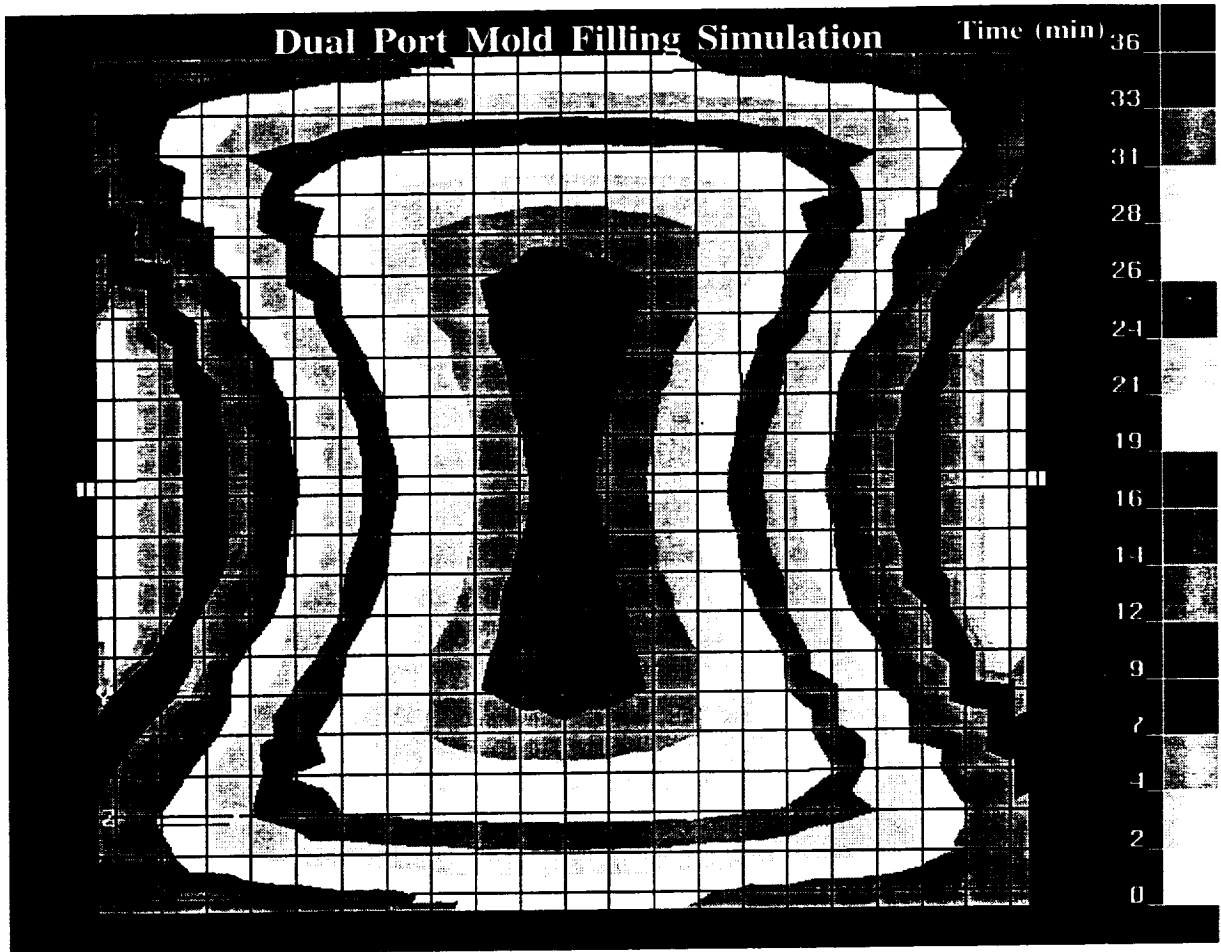


Figure 15: Predicted flow fronts for dual port injection.

1994012384

15-24

1.1.2

p. 15

**INFLUENCE OF FIBER PACKING STRUCTURE
ON PERMEABILITY**

N94-16857

Zhong Cai
Drexel University
Philadelphia, PA 19104

Alexander L. Berdichevsky
CR Industries
Elgin, IL 60123

ABSTRACT

The study on the permeability of an aligned fiber bundle is the key building block in modeling the permeability of advanced woven and braided preforms. Available results on the permeability of fiber bundles in the literature show that substantial difference exists between numerical and analytical calculations on idealized fiber packing structures, such as square and hexagonal packing, and experimental measurements on practical fiber bundles. The present study focuses on the variation of the permeability of a fiber bundle under practical process conditions. Fiber bundles are considered as containing openings and fiber clusters within the bundle. Numerical simulations on the influence of various openings on the permeability have been conducted. Idealized packing structures are used, but with introduced openings distributed in different patterns. Both longitudinal and transverse flow are considered. The results show that openings within the fiber bundle have substantial effect on the permeability. In the longitudinal flow case, the openings become the dominant flow path. In the transverse flow case, the fiber clusters reduce the gap sizes among fibers. Therefore the permeability is greatly influenced by these openings and clusters respectively. In addition to the porosity or fiber volume fraction, which is commonly used in the permeability expression, another fiber bundle status parameter, the ultimate fiber volume fraction, is introduced to capture the disturbance within a fiber bundle.

INTRODUCTION

The permeability of an aligned fiber bundle has been studied extensively since it is an important parameter in the composite manufacturing processes. Different proposed formulas have been suggested and verified by experiments for both longitudinal and transverse permeabilities [1-6]. It was found that the permeability is closely related to the fiber volume fraction or porosity. However, experimental measurements showed large scattering of data. Numerical calculations of the permeability of idealized square and hexagonal packing structures are also reported [7, 8].

The permeability is defined as [9]

$$K = \frac{Q}{A} \frac{\mu}{(\Delta p/L)} \quad (1)$$

where Q is the volume flow rate, A is the total cross-section area, and μ is the viscosity. The pressure difference Δp is across the distance L . Here the positive values of Q and Δp are used although their directions are opposite. In order to use the dimensionless parameter, the permeability K is normalized by using the fiber radius r_f . The normalized permeability K^* is defined as

$$K^* = \frac{K}{r_f^2} \quad (2)$$

When permeability in different directions is discussed, subscript x is used for the fiber direction, and y and z refer to transverse directions. Since a fiber bundle is assumed to be transversely isotropic, only subscript z is used to express the transverse permeability.

The comparison of the permeability of these idealized packing structures and other proposed formulas is summarized in Fig. 1 for both longitudinal and transverse cases. In the longitudinal direction, there is a substantial difference between the model predictions, which are backed by experimental data, and numerical solutions. The disturbance in the fiber bundle under the processing conditions contributes to the discrepancy. In the transverse direction, two models are used in the comparison. Kardos' model [3, 4] only contains fiber volume fraction V_f , while Gutowski's model [2] introduced an additional variable, the ultimate fiber volume fraction V_a . There are some differences between Kardos' model and square packing results, and between Gutowski's model and hexagonal packing results respectively. The difference between these two groups becomes substantial when V_f becomes high.

As a fiber bundle usually contains thousands of filaments, the random distribution of these filaments, and any disturbance within a bundle, can result in the change of permeability of the fiber assembly. In this study, micro-level cell models with introduced disturbance are built to investigate these disturbances using numerical simulations. The variation of the permeability due to these disturbances is then assessed and analyzed.

NUMERICAL SIMULATION

The numerical simulation work was done by using the available finite element packages ANSYS [10] and FIDAP [11]. The automatic meshing capability and the easiness of the pre-processing and post-processing of these FE packages especially with ANSYS greatly help build up various mesh models.

a) Longitudinal Permeability

For the longitudinal permeability, we assume the flow is parallel to the fiber axis, or x direction, and only the velocity component V_x exists. Also we assume the Reynolds number is very small and the gravity can be neglected so that this becomes the so-called Stokes flow. The flow equation can be written as

$$\frac{\partial p}{\partial x} \frac{1}{\mu} = \frac{\partial^2 V_x}{\partial y^2} + \frac{\partial^2 V_x}{\partial z^2} \quad (3)$$

where the terms at the left side are constant over the whole y - z plane. This is equivalent to a 2-D thermal equation with a uniform heat generation over the whole region which can be expressed as

$$\frac{w}{k} = \frac{\partial^2 T}{\partial y^2} + \frac{\partial^2 T}{\partial z^2} \quad (4)$$

When this heat transfer equation is solved, the temperature distribution obtained is equivalent to the velocity field for the flow equation. The longitudinal permeability can be solved accordingly.

2-D thermal elements are used in the calculation. This is a four-node plane element with a single degree of freedom, temperature, at each node. The reference temperature is set as zero at the fiber surface. Therefore the values of the temperature are directly used as the relative magnitude of the temperature rise.

The computational cell is set as a rectangle of L_y by L_z in y and z directions respectively. Symmetry boundary conditions are set at four cell boundaries, $y=0$, $y=L_y$, $z=0$, and $z=L_z$.

b) Transverse Permeability

For the transverse flow with small Reynolds number, the Stokes equation becomes

$$\frac{1}{\mu} \frac{\partial p}{\partial y} = \nabla^2 V_y$$

$$\frac{1}{\mu} \frac{\partial p}{\partial z} = \nabla^2 V_z$$

$$\nabla^2 = \frac{\partial^2}{\partial y^2} + \frac{\partial^2}{\partial z^2} \quad (5)$$

The permeability K is calculated directly from the averaged flow rate according to the definition.

The 2-D 4-node fluid element is used in the simulation. In the calculation the option is set as steady state flow, and the constants for the body force are set to be zero. Also the local Reynolds number for the elements is set to be much smaller than 1. The boundary conditions set on the representative cell (L_y by L_z) are: 1) at the surfaces of $z=0$ and $z=L_z$, $V_z=0$ and $\partial V_y/\partial z=0$; 2) at the surfaces of $y=0$ and $y=L_y$, $V_z=0$ and $\partial V_y/\partial y=0$; and 3) the pressure difference $(p)_{y=0} - (p)_{y=L} = \Delta p$. Along the surfaces of $y=0$ and $y=L_y$, the pressure is also constant.

DENSELY PACKED HOLLOW STRUCTURES

Numerical simulations on hollow hexagonal packing and hollow square packing are reported in [8]. These hollow packing structures possess relatively low ultimate fiber volume fraction, 0.589 for hollow square packing and 0.605 for hollow hexagonal packing. The experimental data of the ultimate fiber volume fraction for an aligned fiber bundle was in the range of 0.78 to 0.85 [2]. In this part of the numerical simulation, hexagonal and square packing structures are still used, with a portion of the fibers removed in a certain pattern. They become densely packed hollow structures. In other words, the

densely packed fibers are assumed to have sparsely distributed voids in the bundle. However, since they are densely packed, there are always "good" lock mechanisms. In other words, these voids are not connected to each other and there is no direct flow path within the bundle.

Since there are different amounts of the fibers removed in different mesh models, the ultimate fiber volume fraction V_a will be different for each of the options. Therefore this simulation reveals more the effect of V_a on the permeability variations.

The computation cells are chosen to be rectangular, so that mirror symmetric boundary conditions can be set at each side. The hollow packing settings are also constructed such that the isotropic behavior of the permeability is always preserved.

Different computational cells are shown in Figs. 2 and 3. Finite element meshes of these computational cells are also shown in these figures. The convergence of the calculations is checked by comparing the results with available "exact" solutions for hexagonal and square packing, and by varying mesh size and increasing element and node numbers. The convergence of the calculation for other structures is also checked on selected samples. Fig. 4 shows the convergence of the calculation versus element number for the mixed packing structure. When determining the mesh size, a compromise is reached by considering both the accuracy and the computational time.

QUASI-RANDOM PACKING MODEL

In studying the transverse stiffness of the unidirectional composites, Adams and Tsai [12] proposed a numerical method which used a random array of cells to represent the micro-level composite structure. We adopt the same approach and build a random set of cells to represent the micro-level fiber assembly with some random disturbance. In other words, the fiber assembly contains closely packed fibers and some open spaces among fibers, which are randomly placed into cells.

The representative volume contains twenty-five unit cells (5 by 5). It is a quarter of the representative volume of 10 by 10, as shown in Fig. 5. Mirror symmetry boundary conditions are imposed on the 5 by 5 cell to reduce the amount of the calculation. It is also assumed that the cell retains the isotropic permeability, which means the permeabilities in the y and z directions are the same. This is realized by the symmetry condition imposed on the +45 degree diagonal.

Two random effects are investigated. One is the random packing pattern, which means some of the cells are filled with fibers while others are empty. The other is the random positioning of fibers within the cell "box", which means fibers are placed at the off-center locations in cells.

The random function in the FORTRAN program language is used to generate the random cell packing and the random center positions. The random function generator in the program is controlled by the seed number. In order to obtain the randomness of the seed number, the time function was used which was related to the time to the one hundredth of a second. The random number obtained from the time function was then transformed into a series of random seed numbers. For each random fiber packing, 15 random numbers were assigned to 25 cells under the rule of symmetry to the diagonal. These cells were ranked according to the magnitude of the random number. Then the lowest N cells were chosen as filled with fibers, where N was determined according to the fiber volume fraction and fiber radius. This program was named as RAND-F. For the random center positions, 15 random numbers were transformed to a value between $-\delta$ and $+\delta$ respectively, where δ was

the maximum offset of the fiber center position determined by the cell mesh condition and the fiber radius. This program was named as RAND-D.

Automatic meshing was used to generate different random packing models. As mentioned earlier, three sets of random packings were tried. The first was the random occupancy of fiber cells, the second was the fully occupied fiber cells with random offset fiber center positions, and the third was the combination of these two, which meant only some cells were randomly filled with fibers which were located at random off-center positions.

For the random occupancy of fiber cells, two basic unit cells were setup to represent the cells with and without fibers, as shown in Fig. 5. The packing pattern generated from the RAND-F program was used as the input, and indices 1 and 0 were assigned to corresponding cells. 25 local coordinate systems were used for these cells and they were located at the center of these cells. Meshing was done for each cell according to the given index (1: with fiber; 0: without fiber). Finally these meshed cells were combined together, repeated nodes were merged, and boundary conditions were set accordingly.

For the random offset position of fiber centers, the fiber center positions were first determined by the RAND-D program. These positions were used to generate the fiber boundaries within the cell. The original cell center positions were used to generate cell boundaries. Then the meshes were automatically generated. Because the offset of the fiber centers sometimes introduced difficulty in automatic meshing, errors did occur and the pre-processing was aborted. Due to the limitation of the automatic meshing used, fibers were always contained in the original cells, which greatly limited the extent of the variation on the permeability.

For the third situation of random fiber cells and random fiber center positions, both programs (RAND-F and RAND-D) were used and automatic meshing was applied accordingly.

The computational error is directly related to the mesh size. This was checked for a particular case by varying the mesh size. As a compromise of the accuracy and the computational time, the mesh model chosen contained 144 elements (12 by 12) for cells without fibers, and 240 or 288 elements (48 in the circumferential direction and 5 or 6 in the radial direction) for cells with fibers. The estimated error in the worst case was less than 1 percent, and in most other cases, the error was around 0.2 to 0.5 percent.

RESULTS AND DISCUSSIONS

The permeability results of the densely packed fibers with introduced openings are shown in Fig. 6 and 7 for longitudinal and transverse directions respectively. These structures have definite packing patterns. All the gaps among fibers are with the same width. All the openings introduced are isolated. Therefore, if we keep squeezing these fiber bundles, the values of V_a will be different in each case. It is shown in the figures that with relatively high fiber volume fraction, the effect of V_a on the permeability increases.

As we mentioned earlier, the effect of the openings on the permeability is different in different flow directions. In the longitudinal flow case, the openings provide the flow path to the fluid. In the transverse flow case, the openings reduce the gap width among fibers, resulting in higher flow resistance. In Fig. 6, the three cases without introduced openings, hexagonal, square, and mixed packings, show relatively low longitudinal permeability.

The variation of the permeability due to different packing is substantial. In the longitudinal direction, at the $V_f=0.5$, the permeability can be about 2.7 times of difference, while in the

transverse direction, the difference can be about 10 times. Therefore, with only one variable, usually the fiber volume fraction V_f , the permeability status of the fiber bundle is possibly still very uncertain.

Fig. 8 shows the permeability variation of random packing structures. As shown in Fig. 5, there are three groups of packing situations with the randomly placed fiber cells. We define them as with fiber locking, without fiber locking, and with direct flow path. In the case of with fiber locking, there exists a row of fibers or a combination of rows of fibers to lock the flow if the maximum packing efficiency of that particular packing is reached. In other words, fluid has to pass through small gaps within the fiber row. In the case of without fiber locking, which means that even at the maximum packing efficiency flow is still possible, the relatively large gaps in the diagonal direction of the cell provide easier flow path for the fluid. In other words, flow paths are mainly in the diagonal directions. In the case of with direct flow path, there exists a row or a combination of rows of open spaces as the flow path.

For each of the selected fiber volume fractions, there are options of number of fiber cells. The percentage of the occurrence of each of these three cases depends on the fiber cell numbers. With 14 fiber cells out of the 25 total cells, there were a few cases of direct flow path, and the rest were with fiber locking or without fiber locking. With 16 fiber cells, the occurrence of direct flow path diminished so that there were mainly cases of with fiber locking and without fiber locking. With 18 or more fiber cells, most of the cases were with the locking of fibers.

The number of cells with fibers is also limited by the fiber volume fraction. With relatively low fiber volume fraction, less fiber cell numbers are possible. For example, for $V_f=0.4$, we tried fiber cell numbers of 14, 16, 18, and 20. For $V_f=0.45$, fiber cell numbers were 16, 18, and 20. For $V_f=0.5$, fiber cell numbers were 17 and 19.

The simulation of the randomly packed fibers was done on these three groups. With 14 to 20 fiber cells, the simulation covers V_f range of 0.2 to 0.5. With 25 fiber cells but random center positions, the range of V_f was from 0.2 to 0.7. With 18 to 20 fiber cells and offset fiber center positions, the range of V_f was 0.4 to 0.55. For each selected case, 25 simulations were performed with different random settings. However, because of the automatic mesh limitation, only meshes with "good" shape were accepted for the finite element calculation. Therefore the successful simulations for each case were usually less than 25. The total simulation cases were over 700 for longitudinal and transverse flow respectively.

Fig. 8a shows the data variation of the permeability when different numbers of the fiber cells are used in the simulation. With each selected fiber cell number, there are about 20 data points. The variations are very substantial. In the longitudinal case, the difference is as high as more than five times. In the transverse direction, the difference can be as high as over a hundred times.

Hexagonal packing is used as a reference in Fig. 8a. In the longitudinal flow case, it is a low limit of the permeability, since it possesses the most uniformly distributed flow channels. In the transverse flow case, however, there were cases that the permeability is higher or lower than that of the hexagonal packing. In the extreme cases, fibers may fully lock the flow path when they contact with each other, or they may be far away from each other so that a large flow path with minimum flow resistance may form within the bundle.

In Fig. 8a about the transverse permeability, three groups of data can be distinguished. In the 14 fiber cell case, the group with locked fibers shows the normalized permeability of

about 0.001, the group without fiber locking shows the normalized permeability of about 0.04, and the group with direct flow path shows the normalized permeability of about 0.2. With 16 fiber cells, only two groups appear, with fiber locking and without fiber locking. The permeability values are about 0.08 and 0.04 respectively. With 18 or more fiber cells, only locked fiber cells exist. Also with the increase of the fiber cells, the permeability data of locked fibers gradually gets close to that of the hexagonal packing.

Fig. 8b shows the variation of the permeability when all 25 cells are filled with fibers, but the fiber center positions are randomly determined. The variation of the permeability in both longitudinal and transverse cases is substantially smaller than that in Fig. 8a. It is also interesting to see that in the longitudinal case, the permeability of these random fiber sets is always higher than that of the original square packing. In the transverse case, however, the variation appears in both directions, resulting in either higher or lower permeability values. This agrees with the results shown in Fig. 1, where the longitudinal permeability data from experiments is substantially higher than that of the idealized packing, and the transverse permeability data from experiments is more close to that of the idealized packing.

For a real fiber bundle under the processing conditions, the macro-level status of the fiber bundle is already determined. In other words, the relative positions of the fibers within the bundle are somewhat settled. Gently squeezing the fiber bundle will not change the macro-level status of the bundle. With this relatively determined fiber bundle status, the variation of the permeability for a certain fiber bundle is limited. However, different fiber bundles may have substantially different status, such as opening size within the bundle. Therefore the permeability from bundle to bundle may be very different. To capture this macro-level fiber bundle status, additional status variables are needed. In [2] and [7], the ultimate fiber volume fraction is introduced in addition to the average fiber volume fraction. More discussions and proposed models on selecting the ultimate fiber volume fraction as the additional permeability parameter are presented in [13].

SUMMARY

Finite element simulations on the variation of the permeability of an aligned fiber bundle have been carried out. These simulations are based on the idealized packing with introduced openings, and based on the quasi-random fiber cell models. The results show that even with the same fiber volume fraction, the permeability variation can vary substantially. The disturbance within a fiber bundle has to be considered in order to reduce the uncertainty in the estimation about the permeability.

The numerical simulation results also suggest that in addition to the average fiber volume fraction, other parameters describing the macro-level status of a fiber bundle are needed. The effect of the ultimate fiber volume fraction on the permeability is investigated through the simulation.

ACKNOWLEDGEMENTS

The authors would like to thank D.J. Lawrie for many helpful discussions and technical supports during the course of this work.

REFERENCES

1. Williams, J.G., Morris, C.E.M., and Ennis, B.C., "Liquid Flow Through Aligned Fiber Beds", *Polymer Engineering and Science*, Vol. 14, No. 6, June, 1974, pp.413-419.
2. Gutowski, T.G., et. al., "Consolidation Experiments for Laminate Composites", *Journal of Composite Materials*, Vol. 21, June, 1987, pp.650-669.
3. Lam, R.C. and Kardos, J.L., "The Permeability of Aligned and Cross-Plied Fiber Beds During Processing of Continuous Fiber Composites", Proceedings of American Society for Composites, Third Technical Conference, Seattle, Washington, September, 1988, pp.3-11.
4. Lam, R.C. and Kardos, J.L., "The Permeability and Compressibility of Aligned and Cross-Plied Carbon Fiber Beds During Processing of Composites", Proceedings of 47th Annual Technical Conference (ANTEC'89), SPE, New York, 1989, pp.1408-1412.
5. Skartsis, L. and Kardos, J.L., "The Newtonian Permeability and Consolidation of Oriented Carbon Fiber Beds", Proceedings of American Society for Composites, Fifth Technical Conference, E. Lansing, Michigan, June, 1990, pp.548-556.
6. Kim, Y.R., McCarthy, S.P., Fanucci, J.P., Nolet, S.C., and Koppernaes, C., "Resin Flow Through Fiber Reinforcements During Composite Processing", *SAMPE Quarterly*, April, 1991, pp.16-22.
7. Sangani, A.S. and Acrivos, A., "Slow Flow Past Periodic Arrays of Cylinders with Application to Heat Transfer", *International Journal of Multiphase Flow*, Vol. 8, No. 3, 1982, pp.193-206.
8. Berdichevsky, A.L. and Cai, Z., "Estimation of the Permeability of Aligned Fibers with the Self-Consistent Method and FE Simulation", accepted by *Polymer Composites*, 1992.
9. Scheidegger, A.E., The Physics of Flow Through Porous Media, University of Toronto Press, 1974, pp.75-78.
10. Kohnke, P.C., ANSYS Engineering Analysis System Theoretical Manual, Swanson Analysis Systems, Inc., 1989.
11. Fluid Dynamics International, FIDAP Theoretical Manual, 1990.
12. Adams, D.F. and Tsai, S.W., "The Influence of Random Filament Packing on the Transverse Stiffness of Unidirectional Composites", *Journal of Composite Materials*, Vol. 3, July, 1969, pp.368-381.
13. Cai, Z. and Berdichevsky, A.L., "An Improved Self-Consistent Method for Estimating the Permeability of a Fiber Assembly", accepted by *Polymer Composites*, 1992.

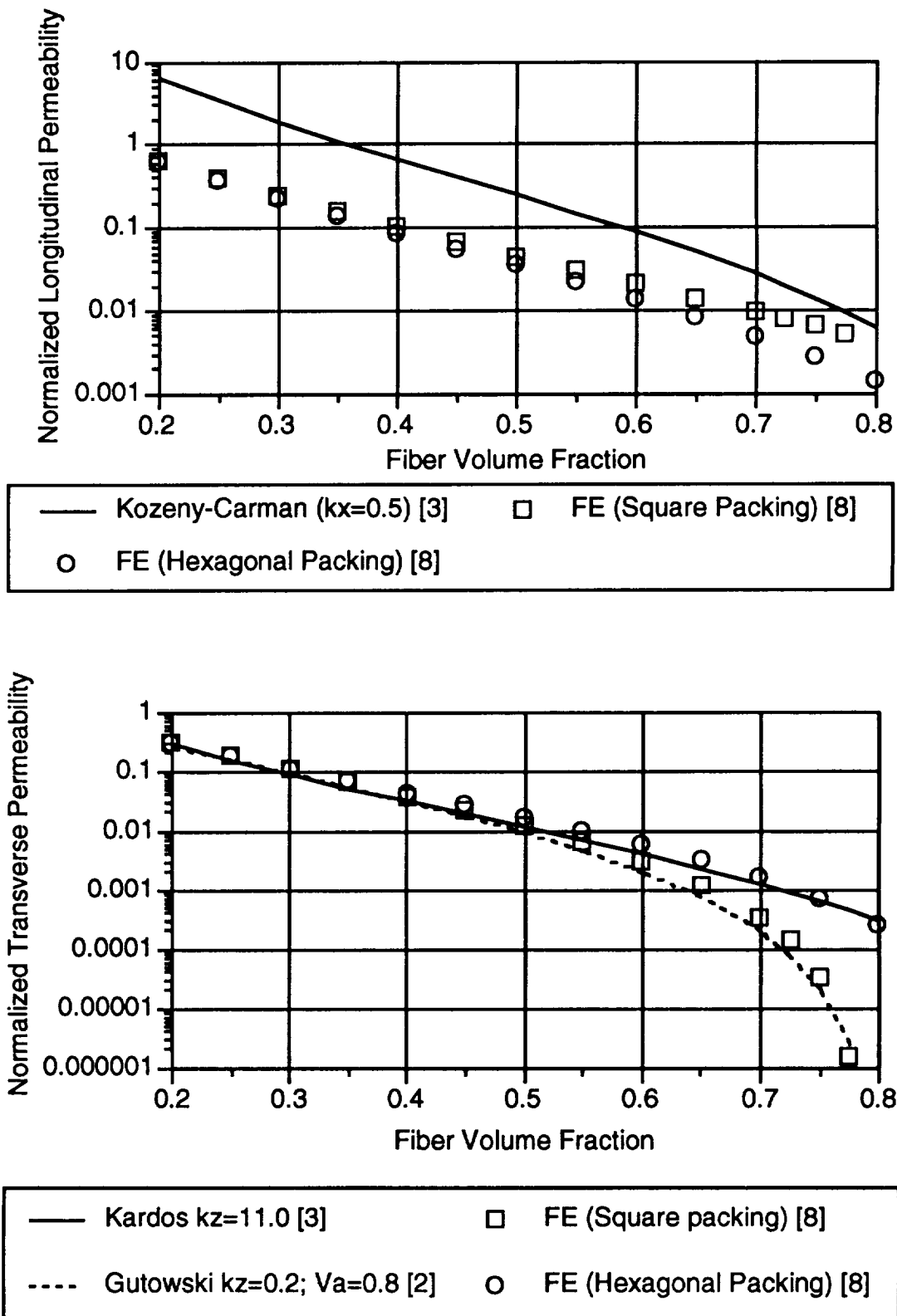


Fig. 1: Comparison of the permeability of idealized packing and other data.

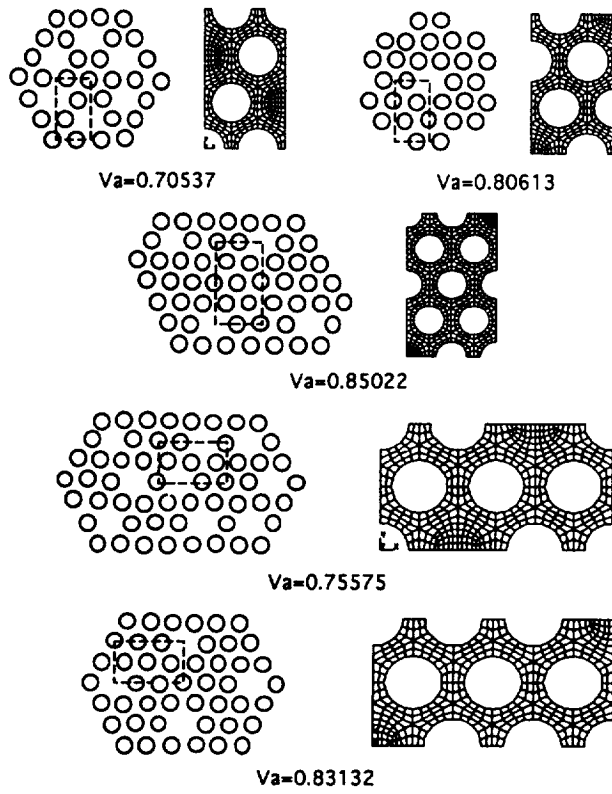


Fig. 2: Densely packed hollow hexagonal structures.

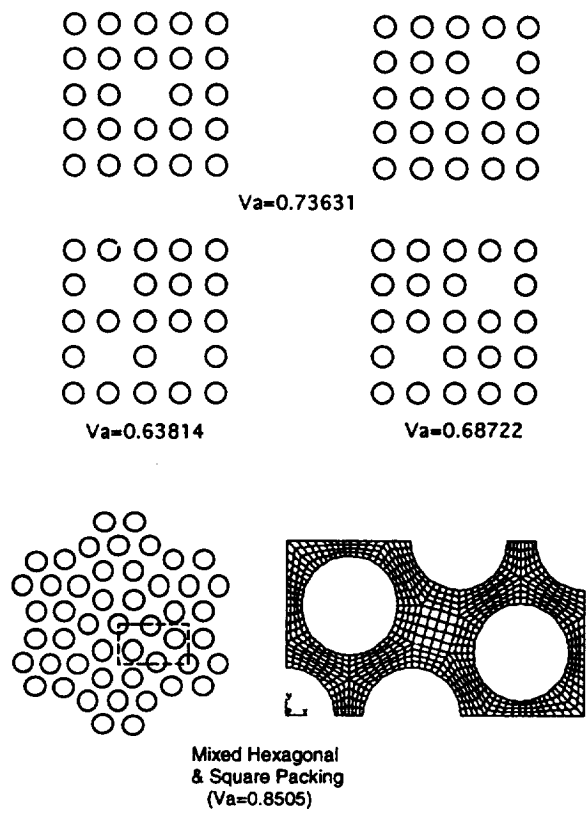


Fig. 3: Densely packed hollow square and mixed structures.

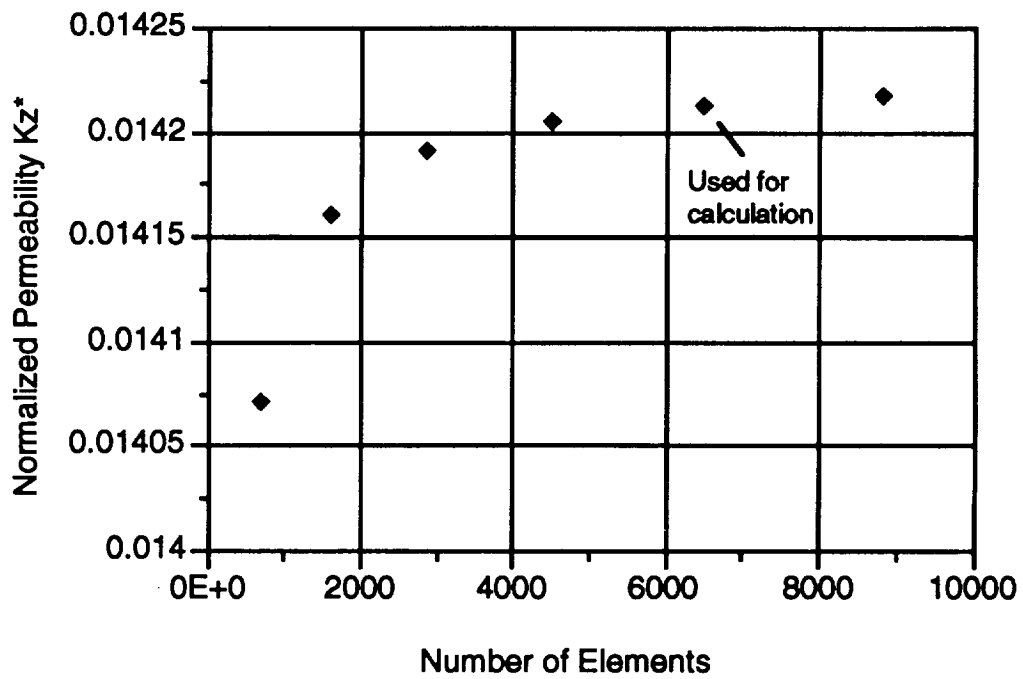
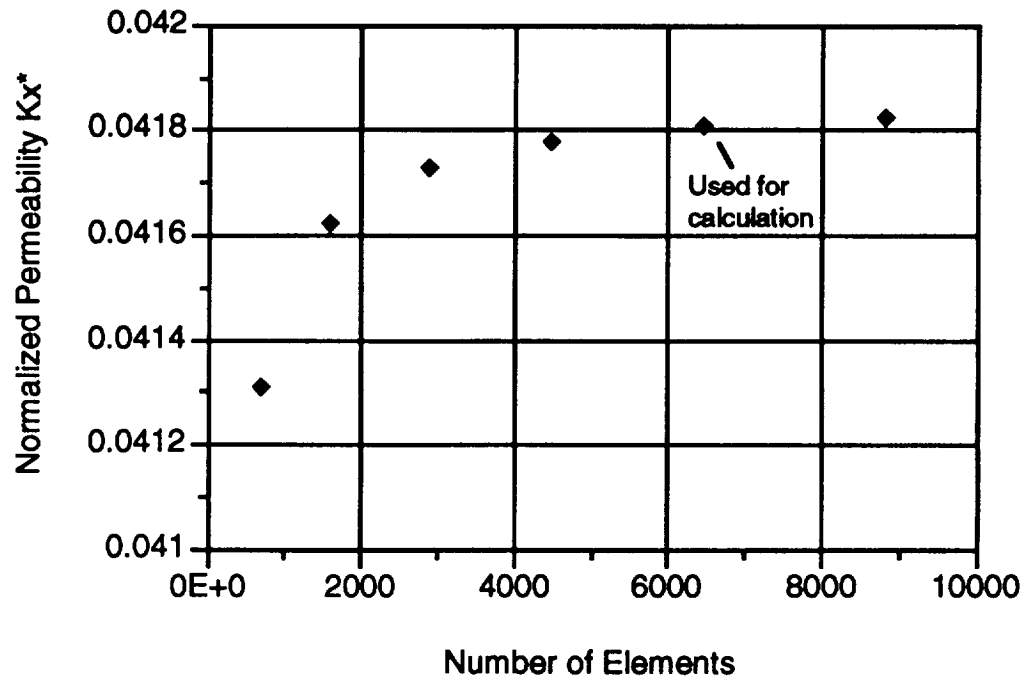
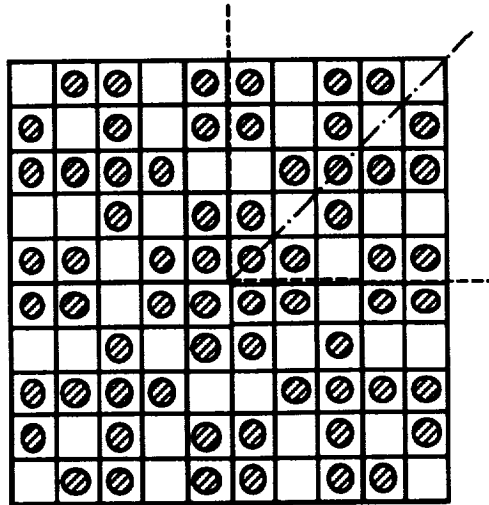
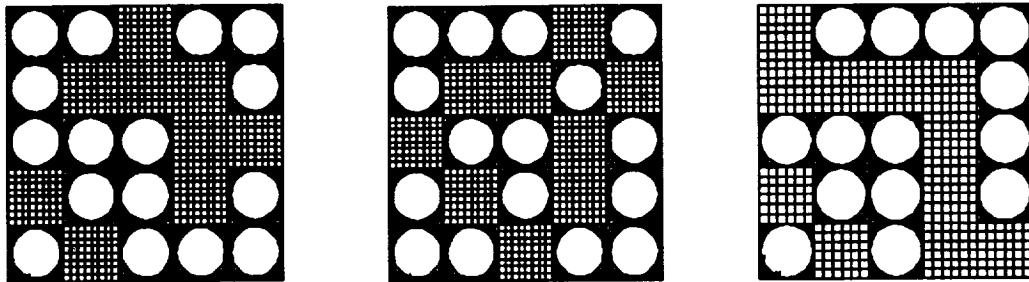


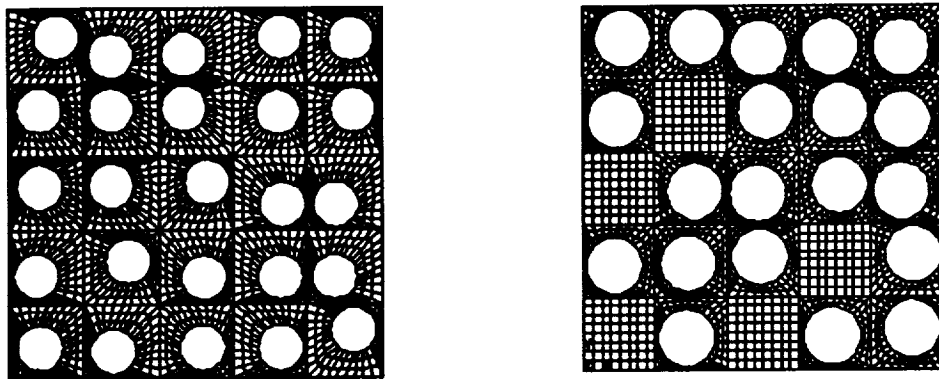
Fig. 4: Convergence of the numerical solution (with mixed packing model).



Computational Cell for "Random" Packing

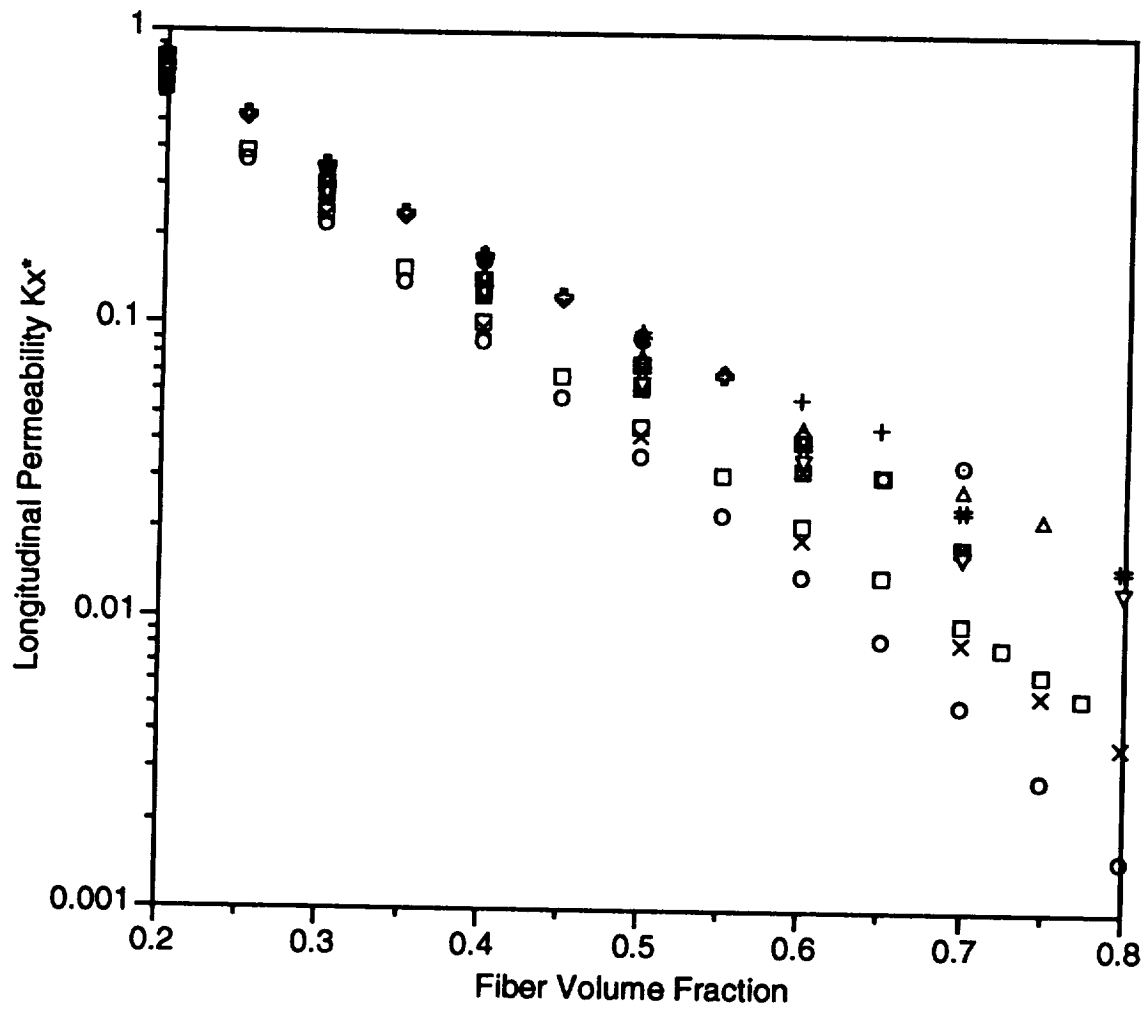


Randomly placed fibers



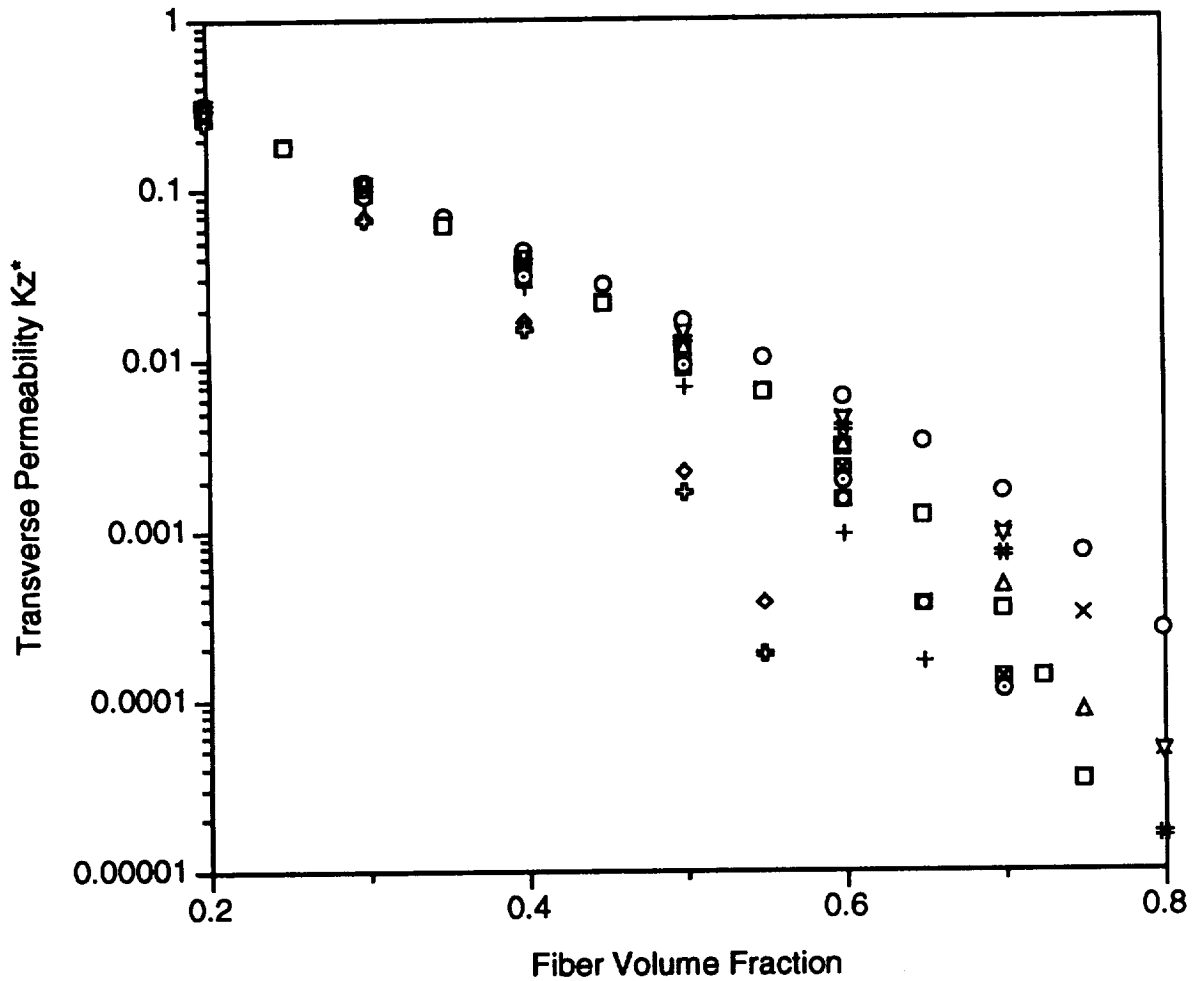
Fibers with random center positions

Fig. 5: Computational cell for "random" packing structures.



○ hex $V_a=0.9069$	× mixed $V_a=0.8505$	△ hol-hex $V_a=0.8061$
□ squ $V_a=0.7854$	■ hol-squ $V_a=0.7363$	▽ hol-hex $V_a=0.8502$
◇ hol-hex $V_a=0.6046$	◻ hol-squ $V_a=0.6872$	○ hol-hex $V_a=0.7558$
⊕ hol-squ $V_a=0.5891$	+ hol-hex $V_a=0.7054$	# hol-hex $V_a=0.8313$

Fig. 6: Normalized longitudinal permeability comparison.



○ hex $V_a=0.9069$	× mixed $V_a=0.8505$	△ hol-hex $V_a=0.8061$
□ squ $V_a=0.7854$	■ hol-squ $V_a=0.7363$	▽ hol-hex $V_a=0.8502$
◇ hol-hex $V_a=0.6046$	◻ hol-squ $V_a=0.6872$	⊙ hol-hex $V_a=0.7558$
⊕ hol-squ $V_a=0.5891$	+ hol-hex $V_a=0.7054$	# hol-hex $V_a=0.8313$

Fig. 7: Normalized transverse permeability comparison.

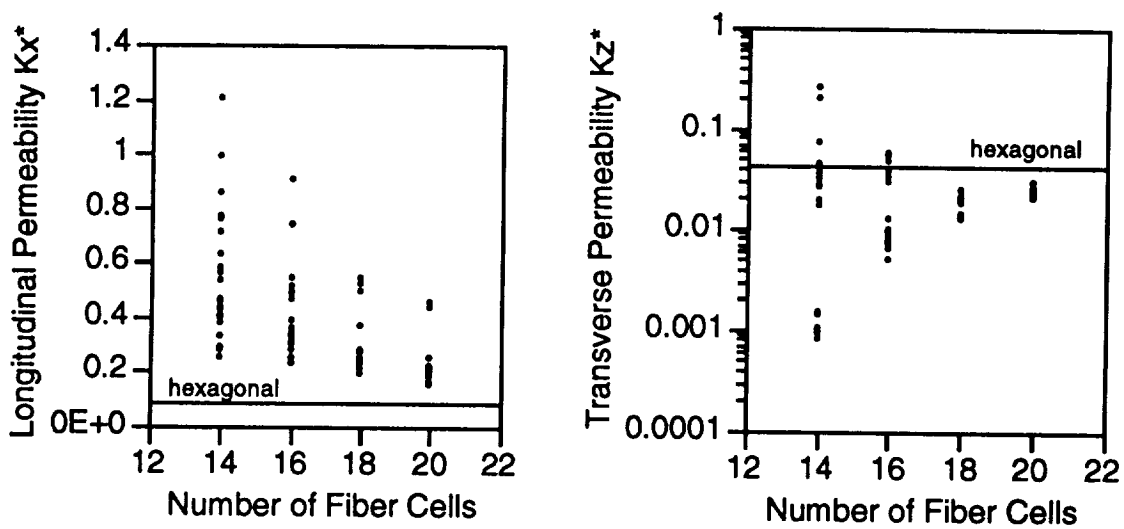


Fig. 8a: Permeability comparison with random model ($V_f=0.4$).

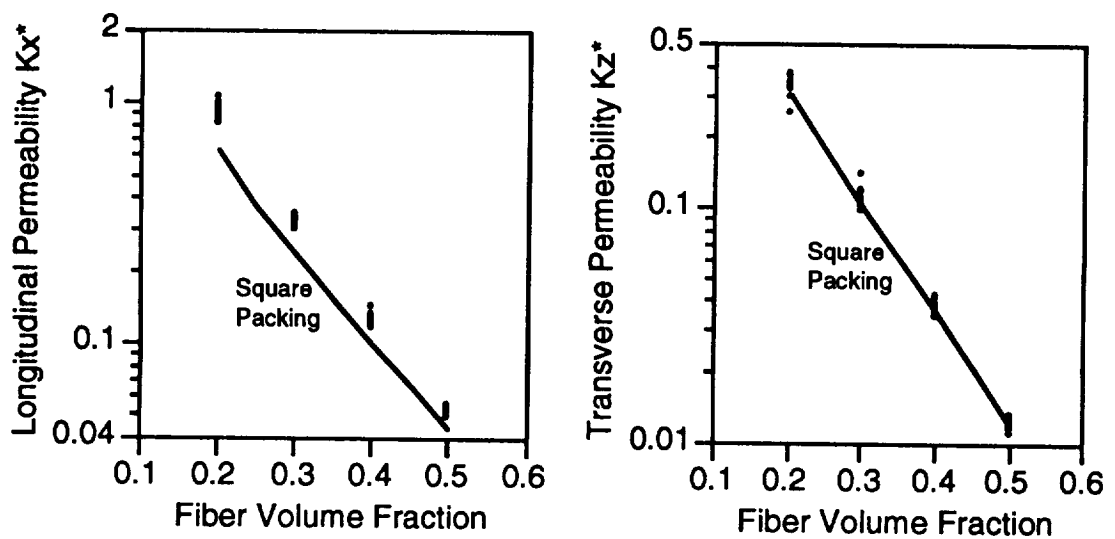


Fig. 8b: Permeability comparison of square packing with disturbances.



1994012385

1324

N94-16858

Characterization of Voids Formed During Liquid Impregnation of Nonwoven Multifilament Glass Networks as Related to Composite Processing

Anant D. Mahale, Robert K. Prud'homme and Ludwig Rebenfeld

TRI/Princeton, and Dept. of Chemical Engineering

Princeton University

Princeton, New Jersey 08544 USA

ABSTRACT

A technique based on matching the refractive index of an invading liquid to that of a fiber mat has been used to study entrapment of air ('voids') that occurs during forced in-plane radial flow into nonwoven multifilament glass networks. The usefulness of this technique is demonstrated in quantifying and mapping the air pockets. Experiments with a series of fluids with surface tensions varying from 28×10^{-3} to 36×10^{-3} N/m, viscosities from 45×10^{-3} to 290×10^{-3} Pa.s, and inlet flow rates from 0.15×10^{-6} to 0.75×10^{-6} m³/s, have shown that void content is a function of the capillary number characterizing the flow process. A critical value of capillary number, $Ca = 2.5 \times 10^{-3}$, identifies a zone below which void content increases exponentially with decreasing capillary number. Above this critical value, negligible entrapment of voids is observed. Similar experiments carried out on surface treated nonwoven mats spanning a range of equilibrium contact angles from 20° to 78°, have shown that there is a critical contact angle above which negligible entrapment is observed. Below this value, there is no apparent effect of contact angle on the void fraction - capillary number relationship described earlier. Studies on the effect of filament wettability, and fluid velocity and viscosity on the size of the entrapment (voids) have also been carried out. These indicate that larger sized entrapments which envelop more than one pore are favored by a low capillary number in comparison to smaller, pore level bubbles. Experiments were carried out on deformed mats - imposing high permeability spots at regular intervals on a background of low permeability. The effect of these spatial fluctuations in heterogeneity of the mat on entrapment is currently being studied.

INTRODUCTION

The resin transfer molding (RTM) process for fabricating fiber reinforced composites requires that a high viscosity liquid resin be forced to penetrate a dense fibrous network (woven or nonwoven). Incomplete penetration of the network by resin leads to permanent entrapment of air in the cured product which has a detrimental effect on its mechanical properties[1,2]. Air pockets entrapped during flow are referred to as 'voids' in keeping with the nomenclature followed by previous researchers. Volatiles arising from the resin system may also cause void formation, but we do not address voids of this nature. Voids of any kind are undesirable, since they act as stress-concentration sites and promote premature failure of the composite. The effects of voids on structural properties have been reported by previous researchers[2,3,4,5].

Voids have been classified as interstitial voids, planar voids (voids between layers of filaments), and general large voids (voids crossing many filament layers)[4]. An investigation on the origin of voids, especially interstitial voids, has been reported by Bascom and Romans[6]. Researchers have used techniques such as density measurements, water absorption, micrography, ultrasonic scan, and radiography to determine void

content. An appraisal and detailed description of these methods has been documented by Judd and Wright[2]. We have previously reported an optical technique for visualization and quantification of air pockets formed during liquid impregnation of a fiber network[7]. This technique involves using a liquid with refractive index identical to that of the filaments composing the network. Fibers in regions saturated with liquid are "optically" dissolved, revealing unoccupied space (voids) that can be distinguished by dark boundaries. A similar technique has been used for investigation of leaks in fiber glass reinforcement of pressure vessels [8]. In this paper we describe experimental work carried out on multifilament glass fiber networks using this technique to study the effect of process variables, fluid properties, and network characteristics on the quantity and nature of air entrapment.

NOMENCLATURE

h	= spacing between plates of flow-cell [mat thickness]
m	= mass per unit area of mat (Kg/m^2)
m_t	= total mass of mat (Kg)
v	= interstitial velocity of liquid (m/s)
Δx	= fluctuation in value of x (units of x)
V_g	= Volume occupied by glass filaments (m^3)
V_t	= Total volume occupied by glass mat (m^3)
V_h	= Total volume occupied by holes or artificially created pores in the glass mat (m^3)

Greek

ϵ	= bulk porosity (-)
ϵ_h	= porosity due to large holes or artificially created pores(-)
ϵ_p	= porosity due to ordinary pores(-)
γ	= surface tension of liquid (N/m)
μ	= viscosity of fluid (Kg/m.s)
θ	= equilibrium advancing contact angle (radians)
ρ_g	= density of glass filaments (Kg/m^3)

EXPERIMENTAL METHODS

In-plane Radial Flow Experiment

A radial in-plane flow geometry is chosen for studying air entrapment under constant inlet flow rates. The main advantages of this geometry are that it closely emulates a 2-dimensional flow system, and that it provides a range of liquid velocities within the same experiment. For the flow rates used, the sample is sufficiently thin to eliminate gravity effects on liquid flow. The experimental system is shown in Figure 1. The system includes a syringe pump which is used to force the liquid through a center-hole into a nonwoven network compressed to a known thickness between parallel glass plates. The refractive index of the invading liquid is adjusted to be equal to that of the glass filaments in the network in order to reveal unoccupied space (voids) that are distinguished by dark boundaries[7]. Motion of the invading liquid, made visible by a light source below the flow apparatus, is captured through a microscope by a camera placed vertically on top, and recorded in real time. The apparatus is placed on a horizontal open linear motion X-Y stage, programmed to scan the network after complete impregnation with liquid. The experimental procedure is described in detail below:

- (i) A centerhole, 0.3 cm diameter, is punched into a 15 cm x 15 cm nonwoven glass filament network (supplied by PPG Industries, P.O.Box 2844, Pittsburgh, PA 15230) which is compressed between two clear glass plates with clamps. Spacers of known thickness are placed on two opposing sides of the mat.
- (ii) The stainless steel syringe (3.18 cm diameter, 25.4 cm stroke, Dev-Air Corp., P.O.Box 30, Paoli, PA 19301) is filled with the refractive-index matching liquid, with care to avoid entrapment of air bubbles in the syringe and connecting flow lines.
- (iii) Setting on the syringe pump (Harvard Apparatus Co. Dover, Mass., Ser No: 6091) is adjusted to the required flow rate.
- (iv) A CCTV camera (Sanyo, VDC 3800 Video Corp. of America, P.O.Box 5480, 7 Veronica Ave., Somerset, NJ 08873) is used with a television zoom lens (Tokina, 12.5-75 mm, F1.8, 6X). Intensity of the light source is adjusted to obtain a sharp picture of the mat on a 13 inch television monitor. Experiments are carried out in a darkened room to avoid reflection of external light from the glass surface.
- (v) Outlet of the syringe pump is connected to a pneumatically operated three way valve which toggles between the flow-cell inlet and purge. A light emitting diode (LED) is used to indicate when the the flow-cell inlet is connected to the pump. This is placed in the field of view of the CCTV camera which records the experiment on a VCR (Panasonic Omnivision VHS-9600).
- (vi) Before beginning the experiment, all lines are completely filled with the operating fluid up to the centerhole of the fiber mat. The three-way valve is positioned so as to isolate the flow-cell (LED off) and the video recorder and pump are started. The valve is then switched, turning the LED on to indicate flow of liquid into the network. Flow is continued until the entire mat is saturated with liquid. The video recorded experiment enables one to analyze temporal data in the form of radial position of the fluid front as a function of penetration time which gives the interstitial velocity as a function of radial position.

The analysis of recorded experiments utilizes an image analysis system developed at TRI/Princeton, which combines image acquisition hardware with prepackaged libraries of graphics routines and data manipulation programs.

Void Analysis

The quantity of entrapped air at any location is expressed in the form of a void fraction, which is defined as a ratio of the volume of air entrapped to the total volume. Volumes are calculated by multiplying the measured area of the air pocket by the thickness of the mat. The air pockets are assumed to extend across the thickness of the mat in this calculation. In case of small bubbles, this assumption gives an overestimate of the actual void fraction.

Other information about voids includes their size distribution. For this purpose, three size ranges are chosen as follows:

$x_1 = [N_1/N_t]$ - Ratio of the number of entrapments in the range of sizes less than $0.32 \times 10^{-9} \text{ m}^3$ per unit area of mat to the total number of bubbles per unit area. This is a range of sizes extending up to about ten times the mean pore size in the mat [$0.02 \times 10^{-9} \text{ m}^3$].

$x_2 = [N_2/N_t]$ - Ratio of the number of entrapments in the range of sizes from $0.32 \times 10^{-9} \text{ m}^3$ to $1.9 \times 10^{-9} \text{ m}^3$ per unit area of mat to the total number of bubbles per unit area.

$x_3 = [N_3/N_t]$ - Ratio of the number of entrapments in the range of sizes greater than $1.9 \times 10^{-9} \text{ m}^3$ per unit area of mat to the total number of bubbles per unit area.

The experimental procedure for void analysis is as follows:

(i) The CCTV camera with an 8X magnification lens is mounted on the eyepiece of a microscope (Olympus) with a magnification range of 0.7 to 4.0 and is used for photographing the network at a total magnification of 645X. At this magnification, the smallest measurable air pocket is of size $0.1 \times 10^{-6} \text{ m}^2$ within an error of 5%. Assuming air pockets to be cylindrical, with height equal to that of the spacing between the plates of the flow cell, the measured area of air entrapment corresponds to a void volume of $0.05 \times 10^{-9} \text{ m}^3$. Smaller air pockets can be identified but cannot be quantified without greater experimental error.

(ii) The horizontal open frame linear motion stage (Daedal Inc., P.O.Box G, Harrison City, PA 15636) is programmed to scan and photograph the saturated network to provide a record of each frame for subsequent analysis. The total domain of study is a $0.112 \text{ m} \times 0.121 \text{ m}$ rectangle.

(iii) The recording of the experiment is played back and a frame is captured on the RGB monitor for study. Each micrograph of the high magnification scan obtained in the experiment is analyzed to obtain the area covered by voids. This is done by enclosing each void by a boundary, filling it with black pixels, and counting the enclosed pixels. This procedure is repeated for all voids in each frame.

(iv) The radial position of each micrograph is taken as the distance of its center from the center hole. Void areas measured at equal radial positions are arithmetically averaged to obtain the mean void area at that radial position. This gives the void fraction as a function of radial position and liquid velocity.

(v) In the analysis of each micrograph, a classification table is maintained to record the size distribution of air entrapments. Data from micrographs at the same radial position are averaged to obtain a relationship between void sizes and fluid velocity.

Characterization of Fluids

Refractive index, viscosity and surface tension characterize the fluids used in the experiments. Wettability of filaments composing the network can be quantified in terms of an equilibrium contact angle formed by the liquid meniscus with the solid surface.

Aqueous zinc iodide solutions were found to give refractive indices in the range of that of glass, depending upon concentration. These solutions were observed to be effective in detecting air pockets, but were not used due to their corrosive character. A series of refractive index matching fluids (manufactured by R.P.Cargille Labs. Inc., Cedargrove, NJ, USA) were used in the flow experiments. In order to adjust the refractive index of the operating liquid to match that of the glass fiber mat, a blend of two optical fluids was used. The liquids used were Cargille 5040 with refractive indices of 1.475 and 1.570 (at 25°C and 5893 Å). A blending correlation was obtained for these through experiments. It is given by

$$\kappa_{\text{mix}} = \kappa_1 \phi_1 + \kappa_2 \phi_2$$

where κ_{mix} is the refractive index of mixture, and κ_i and ϕ_i are the refractive index and volume fraction of the i^{th} solution, respectively. Chloroparaffins (manufactured by Dover Chemical Corp., Dover, OH 44622) with

refractive indices close to those of the optical solutions were blended with the optical solutions to vary the solution viscosities[7].

Liquid viscosity was measured using a Couette geometry on a fluids spectrometer (Rheometrics Inc.) at four shear rates. The fluids were Newtonian; i.e., the viscosities were found to be independent of shear rate.

Wettability of the glass filaments was altered using fluorosurfactant surface treatments on the networks. Surface tension of the liquid and wettability of the filaments were determined using a modified Wilhelmy wetting force measurement technique that has been previously described[9].

Network Characteristics

The nonwoven multifilament glass network is characterized in terms of the following parameters:

Average or bulk porosity (ϵ):

$$\epsilon = 1 - \frac{m}{\rho_g h}$$

where m is mass per unit mat area, ρ_g is the density of the glass filaments, and h is the spacing between the plates of the radial flow cell (mat thickness). Average porosity of the mats fluctuated within about 4-5% (Appendix 1).

Average permeability:

This was determined using the TRI radial in-plane permeability measurement technique[10]. The mats used were found to be isotropic with an average permeability of about 1000 darcy.

Pore Volume Distribution:

Pore structure of the mats was characterized by the liquid extrusion method on the TRI Pore Volume Distribution apparatus[11].

EXPERIMENTAL WORK

Radial in-plane flow experiments were carried out at constant inlet flow rates using three types of mats. These differed in their average filament diameter, and the type of surface sizing. Refractive indices of the filaments ranged between 1.550 and 1.552 for the three mats. Care was taken in choosing samples to minimize variability in their average porosity. Mats of type I were compressed to a thickness of 0.05×10^{-2} m corresponding to a porosity of 0.76, and similarly those of type II and type III, to a thickness of 0.08×10^{-2} m corresponding to a porosity of 0.82 and 0.83 respectively. The experiments spanned a range of inlet volumetric flow rates from 0.15×10^{-6} to 0.75×10^{-6} m³/s providing a range of interstitial velocities. Liquid viscosities ranged from 45×10^{-3} to 290×10^{-3} Pa.s and surface tensions varied from 28×10^{-3} to 36×10^{-3} N/m.

Studies were carried out on mats of type III, after treating these with a series of surfactants. This changed the wettabilities of filaments composing the mats without varying the fluid properties or the network structure. The surface treatments were carried out by saturating a mat with a surfactant solution in a bath for 10 minutes, followed by air drying. The wettability of these treated surfaces was measured in terms of an equilibrium contact angle formed by the test fluid on the surface. Contact angle values ranged from 20° (wetting) to 78° (nonwetting). Table 1 summarizes the different surfactant solutions and the corresponding equilibrium contact angles formed by the test fluids with the filament surface after treatment. Measured contact angle values were averages taken over a random set of 5-6 filaments that were picked out of the surface treated mats.

An attempt was made to study the effect of spatial variations in permeability on air entrapments by imposing known deformities onto the already existing mat structure. Deformation and reorientation was imposed by impinging the mat on a regular rectangular grid of 3 mm. diameter pegs. The reoriented filaments were held in place by exposing the mat to vapors of super glue in the presence of moisture. A schematic of this apparatus is shown in Figure 2. The resultant mat had a uniform spatial distribution of large pores at the location of pegs imposed on the isotropic random structure.

RESULTS AND DISCUSSION

Effect of Capillary Number

Forced flow through fiber networks results from a combination of viscous and surface tension effects. A dimensionless number quantifying the relative magnitude of viscous forces to interfacial forces is the capillary number (Ca) which is defined as follows:

$$Ca = \frac{\mu v}{\gamma}$$

where μ is viscosity, γ is surface tension, and v is interstitial velocity of fluid.

Velocity and viscosity effects on the extent of entrapment, when combined through the capillary number, collapse on to single master curves for mats I, II and III. These are shown as plots of void fraction as a function of capillary number in Figures 3,4 and 5. For all three mat types there is a critical value of capillary number which identifies a zone below which void content increases exponentially with decreasing capillary number. Above this value, negligible entrapment is observed. The critical capillary number at the onset of void formation is 2.5×10^{-3} . Although the volume fraction of trapped voids is roughly comparable for mats I, II and III, the voids in mat II are larger than those in mats I and III. There is also more variability in the results for mat II than for mats I and III.

Sizes of the entrapped regions spanned a wide range, from tiny spherical bubbles (completely trapped in single pores) to larger irregular shaped zones (encompassing several pores). The number fraction of small entrapments [x_1] increases with increasing fluid velocity. At the same time the number fraction of intermediate sized regions [x_2] and the number fraction of larger sized regions [x_3] decreases with increasing fluid velocity, as shown in Figures 6,7 and 8. Viscosity of the liquid also has a strong influence on x_i as shown in Figure 9.

The data from Figure 9 collapse onto a single curve when the velocity and viscosity effects are combined in terms of the capillary number, as shown in Figure 10. Comparable curves for x_2 and x_3 are shown in Figures 11 and 12. Lower capillary numbers favor formation of larger sized entrapments as opposed to the smaller sized ones. The smaller sized entrapments are of the order of the mean pore size in the mat. These entrapments are usually located completely inside a pore and are spherical in shape. Larger sized entrapments span more than a single pore.

Effect of Filament Wettability

It is known from previous work in fluid displacement mechanics in porous media that there is a significant difference between wetting displacement ($\cos \theta = 1$) and non-wetting displacement ($\cos \theta = 0$)[12]. Studies have indicated that poor resin wettability of commercial finished filaments resulted in an increase in the formation of voids[6]. Reducing the contact angle to zero and/or oscillating the tension in the strand as it passed through the resin markedly reduced the number of voids.

Flow experiments carried out using surface treated mats covered a range of contact angles between 20° and 78° . Figure 13 shows void fraction as a function of capillary number for different surface treatments. As seen from these plots, no particular trend in the slope of the curve or in the critical capillary number value is

observed with respect to the surface wettability up to an angle of 57°. Beyond this, as the angle approaches 90°, air entrapment drops to zero; within the same range of capillary numbers. This suggests a critical transition between a zone of entrapment to that of no entrapment as the surface wettability of the filaments composing the mat structure decreases. This result along with the observations of Bascom and Romans[6] suggests that entrapment is high under conditions of extremely low as well as extremely high wettabilities; and is minimal at intermediate contact angles that are close to 90°. Local nonuniformities are one cause of entrapment. The local shape of meniscus between filaments is flatter and has less curvature at contact angles close to 90°, whereas it is sharply curved for angles close to 0° and 180°.

A study carried out on the effect of filament wettabilities on the size distribution of entrapped zones indicates that size distribution data for the range of capillary numbers obtained for different surface wettabilities collapses onto a single curve when plotted against a modified capillary number.

The modified capillary number is expressed as given below:

$$Ca = \frac{\mu v}{\gamma \cos \theta}$$

where θ is the equilibrium contact angle made by the liquid with the filaments composing the network. Experimental data indicating the effect of modified capillary number on void sizes are given in Figures 14, 15 and 16.

Effect of Mat Structure:

The nonwovens used here have groups of filaments bundled together. These bundles are placed randomly to create a structure having a bimodal pore volume distribution, as shown in Figure 17. The smaller pores are created by the spacing between filaments. The larger ones are the pores between multifilament bundles.

In the process of deforming and reorienting the pore structure with the grid of pegs, the filaments are relocated to create open spaces or holes. Hence the structure is modified to have three types of pores. The original bimodal structure still exists along with a third type of pores created by the pegs. The pore volume distribution plot for this deformed network is also shown in Figure 17. The third peak representing the newly created pores is not observed in this measurement. Calculation using the dimensions of the grid indicates that the total volume of large pores created in this restructuring process is 8% of the total pore volume (Appendix 2). The deformation therefore, is insufficient to appear as an additional peak in the pore volume distribution diagram. The results of flow experiments on these deformed mats is the same as those on undeformed mats. These are shown in Figure 18; and simply reproduce results from experiments carried out on undeformed samples that are shown in Figure 5.

CONCLUSIONS

The isorefractive index technique combined with an image analysis system was found to be an elegant method of quantifying air entrapment in glass filament networks. When applied to radial flow geometry, this technique was useful in mapping voids and hence relating them to interstitial velocity and viscosity of the penetrating liquid. The technique provides data that will be useful in designing impregnation and mold filling processes for the production of advanced composite materials. A critical capillary number for void formation was found to be 2.5×10^{-3} . Below the critical capillary number the volume fraction of trapped voids increases exponentially with capillary number. Surface wettability of filaments composing a nonwoven mat measured in terms of an equilibrium contact angle, affects the fluid flow mechanism. Experiments indicate that there is a critical contact angle between 57° and 78° above which air entrapment is minimal. Below this value, there is no change in the relationship between void fraction and capillary number. A modified capillary number that includes the equilibrium contact angle seems to control the mean size of entrapments. Definite answers are yet to be arrived at which would quantitatively express the effect of network properties on void formation.

ACKNOWLEDGMENT

The assistance of Mrs. Susan M. Montgomery of TRI/Princeton with the image analysis system is gratefully acknowledged.

APPENDIX 1

Estimation of bulk porosity variation:

Variation in bulk porosity is related to the variation in specific mass by:

$$[\epsilon + \Delta\epsilon] = 1 - \left[\frac{m + \Delta m}{\rho_g h} \right]$$

Maximum variation of mass in samples used with one operative liquid was 10 Kg/0.0225 m² [Δm] for an average mass of 70 Kg/0.0225 m² [m], ρ_g is of magnitude 2560.0 Kg/m³, and the smallest value of spacing [h] used was 0.05x10⁻²m.

Using these values, variation in bulk porosity is given by:

$$\frac{[\epsilon + \Delta\epsilon] - [\epsilon]}{[\epsilon]} \times 100 = \left[\frac{-\Delta m}{\rho_g h - m} \right] \times 100$$

= 4.6%

APPENDIX 2

Estimation of porosity created by deformation:

$$\epsilon = 1 - \frac{V_g}{V_t}$$

$$\epsilon h = \frac{V_h}{V_t}$$

$$V_g = \frac{m_t}{\rho_g}$$

Substituting in above the values of:

$$m_t = 7.4 \times 10^{-3} \text{ Kg}$$

$$\rho_g = 2.56 \times 10^3 \text{ Kg/m}^3$$

$$V_t = 225 \times 0.08 \times 10^{-6} \text{ m}^3$$

$$V_g = 225 \times 0.08 \times \pi \times (0.15)^2 \times 10^{-6} \text{ m}^3$$

$$\epsilon_t = 0.84$$

$$\epsilon_h = 0.06$$

Therefore the percentage of total porosity due to the deformation is given by:

$$\frac{\epsilon_h}{\epsilon_t} \times 100 = 7.1\%$$

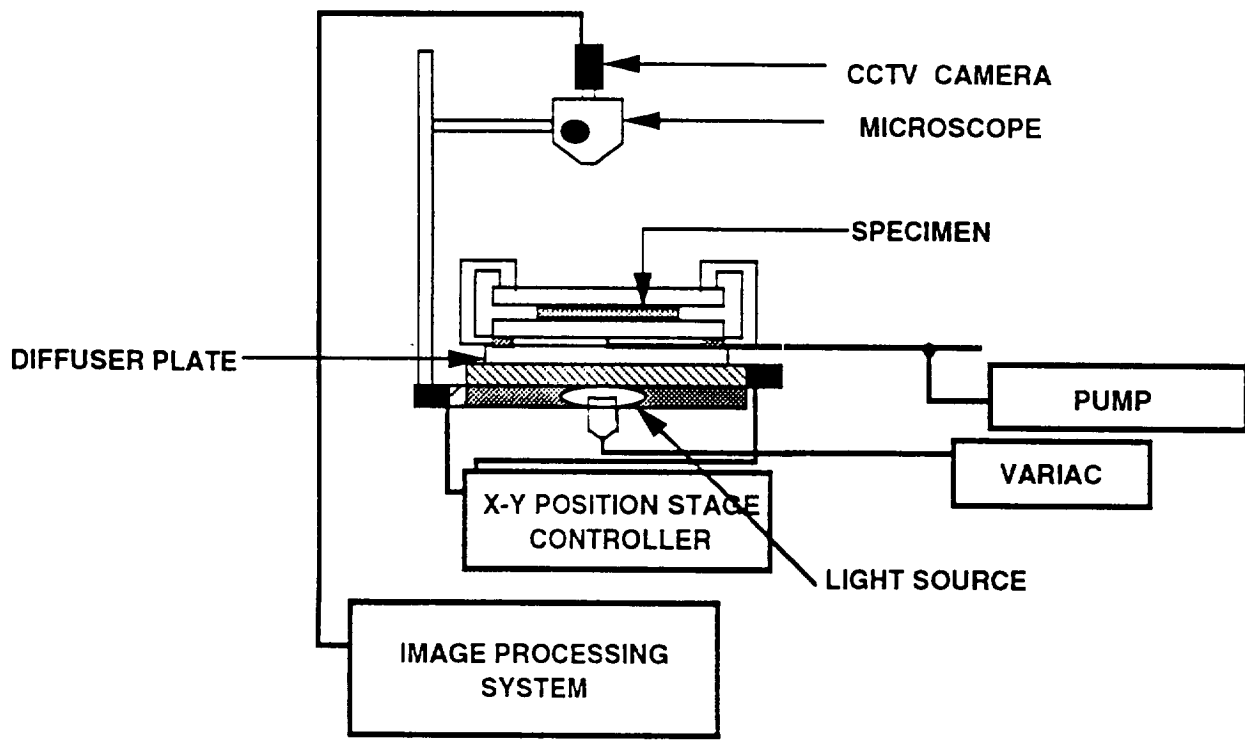
REFERENCES

1. E.J.Kohn, A.G.Sands and R.C.Clark, Ind. and Eng. Chem. Product Research and Development, 7, 179 (1968).
2. N.C.Judd and W.W.Wright, SAMPE, 14, No1, 10 (1978).
3. W.Hand, Proceedings of the 20th Technical Conference, SPI Reinforced Plastics Division, Section 1-E, Feb(1965).
4. J.T.Paul and J.B.Thomson, Proceedings of the 20th Technical Conference, SPI Reinforced Plastics Division, Section 12-C, Feb(1965).
5. I.Petker, Soc. Plastic Eng. Trans, 49 (1965).
6. W.D.Bascom and J.B.Romans, Ind. and Eng. Chem. Product Research and Development, 7, 172 (1968).
7. A.D.Mahale, R.K.Prud'homme, L.Rebenfeld, Polymer Eng. & Sci., 32, No 5, 319 (1992).
8. J.McAdams, Rev. Sci. Instrum. 59 (12), 2617 (1988).
9. B.Miller, in *Absorbency*, edited by P.K.Chatterjee (Elsevier, New York) (1985).
10. K.L.Adams, B.Miller, L.Rebenfeld, Polymer Eng. & Sci., 26, 1434 (1986).
11. B.Miller, I.Tyomkin, Textile Research Jnl., 56, No 1, 35 (1986).
12. D.Wilkinson, American Physical Society, Physical Review A., 34, No 2, 1380 (1986).

TABLE 1
SURFACE TREATED SAMPLES

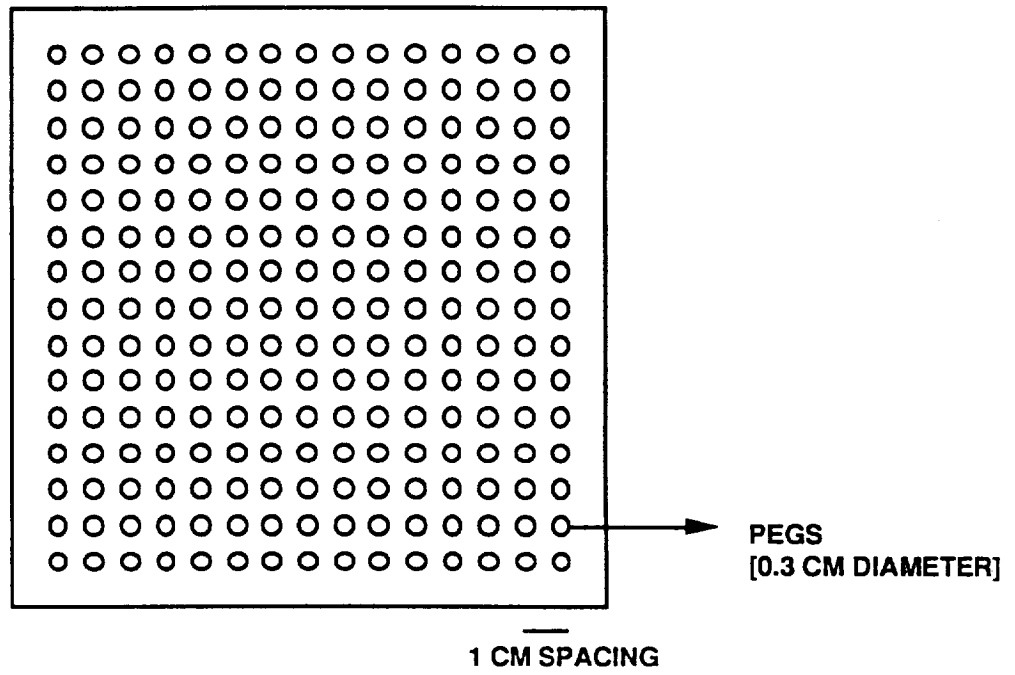
Viscosity = 48 cp. Surface tension = 34 dynes/cm.

cos θ	θ	Surface treatments used
0.2	78	100 ppm Zonyl FSC solution.
0.55	57	0.05% w/w Sodium Laurel Sulfate.
0.64	50	0.1% w/w Sodium Laurel Sulfate.
0.67	48	100 ppm Zonyl FSN solution.
0.90	25	no treatment.

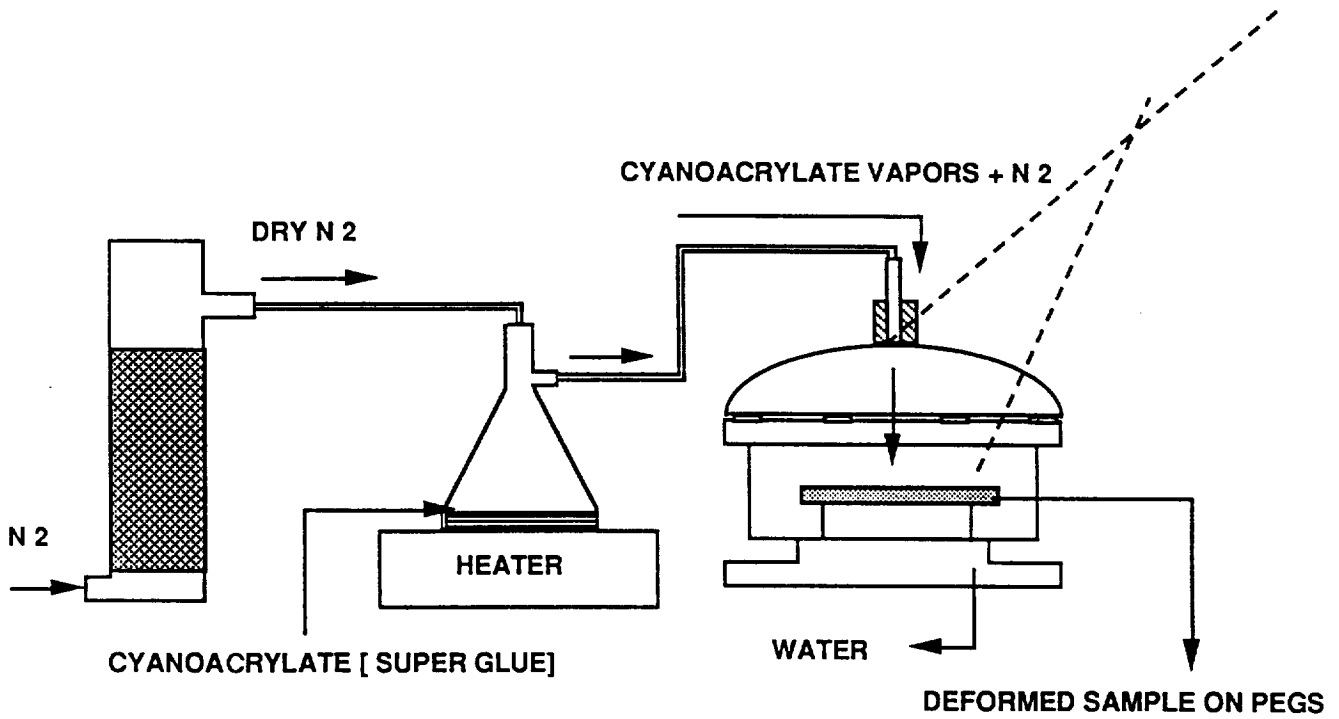


EXPERIMENTAL APPARATUS

FIG 1

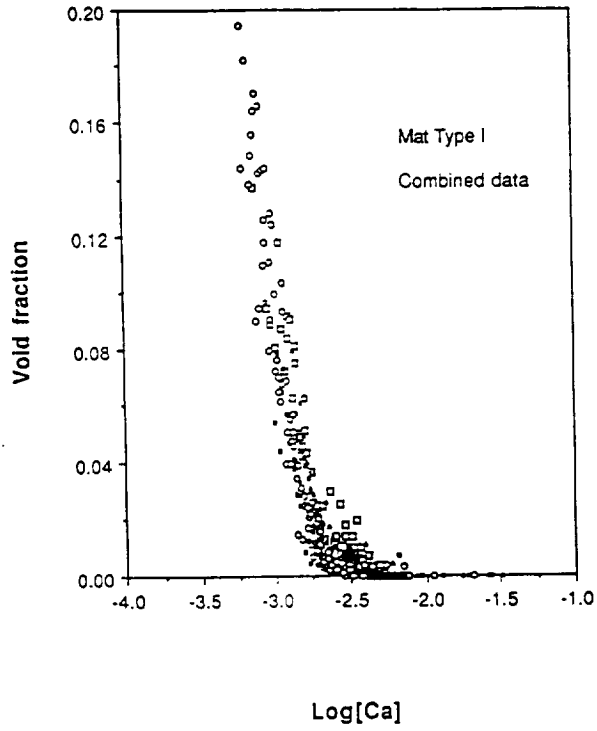


GRID OF PEGS



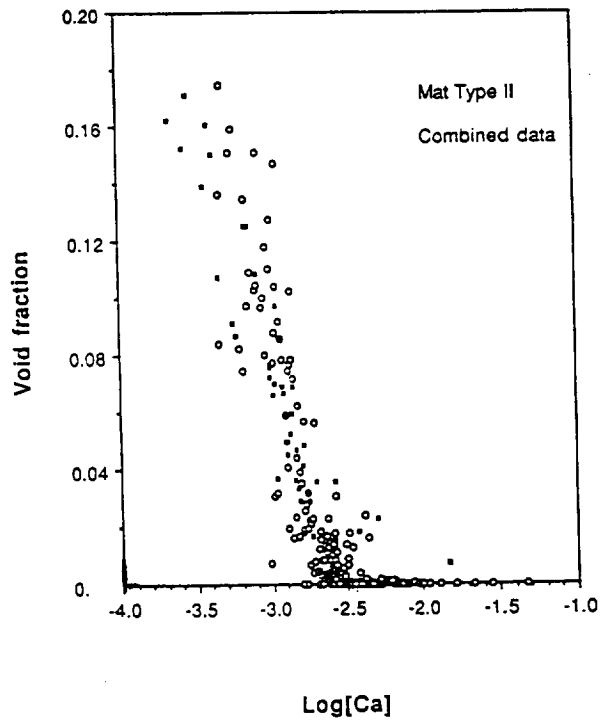
THE PROCEDURE FOR REORIENTATION OF MAT STRUCTURE.

FIG 2



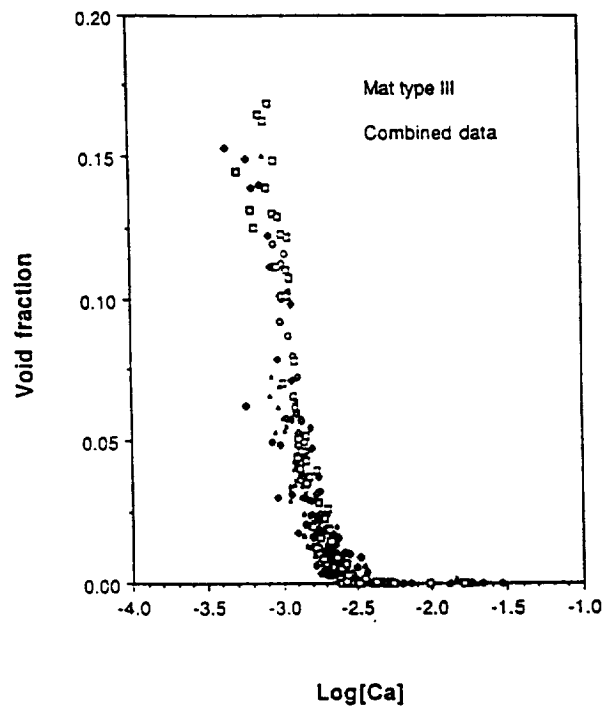
Void fraction vs Capillary number

FIG 3



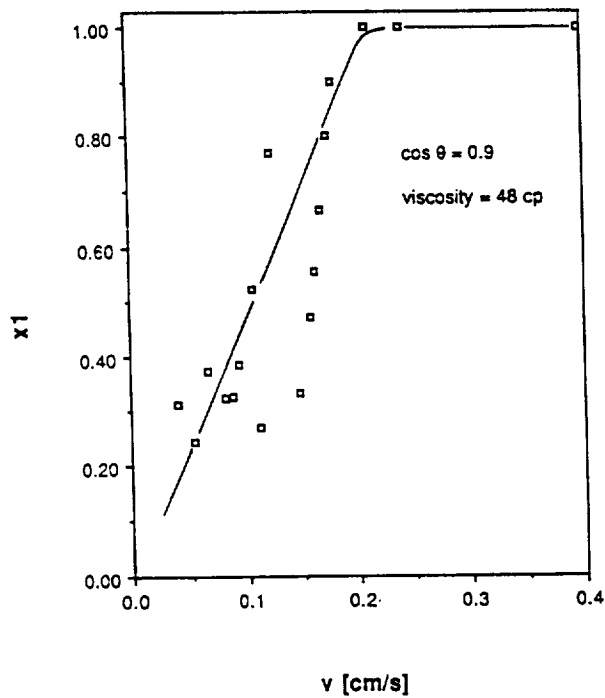
Void fraction vs Capillary number

FIG 4



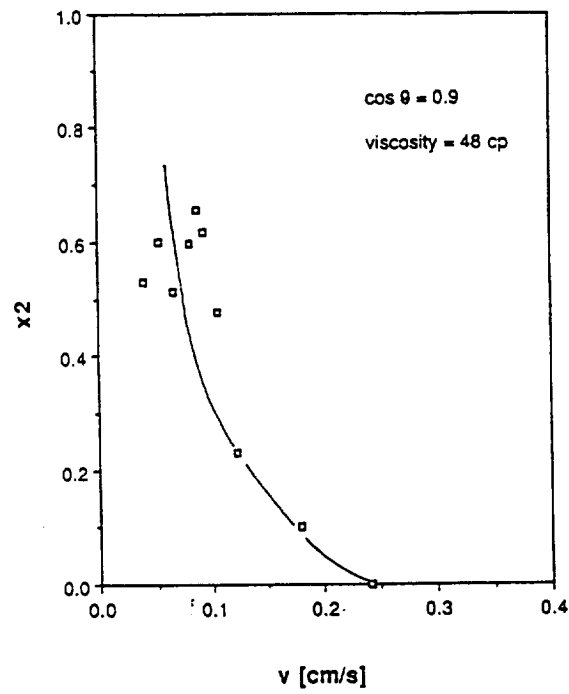
Void fraction vs Capillary number

FIG 5



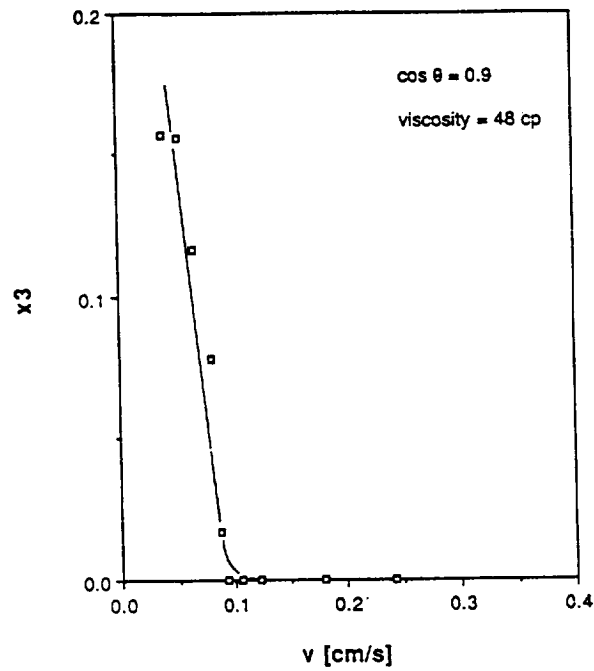
Fraction of total number of bubbles in the range of sizes < 0.32 mm³

FIG 6



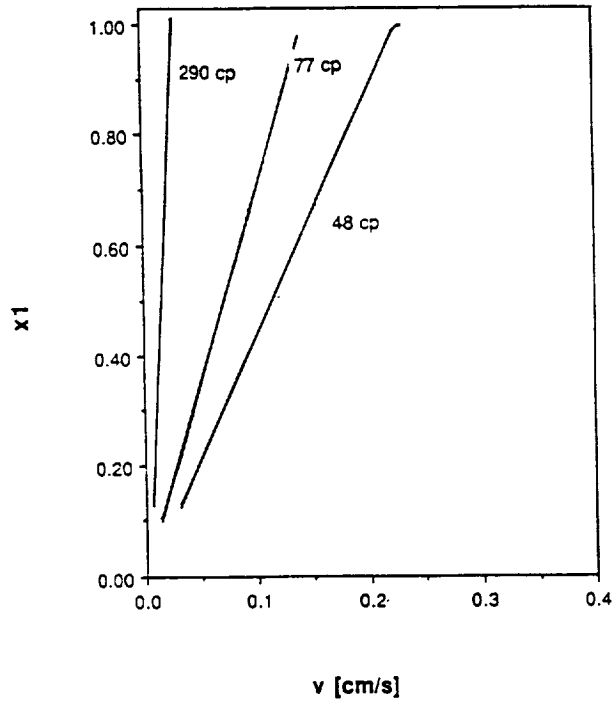
Fraction of total number of bubbles in the range of 0.32 - 1.9 mm³

FIG 7



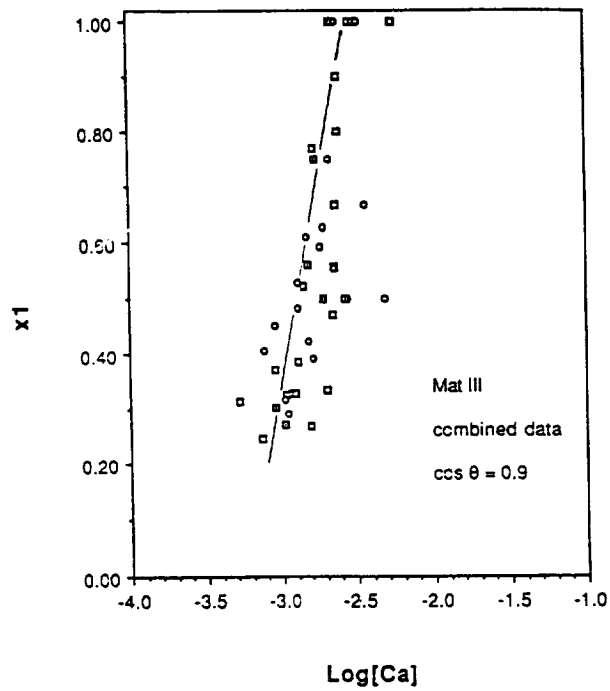
Fraction of total number of bubbles in the range of sizes > 1.9 mm³

FIG 8



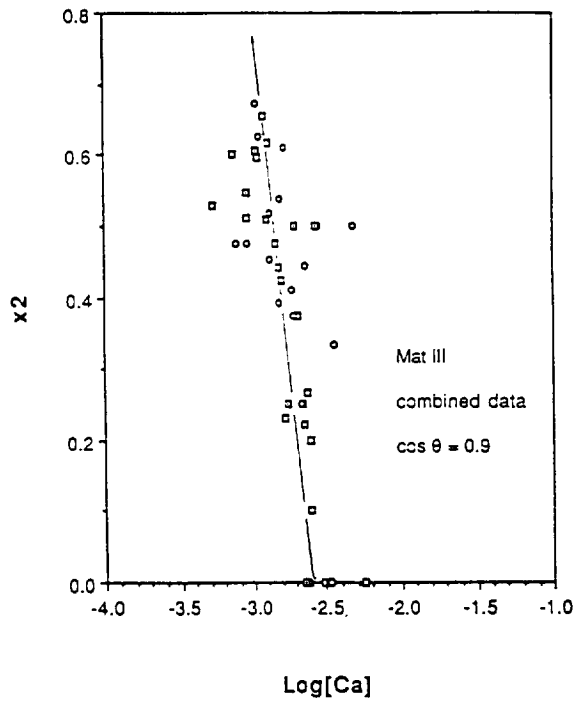
Fraction of total number of bubbles in the range of sizes < 0.32 mm³

FIG 9



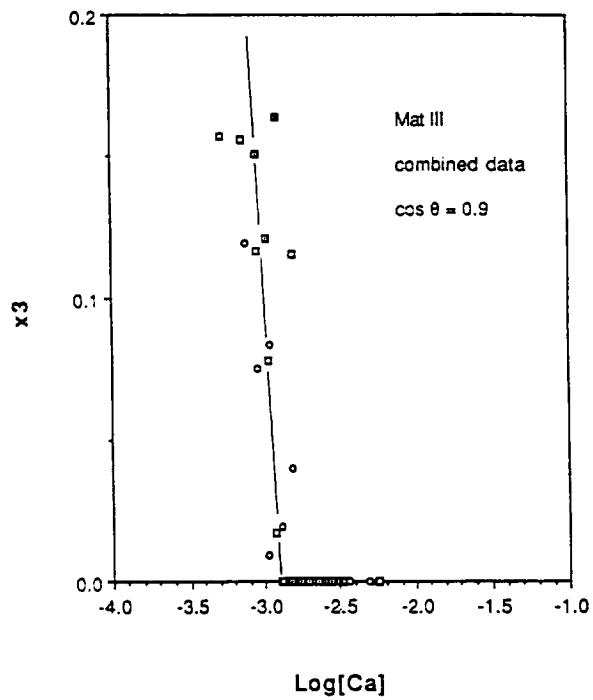
X1 vs Capillary number

FIG 10



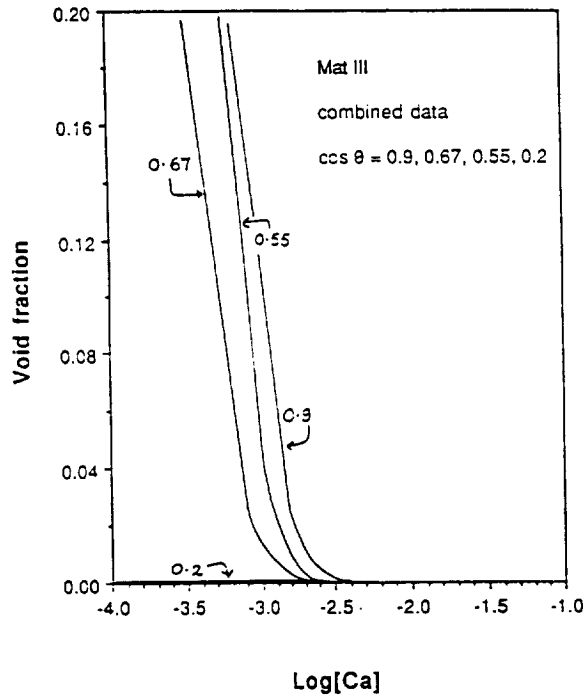
X2 vs Capillary number

FIG 11



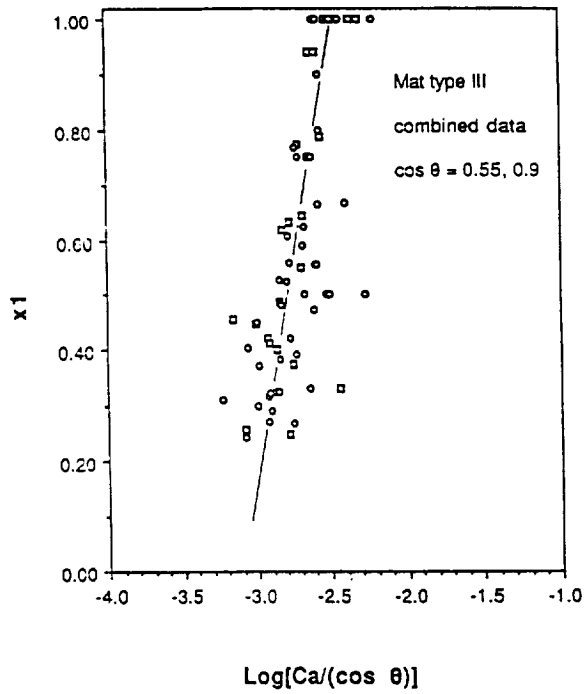
X3 vs Capillary number

FIG 12



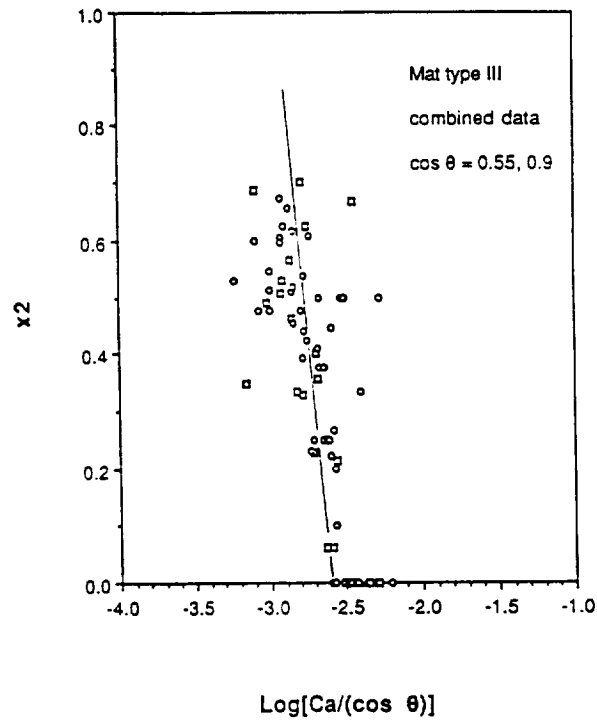
Void fraction vs Capillary number

FIG 13



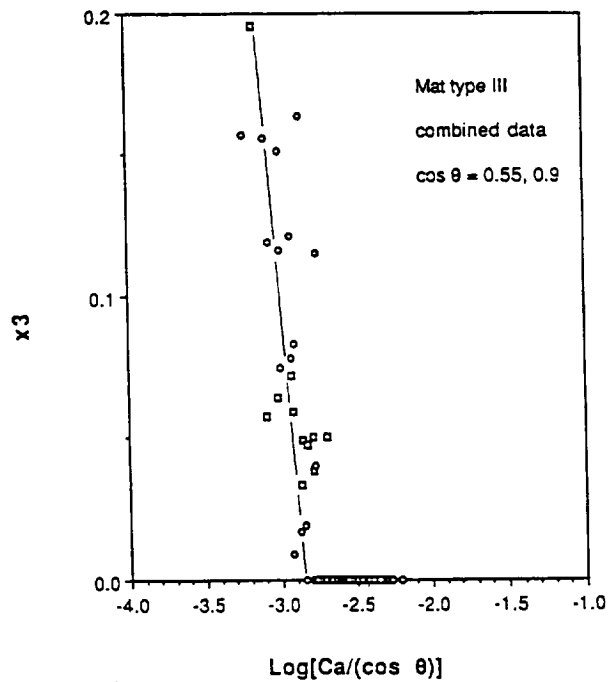
X1 vs Modified Capillary number

FIG 14



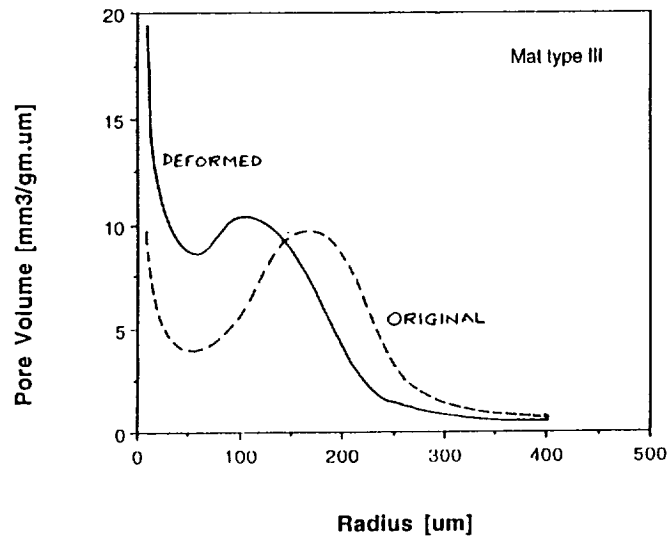
X2 vs Modified Capillary number

FIG 15



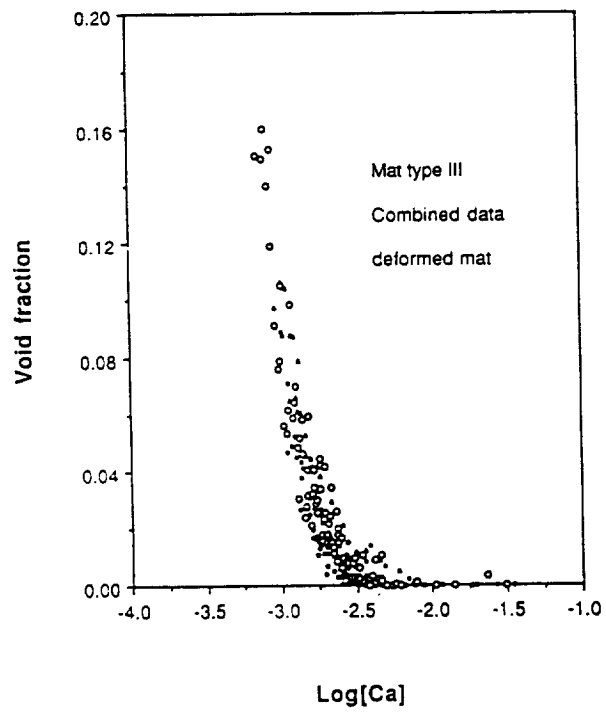
X3 vs Modified Capillary number

FIG 16



Pore Volume Distribution

FIG 17



Void fraction vs Capillary number

FIG 18

1994012386

N94-16859

**DEVELOPMENT OF BRAIDED FIBER SEALS
FOR ENGINE APPLICATIONS**

Zhong Cai, Rajakkannu Mutharasan, Frank K. Ko, Guang-Wu Du
Drexel University
Philadelphia, PA 19104

Bruce M. Steinetz
NASA Lewis Research Center
Cleveland, OH 44135

ABSTRACT

A new type of braided fiber seal has been developed for high temperature engine applications. Development work performed in this study includes seal design, fabrication, leakage flow testing, and flow resistance modeling. This new type of seal utilizes the high flow resistance of tightly packed fibers and the conformability of textile structures. The seal contains a core part with aligned fibers, and a sheath with braided fiber layers. Seal samples are made by using the conventional braiding process. Leakage flow measurements are then performed. Mass flow rate versus the simulated engine pressure and preload pressure is recorded. The flow resistance of the seal is analyzed using the Ergun equation for flow through porous media, including both laminar and turbulent effects. The two constants in the Ergun equation are evaluated for the seal structures. Leakage flow of the seal under the test condition is found to be in the transition flow region. The analysis is used to predict the leakage flow performance of the seal with the determined design parameters.

INTRODUCTION

The primary design of an engine seal is the prevention of hot engine flow path gases and potentially explosive hydrogen/oxygen mixtures from escaping through the seal and damaging the engine panel support and articulation system. A balanced-pressure seal system with positive purging can be designed which ensures engine flow path gases such as unburned hydrogen do not get behind to movable panels. Because pressure differential across the movable panels is minimized, the pressure loads supported by the seals are greatly reduced. An illustration of the seal application system is shown in Fig. 1. More detailed discussion is given in [1].

The general requirements for the seal system for such applications can be summarized as follows: a) minimize seal leakage; b) conform to and seal against distorted adjacent engine walls; c) operate in a high heat flux environment utilizing minimum coolant resources; d) maintain material stability in a chemically hostile hydrogen-oxygen environment; and e) minimize sliding damage over engine life.

New design concepts have been developed to satisfy the seal performance requirements. One of the choices is to use tightly packed fibers. Textile rope structures have long been used in packing materials and seals. Currently a large family of ceramic fibers is available for applications with high temperature and a hostile environment.

The objective of the current study is to evaluate the leakage performance of a range of braided fiber seal architecture/material configurations. The knowledge acquired through the development work provides a solid data base for various seal applications and for the further improvement of the design and fabrication of seals.

SEAL DESIGN AND FABRICATION

Based on the textile engineering experience, a core-sheath system is selected for the seal structure. This core-sheath structure is made by stuffing tubular fabrics with parallel fiber bundles, as shown in Fig. 1. The structure provides the high capacity for the incorporation of longitudinal fibers. Depending on the fiber architecture selected for the seal system, various levels of conformability, abrasion resistance and packing densities can be developed. Of the wide variety of fiber architectures, braided structures provide the highest level of conformability while maintaining a high level of structural integrity and fiber coverage. Therefore the fabrication process for this core-sheath structure is to braid the sheath on top of the aligned core fibers.

The proposed seal configuration consists of a core part of aligned ceramic fibers and a sleeve with braided ceramic or metallic fibers. In the application the leakage flow is transverse to the aligned fibers. When preload is applied transversely to the seal, these aligned fibers are compacted thus providing very high flow resistance. This design employs the conformability of the fiber structures and also utilizes the high temperature performance of ceramic fibers.

The conventional 2-D braiding method is used for the seal construction. As discussed in [2], 2-D braiding can produce a wide range of braiding angles ($\theta = \pm 10^\circ$ to $\pm 80^\circ$). The physical and mechanical behavior of braided structures depends upon the fiber orientation, fiber properties and fiber volume fraction. The governing equations for 2-D braiding are

$$d_o = \frac{N_{ys} A_{ys}}{\pi t_s V_{fs} \cos \theta} + t_s \quad (1)$$

$$d_i = \frac{N_{ys} A_{ys}}{\pi t_s V_{fs} \cos \theta} - t_s \quad (2)$$

$$d_o - d_i = 2 t_s \quad (3)$$

where d_o is the outside braid diameter, d_i is the inside braid diameter, t_s is the sheath thickness and usually t_s is much smaller than d_i and d_o . N_{ys} is the number of yarns in the sheath, A_{ys} is the nominal yarn cross sectional area along the yarn axis, and V_{fs} is the fiber volume fraction of the sheath. The number of yarns is related to the carrier number N_r , the sheath layer number N_L , and the number of yarns or plies on each carrier N_{yr} as

$$N_{ys} = N_r N_{yr} N_L \quad (4)$$

N_L is also the number of braiding passes in the operation.

As shown in Fig. 1, before installation or after braiding, the seal cross section is in a circular shape. After installation the seal shape becomes close to a rectangle. The dimensions of the rectangle are set by the application requirements. We assume the seal

width and height after the installation are w_s and h_s respectively; the area relation can be expressed approximately as

$$h_s w_s = \pi d_0^2 / 4 \quad (5)$$

From this relation, the nominal seal diameter d_0 can be determined. If the yarn number and yarn cross section area in the core N_{yc} and A_{yc} are chosen, the overall porosity of the seal is

$$\epsilon = 1 - V_f = 1 - \frac{N_{yc} A_{yc} + N_{ys} A_{ys} / \cos \theta}{\pi d_0^2 / 4} \quad (6)$$

The relation for the core fiber volume fraction V_{fc} is

$$N_{yc} A_{yc} = V_{fc} (\pi d_i^2 / 4) \quad (7)$$

The sheath layer thickness t_s is related to the braiding operation parameters, such as braiding angle, yarn tension, and sheath layer number. Usually t_s needs to be estimated empirically. The other important seal design parameter, the core percentage of the fiber volume, can be calculated as

$$V_c = \frac{A_{fc}}{A_{ft}} = \frac{A_{fc}}{A_{fs} + A_{fc}} \quad (8)$$

where A_{fc} and A_{fs} are the fiber cross section area along the seal axis for the core and the sheath respectively, and can be calculated as

$$A_{fc} = N_{yc} A_{yc} \quad (9)$$

$$A_{fs} = N_{ys} A_{ys} / \cos \theta \quad (10)$$

We should emphasize that all the calculations involved above are for the nominal values only. Since the yarn size changes during the braiding operation, the final dimension of the seal may vary depending on the fabrication conditions.

LEAKAGE FLOW ANALYSIS

The problem of flow through porous media can be described by the Ergun equation [3, 4]. The differential form of the Ergun equation is

$$-\frac{dp}{dx} = C_L \frac{\mu q (1 - \epsilon)^2}{D_p^2 \epsilon^3} + C_T \frac{\rho q^2 (1 - \epsilon)}{D_p \epsilon^3} \quad (11)$$

where p , μ , and ρ are fluid pressure, viscosity, and density respectively, q is the average flow rate, ϵ is porosity of the medium, and D_p is the characteristic particle dimension. The two dimensionless constants C_L and C_T account for the viscous and turbulent effect respectively, and are determined semi-empirically. For the packed spherical particles, D_p is chosen as the sphere diameter, and C_L and C_T are found to be 150 and 1.75 respectively.

If the viscous flow is dominant, the turbulent flow term can be dropped. This leads to the well-known Kozeny-Carman equation for the laminar flow through porous media. The constant after some conversion becomes the Kozeny constant. However, a large number of experiments show that the constant term varies in different situations, and generally is lower than that in the Ergun equation [5, 6].

Viscous flow through aligned fiber bundles has also been studied in the composite processing field [7, 8, 9, 10]. For aligned fiber bundles, the permeability is not isotropic. The flow resistance in the transverse direction is much higher than that in the longitudinal direction [7, 8, 9]. Also in the transverse direction, flow can stop at the maximum packing efficiency which is less than one [10]. The stop-flow phenomenon is in general not true for other packed beds. Therefore, the Ergun equation or the Kozeny-Carman equation cannot predict this stop-flow behavior. However, in the middle range of the porosity or fiber volume fraction, the Kozeny-Carman equation has been used to give reasonable predictions. Estimations of the Kozeny constant for the longitudinal and transverse flow are presented in [7, 8, 9].

In applying the Ergun equation here, we choose the fiber diameter d_f as the characteristic length to replace D_p . The conversion factor from D_p to d_f is left in the two constants C_L and C_T . For flow through seal structure including packed aligned fibers in the core and braided fiber sheath, we expect C_L and C_T to be different from those in the original Ergun equation [3, 4] because of the geometry configuration. In the seal application, only part of the seal section is exposed to the flow path, as shown in Fig. 1. This will also affect the magnitude of C_L and C_T .

We can also write the flow equation using the form of Darcy's law as

$$-\frac{dp}{dz} = q \frac{\mu}{K} \quad (12)$$

where K is the permeability which has the units of length squared, and z is used for the transverse flow. Alternatively the flow resistance R can be used as

$$-\frac{dp}{dz} = q \mu R \quad (13)$$

where R has the units of one over length squared and is defined as

$$R = (C_L + C_T Re) \frac{1}{d_f^2} \frac{(1 - \epsilon)^2}{\epsilon^3} = \frac{C_L}{d_f^2} \frac{(1 - \epsilon)^2}{\epsilon^3} \left(1 + Re \frac{C_T}{C_L} \right) \quad (14)$$

where the Reynolds number Re for the flow is defined as

$$Re = \frac{\dot{m} d_f}{\mu (1 - \epsilon)} = \frac{\rho q d_f}{\mu (1 - \epsilon)} \quad (15)$$

The mass flow rate \dot{m} is calculated using the seal cross section area transverse to the flow, and is a constant over the flow length. In the viscous flow case, this flow resistance R is only a function of the fibrous structure which is represented by d_f , ϵ , and C_L . However, if the turbulent flow cannot be neglected, then the fluid property and the velocity also enter the expression through Re .

From the above discussion, it is clear that in the seal design, both the porosity and the fiber diameter strongly influence the flow resistance. Also with the turbulent effect, the overall seal resistance is increased.

To solve for the seal leakage rate, we applied the ideal gas law for the relation between ρ and p as

$$\rho = \frac{M_w}{R_g T} p = \frac{\rho_o}{p_o} p \quad (16)$$

where M_w is the molecular weight, R_g is the gas constant, T is the temperature, and ρ_o and p_o are the reference values at the temperature. The viscosity of the gas is considered to be constant over the seal length for the simplification of the problem. By applying these relations and rearranging various terms, we can obtain

$$C_L \left[\frac{\mu (1 - \epsilon)}{d_f \dot{m}} \right] + C_T = \frac{1}{2} \frac{p_{in}^2 - p_{out}^2}{w_s} \frac{\rho_o}{p_o} \frac{d_f}{\dot{m}^2} \frac{\epsilon^3}{(1 - \epsilon)} \quad (17)$$

where subscripts *in* and *out* indicate the inlet and outlet locations of the seal respectively, w_s is the seal width after installation, and the engine pressure $p_e = p_{in} - p_{out}$.

With this leakage flow equation, we can set up experiments to measure the leakage mass flux versus the engine pressure, then evaluate the unknown constant terms C_L and C_T for the designed seal structure. Since the leakage flow equation is in the linear form for C_L and C_T , a linear regression of the test data can be conveniently performed. After we obtained these constant values, the seal leakage rate under the application conditions can be predicted.

LEAKAGE FLOW TEST

Leakage test setup is illustrated in Fig. 2. Flow media included air and helium since they represent different transport properties. Engine pressure p_e was simulated using the compressed gases, and was regulated using a series of valves. The seal was placed into a groove of 0.5 inch (0.0127 m) wide in the lower platen of the test fixture. An expandable soft-tube bladder was inserted at the bottom of the groove. This bladder tube was connected to another compressed air line, and the pressure in this line was also regulated. In the test this line pressure, which was the preload pressure p_p for the seal, was set at different levels, typically 20, 40, 80, and 130 psig (0.138, 0.276, 0.552, and 0.896 MPa) respectively. When the bladder tube was pressurized, it pushed the seal upwards against the top plate. A gasket was installed between the top plate and the bottom part of the fixture to ensure that leakage occurred only through the seal. The seal sealed an inter-panel gap that was 4 inch (0.102 m) long and 0.2 inch (0.0508 m) high.

The measurement devices include a digital pressure gage, Model PX-623, a pressure conditioner, Model DP41-V-A, a mass flow meter, Model FMA-875-V, and a conditioner, Model FMA-78P2, all of them from Omega Engineering. The mass flow meter was connected to the gas input line. The pressure gage was positioned at the inlet side of the seal. The outlet pressure was atmospheric pressure. Therefore the recorded pressure difference was used to simulate the engine pressure.

In the leakage test, seals are carefully placed into the groove. After that the top plate was installed. Preload pressure of 130 psi (0.896 MPa) was first applied to consolidate the seal structure. This preload pressure was maintained for about a minute, and then released. This was to ensure the consistency of the initial test condition of the seal. Then the flow gas, either helium or air, was introduced. A regulator on the gas input line was used as the control device to obtain the desired engine pressure values. After the readings reached the steady state (usually in less than a minute), the mass flow rate was recorded. The simulated engine pressure was increased from 0 to 50 psig (0.345 MPa), and maintained at a series of preset values for the reading. Because the mass flow meter can handle about 200 liters per minute maximum flow rate, for some seals the maximum pressure values were lower than 50 psig (0.345 MPa). Tests were first done at the lower preload pressure values, for example, 20 psig (0.138 MPa), and then increased to the next higher level. A systematic application of preload was used to eliminate the potential hysteresis effects in the measurement. When tests at various preload levels were completed, preload line pressure was released. The seal sample was then taken out of the apparatus, and the dimensions of the seal were measured at five locations along the seal length using a caliper.

SEAL PERFORMANCE

The effect of the main design parameters, such as fiber diameter, braiding angle, sheath layer number, and seal porosity, on the seal leakage performance has been observed in the seal leakage tests. As discussed earlier, seal porosity and fiber diameter showed great influence in the overall seal leakage performance.

Sample to sample variation of the seal leakage rate was one of the main concerns of the seal performance. In the fabrication process, a long braided structure was made, then seal samples with 5.6 inch (0.142 m) lengths were cut from the long structure. Theoretically, these seal samples had the same porosity and fiber architecture. The variation among different seal samples with the same structure reflected the influence of random operating conditions in the fabrication process, which is not unusual in the textile process. The variation is important to the quality control of the seal performance.

Fig. 3 shows the mass flow rate of four seals M1-(1) to M1-(4) under the preload pressures 40 psi (0.276 MPa). Data of both air and helium is included. The results show that the variation among these seal samples is relatively small, with readings within $\pm 15\%$ of the sample average. The variation was also checked for the eight seals of batch M1. At the preload $p_p=40$ psig (0.276 MPa) and the engine pressure $p_e=5$ psig (0.0345 MPa) with helium as the medium, the mass flow rate of the sample average is 0.00196 (lb/ft/sec), and the standard deviation is 0.00024 (lb/ft/sec).

The other variation checked is in the measurement of the flow leakage test. This was performed on the M6c batch seals. Each sample was measured three times. The consecutive measurements were made after the seal was taken out of the test fixture for at least 24 hours, allowing the seal to essentially return to its initial condition. Sample average and variance were calculated. A flow parameter is used which is defined as the mass flow rate of helium per second per foot of seal multiplied by the square root of the absolute temperature, divided by the absolute inlet pressure. This flow parameter has the units of $[\text{lb (He)} \cdot \text{R}^{1/2}]/[\text{s ft psia}]$. The test condition is set at the preload pressure of 40 psig and engine pressure of 15 psig. The sample average of the flow parameter of M6c-(1) seal is 0.001290 and the sample variance is 0.000025. Correspondingly these values of sample M6c-(2) are 0.001166 and 0.000054 respectively. These results show that the variation of the measurement is acceptable.

A typical response of the seals using the permeability versus the applied preload p_p and the simulated engine pressure p_e is shown in Fig. 4. The seal permeability decreases when the engine pressure or the preload pressure increases. It appears that the effect of the engine pressure on the permeability is stronger than that of the preload pressure. As we discussed in the previous section, the seal structure Re was controlled by p_e which determined the mass flow rate. The turbulent part of the flow resistance is therefore strongly related to p_e . The viscous flow resistance was greatly influenced by the seal porosity which is related to the preload p_p . In the case of relatively high fiber volume fractions, which was true for the seal design, applying p_p can only change the porosity to a very limited extent. When p_e was increased during the flow leakage test, the change of Re was significant.

To determine the seal response to the transverse preload pressure, another experimental measurement was conducted, in which an Instron machine was used to compress the seal placed into a mold with the same dimensions as the leakage flow test device. Both the deflection and the load were monitored. Load was applied up to 1100 lbf (500 kg), for the seal sample of about 5.6 inch (0.142 m) length. Seal porosity was determined using the measured mold height and the nominal fiber content.

Since seals were designed with different parameters, such as fiber content, core percentage, braiding angle, and fiber type, the load-deflection responses of these seals were very different. However, they all showed nonlinear response as other fibrous preforms reported in the literature [9-15]. A comparison of the seal response with the available fiber deflection model proposed in [14] is shown in Fig. 5. A good agreement can be seen for most part of the fiber volume fraction range.

LEAKAGE FLOW MODELING

To determine the constants C_L and C_T for the designed seal structure, leakage flow test data was used. As we mentioned above, if the measurements are taken correctly, and the Ergun equation is valid, then the values of C_L and C_T will be constant for a specific seal sample under the test condition. Also the leakage flow equation has the form of $y = ax+b$, with x and y defined as

$$x = \frac{\mu (1 - \varepsilon)}{d_f \dot{m}} = \frac{1}{Re} \quad (18)$$

$$y = \frac{1}{2} \frac{p_{in}^2 - p_{out}^2}{w_s} \frac{\rho_o}{p_o} \frac{d_f}{\dot{m}^2} \frac{\varepsilon^3}{(1 - \varepsilon)} \quad (19)$$

and the equation becomes

$$y = C_L x + C_T \quad (20)$$

The measurement data of different gases, helium and air, will then fall on one straight line. The values of these two constants can also be determined using the linear regression approach.

Fig. 6 shows two selected seal samples using the x - y plot. Although there are data scattering in the figure, it is reasonable to conclude that the Ergun equation is valid for the seal leakage flow. The constant values of C_L and C_T for these two seals are 3.4 and 4.4 for M2-(1), and 85 and 170 for M5-(1) respectively, using the least square regression for each test batch and averaged value for the seal sample. The correlation coefficient of the linear

regression in most cases is larger than 0.99. However, variations of C_L and C_T under different preloads can also be seen in Fig. 6. The overall seal performance is still related to other parameters, such as fiber diameter or porosity. If other parameters are all the same, then the higher the values of C_L and C_T are, the higher the seal resistance is.

The ratio of C_T/C_L is also important in evaluating the turbulent effect of the leakage flow process. As we discussed earlier, the seal resistance is the summation of the laminar and turbulent flow resistances. The relative magnitude of the turbulent effect can be determined using the index $Re \cdot (C_T/C_L)$, not just Re . In the original Ergun equation [3, 4], with the given values of $C_L=150$ and $C_T=1.75$, the requirement to neglect the turbulent effect is that $Re < 10$. In the seal structure and test setup, the values of C_L and C_T were significantly different. Therefore $Re < 10$ was no longer a valid criterion in determining whether the turbulent flow was negligible. As shown in equation (14), the contribution of the turbulence effect to the flow resistance can be measured by the term $Re \cdot (C_T/C_L)$. Therefore the correct criterion should be $Re \cdot (C_T/C_L) \ll 1$. The ratio of C_T/C_L for most of the seal samples was found to be at the range of 1 to 2 from experiments. Therefore the corresponding requirement for Re is $Re < 0.1$, which is much more severe than other cases.

In the leakage flow test, the range of Re was found to be between 0.1 to 5. Therefore, the flow is in the transition region. The ratio of mass flow rate of air to helium was used to check the flow status. The theoretical value of this ratio for laminar flow is $(\mu/\rho)_{\text{helium}}/(\mu/\rho)_{\text{air}} = 7.86$, and that of turbulent flow is $(\rho_{\text{air}}/\rho_{\text{helium}})^{1/2} = 2.69$. This ratio of all the seals tested was in the range of 3 to 7.

SUMMARY

The work performed in this study showed that the application of braided fiber seal is feasible. Seals were designed and fabricated using different fiber architectures, and then tested for the leakage flow. It was found that many design parameters, such as the seal porosity, the percentage of the core part, layer number of the sheath, fiber diameter, sheath braiding angle, and sheath thickness, all contribute to the seal leakage performance. Qualitative relationships have been established between the design parameters and seal performance.

The Ergun equation is applied to the leakage flow analysis. The two constants in the Ergun equation, C_L and C_T which accounted for laminar and turbulent effects respectively, are found to be substantially different from those suggested in the literature for other packed geometries. Test data show that C_L and C_T have about the same order for the seal structure and the flow leakage test setup. The relative magnitude of the turbulent effect versus laminar effect can be correctly evaluated using an index $(Re \cdot C_T/C_L)$, not just Re . In the seal leakage flow case this leads to a conclusion that only if Re is less than 0.1 or so, can the turbulent effect be neglected. The leakage flow of the seal under the test condition was found to be in the transition region.

ACKNOWLEDGEMENT

The authors would like to thank Hon Wong, Dan Luu, John McKelvie, and Tim Tezak of Drexel University for their help in the seal design, fabrication, and testing, and Christopher Pastore, Susan Marr and Xiaoming Tao for their work in the preliminary design experiments. The project funding by NASA Lewis Research Center is gratefully acknowledged.

REFERENCES

1. Steinetz, B.M., DellaCorte, C., and Sirocky, P.J., "On the Development of Hypersonic Engine Seals", NASA TP-2854, 1988.
2. Ko, F.K., "Braiding", *Engineering Materials Handbook*, Vol. 1, Composites, Edited by Reinhart, T.J., American Society for Materials International, Metal Park, OH, 1988.
3. Bird, R.B., Stewart, W.E., and Lightfoot, E.N., *Transport Phenomena*, John Wiley & Sons, 1960, pp.181-200.
4. Denn, M.M., *Process Fluid Mechanics*, Prentice-Hall, 1980, pp.67-71.
5. Carman, P.C., *Flow of Gases through Porous Media*, Academic Press, 1956.
6. Van Den Brekel, L.D., and De Long, E.J., "Hydrodynamics in Packed Textile Beds", *Textile Research Journal*, August, 1989, pp.433-440.
7. Williams, J.G., Morris, C.E.M., and Ennis, B.C., "Liquid Flow Through Aligned Fiber Beds", *Polymer Engineering and Science*, Vol. 14, No. 6, June, 1974, pp.413-419.
8. Lam, R.C. and Kardos, J.L., "The Permeability of Aligned and Cross-Plied Fiber Beds During Processing of Continuous Fiber Composites", *Proceedings of American Society for Composites*, Third Technical Conference, Seattle, Washington, September, 1988, pp.3-11.
9. Lam, R.C. and Kardos, J.L., "The Permeability and Compressibility of Aligned and Cross-Plied Carbon Fiber Beds During Processing of Composites", *Proceedings of 47th Annual Technical Conference (ANTEC'89)*, SPE, New York, 1989, pp.1408-1412.
10. Gutowski, T.G., et. al., "Consolidation Experiments for Laminate Composites", *Journal of Composite Materials*, Vol. 21, June, 1987, pp.650-669.
11. van Wyk, C.M., "Note on the Compressibility of Wool", *Journal of Textile Institute*, Vol. 37, 1946, T285-292.
12. Dunlop, J.I., "On the Compression Characteristics of Fiber Masses", *Journal of Textile Institute*, Vol. 74, 1983, pp.92-97.
13. Carnaby, G.A. and Pan, N., "Theory of the Compression Hysteresis of Fibrous Assemblies", *Textile Research Journal*, Vol. 59, 1989, pp.275-284.
14. Gutowski, T.G., Morigaki, T., and Cai, Z., "The Consolidation of Laminate Composites", *Journal of Composite Materials*, Vol. 21, February 1987.
15. Kim, Y.R., McCarthy, S.P., and Fanucci, J.P., "Compressibility and Relaxation of Fiber Reinforcements During Composite Processing", *Polymer Composites*, Vol. 12, No. 1, February 1991, pp.13-19.

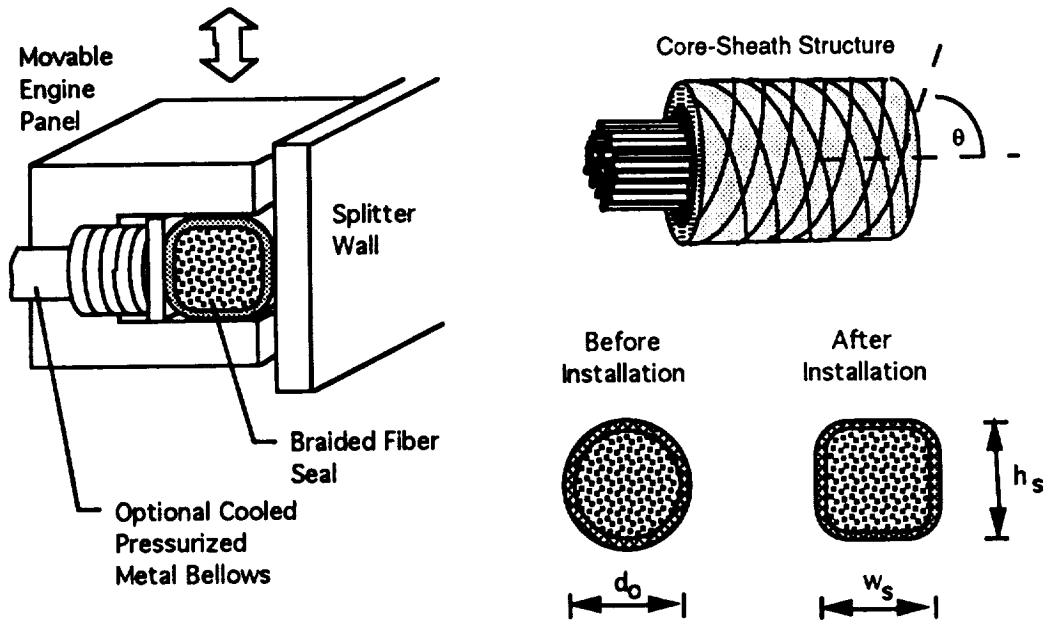


Fig. 1: Illustration of the seal structure and applications.

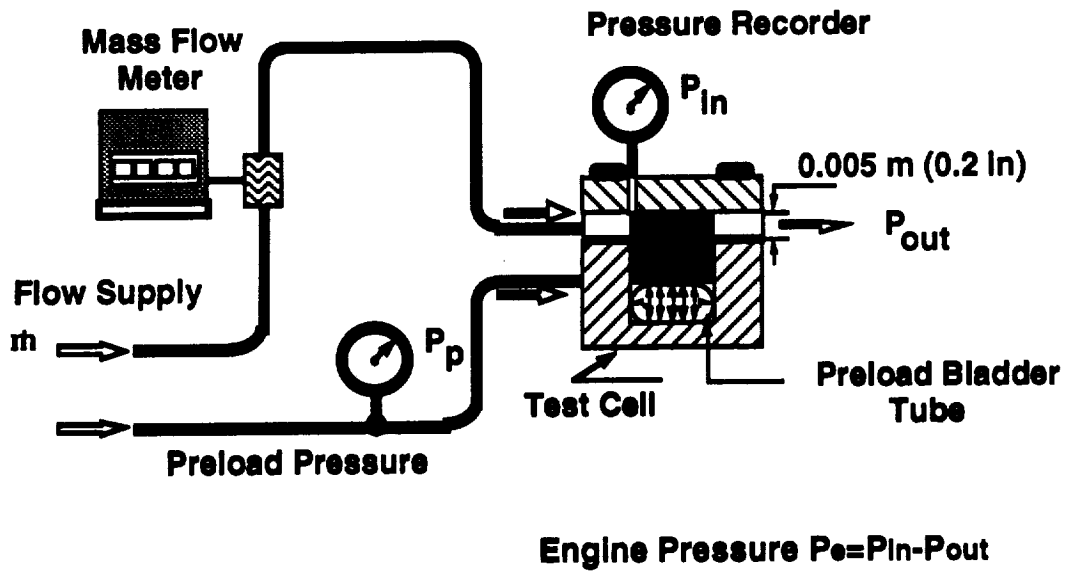


Fig. 2: Leakage flow test setup.

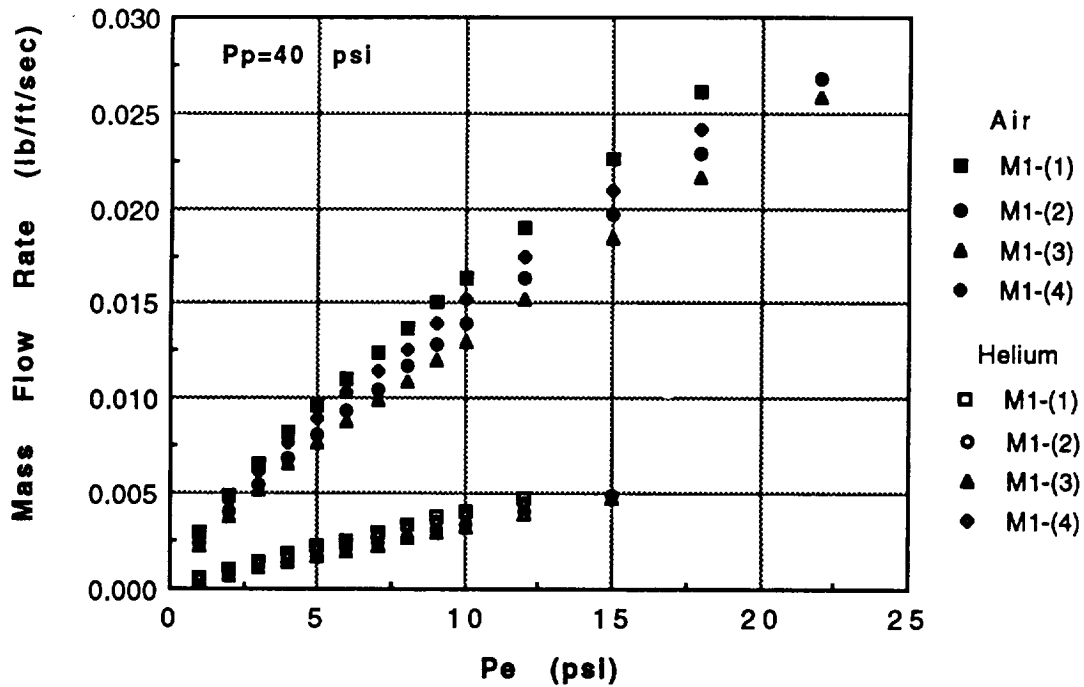


Fig. 3: Variation among the same batch of seal samples.

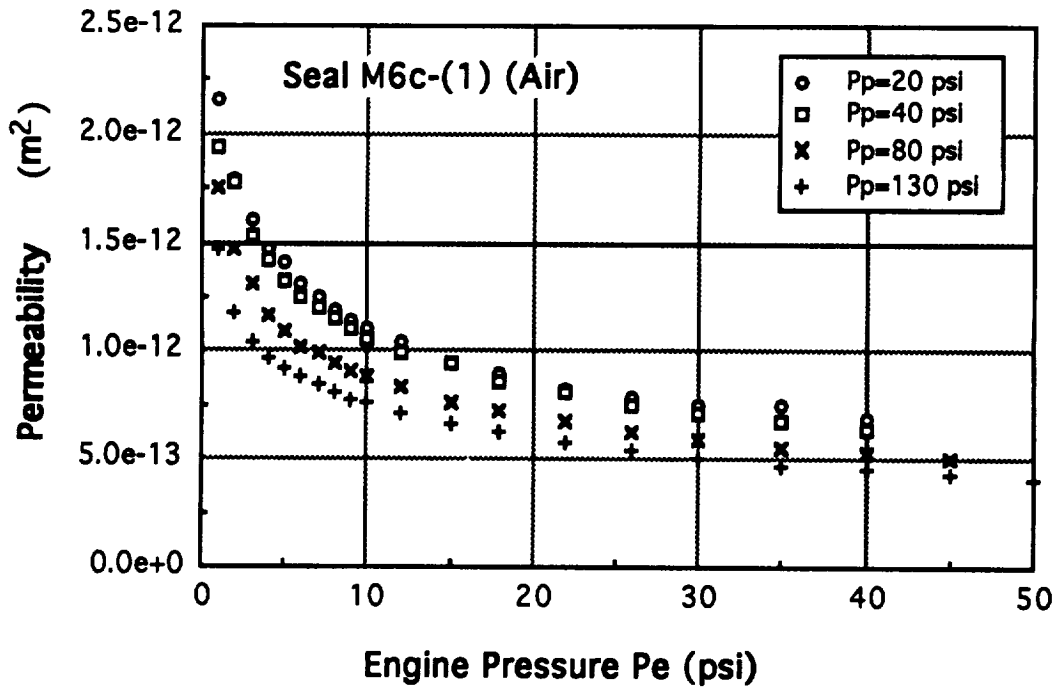


Fig. 4: Permeability versus the engine pressure p_e and the preload p_p .

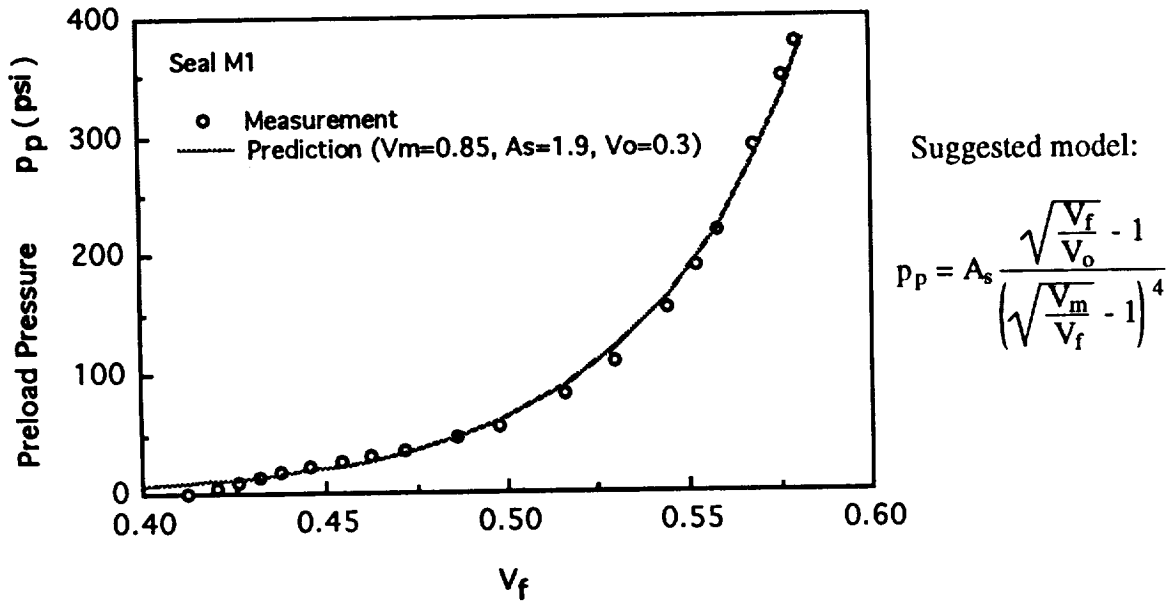


Fig. 5: Comparison of test data and model prediction [14] on seal porosity.

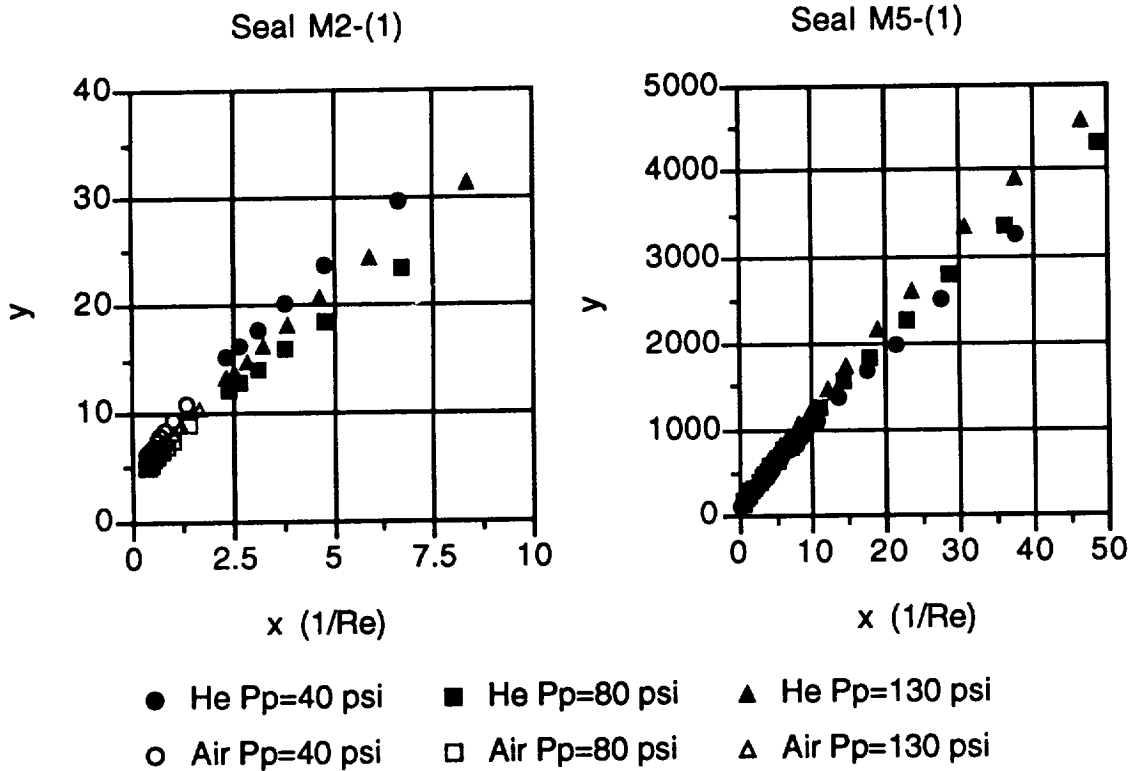


Fig. 6: Flow test data using dimensionless variables.

199402 387

QUANTIFICATION OF PROCESSING ARTIFACTS IN TEXTILE COMPOSITES

Christopher M. Pastore
North Carolina State University
Textile Materials Science

215-24
N 94 - 16860

ABSTRACT

One of the greatest difficulties in developing detailed models of the mechanical response of textile reinforced composites is an accurate model of the reinforcing elements. In the case of elastic property prediction, the variation of fiber position may not have a critical role in performance. However when considering highly localized stress events, such as those associated with cracks and holes, the exact position of the reinforcement probably dominates the failure mode.

Models have been developed for idealized reinforcements which provide an insight into the local behavior. However, even casual observations of micrographical images reveals that the actual material deviates strongly from the idealized models. In this paper, some of the deviations and causes are presented for triaxially braided and three dimensionally woven textile composites. The necessary modelling steps to accommodate these variations are presented with some examples. Some of the ramifications of not accounting for these discrepancies are also addressed.

INTRODUCTION

One of the principal objectives of composite materials is to replace catastrophic failure, typical of metal structures, with dispersive failure. This is accomplished by physically separating the brittle and ductile phases (fiber and matrix) within the composite.

The goal is realized to the greater part in the case of laminated composite materials. It has been demonstrated that dispersive failure occurs. However, a new problem arises with the introduction of these laminated materials: damage tolerance. When subject to impact, some local delamination of the composite is likely to occur, and when subsequently put in compression, the composite suffers a premature failure associated with this delamination zone. This low compression-after-impact (CAI) strength becomes the design allowable for this material, and greatly reduces the benefits associated with the material.

Improved CAI strength is one of the driving forces for textile reinforced composites. In addition to the labor-reduction and shape formation ability of these materials, the intertwined nature of the reinforcing elements (fibers and yarns) hinders delamination. In fact, in the case of 3-D fabrics, delamination cannot occur due to the lack of lamina. Clearly the entanglement of yarns within the fabric structure reduces in-plane properties, but if the CAI strength is superior to the equivalent laminate, the design allowable has increased, making the textile composite the more attractive candidate.

However, if some particular architectural phenomena within the composite material detract from this dispersive failure, then one might conclude that the main goal has been defeated. Thus it is necessary when modelling textile reinforced composites to guarantee that failure modes are not catastrophic. It is conceivable that particular architectures combined with some local deformation events will combine to create an unfavorable failure mode.

It is the intent of this paper to consider process variations (intentional and accidental) which may have an impact on the local performance of the textile composite. Performance may be characterized by stiffness, variation in properties, or mode of failure. In any of these cases, it is necessary to have some handle on the performance of the textile composites. This performance is dictated by the reinforcing material, and consequently deviations from the "expected" material must be examined. The types of deviations typically associated with different fabric structures are presented and discussed. Localized deformation events which correlate to particular architectural variations are introduced. In most of these cases, the actual impact of architecture on performance is not known. Thus, some analytical tools are proposed to examine these phenomena in more detail.

PROCESS DEVIATIONS

Process deviations can be the result of an error in processing, the natural random events associated with fabrication, or the consequences of particular manufacturing schemes. In any of these events, it is useful to have some model of the corresponding material response. There are many types of process deviations, and each fabric system has distinct particulars of deviation types and effects.

In this section, both types of deviations (random and fixed) are discussed with some examples. As is frequently the case when studying textile reinforced structures, the author is left with more questions than answers when investigating these issues.

Yarn Mis-Orientation

One typical process deviation is the mis-orientation of the yarns within the fabric specimen. This can occur from the natural deviation of the fabrication equipment or as a result of post-fabrication handling. To get some understanding of how this impacts the composite performance, an idealized model was run. The intention is to determine the distribution of yarn orientations within the specimen and then calculate the effects of these orientation distributions on the elastic properties of the unit cell.

In this case, a plain weave fabric was considered. The fabric is a standard 12K carbon fabric with 12 epi and 12 ppi. Composites were made with 1, 2, and 4 layers of fabric. The composite structures were subject to neutron tomography to create a rendering of the internal structure of the actual composite. It is worth pointing out that the application of neutron tomography to textile composites is not a traditional method of inspection. Composites are usually examined with ultrasonics (C-scan), or with X-radiography to determine damage. C-scan is based upon the consideration that the material under inspection is a layered system, and reflections are caused by delaminations. Since the general textile is not a layered construction, these assumptions are invalid, and it is not clear exactly what the ultrasonic responses reveal. X-radiography is not sufficient for composite materials since epoxies and carbon fibers have similar diffraction patterns when subject to X-rays. X-radiography is most commonly used by applying some radio-opaque liquid to the cracks and delaminations on the surface and then taking an image of the opaque liquid. Since we are interested in determining the reinforcing architecture in a complex structure, it is not useful to look only for cracks. Neutron tomography is intriguing in that the epoxies and the carbon fibers may have sufficiently distinct diffraction patterns at work.

Using this philosophy, some woven composite specimens were exposed to a collimated neutron beam and a photographic plate was held on the other side. (True tomography will involve rotating the target specimen and creating a series of images for 3-D reconstruction.) Figure 1 shows the un-processed neutron radiogram for a

single layer woven composite. This is not the complete tomographical image, but rather a simple planar projection of neutron penetration of the specimen.

From this picture, it is possible to determine more information about the reinforcing structure. Since the issue of importance at this moment is simply the yarn orientation, image analysis techniques were used to highlight the yarn structure (difference of Gaussians), distinguish between warp and fill yarns (derivative operators and Laplacian transforms), and finally reduce the grey scale images to line structures (skeletonization). Figure 2 shows the yarn structure after image analysis techniques have reduced the fabric to line elements. As can be seen in these figures, there is a fair amount of random orientation of the yarns within the fabric.

From these images, it is possible to determine the orientation parameters associated with the fabric structure. Figure 3 shows the distribution of in-plane warp yarn orientation (θ_{warp}), and in-plane fill yarn orientation (θ_{fill}). It can be seen in these figures that the filling yarns generally had a tighter dispersion of orientation than the warp yarns. This may be due to handling of the fabric, wherein a shear displacement was applied to the fabric. These distributions are not intended to be typical of plain weave composites, but rather indicate a specific material under investigation for this study.

Additionally, from photomicrographs of the composite specimens, the out-of-plane orientations (ϕ_{warp} and ϕ_{fill}) were measured. When measuring ϕ , the measurements can take on the total average of the out-of-plane, or distinguish between the relatively flat portions which correspond to the floating region of the interlacing yarn. If the entire yarn path is measured, the mean of ϕ is around 0. However, if the flat component of the yarns is taken as a separate element, the means are non-zero. In this research, the total arc length of the yarns was used for determining the distribution of angles. The distribution of properties is accounted for in the Monte-Carlo simulation (described below). Figure 4 shows the distribution of the out-of-plane components for the warp and filling yarns.

Numerically, the means and standard deviations of these orientation parameters are given in Table 1. An illustration of the angles measured is shown in Figure 5.

For example, if we consider a plain weave fabric allowing random variations in architectural parameters, we can calculate the expected distribution of elastic properties. This was accomplished through a Monte-Carlo simulation using a geometry based stiffness averaging calculation of elastic properties [12]. For the purposes of this discussion, the probability distribution functions of the in-plane and out-of-plane orientations described above were used. The material was modelled with carbon yarns and epoxy resin as the matrix. A fiber volume fraction of 55% was assumed for calculation purposes.

In addition to modelling the particular p.d.f.'s generated, the modelling was extended to include the effects of increasing the freedom of out-of-plane orientation. For these cases, the out-of-plane distribution was assumed to be Gaussian, and the standard deviation of this distribution was the variable parameter for the modelling. A total of 100,000 trials were carried out for each particular distribution. Figure 6 shows the frequency distribution of E_{11} for this plain weave fabric. It can be seen here that the distribution of properties is fairly Gaussian. As the freedom of the out-of-plane angle, ϕ , increases (*i.e.* the standard deviation of ϕ increases), the distribution becomes less Gaussian, tending more towards a uniform distribution, as might be expected.

However, when considering the distribution of E_{22} (which has a smaller standard deviation of both the in-plane and out-of-plane angles) the distribution is distinctly non-Gaussian, as illustrated in Figure 7. The behavior shows a distinctly non-symmetric peak when the out-of-plane angle is restricted, as in the data generated from image analysis. This looks something like a χ -squared type distribution, and is directly related to the restricted out-of-plane orientation for the filling yarns. When the out-of-plane distribution is increased, the distribution

becomes more Gaussian.

When considering the shear modulus distribution, G_{12} , in Figure 8, the distribution is Gaussian until the standard deviation of the out-of-plane angle reaches high values. When the out-of-plane angle has substantial freedom of movement, the shear modulus takes on a relatively uniform distribution of properties.

Clearly these distributions of elastic properties will influence the performance of a structural part formed from these materials. The important factor is to account for these distributions as actual material deviations and develop stochastic models of reliability when the deviations are significant.

It must also be determined if it is possible to reduce the variations in these materials. Clearly, if the distributions are significant, the design criteria for these materials will make them unacceptable for application in structural components. Thus it is necessary to examine both the influence of these variations on a component (rather than the unit-cell level analysis presented herein) as well as determining the processing and handling procedures to reduce the orientational variations in the first place.

Fixed Processing Errors

Occasionally, there are fundamental processing errors associated with the manufacture of textile composites. Unfortunately, at the current time this is not as uncommon as would be desired. Some processing errors, such as yarn mis-orientation, are statistical in nature, and can be addressed as indicated previously. Others are not statistical phenomena, but rather some "fixed" error. Processing errors of this kind are generally not easy to detect. If the error is associated with a yarn which is completely contained within the fabric (in the case of a three dimensional fabric), it will only be detected by destructive evaluation, since there are currently no adequate non-destructive testing techniques for determining the position of yarns within a complex fabric, as discussed above. This leaves only destructive testing, in which case, the defect will only be detected if it lies within the region analyzed.

The general family of fixed processing errors can be subdivided into two principal classes of defects:

- i. Flawed yarns
- ii. Misplaced yarns

The defects in class (i) include things such as slubs on the surface of the yarns, broken yarns, and spliced yarns. Since spliced yarns are necessarily the result of an action carried out by the manufacturer, these defects are identifiable in advance of making the composite. However, slubs and breaks may occur without the knowledge of the manufacturer and thus be included in the composite structure.

Class (ii) errors can occur from problems such as "false twist" of two yarns during the processing, or from a manufacturing plan error. The twisting of two yarns, while unlikely for yarns under tension, can occur to yarns which are only lightly loaded during manufacturing. This can result in a locally dense region of the fabric with unknown fiber orientations. Furthermore, the distortion associated with this locally dense region may extend beyond the boundaries of the defect zone, thus having some more global effect on the fabric in terms of overall orientation and density. Manufacturing plan errors are currently more common. These come about from an improperly designed manufacturing machine or an error in deriving the machine control parameters.

By carrying out destructive testing on a variety of fabrics made from a new or modified machine, it may be possible to identify fundamental flaws associated with that machinery. As an example, consider the three dimensional braiding process. In this type of machinery, the yarns are attached to carriers connected to a "loom" which typically lies in a plane. The yarns connected to the carriers are under tension to provide a good fabric. If the carriers are providing some spring-type tension (fairly common), then the tension will be a function of the distance the spring has extended. This implies that the yarn providing the greatest crimp, and/or those farthest from the center of the loom, will be applying greater tension to the fabric than others. This will result in an uneven fell formation on the braid. This type of phenomenon has been observed. It manifests itself as a curved row of picks across the face of the fabric, rather than a straight line, perpendicular to the edges of the braid. There are solutions to this problem, and these have been developed in response to such a distortion of the fabric.

Errors in machine control parameters are more difficult to identify since unlike the improper machine design, they are specific to the particular fabric being formed. Thus, there is no way to determine *a priori* if a problem should be expected. A typical control parameter defect might be the lifting of a harness or hook at the wrong time in a three dimensional weaving process. This could result in a fairly "harmless" error, or perhaps a more severe problem. The difficulty arises when these defects are located within the volume of the fabric and do not appear on the surfaces. Thus they are detectable only by destructive testing.

Fortunately, since these types of defects are associated with hook or harness lifting, they are repeatable. If the fabric being formed is fairly simple, that is, either the hooks have multiple linkages across the width of the fabric or the weave pattern repeats along the length, the chances of finding the defect through destructive testing are good. Additionally diagnosis of the defect is tangible because of the systematic appearance of the defect. However, if the fabric is highly complex, it is possible that every pick is unique. In this case, it is necessary to destroy one entire specimen for investigation and then weave another for application. Also diagnosis of a defect in such a fabric will be extremely difficult.

These types of defects could be eliminated through the application of a feed-back system which would check the controls being sent to the harnesses or hooks, and reconstruct the idealized geometry of the woven fabric from this information. Although such a technique does not eliminate class (i) type defects, it does eliminate fundamental process control problems. If the machinery is controlled by mechanical means (chains, punch cards, *etc.*), it will be necessary to electronically reproduce the harness/hook motion and process it independently.

STRUCTURAL INHOMOGENEITIES

In addition to the process deviations discussed above, it is also necessary to consider the variations of fiber architecture that are fundamental to the fabrication of the structure under consideration. These variations may be on a fairly large scale, or within the unit cell of the structure. These structural inhomogeneities are assumed to be associated with idealized textile structures, and as such can be considered part and parcel of the general problem of analysis of textile reinforced composites.

Textile composites have strong advantages over laminates by their ability to be formed in near-net-shape structures. Furthermore, the three dimensional reinforcement available with textiles provides the damage tolerance mechanisms. Both of these advantages create difficulties when trying to analyze the behavior of the material.

In this paper, we will consider three types of structural inhomogeneities: architectural variations (change in fabric structure throughout a component), sub-unit-cell characteristics (events associated with behavior smaller than a unit-cell), and the formation of holes (an unanswered debate about the merits of cutting versus forming).

Architecture Variation

In the case of a complex shaped textile reinforced composite, it is necessary to consider the distribution of fiber architecture throughout the structural component. The need for such a subdivision of the structure into distinct zones of mechanical properties has been investigated previously [14, 13]. What is needed is a method for combining these properties in a material-smart fashion in order to achieve correct solutions to the analytical problem.

The correct solution of the problem begins with the correct discretization of the component into meso-volumes [1]. This must be carried out with attention paid to both the material being examined and the structural analysis code. If we consider a braided stiffened panel, as illustrated in Figure 10, we can see that the braided material has a distinctly inhomogeneous arrangement throughout the component. Not only is there a clear rotation of properties between skin and stiffener, but there are also transitional zones between them. The mesh shown in this figure corresponds to a potential analytical description of the material. The gray levels are intended to indicate differing stiffness (and strength) characteristics of the structure. This description is based on treating the braided structure as a three layer system.

It should be pointed out that this variation in properties is probably beneficial to the response of the structure. As is well known, the interface of distinct materials, particularly at a sharp corner, is a stress raiser. Having an architecture which effectively blends the materials between panel and stiffener is likely to somewhat reduce the stress concentration. In order to identify if there is a beneficial effect from this type of construction, it is necessary to use a detailed material model along with an appropriate structural analysis code which takes into consideration the material properties and distributions thereof.

Sub-Unit Cell Inhomogeneities

Traditional analysis of textile reinforced composites, and composites in general, assumes that there is a unit-cell associated with the material under investigation. However, if the event under consideration has some highly localized effects, the response of the composite may be dictated by sub-unit-cell architectures. Also, the integrated 3-D nature of many textile reinforcements requires the analyst to either accept the composite as having no property variation through the entire thickness of the part, or to subdivide the material in the thickness direction and then model the material as some layered structure which does not have physical discontinuities between the layers.

Even in the condition of simple tension, the inhomogeneities associated with the unit cell may play an important role. As an example, consider a triaxially braided composite. When a braided composite is loaded under simple tension, there exists distinct stripes of opposing shear (γ_{xy}) across the width of the specimen.

Tests carried out by Dr. Peter Ifju using Moire interferometry [10] have identified these phenomena. The cause of these bands of shear is the sub-unit-cell architecture of the braided material at the free surface ($z = 0$, $z = h$). In order to model this behavior, it is useful to treat the braid as stripes of three layer material, each stripe having the inverse stacking sequence of its neighbors. A schematic representation of this type of model is presented in Figure 11. In this case, the outer layer of the braid appears as bands of $+\theta$, $-\theta$ across the width. For some increased level of modelling, it is possible to include the out-of-plane orientation associated with the crimp of the yarns in each layer. In either case, each of these stripes is clearly anisotropic, with C_{16} terms and others non-zero. It is necessary to treat this as a general in-plane anisotropic material (13 constants).

To model the surface shear striping effects, the braid was treated as a 3 layer composite material. The first and last

layers consist of bands of anisotropic material, while the middle layer is a homogeneous braid. The detailed material model is shown in Figure 12. To simulate tension testing, the braid was sandwiched between clamps at the ends, and a soft material was applied to the surface to provide rectangular continuity. The clamping and location of unit displacements are shown in Figure 13. The structural analysis was carried out using a “material smart” structural analysis code developed by the author and his colleagues [1]. Carrying out the analysis, the shear stress distribution on the surfaces becomes apparent. Figure 9 shows the distribution of τ_{xy} on the upper surface of the braid. This corresponds very well to the experimental data achieved by Ifju.

Hole Formation

The ability to form near-net-shape structures greatly reduces the labor intensity in many applications. However, in certain instances, it is not clear if near-net-shape provides a better solution than machining. A case in point is the formation of holes in textile composite materials. With most textile composites, it is quite possible to form the hole directly in the structure.

Determining the benefits of manufacturing holes in this manner is not simple. Figure 14 shows a schematic rendering of holes in a plain weave fabric. The left diagram shows machined holes, while the right shows a formed hole.

The considerations of benefits/risks associated with both are not finalized. The issues range from actual manufacturing costs to performance characteristics.

In terms of manufacturing, it can be argued that the formed hole reduces labor in that the hole can be formed in the composite during densification (by inclusion of a pin in the tool). Conversely, if there is some small tolerance error in the consolidation, it cannot be corrected easily. Forming the hole through machining operations allows the assembly engineer to guarantee that the part fits correctly each time it is assembled. If there is some small fluctuation in part dimensions, it can be accounted for in machining.

The machined hole has problems in terms of hole location with respect to the unit cell. Clearly the deformation processes associated with an open hole are highly localized. Thus the problem becomes one of sub-unit cell analysis. Holes “A” and “B” on Figure 14 show the problem of machining. The holes can be located in an arbitrary position with respect to the unit cell. From the analysis and testing point of view, this means that every possible position must be considered, and the worst case must be used for design. When the hole is formed, it will be located in the same place every time.

However, the formation of a hole in the structure causes disruption to the surrounding architecture. Hole “C” indicates an extreme example of this kind of disruption. Clearly the fiber volume fraction changes with position around the hole, as does the fiber orientation. This means that the elastic properties are varying around the hole. From the testing point of view, this problem is relatively straight-forward, but for the analyst, this is a difficult task indeed.

Considering failure, having cut yarns (free fiber ends) at the points of stress concentration seems to be a likely place for crack initiation and subsequent failure. This indicates that the cut hole is probably not good for strength. On the other hand, the locally high fiber volume fractions associated with the formed holes provide an ideal place for failure initiation, as it is well known that fracture typically occurs at the points of highest fiber volume fraction.

This leads to a request for the experimentalist to make the determinations. Several studies have been carried out in laboratories to determine the advantages/disadvantages of formed holes versus machined holes. In several studies

brought to the attention of the author, the results have varied dramatically. Sometimes the machined holes show higher open-hole-tension strengths, and other times the formed holes are stronger. Clearly the “truth” of this matter is complex. The fiber orientation, fiber/matrix bonding strength, dimension of hole relative to coupon, dimension of hole relative to unit cell, and other factors determine the optimal selection of material.

ANALYSIS

Having identified several problems and levels of complexity for the general problem of textile structural composites, it is only appropriate to also present some opportunities for addressing these issues.

In order to use these materials, it will be necessary to acquire a substantial data base of properties, and to develop analytical tools for screening materials before testing. The costs of manufacturing these composites is currently too high to have a large experimental program looking into many aspects of performance.

Depending on the properties of interest, there are several approaches available to prediction of performance. The following represent four categories which the author has identified as holding promise for the successful application of these materials:

- i. Unit cell modelling (elastic properties)
- ii. Material-smart structural analysis (deformation and strength)
- iii. Stochastic structural analysis (reliability)
- iv. Neural network modelling (speed, non-intuitive solutions)

Each of these analytical methods is addressed briefly below.

Unit Cell Modelling

Much has been written about unit cell modelling [5, 9, 11, 15, 8]. In many cases, unit cell modelling refers to the calculation of elastic properties of the textile composite on the basis of the reinforcing geometry [6]. Thus, in order to carry out this analysis, it is necessary to have a good description of the unit cell in terms of the reinforcing geometry.

A processing science model can be used to create a geometric description of the reinforcement [13, 7]. The difficulty is in making this geometric model correspond well with the reality of the reinforcement. This means including variations of yarn path through the structure, predicting accurate orientation angles (in-plane and crimp), ensuring proper fiber volume fraction, and including the correct fiber volume fraction within a yarn. In many laminated textiles (wherein layers of fabric are stacked to form the thickness), as well as in three dimensional textiles wherein some de-bulking of the fabric has been carried out, the yarn paths and positions are not ideal. There is nesting of layers and buckling of yarns in the structure. To carry out a detailed unit cell model, these parameters must be accounted for in the geometry.

This is not a trivial task. The implications are that each individual textile composite must be examined independently. This clearly will not allow textile reinforcements to be used as structural materials. Thus, some alternative must be found.

The approach would be to carry out an “effects of defects” study on the unit cell level. Analytically, it can be determined how important parameters such as nesting are on the overall stiffness characteristics of the reinforcement. If, as expected, small variations in nesting do not have dramatic influences on the performance of the composite, it will be possible to carry out the analysis with such a tedious level of detail.

This approach can be coupled with experimental tests to verify the results. Only by eliminating the questions can these materials be adopted.

Material Smart Structural Analysis

In order to carry out a structural analysis of some textile composite component, a division of the component into discrete elements is desirable. Then, the analysis can be carried out using some elemental type analysis. This division into elements will typically be in terms suitable to the analyst, and from the textile point of view, is constructed in terms of arbitrary volume, called *meso-volumes*. These elements may or may not be directly related to the “natural” under-lying textile structure, and it is necessary for the analysis to account for this. It is important to realize that in the case of a “general” textile composite (*i.e.* when a unit-cell model is insufficient for the component), the elastic properties, density, and strength properties of each element may be unique. Thus, we must consider the k^{th} meso-volume as being characterized by some unique stiffness matrix, $C_{ij}(k)$, and some unique density, $\rho(k)$.

Thus, the solution becomes rather complicated, since it must be constructed in such a way to satisfy the necessary continuity conditions between adjacent meso-volumes. These adjacent meso-volumes may have equal or distinct properties depending on their location. The continuity conditions change depending on whether the adjacent meso-volumes have equal or distinct characteristics. Simply applying these discrete $C(k)$ values to a standard finite element analysis will not guarantee that all continuity conditions are met. Thus it is necessary to develop an analytical procedure that can accommodate some “understanding” of the material being modelled. Some techniques have been developed for this purpose [2, 3, 4] and are currently being employed and developed further for the specific problems associated with textile reinforced composites.

One of the issues to be resolved in this analysis is the technique for addressing adjacent meso-volumes which have different elastic characteristics, but this distinction is purely artificial. In this case, some smoothing of stresses and strains must be achieved. Currently two approaches are being considered for the solution. In the first case, the idea of introducing interfacial elements between such meso-volumes is proposed. These interfacial meso-volumes can have smoothed stress/strain relationships which effectively make the problem one of developing these elements and incorporating them into the global analysis. In such a case of an interfacial element analysis, the whole volume of a structural part consists of meso-volumes and interfacial sub-elements characterized by distinct C_{ij} and ρ values.

Another approach, based on a global smoothing of textile properties can be realized in a similar way. By use of some interpolating/approximating techniques, the spatial distribution of mechanical properties associated with each meso-volume can be smoothed. This results in continuous C_{ij} and ρ values depending on x , y , and z coordinates. The discretization of the structural part’s volume in this case will be controlled by global boundary and loading conditions as well as by global variation of textile properties. This kind of solution would be efficient for a global type problem (traditional deformation, low-frequency vibration, buckling) for which detailed local stress analysis is not of primary concern.

Stochastic Structural Analysis

In order to predict reliability of a structure, it is necessary to have some description of the probability of failure. These statistical phenomena can be derived through a combination of activities. Unidirectional materials (representing composite yarns) can be tested extensively and distributions of stiffness and strength in various directions can be compiled.

These data can then be linked to the random distribution of orientation throughout the composite structure, creating a distribution of stiffnesses and strength properties for the textile structure.

The structure can be analyzed in a stochastic model including fluctuating loading conditions to make predictions of failure probability under specific loading.

This approach is rather complex. Existing stochastic models of reliability separate the stiffness variations and the strength variations. Even more, the stiffness characteristics are modelled as independent events.

In order to fully understand the reliability of the textile reinforced structure, new stochastic models are required, which may, for instance, treat the stiffness tensor as the random variable, rather than the 21 constants as independent variables.

It should be pointed out that stochastic modelling is not Monte-Carlo type simulation. Although it is much easier to construct a Monte-Carlo simulation, it has short comings, particularly in terms of quantification of the "goodness" of the probabilistic results. Stochastic modelling, on the other hand, is analytical in nature and thus provides a complete track of the error associated with the analysis.

Although much more difficult, the stochastic modelling provides an excellent opportunity for developing detailed understanding of the critical parameters which affect the performance of textile reinforced composites.

Neural Network Modelling

Another approach is the use of neural networks for the prediction of properties. A neural network is a complex relationship building algorithm. The advantage (and disadvantage) of these constructions is that they have no mechanistic description of the relationships being constructed. The network will map a set of input parameters onto a set of output parameters by constructing rules of relationships through transcendental functions.

The idea of applying neural nets is to create a quick, unbiased model of performance. These nets can be built from experimental data or from predicted response, or a combination of both. The author is currently working with a colleague on the development of a neural net which uses geometric parameters and physical properties as input, and outputs stiffness, crack initiation, and failure stress for a simple tension test.

The net can be trained to some maximum precision, after which the net can be queried. Structural analysis is generally non-invertible, but the neural net construction provides a "back-propagation" algorithm which allows the user to request a set of inputs which meet some specified output set. This provides a degree of freedom to the designer not available with traditional analytical tools.

Clearly the lack of mechanistic descriptions causes some concern, but a sufficiently trained net will demonstrate its accuracy on unknown data sets, and should be able to make predictions as accurate as any other technique, given sufficient input data.

CONCLUSIONS

The relative novelty of textile reinforcements is directly associated with the high level of variations and processing defects in the materials. However, one must be careful when considering these variations not to “throw out the baby with the bath water.” The structural inhomogeneities associated with textile composites are beneficial to the performance characteristics, but provide complexities to analysis and manufacturing. We should be aware that metal structures have comparable levels of complexity, but the scale and randomness, coupled with the long history of study, allow the designer to use these materials readily. Presumably with improvements in understanding, testing, and manufacturing, it will soon be possible to design textile composites with the same level of confidence metals currently enjoy.

There are two basic approaches needed to optimize these materials and make them acceptable to designers as structural materials:

- i. Reduce manufacturing variability
- ii. Identify *effects of defects* for textile composites

It is not clear which approach takes priority; rather, both should be pursued simultaneously. As with any manufacturing process, there is no theoretical limit to the controls available, but this reduces productivity and increases cost. What is necessary is to determine the critical manufacturing flaws and eliminate them.

Many manufacturing defects can be resolved by careful processing science modelling of the material, employing a real-time data acquisition system to verify the architecture of the fabric.

The identification of processing errors requires the development of better non-destructive testing, development of statistical models in order to create a quality assurance and testing program for manufacturing, and application of total quality management (TQM) procedures to the entire process flow.

The determination of “critical” flaws should be made by a combination of testing and analysis. Testing must be developed not on the history of metals, but with an understanding of the actual material. Just improving testing and correlating the data acquisition system to the material may show a dramatic reduction in reported property scatter.

By understanding the interaction of local defects and the performance of the structure, it will be possible to carry out sensitivity studies on the manufacturing parameters and identify the proverbial “20%” of the flaws which create “80%” of the problems.

Clearly the advantages of textile reinforced composites outweigh the current problems in manufacturing and analysis. Many of the existing defects will be identified and removed in a short time, and analytical tools are rapidly developing to handle these materials. The complexity of the material and the implicit hierarchical nature of the corresponding analysis should be considered as an opportunity for the advancement of the science of composites.

ACKNOWLEDGEMENTS

The author wishes to extend his thanks to several individuals for assistance in the development of this paper. Mr. Kip Clyburn provided the neutron tomography images, Mr. Alexander Birger provided the numerical solutions to

the braid shear stripes problem, and Mr. Wade Jackson provided the photomicrographs of the plain weave specimens. Professor Alexander Bogdanovich was of critical assistance in discussing the problems and possible solutions in all aspects.

The numerical solutions were carried out on a Convex supercomputer through a grant from the North Carolina Supercomputing Association.

References

- [1] A. Bogdanovich, C. Pastore, and A. Birger. *Analysis of Composite Shallow Shell Structures Reinforced with Textiles*, volume 2, pages 35--44. Editions Pluralis, Paris, 1992.
- [2] A. E. Bogdanovich and E. V. Yarve. Stress analysis in multilayered beams under transverse dynamic bending. *Mechanics of Composite Materials*, (5):824--837, 1983.
- [3] A. E. Bogdanovich and E. V. Yarve. Numerical solution of the two-dimensional transient deformation problem for a laminated media. *Mechanics of Composite Materials*, (1):36--44, 1988.
- [4] A. E. Bogdanovich and E. V. Yarve. Numerical analysis of impact deformation of laminated composite plates. *Mechanics of Composite Materials*, (5):804--820, 1989.
- [5] R. L. Foye. Finite element analysis of unit cells. In J. Buckley, editor, *Fiber Tex '90*, pages 45--53, Hampton, VA, May 1992. NASA Langley Research Center.
- [6] Y. A. Gowayed and C. M. Pastore. Analytical techniques for the prediction of elastic properties of textile reinforced composites. *Mechanics of Composite Materials*, :accepted for publication, . .
- [7] Yasser A. Gowayed. *An Integrated Approach to the Mechanical and Geometrical Modeling of Textile Structural Composites*. PhD thesis, North Carolina State University, Raleigh, NC, May 1992.
- [8] A. F. Kregers and Yu. G. Melbardis. Determination of the deformability of three-dimensionally reinforced composites by the stiffness averaging method. *Polymer Mechanics*, 1:3--8, January 1978.
- [9] C. Lei, A.S. Wang, and F. Ko. A finite cell model for 3-D braided composites. In *Proceedings of ASME Winter Annual Meeting*, pages 123--132, Chicago, IL, June 1988. ASME, ASME.
- [10] J. Masters, R. Foye, C. Pastore, and Y. Gowayed. Mechanical properties of triaxially braided composites: Experimental and theoretical results. In *Proceedings of the NASA/DOD Advanced Composites Technology Conference*, pages 34--41, Hampton, VA, Nov. 1991. NASA/DOD, NASA.
- [11] C. Pastore and Y. Gowayed. A self consistent fabric geometry model : Modification and application of a fabric geometry model to predict the elastic properties of textile composites. *Journal of Composites Technology and Research*, Accepted for publication: 1992.
- [12] C. M. Pastore, A. E. Bogdanovich, and Y. A. Gowayed. Applications of a meso-volume based analysis for textile composite structures. *Composites Engineering*, 3(2):181--194, 1993.
- [13] C.M. Pastore, Y.A. Gowayed, and Y. J. Cai. *Applications of Computer Aided Geometric Modelling for Textile Structural Composites*, pages 45--53. Computational Mechanics Publications, Southampton, UK, 1990.

- [14] T. Tan, C. Pastore, and F. Ko. Engineering design of tough ceramic matrix composites for turbine components. *Journal of Engineering for Gas Turbines and Power*, 113(2):312--317, April 1991.
- [15] Dennis W. Whyte. *On the Structure and Properties of 3-D Braided Composites*. PhD thesis, Drexel University, Philadelphia, PA, June 1986.

Table 1: Geometric Parameters of Plain Weave Fabric

System	Mean (deg)	Standard Deviation (deg)
θ_{warp}	0.4399	6.3451
ϕ_{warp}	0.2495	1.0121
θ_{fill}	90.1724	4.9632
ϕ_{fill}	0.2195	0.1225

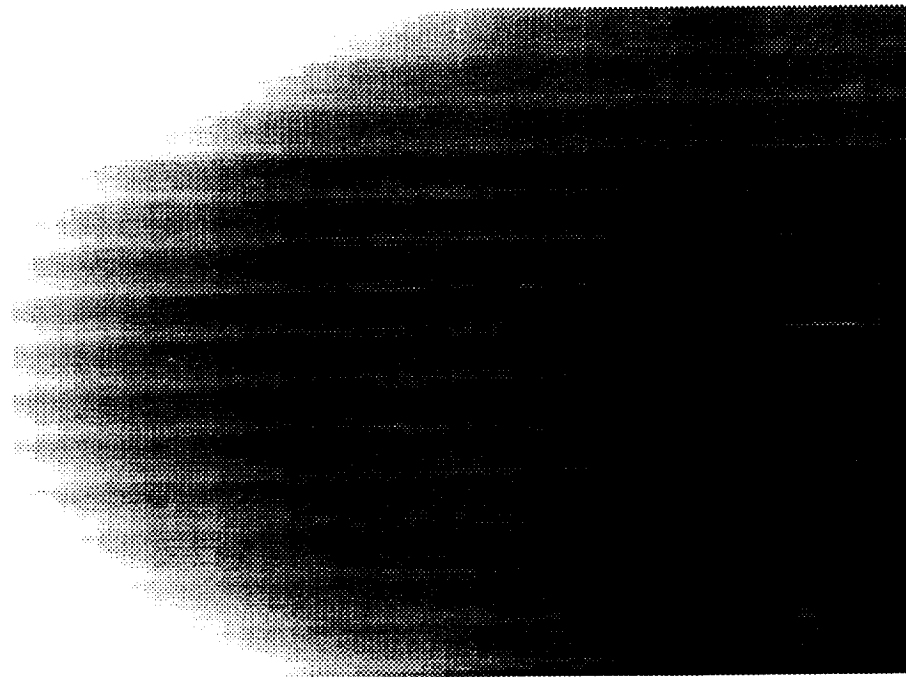


Figure 1: Neutron Radiogram of Plain Weave Fabric Showing In-Plane Projection of Fabric Structure

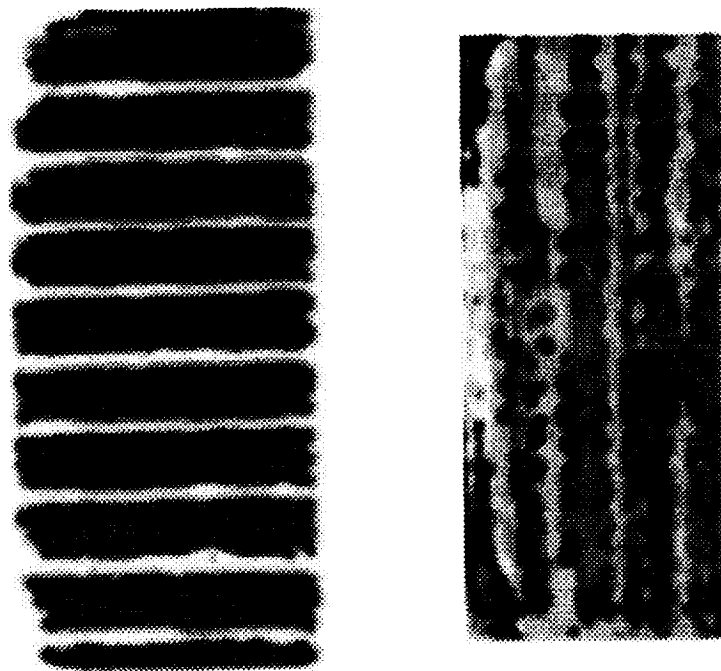


Figure 2: Image Analysis rendering of in-plane warp and fill yarn paths for a plain weave composite

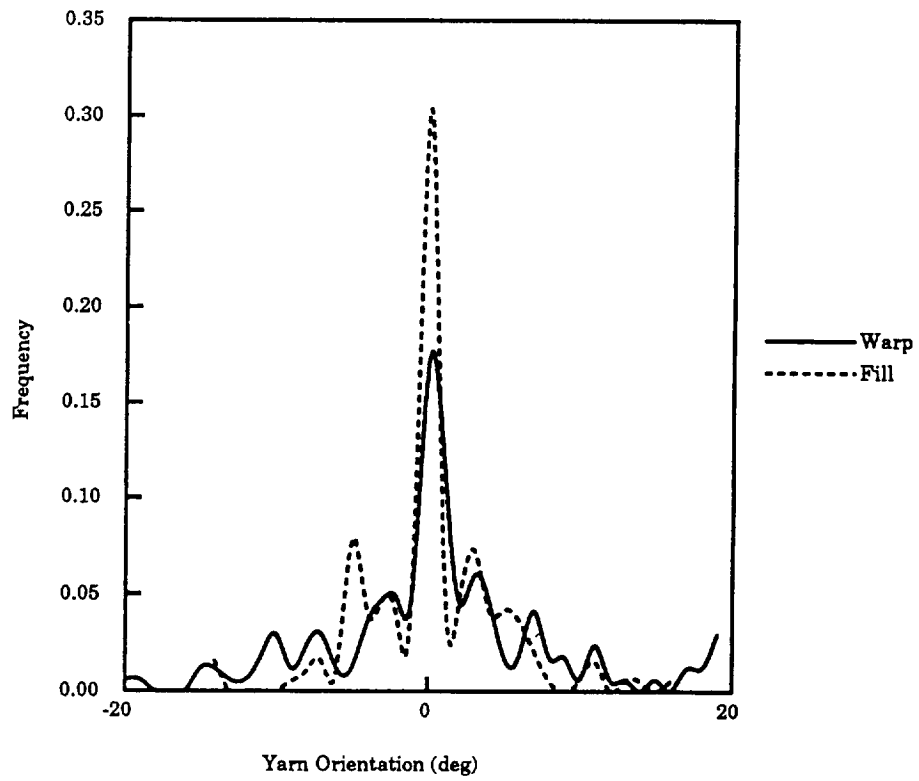


Figure 3: Distribution of In-Plane Angles, θ_{warp} and θ_{fill} for a Plain Weave Fabric

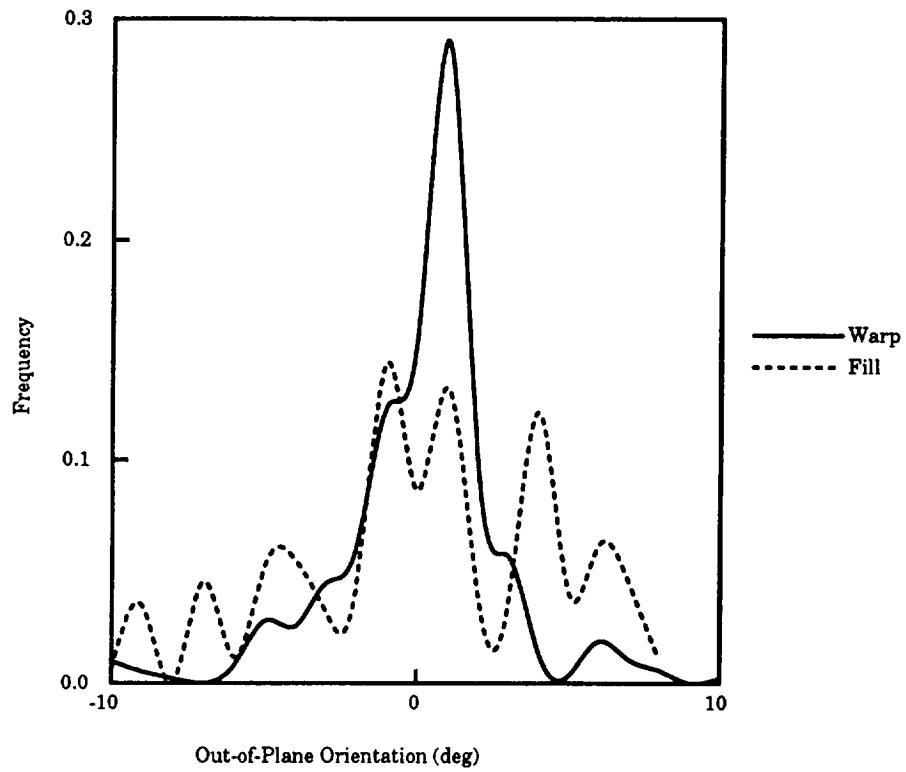


Figure 4: Distribution of Out-Of-Plane Angles, ϕ_{warp} and ϕ_{fill} for a Plain Weave Fabric

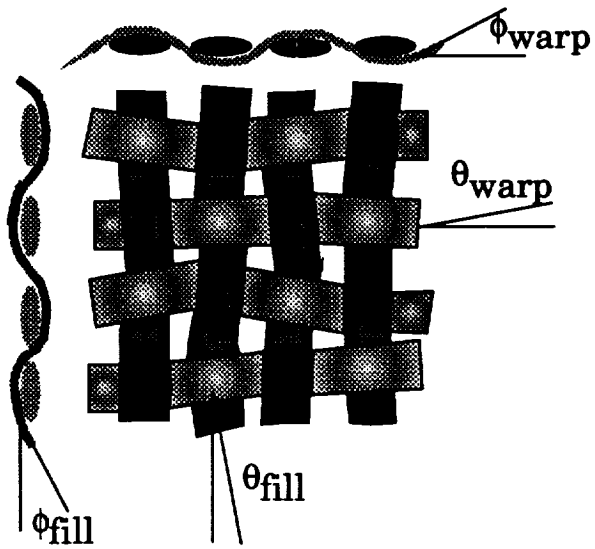


Figure 5: Schematic Diagram of Plain Weave Fabric Showing Orientations Measured

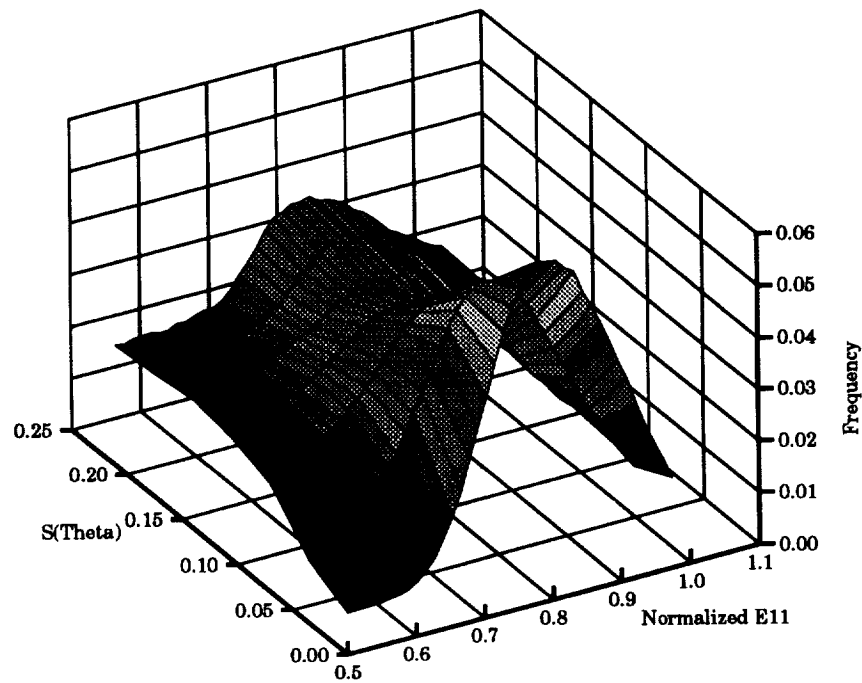


Figure 6: Frequency of Normalized E_{11} Value for a Plain Weave Fabric With a Range of Standard Deviations of ϕ_{fill}

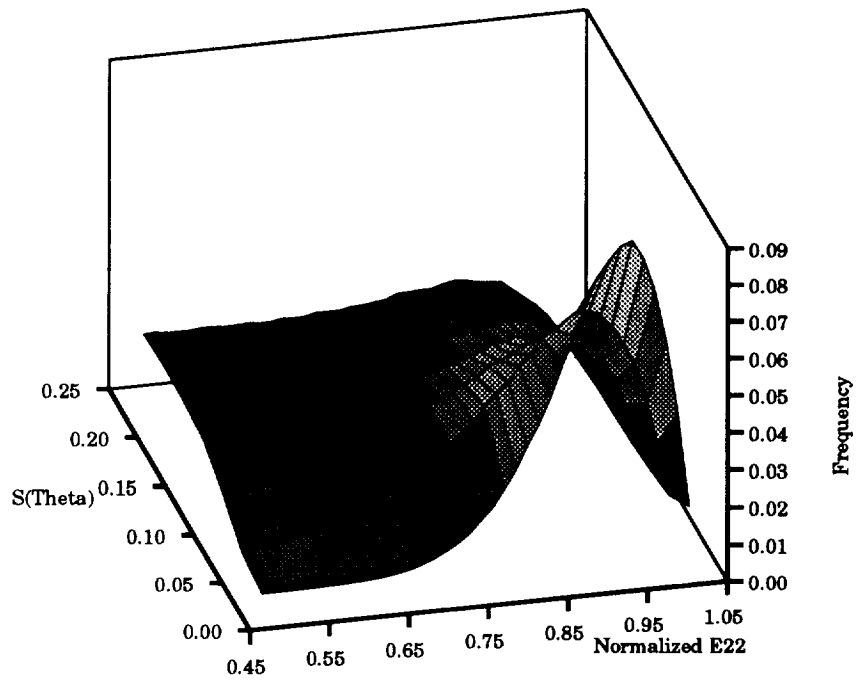


Figure 7: Frequency of Normalized E_{22} Value for a Plain Weave Fabric With a Range of Standard Deviations of ϕ_{fill}

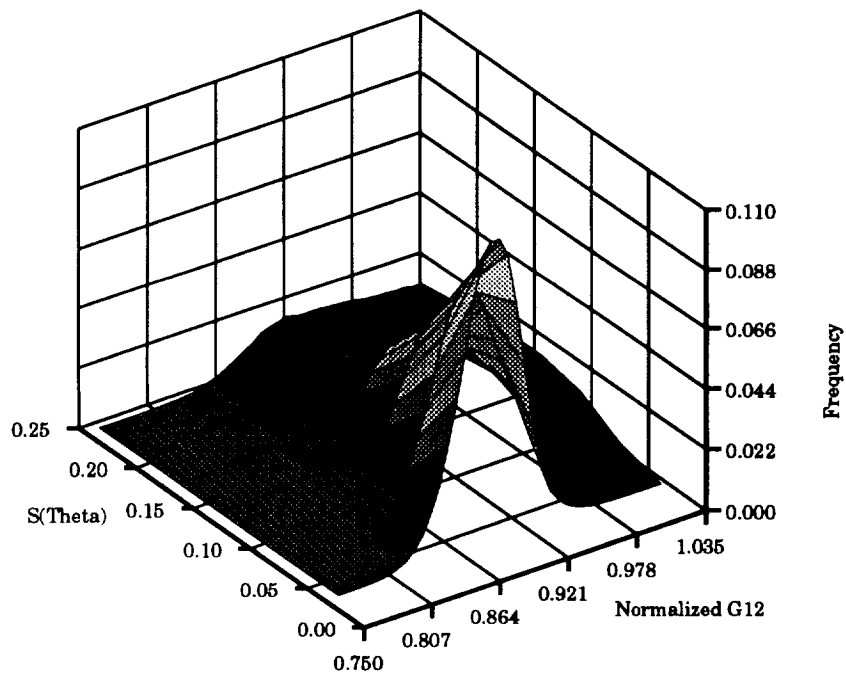


Figure 8: Frequency of Normalized G_{12} Value for a Plain Weave Fabric With a Range of Standard Deviations of ϕ_{fill}

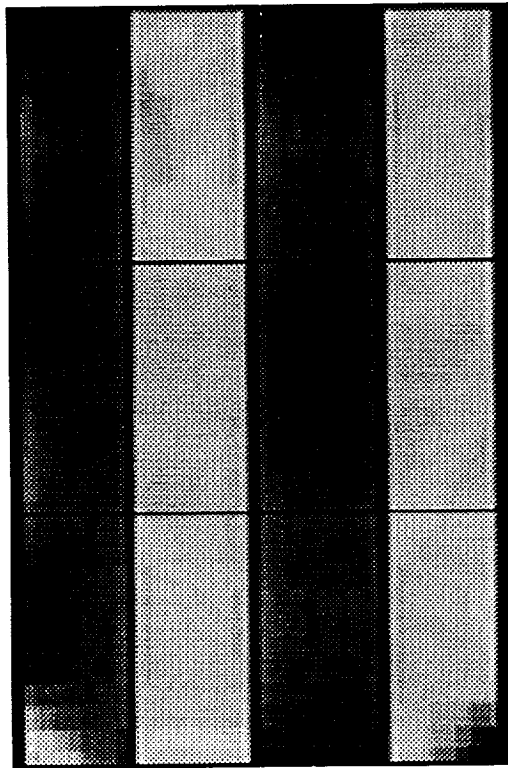


Figure 9: Numerical Predictions of Shear Band Formation in Biaxially Braided Composite Specimen Subject to Simple Axial Tension: *Dark bands indicate negative shear; light bands show positive shear*

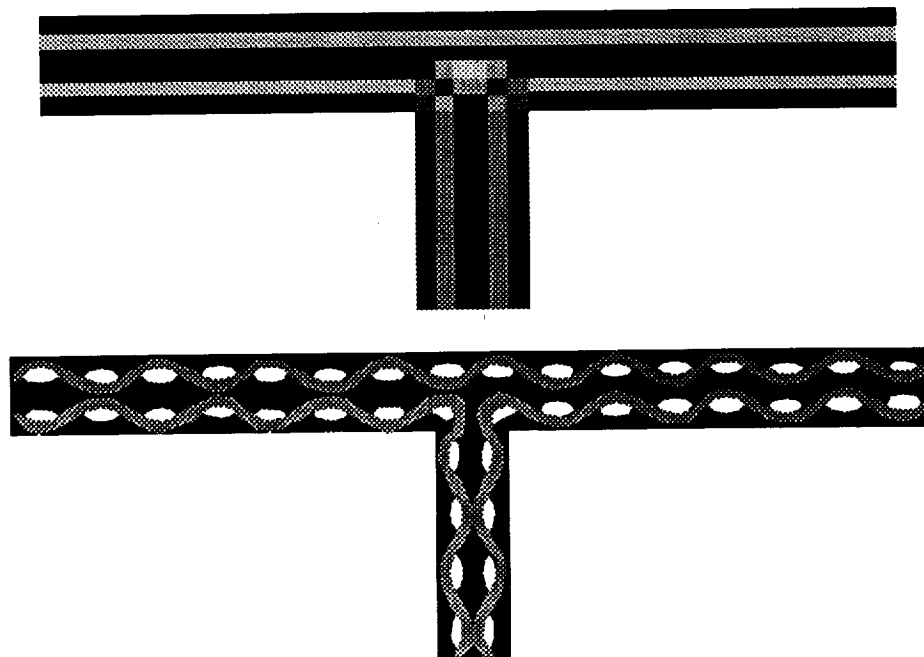


Figure 10: Schematic Representation of Braided Stiffened Panel and Possible Analytical Mesh for Analyzing this Structure

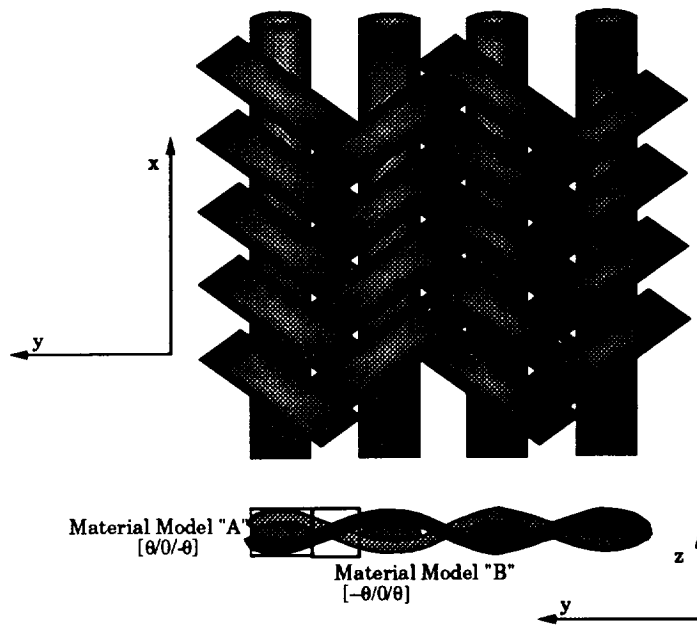


Figure 11: Schematic Diagram of Braided Fabric Showing Cut Sections Used for Analysis

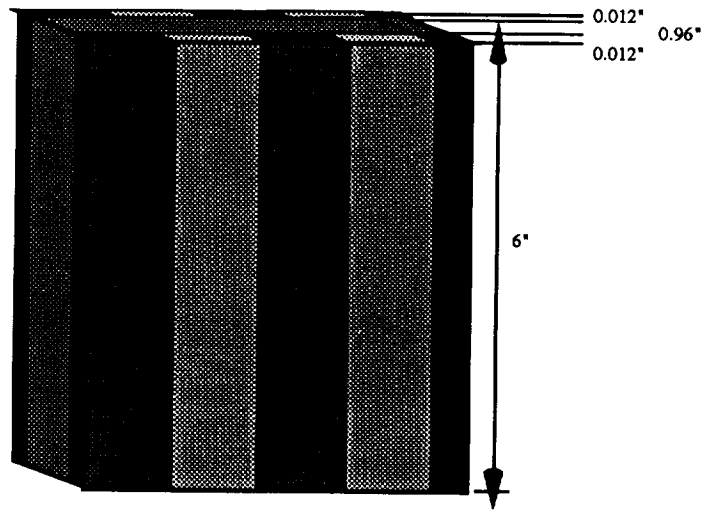


Figure 12: Schematic Diagram of Material Model Used for Braided Composite Subject to Simple Tension

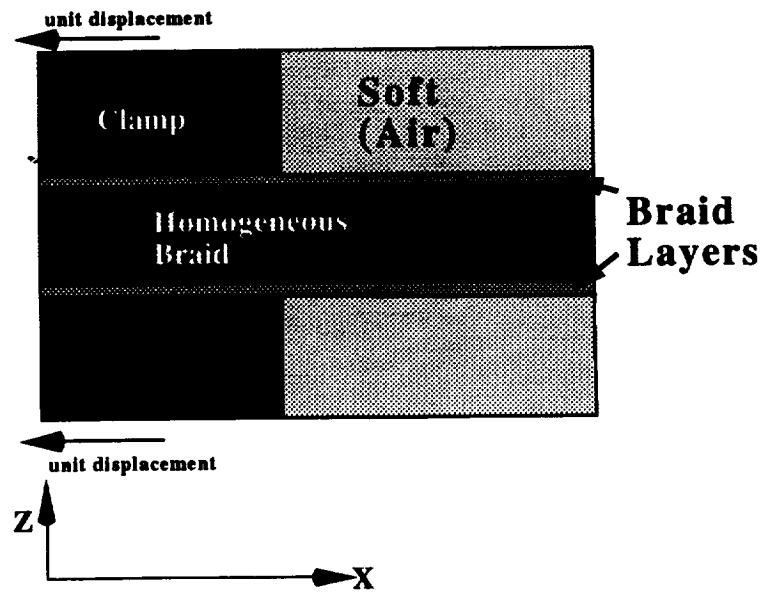


Figure 13: Schematic Diagram of Structural Analysis Configuration Used for Braided Composite Subject to Simple Tension

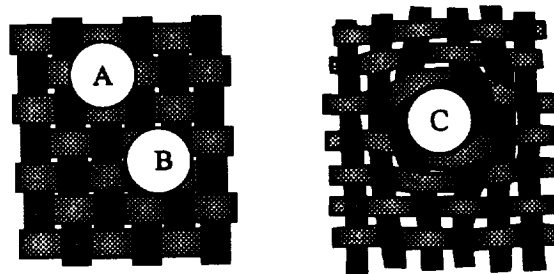


Figure 14: Possible Locations and Types of Holes in a Plain Weave Fabric

1994012388

STOCHASTIC DAMAGE EVOLUTION IN TEXTILE LAMINATES

Yuris A. Dzenis

N 9 4 - 1 6 - 8 6 1

Center for Composite Materials
Department of Mechanical and Aerospace Engineering
University of Texas at Arlington
Arlington, TX 76019

Alexander E. Bogdanovich and Christopher M. Pastore

College of Textiles
North Carolina State University
Raleigh, NC 27695-8301

SUMMARY

A probabilistic model utilizing random material characteristics to predict damage evolution in textile laminates is presented in this paper. Model is based on a division of each ply into two sublaminas consisting of cells. The probability of cell failure is calculated using stochastic function theory and maximal strain failure criterion. Three modes of failure, i.e. fiber breakage, matrix failure in transverse direction, as well as matrix or interface shear cracking are taken into account. Computed failure probabilities are utilized in reducing cell stiffness based on the meso-volume concept. A numerical algorithm is developed predicting the damage evolution and deformation history of textile laminates. Effect of scatter of fiber orientation on cell properties is discussed. Weave influence on damage accumulation is illustrated with the help of an example of a Kevlar/epoxy laminate.

INTRODUCTION

Textile reinforced composites represent an important class of advanced composite materials. Although their structural performance under uniaxial loading yields to that of unidirectional composites, better impact resistance and balanced in-plane properties of these materials as well as ease of application and the resulting low manufacturing cost make them superior for a variety of applications [1]. Ishikawa and Chou [1-3] have developed several micromechanical models for textile laminates. Unidirectional mosaic and fiber undulation models are used for effective thermoelastic properties calculation of plain weave fabric composites. The bridging model is developed to simulate the load transfer between the interlaced regions in satin weave composites. Although the elements of stress-strain analysis can be incorporated in the models and effects like "knee behaviour" of textile composites can be described [2], these models do not allow to analyze the damage evolution in textile laminates.

It is well-known that textile composites under loading undergo multiple damage formation on several structural levels that corresponds to their complex structural hierarchy. The process of damage accumulation in these materials is of stochastic nature due to a number of random factors, such as inevitable scatters in stiffness and strength properties of components, local structural inhomogeneities, and random loading. A combined effect of the above mentioned

factors causes scatter in static and dynamic strength of finite size specimens. On the other hand, for large specimens, where all the combinations of random factors are present, their effect may result in gradual accumulation of damage and a definite failure strength. In general, failure analysis of textile composites should involve consideration of several consecutive geometrical models, corresponding to micro-, meso-, and macrolevels of composite structure [4].

Numerous scientists have studied composite strength problems with the help of statistical modeling (see [5-7] and references therein). Ovchinskii [5] proposed and worked out the fundamental principles, models, and algorithms for stochastic simulation of fracture processes in reinforced composites, starting with micro-level consideration. However, the simulation procedures with micro-level consideration require extensive computational resources for laminate analysis.

A statistical method for reliability analysis of laminates was developed in [8-10]. In these papers, theory of random scalar and vector field excursions was applied for computing the probability of excursions of a random stress-strain field beyond the limiting surface. The method was applied in [11-13] for ply-by-ply stochastic failure analysis and reliability calculation of laminated composite plates and shells. In these papers the whole composite layer was considered as a basic element and maximum probability criterion was used for determination of damage sequence.

Another approach for damage analysis of laminates was developed in [14,15]. The model is based on a division of each layer into statistically large number of mesovolumes. Concentration of broken mesovolumes in plies is calculated as a probability of ply random strains to exceed the limiting failure strains. These concentrations are utilized in ply stiffness reduction. The model allows to predict the gradual damage accumulation and deformation history of composite laminates.

At present, paper probabilistic modeling of damage evolution in textile laminates is performed based on the approach developed in [14,15].

PROBLEM FORMULATION

Consider a textile reinforced laminated composite sketched in Figure 1,a. Each ply of this laminate consists of two sublaminas, made of a set of cells of two types (Figure 1,b). The orientation of fibers in cell with respect to laminate axes, referred further as cell orientation, is described by angle θ . The relative orientation of cells within the same lamina is not necessarily perpendicular, in general. The weave type in this model is described by fraction of cells of particular orientation in sublamina ν . The fraction of cells of the other orientation is, obviously, $1 - \nu$. Material properties of cells of different orientations within the same lamina can also be different, in general.

Now, the problem can be formulated as follows. Assume that initial elastic material properties of cells are random $\tilde{E}^k, \tilde{E}_{20}^k, \tilde{G}_{120}^k, \tilde{\nu}_{120}^k$. Index k is the cell identification number. Here and further tilda sign \sim , upper bar $\bar{\cdot}$, and D denote random characteristic, mathematical mean, and dispersion of characteristic, respectively. Load increment applied to such a laminate results in random stress-strain field in each ply, sublamina, and, consequently, in each cell. Even at very low levels of applied load a nonzero probability of cell failure exists and damages start to accumulate in composite. Accumulation of damages causes reduction in laminate stiffness and redistribution of stresses between cells and plies.

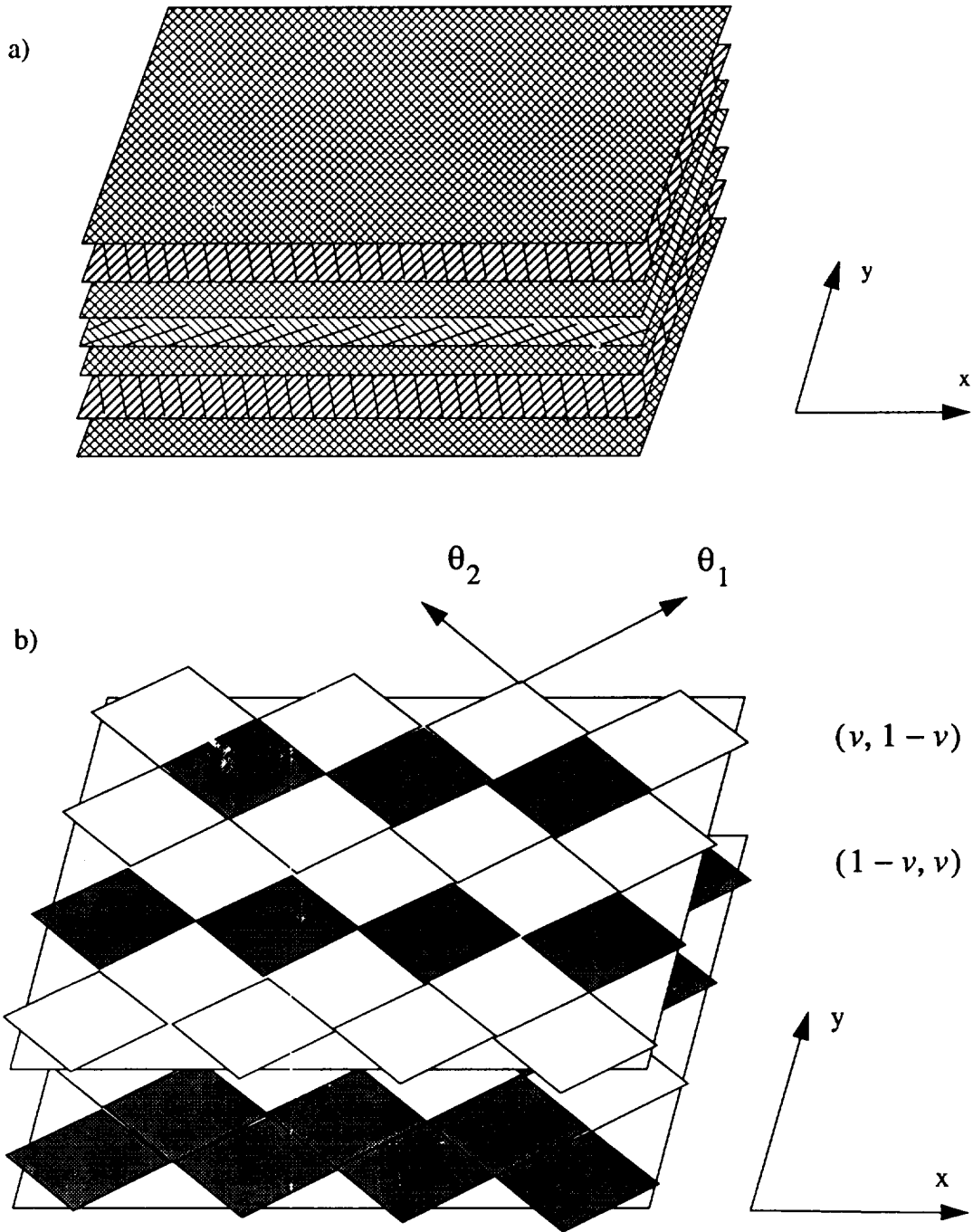


FIGURE 1. Schematic representation of textile laminate (a) and lamina subdivision (b).

Assume that in-plane stresses applied to composite are monotonically increasing functions of a parameter t . $\sigma_i(t) = [\sigma_{11}(t), \sigma_{22}(t), \tau_{12}(t)]$, with parametric derivatives $\dot{\sigma}_i(t)$. Random deformations of composite can then be calculated using integral equations

$$\bar{\epsilon}_i(t) = \int_0^t \bar{S}_{ij}(\tau) \dot{\sigma}_j(\tau) d\tau \quad (1)$$

where \bar{S}_{ij} are current effective laminate compliances. They depend on cell current elastic properties, ply weave and composite lay-up.

$$\bar{S}_{ij}(\tau) = L[\bar{E}_1^k(\tau), \bar{E}_2^k(\tau), \bar{G}_{12}^k(\tau), \bar{v}_{12}^k(\tau), \theta^k, v^k] \quad (2)$$

The current elastic constants are functions of the initial elastic constants and current damage functions in cells.

$$\begin{aligned} \bar{E}_1^k(\tau), \bar{E}_2^k(\tau), \bar{G}_{12}^k(\tau), \bar{v}_{12}^k(\tau) = \\ M[\bar{E}_{10}^k, \bar{E}_{20}^k, \bar{G}_{120}^k, \bar{v}_{120}^k, r_i^k(\tau)] \end{aligned} \quad (3)$$

Damage functions may be calculated using cell random stress-strain field parameters and some appropriate failure criteria.

$$r_i^k(\tau) = R[\bar{\epsilon}_i^k(\tau), \bar{\sigma}_i^k(\tau)] \quad (4)$$

Cell stress-strain field parameters are calculated, in turn, from known composite strains $\bar{\epsilon}_i$ (eq. 1).

$$\bar{\epsilon}_i^k(\tau), \bar{\sigma}_i^k(\tau) = K[\bar{\epsilon}_i(\tau), \bar{E}_1^k(\tau), \bar{E}_2^k(\tau), \bar{G}_{12}^k(\tau), \bar{v}_{12}^k(\tau), \theta^k, v^k] \quad (5)$$

L, M, R, K, P are stochastic functional operators to be specified. According to this approach, current composite elastic properties, and therefore composite deformations and damage functions, are dependent on loading history. In order to integrate eq.(1), we have to calculate stochastic stress-strain field parameters in cells which depend on stochastic material properties and loading, as well as deformation history. The failure criterion (eq. 4) should be chosen to obtain probabilities of ply failure (damage functions). The stiffness reduction algorithm due to damage accumulation in plies (eq. 3) has to be specified.

FAILURE PROBABILITY CALCULATION

Assume, that cell stochastic elastic characteristics $\bar{E}_1^k, \bar{E}_2^k, \bar{G}_{12}^k, \bar{v}_{12}^k$ are statistically independent and normally distributed random numbers. They can be described using mathematical mean values $\bar{E}_1^k, \bar{E}_2^k, \bar{G}_{12}^k, \bar{v}_{12}^k$ and dispersions $D_{E_1^k}, D_{E_2^k}, D_{G_{12}^k}, D_{v_{12}^k}$. Mathematical mean value and dispersion of a function of independent random variables $\bar{y} = f(\bar{x}_1, \bar{x}_2, \dots, \bar{x}_n)$ can be evaluated as follows:

$$\bar{y} = f(\bar{x}_1, \bar{x}_2, \dots, \bar{x}_n)$$

$$D_y = \sum_{i=1}^n \left(\frac{\partial y}{\partial x_i} \right)^2 D_{x_i} \quad (6)$$

Stochastic cell strain response to the incremental laminate loading is calculated using normally distributed numbers properties. Mean values and dispersions of the following random variables are computed in sequence (see [14,15] for some of the formulas involved):

- (i) cell current technical elastic characteristics
- (ii) cell stiffness coefficients in material axes
- (iii) cell stiffness coefficients in laminate axes
- (iv) sublaminas stiffness coefficients
- (v) laminate stiffness coefficients
- (vi) laminate compliance coefficients
- (vii) laminate strain increments
- (viii) total laminate strains
- (ix) sublaminas stresses
- (x) cell strains in laminate axes
- (xi) cell strains in material axes

Cell properties averaging procedure according to weave parameter ν (iv), and classical lamination theory are used in the calculation. Procedure for current elastic properties estimation (i) is described below.

Maximal strain criterion is applied to calculate the failure probability of individual cells. We will describe damage criterion for deterministic and stochastic failure strains. In case of deterministic failure strains, each cell is assigned limiting failure strains in tension and compression, ϵ_i^k , $\epsilon_i^{k'}$, respectively. These limiting values are the same in magnitude for shear strain. In case of stochastic failure strains these are normal distributions. The probability of $\tilde{\epsilon}_i^k$ to exceed deterministic border ϵ_i^k is simply the area under differential distribution of $\tilde{\epsilon}_i^k$ on the right side of the upper bound ϵ_i^k , and can be calculated from integral distribution $F_{\tilde{\epsilon}_i^k}$ of ply strain by using eq.(7).

$$r_i^k = 1 - F_{\tilde{\epsilon}_i^k}(\epsilon_i^k) \quad (7)$$

For stochastic failure strains $\tilde{\epsilon}_i^k$, probability $\tilde{\epsilon}_i^k$ to exceed $\tilde{\epsilon}_i^k$ can be calculated as probability of random difference $\tilde{\epsilon}_i^k - \tilde{\epsilon}_i^k$ to be negative.

$$r_i^k = F_{\tilde{\epsilon}_i^k - \tilde{\epsilon}_i^k}(0) \quad (8)$$

Parameters of integral distribution $F_{\tilde{\epsilon}_i^k - \tilde{\epsilon}_i^k}$ can be calculated as

$$\overline{\tilde{\epsilon}_i^k - \tilde{\epsilon}_i^k} = \tilde{\epsilon}_i^k - \tilde{\epsilon}_i^k$$

$$D_{\tilde{\epsilon}_i^k - \tilde{\epsilon}_i^k} = D_{\tilde{\epsilon}_i^k} + D_{\tilde{\epsilon}_i^k} \quad (9)$$

Taking into account both upper and lower bounds ϵ_i^k and $\epsilon_i^{''k}$, and assuming that strain field excursions beyond the two bounds are statistically independent events, the following expressions for r_i^k can be derived

(a) deterministic bounds $\epsilon_i^k, \epsilon_i^{''k}$

$$r_i^k = 1 - F_{\epsilon_i^k}(\epsilon_i^k) + F_{\epsilon_i^k}(\epsilon_i^{''k}) \quad (10)$$

(b) random bounds $\tilde{\epsilon}_i^k, \tilde{\epsilon}_i^{''k}$

$$r_i^k = F_{\epsilon_i^k - \tilde{\epsilon}_i^k}(0) + F_{\epsilon_i^k - \tilde{\epsilon}_i^{''k}}(0) \quad (11)$$

It is easy to show that second case is reduced to first one when $D_{\epsilon_i^k} = D_{\epsilon_i^{''k}} = 0$. Thus, damage state of each cell is described by three damage parameters $r_i^k = \{r_1^k, r_2^k, r_{12}^k\}$. Note, that according to the developed model damage state in cells depends on weave of textile reinforcement and for $\nu \neq 0.5$, cells with the same orientation in top and bottom sublaminas, which have identical initial elastic characteristics, may become fairly distinct due to damage. Hence, each ply of textile laminate in the proposed model is composed of cells of four different types.

EFFECT OF DAMAGE ON CELL PROPERTIES: MESOVOLUME CONCEPT

In order to use the information about the failure probability we need to specify how is it realized in the composite, i. e. when and how much damages of different types do emerge and how do they effect the current mechanical properties of composite. Assume that there are three types of damages related to three in-plane deformations in each cell $\epsilon_i^k = [\epsilon_{11}^k, \epsilon_{22}^k, \gamma_{12}^k]$. Failure type due to ϵ_{11}^k exceeding the critical bound can be associated with fiber breakage, and those due to ϵ_{22}^k and γ_{12}^k - with matrix cracking in transverse to fiber direction and in shear, respectively.

Assume that each cell consists of certain number of mesovolumes. The mesovolume has to be structurally homogeneous, i.e. to contain sufficient amount of reinforcing fibers to be considered as a continuum, and at the same time it has to be comparatively small in order to satisfy the condition of stochastic homogeneity of stress and strain fields inside its envelope. Initial random characteristics of cells are equal to respective mesovolumes characteristics. Assume that each of the mesovolumes can be either perfect or broken in any of three ways, namely in fiber direction, in transverse direction and in shear. Therefore, we can suppose that at every current state of loading, the relative numbers of broken mesovolumes in cells for each type of failure are proportional to probabilities of failure r_i^k . In the limiting case of the infinite number of mesovolumes in cell the proportionality becomes equality. So, we can interpret the numbers $r_i^k = [r_1^k, r_2^k, r_{12}^k]$ as relative counts of broken meso-elements of three types in each cell.

Accumulation of damages in cells causes stiffness reduction of laminate and stress redistribution around the microcracks and between the cells and plies. This process is very complicated and modeling damage accumulation using micro-level consideration is, in general, not amenable to analytical studies. Probabilistic imitation approach [5] has lead to certain success in the area but it is computationally extensive and needs many simplifying assumptions to be

made as well.

It is assumed in this paper that meso-element failure in certain direction causes deterioration of properties in the same direction. Failure of r_i^k fraction of all meso-elements in i -th direction of k -th cell will result in reduction of cell elastic modulus in this direction. It is proposed that mathematical mean values of cell elastic moduli decrease with damage accumulation according to following hypothesis,

$$\begin{aligned} \bar{E}_1^k(t) &= \bar{E}_{1_0}^k (1 - r_{11}^k(t)) & \bar{E}_2^k(t) &= \bar{E}_{2_0}^k (1 - r_{22}^k(t)) \\ \bar{G}_{12}^k(t) &= \bar{G}_{12_0}^k (1 - r_{12}^k(t)) & \bar{v}_{12}^k(t) &= \bar{v}_{12_0}^k (1 - r_{11}^k(t)) \end{aligned} \quad (12)$$

but relative standard deviations remain constant

$$\frac{\sqrt{D_{E_1^k(t)}}}{\bar{E}_1^k(t)} = \frac{\sqrt{D_{E_{1_0}^k}}}{\bar{E}_{1_0}^k} \quad \frac{\sqrt{D_{E_2^k(t)}}}{\bar{E}_2^k(t)} = \frac{\sqrt{D_{E_{2_0}^k}}}{\bar{E}_{2_0}^k} \quad \frac{\sqrt{D_{G_{12}^k(t)}}}{\bar{G}_{12}^k(t)} = \frac{\sqrt{D_{G_{12_0}^k}}}{\bar{G}_{12_0}^k} \quad \frac{\sqrt{D_{v_{12}^k(t)}}}{\bar{v}_{12}^k(t)} = \frac{\sqrt{D_{v_{12_0}^k}}}{\bar{v}_{12_0}^k} \quad (13)$$

According to this algorithm damage accumulation in cell during laminate loading evokes the shift of cell moduli distributions towards zero direction and narrows these distributions proportionally to stiffness decrease. Changes in statistical distributions of stiffness resulting from damage accumulation according to the proposed algorithm of stiffness reduction are illustrated in Figure 2.

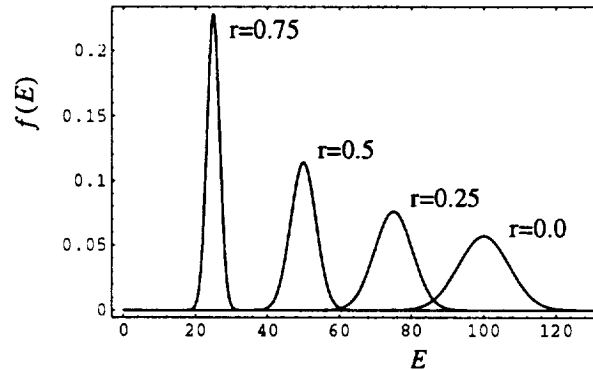


FIGURE 2. Stiffness distributions at various damage levels.

This simple approach does not take into consideration micromechanical phenomena like stress redistribution around the single cracks or cracks interaction, but does take into account gradual stiffness reduction due to damage accumulation in cells and stress redistribution between them.

DISTRIBUTIONS OF CELL MATERIAL CHARACTERISTICS

The basic feature of the proposed method is the consideration of stochastic nature of stress-strain field in the laminate due to stochastic stiffness and strength properties of laminate constituents. In addition, the concept of mesovolume as a building element for textile composites is introduced. Initial random properties of cells should be known to perform analysis. They can be obtained experimentally on small unidirectional specimens or can be calculated using some appropriate micromechanical models. In textile laminate, the scatter of angle of cell orientation

in ply should be taken into account. Experimental inspection of specimens of fabric laminates shows that scatter of orientation depends essentially on the weave type and manufacturing technique.

Experimental statistical data for Kevlar/epoxy unidirectional composite presented in reference [16] are used in the following analysis. The random elastic and strength (critical strain bounds) characteristics are listed in Tables 1 and 2 (first line corresponds to zero deviation of angle). The standard deviations of random characteristics were calculated from their 95% confidential intervals given in [16], using well known statistical formulas.

Effect of scatter of orientation on distribution of cell properties was analyzed using the Monte-Carlo method. First, properties of unidirectional material and angle orientation were chosen at random according to their distributions. Then cell properties were calculated using rotational dependencies of the elastic and strength characteristics. Sets of several thousand samples were computed for each angle deviation value. Resulting mean values and standard deviations of variables are shown in Tables 1,2. Some distributions of material characteristics obtained at 5 degree orientation deviation are shown in Figures 3,4.

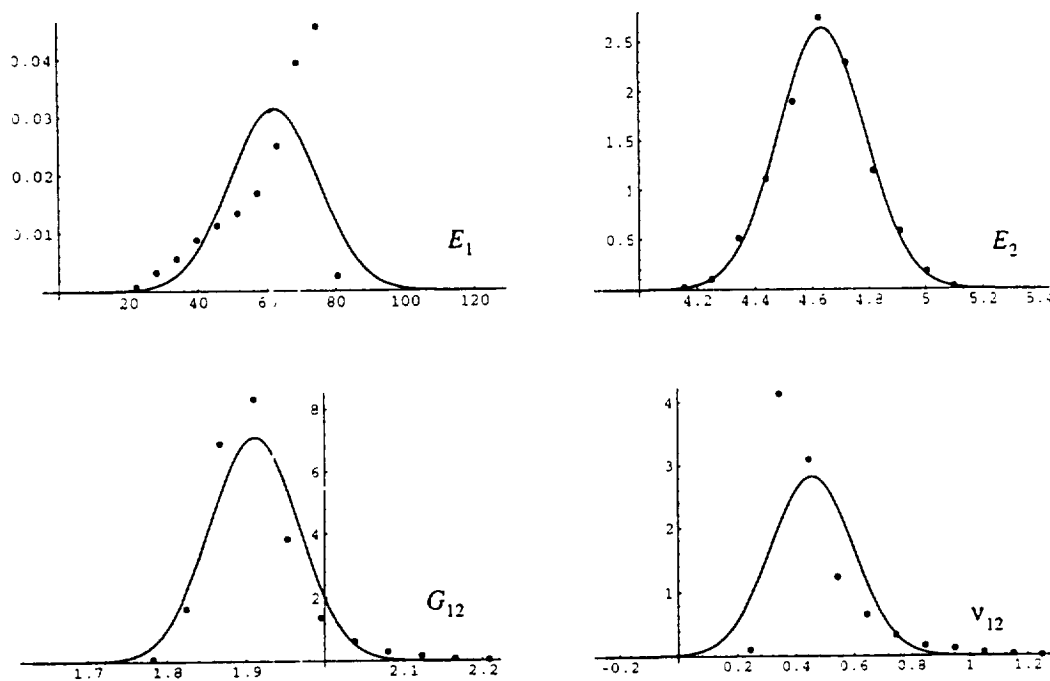


FIGURE 3. Calculated distributions of cell elastic characteristics (points) and their normal approximations (lines)

Analysis shows that scatter of orientation influences considerably the distributions of material properties. The strongest effect is observed for modulus E_1 and Poisson's ratio ν_{12} of the material. The increase of scatter of cell orientation causes decrease in tensile stiffness and slight increase in shear stiffness and failure strain of cell. In all cases, essential increase in deviation of material parameters is observed. Shape analysis of the resulting distributions shows that at larger deviations, some of them become significantly non-Gaussian. The reason for that is an extremal dependence of material properties on orientation angle around zero orientation. Fig-

TABLE 1. Mean Value and Deviation of Cell Elastic Characteristics for Different Orientation Scatter

Angle St. Deviation deg	E_1 GPa	E_2 GPa	G_{12} GPa	ν_{12}
0	74.9/2.22	4.65/0.16	1.88/0.03	0.35/0.031
1	74.0/2.48	4.65/0.16	1.88/0.03	0.35/0.032
2	71.9/4.28	4.65/0.16	1.88/0.03	0.36/0.039
5	62.0/12.9	4.63/0.16	1.91/0.05	0.46/0.14
10	47.1/20.5	4.60/0.16	2.03/0.22	0.71/0.37

* mean / standard deviation

TABLE 2. Mean Value and Deviation of Cell Failure Strains for Different Orientation Scatter

Angle St. Deviation deg	ϵ'_{11} %	ϵ''_{11} %	ϵ'_{22} %	ϵ''_{22} %	$\gamma'_{12}, \gamma''_{12}$ %
0	1.71/.2	-.478/.024	.283/.016	-1.41/.11	2.56/.79
1	1.71/.2	-.478/.024	.284/.016	-1.41/.11	2.55/.82
2	1.72/.2	-.478/.024	.283/.015	-1.41/.11	2.60/.76
5	1.72/.2	-.482/.026	.285/.016	-1.42/.11	2.49/.78
10	1.76/.21	-.494/.035	.292/.021	-1.45/.13	2.35/.92

* mean / standard deviation

Figure 5 shows the variation of elastic characteristics of unidirectional composite with orientation. Figure 6 represents the variation of tensile and compressive deformations at failure with angle, and Figure 7 - the variation of shear failure strain. These extremal dependencies cause the shape change of distributions. In case of low initial scatter the distributions may become one-sided.

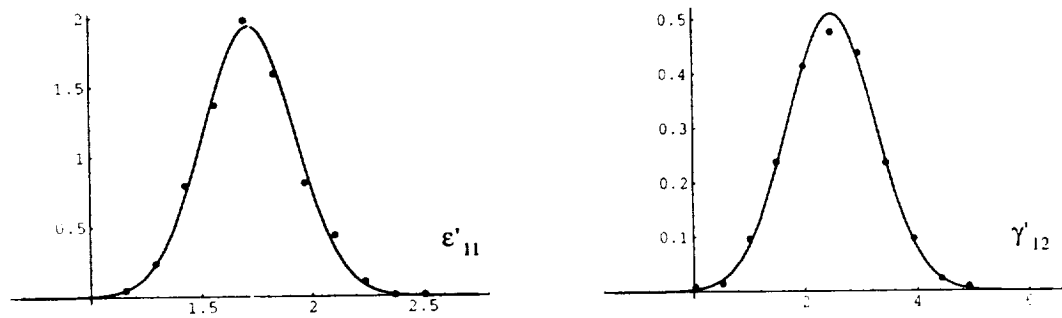


FIGURE 4. Calculated distributions of cell failure strains (points) and their normal approximations (lines).

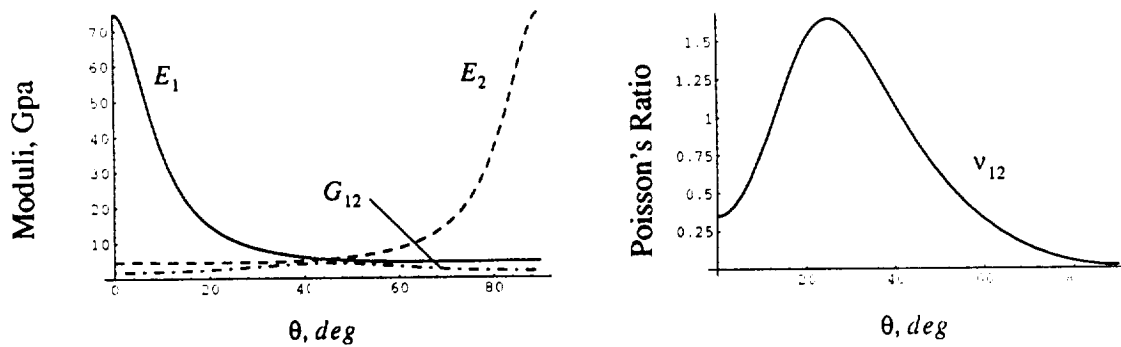


FIGURE 5. Variation of cell elastic characteristics with fiber orientation.

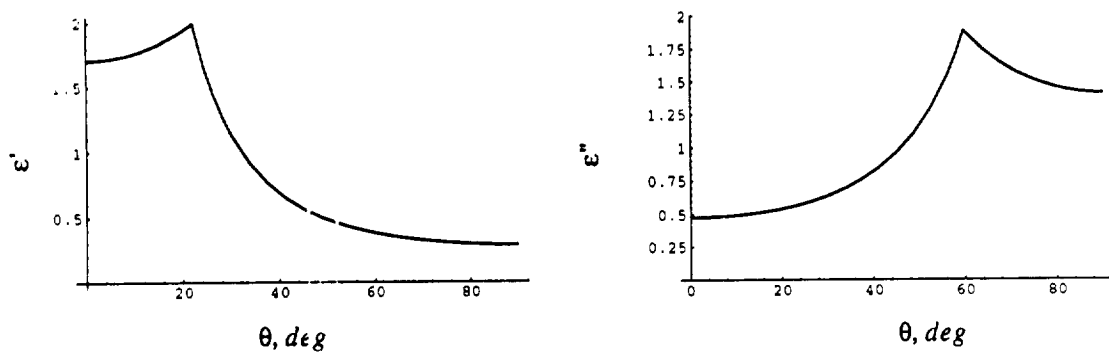


FIGURE 6. Variation of cell failure strains in tension ϵ' and compression ϵ'' with fiber orientation.

The performed calculation of third and fourth moments of distributions (i.e., coefficients

of skewness and kurtosis) and their comparison with literature data [17] have shown that for the material under consideration the 5 deg deviation of angle makes some of material distributions to deviate significantly from normal distribution. Further development of method is required to deal with these situations.

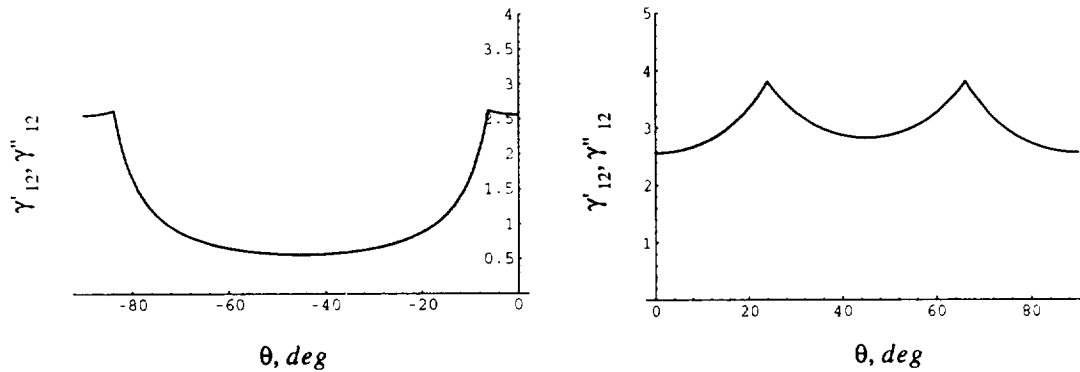


FIGURE 7. Variation of cell failure strain in shear with orientation.

ILLUSTRATIVE EXAMPLE

Computer code is developed for calculating laminate response under the in-plane loading. Incremental loading is set in the program according to given derivatives $\dot{\sigma}_i$ and equation (1) is integrated numerically. On each step of loading the damage functions in cells r_i^k accumulated up to the previous step are used to calculate the current elastic properties of cells and laminate strain increments. It is assumed that complete failure of composite occurs when any of the current effective elastic moduli of laminate $\bar{E}_1, \bar{E}_2, \bar{G}_{12}$ becomes equal to zero (in program - equal to small number). The program is written in "Mathematica" and handles general case of arbitrary ply number, weave and arbitrary cell orientations in plies. Detailed information on damage functions and data on laminate strains and current effective properties are recorded to the data file on each loading step and plotted after completing the computation.

The capability of program is illustrated on an example of Kevlar/epoxy laminate consisting of identical textile reinforced plies. Orientation of cells in the laminate is $[\pm 45]$. Characteristics of Kevlar/epoxy composite with 2 deg orientation deviation (Tables 1,2) are used as cell material properties. The following values of weave parameter ν were used in the analysis - 0.5, 0.33, 0.25, and 0.11, which correspond to plain weave, twill weave, 4 harness satin and 8 harness satin weave, respectively.

Calculated stress-strain diagrams due to shear loading and cumulative damage functions of the composite are shown in Figure 8. Continuous lines, dashed lines and dash-dot lines in the following figures correspond to 11, 22 and 12 variables, respectively. Arrow points toward the lower values of ν . Figure 9 shows the evolution of damages of different type in the laminate, obtained by averaging the damage functions over all cells. One can see that the more inhomogeneous distribution of cells between sublaminas is (lower ν), the greater delay is observed for severe damage formation onset. The axial compressive deformations of laminate seen on the stress-strain diagrams (Figure 8) are due to damage induced anisotropy effect (see discussion in [15]).

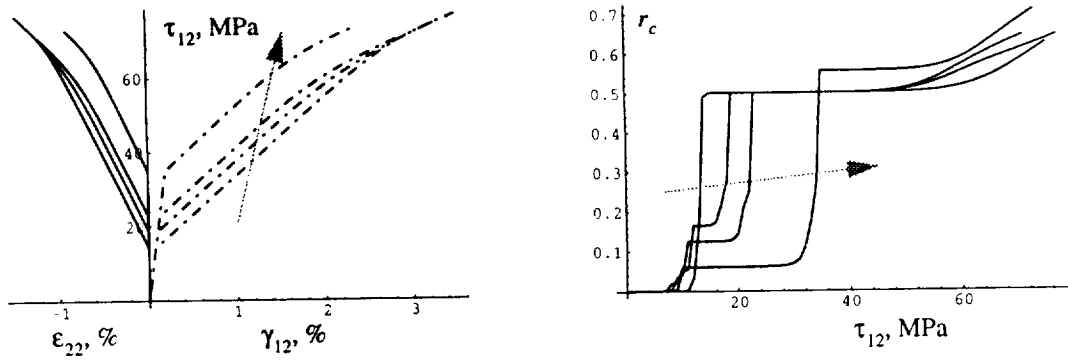


FIGURE 8. Stress-strain diagrams and cumulative damage functions of textile laminate at shear.

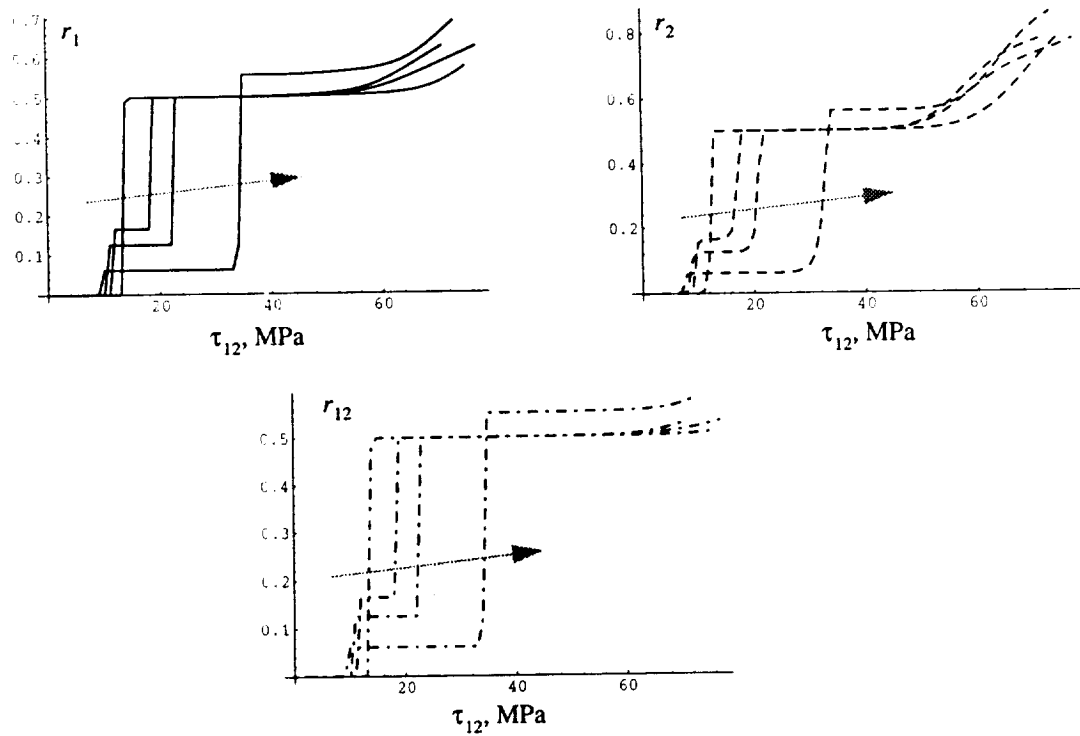


FIGURE 9. Average accumulation of damages of three types in textile laminate.

CONCLUSIONS

Damage evolution in textile laminates under the in-plane loading is discussed in this paper. A laminate model based on the special lamina subdivision is presented which predicts variation of properties with weave parameter. The damage accumulation in such a system is calculated based on the random function theory. Numerical algorithm and computer code for damage accumulation and deformation history prediction are developed. The effect of orientation scatter on the statistical distributions of cell material properties is discussed.

ACKNOWLEDGEMENTS

Yu. A. Dzenis would like to thank his wife, Natasha, for patience.

REFERENCES

1. Ishikawa, T. and Chou, T.W., "One-Dimensional Micromechanical Analysis of Woven Fabric Composites", *AIAA Journal*, 1983, 21, pp.1714-1721.
2. Ishikawa, T. and Chou, T.W., "Stiffness and Strength Behaviour of Woven Fabric Composites", *Journal of Material Science*, 1982, 17, pp.3211-3220.
3. Ishikawa, T. and Chou, T.W., "In-Plane Thermal Expansion and Thermal Bending Coefficients of Fabric Composites", *Journal of Composite Materials*, 1983, 17, pp.92-104.
4. Bogdanovich, A.E. and Pastor, C.M., "On the Structural Analysis of Textile Composites" -In: *Topics in Composite Materials and Structures*, AE-Vol 26, ASME,1992, pp.13-91.
5. Ovchinskii A.S., "Fracture Processes in Composite Materials: Computer Imitation of Micro- and Macromechanisms", (in Russian). Nauka Publ. (Moscow),1988.
6. Wagner H.D., "Statistical Concepts in the Study of Fracture Properties of Fibres and Composites" - In: *Composite Materials Series. Vol. 6. Application of Fracture Mechanics to Composite Materials*, K. Friedrich, ed., Elsevier, 1989, pp.39-77.
7. Argon A., "Statistical Aspects of Fracture" - In: *Composite Materials. Vol. 5. Fracture and Fatigue*, Acad. Press, 1974, pp. 166-205.
8. Bogdanovich, A.E. and Yushanov, S.P., "Buckling Analysis of Cylindrical Shells Having Random Field of Initial Imperfections Under Axial Dynamic Compression", *Mechanics of Composite Materials (Riga)*, 1981, 5, pp. 821-831.
9. Bogdanovich, A.E. and Yushanov, S.P., "On the Calculation of Reliability Function of Anisotropic Shells by Using Technique of Seldom Outbursts of a Stochastic Vector Field Out of the Limiting Surface", *Mechanics of Composite Materials (Riga)*, 1983, 1, pp. 80-89.
10. Yushanov, S.P. and Bogdanovich, A.E. "Method of Reliability Calculation for Imperfect Laminated Cylindrical Shells with Account for Scatter of Composite Strength Characteristics", *Mechanics of Composite Materials (Riga)*, 1986, 6, pp. 1043-1048.
11. Yushanov, S.P., "On Reliability Calculation of Laminated Composite Shells with Random Elastic and Strength Characteristics", *Mechanics of Composite Materials (Riga)*, 1985, 1, pp. 87-96.
12. Yushanov, S.P., "Probabilistic Model of Composite Ply-by-Ply Failure and Reliability Calculation of Laminated Cylindrical Shells", *Mechanics of Composite Materials (Riga)*, 1985, 4, pp. 642-652.
13. Bogdanovich, A.E. and Yushanov, S.P., "A Reliability Analysis of Laminated Composites and Cylindrical Shells" - *Proc. of the Sixth Int. Conf. on Compos. Mater. and Second Europe. Conf. on Compos. Mater.*, London, 1987. Elsevier Appl. Sci. Publ., 1987, vol. 5, pp. 5.525-5.535.

14. Dzenis Yu.A., Joshi S.P., Bogdanovich A.E., Damage Evolution Modeling in Orthotropic Laminated Composites - Proceedings of the 33rd AIAA/ASME/ASCE/AHS/ASC Structures, Structural Dynamics and Material Conference, April 13-15, 1992, Dallas. Part 5, p.2887-2897.
15. Dzenis Yu.A., Joshi S.P., Bogdanovich A.E., Damage Evolution Analysis of Laminates Subjected to Random Quasistatic Loading - Proceedings of the 7th ASC Technical Conference on Composite Materials, October 13-15, 1992, University Park, Pennsylvania, p.1084-1093.
16. Clements, L.L. and Chiao, T.T., "Engineering Design Data for an Organic Fiber/Epoxy Composite", Composites, Vol. 8, No. 2, April 1977, pp. 87-92.
17. Pearson, E.S. and Hartley, H.O., "Biometrika Tables for Statisticians. Vol 1", Campridge, 1966.

1994012389

DEVELOPMENT OF TEST METHODS FOR TEXTILE COMPOSITES

John E. Masters
Lockheed Engineering and Science
Hampton, VA

Peter G. Ifju
Virginia Polytechnic Institute
Blacksburg, VA

Mark J. Fedro
Boeing Defense and Space Group
Philadelphia, PA

57-24

1-21
N94-16862

INTRODUCTION

NASA's Advanced Composite Technology (ACT) Program was initiated in 1990 with the purpose of developing less costly composite aircraft structures. A number of innovative materials and processes have been evaluated as a part of this effort. Chief among them are composite materials reinforced with textile preforms.

These new forms of composite materials bring with them potential testing problems. Methods currently in practice were developed over the years for composite materials made from prepreg tape or simple 2-D woven fabrics. A wide variety of 2-D and 3-D braided, woven, stitched, and knit preforms have been suggested for application in the ACT program. The applicability of existing test methods to the wide range of emerging materials bears investigation. The overriding concern is that the values measured are accurate representations of the true material response.

The ultimate objective of this work is to establish a set of test methods to evaluate the textile composites developed for the ACT Program.

OUTLINE OF PRESENTATION

The figures contained in this paper reflect the presentation made at the conference. They may be divided into four sections as the outline listed below illustrates. A definition of the problem serves as the introduction to the paper. This is contained in the next three figures which outline the methods being investigated and summarize items of concern in applying them to textile composites. This section will be followed by a review of results obtained in a related study of 2-D triaxially braided textile composite materials. These results illustrate the concerns outlined in the introduction. A description of the on-going test methods development effort will be reviewed in the third section. This program, which is in its initial stages, involves a number of investigators in government, universities, and the aircraft industry. The approach taken in the program will be defined. This will be accompanied by an inventory of the material systems being investigated and a list of test methods and investigators. Finally, a short summary will conclude the paper.

> INTRODUCTION

Mechanical Tests Applied to Current Materials

Statement of Problem

Textile Composite Concerns

> 2-D BRAID TEST RESULTS

Material Description

Moiré Interferometry

Strength and Modulus Measurements

> ON-GOING TEST METHODS DEVELOPMENT EFFORT

> SUMMARY

STATEMENT OF PROBLEM

The problem to be addressed is summarized in the two bullet statements given below. Simply stated, the test methods listed in the previous figure were developed to evaluate composite materials formed by laminating layers of pre-impregnated fiber-reinforced tape. The microstructure of these laminated composite materials differs significantly from the braided, woven, and stitched materials to be evaluated in this program. The fiber architecture will play a prime roll in determining the mechanical response of these textile composite materials. Will existing methods and practices accurately reflect the material response of these materials?

- **TEST METHODS DEVELOPED FOR
LAMINATED TAPE COMPOSITES**

- **TEXTILE ARCHITECTURE CONTROLS
MATERIAL RESPONSE**

SCREENING AND CHARACTERIZATION TESTS APPLIED TO LAMINATED TAPE COMPOSITES

The first step taken to meet the program objective was to survey the aircraft manufacturers who were active participants in the ACT program. All organizations were asked to identify the mechanical and physical properties they typically measured to evaluate a new material system. Their response formed the basis for efforts to develop test methods for composite materials reinforced with textile preforms.

Six organizations responded to the inquiry. Each has its own distinct identity and design philosophy. Their approaches to evaluating new materials, however, had many common elements.

The common theme that emerges is that testing of a new material system is conducted in three stages: material screening, material characterization, and development of design allowables. Although none of the test matrices were identical, a number of the tests were common to all lists. The practices employed by the manufacturers in the screening and characterization phases of investigation are listed below in the figure.

<u>TEST TYPE</u>	<u>TEST METHOD</u>
• TENSION:	
Unnotched	ASTM D3039, D3518 MISC. COMPANY METHODS
Notched	SACMA SRM 5 NASA 1142- B9
• COMPRESSION:	
Unnotched	ASTM 3410 SACMA SRM1 NASA SHORT BLOCK MISC. COMPANY METHODS
Notched	SACMA SRM 3 NASA 1092 ST-4 MISC. COMPANY METHODS
• COMPRESSION AFTER IMPACT	SACMA SRM 2 NASA 1142 B11
• BOLT BEARING	MISC. COMPANY METHODS
• INTERLAMINAR TENSION	FLATWISE TENSION CURVED BEAM
• INTERLAMINAR SHEAR	ASTM D2344
• MODE I DELAMINATION	DOUBLE CANTILEVER BEAM
• MODE II DELAMINATION	END NOTCHED FLEXURE

TEXTILE COMPOSITE TESTING ISSUES

It is not difficult to identify a number of specific testing issues relative to textile composites. Several of these concerns, which are applicable to virtually all of the test methods listed on the previous page are listed below.

The first two reflect the unique size effects these materials may present. A unit cell is defined as the smallest unit of repeated fiber architecture. It may be considered the building block of the material. The size of the unit cell is dependent on a number of factors including the size of the yarns, the angle at which they are intertwined or interwoven, and the intricacy of the braid or weave pattern. A representative volume of material must be tested and monitored to accurately reflect true material response. Specimen geometry and strain gage sizes must be reexamined in terms of unit cell size. The effect of the sizes of the yarn bundles must also be considered since they may also effect the performance and the measurements. This is expressed in the third statement.

The final three items on the list reflect concerns over specimen geometry. Test specimen dimensions established for tape type composites may not be applicable to textile composites. The degree of heterogeneity present in the latter materials is quite different than that encountered in the former. The potential effects of these differences must be also quantified.

A limited amount of relevant data has been developed for 2-D triaxially braided textile composites. These results will be reviewed in the following section. They include Moiré interferometry and strength and modulus measurements.

- **EFFECT OF UNIT CELL SIZE ON MECHANICAL PERFORMANCE**

- **EFFECT OF UNIT CELL SIZE ON STRAIN GAGE AND DISPLACEMENT MEASUREMENTS**

- **EFFECT OF TOW SIZE AND FIBER ARCHITECTURE ON MECHANICAL PERFORMANCE**

- **EFFECT OF FINITE WIDTH ON UNNOTCHED AND OPEN-HOLE SPECIMENS**

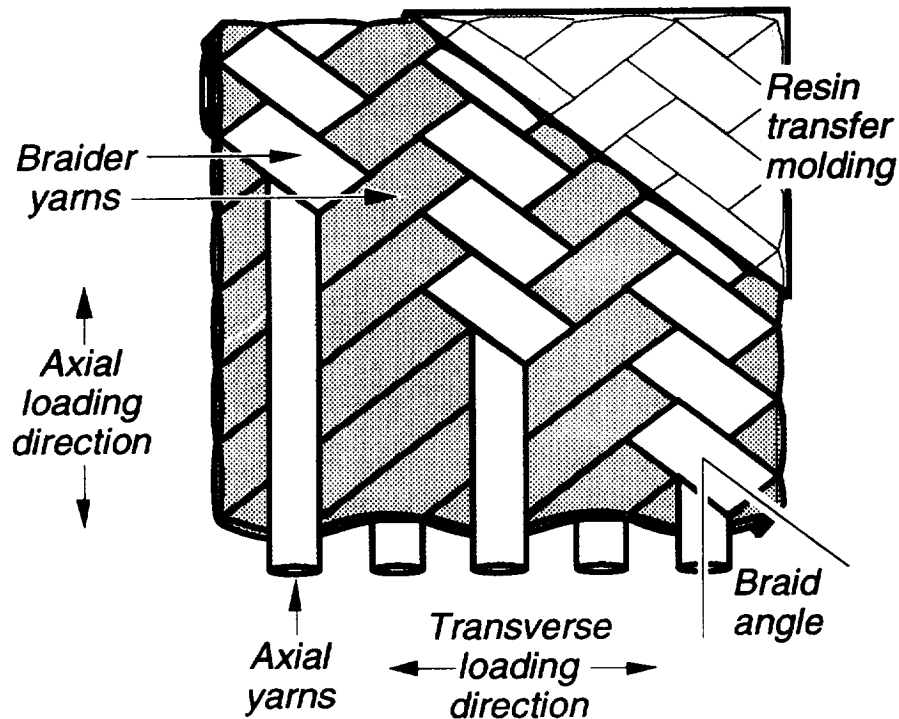
- **EFFECT OF EDGE CONDITIONS ON MECHANICAL PERFORMANCE**

- **EFFECT OF TEXTILE THICKNESS ON MECHANICAL PERFORMANCE**

TRIAXIAL BRAID PATTERN: DESCRIPTION OF MATERIAL TESTED

The specimens studied in this investigation featured 2-D triaxially braided AS4 graphite fiber preforms impregnated with Shell 1895 epoxy resin. In a triaxially braided preform three yarns are intertwined to form a single layer of $0^\circ/\pm\Theta^\circ$ material. In this case, the braided yarns are intertwined in a 2 x 2 pattern. Each $+\Theta$ yarn crosses alternatively over and under two $-\Theta$ yarns and vice versa. The 0° yarns were inserted between the braided yarns. This yields a two dimensional material. The figure below schematically illustrates the fiber architecture and establishes the nomenclature used in the paper.

The yarns were braided over a cylindrical mandrel to a nominal thickness of 0.125 in. The desired preform thickness was achieved by overbraiding layers; there are no through-the-thickness fibers. After braiding, the preforms were removed from the mandrel, slit along the 0° fiber direction, flattened, and border stitched to minimize fiber shifting. The resin was introduced via a resin transfer molding process.



TRIAXIAL BRAID CONFIGURATIONS

Three preform parameters, braid angle, yarn size, and 0° yarn content, were varied in this study. The last parameter listed is typically expressed as a percentage of 0° yarns. It is the volumetric proportion of longitudinal yarns to total yarn content and is a function of braid angle and yarn size. Yarn size is expressed in terms of the number of filaments per yarn. The AS4 fibers used in these materials have a nominal diameter of 7 microns. The longitudinal yarns were larger than the braided yarns in all cases. The B1 and B2 architectures had the same yarn sizes; they differed in braid angle and 0° yarn content. The preform parameters are listed in the table.

The fabrics were formed with a 144 carrier New England Butt triaxial braider, incorporating 72 longitudinal yarns. The mandrel diameters varied for each architecture. Since the number of carriers was constant, this had the effect of changing the yarn spacing. These parameters are also listed in the table.

MATERIAL	BRAID PATTERN	BRAIDER YARN SIZE	0° YARN SIZE	0° YARN CONTENT (%)	0° YARN SPACING (Yarn/In.)	BRAID YARN SPACING (Yarn/In.)
A1	0/± 63°	12K	24K	31.5	4.17	9.16
B1	0/±66.5°	6K	18K	37.6	4.77	11.98
B2	0/±70°	6K	18K	34.0	4.37	12.74

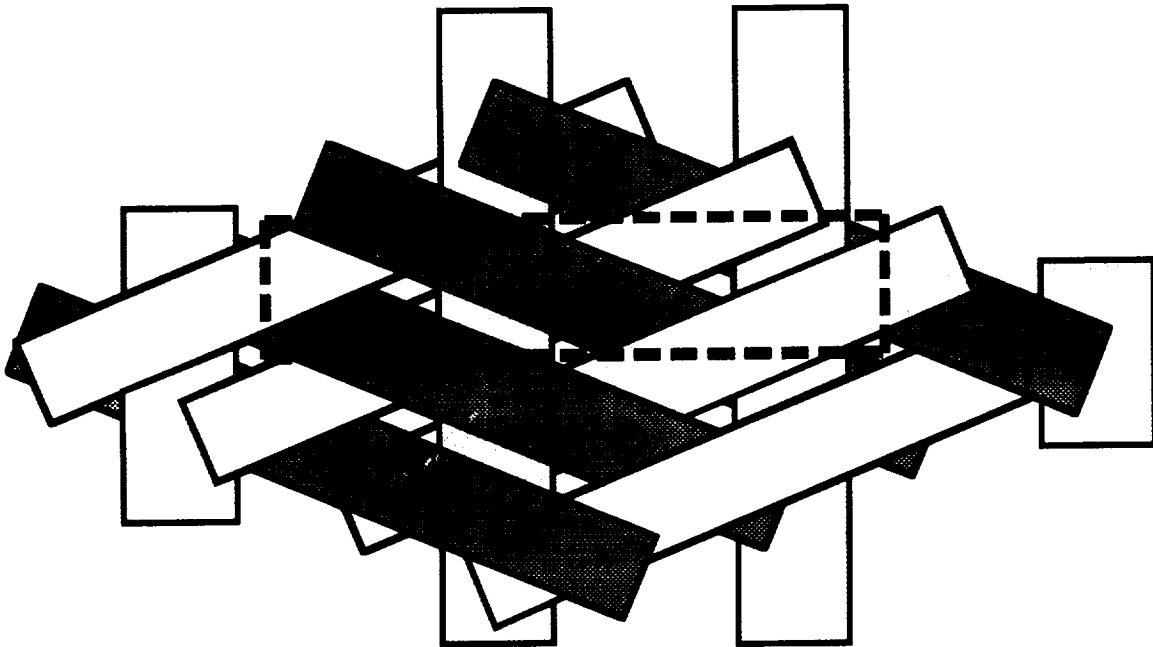
Note: K indicates thousands. For the AS-4 yarns, each filament is 7 microns in diameter

UNIT CELL DEFINITION

A convenient way to describe textile preforms is to identify a unit cell of material - a repeatable unit of fabric geometry. The unit cell represents the complete yarn intertwinement pattern. The unit cell approach has become the foundation of textile analysis and serves as a convenient framework in which to interpret experimental data.

The rhombic frame shown in the figure defines a unit cell for the 2-D triaxially braided material studied in this program. For computational purposes, it is desirable to define the smallest unit cell possible. In some analyses, rectangular unit cells are also required. The rectangular section shown in the figure represents the smallest unit cell identified.

The table shown below contains the dimensions of the unit cells for the three architectures tested. The unit cell width is dependent on the mandrel diameter and the number of yarns braided. The height of the unit cell is dependent on the cell width and the braid angle. Even though a conservative definition of the unit cell was applied in this case, the data in the table indicate that the unit cells can be quite large compared to typical specimen and strain gage dimensions.



UNIT CELL DIMENSIONS

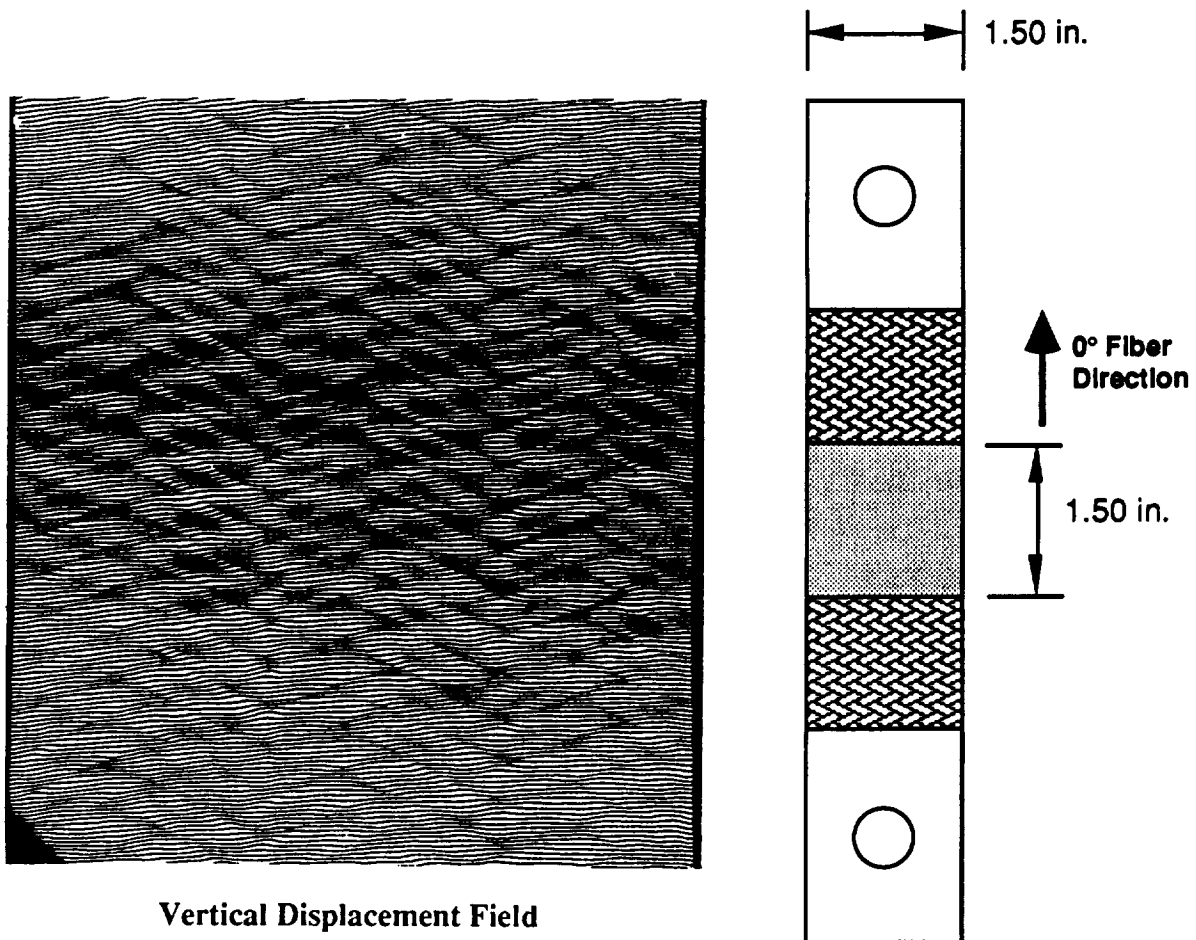
MATERIAL	WIDTH (in.)	HEIGHT (in.)
A1	0.48	0.12
B1	0.42	0.09
B2	0.46	0.08

MOIRÉ INTERFEROMETRY Axial Load - Vertical Displacement Field

As indicated earlier, Moiré interferometry was used to define the full field strain distribution in these braided specimens. The technique defines deformation patterns in both the vertical and horizontal directions. The technique was applied to specimens subjected to longitudinal and transverse loading. These results are shown in this and the following figures.

The figure below illustrates the specimen geometry and highlights the section studied. The vertical displacement field that resulted when a specimen was loaded to 1200 micro-strain along the 0° fiber direction is also shown in the figure.

The vertical displacement fields (V fields) consist of basically horizontal fringes; this indicates specimen extension where points along one fringe have been displaced vertically with respect to points along a neighboring fringe. For a uniform extension the fringes should be evenly spaced and straight. The fringes for the specimens tested, however, are wavy and the spacing between them varies. The variation is cyclic and coincides with the repeated unit of the textile architecture.

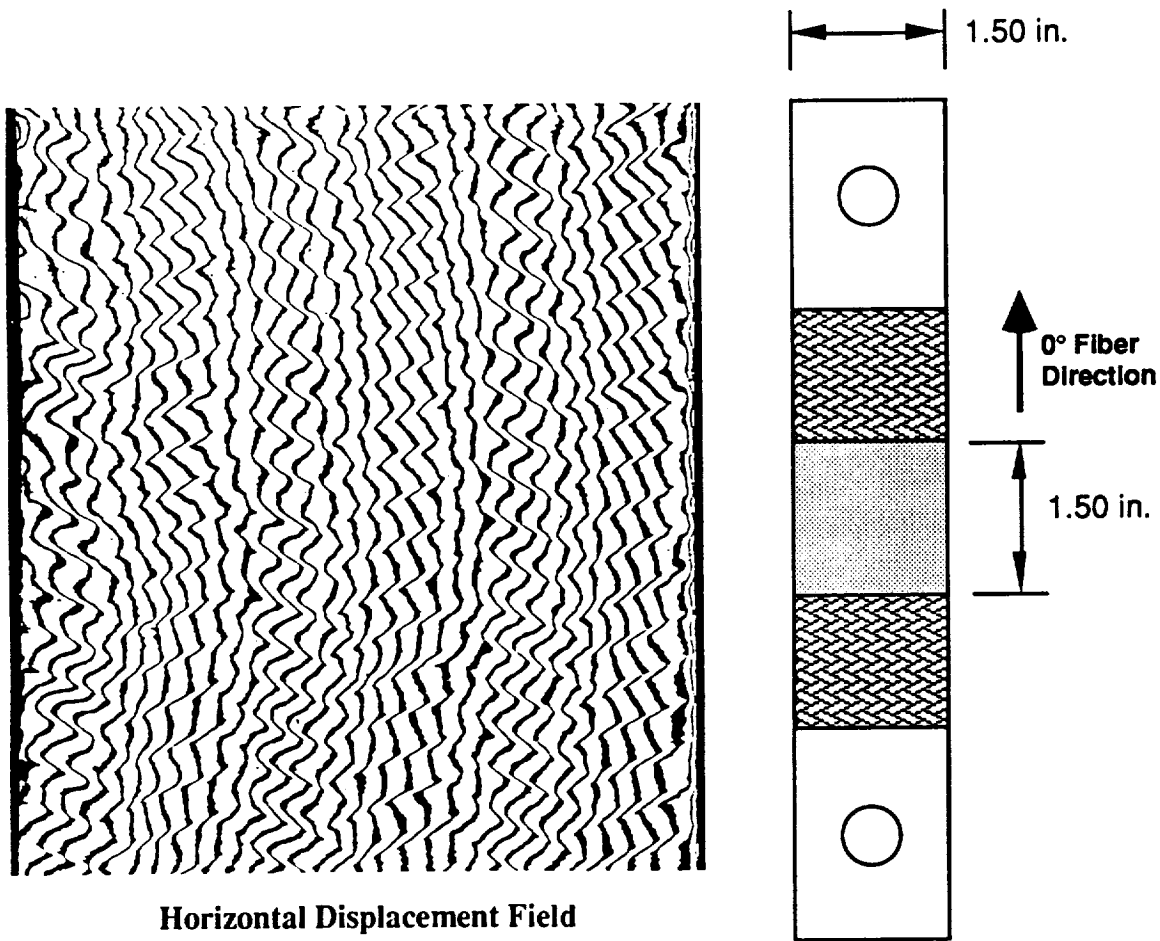


Vertical Displacement Field

MOIRÉ INTERFEROMETRY

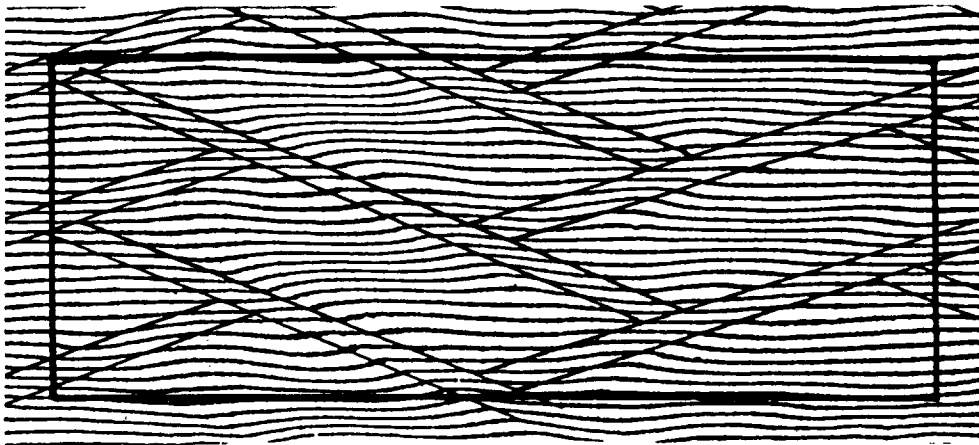
Axial Load - Horizontal Displacement Field

The horizontal displacement patterns (U fields) consist of zigzag vertical fringes that display the Poisson's effect. For uniform contraction the fringes should be straight and the spacing constant. The fringes however display a variation which is cyclic, and matches that of the braid geometry. The sharp kinks in the U field fringes reveal the presence of shear strains between the fiber bundles.

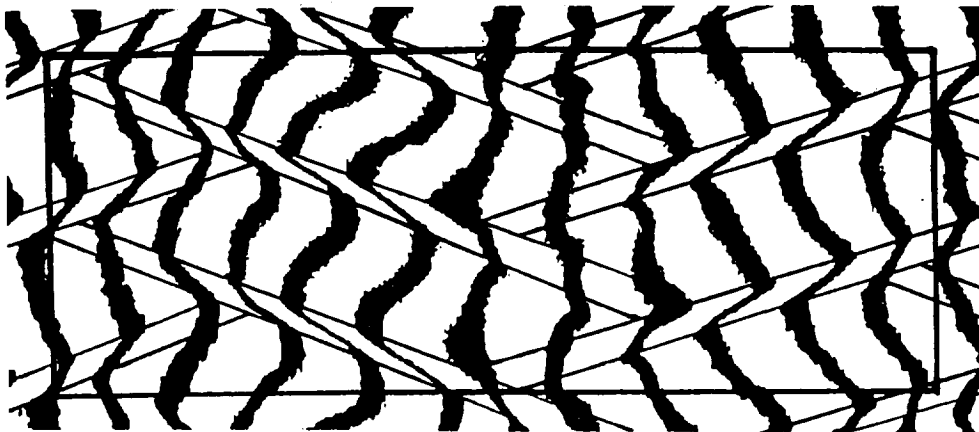


ENLARGED VIEW OF TWO UNIT CELLS OF SPECIMEN (Axial Loading)

The figure shows the V and U fields of a highly magnified region of specimen that consists of two unit cells. The boundaries between adjacent fiber bundles and the outline of the cells are marked. It was revealed that the shear deformation at interfaces between the fiber bundles occurred over a finite width. This width is illustrated in the patterns as the distance between the closely spaced lines. This is consistent with the presence of the resin rich areas between the fiber bundles, which was on the order of one fifth of the width of the fiber bundle itself. The U field shows that the shear strain γ_{xy} in the resin rich zones was on the order of 0.5 times that of the average applied normal strain ϵ_y . Additionally, the U field shows that the Poisson effect was nearly constant across the unit cell. The V displacement pattern clearly shows that the strain ϵ_y varies significantly within each unit cell as can be seen by the nonuniform fringe spacing. The ratio of maximum strain ϵ_y to minimum strain was about 2 to 1. The normal strain varies on top of the fiber bundles and is nearly constant throughout all of the resin rich zones.



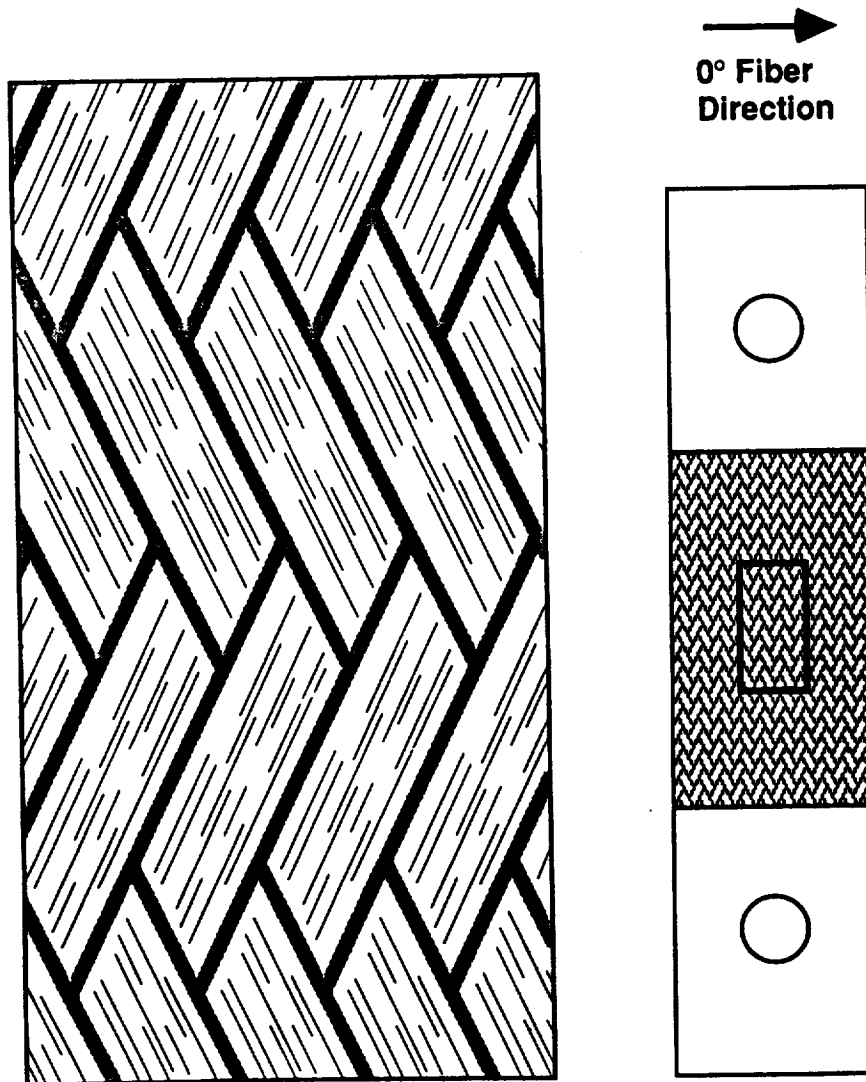
Vertical Displacement Field



Horizontal Displacement Field

**SPECIMEN SECTION COINCIDING WITH
MOIRÉ FRINGE PATTERNS
(Transverse Loading)**

Interferometry was also performed on specimens loaded in the transverse direction (i.e. at 90° to the axial direction). This figure shows the region investigated in these specimens. The pattern of the surface braided yarns is shown schematically in the figure. The deformation fields that developed in these coupons are shown in the next two figures.

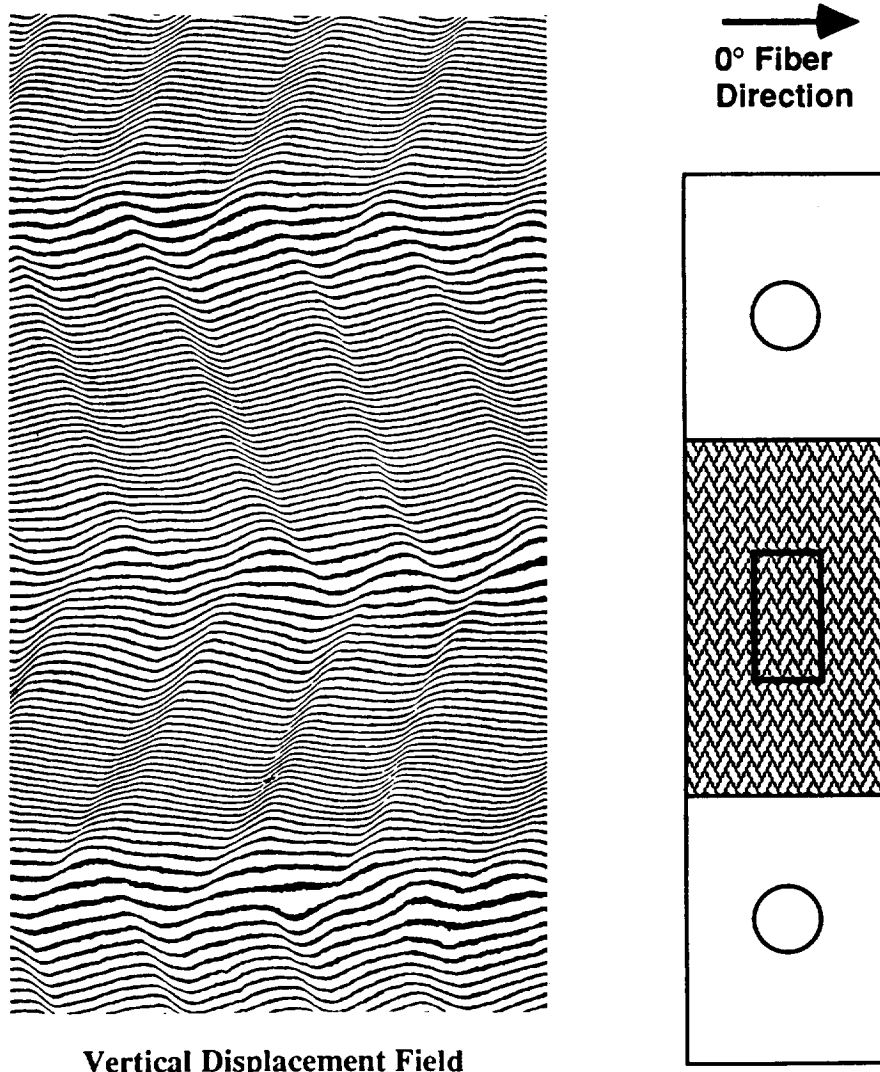


MOIRÉ INTERFEROMETRY Transverse Load - Vertical Displacement Field

In general, the interferometry results indicate that greater variations in normal and shear strains existed in specimens loaded in the transverse direction than in the axial direction.

This figure displays the vertical displacement field for a coupon loaded in the transverse direction. The location of the yarns are evident in the vertical displacement fringe patterns, where sudden jogs in the fringes represent strong shear strains in the resin rich regions between the yarns. From the V displacement pattern, the spacing of the fringes in the vertical direction displays a cyclic variation. The strains are highest over the region where there are 90° fibers under the braider yarns. They are lowest over the regions where the braider yarns cross. The difference between the average strains in these areas is on the order of 3 times.

Unlike the axial loading case, the cyclic variation is not confined to the dimensions of the unit cell. The variation breaches the unit cell to form a global material response that covers the entire specimen. This is illustrated by the horizontal bands seen in the figure. They span several unit cells and extend across the specimen width.



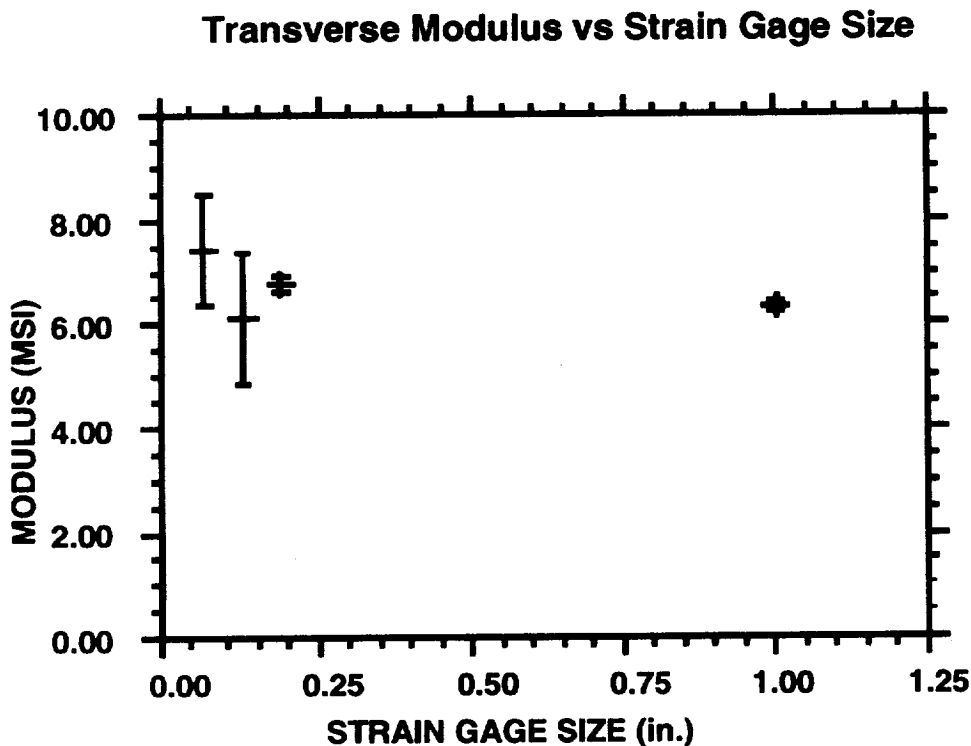
Vertical Displacement Field

CONSIDER STRAIN FIELD INHOMOGENEITY WHEN CHOOSING INSTRUMENTATION

The inhomogeneity in the strain fields demonstrated in the Moiré interferometric results discussed in the previous slides has significant implications with regard to specimen instrumentation. The large strain gradients seen within the unit cell graphically illustrate the need to measure strain over a truly representative volume of material to get an accurate determination of the global material response. Local strain readings can be misleading and confusing.

The data shown in the figure below demonstrate these points. The figure plots the measured transverse modulus of several B1 laminates vs. the size of the gages used to measure the strain. The gages ranged in length from 0.062 in. to 1.0 in.; the preform's unit cell measures 0.42 in. in this direction. The average modulus and the standard deviation of the data are shown in the figure. As the figure indicates, significant scatter was evident in the results obtained using the small gages. These effects were reduced as the length of the gage increased. The results also indicate that average value also decreased as strain gage size increased.

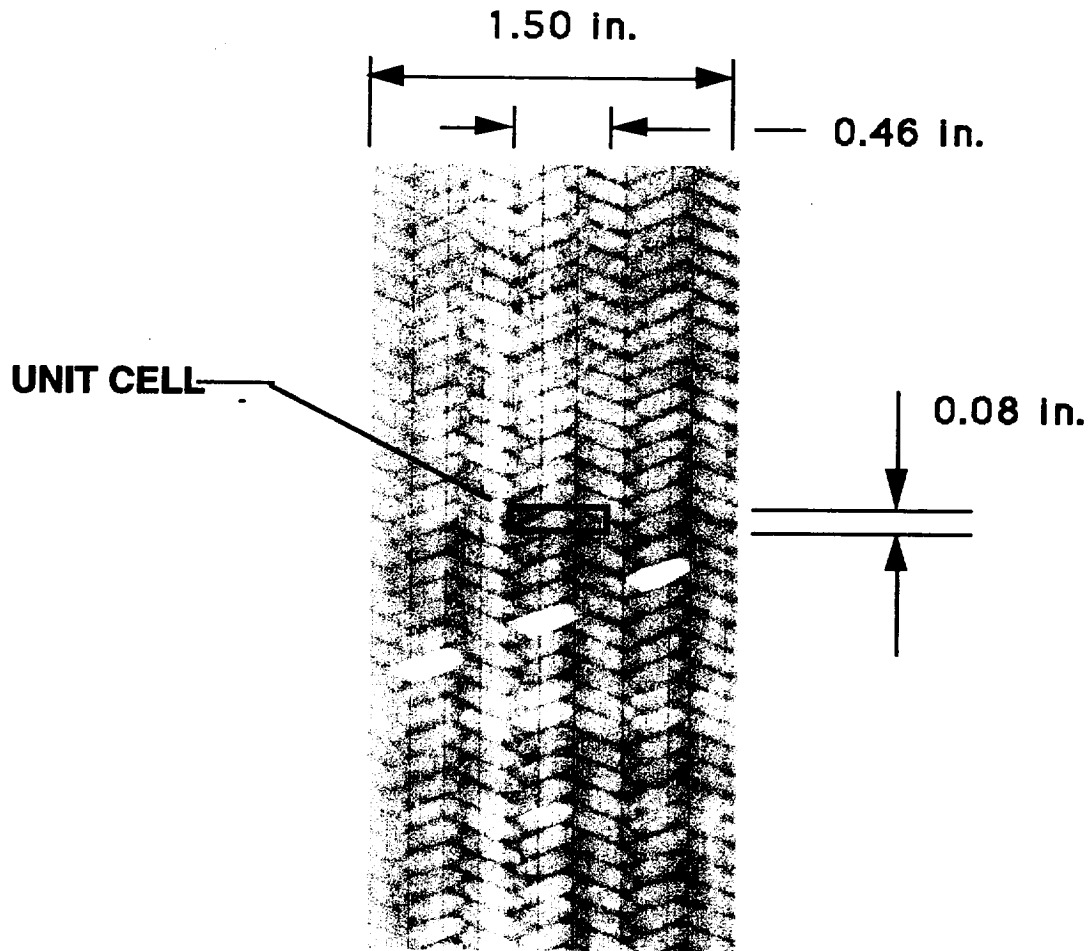
The results illustrate the need to consider the textile architecture when choosing instrumentation for a specimen.



MATERIAL ARCHITECTURE AND TEST COUPON GEOMETRY

The preform architecture must also be considered when designing test specimens. The figure below contains a photograph of a tensile test coupon. The specimen, which is typical of those commonly used in screening and evaluation test programs, is 1.5 in. wide and 10 in. long. Superposed on the photograph are the B2 architecture's unit cell dimensions. As the figure illustrates, when oriented in this direction, the specimen is only three unit cells wide. This again raises the question of whether a representative volume of material is being sampled in the test.

Specimen width and thickness must be considered when designing test specimens to attain true measures of modulus and strength. Unfortunately, design criteria have not yet been established for these materials.

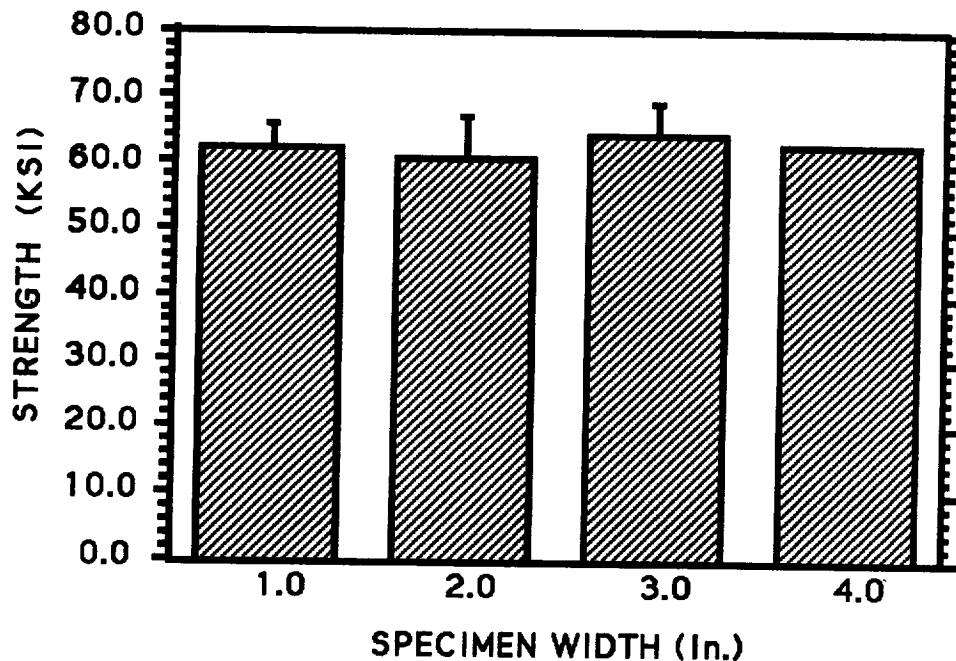


EFFECT OF SPECIMEN WIDTH ON STRENGTH (Data Normalized to 55% Fiber Volume)

A series of longitudinal tensile tests were conducted to judge cursorily the effect of specimen width on strength of the B2 type 2-D triaxially braided laminates defined in an earlier figure. In these tests specimen width was varied from 1.0 in. (2 unit cells wide to 4.0 in. (8 unit cells wide).

The results of these tests are shown in the figure below. The data, which have been normalized to 55% fiber volume to simplify the comparison, indicate that specimen width had no apparent effect on the test results for this architecture. The average strengths and the standard deviations of the results (indicated by the bars in the figure) were comparable for each group of tests (note: the 4.0 in. data represents the average of two tests; the standard deviation was not computed).

A larger, more complete examination of the interaction of textile architecture and test laminate geometry is underway as a part of an effort to develop test methods for textile composites. This effort will be outlined in the following pages.



TEST METHODS DEVELOPMENT: PROGRAM OBJECTIVE

As indicated below, the objective of this on-going effort, simply stated, is to develop a set of test methods and guidelines to be used to measure the mechanical and physical properties of composite materials reinforced with fibrous textile preforms. Investigations conducted to date have indicated that existing methods, which were developed largely to evaluate laminated tape type composites, may not adequately address the subtleties of these new material forms.

**DEVELOP AND VERIFY NASA RECOMMENDED MECHANICAL TEST
PROCEDURES AND INSTRUMENTATION TECHNIQUES
FOR TEXTILE COMPOSITES**

TEST METHODS DEVELOPMENT: PROGRAM APPROACH

A straightforward approach has been adopted to meet the objective outlined in the previous figure. An extensive test program will be conducted to gather data addressing the concerns listed earlier. The program, which will include a wide variety of woven, braided, and stitched preform architectures, will consider several loading conditions.

The general approach is outlined in the figure below. Details of material tested and test methods are supplied in the following pages.

- **IDENTIFY AND/OR DESIGN AND DEVELOP SPECIMEN CONFIGURATIONS AND TEST FIXTURES**

- **CONDUCT MECHANICAL TEST PROGRAM**
 - **Variety of Test Methods**
 - **Variety of Instrumentation Techniques**
 - **Full Field Strain Measurements**
 - **Analytical Support**

- **IDENTIFY SMALLEST LEVEL OF HOMOGENEITY**

- **IDENTIFY APPROPRIATE TEST METHODS AND INSTRUMENTATION GUIDELINES**

MATERIAL SYSTEMS FOR TEST METHOD DEVELOPMENT

Fifteen woven, braided, and stitched preforms will be evaluated in the program. The preform types are listed below in the table; the number of each type to be tested is indicated in parentheses. The table also lists the braid parameter that will be varied for each preform type. The list of materials reflects the material forms that are being evaluated by the aircraft manufacturers in the ACT program.

TEXTILE PREFORM TYPES:

- **2-D TRIAXIAL BRAIDS - (4)**
 - Tow Size
 - % Longitudinal Tows
 - Braid Angle
- **3-D INTERLOCK WEAVE - (6)**
 - Weave Type - (3)
 - Warp, Weft, and Weaver Tow Size
- **STITCHED UNIWEAVE - (5)**
 - Stitch Material
 - Stitch Spacing
 - Stitch Yarn Size

MATERIALS:

FIBER: HERCULES AS4

RESIN: SHELL 1895

STANDARD TEST METHOD PROGRAM FOR TEXTILE COMPOSITES

The types of tests being developed and the organizations involved in their development are listed in the table below.

<u>TEST TYPE</u>	<u>ORGANIZATION</u>
• STRAIN GAGE GUIDELINES	BOEING DEFENSE & SPACE LOCKHEED ENG. & SCIENCE
• TENSION Unnotched Notched	BOEING DEFENSE & SPACE
• COMPRESSION Unnotched Notched	BOEING DEFENSE & SPACE NASA/LANGLEY
• IN-PLANE SHEAR	BOEING DEFENSE & SPACE VA. TECH
• BOLT BEARING	BOEING DEFENSE & SPACE
• COMPRESSION AFTER IMPACT	NASA LOCKHEED ENG. & SCIENCE
• OUT-OF PLANE LOADS	NASA UNIVERSITY OF DELAWARE

SUMMARY

A brief summary of the technical results reviewed in the presentation is given below. The experimental investigation conducted on 2-D braided materials indicated that significant strain gradients existed within the materials unit cell as a result of the braid architecture. This inhomogeneity in the strain field is an important factor that must be considered when choosing instrumentation for a test specimen. Although the 2-D braided laminates tested did not demonstrate a width effect, the size of the unit cell must also be considered when designing a test specimen.

Finally, the concerns discussed above and others listed in an earlier figure will be addressed in an on-going test method development effort.

- **MOIRÉ INTERFEROMETRY IDENTIFIED LARGE STRAIN GRADIENTS WITHIN THE UNIT CELL**
- **INHOMOGENEITY IN STRAIN FIELD EFFECTS INSTRUMENTATION**
- **UNIT CELL SIZE MAY AFFECT TEST RESULTS**
- **ON-GOING INVESTIGATION TO DEFINE TEXTILE TEST METHODS UNDERWAY**



1994012390

513-24

Three-Dimensional Analysis of Anisotropic Spatially Reinforced Structures

Alexander E. Bogdanovich

N 94-16863

Latvian Academy of Sciences, Riga, Latvia
(Currently: Visiting Research Associate Professor, North Carolina State University
Raleigh, NC 27695-8301, USA)

SUMMARY

The material-adaptive three-dimensional analysis of inhomogeneous structures based on the meso-volume concept and application of deficient spline functions for displacement approximations is proposed. The general methodology is demonstrated on the example of a brick-type mosaic parallelepiped arbitrarily composed of anisotropic meso-volumes. A partition of each meso-volume into sub-elements, application of deficient spline functions for a local approximation of displacements and, finally, the use of the variational principle allows one to obtain displacements, strains and stresses at any point within the structural part. All of the necessary external and internal boundary conditions (including the conditions of continuity of transverse stresses at interfaces between adjacent meso-volumes) can be satisfied with requisite accuracy by increasing the density of the sub-element mesh. The application of the methodology to textile composite materials is described. Several numerical examples for woven and braided rectangular composite plates and stiffened panels under transverse bending are considered. Some typical effects of stress concentrations due to the material inhomogeneities are demonstrated.

INTRODUCTION

Unlike traditional laminated materials, textile reinforced composites are characterized by a variation of their physical properties in all three directions. Therefore, textile composites have to be treated as complex three-dimensional hierarchical structures rather than as traditional, structurally quasi-homogeneous materials. However, the direct application of numerical analysis to a textile composite structural part starting with the hierarchical level "single fiber - matrix" seems to be unrealistic even when utilizing the most advanced super-computing facilities. Obviously, the analysis of a multi-level structured material has to be specified for the particular engineering problem.

For the case when only displacements are of interest, the analysis of a "fully homogenized" textile structural part may be useful in many practical situations. The whole part can thus be identified as a single "meso-volume" in the terminology of [1-3]. If the information about all six stress components in the structural part is needed, the internal interfaces gain importance and, correspondingly, the next hierarchical level has to be considered. At this level, the whole structure can be treated as an assemblage of distinct, anisotropic structurally homogeneous elements (meso-volumes). Starting at this level, some "global" failure effects in a structural part can be predicted using traditional phenomenological failure criteria. In the case when "local" failure effects are of interest, one has to start at the next hierarchical level, namely, the level of a single yarn surrounded by matrix material. The same concept of a meso-volume can be applied to this analysis supposing that a structurally homogeneous yarn element and matrix element represent two distinct types of meso-volumes [1]. Finally, the yarn itself can be considered as a complex structure. When the aim is predicting fracture initiation inside a single yarn, fiber elements surrounded by resin can be

considered as meso-volumes. Note that for traditional laminated composite structural parts there are three typical hierarchical levels: (i) an anisotropic homogenized structural part; (ii) an anisotropic structurally homogeneous layer; (iii) a single fiber surrounded by a matrix material. It is important to point out that the internal reinforcement architecture of textile composites at any of the sub-structural hierarchical levels is considerably more complex than reinforcement architecture of traditional laminated composites [4-7].

It follows from the above considerations that textile composite structures need a special approach for stress and failure analyses. Neither common theories of laminated structures with their corresponding finite element approaches nor strength-of-materials methodologies are usable.

In a "perfect" model of a composite laminate, as well as in a model for a spatially reinforced material, both the conditions of continuity of displacements and transverse stresses must be satisfied through the entire structural part. The continuity of transverse stresses can be achieved only if transverse strains are assumed to be discontinuous at each physical interface, as follows from Hooke's law. This leads to the requirement for the discontinuity of the first derivatives of displacements. Therefore, only those kinematic models which incorporate the above mentioned discontinuities can be considered valid. In [1] this topic was thoroughly discussed in the context of finite element modelling of laminated composite structures. According to the concept proposed, there is an opportunity to develop a rather general displacement-assumed computational model for a complex reinforced composite structural part using its primary "material-adaptive" partition into meso-volumes, then additional, purely computational partition into sub-elements inside each meso-volume. Afterwards, an approximation of the unknown displacement fields with respect to the whole discretization introduced by these two partitions in terms of deficient spline functions can be realized.

In the present paper this idea is used for the analysis of spatially reinforced rectangular plates and stiffened panels. To demonstrate the functionality of the method, several examples are considered. The first example models the behavior of a triaxially braided composite when the material is treated: (i) as a homogeneous material and (ii) as a six layer material. The structural responses predicted by modelling the material as an anisotropic homogeneous solid as opposed to a "laminate" are analyzed. The second example studies the behavior of a plain weave plate having geometrical parameters of the unit cell when modelled as a three-dimensional "brick" system. In the brick model presented herein, the material-adaptive aspect of the analysis is employed to maintain the continuity of displacements and stresses throughout the plate. Finally, a triaxially braided "skin - stiffener" structure is modelled using brick-type elements with elastic properties of distinct bricks derived from the homogenized properties of the triaxially braided material.

MATERIAL - ADAPTIVE ANALYSIS OF COMPOSITE STRUCTURES

Spline approximations

A general methodology for the analysis of inhomogeneous materials and structures can be demonstrated on the example of a brick-type mosaic parallelepiped shown in Figure 1, a. In this case the internal boundaries separate adjacent bricks (each brick having unique physical properties), and the boundaries are parallel to the side planes of the parallelepiped. Let us designate the set of planes containing all of these boundaries as $P_x = \{x=x_0=0, x=x_1, \dots, x=x_K=a\}$, $P_y = \{y=y_0=0, y=y_1, \dots, y=y_L=b\}$, and $P_z = \{z=z_0=0, z=z_1, \dots, z=z_M=c\}$. Thus, the parallelepiped contains $K \times L \times M$ structurally homogeneous meso-volumes. In general, each meso-volume has distinct properties, but in certain obvious practical situations some adjacent meso-volumes have identical properties. Accounting for this possibility is one of the key features of the algorithm to be developed.

A system of spline functions suitable for approximation of displacements in the parallelepiped must satisfy the following conditions:

- (i) Spline functions dependent on each of the x , y , and z coordinates are continuous with respect to the corresponding coordinate inside the whole parallelepiped. This guarantees continuity of displacements inside the structurally inhomogeneous body;
- (ii) At least one of the x - coordinate set of spline functions is characterized with discontinuous first derivative at each of the points $x=x_1, x=x_2, \dots, x_{k-1}$ where physical properties of adjacent meso-volumes are distinct. Analogous procedure is applied to the spline functions from the y - and z - coordinate sets. This is a necessary condition for satisfying the continuity of the corresponding transverse stresses (the detailed discussion on the problem of approximating functions can be found in [1]);
- (iii) At any internal point of each meso-volume all of the approximating splines have the highest possible degree of continuity.

Construction of the approximation splines starts by generating another three sets of mutually parallel planes: $P_\xi = \{x=\xi_0=0, x=\xi_1, \dots, x=\xi_\lambda=a\}$, $P_\eta = \{y=\eta_0=0, y=\eta_1 \dots, y=\eta_\mu=b\}$, and $P_\zeta = \{z=\zeta_0=0, z=\zeta_1, \dots, z=\zeta_\nu=c\}$ that are of a purely computational meaning. The purpose of these planes is the same as for the sub-division planes introduced in [8] for a laminated plate, Figure 2. Note that all of the planes from the sets P_x, P_y , and P_z coincide with certain planes from the sets P_ξ, P_η , and P_ζ . The recursive procedure used here for derivation of the deficient splines of an arbitrary degree follows in its principal features the procedure worked out in [9], [10] for the case of second degree deficient splines.

The displacement field in the parallelepiped can be represented in the same form as for a laminated plate [8]:

$$\begin{aligned}
 u_x(x,y,z) &= \sum_i \sum_j \sum_k U_{ijk} X_i^u(x) Y_j^u(y) Z_k^u(z) \\
 u_y(x,y,z) &= \sum_i \sum_j \sum_k V_{ijk} X_i^v(x) Y_j^v(y) Z_k^v(z) \\
 u_z(x,y,z) &= \sum_i \sum_j \sum_k W_{ijk} X_i^w(x) Y_j^w(y) Z_k^w(z)
 \end{aligned} \tag{1}$$

The difference appears only in the properties of the spline functions of the first and the second sets, namely $X_i^u(x), X_i^v(x), X_i^w(x)$ and $Y_j^u(y), Y_j^v(y), Y_j^w(y)$. They are not continuous like in the case of a laminated plate, but have selected discontinuous first derivatives.

Basic equations

The stress-strain equations for a generally anisotropic mosaic parallelepiped (Figure 1, a) can be written in the form

$$\begin{aligned}
 \sigma_x &= Q_{11}(\mathbf{r}) \epsilon_x + Q_{12}(\mathbf{r}) \epsilon_y + Q_{13}(\mathbf{r}) \epsilon_z + Q_{14}(\mathbf{r}) \gamma_{yz} + Q_{15}(\mathbf{r}) \gamma_{xz} + Q_{16}(\mathbf{r}) \gamma_{xy} \\
 \sigma_y &= Q_{12}(\mathbf{r}) \epsilon_x + Q_{22}(\mathbf{r}) \epsilon_y + Q_{23}(\mathbf{r}) \epsilon_z + Q_{24}(\mathbf{r}) \gamma_{yz} + Q_{25}(\mathbf{r}) \gamma_{xz} + Q_{26}(\mathbf{r}) \gamma_{xy} \\
 \sigma_z &= Q_{13}(\mathbf{r}) \epsilon_x + Q_{23}(\mathbf{r}) \epsilon_y + Q_{33}(\mathbf{r}) \epsilon_z + Q_{34}(\mathbf{r}) \gamma_{yz} + Q_{35}(\mathbf{r}) \gamma_{xz} + Q_{36}(\mathbf{r}) \gamma_{xy} \\
 \tau_{yz} &= Q_{14}(\mathbf{r}) \epsilon_x + Q_{24}(\mathbf{r}) \epsilon_y + Q_{34}(\mathbf{r}) \epsilon_z + Q_{44}(\mathbf{r}) \gamma_{yz} + Q_{45}(\mathbf{r}) \gamma_{xz} + Q_{46}(\mathbf{r}) \gamma_{xy} \\
 \tau_{xz} &= Q_{15}(\mathbf{r}) \epsilon_x + Q_{25}(\mathbf{r}) \epsilon_y + Q_{35}(\mathbf{r}) \epsilon_z + Q_{45}(\mathbf{r}) \gamma_{yz} + Q_{55}(\mathbf{r}) \gamma_{xz} + Q_{56}(\mathbf{r}) \gamma_{xy} \\
 \tau_{xy} &= Q_{16}(\mathbf{r}) \epsilon_x + Q_{26}(\mathbf{r}) \epsilon_y + Q_{36}(\mathbf{r}) \epsilon_z + Q_{46}(\mathbf{r}) \gamma_{yz} + Q_{56}(\mathbf{r}) \gamma_{xz} + Q_{66}(\mathbf{r}) \gamma_{xy}
 \end{aligned} \tag{2}$$

where $Q_{lm}(\mathbf{r})$ are step-wise functions of the position vector \mathbf{r} . Then the linear strain-displacement equations are taken as:

$$\begin{aligned} \epsilon_{xx} &= \frac{\partial u_x}{\partial x}, & \epsilon_{yy} &= \frac{\partial u_y}{\partial y}, & \epsilon_{zz} &= \frac{\partial u_z}{\partial z}, \\ \gamma_{xy} &= \frac{\partial u_x}{\partial y} + \frac{\partial u_y}{\partial x}, & \gamma_{xz} &= \frac{\partial u_x}{\partial z} + \frac{\partial u_z}{\partial x}, & \gamma_{yz} &= \frac{\partial u_y}{\partial z} + \frac{\partial u_z}{\partial y} \end{aligned} \quad (3)$$

The potential energy of the plate can be written as

$$P = \frac{1}{2} \int \int \int_V Q_{lm}(x, y, z) \epsilon_l \epsilon_m \, dx \, dy \, dz \quad (4)$$

with $l, m = 1, \dots, 6$; $\epsilon_1 = \epsilon_{xx}$, $\epsilon_2 = \epsilon_{yy}$, $\epsilon_3 = \epsilon_{zz}$, $\epsilon_4 = \gamma_{yz}$, $\epsilon_5 = \gamma_{xz}$, $\epsilon_6 = \gamma_{xy}$.

The work of external force is expressed as follows

$$W = \int_S q(x, y) u_z(x, y, h) \, dx \, dy \quad (5)$$

where S is a loaded part of the surface $z = h$.

The solution procedure

The unknowns U_{ijk} , V_{ijk} , W_{ijk} can be calculated from the variational equation

$$\delta H = \delta(P - W) = 0 \quad (6)$$

through the usual procedures.

It can be shown that the function $H = P - W$ with the P and W defined accordingly to (4) and (5) can be written, after substitution of (1) and (2), (3), in the tensor form

$$\begin{aligned} H = & (A_{ijklmn} U_{ijk} U_{lmn} + B_{ijklmn} V_{ijk} V_{lmn} + C_{ijklmn} W_{ijk} W_{lmn} \\ & + D_{ijklmn} U_{ijk} V_{lmn} + E_{ijklmn} U_{ijk} W_{lmn} + F_{ijklmn} V_{ijk} W_{lmn}) \\ & + (a_{ijk} U_{ijk} + b_{ijk} V_{ijk} + c_{ijk} W_{ijk}) \end{aligned} \quad (7)$$

where A_{ijklmn} , B_{ijklmn} , C_{ijklmn} , D_{ijklmn} , E_{ijklmn} , F_{ijklmn} , a_{ijk} , b_{ijk} , and c_{ijk} - unknown constants.

The first six of them depend on mechanical properties of the materials forming the parallelepiped while the other three depend on the surface and volumetric loads. The summation indices in (9)

run: i and l from 1 to l_x , j and m from 1 to l_y , k and n from 1 to l_z . Here, $l_x = \lambda + 1 + K(m_x - 1)$,

$l_y = \mu + 1 + L(m_y - 1)$, and $l_z = \nu + 1 + M(m_z - 1)$.

The formulation of the solution procedure described above is not totally sufficient: it is applicable only if all of the meso-volumes have distinct properties. Hence, it does not allow one to correctly solve the particular case of the particular parallelepiped shown in Figure 1, a. For example, there is the surface element $\{x=x_2, y_0 \leq y \leq y_1, z_0 \leq z \leq z_1\}$ along which two identical meso-volumes interact. This means that the displacements here must have continuous first derivatives

with respect to x -coordinate. At the same time, this surface element belongs to the border between two meso-volumes and, according to the above procedure, the x -coordinate splines deficient at $x=x_2$ would be applied automatically (see Figure 1, b). Thus, the algorithm should be generalized in order to delete deficiencies along all surface elements separating distinct meso-volumes inside a mosaic parallelepiped. Mathematically it means that some constraints in the form of linear algebraic equations with respect to the unknown displacement coefficients U_{ijk} , V_{ijk} , and W_{ijk} are imposed on the original system of spline functions :

$$\alpha_{ijk}^p U_{ijk} + \beta_{ijk}^p V_{ijk} + \gamma_{ijk}^p W_{ijk} = \phi_{ijk}^p \quad (8)$$

where α_{ijk}^p , β_{ijk}^p , γ_{ijk}^p , and ϕ_{ijk}^p are predetermined constants, p is a number of constraints.

The procedure worked out for this purpose is illustrated graphically in Figure 1. At the first stage the original defects of the splines X_{s-1} and X_{s+1} at $x=x_2$ (see Figure 1, b) are eliminated.

The new system of splines is shown in Figure 1, c. Then, the defect of the spline X_s is eliminated, and the final system shown in Figure 1, d is obtained. It is easy to prove that this procedure is equivalent to the following constraint:

$$U_{s-1jk} \left(\frac{\partial X_{s-1}(x_2+0)}{\partial x} - \frac{\partial X_{s-1}(x_2-0)}{\partial x} \right) + U_{sjk} \left(\frac{\partial X_s(x_2+0)}{\partial x} - \frac{\partial X_s(x_2-0)}{\partial x} \right) + U_{s+1jk} \left(\frac{\partial X_{s+1}(x_2+0)}{\partial x} - \frac{\partial X_{s+1}(x_2-0)}{\partial x} \right) = 0 \quad (9)$$

Here, j and k run only the numbers corresponding to the splines of the sets $Y_j(y)$ and $Z_k(z)$ which have their supports inside the intervals $[y_0, y_1]$ and $[z_0, z_1]$ accordingly.

There is another problem with the construction of correct splines for the problem under consideration. In the particular case shown in Figure 1, a is a concern about the line segments $\{x=x_2, y=y_1, z_0 \leq z \leq z_1\}$ and $\{x=x_2, z=z_1, y_0 \leq y \leq y_1\}$ along which three different materials interact. For example, when moving to the second of these line segments in the vertical direction from the bottom ($z < z_1$) along any line $\{x=x_2, y=y^*\}$, $y_0 \leq y^* \leq y_1$, we have, under condition (9), that the displacements have continuous first derivatives with respect to x -coordinate. In the contrary, when moving to the same line segment from the top ($z > z_1$) along the line $\{x=x_2, y=y^*\}$, $y_0 \leq y^* \leq y_1$, we still have (and must have) displacements with discontinuous first derivatives with respect to x -coordinate. Therefore, at $z=z_1$ we have to satisfy the contradictory requests for the properties of $X_i(x)$ spline functions. It seems that this contradiction is of fundamental value and is related to the specific nature (possibly, singular behavior) of stress fields at the interactions of three different materials. This can not be principally improved in the current numerical approach, but can be localized in a small vicinity of the line segment using a partition of each meso-volume into sub-elements with three sets of planes P_ξ , P_η , and P_ζ . The effect of the named contradiction will be limited, for example, to the length of the support of the "transitional" spline $Z_t(z)$ (see, Figure 1, a).

The same form of constraints (8) can be used to specify the initial sets of approximating splines for some particular case of external boundary conditions at the edges of the mosaic parallelepiped. Formulation of various "global" and "local" edge boundary conditions in the context of the sub-layer/spline approximation method was discussed in [8, 11]. Clearly, the formulation of boundary conditions at the edges of a mosaic parallelepiped requires some additional discussion. However, we shall omit this discussion here, rather focusing only on some illustrative examples.

ANALYSIS OF TRIAXIALLY BRAIDED RECTANGULAR PLATES

In this study, a comparison is made for two models of a triaxially braided textile reinforced composite. The braid was modelled with a braiding angle of 63° , and the constituents were AS-4 carbon yarn as the reinforcement and Shell 1895 epoxy resin as the matrix.

The first model is based on a unit cell approach using a three dimensional representation of the reinforcing structure. The elastic properties of the unit cell were determined on the basis of a geometrical rendering of the reinforcement architecture. The geometrical rendering is illustrated in Figure 3. The stiffness matrix was determined by applying a Geometrically Integrated Numerical Analysis (GINA) technique [12]. Using this technique it is possible to evaluate the elastic properties of an arbitrary meso-volume. For the purposes of this analysis, the meso-volume was set to be the unit cell. The stiffness matrix predicted by this model is given below:

$$\mathbf{Q} = \begin{pmatrix} 56.46 & 17.68 & 8.88 & 0.004 & 0.058 & 1.299 \\ & 35.92 & 7.55 & -0.003 & 0.057 & 0.553 \\ & & 14.13 & 0.010 & 0.031 & 1.05 \\ & & & 12.99 & 0.206 & 0.055 \\ & sym & & & 3.32 & 0.010 \\ & & & & & 4.13 \end{pmatrix} \text{ GPa} \quad (10)$$

The second model provides a representation of the braided composite as a 6 layer symmetric angle-ply laminate. The ply lay-up assumed is $[63/0/-63^\circ]_s$. The unidirectional (0°) layer properties were derived using the same fiber and resin materials properties as mentioned above through the micromechanics approach [10]. The properties of 63° and -63° layers were calculated from the properties of the 0° layer through the standard tensor transformation technique.

It should be pointed out that these two materials are not identical in terms of constituent ratios. The materials were modelled on the basis of realistic manufacturing processes. For the braiding system this assumed that the braider yarns were 12K, and the triaxial yarns were 24K tows. This results in 38.1% longitudinal yarns. In the case of the laminate, it was assumed that the plies each had the same thickness, thus 33% were longitudinals. The principal difference between these models is obvious: in the first model yarns have out-of-plane orientations, while the second model implies the in-plane reinforcement only. It is important to note that in the case of anisotropic, 3-D braided plate there is only one meso-volume within the plate which is identical, in its turn, to the unit cell, while the lamination model assumes 6 meso-volumes within the plate represented by distinct layers.

Numerical results were obtained for the square plate. The geometry parameters and the coordinate system used were taken the same as in the previous Section. Three combinations of the boundary conditions were considered:

$$\begin{aligned} \text{ss-ss: at } x=0 \text{ (s), at } x=a \text{ (s), at } y=0 \text{ (s), at } y=a \text{ (s)} \\ \text{cc-ss: at } x=0 \text{ (c), at } x=a \text{ (c), at } y=0 \text{ (s), at } y=a \text{ (s)} \\ \text{cs-ff: at } x=0 \text{ (c), at } x=a \text{ (s), at } y=0 \text{ (f), at } y=a \text{ (f)} \end{aligned} \quad (11)$$

where the following designation used: (s): $\sigma_x = u_y = u_z = 0$ ($\sigma_y = u_x = u_z = 0$); (c): $u_x = u_y = u_z = 0$; (f): $\sigma_y = \tau_{xy} = \tau_{zy} = 0$. The external load applied to the top surface $z = h$ was prescribed by the equation

$$q = q_0 \sin\left(\pi \frac{x}{a}\right) \sin\left(\pi \frac{y}{b}\right) \quad (12)$$

with a negative magnitude of q_0 .

The symmetry of the solution can be used in the case of the boundary conditions "ss-ss" and a "braid" model only. In all the other cases full length and width of a plate have to be taken into consideration. The uniform divisions into 8 intervals in both x and y directions, as well as uniform divisions into 3 sub-layers of a homogeneous "braid" and each layer in a "laminate" were used. The third degree spline functions were employed.

Figure 4 shows the variation of σ_x as a function of x coordinate for $y = 0.5a$, $z = 0$. Figure 5 depicts the variation of σ_x throughout the thickness of a plate for $x = 0.5a$ and $y = 0.5a$. Figure 6 demonstrates the dependency of $\tau_{xz}(z)$ for $x = 0.25a$ and $y = 0.25a$.

From Figure 4, it is interesting to note that σ_x changes its sign along the length of the plate for the cases of boundary conditions “cc-cc” and “cs-ff”. This stress component takes identical magnitudes for the values of $x \in [0.7a, a]$. This example demonstrates that for moderately thick anisotropic braided structure (with the aspect ratio $a/h=10$) the edge effect zones extend through its whole length.

Through-the-thickness distributions of both the stresses σ_x and τ_{xz} (Figures 5 and 6) are rather distinct for the “braid” and “laminated” models. The single-ply anisotropic material shows a smooth distribution, while for the 6-ply laminated material there are sharp “knees” at the ply interfaces. These results indicate that the structural response of a braided composite plate is influenced significantly by the number of meso-volumes representing the structure and the method used when modelling mechanical properties of a meso-volume.

APPLICATION OF THE THREE-DIMENSIONAL “BRICK” MODEL TO THE PLANE WEAVE RECTANGULAR PLATE

The meso-volume approach can also be applied to the unit cell problem to develop a picture of highly localized stress distributions associated with the cell. To examine the effectiveness of applying this approach, the plain weave unit cell shown in Figure 7 was modelled. The unit cell was divided into 32 meso-volumes (4 in x , 4 in y , and 2 in z) uniformly. Figure 7 illustrates the position of the meso-volumes within the unit cell, with sub-meso-volume divisions indicated by gray lines. Each meso-volume had distinct material properties. Figure 8 is a figurative representation of the Q_{11} , and Q_{22} values for the meso-volumes. There were no sub-divisions into sub-meso-volumes in the z direction. For both top and bottom, the meso-volumes A, D, M, and P (as well as A', D', M' and P') were divided into 9 sub-meso-volumes (3x3x1) nonuniformly. Meso-volumes B, C, E, H, I, L, N, and O were divided into 12 sub-meso-volumes (4x3x1 or 3x4x1). Meso-volumes F, G, J, and K were represented in terms of 16 sub-meso-volumes (4x4x1).

The structure was loaded sinusoidally, according to the equation (12), with a negative magnitude of q_0 . The boundary conditions corresponded with simple support on all edges. The dimensions of the plate were $a \times b \times h$, with $a/b = 0.75$, and $a/h = 24$.

The most critical continuity concerns arise at the line of intersection of 4 distinct meso-volumes. Figure 9 illustrates the distribution of τ_{xz} as a function of z taken at two x values with $y = 0.1875 b$. The first case is $x = 0.2499 a$, and the second $= 0.5001 a$, which are just left and right of the interface between meso-volumes D-H, and D'-H'. It can be seen that the stress distribution for the two coordinates is extremely close.

Figure 10 examines the distribution of τ_{xy} as a function of x at the bottom surface ($z=0$). The first case is for $y=0.2499 b$, and the second for $y=0.2501 b$. This corresponds with lines running just beyond and just before the interfaces between meso-volumes A'-E', B'-F', C'-G', and D'-H'. In this case, the stress-concentrations associated with a material joint are revealed. This stress concentration can be considered a singularity contained within the border of sub-meso-volumes, but this has to be proved separately. By making the sub-meso-volume mesh denser in this region it is possible to localize the effect of this stress concentration within an arbitrary degree of precision. Beyond the stress concentration regions, the stress distributions on either side of the interface demonstrate continuity. This example shows that complex, structurally inhomogeneous parts can

be effectively analyzed by the numerical method presented in this paper, while satisfying all of the necessary continuity conditions.

APPLICATION OF THE THREE-DIMENSIONAL "BRICK" MODEL TO THE TRIAXIALLY BRAIDED SKIN-STIFFENER STRUCTURE

Problem formulation and solution procedure

Consider a rectangular laminated composite plate stiffened with a set of mutually parallel laminated composite beam elements having rectangular cross-sections (Figure 11). The stiffeners are, in general, non-equidistant. Geometric parameters and mechanical properties of any stiffener can be considered unique. A general type of anisotropic properties for a skin plate as well as for each of the stiffeners is assumed. It should be mentioned that another set of mutually parallel stiffeners (orthogonal to the first one) can be included without any changes in the analysis. For simplicity, only one set of stiffeners is shown in Figure 11.

In this analysis we shall focus on the skin-stiffener interaction problem. For this problem it is sufficient to analyze some representative element with its boundaries along the mid-lines between adjacent stiffeners (Figure 12). In general, the representative element can not be considered as a "unit cell" of a stiffened structure because of a distance variation between adjacent stiffeners as well as variations of an individual stiffener's characteristics. Nevertheless, the results obtained in the analysis of a single representative element should reveal all the main specific features of the interaction problem mentioned above.

Obviously, the analysis of stiffened panel element shown in Figure 13 can be developed in a direct way, by generalizing the analysis of [8]. Actually, this element is composed of the two 3-D anisotropic parallelepipeds (the skin and the stiffener). At the first step, both of them can be analyzed separately using the same approach [8]. At the second step, the specific boundary conditions imposed on displacements and transverse stresses at the interaction surface between these parallelepipeds must be satisfied, and the solution would be completed. When applying this approach, two distinct discretization meshes would possibly be used at the first stage assuming that the properties of the parallelepipeds are rather different. These meshes have to be chosen in order to satisfy the variational equation and all the external and internal boundary conditions for each of them [8]. The displacements and stresses obtained at the first stage still will contain some unknowns to be calculated from the continuity conditions at the interaction surface. This means that some functions referring to different meshes have to be matched. The described procedure, applied to all of the skin-stiffener interaction surfaces, may be cumbersome and computationally inefficient.

Another possible computational approach seems to be more elegant. By adding some fictitious "soft" material, the original, irregularly stiffened panel is completed up to the regular-shape parallelepiped (see Figure 11). Its thickness is equal to the total thickness of the skin and the highest stiffener. A filling material has to be chosen which will have no effect on the stress/strain state in the skin and stiffeners.

The "representative" element for this new structure can be extracted following Figures 12 and 13. This is an internally structured complex parallelepiped containing 3 different materials (the skin, the stiffener and the filler). Its structure can be characterized as a brick-type mosaic. The general "meso-volume" approach proposed in [1] can be applied to this type of structurally inhomogeneous material. In this particular case, the skin, the stiffener and the surrounding soft filler can be treated as three distinct meso-volumes. A unified discretization mesh can be introduced for the parallelepiped as a whole, and the appropriate system of 3-coordinate deficient spline functions has to be constructed for the analysis.

Orthotropic skin stiffened with an orthotropic stiffener

First consider a single-layer orthotropic plate stiffened with a single-layer orthotropic stiffener. Both the skin and the stiffener are made of the same carbon/epoxy unidirectionally reinforced composite material having the following elastic properties [13]:

$$E_1=25.0 \text{ Msi}, E_2=E_3=1.7 \text{ Msi}, G_{12}=G_{13}=G_{23}=0.65 \text{ Msi}, \nu_{12}=\nu_{13}=\nu_{23}=0.30. \quad (13)$$

For the skin the "1" direction goes along the x -axis; for the stiffener it goes along the y -axis. The fictitious "filler" is an isotropic material, its modulus E will be varied in magnitude, and Poisson's ratio is taken as 0.3.

Notations for the stiffened element are shown in Figure 13. The thickness of a skin $h=a/20$, the thickness of a stiffener $h_s=a/20$, and the width of a stiffener $d=a/10$. The element is under a sinusoidally distributed normal compressive load (12) applied to the top surface. In the following calculations it is taken $a=b$.

Due to the symmetry of a problem, a quarter of a stiffened panel, $0 \leq x \leq a/2$, $0 \leq y \leq b/2$ is solved. Boundary conditions at the side edges are:

$$\text{at } x=0: u_z = 0, u_y = 0, \sigma_x = 0; \quad (14)$$

$$\text{at } y=0: u_z = 0, u_x = 0, \sigma_y = 0. \quad (15)$$

Correspondingly, condition (15) is used at the stiffener's surface $y=0$.

The first task is to analyze an effect of a fictitious filler on a stress/strain state in the skin and the stiffener. The following partition of the skin, the stiffener and the filler is taken:

in x-direction: for any y and z values the interval $[0, a/2-d/2]$ is divided uniformly into 6 parts, and the interval $[a/2-d/2, a/2]$ is divided uniformly into 5 parts;

in y-direction: for any x and z values the interval $[0, b/2]$ is divided uniformly into 4 parts;

in z-direction: for any x and y values both the intervals $[0, h_s]$ and $[h_s, c]$ are divided uniformly into 4 parts.

The distributions of σ_z , σ_x , and τ_{xz} along the x -coordinate at $y=b/2$, $z=h_s$ are presented in Figure 14 for three magnitudes of the filler's elastic modulus: $E/E_2 = 0.001$ (case "a"), 0.01 (case "b"), and 0.1 (case "c"). A small difference between the curves "c" and "b" can be recognized, but the curves "b" and "a" absolutely coincide. The stresses σ_z and τ_{xz} are very close to zero at the main part of the free surface of the skin ($z=h_s$, $0 \leq x \leq 0.45a$). Small oscillations and non-zero values of σ_z and τ_{xz} in a vicinity of the point $x=0.45a$ can be explained by the rather coarse x -direction mesh used in the analysis.

Another group of results for the same three magnitudes of E is presented in Figure 15. The dependencies $\sigma_x(z)$, $\tau_{xz}(z)$ at $x=0.45a$, $y=0.5b$ as well as the dependency $\sigma_y(y)$ at $x=0.45a$, $z=h_s/2$ demonstrate the similar effect of the E magnitude as it results from Figure 7: there is some small difference in the curves for the cases "c" and "b", but no difference between the cases "b" and "a". As it is seen, the free surface condition for the stresses $\sigma_x(z)$ and $\tau_{xz}(z)$ at the side surface of the stiffener is fairly satisfied.

The results presented in Figures 14 and 15 lead to the conclusion that the value $E = 0.01E_2$ is sufficiently small. This value will be used in all of the following calculations.

It can be seen from Figures 14 and 15 that there are high stress gradients in the vicinity of the corner $x=0.45a$, $z=h_s$. The results obtained with the previous, rather coarse x -direction mesh are probably not accurate there. Convergence of stresses when increasing density of the mesh in x -direction has to be analyzed. In this analysis the above described meshes in y - and z -directions will be retained. The following node coordinates for the four meshes in x -direction will be used:

- (i) $2x/a = 0.18, 0.36, 0.54, 0.72, 0.84, 0.87, 0.90, 0.93, 0.96, 0.98, 1.0$
- (ii) $2x/a = 0.18, 0.36, 0.54, 0.72, 0.86, 0.88, 0.90, 0.92, 0.94, 0.96, 0.98, 1.0$
- (iii) $2x/a = 0.18, 0.36, 0.54, 0.72, 0.868, 0.884, 0.900, 0.916, 0.932, 0.960, 0.980, 1.0$
- (iv) $2x/a = 0.18, 0.36, 0.54, 0.72, 0.876, 0.888, 0.900, 0.912, 0.924, 0.960, 0.980, 1.0$

In each of these meshes there are two divisions to the left of the point $x=0.45a$ ($2x/a=0.9$) and two divisions to the right of this point having the same lengths, designated Δ . The value $2\Delta/d$ is equal to 0.3, 0.2, 0.16, and 0.12 for the meshes (i)-(iv) correspondingly.

The dependencies of σ_z , τ_{xz} , σ_x , and σ_y on $2\Delta/d$ at the corner point $x=0.45a$, $y=0.5b$, $z=h_s$ are presented in Figure 16. It looks like there are no finite limits of σ_z , τ_{xz} , and σ_y with Δ going to zero. This indicates, probably, a singular behavior of these functions along the line $x=0.45a$, $z=h_s$. On the contrary, σ_x does not depend on Δ . This reasonable result encourages the belief that the tendencies shown by the other three curves have some physical meaning. Note also that σ_z is tensile, and σ_x considerably exceeds the other three stresses. Undoubtedly, the effects revealed ask for a more detailed analysis.

The next issue of a certain interest is the behavior of contact stresses σ_z , τ_{xz} , and τ_{yz} at the skin-stiffener interaction area. They were calculated with the same y - and z - meshes as before and with the following three x -meshes:

- (I) uniform for both the skin and the stiffener; each of the intervals $[0, 0.45a]$ and $[0.45a, 0.5a]$ is divided into 9 parts;
- (II) $2x/a = 0.15, 0.30, 0.45, 0.60, 0.70, 0.825, 0.850, 0.875, 0.900, 0.911, 0.922, 0.933, 0.944, 0.955, 0.966, 0.977, 0.988, 1.0$.
- (III) $2x/a = 0.15, 0.30, 0.45, 0.60, 0.80, 0.87, 0.88, 0.89, 0.90, 0.911, 0.922, 0.933, 0.944, 0.955, 0.966, 0.977, 0.988, 1.0$.

Distributions of σ_z , τ_{xz} , and τ_{yz} along the half-width of the stiffener at $z=h_s$, $y=0.5b$ (for σ_x and τ_{xz}) and $y=0.25b$ (for τ_{xy}) are presented in Figure 17. For any of these stresses, the three curves corresponding to the mesh (I) and the meshes (II) and (III) are distinct only inside a small x interval adjacent to the corner $x=0.45a$, $z=h_s$ where the contact stresses increase sharply. However, even near this corner the curves corresponding to the meshes (II) and (III) coincide. Note that the normal contact stress σ_z changes its sign and becomes tensile at $x < 0.458a$. These results demonstrate that the realistic distributions of contact stresses in the problem of skin-stiffener interaction are very complex. Definitely, they would play a major role in the predictions of failure initiation in stiffened structures.

Triaxially braided T-section plate

A structural element of the same type as in Figure 13 is considered here. It is made of a triaxially braided composite characterized with the stiffness matrix (10). The element is modelled with both version "a" and version "b" brick-type mosaic structures shown in Figure 18. In both cases the meso-volume "A" has the stiffness (10) with material axes 1, 2, and 3 going along the plate axes x , y , and z correspondingly. The meso-volume "B" is characterized with the same stiffness matrix, but the material axes 1 and 3 correspond to the plate axes z and x in this case. Still, axis 2 goes along with axis y . All the other meso-volumes involved in the analysis, namely, C, D, E, and C', C'', D', D'', E', E'', have their stiffness matrices generated from the matrix (10) as something intermediate between the matrices for the meso-volumes "A" and "B". The purpose of these intermediate meso-volumes is to provide a smooth transition inside the zone between meso-volumes "A" and "B". It is assumed that all of them have distinct elastic characteristics.

The element shown in Figure 18 is loaded with a sinusoidally distributed surface pressure (12) (see Figure 13). All four side edges are assumed to be simply supported. The full length of the plate is $a=100$, its full width $b=200$, and the skin stiffness $h=10$. The stiffener width is $d=20$ and its thickness $h_s=40$. Due to the symmetry, one quarter of the element was solved. The numerical results obtained for the element divisions into meso-volumes, cases "a" and "b", are presented in Figures 19-25.

As can be seen in Figure 19, the distribution of σ_z along z inside the skin and stiffener is a smooth curve with a maximum on the skin-stiffener contact point. There is no difference between the variants "a" and "b". On the contrary, the distribution of the same stress along z at the stiffener's side surface (Figure 20) has a pronounced spike at the corner $x=0.4a$, $z=z_s$. Note that in this case the maximum of σ_z is tensile. The same character of distributions can be seen for τ_{xz} in Figure 21 and for σ_x in Figure 22. There is an almost negligible difference between the variants "a" and "b".

The distributions of σ_x and τ_{xz} along the x coordinate presented in Figures 23 and 24 show again sharp spikes around the corner of the skin and the stiffener. Finally, the monotonic curve shown in Figure 25 characterizes the distribution of σ_y on y coordinate inside the skin and the stiffener.

The stress fields σ_z and σ_x along the plane $z=40$ are shown in Figures 26 and 27. They clearly demonstrate a high stress concentration around the skin-stiffener contact area.

The problem treated in this Section is very complex. The results presented can be considered as preliminary. A detailed convergence analysis when using finer meso-volumes as well as sub-meso-volume meshes is needed. It can be expected from the results above that there are singularities of some stress components at the corner $x=0.4a$, $z=z_s$. Still, to the author's best knowledge there are no other formulations and solutions for the class of problems addressed in this paper.

CONCLUSIONS

The sub-layer/spline approximation method developed in the previous works for a 3-D analysis of laminated plates has been generalized in this work for the solution of 3-D elasticity problems for a brick-type mosaic structure. The material-adaptive approximation of displacements with deficient spline-functions is used. It allows one to eliminate, or at least localize, the unwanted jumps of transverse stresses at the interfaces. The development of internal continuity conditions depend on the physical description of the structural part, and is specifically constructed for inhomogeneous structural materials (laminates, 3-D woven, triaxially braided, and 2-D woven composites). Calculation of material properties of each meso-volume are based upon the geometry of the actual material. Incorporating the geometric description of the reinforcement into the structural analysis

yields a precise and complete theoretical description of the material without depending upon data from other sources, which may not be available.

A representative element of a stiffened laminated or textile-reinforced composite panel can be considered as a particular case of a brick-type mosaic parallelepiped. In order to use this approach in the analysis, a fictitious "soft" material was added to the stiffened panel. The procedure of developing the correct spline approximation functions for this problem was discussed. The stress concentrations at the contact zone between the stiffener and the skin have been investigated for the "orthotropic skin-orthotropic stiffener" structure. It was found that the spike values of σ_z , τ_{xz} , and σ_y stresses do not converge when increasing mesh density. This indicates that singularities can be expected at the contact zone.

The analysis carried out for the T-profile triaxially braided plate revealed high stress concentrations around the corner. This zone has to be considered as the most suspicious for the failure initiation. It was shown also that the stress concentrations are sensitive to the number of meso-volumes used in the representation of a "transitional zone". The method has been shown to be successful in analyzing three different types of textile composite structures. With this tool there are many problems that can be addressed which have not been solved previously.

ACKNOWLEDGEMENTS

The author wishes to extend thanks to Dr. Christopher M. Pastore who provided the mechanical characteristics of braided and woven materials used in the numerical examples, and to Mr. Alexander Birger who coded the structural analysis program and carried out the computational work.

The author would like to acknowledge the North Carolina Supercomputing Association for use of their super-computing facilities in the solution of the numerical problems.

REFERENCES

1. Bogdanovich, A. E. : Spline Function Aided Analysis of Inhomogeneous Materials and Structures. Proceedings of the IUTAM Symposium "Local Mechanics Concepts for Composite Material Systems", Blacksburg, Virginia, USA, October 28-31, 1991. Berlin-Heidelberg-New York: Springer-Verlag, J. N. Reddy, K. L. Reifsnider (Eds.), 1992, pp. 355-382.
2. Bogdanovich, A. E. ; Pastore, C. M. : On the Structural Analysis of Textile Composites. Topics on Composite Materials and Structures, AE - vol. 26, AMD - vol. 133, ASME Publications, 1992, pp. 13-19.
3. Pastore, C. M. ; Bogdanovich, A. E. ; and Gowayed, Y. A. : Applications of a Meso-Volume-Based Analysis for Textile Composite Structures. Composites Engineering, vol. 3, no. 2, 1993, pp. 181-194.
4. Tarnopol'skii, Yu. M. ; Zhigun, I. G. ; and Polyakov, V. A. : Spatially Reinforced Composite Materials. Moscow, Mashinostrojenije Publishers, 1987 (in Russian). English translation by Technomic Publishers, 1992.
5. Chou, T. W. ; and Ko, F. K. : Textile Structural Composites. Elsevier, Essex, UK, 1988.
6. Ko, Frank K. : Preform Fiber Architecture for Ceramic - Matrix Composites. American Ceramic Society Bulletin, vol. 68, no. 2, February 1989, pp. 401-414.

7. Tan, T. M. ; Pastore, C. M. ; and Ko, F. K. : Engineering Design of Tough Ceramic Matrix Composites for Turbine Components. *Journal of Engineering for Gas Turbines and Power*, vol. 113, no. 2, April 1991, pp. 312-317.
8. Bogdanovich, A. E. ; and Birger, A. B. : Application of Spline Functions to the 3-D Analysis of Laminated Composite Plates Subject to Static Bending. *Proceedings of the Second International Symposium on Composite Materials and Structures, Beijing, China, August 2-5, 1992*. Peking University Press, pp. 719-725.
9. Bogdanovich, A. E. ; and Yarve, E. V. : Numerical Solution of a Two-Dimensional Problem of Nonsteady Deformation of Laminated Media. *Mechanics of Composite Materials (in Russian)*, translated by Consultants Bureau. New York: Plenum Publishing Corporation, no. 1, 1988, pp. 31-38.
10. Bogdanovich, A. E. ; and Iarve, E. V. : Numerical Analysis of Impact Deformation and Failure in Composite Plates. *Journal of Composite Materials*, vol. 26, no. 4, 1992, pp. 520-545.
11. Bogdanovich, A. E. ; and Birger, A. B. : Application of Spline Functions to the Analysis of Local Boundary Effects in Laminated Composite Plates. To be published in *Proceedings of the ASME Winter Annual Meeting, Anaheim, California, November 8-13, 1992*.
12. Gowayed, Y.A. : An integrated approach to the mechanical and geometrical modelling textile structural composites. Ph.D. Thesis, North Carolina State University, Raleigh, N.C. USA, 1992.
13. Humpreys, E. A. ; and Rosen, B. W. : Properties Analysis of Laminates. *Engineering Materials Handbook*, vol. 1. Composites. ASM International, 1987, p. 223.

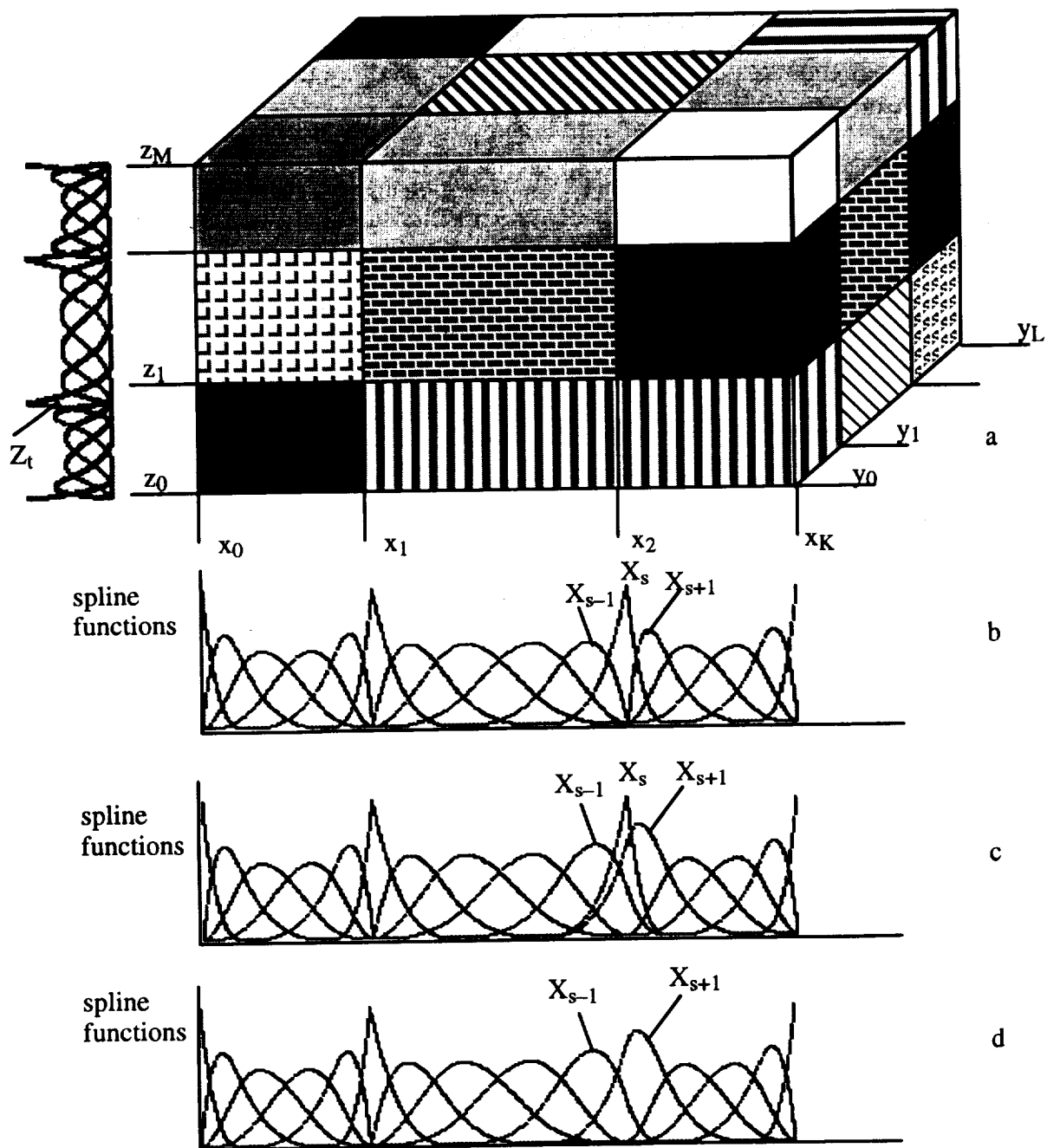


Figure 1. Brick-type mosaic parallelepiped (a) and illustration of the procedure used for removing the defect at the surface $x=x_2$, $y_0 \leq y \leq y_1$, $z_0 \leq z \leq z_1$ (b,c,d).

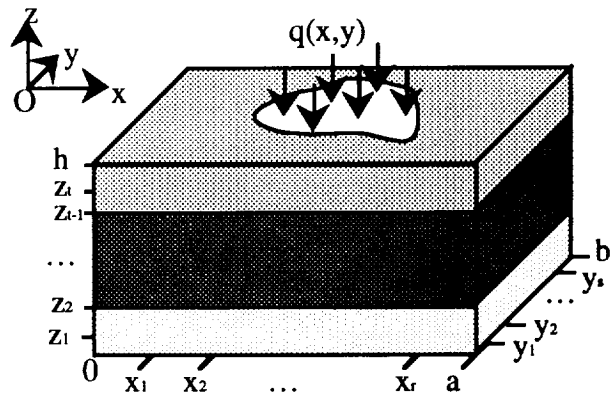


Figure 2. Notations used in a plate analysis.

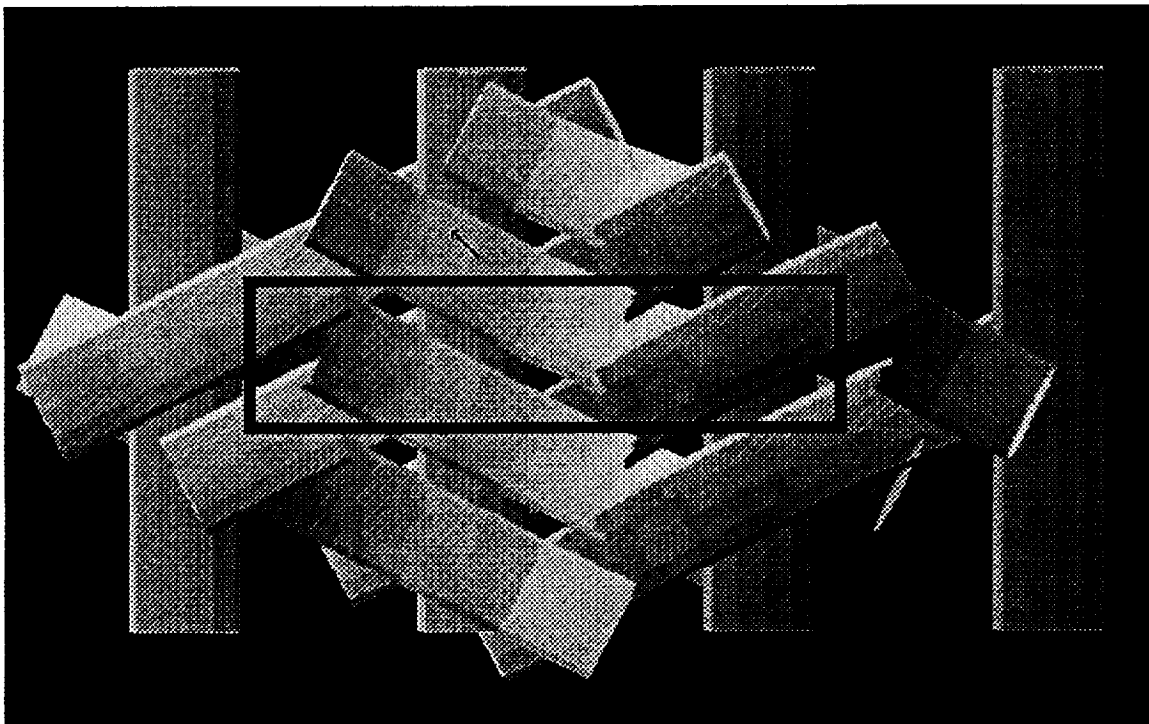


Figure 3. Schematic Illustration of Triaxially Braided Fabric Structure Showing Unit Cell Dimensions Used for Calculation.

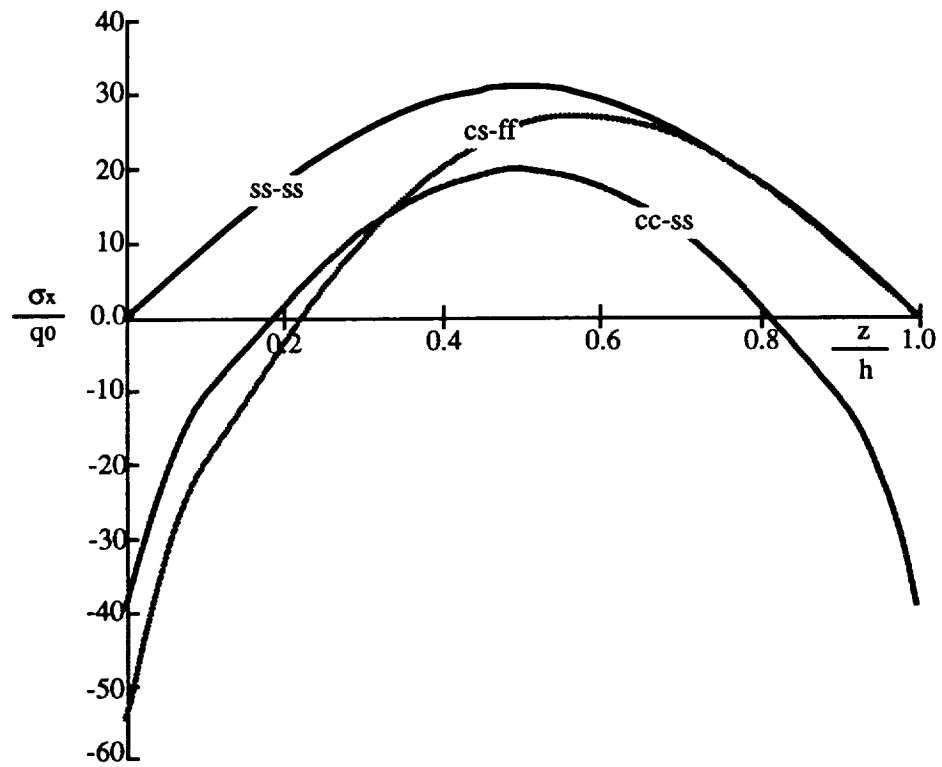


Figure 4. Variation of σ_x as a function of length coordinate for the “braid” model under three combinations of boundary conditions.

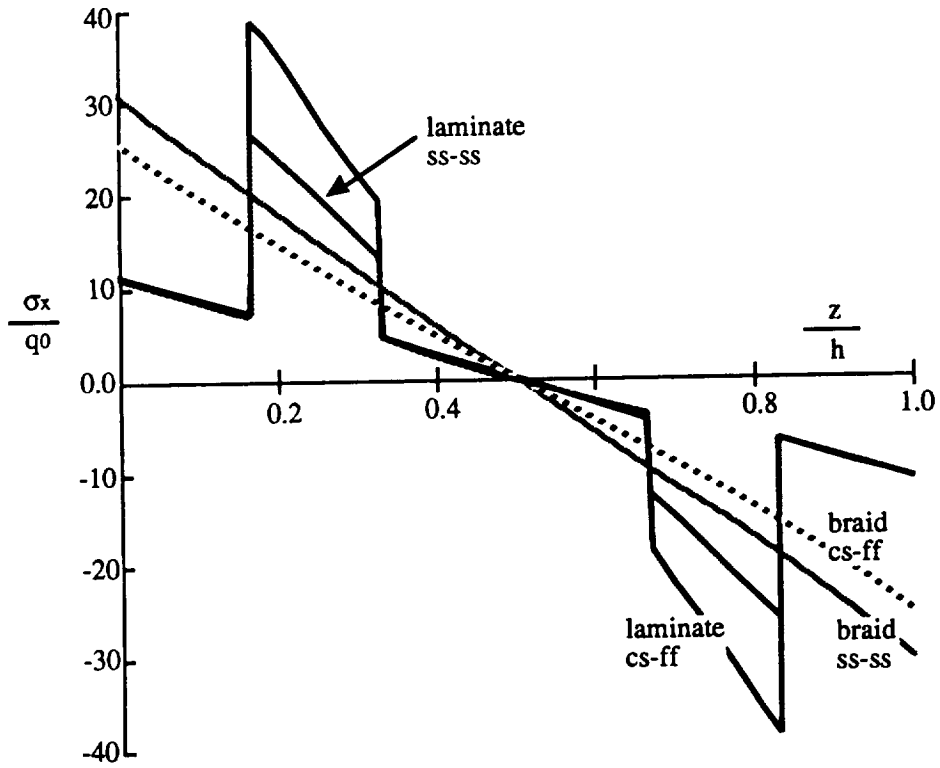


Figure 5. Variation of σ_x as a function of length coordinate for "laminar" and "braid" models under two combinations of boundary conditions.

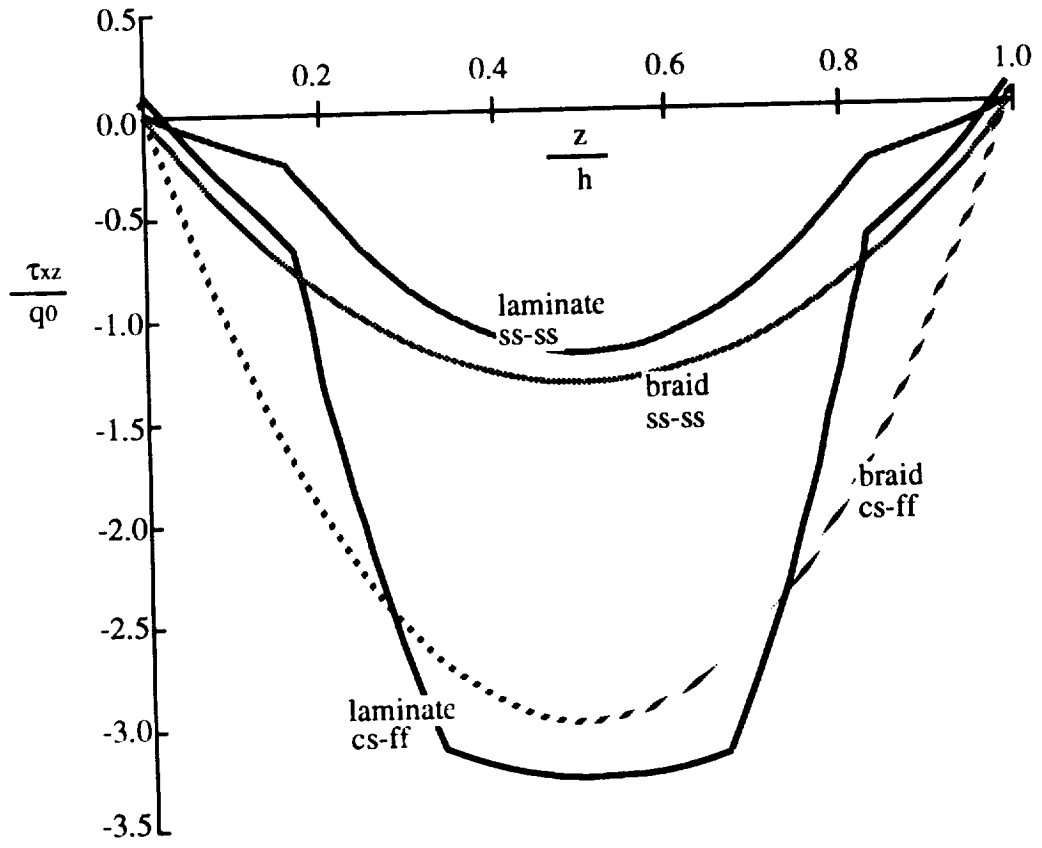
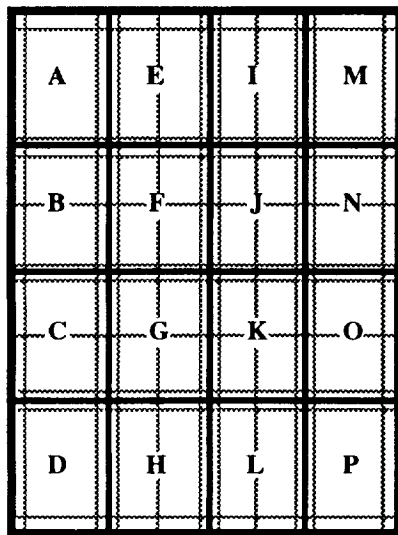
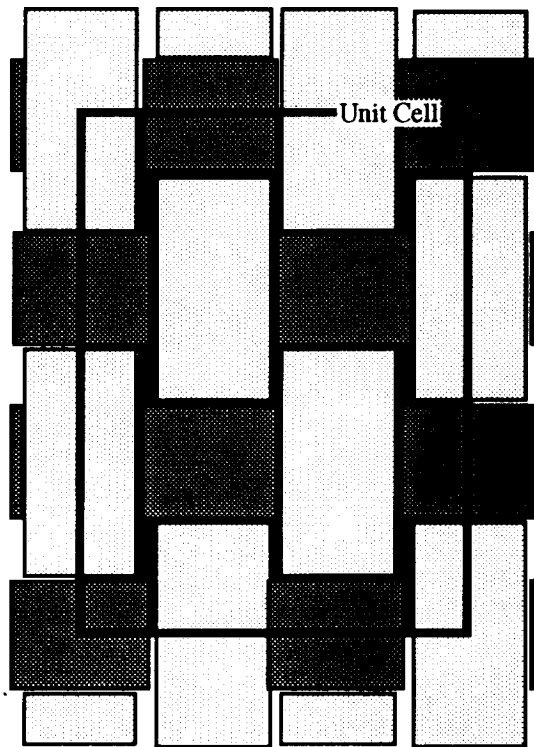
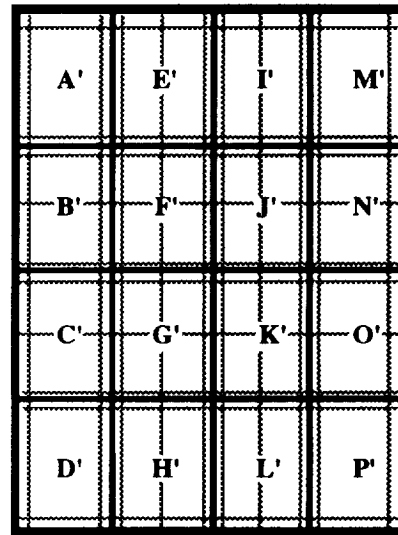


Figure 6. Variation of τ_{xz} as a function of thickness coordinate for "laminar" and "braid" under two combinations of boundary conditions.



Meso-Volume Mesh
Upper Layer



Meso-Volume Mesh
Lower Layer

Figure 7. Schematic Illustration of Weave Unit Cell and the Meso-Volume Mesh.

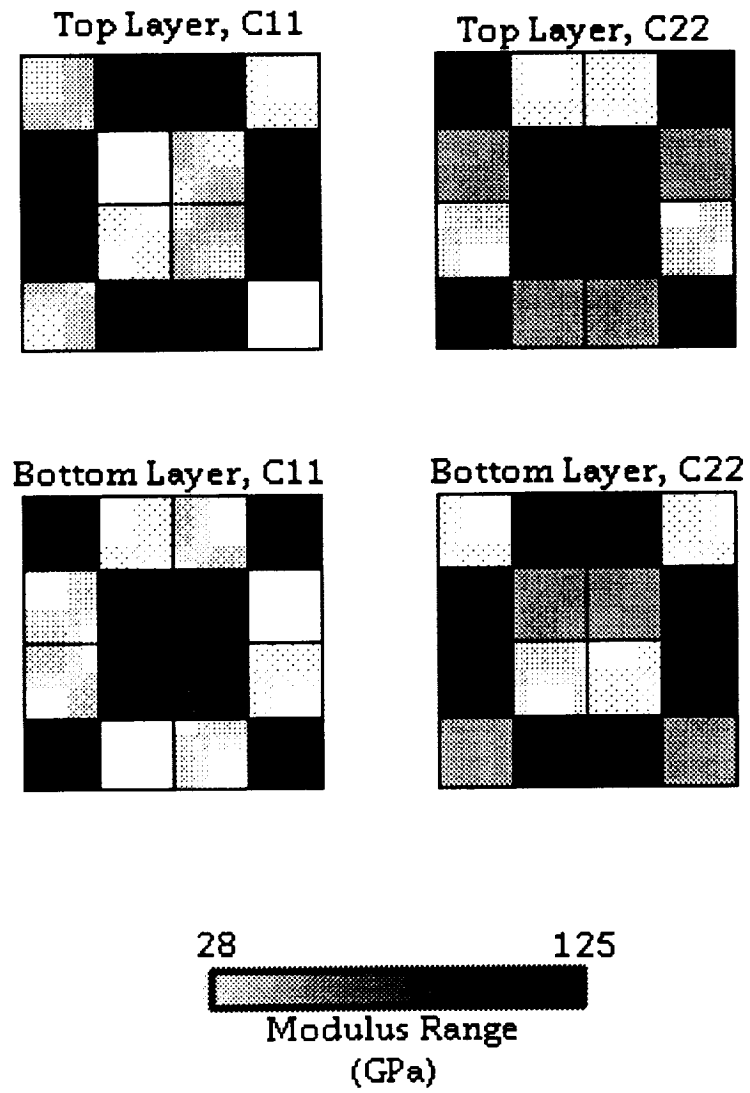


Figure 8. Schematic Drawing Showing Q_{11} and Q_{22} Values Associated with the Meso-Volumes for the Plain Weave Brick Model.

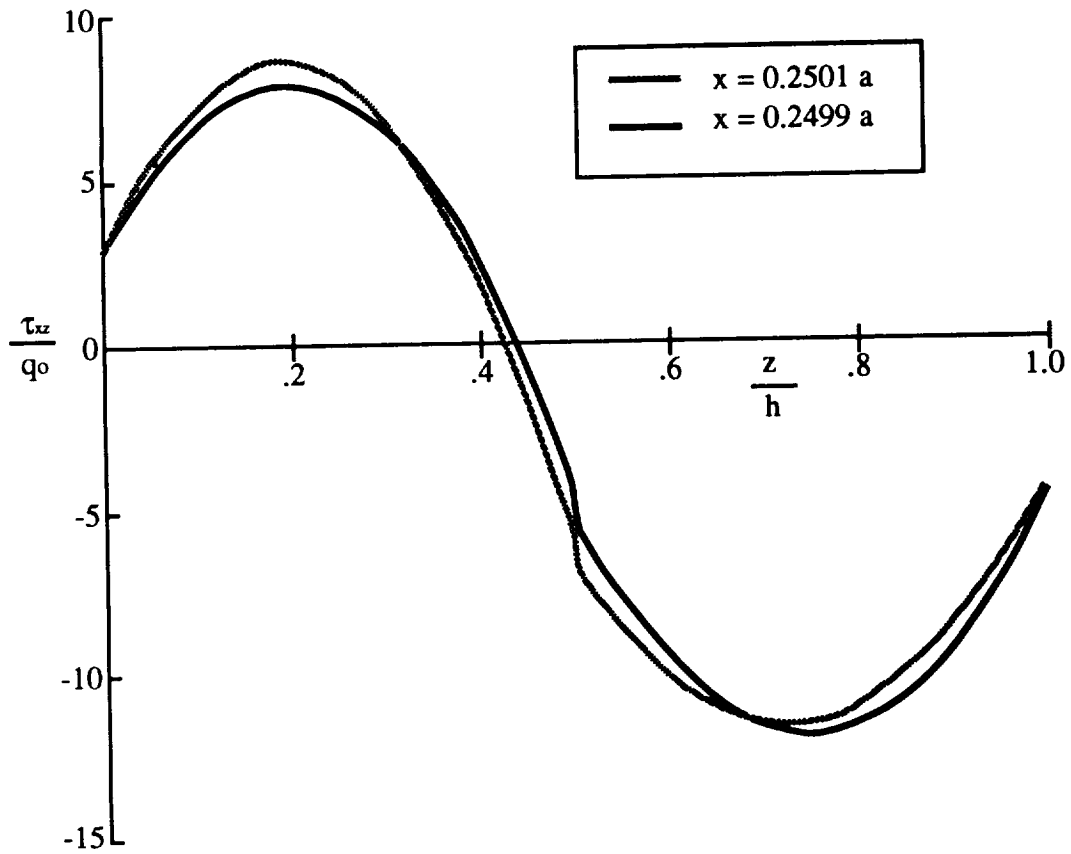


Figure 9. Distribution of τ_{xz} as a function of z , for $y = 0.1875 b$, at the lines on either side of the meso-volume interface.

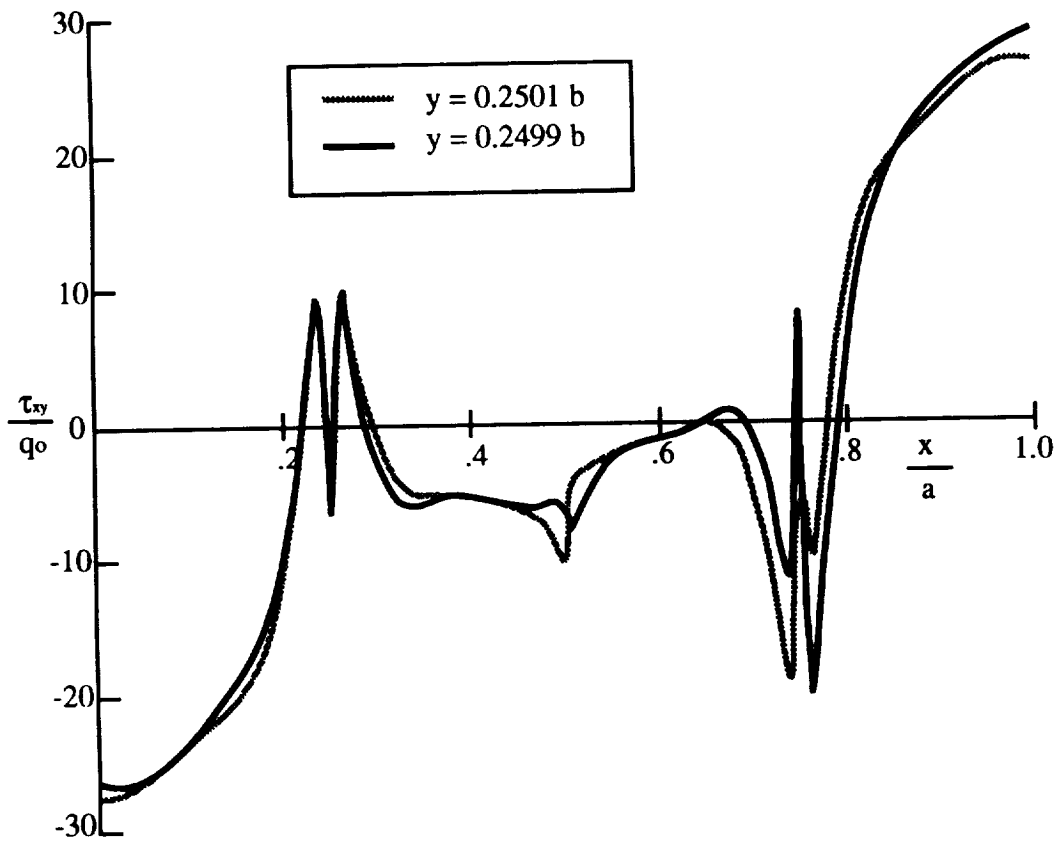


Figure 10. Distribution of τ_{xy} as a function of x , for $z = 0$, at the lines on either side of the meso-volume interface.

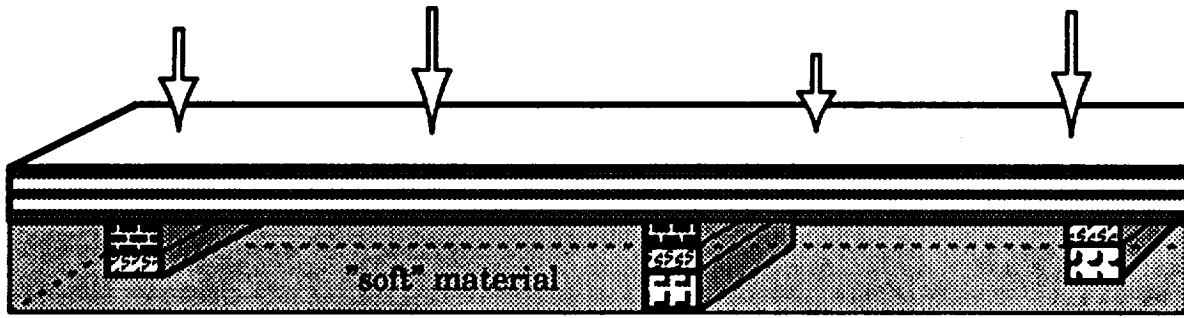


Figure 11. Stiffened composite panel structure filled with a "soft" material.

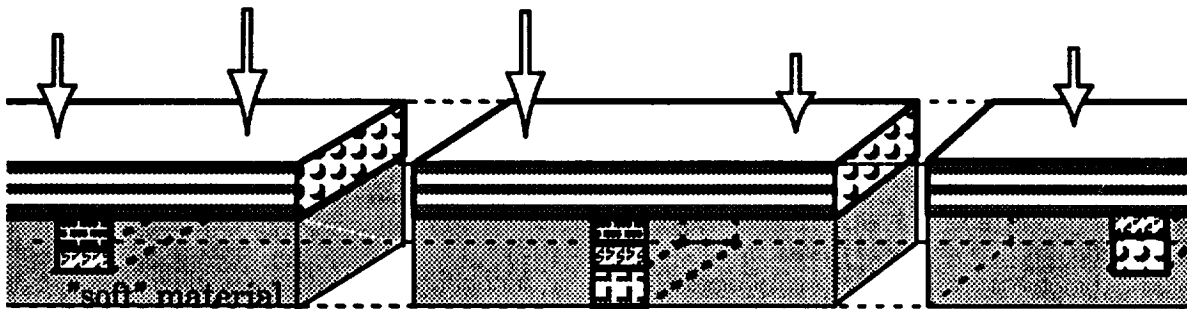


Figure 12. Division of the filled panel into representative elements.

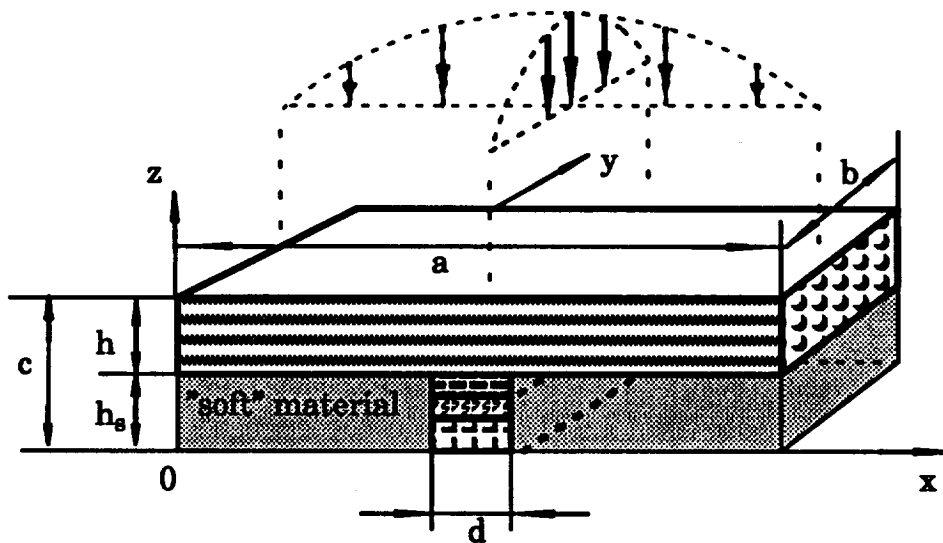


Figure 13. Notation used for the representative element.

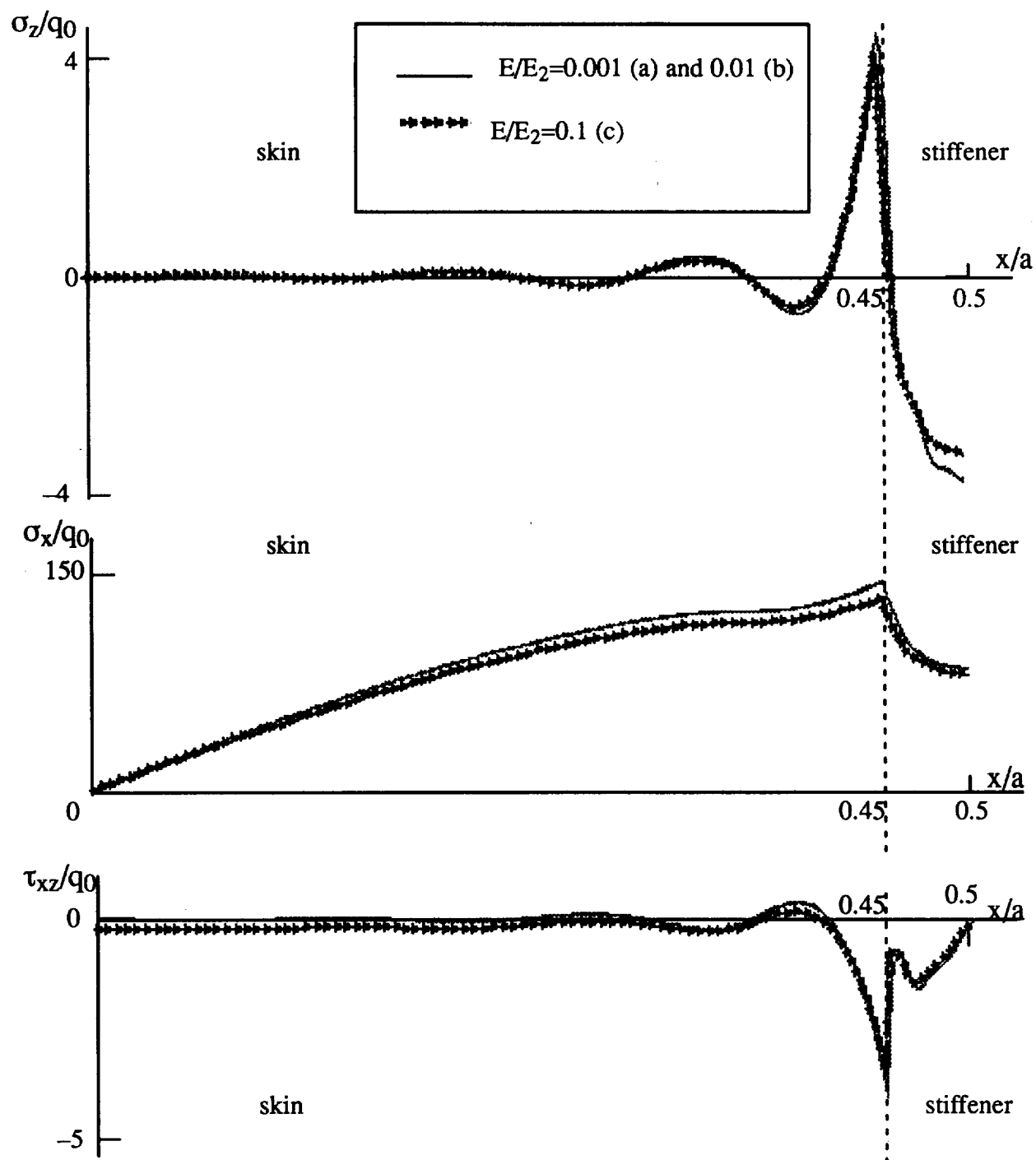


Figure 14. Variations of σ_z , σ_x , and τ_{xz} along x -coordinate for three magnitudes of the filler's modulus E .

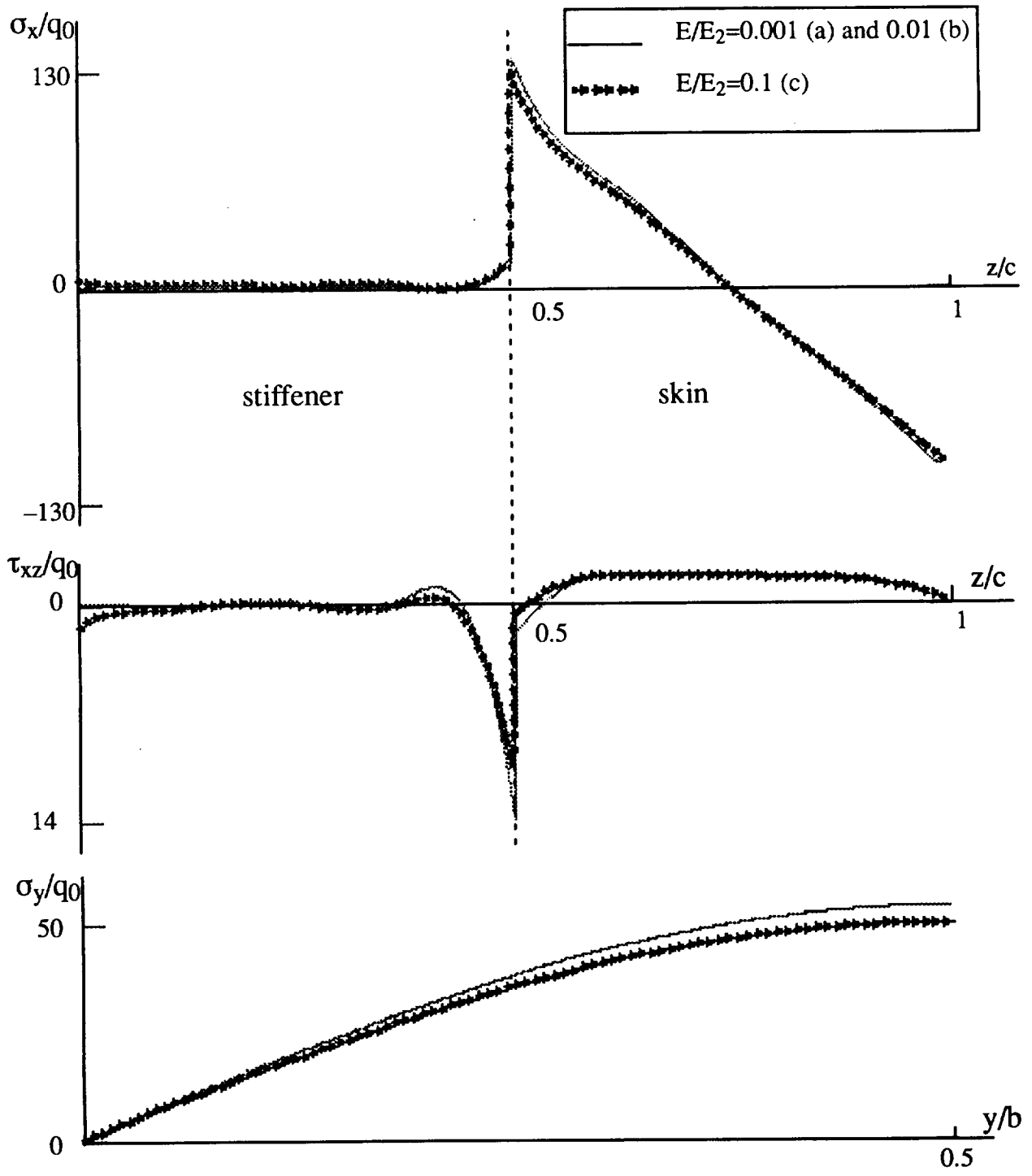


Figure 15. Variations of σ_x , τ_{xz} along z -coordinate and σ_y along y -coordinate for three magnitudes of the filler's modulus E .

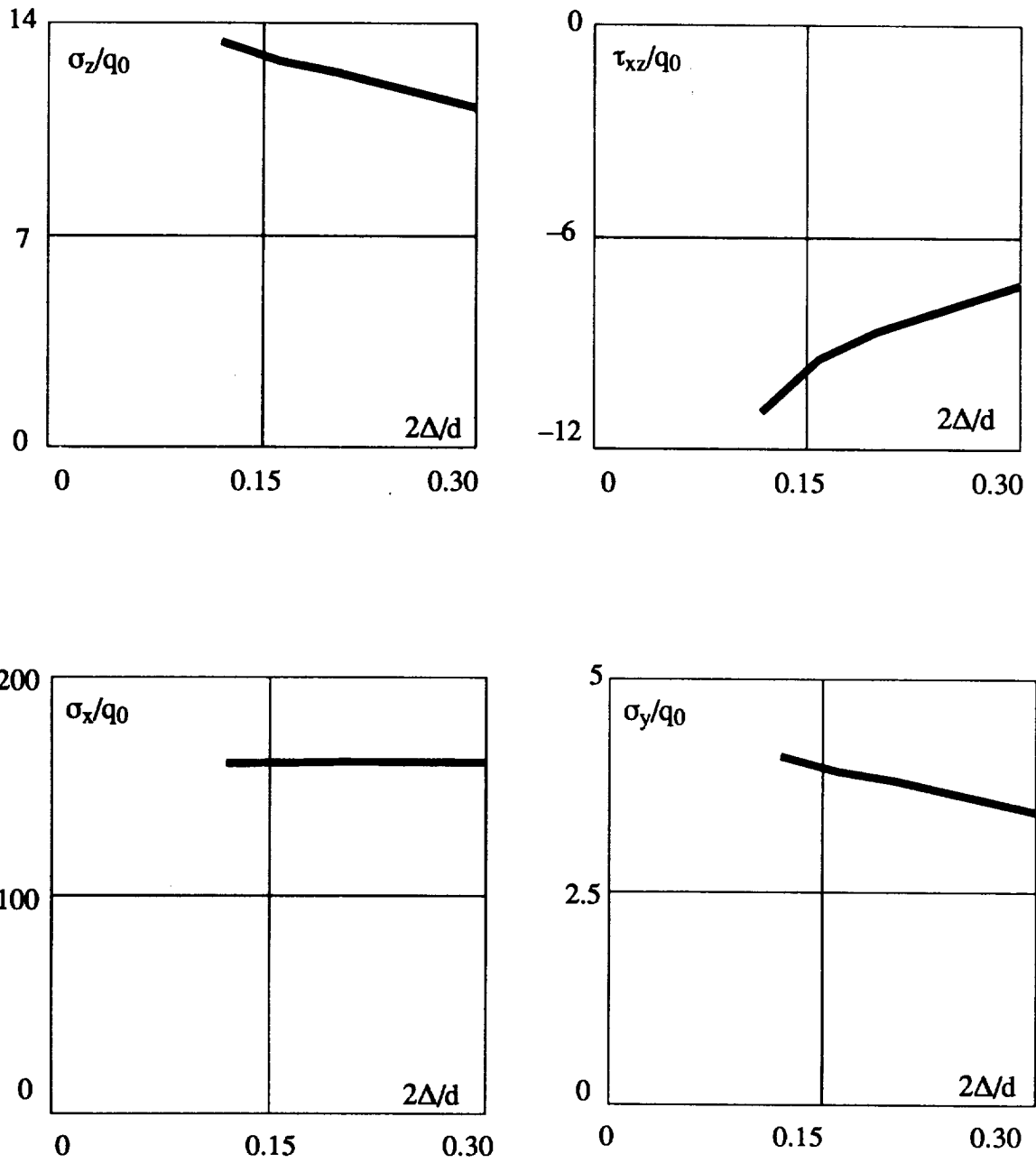


Figure 16. Dependencies of the σ_z , τ_{xz} , σ_x , and σ_y values at $x=0.45a$, $y=0.5b$, $z=h_s$ on the mesh step Δ in x -direction.

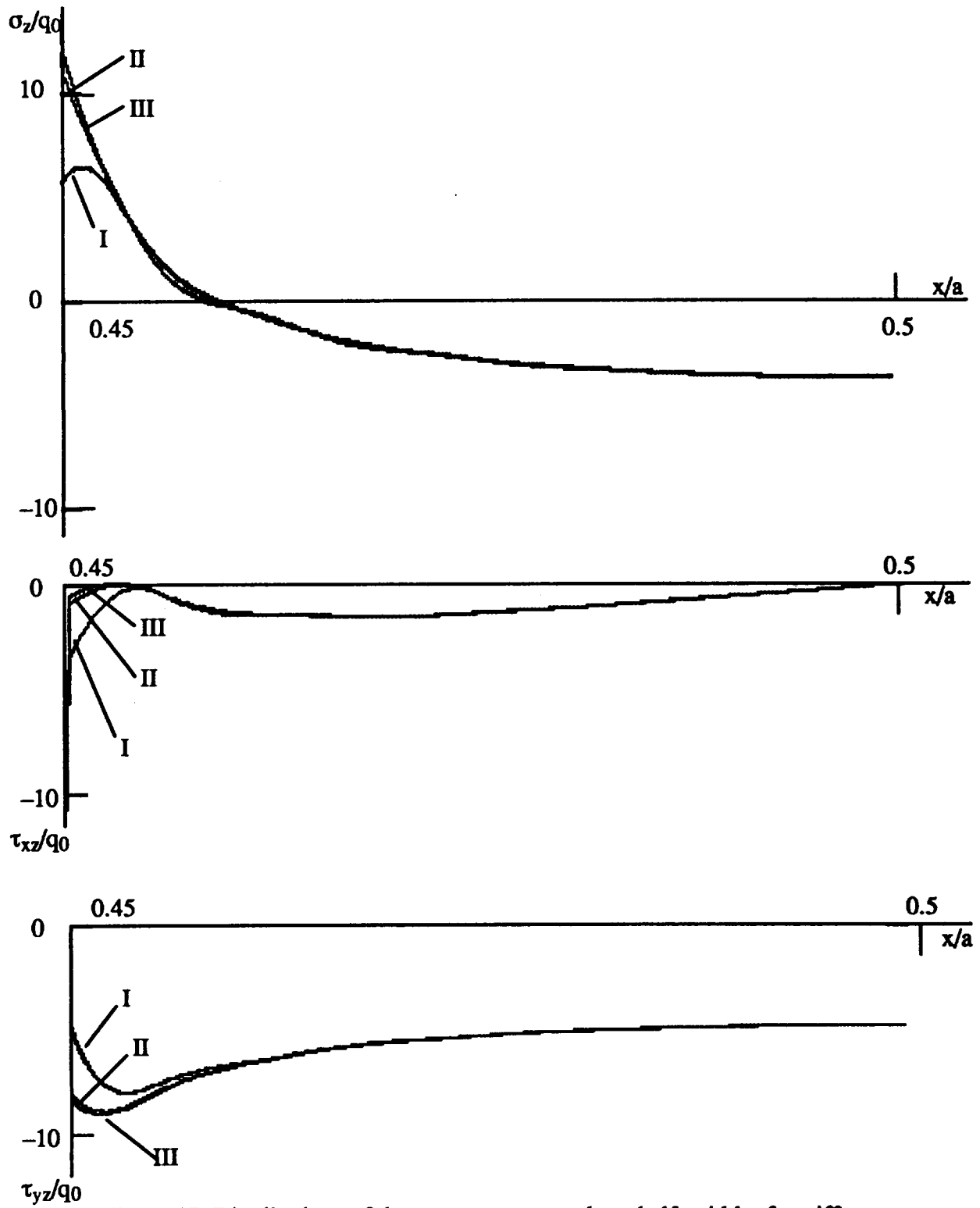


Figure 17. Distributions of the contact stresses along half-width of a stiffener for the divisions I, II, and III.

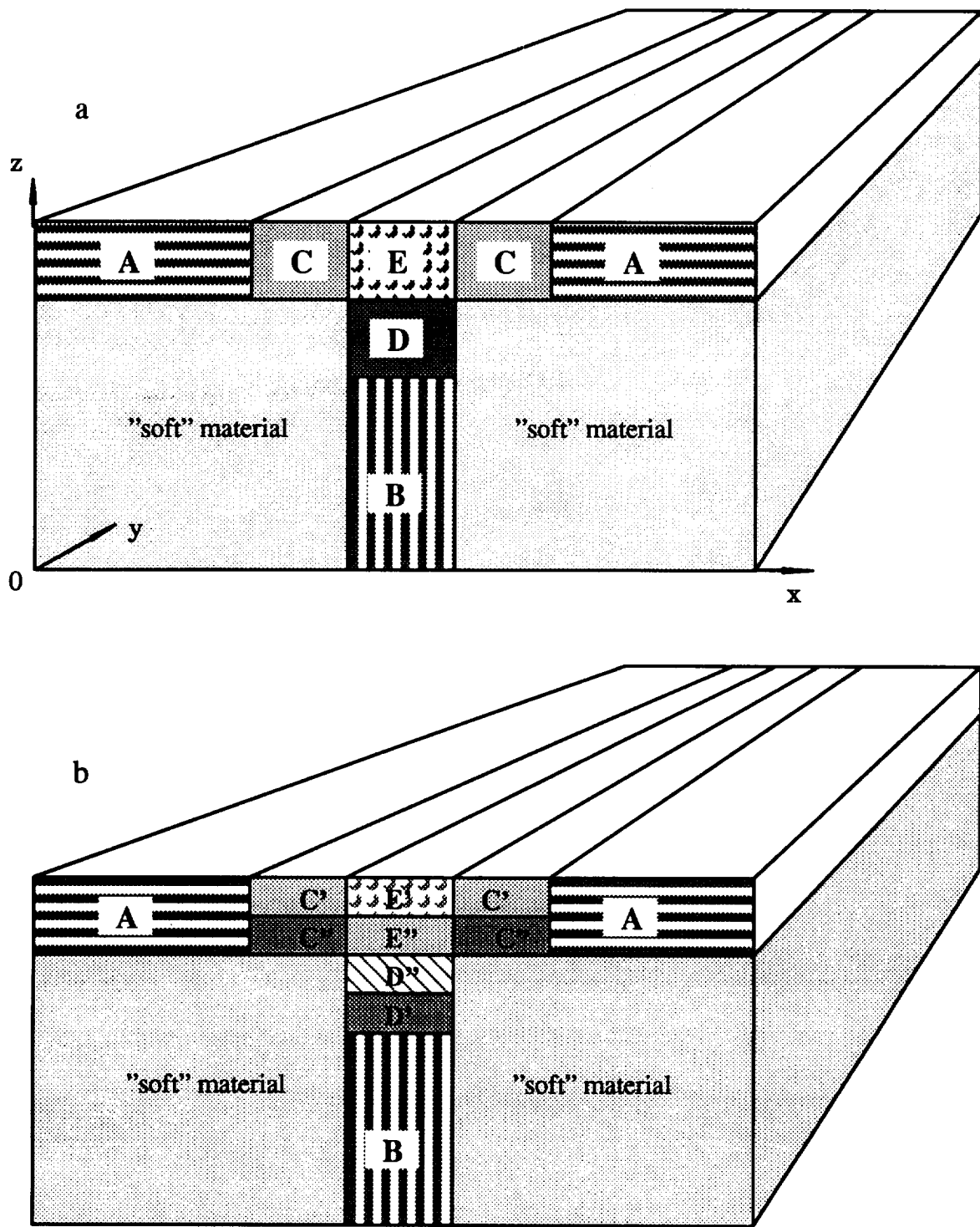


Figure 18. Meso-volume modelling of T-section triaxially braided plate.

Figure 19. Variation of σ_z along z coordinate at $x=0.5a, y=0.5b$.

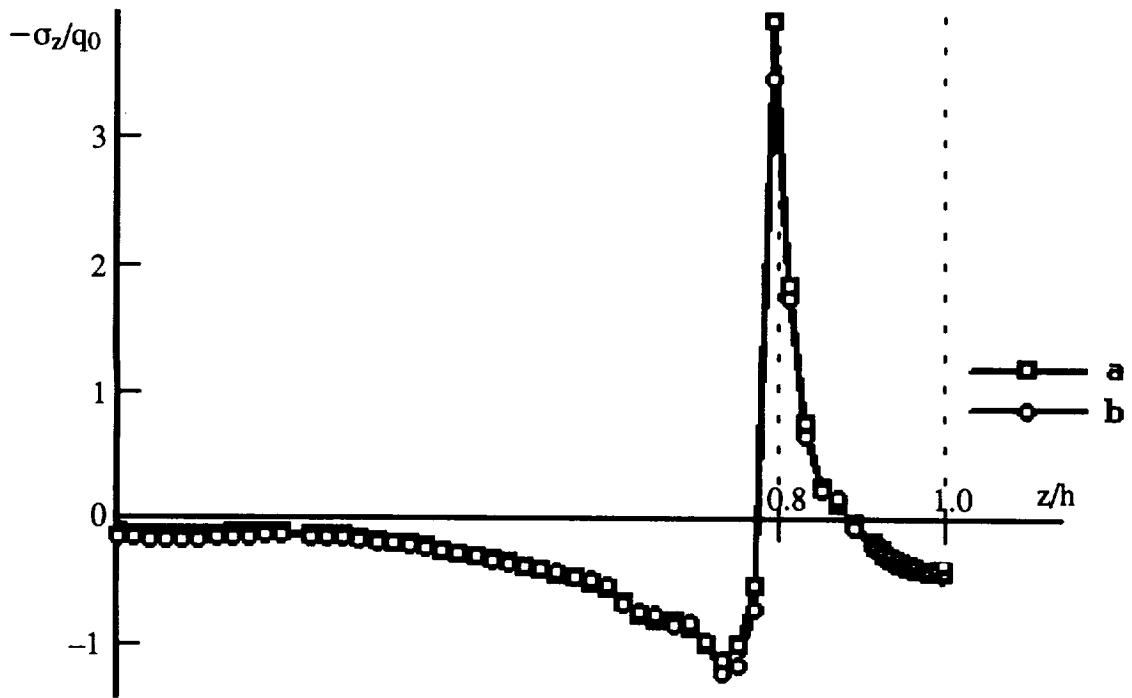
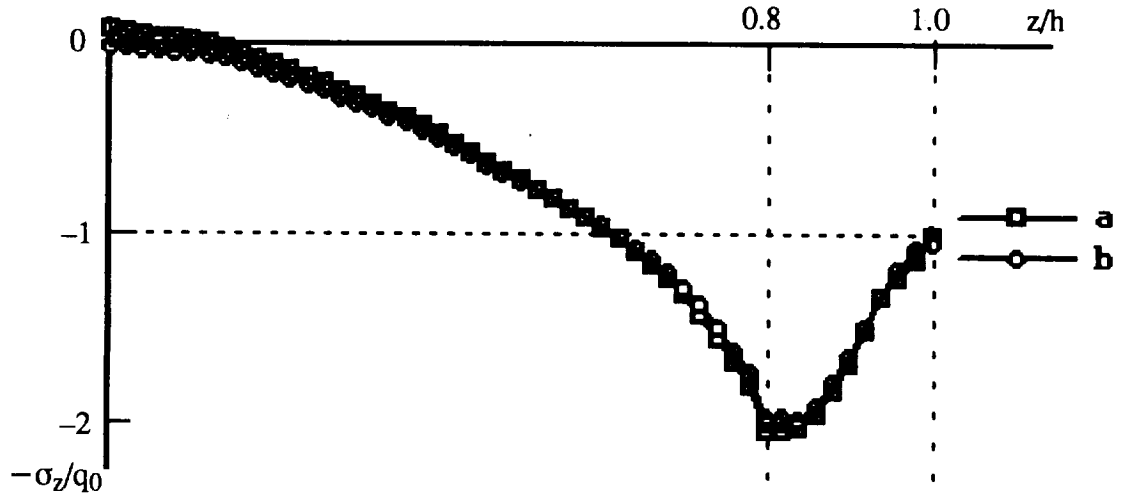


Figure 20. Variation of σ_z along z coordinate at $x=0.4a, y=0.5b$.

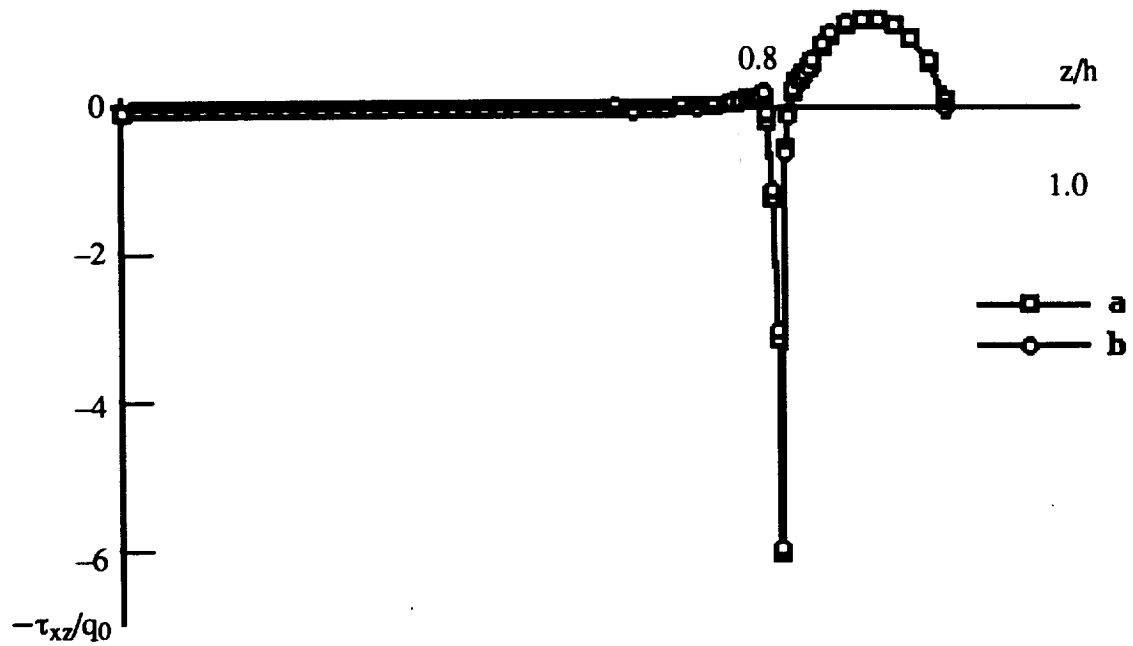


Figure 21. Variation of τ_{xz} along z coordinate at $x=0.4a, y=0.5b$.

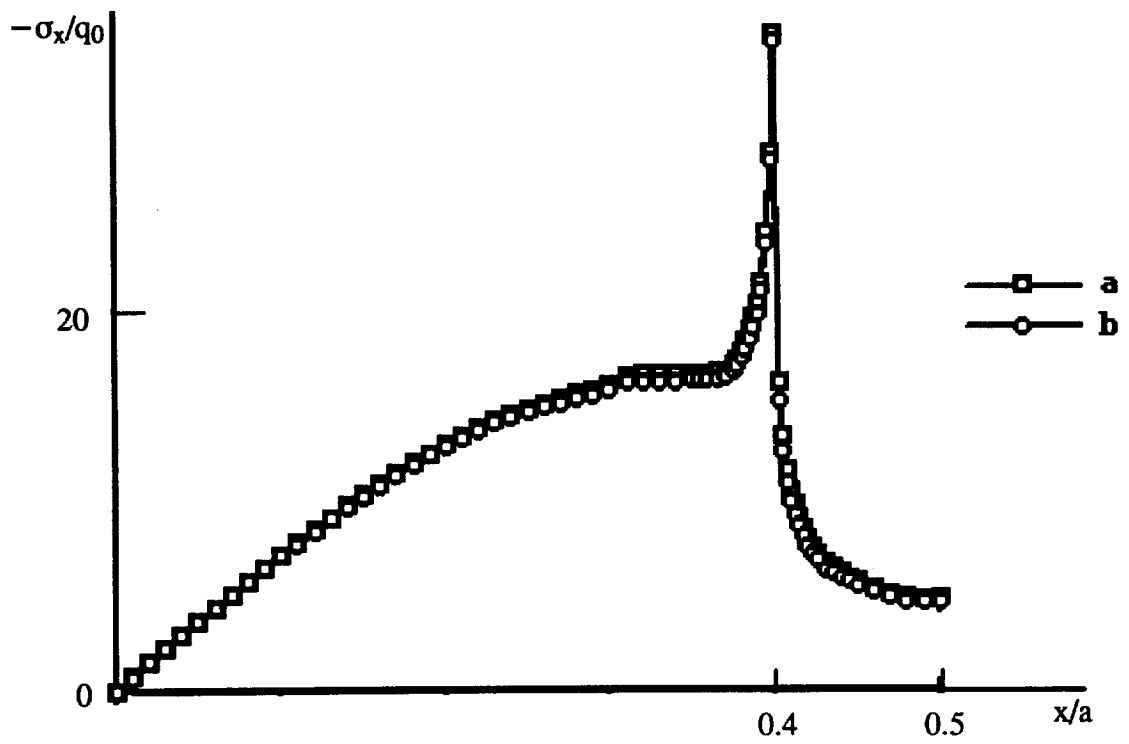


Figure 22. Variation of σ_x along x coordinate at $y=0.5b, z=0.8h$.

Figure 23. Variation of σ_z along x coordinate at $y=0.5b, z=0.8h$.

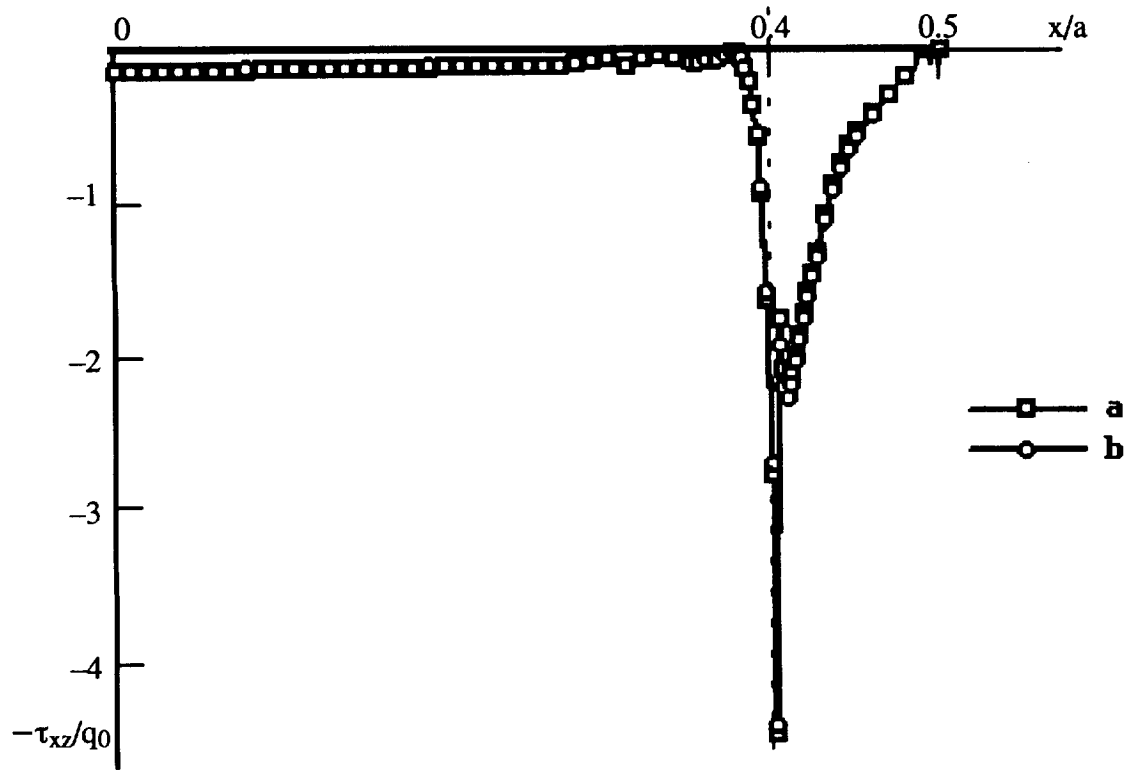
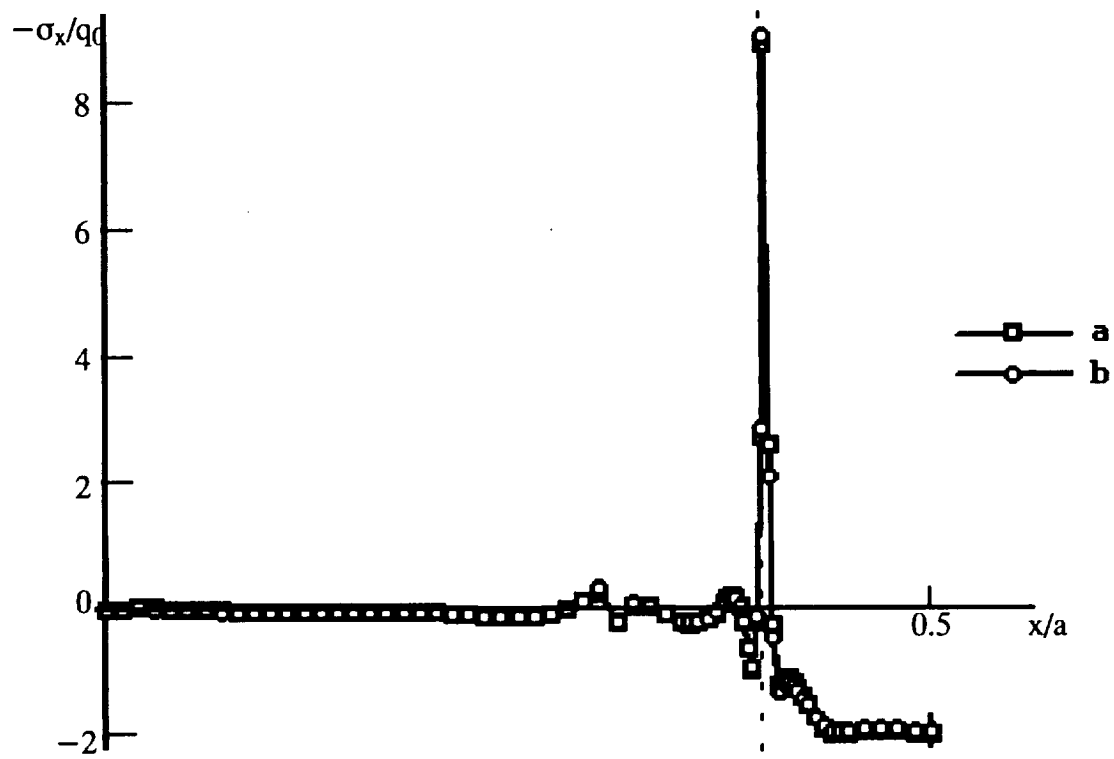


Figure 24. Variation of τ_{xz} along x coordinate at $y=0.5b, z=0.8h$.

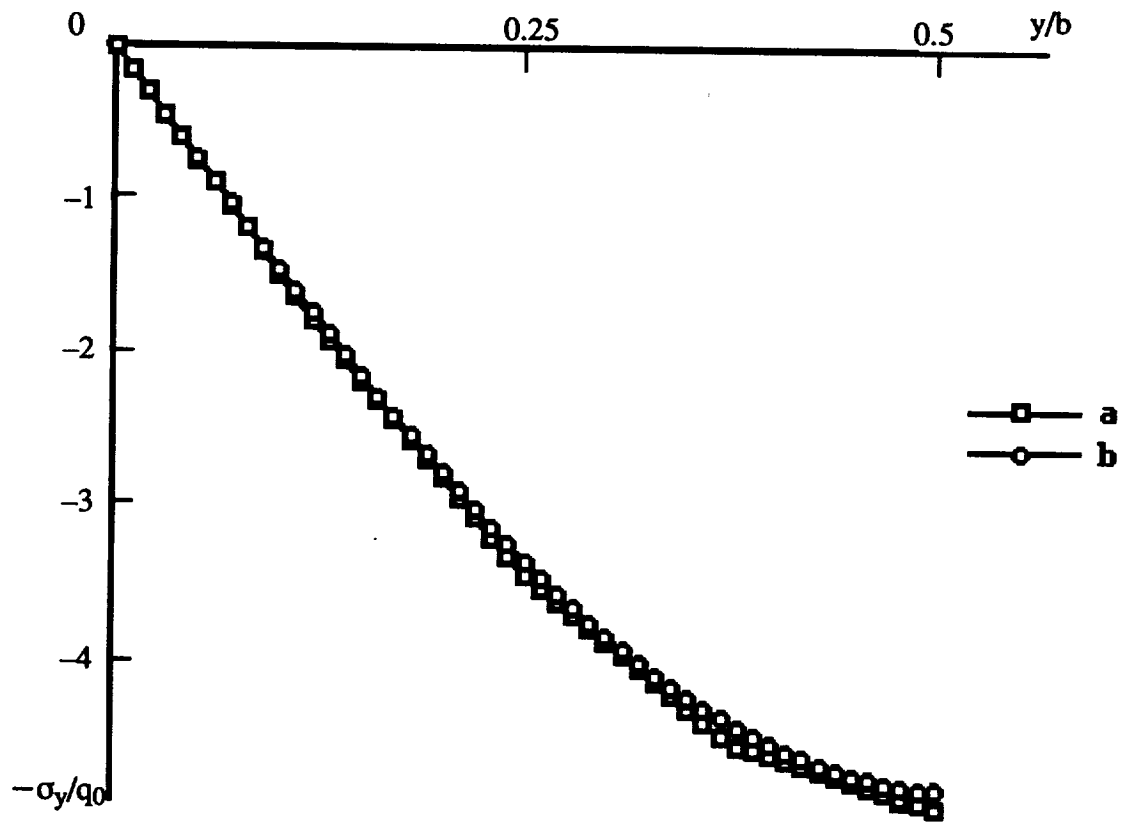


Figure 25. Variation of σ_y along y coordinate at $x=0.5a$, $z=0.9h$.

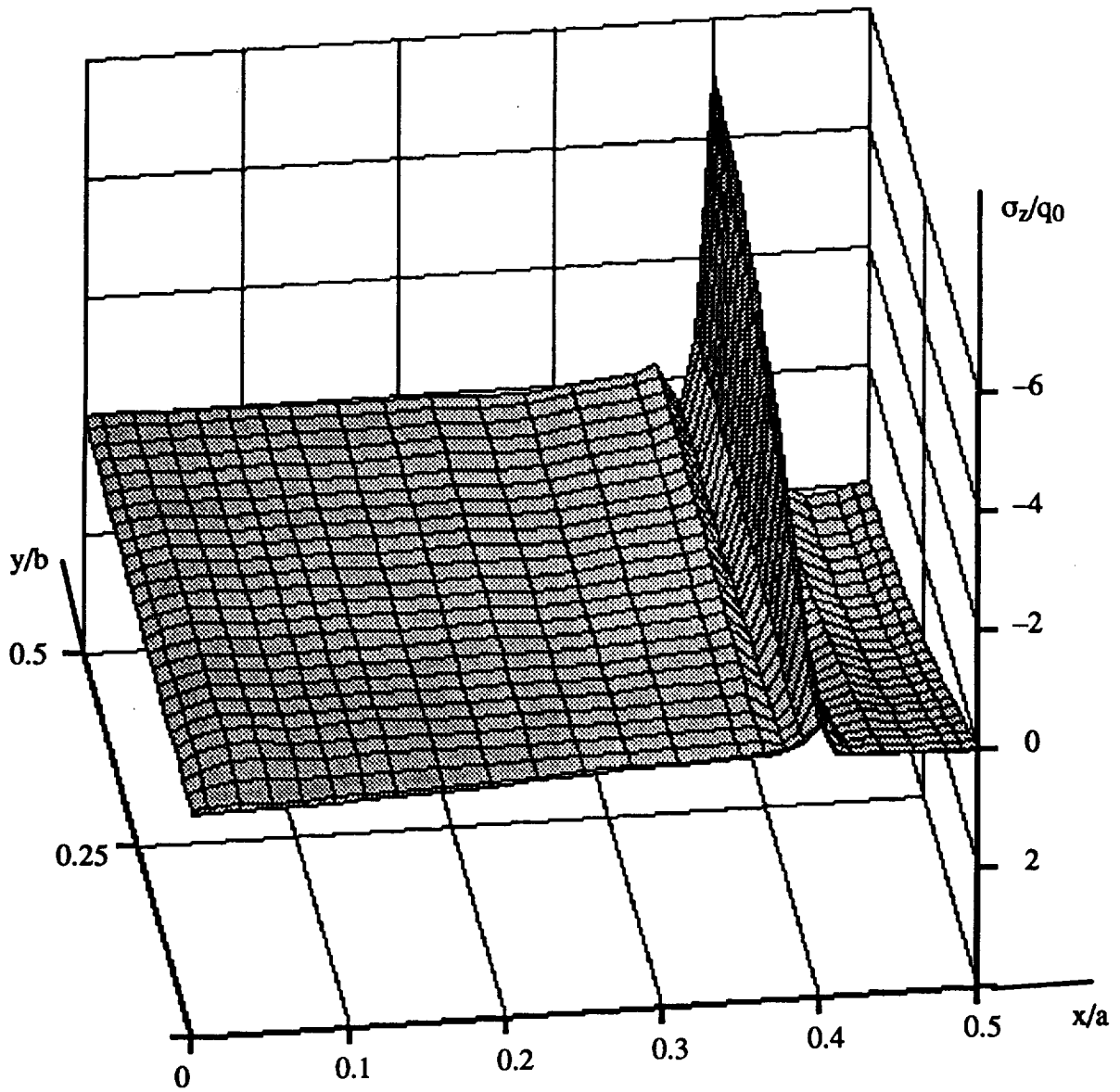


Figure 26. σ_z field in the plane $z=0.8h$.

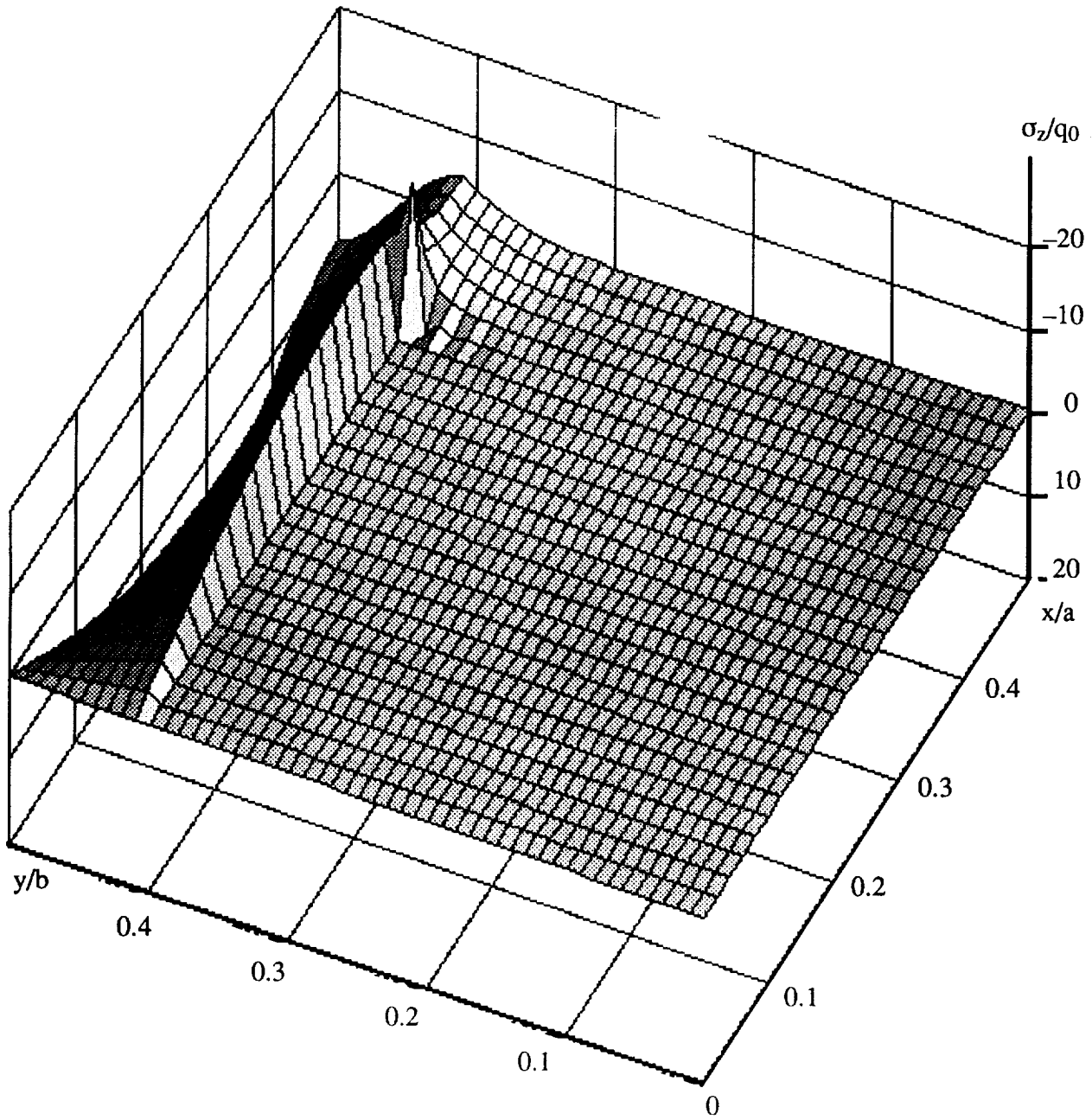


Figure 27. σ_x field in the plane $z=0.8h$.

1994012391

**TECHNO-ECONOMIC REQUIREMENTS FOR
COMPOSITE AIRCRAFT COMPONENTS**

Ray Palmer
Douglas Aircraft Company
Long Beach, California
(310) 593-0439

519-24
N94-16864

This paper presents information obtained in the performance of NASA contract NAS1-18862, "Innovative Composite Aircraft Primary Structure" (ICAPS).

INTRODUCTION

- **WHY COMPOSITES**
- **AIRCRAFT APPLICATIONS**
- **RESTRAINTS**
- **OBJECTIVE**
- **DAC APPROACH**
- **NEAR NET SHAPE DRY FIBER PREFORM**
- **RESIN INFUSION**
- **DAMAGE TOLERANCE**
- **COSTING ESTIMATES**

Why Composites?

The primary reason for use of composites is to save structural weight. A well designed composite aircraft structure will usually save 25-30 percent of a well designed metal structure. The weight savings then translates into improved performance of the aircraft in measures of greater payload, increased flying range or improved efficiency - less use of fuel.

Composite materials offer technical advantages. Key technical advantages that composites offer are high stiffness, tailored strength capability, fatigue resistance, and corrosion resistance. Low thermal expansion properties produce dimensionally stable structures over a wide range of temperature. Specialty resin "char" forming characteristics in a fire environment offer potential fire barrier application and safer aircraft.

The materials and processes of composite fabrication offer the potential for lower cost structures in the near future.

- **SAVE STRUCTURAL WEIGHT**
- **HIGH STIFFNESS**
- **IMPROVED STRUCTURAL PERFORMANCE**
- **TAILORED STRENGTH**
- **FATIGUE RESISTANCE**
- **CORROSION RESISTANCE**
- **LOW THERMAL EXPANSION**
- **RETAINED STRENGTH IN FIRE**
- **COMPLEX SHAPE FABRICATION**
- **POTENTIAL FOR LOWER COST**
- **UNLIMITED BUSINESS OPPORTUNITIES**

***AIRCRAFT
COMPOSITE
APPLICATIONS***

The first military aircraft production composite part was the stabilizer on the Grumman A-4 in 1970. This part, not shown on the view graph, represented only about 1 percent of the structural weight of the aircraft.

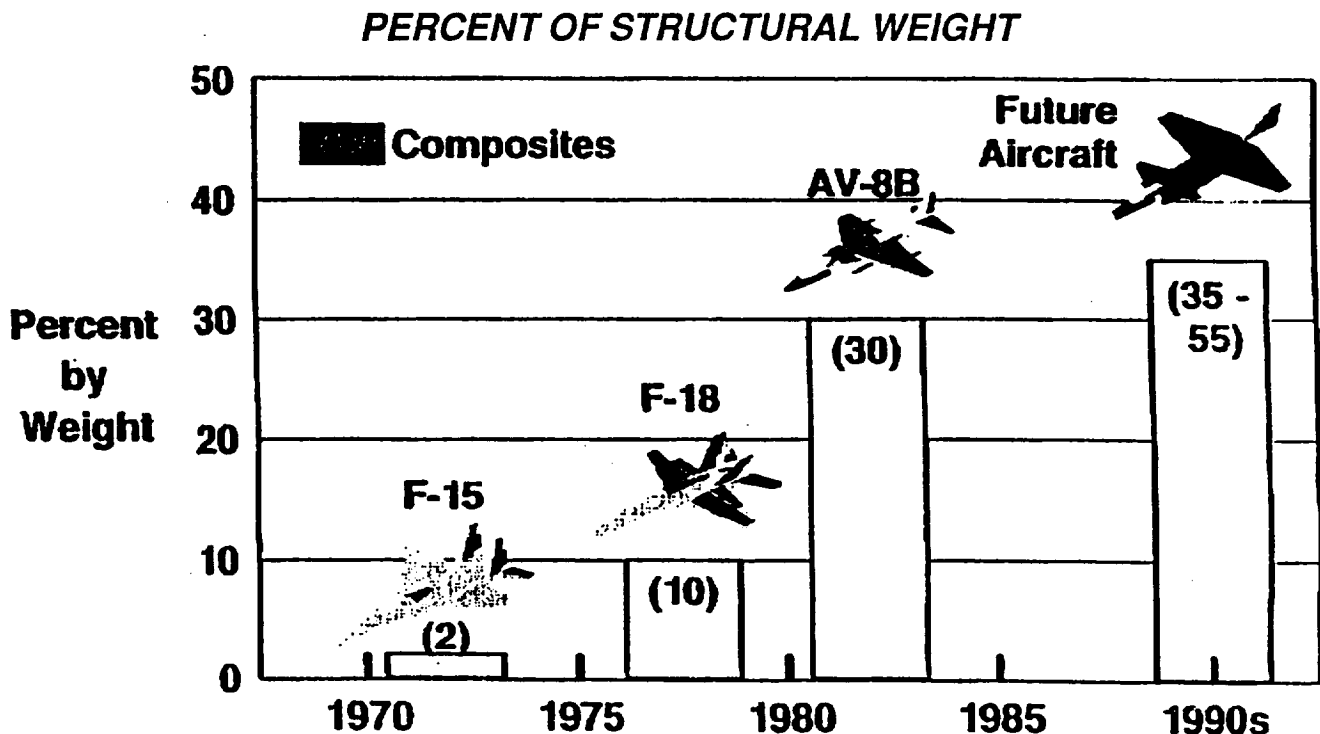
In 1972, McAIR introduced the F-15 applications of speed brake, horizontal and vertical stabilizer skins as composite materials that represented about 3 percent of the aircraft structural weight.

In 1978 McAIR introduced additional composite applications on the F-18. Horizontal and vertical stabilizer skins, wing skins, and control surfaces that represented almost 11 percent of the aircraft structural weight.

In 1982 McAIR added more composite materials than ever before to the AV8-B fighter aircraft. Wing skins and sub-structure, horizontal stabilizer skins and sub-structure, nose fuselage structure, control surfaces made of composite material represented almost 30 percent of the total primary structure. The vertical stabilizer reverted to metal structure to allow its use as an antennae.

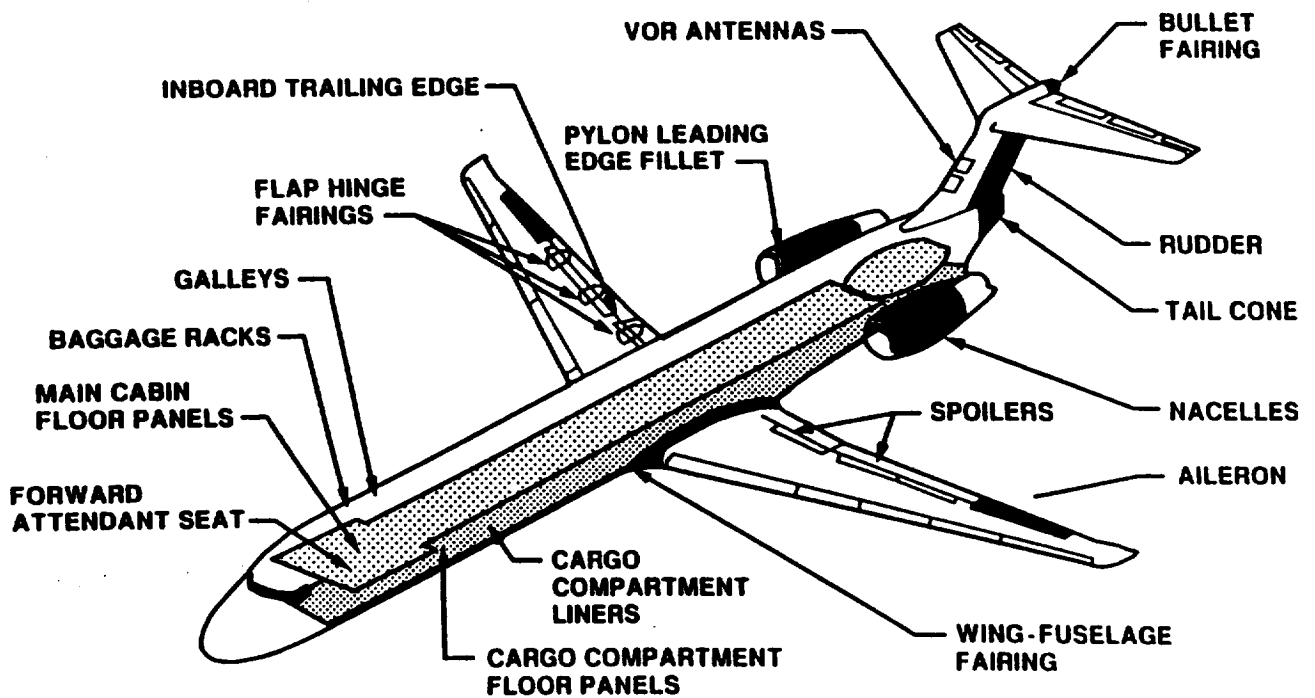
It is predicted that the next generation fighter aircraft will have over 50 percent composite material structural weight.

McAIR COMPOSITES - EXPERIENCING GROWTH



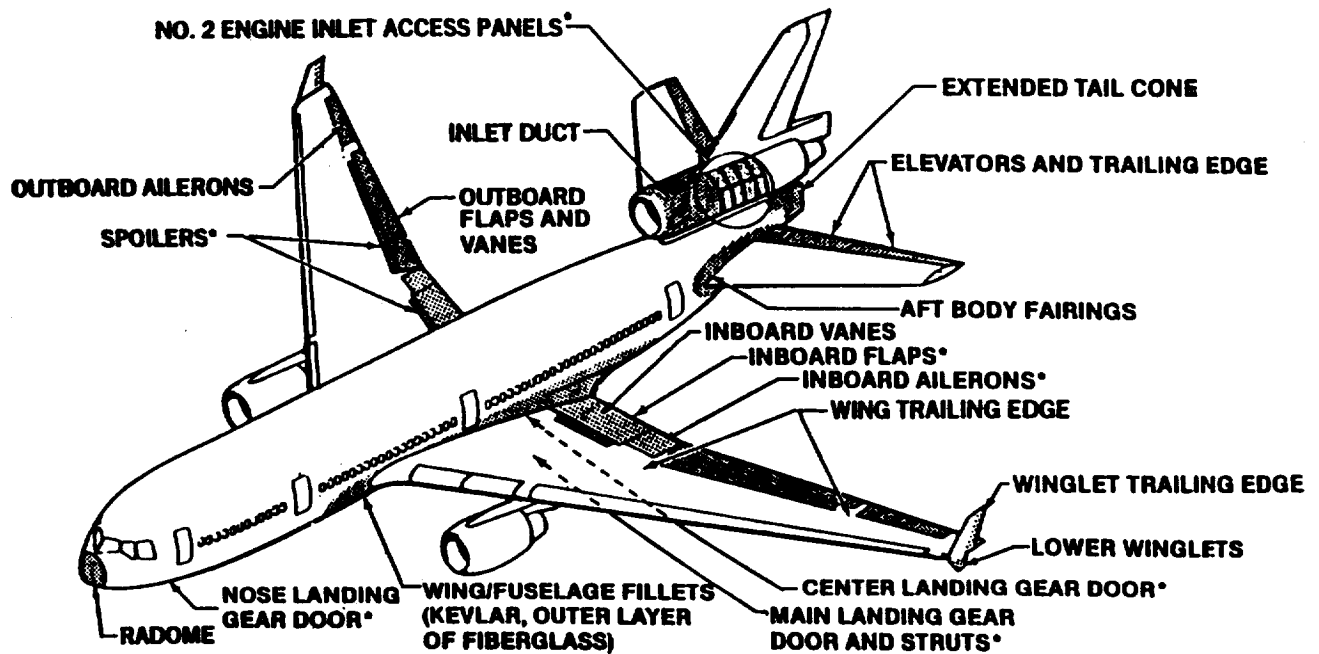
The original MD-80 series aircraft was an all metal primary structure design. Once an aircraft is in production, it is very difficult to change to a more expensive, even though lower weight component made from composite materials. Many of the *feathers* of the aircraft, representing 3 percent of the overall structural weight, were eventually converted to composite materials that included spoilers, ailerons, rudder, engine nacelles, wing trailing edges, and tail cone. No primary structure is of composite materials.

MD-80 ADVANCED COMPOSITES



Composite secondary structural components were designed into the original MD-11 production design that represents approximately 5 percent of the overall structural weight of the aircraft. Most control surfaces such as outboard ailerons, flaps and vanes, and spoilers and wing trailing edge panels are carbon fiber composites. Horizontal stabilizer elevators and trailing edge panels are composites. Winglet skins are carbon fiber composites, Wing fuselage fairings and aft body fairings are Kevlar fiber composites. All considered, composites are still considered as "feathers" of the aircraft and there is no true primary structure.

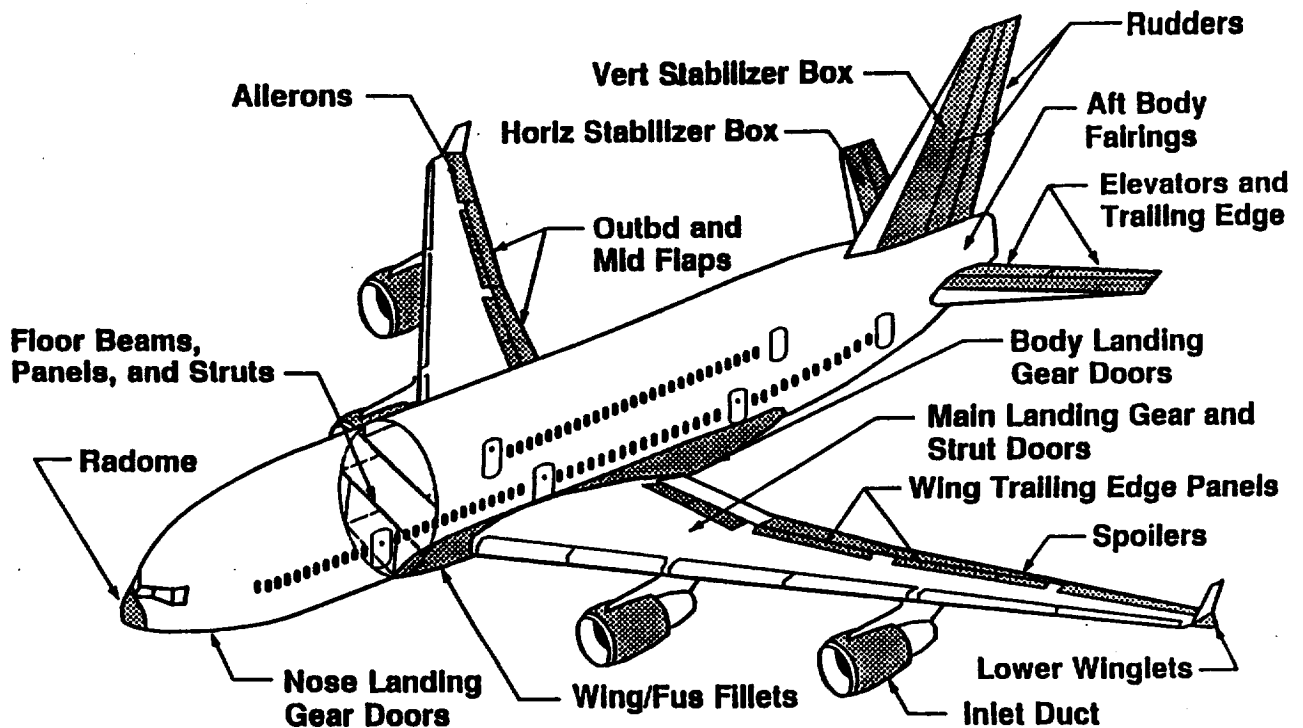
MD-11 COMPOSITE CONSTRUCTION



*UNDER CONSIDERATION

The final design of the MD-12X has not yet been completed. However, almost 11 percent overall composite structural weight is being proposed for this aircraft. All control surfaces are proposed to be carbon fiber composite. Fairings and various "feathers" are also proposed in a manner similar to the MD-11. In addition, primary structure (carbon fiber) is proposed for horizontal and vertical stabilizers. Internal fuselage cargo and passenger floor beams and support struts are proposed carbon fiber.

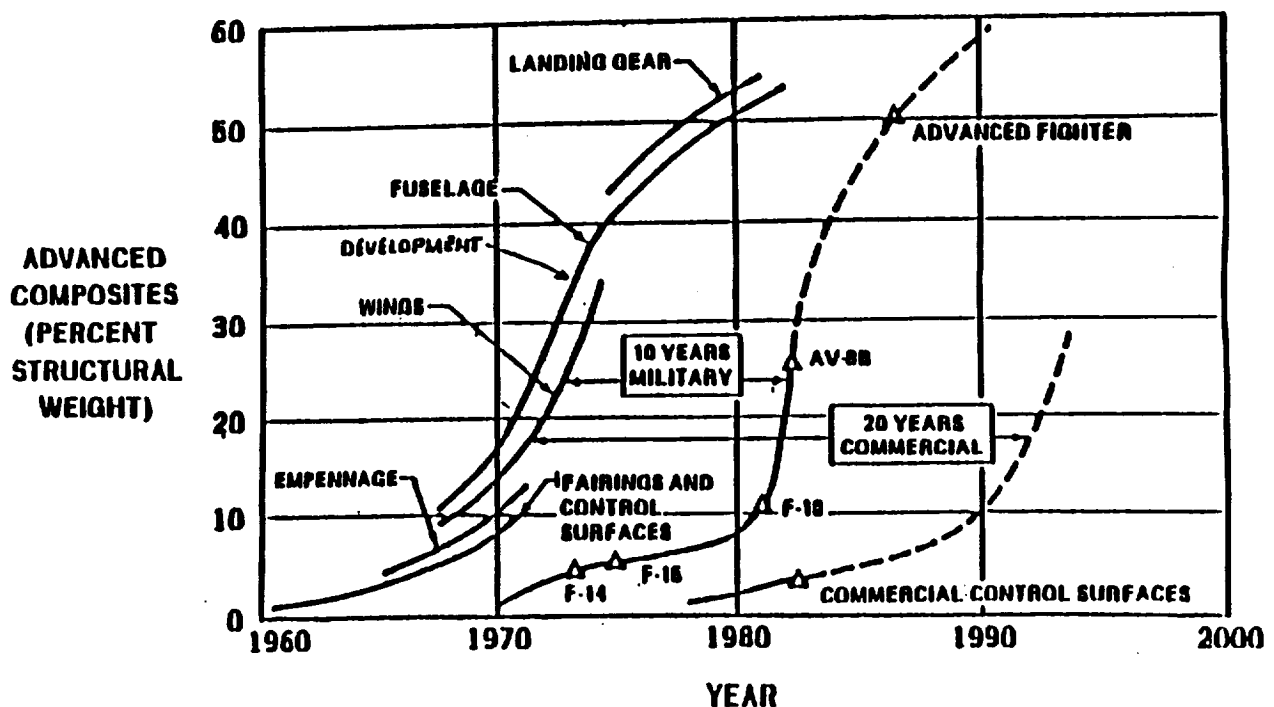
MD-12X COMPOSITE STRUCTURES



The primary message in this chart is that it has taken approximately 10 years from start of composite development activities at Wright Field until equivalent structure was applied to production military fighter aircraft. Grumman aircraft placed the first production composite structure in service, the Tom Cat stabilator in 1970 and McDonnell Aircraft Company placed the F-15 speed brake and stabilizer skins in production in 1972. Primary wing structure took the same 10-year period from development in 1970 at Wright Field to F-18 and then AV-8B wing structure at McDonnell Aircraft Company in 1978-1982 time period. It is projected that the next fighter aircraft will have over 50 percent primary structure of composite material.

It took almost 20 years from initial development at Wright Field until voluntary commercial production of carbon fiber composite control surfaces started at Boeing and DAC transport divisions. If this 20-year trend holds true, and NASA ACT activity and support continues, it appears that a major jump into primary commercial transport wing application can be expected in the mid 1990's.

IMPLEMENTATION OF ADVANCED COMPOSITES ON AIRCRAFT



The greatest restraints to application of composites in commercial aircraft are the high cost of composite structure (materials plus fabrication and qualification costs), and the marginal resistance to damage tolerance and reduced compression after barely visible surface impact damage.

GREATEST RESTRAINTS TO APPLICATION OF COMPOSITES ON AIRCRAFT STRUCTURE

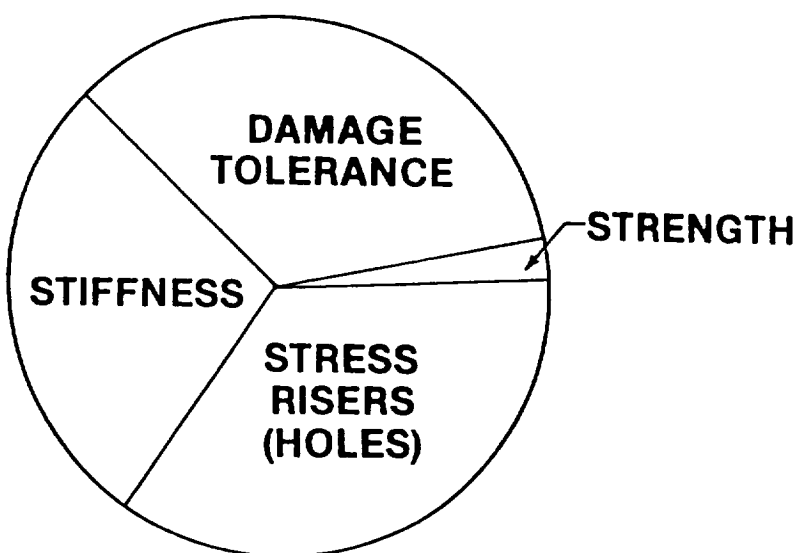
- **HIGH COST**

- **DAMAGE TOLERANCE**

Technical factors were identified that will limit the application of composites to transport aircraft primary structure. The analysis was based on the strength/stiffness capability of a 35m modulus, 520,000 tensile fiber, and a typical production resin system, Hercules 3501-6.

The analysis indicated that approximately one-third of the overall primary structure was critical in stiffness, one-third was critical in stress risers (cut-outs or bolted joints), one-third was critical in damage tolerance, and that only 2 or 3 percent was critical in strength.

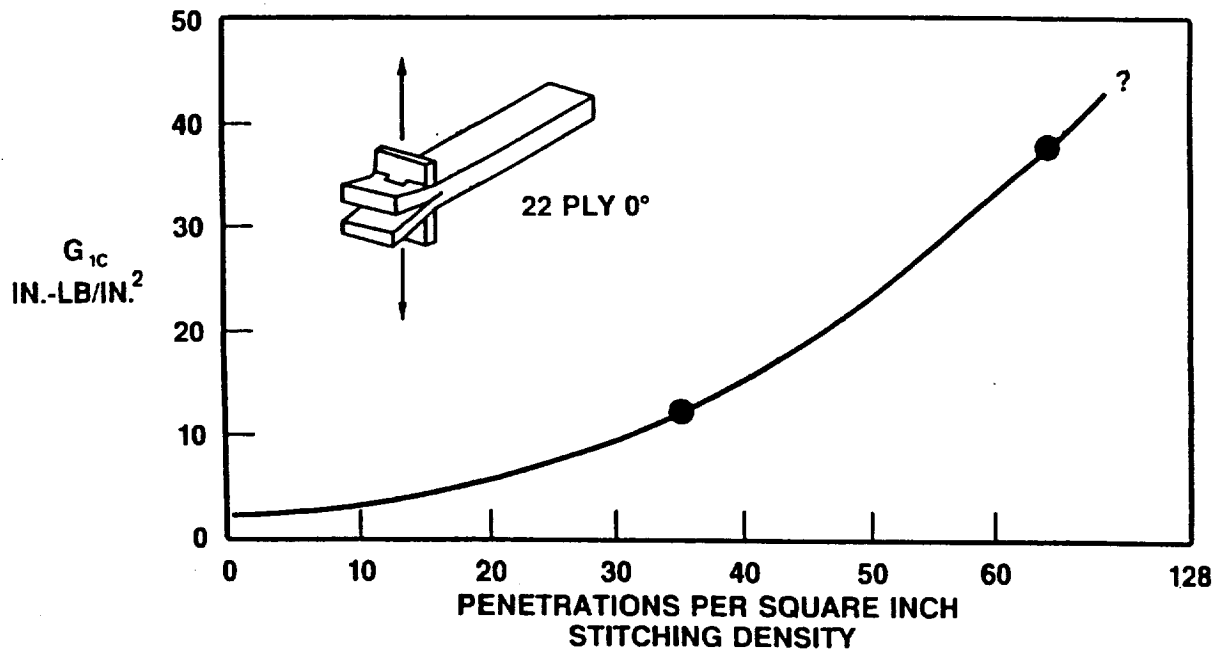
FACTORS THAT LIMIT APPLICATION OF COMPOSITE STRUCTURES IN A TYPICAL TRANSPORT AIRCRAFT



**BASED ON CARBON FIBERS WITH 520,000 PSI TENSILE/
35 M PSI MODULUS AND PRESENT PRODUCTION RESIN
SYSTEMS (HERCULES 3501-6/AS-4)**

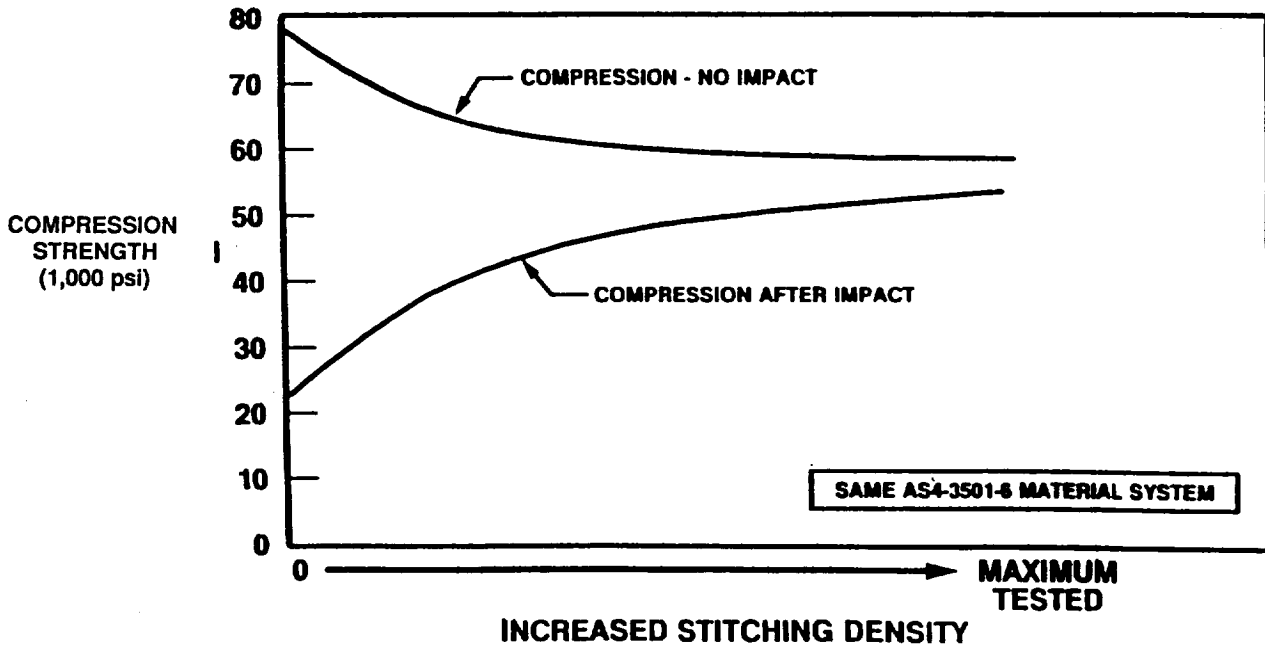
One measure of damage tolerance is resistance to peel or delamination forces. G_{1C} , crack growth rate, is a measure of delamination force. Through thickness stitching, using high strength glass or Kevlar thread, can improve G_{1C} from less than 1 in. lb/in. to over 36 in. lbs/in. while using the same structural fiber and matrix resin system. At near 36 in. lbs/in. G_{1C} peel force, specimen failure changes from peel or delamination to flexure failure at a row of stitching. Thus, it appears that stitching can eliminate G_{1C} or peel as a mode of propagation of failure in a composite laminate.

G_{1C} VERSUS STITCHING DENSITY



Retained strength in compression after barely visible impact damage is a critical mechanical property. As shown in this viewgraph, an undamaged compression panel with approximately 80,000 psi compression strength will have only about 20,000 psi compression strength after just visible impact damage. Through thickness "Z" axis stitching, with increasing stitch penetration density (penetrations per square inch) can improve CAI to over 55,000 psi while using the original reinforcement fibers and matrix resin system. Thus, structure that is damage tolerance critical can be much lighter in weight when the through thickness stitched fiber reinforcement is included in the design and fabrication.

INCREASED STITCHING DENSITY VERSUS COMPRESSION AFTER IMPACT



There are two major objectives in the DAC/NASA composites development program.

1. *Reduce Manufacturing Costs by 50 Percent*

The cost is compared to the best procedures for "B" stage material layup and autoclave cure. This includes hand layup and automated equipment tape, tow or filament layup. The final goal is to produce composite structure that is comparable in cost to aluminum structure and gain a weight savings of 25 to 30 percent.

2. *Improve damage Tolerance by 100 Percent*

The goal is to use the same lower cost resin system/fiber combination, and with the addition of "Z" axis stitched through thickness fibers, improve CAI by 100 percent. This will allow lighter weight structure to be designed where damage tolerance is critical.

OBJECTIVES

REDUCE MANUFACTURING COST BY 50 PERCENT

IMPROVE DAMAGE TOLERANCE BY 100 PERCENT

Many methods of producing near net shape preforms are under investigation by various developers. At DAC, after a study of each of the listed potential process, we have selected the knitting/stitching and the weaving/stitching as having the best overall potential to produce the large complex shape preforms required for the proposed transport aircraft structural components.

METHODS FOR NEAR NET PREFORM FABRICATION

- TWO-DIMENSIONAL ADVANCED WEAVING
- THREE-DIMENSIONAL WEAVING
- WEAVING KNITTING
- KNIT / KNIT
- IN-LINE MULTI-PLY KNIT
- BRAIDING
- IN-LINE MULTI-PLY THERMOPLASTIC HEAT SET
- **KNITTING / STITCHING**
- **WEAVING / STITCHING**
- FILAMENT WINDING

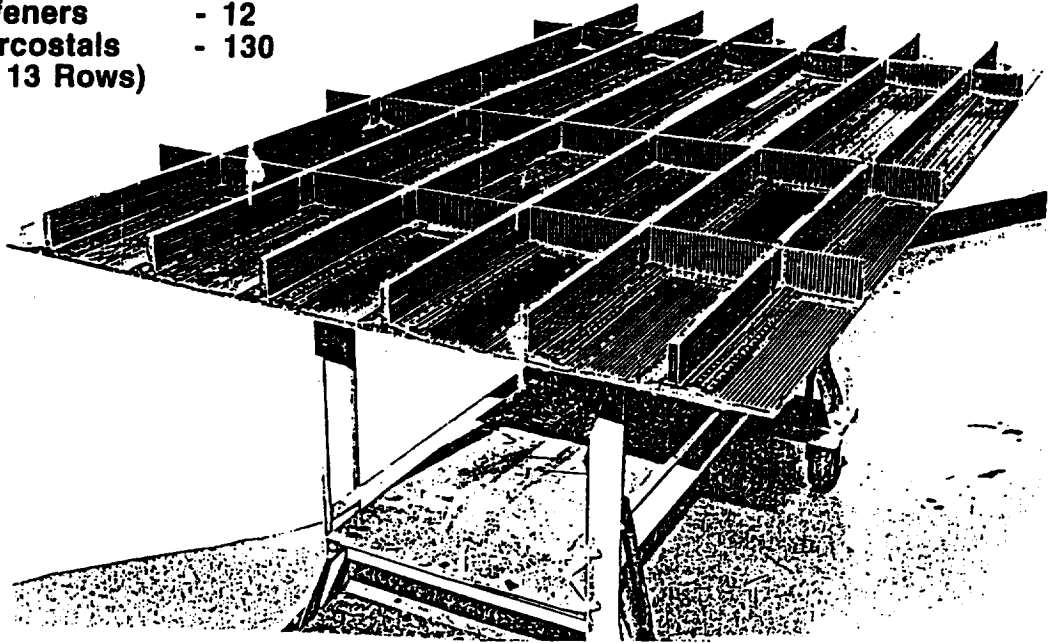
The blade stiffened panel design with 90° intercostal blade reinforcements used to demonstrate the dry fiber near net shape preform/resin infusion process (RIP) is shown in this viewgraph. This NASA demonstration wing subcomponent panel is 4-ft. x 6-ft. with 6 blade stiffeners and 3 rows of 7 individual intercostals that were all stitched together and then impregnated by the RIP (developed at DAC) and cured in the autoclave.

A similar wing panel design 8-ft. by 20-ft. with 12 stiffeners and 130 intercostals was used for later comparative cost estimating purposes.

SELECTED STIFFENED PANEL DESIGN

ASSUME:

Stiffened Panel	- 8' X 20'
Skin Thickness	- 0.360"
Stiffeners Thickness	- 0.480"
Stiffener Height	- 2.5"
Intercostals Thickness	- 0.120"
Intercostal Height	- 2.5"
Number Stiffeners	- 12
Number Intercostals (10 Rows x 13 Rows)	- 130



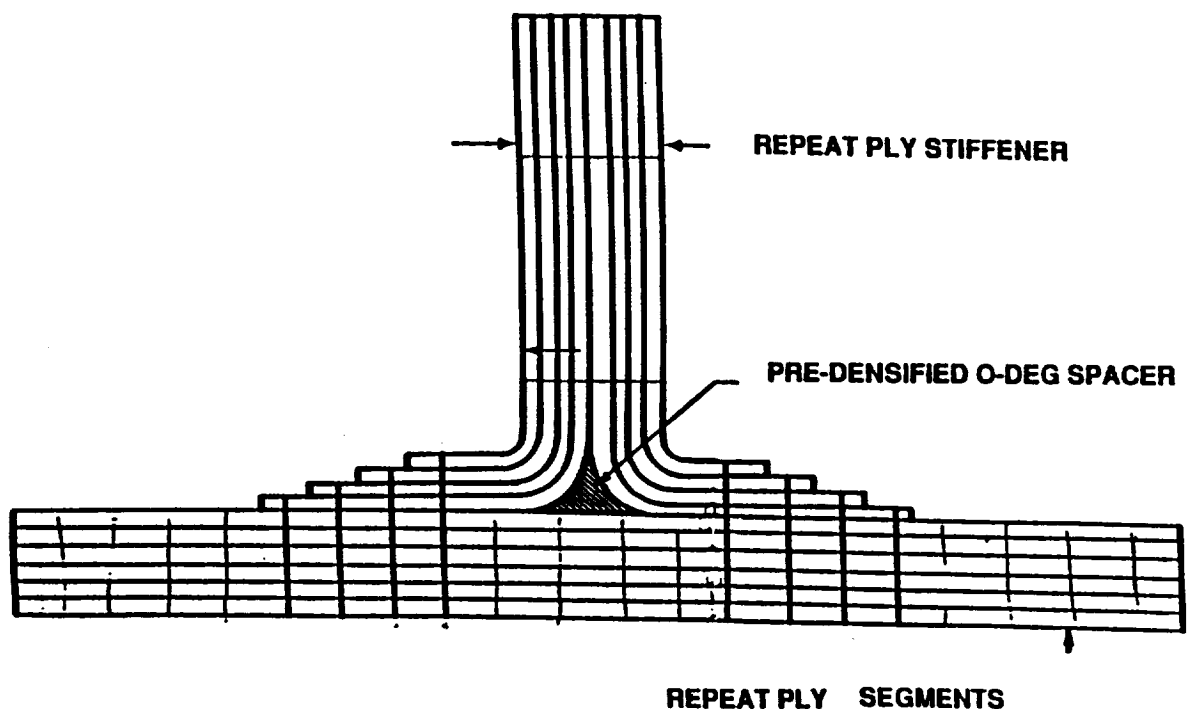
The basic design concept for the stiffened panel is shown in this viewgraph. The design is based on a 9-layer repeat pattern that is "lightly" stitched together as the first processing step. The skin is then made from 6 layers of this 9-ply material (54-ply total) and is high density stitched together to secure the 54 total layers and add damage tolerance to the skin.

The stiffener shown consists of 8 layers of 9-ply material (72-ply total) that are high density stitched together in the web area of the stiffener. The stiffeners are trimmed from the 72-ply sheet and flanges folded left and right and trimmed with four 9 layer steps. The flanges of the stiffener are then high density stitched to the skin for stiffener location and damage tolerance of stiffener to skin bond.

TEXTILE PREFORM - RTM

STITCHING OF BLADE STIFFENER TO SKIN

EXAMPLE

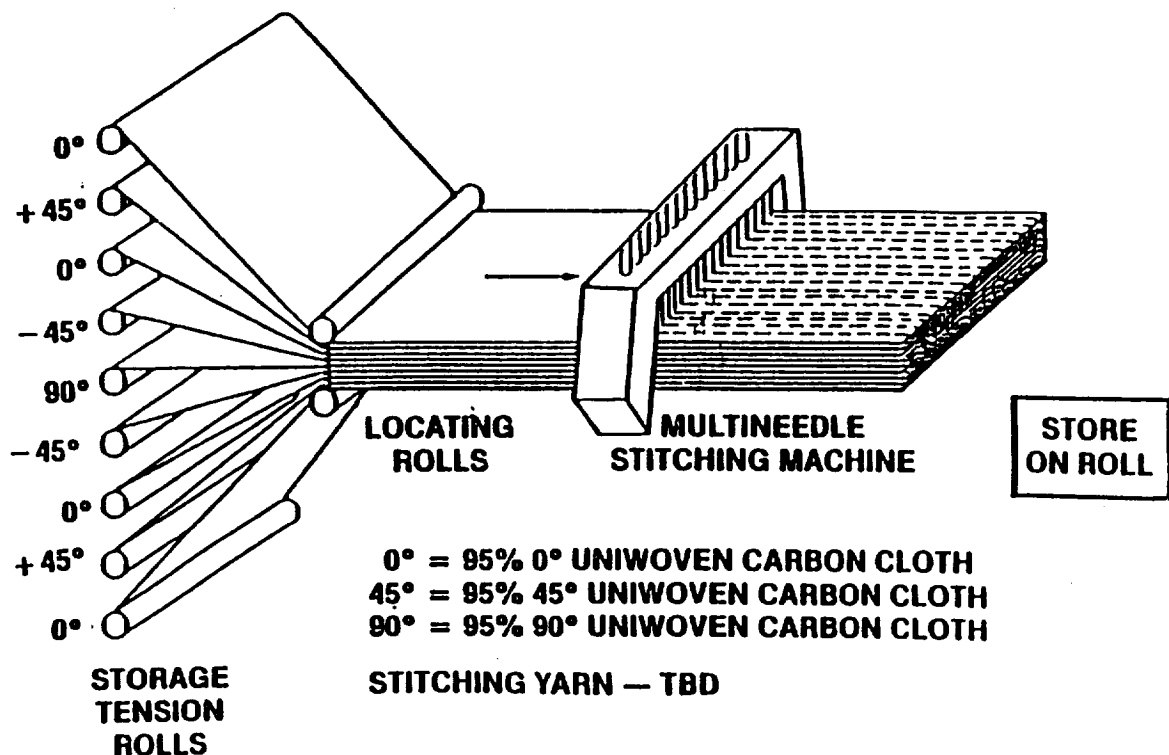


Uniwoven carbon fiber fabric can be manufactured by the weaving companies with 95 to 98 percent of the structural fibers in the 0°, the 45° or the 90° fiber directions. The remaining 2 to 5 percent fibers are fiberglass or polyester material to tie the fabric together.

This viewgraph shows one concept where 9 layers of material are metered from a tension storage rack through locating rolls and through a multi-needle stitching machine to stitch the 9 layers together. In this case, the needles are 1-in. apart and a light weight polyester or nylon thread is used. This stitching neither adds or subtracts from later laminate mechanical properties, but is merely to secure the 9 layers together so they can be later processed and handled as a single ply.

After light density stitching, the 9-layer material is stored on a large diameter roll and is ready for the next manufacturing step.

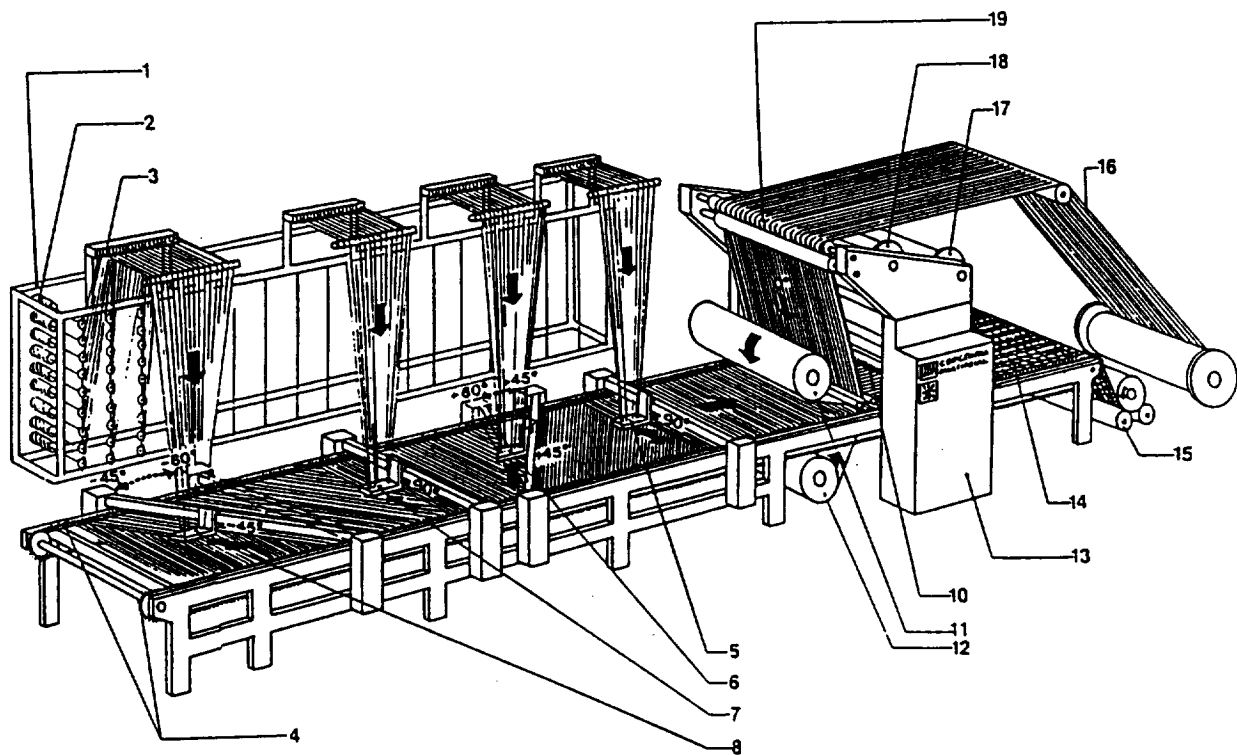
NINE-PLY BASIC STITCHED SUB-ELEMENT EXAMPLE



The Liba warp/knit machine is an alternate method of producing multi-oriented fiber layers of material. The 45° and the 90° layers are placed directly from the spools of fiber "tow" onto a moving belt with support pins along each edge. The 0° layer is first placed on a warp beam and then from the warp beam to the traveling belt with the 90° and 45° layers. The layers are all knit together immediately after the warp 0° layer insertion using a light polyester thread. As with the stitched uniwoven layers, the knit thread merely secures the layers of material together for later processing and adds nothing to the mechanical properties.

If the fiber pattern is acceptable, the Liba process of warp/knit is lower cost than an equivalent amount of uniwoven/stitched layered material and is a more desirable material form.

**FUNCTIONAL DESCRIPTION OF THE LIBA-MULTI-AXIAL SYSTEM
COPCENTRA MULTI-AXIAL, Version 5 (4 weft insertion systems):**

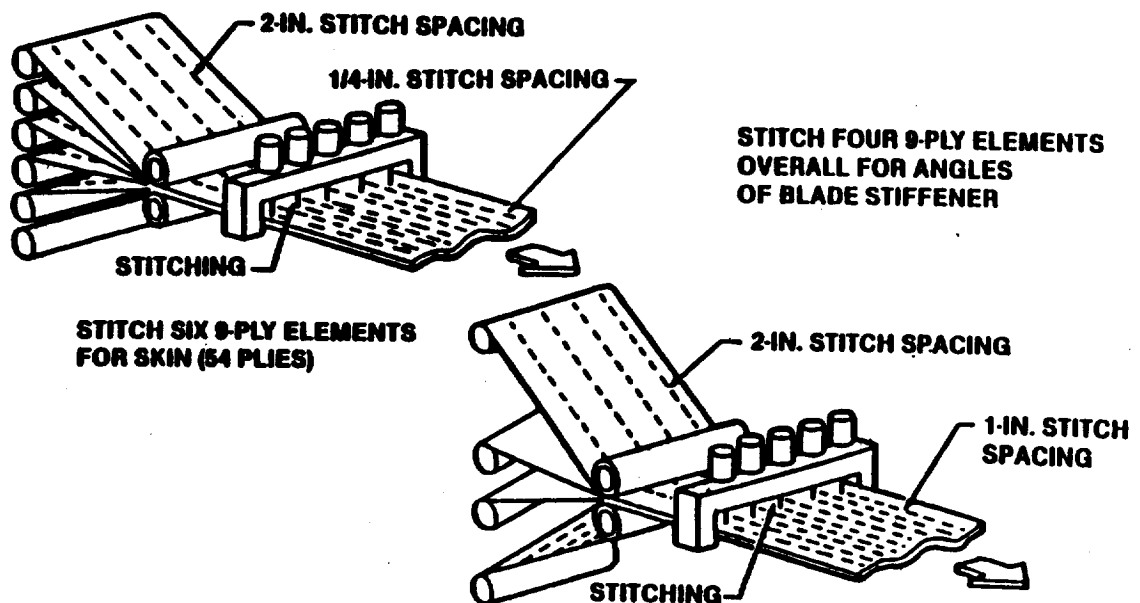


The figure on the left shows six 9-ply lightly stitched (54-ply total) layers of material passing from the tension storage rack through the multi-needle stitching machine. The stitch pattern is 0° rows, 1/4-in. apart as shown, and a high strength fiberglass or Kevlar thread is used. The resultant through thickness threads add damage tolerance to the finished panel.

The figure on the right shows four 9-ply lightly stitched (36-ply total) layers being stitched together on the multi-needle machine. This second step in preparation of panel blade stiffeners uses light-weight nylon or polyester thread merely to secure the 36 layers together but adds no mechanical properties to the final stiffeners.

STITCHING CONCEPT FOR BLADE-STIFFENED PANEL

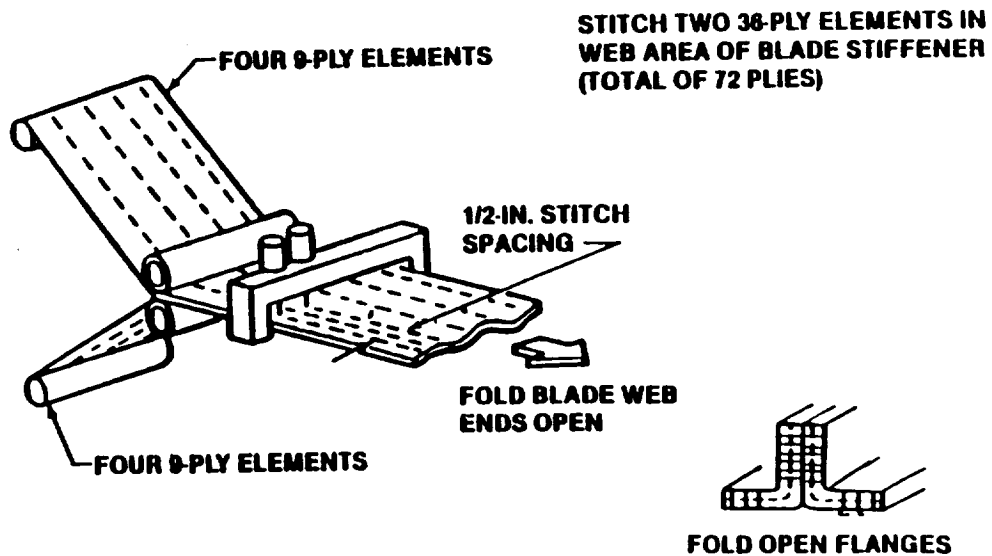
EXAMPLE



Two layers of 36-ply lightly stitched material are shown passing through the multi-needle machine. In this case the web area of the stiffener is the only area stitched (72-ply) using high density stitching and fiberglass or Kevlar thread to gain damage tolerance in the stiffener web area. As shown on the right, the stiffeners are cut to the desired width and flanges folded left and right to make the blade stiffeners.

STITCHING CONCEPT FOR BLADE-STIFFENED PANEL

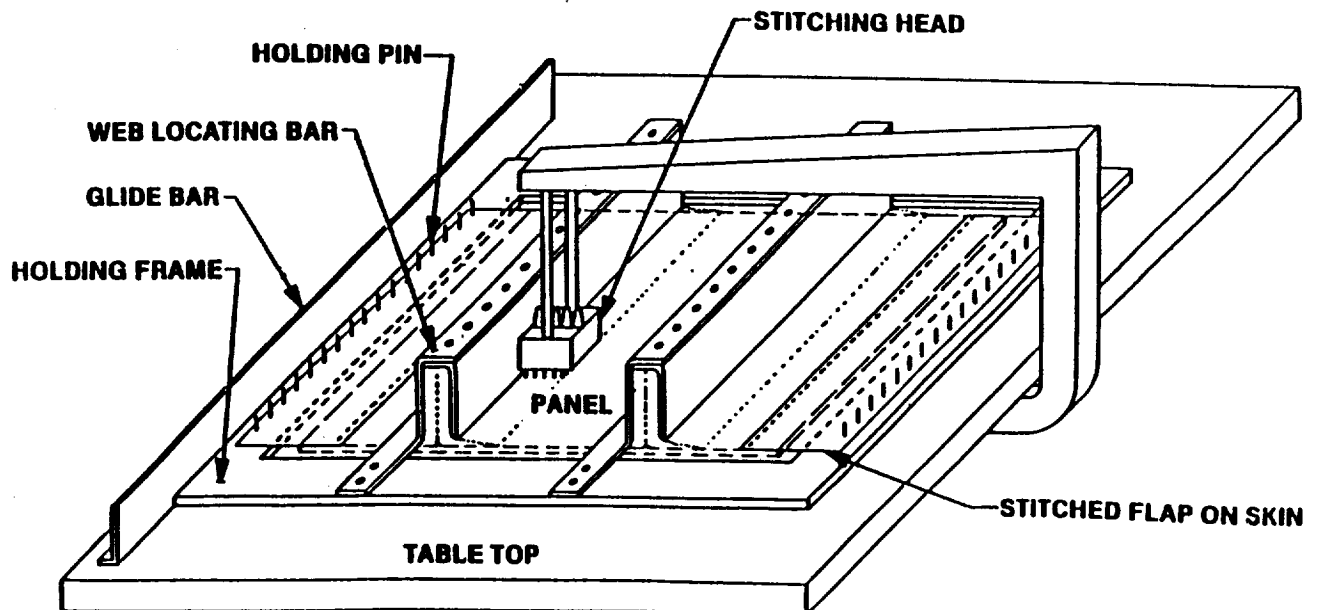
EXAMPLE



The 54-ply stitched skin is shown mounted in a holding picture frame in a long arm single needle stitching machine. The stiffener webs are secured in individual holding frames and the stiffener frames pin located to the skin picture frame. This viewgraph shows the stiffener flange being stitched to the skin using a 4-needle sewing head. In this case, the sewing head is in a fixed location and the work passed by the stitching head with stitching location achieved by the edge of the skin picture frame and a guide bar on the stitching machine.

STITCHING "T" FLANGE TO SKIN

EXAMPLE



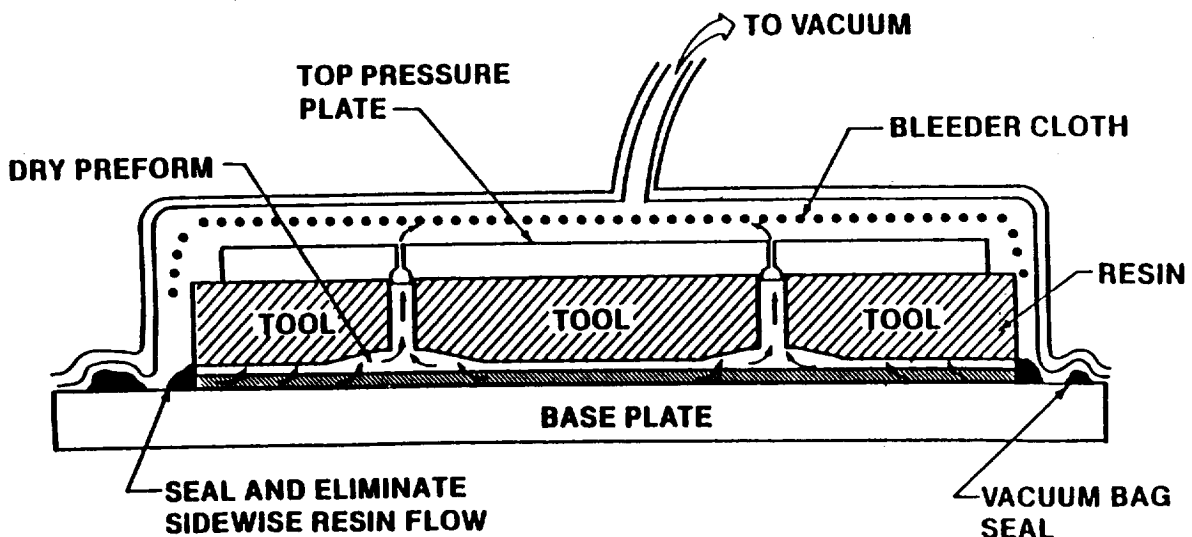
The stitched preform is next trimmed to final size to fit the tooling and weighed. A "B" stage resin slab is weighed and cast to the size of the skin and will give approximately 34 percent panel resin content.

The cast film of resin is located on the tool base plate. The preform is located over the resin. The tooling mandrels (3 shown) are located in position between the stiffener webs. The top pressure plate is located over the tool mandrels. The tooling mandrels are pin located through the top pressure plate to assure accurate location and thickness of the final cured stiffeners.

Bleeder cloth and a vacuum bag are placed over the entire assembly. The assembly is then placed in an autoclave for final heat and pressure cycle to impregnate the preform and cure the panel.

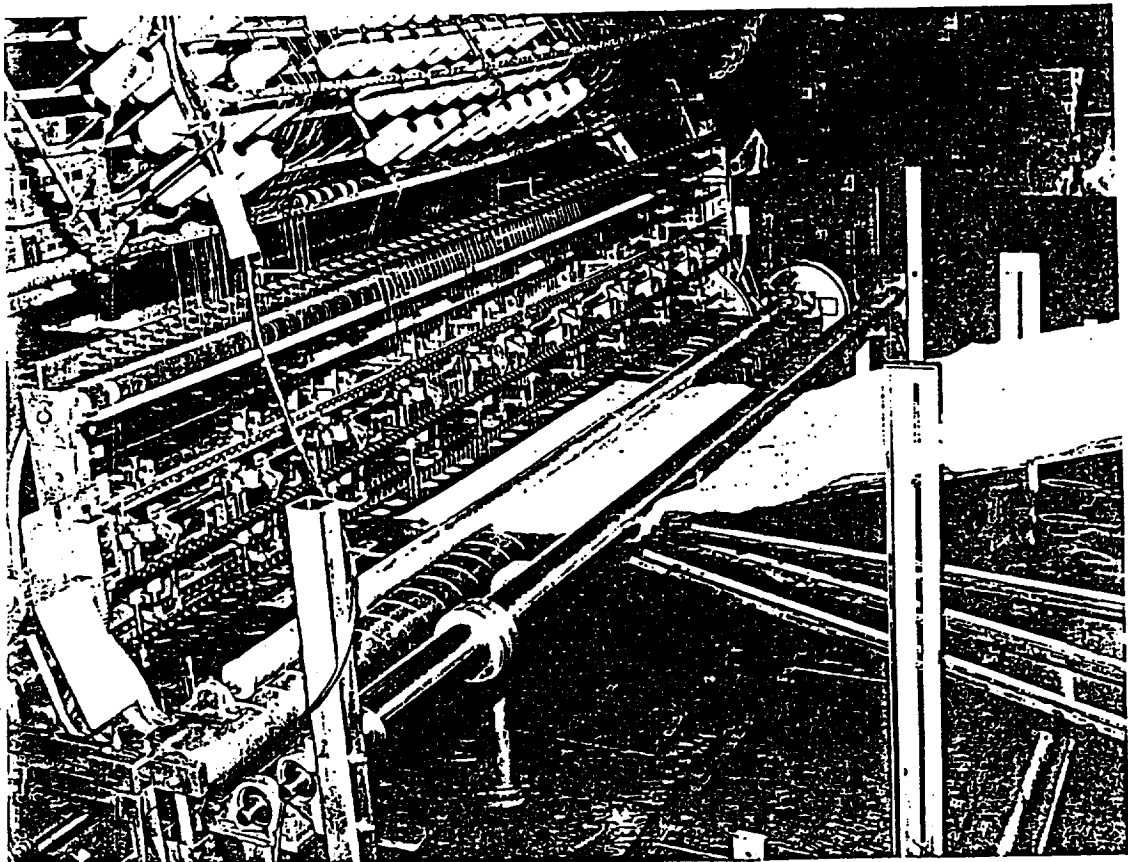
With heat, the resin becomes very thin and impregnates up through the skin, the blade stiffeners, and into the upper bleeder cloth. At this time the resin gels, and the cure cycle is completed with a standard autoclave curing cycle.

VACUUM IMPREGNATION OF STIFFENED PANEL



This is a photograph of the DAC multi-needle stitching machine, 128" wide, that was made by Pathe, Inc., Irvington, New Jersey. The machine has 128 needles and is shown with material feeding into the machine from a 12 roll tension storage rack. The stitching rate can be controlled from a few penetrations per minute to over 200 penetrations per minute - depending on the number of layers or thickness of material being stitched.

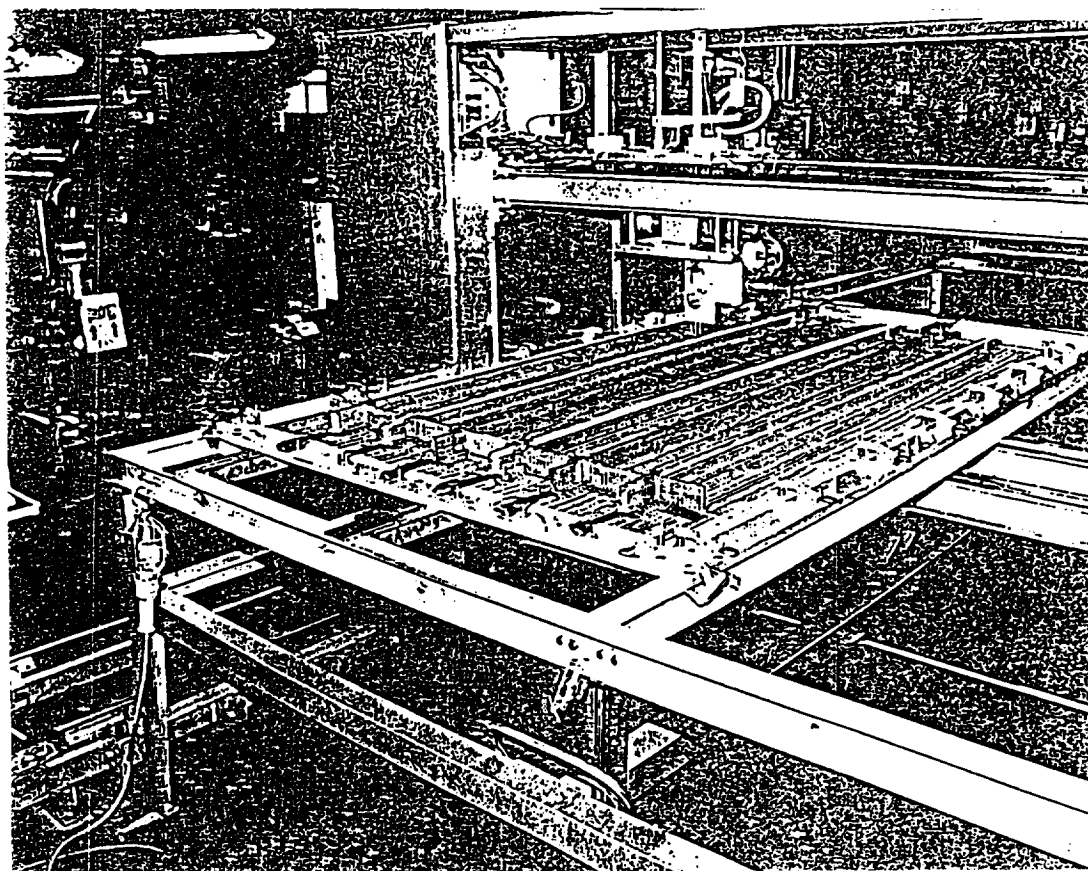
MULTI-NEEDLE STITCHING MACHINE 128" WIDE



(Original photo unavailable)

This is a photograph of the DAC single needle stitching machine, fully computer controlled for x - y -motion over an area 9-ft. wide and 15-ft. long. The material to be stitched is mounted in a holding frame, in a fixed location, and the stitching head moves to create the desired stitch pattern. A "lock" type stitch is used to allow stitching in any direction. This machine will stitch at rates between a few penetrations per minute, and over 400 penetrations per minute, depending on the thickness of the material being stitched.

COMPUTER CONTROL SINGLE NEEDLE STITCHING MACHINE 9' X 15' AREA



(Original photo unavailable)

A cost estimate has been made to produce an arbitrary size panel 8-ft. by 20-ft. in size with 12 lengthwise stiffeners and 10 rows of 13, each 90° intercostals (total 130).

Assumptions used in the preparation of cost estimates for material and stitching tape layup and tow placement labor are shown. Special note should be taken that all stitching tape layup and tow placement estimates are loaded with a 50 percent efficiency factor. Note also, that all equipment is assumed to be in working order and that repeat part fabrication is occurring so that no individual set up time is included and that no Quality Control (QC) costs are included in any of the estimates.

The estimates include all layup, bagging, and curing but no time is included for NDI, part trim, part finish, or part assembly.

COST ESTIMATE

THIS IS NOT A REAL PANEL. SIZE, THICKNESS AND PLY PATTERN ARE ARBITRARY.

COST ASSUMPTIONS:

MATERIAL	<table style="width: 100%; border: none;"> <tr> <td style="padding-right: 10px;">3K 35M FIBER</td> <td>= \$32 / POUND</td> </tr> <tr> <td>12K 35M FIBER</td> <td>= \$18 / POUND</td> </tr> <tr> <td>UNIWOVEN FABRIC</td> <td>= 2 x FIBER</td> </tr> <tr> <td>"B" STAGE FABRIC</td> <td>= 2 x FABRIC</td> </tr> <tr> <td>WARP/KNIT</td> <td>= 2 x FIBER</td> </tr> <tr> <td>RESIN</td> <td>= \$20 / POUND</td> </tr> </table>	3K 35M FIBER	= \$32 / POUND	12K 35M FIBER	= \$18 / POUND	UNIWOVEN FABRIC	= 2 x FIBER	"B" STAGE FABRIC	= 2 x FABRIC	WARP/KNIT	= 2 x FIBER	RESIN	= \$20 / POUND				
3K 35M FIBER	= \$32 / POUND																
12K 35M FIBER	= \$18 / POUND																
UNIWOVEN FABRIC	= 2 x FIBER																
"B" STAGE FABRIC	= 2 x FABRIC																
WARP/KNIT	= 2 x FIBER																
RESIN	= \$20 / POUND																
STITCHING	<table style="width: 100%; border: none;"> <tr> <td style="padding-right: 10px;">SET-UP TIME</td> <td>= NOT ESTIMATED</td> </tr> <tr> <td>ALL STITCHING</td> <td>= 50% EFFICIENCY</td> </tr> <tr> <td>THIN STITCHING</td> <td>= 112 ppm</td> </tr> <tr> <td>THICK STITCHING</td> <td>= 32 ppm</td> </tr> <tr> <td>MULTI-NEEDLE MACHINE</td> <td>= 100 NEEDLES 1" APART</td> </tr> <tr> <td>SINGLE NEEDLE MACHINE</td> <td>AUTOMATED CONTROL</td> </tr> <tr> <td>AUTOMATED TAPE</td> <td></td> </tr> <tr> <td>LAYUP/TOW PLACEMENT</td> <td>= 50% EFFICIENCY</td> </tr> </table>	SET-UP TIME	= NOT ESTIMATED	ALL STITCHING	= 50% EFFICIENCY	THIN STITCHING	= 112 ppm	THICK STITCHING	= 32 ppm	MULTI-NEEDLE MACHINE	= 100 NEEDLES 1" APART	SINGLE NEEDLE MACHINE	AUTOMATED CONTROL	AUTOMATED TAPE		LAYUP/TOW PLACEMENT	= 50% EFFICIENCY
SET-UP TIME	= NOT ESTIMATED																
ALL STITCHING	= 50% EFFICIENCY																
THIN STITCHING	= 112 ppm																
THICK STITCHING	= 32 ppm																
MULTI-NEEDLE MACHINE	= 100 NEEDLES 1" APART																
SINGLE NEEDLE MACHINE	AUTOMATED CONTROL																
AUTOMATED TAPE																	
LAYUP/TOW PLACEMENT	= 50% EFFICIENCY																
LABOR	\$50 / HOUR																

This viewgraph shows the methodology used to estimate the cost of 100-in. wide unidirectional fabric (not yet purchased). All material costs followed this format.

Dry fiber 3k carbon cost of \$32/lb was supplied by the fiber manufacturer. Cost of 2x fiber cost for uniwoven fabric was considered proper by the fiber supplier/weaver at \$64/lb. The weight of 100-in. wide fabric, at 145 gm/m² fiber areal weight was calculated at 0.76 lbs/linear yard x \$64/lb = \$48.64/linear yard.

IM-7, higher modulus fiber at \$47/lb, for example uniwoven fabric with the same fiber areal weight would cost 0.76 lbs/linear yard x \$94/lb = 71.44/linear yard.

MATERIAL COST ESTIMATE

EXAMPLE

Dry Fiber Uniwoven 100" Wide

Assume:	3K 35M Modulus fiber	\$32.00/lb
	Uniwoven fabric 0°,45°,90°	145 gm/m ²
	Fabric width	100 inches
	Fabric cost = 2 x fiber cost	\$64.00/lb

Weight: 100" Wide fabric at 145 gm/m²

$$\frac{145 \text{ gm}}{\text{m}^2} \times \frac{1 \text{ m}}{39''} \times \frac{1 \text{ m}}{39''} \times \frac{100''}{36''} \times \frac{1 \text{ lb}}{454 \text{ gm}} = 0.76 \text{ lb/lin yd}$$

$$\text{Cost/linear Yard} = \frac{0.76 \text{ lb}}{\text{lin yd}} \times \frac{\$64.00}{\text{lb}} = \$48.64/\text{lin yd}$$

"B" Stage Layup - 8-ft. by 20-ft. Panel

This is a summary of material and labor costs for an 8-ft. by 20-ft. 12 stiffener, 130 intercostal stiffened panel made by the "B" stage layup autoclave curing process. It includes individual breakdown of cost for skin, stiffeners, intercostals, and bonding costs for stiffeners and intercostals to skin.

The cost of materials was estimated following the procedure identified in viewgraph 25 and 26, cost estimate, and material cost estimate. An estimate of total square feet of "B" stage material was made and then reduced to pounds of carbon fiber. This weight was multiplied by 4 times the cost of fiber per pound to estimate total "B" stage material cost.

The labor cost for the 60-ply skin was 2 man hours estimate per ply, 8-ft. by 20-ft. x 60 plies. In addition, densification was estimated as vacuum for 1 hour, each 10 layers. The skin was estimated to be cured in a separate cure cycle. All 12 stiffeners and 130 intercostals were laid up, densified every 10 plies, and cured in separate cure cycles. The stiffeners and intercostals were trimmed to specification and secondary bonded to the skin.

Note that the cost estimate of \$166,053 is the highest cost of all processes estimated and is over 5 times the cost estimate for equivalent aluminum structure. It should also be noted that most current composite production is by this method. We believe that great savings in composite fabrication cost is right around the corner.

The fiber/resin system used for this estimate was a 35m modulus fiber (Hercules AS-4 3k and a general purpose brittle resin, Hercules 3501-6 in "B" stage uniwoven form.

A toughened resin system such as Hercules 8551-2 resin, to achieve some damage tolerance would add about 50% to the material cost but no change in the labor cost.

MATERIAL AND LABOR COST ESTIMATE

"B" STAGE LAYUP 8' x 20' DRY FIBER PREFORM

	MATERIAL	LABOR	TOTAL
60-PLY 8' x 20' SKIN	28,493	7,200	35,693
12 STIFFENERS	14,246	25,200	39,446
130 INTERCOSTALS	2,714	45,500	48,214
	\$45,453	\$77,900	\$123,353

**+ ROM ESTIMATE: BAG AND CURE PARTS
 TRIM PARTS
 SECONDARY BOND PARTS**

TO COMPLETE SKIN: 854 HOURS x \$50/HR = \$42,700

TOTAL STIFFENED SKIN = \$166,053

Dry Fiber Uniwoven/RIP 8-ft. by 20-ft. Panel

This is a summary of material and labor costs for an 8-ft. by 20-ft. 12 stiffener, 130 intercostal stiffened panel made by the dry fiber uniwoven/stitched preform Resin Infusion Process (RIP). It includes an individual breakdown of cost for skin, stiffeners, intercostals, bagging, and curing the complete assembly.

The uniwoven fabric material cost was estimated by first determining the number of square feet of material required, reduce this to pounds of fiber and then multiplying the pounds of fiber by 2x the fiber cost. This equaled the total cost of 9-ply material. The stitching cost was estimated for skin and stiffeners using a 100-needle machine, operating at 112 penetrations per minute plus a 50 percent efficiency factor. The intercostals and the stitching of stiffener and intercostal flanges to the skin were estimated using an automated single needle machine operating at 32 penetrations per minute plus a 50 percent efficiency factor. Total hours were multiplied by \$50/hour to get the cost.

The dry preform has integral stitched skin, stiffeners, and intercostals that are all processed in one RIP cycle.

Note that the cost estimate of \$66,722 is only 42 percent of the standard "B" stage uniwoven hand layup autoclave cure process, but still more than 2 times the cost of equivalent aluminum structure.

MATERIAL AND LABOR COST ESTIMATE

DRY FIBER UNIWOVEN - 100" WIDE
8' x 20' DRY FIBER PREFORM

	MATERIAL	LABOR	TOTAL
LIGHT DENSITY STITCH 10-PLY MATERIAL		8,400	8,400
60 PLY 8' x 20' SKIN	24,093	1,950	26,043
12 STIFFENERS	12,046	975	13,021
130 INTERCOSTALS	2,008	1,450	3,458
STITCH 12 STIFFENERS TO SKIN		9,400	9,400
STITCH 130 INTERCOSTALS TO SKIN		1,800	1,800
RESIN COST	2,200		2,200
TOTAL:	\$40,347	\$23,975	\$64,322

+ ROM ESTIMATE: WEIGH RESIN - LOCATE
BAG AND CURE PANEL
TRIM TO SIZE

TO COMPLETE SKIN: 48 HOURS x \$50/HR = \$2,400.00

TOTAL STIFFENED SKIN = \$66,722

Dry Fiber Warp/Knit/RIP 8-ft. by 20-ft. Panel

This is a summary of material and labor costs for an 8-ft. by 20-ft. 12 stiffener, 130 intercostal stiffened panel made by the dry fiber warp/knit/stitched preform Resin Infusion Process (RIP). It includes an individual breakdown of cost for skin, stiffeners, intercostals, bagging, and curing the complete assembly by RIP. The dry fiber preform has integral stitched skin, stiffeners, and intercostals that are all processed in one RIP cycle. The warp/knit fabric material cost was estimated as 2x the total fiber cost. This is the same method of material cost estimate as uniwoven fabric. The big difference in lower cost for warp/knit is that 12k tow is used in warp/knit and 3k tow is used in uniwoven fabric.

The stitching costs were estimated, using the 100-needle machine operation at 112 penetrations/minute plus a 50 percent efficiency factor for skins and stiffeners. The intercostals and the stitching of intercostals and stiffener flanges to skin were estimated using a 2-needle automated stitching machine at 32 penetrations per minute plus a 50 percent efficiency factor.

Note that the cost estimate of \$30,915 is only 18 percent of the standard "B" stage uniwoven hand layup autoclave cure process, and in addition, is only 95 percent of the estimated cost of a similar aluminum structure.

MATERIAL AND LABOR COST ESTIMATE

DRY FIBER WARP/KNIT - 100" WIDE 12k
8' x 20' DRY FIBER PREFORM

ASSUME: 12k tow = \$18/lb
Warp/knit 10-ply fabric - 100" wide
50 percent stitching efficiency - no set up time
100 multi-needle machine - operational
Two needle computer controlled machine - operational

	MATERIAL	LABOR	TOTAL
60 PLY 8' x 20' SKIN	11,415	950	12,365
12 STIFFENERS	5,708	475	6,183
130 INTERCOSTALS	1,087	1,050	2,137
STITCH 12 STIFFENERS TO SKIN		4,200	4,200
STITCH 130 INTERCOSTALS TO SKIN		1,430	1,430
RESIN COST	2,200		2,200
IMPREGNATE/CURE/TRIM		2,400	2,400
TOTAL:	20,410	10,505	30,915

TOTAL STIFFENED SKIN = \$30,915

Automated Tape Layup - Standard 8-ft. by 20-ft. Panel

This is a summary of material and labor cost for an 8-ft. by 20-ft. 12 stiffener, 130 intercostal stiffened panel made by the standard automated "B" stage tape layup/autoclave cure procedure. Six inch wide tape is laid up at a rate of 10 ft. per minute. It includes an individual breakdown of cost for skin, stiffeners, intercostals, bagging, and curing the complete assembly in the autoclave. This process assumes no stitching. The skin is automated tape layup. The stiffeners and intercostals have automated tape layup 4-ply material that is then hand laid up and densified on the mandrels. All individual "B" stage layups are then assembled on the "B" stage tape layup skin and cured together in one autoclave cure cycle.

Note that the cost estimate of \$46,242 is only 35 percent of the standard "B" stage uniwoven hand layup autoclave cure process but is still 43 percent higher than the cost of equivalent aluminum structure.

MATERIAL AND LABOR COST ESTIMATE

AUTOMATED TAPE LAYUP - STANDARD

12 STIFFENER 8' x 20' PANEL

ASSUME: 12k tow = \$18/lb - "B" Stage x 2 = \$36/lb
Tape width = 6 in.
10 ft. per minute layup speed, 10-second turn time
Apply 50 percent efficiency
Co-cure skin/stiffeners/intercostals

	MATERIAL	LABOR	TOTAL
60 PLY 8' x 20' SKIN	19,051	3,500	22,551
12 60-PLY STIFFENERS	9,525	5,350	14,875
130 20-PLY INTERCOSTALS	1,116	4,650	5,716
ASSEMBLE ON TOOL		1,500	1,500
BAG, CURE, TRIM		1,600	1,600
TOTAL:	\$29,692	\$16,600	\$46,242

TOTAL STIFFENED SKIN = \$46,242

Automated Tape Layup - Advanced 8-ft. by 12-ft. Panel

This is a summary of material and labor cost for an 8-ft. by 20-ft. 12 stiffener, 130 intercostal stiffened panel made by the advanced automated "B" stage tape layup/autoclave cure process. Six inch wide tape is laid up at a rate of 30 ft. per minute. It includes an individual breakdown of cost for skin, stiffeners, intercostals, bagging, and curing the complete assembly in the autoclave. This process assumes no stitching. The skin is automated tape layup. The stiffeners and intercostals have automated tape layup 4-ply material that is then hand laid up and densified on the mandrels. All individual "B" stage layups are then assembled and cured together in one autoclave cure cycle.

Note that the cost estimate of \$42,748 is only 26 percent of the standard "B" stage uniwoven hand layup autoclave cure process but it is still 32 percent higher than the cost of equivalent aluminum structure.

MATERIAL AND LABOR COST ESTIMATE

AUTOMATED TAPE LAYUP - ADVANCED 12 STIFFENER 8' x 20' PANEL
--

ASSUME: 12k tow = \$18/lb - "B" Stage x 2 = \$36/lb
 Tape width = 6 in.
 30 ft. per minute layup speed, 3-second turn time
 Apply 50 percent efficiency
 Co-cure skin/stiffeners/intercostals

	MATERIAL	LABOR	TOTAL
60 PLY 8' x 20' SKIN	19,051	1,383	20,434
12 60-PLY STIFFENERS	9,525	4,123	13,648
130 20-PLY INTERCOSTALS	1,116	4,450	5,566
ASSEMBLE ON TOOL		1,500	1,500
BAG, CURE, TRIM		1,600	1,600
TOTAL:	\$29,692	\$13,056	\$42,748

TOTAL STIFFENED SKIN = \$42,748
--

Automated "B" Stage Tow Placement 8-ft. by 20-ft. Panel

This is a summary of material and labor cost for an 8-ft. by 20-ft. 12 stiffener, 130 intercostal stiffened panel made by the automated "B" stage tow placement autoclave cure process. It assumes a band of tow 6 in. wide and tow lay down at 30 ft. per minute. It includes an individual breakdown of cost for skin, stiffeners, intercostals, bagging, and curing the complete assembly in the autoclave. This process assumes no stitching. The skin is made by automated tow placement, the stiffeners and intercostals made from 4-ply tow placement "sheets" that are then hand laid up and densified on individual mold mandrels. All individual details of skin, stiffeners, intercostals, and tooling mandrels are assembled and cured together in one autoclave curing process.

Note that the cost estimate of \$42,795 is only 25 percent of the standard "B" stage uniwoven hand layup autoclave cure process but it is still 29 percent higher than the cost of equivalent aluminum structure.

MATERIAL AND LABOR COST ESTIMATE

TOW PLACEMENT
12 STIFFENER 8' x 20' PANEL

ASSUME: 12k tow = \$18/lb - "B" Stage x 2 = \$36/lb
Note: Use of multiple spools of tow to equal 6-in. band makes tow cost and 6-in. tape cost the same.
30 ft. per minute layup speed, 3 second turn time
Apply 50 percent efficiency
Co-cure skin/stiffeners/intercostals

	MATERIAL	LABOR	TOTAL
60 PLY 8' x 20' SKIN	19,051	1,383	20,434
12 60-PLY STIFFENERS	9,525	4,170	13,695
130 20-PLY INTERCOSTALS	1,116	4,450	5,566
ASSEMBLE ON TOOL		1,500	1,500
BAG, CURE, TRIM		1,600	1,600
TOTAL:	\$29,692	\$13,103	\$42,795

TOTAL STIFFENED SKIN = \$42,795
--

Aluminum Riveted Stiffener 8-ft. by 20-ft. Panel

This is a summary of material and labor cost for an 8-ft. by 20-ft. 12 stiffener, 130 intercostal all aluminum riveted stiffened panel. It includes an individual breakdown of cost for skin, stiffeners, intercostals, drilling and riveting of stiffeners and intercostals to the skin.

This estimate was prepared by a professional metal component production estimator and was sized to be equal structural performance to the composite panels.

The skin cost was extrapolated from real production cost of similar size/thickness metal structure. The machined-to-thickness skin was estimated as a purchase part that includes material and outside machining labor cost (all reported as material cost).

The stiffeners were priced as extruded aluminum details, extrapolated from existing production records plus final machine to size and flange taper labor.

The intercostals estimate was extrapolated from similar "purchased part records and included both material and outside source labor all as material cost.

The drilling and riveting of stiffeners and intercostals to skin assumes automated drivematic production rates for 90 percent of the rivets. The remaining 10 percent are estimated for hand drill and set of rivets.

Note that these are all production quantity estimates for the aluminum stiffened panel and there is *not* a 50 percent efficiency factor placed on any of the fabrication operations.

Note also that the cost estimate of \$32,392 is only 20 percent of the standard "B" stage uniwoven hand layup autoclave cure process.

Equal performance aluminum structure cost is the target cost for our innovative composite materials, design, fabrication program at DAC.

MATERIAL AND LABOR COST ESTIMATE

ALUMINUM 12 STIFFENER 8' x 20' PANEL

	MATERIAL	LABOR	TOTAL
8' x 20 SKIN	4,156		4,156
12 STIFFENERS	3,870	8,966	12,836
130 INTERCOSTALS	13,000		13,000
ASSEMBLY		2,400	2,400
TOTAL:	\$21,056	\$11,366	\$32,392

**ASSUMES: SKIN - PURCHASED
STIFFENERS - MATERIAL AND MACHINING
INTERCOSTALS - PURCHASED
ASSEMBLY - 90% AUTOMATED DRILL/RIVET (DRIVEMATIC)**

Estimated Cost Summary - Material + Labor

8-ft. by 20-ft. Stiffened Panel

The viewgraph presents a materials and labor cost summary for fabrication of an aluminum 8-ft. by 20-ft. stiffened panel with six different methods of fabrication of similar composite structure.

These estimated cost numbers do not reflect the total panel cost - only materials and fabrication labor cost are included. There is no consideration for design, analysis, tooling, equipment, individual process set up time, quality control, or finishing costs included in this estimate.

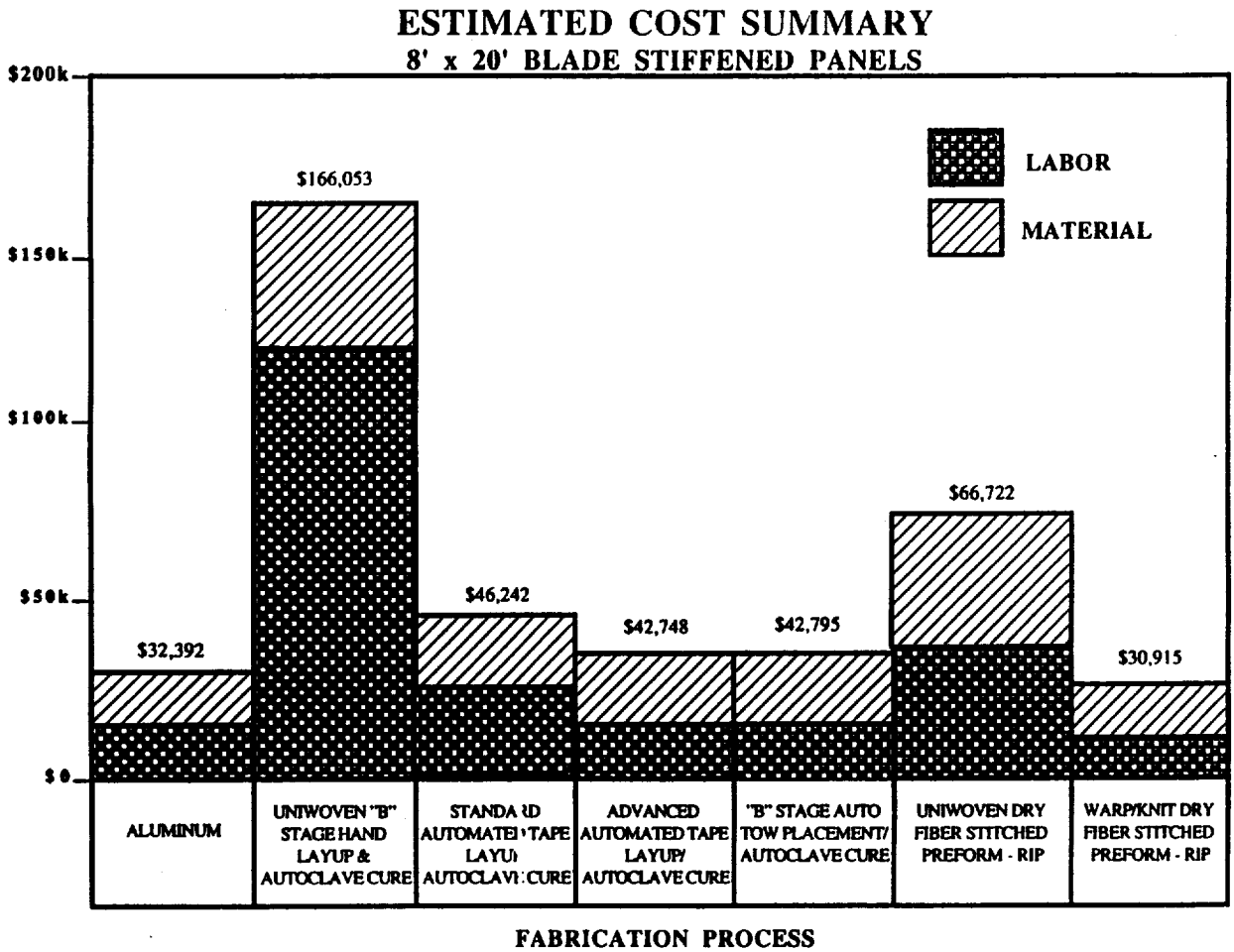
Note that the aluminum structure is estimated from large-scale production records. The composite cost estimates are conservative as shown by the use of automated equipment - 50 percent efficiency factors added to the processing time.

Note that the warp/knit/stitched dry fiber preform/RIP concept is the only composite materials and process method that was cost competitive with the aluminum structure.

8' x 20' BLADE STIFFENED PANELS

FABRICATION METHOD	MATERIAL	LABOR	TOTAL	% OF ALUMINUM
ALUMINUM	21,056	11,366	\$32,392	100%
UNIWOVEN "B" STAGE HAND LAYUP & AUTOCLAVE CURE	45,453	120,600	\$166,053	512%
STANDARD AUTOMATED TAPE LAYUP/AUTOCLAVE CURE - 12k TOW	29,692	16,550	\$46,242	143%
ADVANCED AUTOMATED TAPE LAYUP/AUTOCLAVE CURE - 12k TOW	29,692	13,056	\$42,748	132%
"B" STAGE AUTOMATED TOW PLACEMENT/AUTOCLAVE CURE - 12k TOW	29,692	13,103	\$42,795	132%
UNIWOVEN DRY FIBER STITCHED PREFORM RIP IMPREGNATION AND CURE - 3k TOW	40,347	26,375	\$66,722	205%
WARP/KNIT DRY FIBER STITCHED PREFORM RIP IMPREGNATION AND CURE - 12k TOW	20,410	10,505	\$30,915	95%

This viewgraph is a bar chart showing all of the data presented in the previous viewgraph.



This review covered the following topics:

- There was a detailed discussion of the benefits that composites can bring to the aircraft
- Current applications of composites were identified for the McDonnell Douglas series of aircraft
- Critical issues of marginal composite damage tolerance and high cost were identified
- A DAC fabrication process for composite structure with affordable cost potential was described
- A series of cost estimates for different automated composite processing methods to fabricate an 8-ft. by 20-ft. stiffened panel were presented and compared to similar aluminum structure
- We feel we can meet the target of 100 percent improvement in composite damage tolerant structure
- We feel we can meet the challenge of composite structure cost near to similar metal structure cost

SUMMARY

DISCUSSED BENEFITS OF COMPOSITES - INCLUDES OTHER THAN WEIGHT SAVINGS

- **DISCUSSED AIRCRAFT APPLICATIONS - PRESENT AND FUTURE**
- **IDENTIFIED CRITICAL ISSUES - COST, DAMAGE TOLERANCE**
- **PRESENTED DAC LOW COST FABRICATION APPROACH**
- **PRESENTED COMPARATIVE COST ESTIMATES**

WE CAN MEET THE CHALLENGE OF EQUAL TO METAL COST.

WE CAN MEET THE CHALLENGE FOR 100% IMPROVED DAMAGE TOLERANCE.



1994012392

-20-05

AEROELASTIC AIRFOIL SMART SPAR

Skott Greenhalgh and Christopher Pastore
Department of Textile Engineering, Chemistry & Science
North Carolina State University, Raleigh, NC 27695

1994012392
N 94-16865
P-9

Moishe Garfinkle
Department of Materials Engineering
Drexel University, Philadelphia, PA 19104

SUMMARY

Aircraft wings and rotor-blades are subject to undesirable bending and twisting excursions that arise from unsteady aerodynamic forces during high speed flight, abrupt maneuvers or hard landings. These bending excursions can range in amplitude from wing-tip flutter to failure. A continuous-filament construction "smart" laminated composite box-beam spar is described which corrects itself when subject to undesirable bending excursions or flutter. The load-bearing spar is constructed so that any tendency for the wing or rotor-blade to bend from its normal position is met by opposite twisting of the spar to restore the wing to its normal position. Experimental and theoretical characterization of these spars was made to evaluate the torsion-flexure coupling associated with symmetric lay-ups. The materials used in this study were uniweave AS-4 graphite and a matrix comprised of Shell 8132 resin and U-40 hardener. Experimental tests were conducted on five spars to determine spar twist and bend as a function of load for 0°, 17°, 30°, 45° and 60° fiber angle lay-ups. Symmetric fiber layups do exhibit torsion-flexure couplings. Predictions of the twist and bend versus load were made for different fiber orientations in laminated spars using a spline function structural analysis. The analytical results were compared with experimental results for validation. Excellent correlation between experimental and analytical values was found.

INTRODUCTION

Cantilevered airfoils with high aspect ratios such as wings or rotor blades are generally soft in flexure. The presence of unsteady aerodynamic forces and a lack of flexural stiffness can lead to airfoil oscillations in bending and twist. The magnitudes of such instabilities depend both on aeroelastic and aerodynamic factors, and can range from the imperceptible to the destructive.

Rotor blades of helicopters in forward flight are subject to periodic aerodynamic forces that are required for lift, thrust and control. However these periodic forces can induce fluctuating bending loads and twisting moments on the blades not associated with flight requirements. If the resultant bending excursions through an angle Δ are aerodynamically imposed so that a twisting moment through an angle α results which tends to increase the magnitude of the excursion then the effect is divergence ($d\alpha/d\Delta > 0$) with respect to such oscillations. It follows therefore that an upwards bending accompanied by a decreasing pitch angle should lead to convergence ($d\alpha/d\Delta < 0$) and static stability, and could improve dynamic stability, depending on the frequency and amplitude of the oscillations.

A common form of such instabilities is flutter which primarily manifests itself as rotor tip oscillations. In terms of aeroelastic factors, the amplitude of such bending excursions is inversely proportional to airfoil stiffness in torsion and flexure. Considering aerodynamic factors, the amplitude is dependent on airfoil section, thickness ratio and pitch angle. Moreover, the amplitude increases with increasing helicopter flight speed, becoming pronounced as advancing and retreating blades approach the limiting extent of their normal lift behavior at the onset of compressibility and stall effects, respectively.

With conventional blade construction bending and twisting excursions are uncoupled ($da/d\Delta=0$). Accordingly no aerodynamic constraints are present to damp the extent of any bending excursion, although rotor blades are subject to unsteady aerodynamic loading.

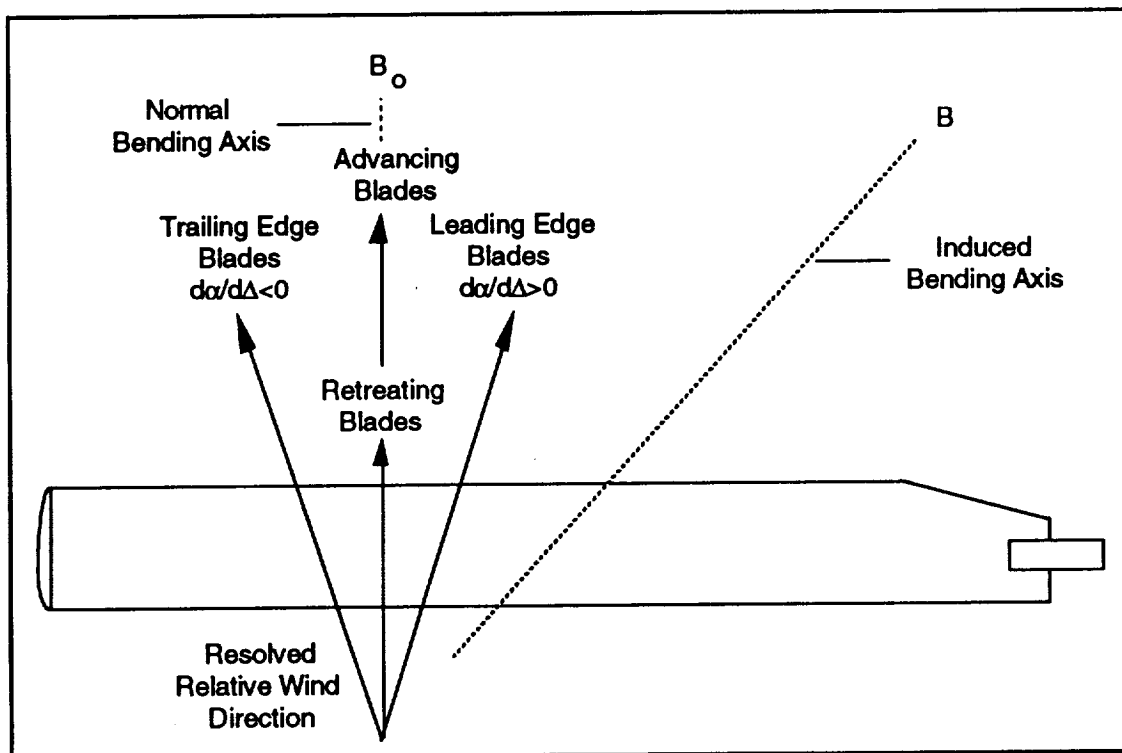


Figure 1. Rotor Blade Resolved Wind

The varying loads to which rotor blades are subject arise from unsteady air forces which have an in-plane component and a normal component relative to the rotor disc. In forward flight the rotor disc can be divided roughly into four azimuth sectors: a trailing blade sector, an advancing blade sector, a leading blade sector, and a retreating blade sector.

In all of these sectors the blades are subject to both the relative wind arising from forward flight and that from blade rotation. When resolved, the relative in-plane wind to which the blades are subject intersects the blade at various angles. In the trailing blade sector the blade is swept backward relative to the wind, and in the leading blade sector it is swept forward. The former condition is stabilizing in regard to flutter (effective $da/d\Delta < 0$) as in the case of swept-back wings, and the latter condition is destabilizing in regard to flutter (effective $da/d\Delta > 0$) as in the case of swept-forward wings [1,2].

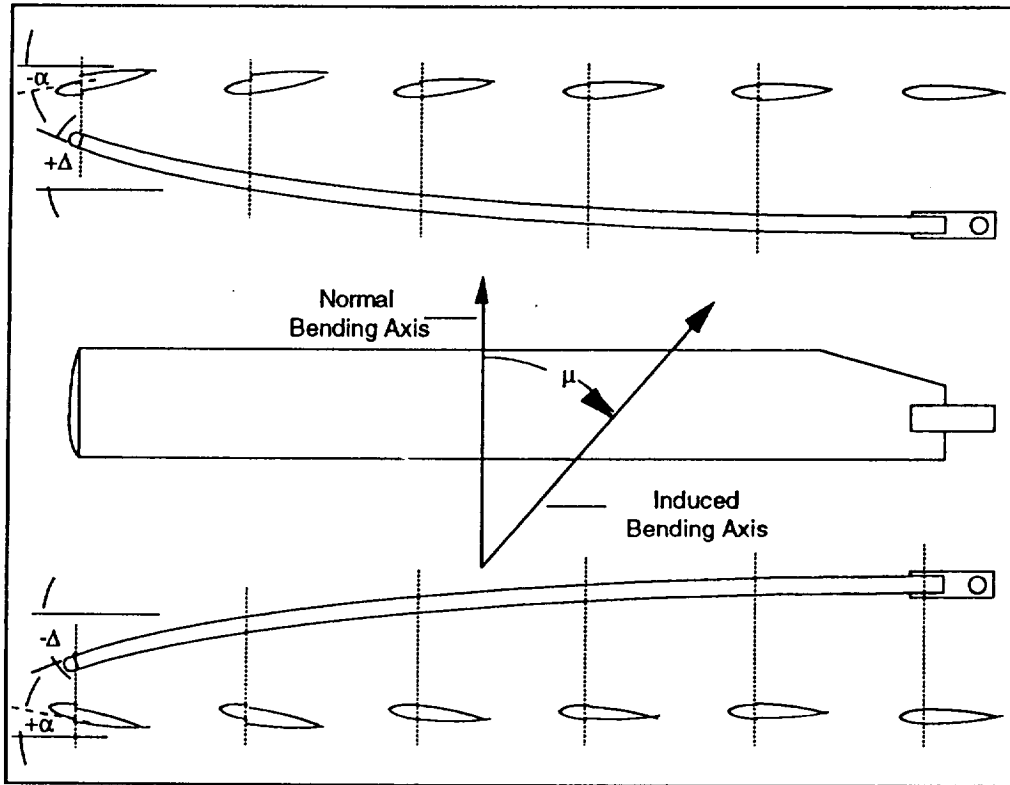


Figure 2a. Effect of Beneficial bend-twist coupling

In the advancing sector the resolved wind is essentially the sum of the rotational wind and the flight wind while in the retreating sector the resolved wind is essentially the difference between the rotational wind and the flight wind. Hence the resolved wind changes both in velocity and direction relative to the normal bending axis of the blades as the blades pass through the azimuth sectors, as shown in Figure 1. With conventional blade construction the normal bending axis B is normal to blade span so that effectively $da/d\Delta=0$, resulting in no beneficial coupling.

Further complicating the aerodynamic loading, because the blades are twisted, the outboard section of the advancing blade can be subject to an updraft while the in-board section is subject to the downwash. Moreover, compressibility in the advancing blade and stall in the retreating blade can directly lead to blade flutter.

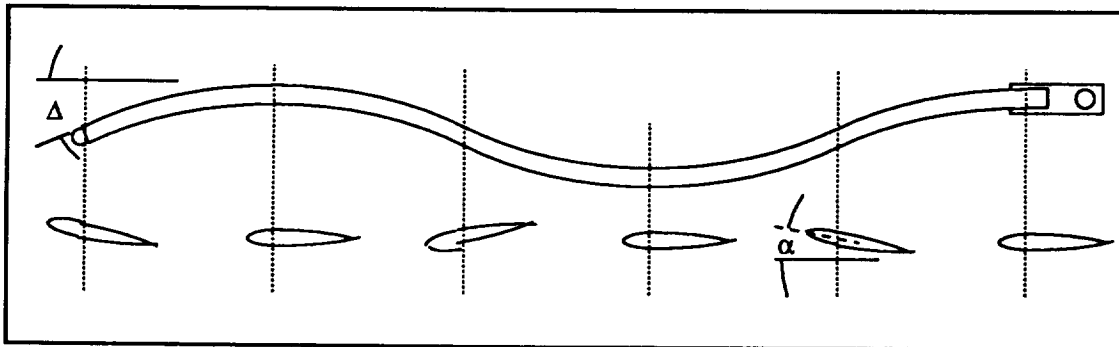


Figure 2b. Effect of Beneficial bend-twist coupling

Furthermore, rotor blades can also be subject to significant bending loads and twisting moments which do not depend on sector. Gust loading can subject rotor blades to high loads at high flight speeds which can result in significant bending excursions. Ice accumulation can so distort the airfoil section that flutter can be induced. Abrupt maneuvers can cause a rotor blade root to contact its flapping stops, as can hard landings. Resulting blade bending can bring a blade in contact with portions of the fuselage.

Essentially, the highly unsteady aerodynamic forces to which rotor blades are subject arise from these diverse sources and lead to blade flutter and even possibly dangerous blade bending excursions. Because in normal blade construction $da/d\Delta=0$, little damping is available.

It is evident that the amelioration of the effects of these fluctuating aerodynamic forces on blade bending and twisting beyond those required for lift, thrust and control would improve helicopter safety and reliability. One means is to employ aeroelastic constraint wherein the blades are made sufficiently stiff to largely resist such bending and twisting or to significantly increase blade flapping-hinge offset. However this brute strength approach results in excessive blade weight and might raise rotor hub stress levels beyond safe limits.

An alternative means is to employ aerodynamic constraint wherein convergent torsional-flexural coupling would diminish the amplitude of fluctuating blade bending and twisting, particularly at high flight speeds, and might result in a noticeable reduction in fuselage vibration.

Accordingly, if an airfoil could be so constructed that a bending excursion through section angle $d\Delta$ structurally induces a twisting moment through section angle $d\alpha$ then the airfoil exhibits torsional-flexural coupling: $d\alpha/d\Delta \neq 0$. Furthermore, if $d\alpha/d\Delta < 0$ a rotor blade would exhibit convergent behavior with upwards bending ($+d\Delta$) accompanied by decreasing pitch angle ($-d\alpha$) and vice versa, which denotes beneficial torsional-flexural coupling. Such beneficial coupling could be induced in a rotor blade if the normal bending axis were skewed through an angle μ . Such an induced bending axis is also shown in Figure 1.

Considerable work has been done on developing spars which impose a beneficial coupling on rotor blades, thereby improving the performance of helicopter rotors under extreme flight conditions, particularly abrupt maneuvers [3,4,5,6].

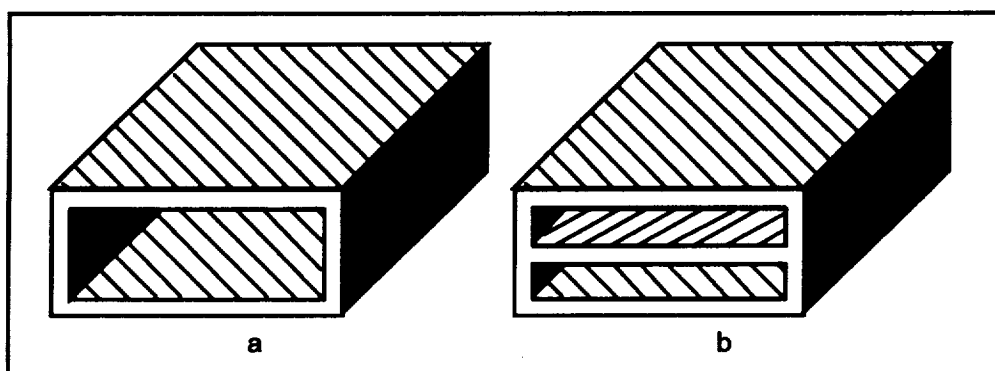


Figure 3. Alternative symmetric laminate construction

The effect of torsion-flexure convergence on a blade subject to first order bending is shown in Figure 2a for any azimuth sector. Hence a bending excursion always results in twisting so as to oppose the bending: $d\phi/d\Delta < 0$. The possible effect of beneficial torsion-flexure coupling on higher orders of bending is shown in Figure 2b.

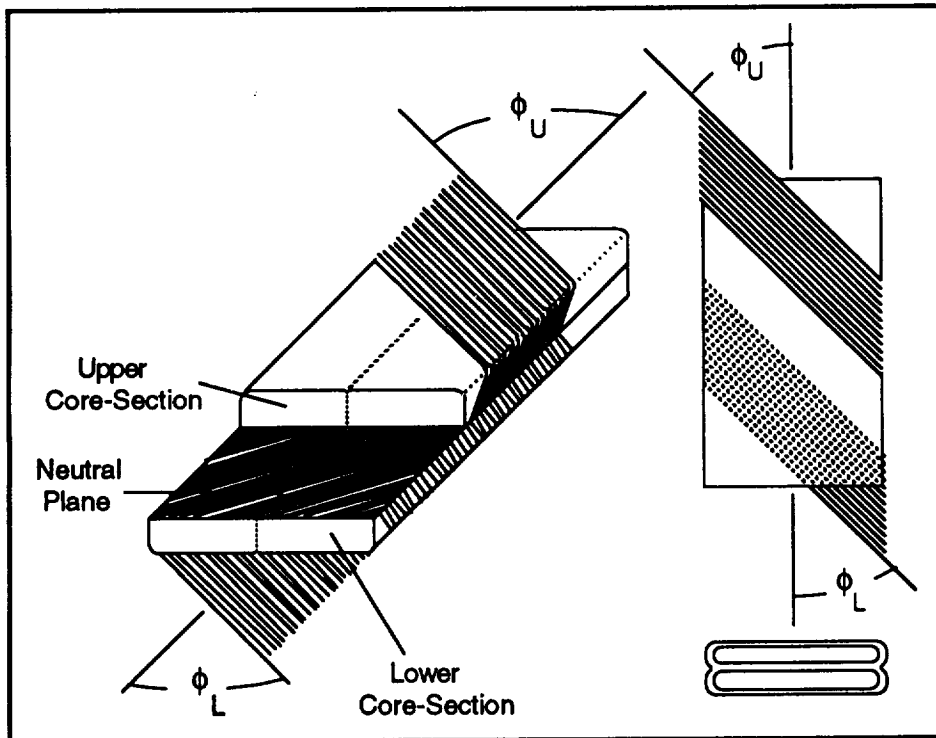


Figure 4. Sected-core spar

EXPERIMENTAL RESULTS

To construct a rotor blade whose actual bending axis is skewed from its normal bending axis requires a spar construction in which the flexural modulus of the spar can be controlled in different directions relative to the longitudinal axis of the spar, characterized as aeroelastic tailoring [7].

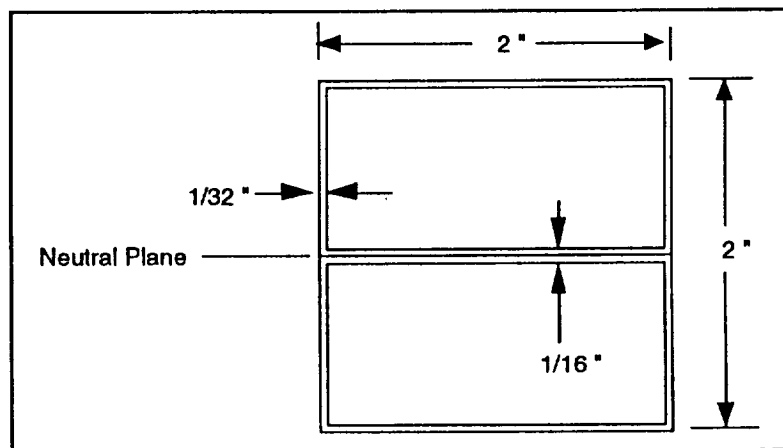


Figure 5. Box-beam cross-section

This behavior can be induced in the spar through an unbalanced symmetric sandwich laminate, such as [q/core/q] as shown in Figure 3a. However, this lay-up sequence cannot be achieved through continuous filament winding processes [8,9].

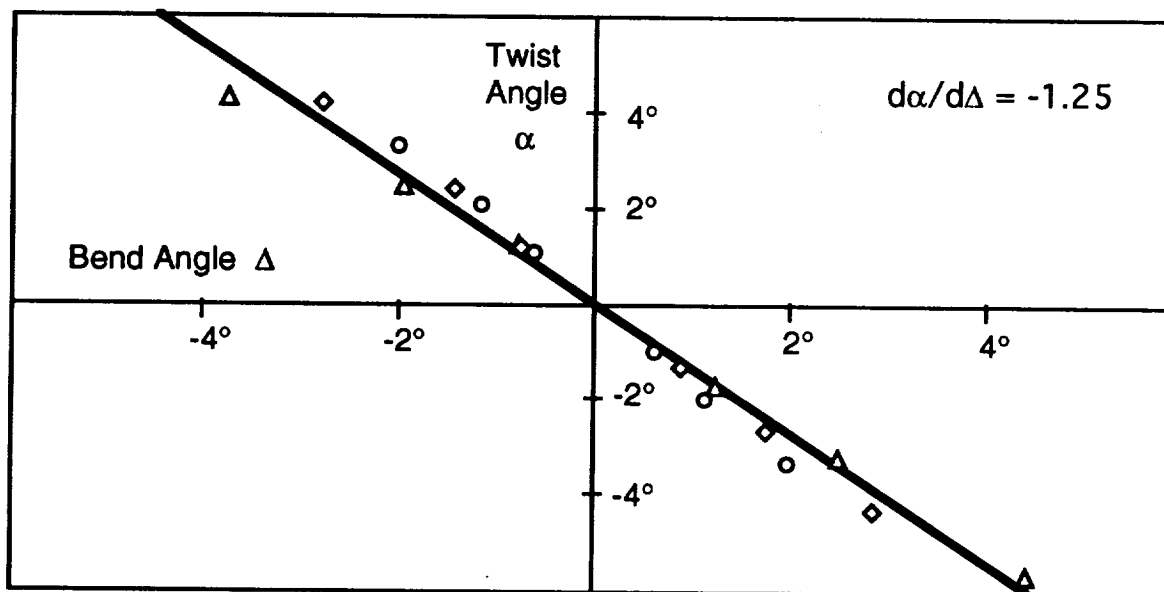


Figure 6. Coupling behavior of a $\phi=45^\circ$ sectored-core symmetrical wound spar

This shortcoming is circumvented by forming the spar of two box-beams joined at the center as shown in Figure 3b. The individual box elements are wound in opposite directions and joined as shown in Figure 4. The resulting sectored-core lamination sequence formed by this process is [q/core/-q/core/q]_s. The central -q ply sequence does not detract significantly from the bending-torsion coupling [10].

A series of prototype spars were fabricated with this construction to demonstrate the behavior. The spars were fabricated using continuous uniweave carbon (<1% 90° glass) and Shell 828 Resin with V-40 curing agent. A single ply was wound about each 36 inch long core at ϕ angles of 0, 17, 30, 45, 60° and then joined to form a box-beam as shown in Figure 5.

The uni-weave material is primarily unidirectional carbon fiber with a small (<2%) amount of glass running in the 90° direction to maintain fabric stability. Winding the fabric onto the cores was a relatively simple matter.

As is evident from the twisting-bending behavior exhibited by the prototype smart spar as illustrated in Figure 6, beneficial torsional-flexural coupling can be realized using sectored-core symmetrical sequence construction and conventional continuous-filament fabrication techniques. The torsion-flexure coupling associated with spars formed from a $\phi=45^\circ$ winding is illustrated.

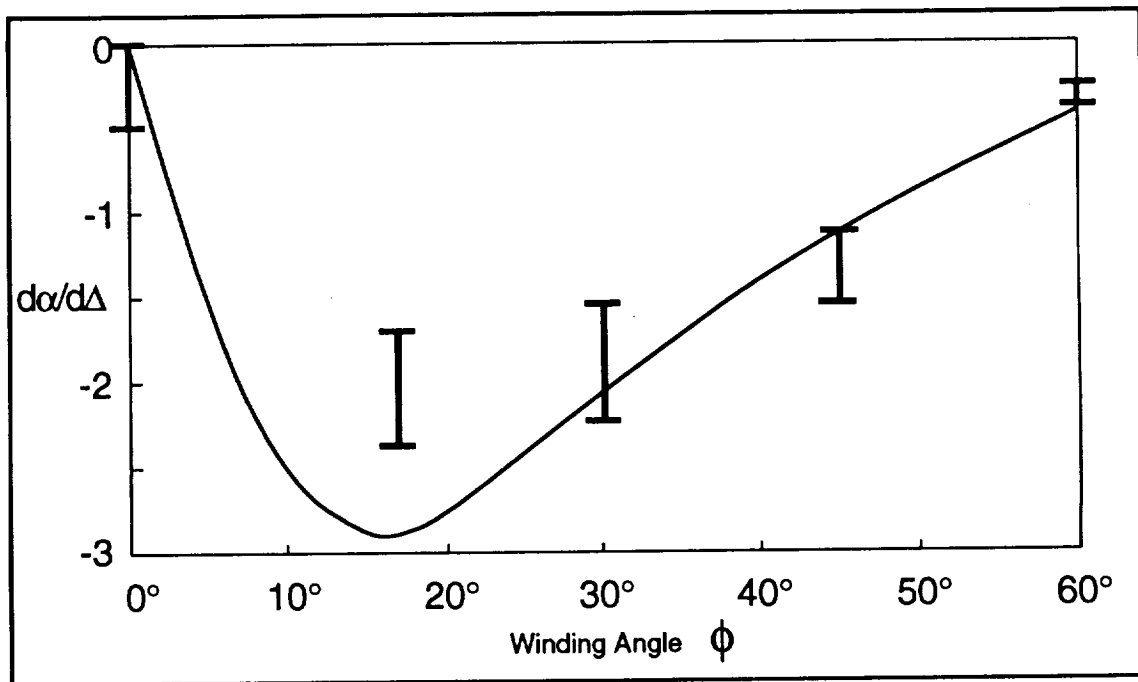


Figure 7. Coupling behavior of the sectored-core wound spars examined

A spline-function aided structural analysis has been developed expressly for the study of composite materials by accounting for the physical material inhomogeneities between plies. Initial efforts of applying this model to prototype spars with ply orientations ranging from 0° to 60° shows promising results, as illustrated in Figure 7.

The solid line in Figure 7 indicates the predicted results. Although the $\phi \approx 45^\circ$ winding showed the greatest twist per unit of bending load, the peak coupling $d\alpha/d\Delta \approx 2$ occurs at $\phi \approx 17^\circ$ for the configuration shown in Figure 5.

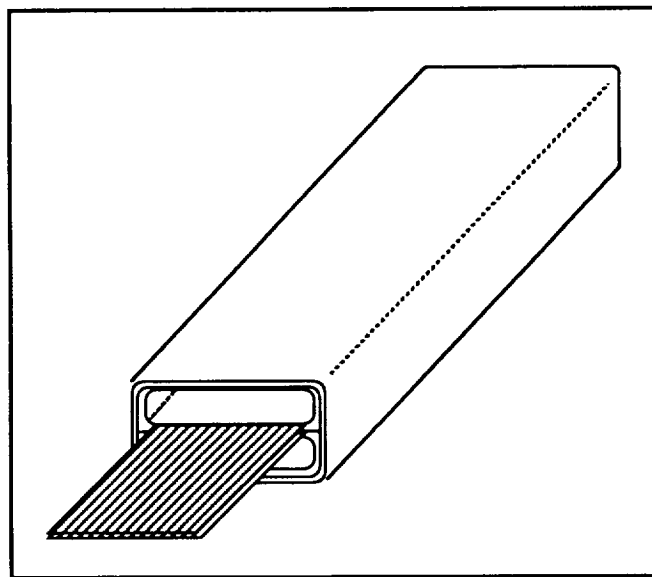


Figure 8. Placement of longitudinal yarns

In actual service rotor blade spars are subject to high centrifugal loading, a condition that must be accounted for by longitudinal yarn layups. To account for this spanwise loading on the spars longitudinal yarns can be inserted adjacent to the neutral plane, as shown in Figure 8. With longitudinal yarns it is expected that the winding angle ϕ which corresponds to the maximal torsion-flexure coupling will be displaced to higher values.

CONCLUSION

A continuous-filament construction "smart" laminated composite box-beam spar for helicopter rotor blades is described which corrects itself when subject to undesirable bending excursions or flutter. Experimental and theoretical characterization of these spars was made to evaluate the torsion-flexure coupling associated with symmetric lay-ups.

Five laminated composite box spars were constructed from a uniweave graphite fiber and epoxy matrix. The spars were made with 0° , 17° , 30° , 45° , and 60° fiber orientation angles with respect to the longitudinal axis. The analytical modeling involved spline function displacement approximations to predict the deformation properties of laminated spars.

From the results of the analytical work, stresses and relevant deflections were found and compared to the test results conducted. Correlations were determined and plotted for each case tested. The greatest twist per unit bending load was found at $\phi=45^\circ$ and maximum tension-flexure coupling at $\phi=17^\circ$.

REFERENCES

1. Shirk, M. H., et. al. "On the Track of Practical Forward-Swept Wings." *J. Astronautics and Aeronautics*, January 1982.
2. Weisshaar, T. A. "Divergence of Forward Swept Composite Wings." *J. Aircraft*, Article No. 79-0722R, Vol. 17, No. 6, pp. 442-448, June 1980.
3. Smith, E. C. and I. Chopra "Formulation and Evaluation of an Analytical. Model for Composite Box-Beams." *AIAA/ASME/AHS/ASC, 28th Structures, Structural Dynamics and Materials Conference*, 1989.
4. Chandra, C., A. D. Stemple, and I. Chopra "Thin-Walled Composite Beams Under Bending, Torsional, and Extensional Loads." *J. Aircraft, AIAA, SDM Conference*, 1990.
5. Hong, Chang-Ho and I. Chopra "Aeroelastic Stability Analysis of a Composite Rotor Blade." *J. American Helicopter Society*, pp. 57-67, April 1985.
6. Smith, E. C. and I. Chopra "Formulation and Evaluation of an Analytical Model for Composite Box-Beams." *AIAA/ASME/AHS/ASC, 28th Structures, Structural Dynamics and Materials Conference*, 1989.
7. Shirk, M. H. and T. J. Hertz "Aeroelastic Tailoring-Theory, Practice, and Promise." *J. Aircraft*, Vol. 23, No. 1, pp. 6-17, 1984.

8. Atanasoff, H. and A. J. Vizzini "A Manufacturing Process for Open Mold Mechanically Coupled Composite Box Beams With Foam Tooling." AIAA/ASME/AHS/ASC, 28th Structures, Structural Dynamics and Materials Conference, pp. 798-808,1989.
9. Stemple, A. D. and S. W. Lee "Large Deflection Static and Dynamic Finite Element Analysis of Composite Beams With Arbitrary Cross-Sectional Warping." AIAA/ASME/AHS/ASC, 28th Structures, Structural Dynamics and Materials Conference, pp. 1788-1797,1989.
10. Greenhalgh, S. "Mechanical Characterization of Twisting-Bending Coupling of Composite Box-Beam Structures", Masters Thesis, North Carolina State University, Raleigh, 1992.



<p>Keith Burgess Techniweave, Inc. P.O. Box 6314 East Rochester, NH 03687</p> <p>(603) 335-2115 (603) 335-3200 Fax</p>	<p>Anant T. Mahale Textile Research Institute 601 Prospect Ave P.O. Box 625 Princeton, NJ 08542</p> <p>(609) 924-3150 Fax:(609) 683-7836</p>	<p>Janice Maiden Textile Technologies, Inc 2800 Turnpike Drive Hatboro, PA 19040</p> <p>(215) 443-5325 FAX: 675-4580</p>
<p>Hiroshi Tamaki Three-D Composites Research Corp. C-B3 TCI 2-1-6, Sengen Tukuba-shi, Ibari-ken 305 Japan</p> <p>0298-58-6170 0298-58-6218 (FAX)</p>	<p>Eric Lang University of Delaware 126 Spencer Lab 4DEL Newark, DE 19701</p>	<p>Tim Kostar University of Delaware 126 Spencer Lab 4DEL Newark, DE 19701</p>
<p>Tsu Wei Chou University of Delaware Department of Mechanical Engr. Newark, DE 19716</p> <p>(302) 831-2421 (FAX) 831-8525</p>	<p>Yuris A. Dzenis University of Texas at Arlington Department of Aerospace Engineering Box 19018 Arlington, TX 76019-0018</p> <p>dzenis@stress.uta.edu Fax: (817)794-5010</p>	<p>Brian J. Hill University of Ulster at Belfast Engineering Composite Rsch. Centre Belfast BT15 1ED Northern Ireland</p> <p>(0232) 328515 FAX: (0232) 321048</p>
<p>John Morton Virginia Polytechnic Institute ESM Dept., VPI & SU Blacksburg, VA 24061</p> <p>(703) 961-6051 FAX: (703) 951-8972</p>	<p>Alfred C. Loos Virginia Polytechnic Institute State University Blacksburg, Virginia 24061</p> <p>(703) 231-4713 (703) 951-8972</p>	<p>Timothy Norman West Virginia State University Department of Mechanical and Aerospace Engineering P.O. Box 6101 Morgantown, WV 26506-6101</p> <p>(304) 293-3111 (304) 293-6689 FAX</p>

**INTERNATIONAL
TECHNICAL TEXTILES**
2085 Harts Lane
Conshohocken, PA 19428 USA
Phone: (215) 825-0961
Fax: (215) 825-9262

<p>Sam Raz Phila. College of Textiles and Science School Hse. La. & Henry Ave. Phila., Penna. 19144</p> <p>(215) 951-2769 FAX: 951-2615</p>	<p>Daryl Chapman Pratt & Whitney P.O. Box 10600 W. Palm Beach, FL 33410</p> <p>(407) 796-5970</p>	<p>John Devlin Pressure Technology, Inc. 7526 Connelly Drive Hanover, MD 21076</p> <p>(301) 760-9856 FAX: (301) 760-9858</p>
<p>Michael Higgins Pressure Technology, Inc. 7526 Connelly Drive Hanover, MD 21076</p> <p>(301) 760-9856 FAX: (301) 760-9858</p>	<p>Mark D. Mello Quadrax Corporation 300 High Point Ave. Portsmouth, RI 02871</p> <p>(401)683-6600 Fax (401)683-6606</p>	<p>Warren La Pointe Quadrax Corporation 300 High Point Ave. Portsmouth, RI 02871</p> <p>(401)683-6600 Fax (401)683-6606</p>
<p>Tim Kniveton Rockwell International 2135 W. Maple Rd. M/S A-261 Troy, MI 48084</p> <p>(313) 435-5585 (313) 435-1366 FAX</p>	<p>Martyn G. Roberts Rolls-Royce, Inc. 2849 Pacesferry Rd. Atlanta, GA 30339</p> <p>(404) 996-8400 FAX (404) 996-5796</p>	<p>Patrick Spriet SEP Division Propulsion a Poudre et Composites Le Haillan B.P. 37 F 33165 St Medard en Jalles France</p> <p>56.55.30.11 Telex: SEP 560678F</p>
<p>Pierre Olry SEP Division Propulsion a Poudre et Composites Le Haillan B.P. 37 F 33165 St Medard en Jalles France</p> <p>fax 011-33-56-55-89-95</p>	<p>Tetsuro Hirokawa Shikibo, Ltd. Research and Development Dept. 1500-5 Shibahraminami Yokaichi, Shiga 547 Japan</p> <p>0748-25-1732 0748-25-1763 FAX</p>	<p>L.I. Fridman St. Petersburg Scientific Research Institute of Chemical Fibers and Composite Materials, Russia</p>
<p>P. Michailov St. Petersburg Scientific Research Institute of Chemical Fibers and Composite Materials, Russia</p>	<p>R.M. Levit St. Petersburg Scientific Research Institute of Chemical Fibers and Composite Materials, Russia</p>	<p>Juha Sarlin Technical Research Centre of Finland Textile Laboratory P.O. Box 635 SF-33101 Tampere, Finland</p> <p>358-3116-3540 358 31 163 498 FAX</p>

<p>Larry C. Dickinson Lockheed Engineering and Sciences Co. 144 Research Dr. M/S 188B Hampton, VA 23666</p> <p>(804) 864-3094 (FAX) 864-7893</p>	<p>Klaus Drechsler MBB Deutsche Aerospace P.O. Box 801109 D-8000 Munchen 80 Germany</p> <p>(089) 607-229 66 FAX: (089) 607-277 96 Telex: 5287-068 mbb d</p>	<p>Ray Palmer McDonnell Douglas Aircraft Dept. E-84, Mail Code 36-52 3855 Lakewood Blvd. Long Beach, CA 90846</p> <p>(310) 593-0439 (310) 982-0815 FAX</p>
<p>H. Benson Dexter NASA Langley Mail Stop 188B Hampton, VA 23681</p> <p>(804) 864-3094 (FAX) 864-7893</p>	<p>John Buckley NASA/Langley Research Center MS 387 Hampton, VA 23681</p> <p>(804) 864-4561</p>	<p>John Master NASA/Langley Research Center MS 387 Hampton, VA 23681</p> <p>(804) 864-1000 (804) 864-3460 FAX</p>
<p>J.W. Weber NorFab Corporation</p>	<p>H.N. Lilani NorFab/Amatex Corporation</p>	<p>Alex Bogdonavich North Carolina State Univ. College of Textiles Raleigh, NC 27695-8301</p> <p>(919) 515-2011 (919) 515-6532 FAX</p>
<p>Christopher Pastore North Carolina State Univ. College of Textiles Raleigh, NC 27695-8301</p> <p>(919) 515-2011 (919) 515-6532 FAX</p>	<p>Joseph M. Marchello Old Dominion University Kaufman Hall Hampton Blvd. Norfolk, VA 23529</p> <p>(804) 683-3759 (804) 683-5354 FAX</p>	<p>Maylene K. Hugh Mail Stop 226 NASA Langley Research Center Hampton, VA 23681</p>
<p>Ronald W. Biberstine On Site Consulting Service, Inc.</p> <p>(914) 896-4159</p>	<p>Timothy L. Collins Owens-Corning Industrial Materials Group 900 W. Valley Road, Suite 1101 Wayne, PA 19087</p> <p>(215) 688-8647 (215) 688-7918 FAX (800) 733-1551 Voice Mail ID# 901.5459</p>	<p>Frank Scardino Phila. College of Textiles and Science School Hse. La. & Henry Ave. Phila., Penna. 19144</p> <p>(215) 951-2769 FAX: 951-2615</p>

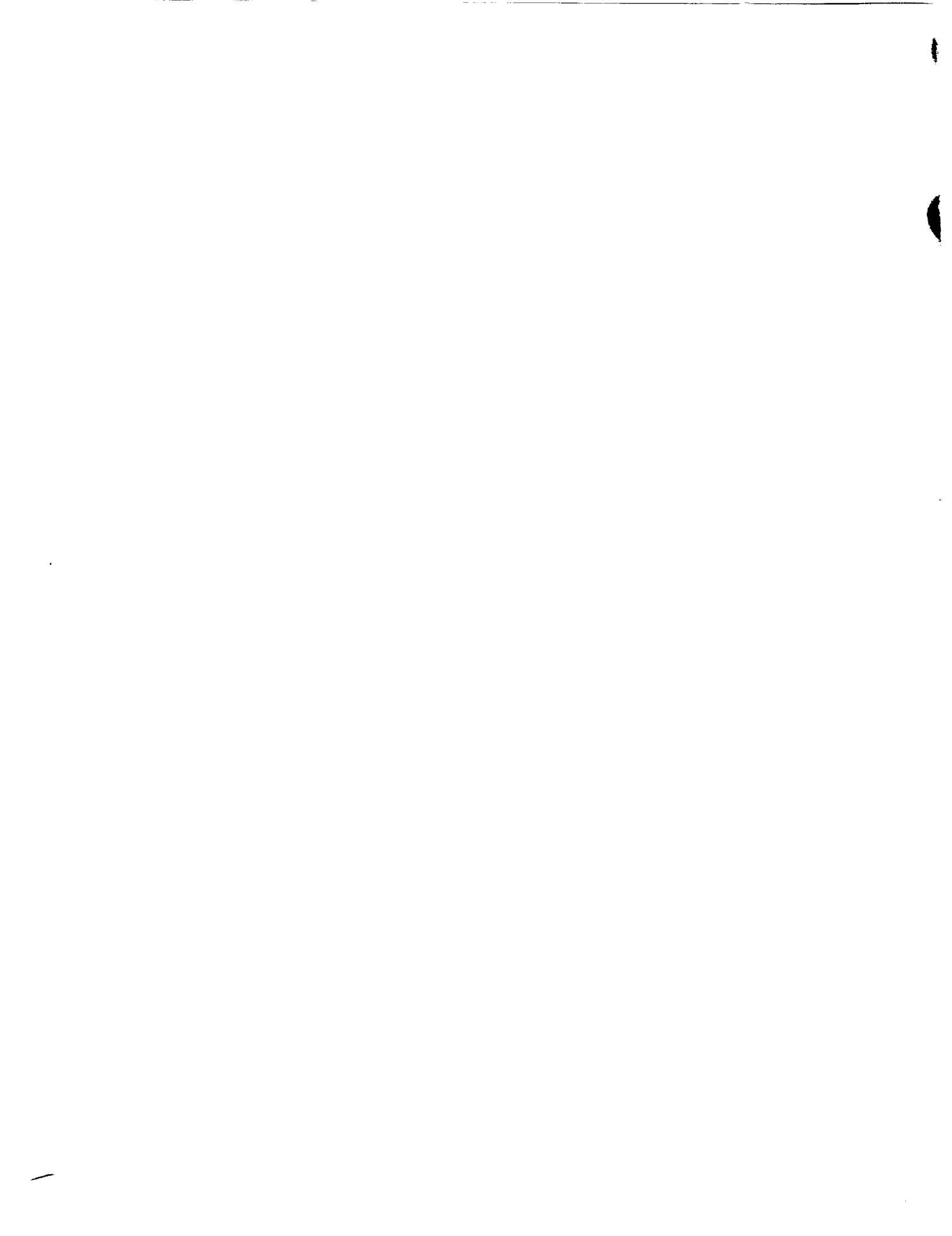
<p>Maggie D'Aversa Ethicon, Inc. Rt. 22 Somerville, NJ 08836-0151</p> <p>(908) 218-3059 (FAX) 218-3525</p>	<p>Vish Agarwal Ethicon, Inc. Rt. 22 Somerville, NJ 08836-0151</p> <p>(908) 218-3059 (FAX) 218-3525</p>	<p>Garrett C. Sharpless Fiber Innovations, Inc. 588 Pleasant St. Unit 3 Norwood, MA 02062</p> <p>(617) 769-2400 FAX (617) 769-7547</p>
<p>Carl Smith Fiberite 2055 E. Technology Circle Tempe, AZ 85284</p> <p>(602) 730-2380</p>	<p>Alberto Morales Fiberite 4300 Jackson St. Greenville, TX 75401</p> <p>(903) 455-6550 (903) 455-0315</p>	<p>Scot Arnold Ford Motor Company PO Box 2053, Rm S-2923 Dearborn, MI 48121</p> <p>(313) 390-3521</p>
<p>Dr. Virendra Kumar GE Corporate Research and Development Bldg. K1/3A26 P.O. Box 8 Schenectady, NY 12301</p> <p>(518) 387-5078</p>	<p>Brian K. Gracias General Electric Aircraft Engines M/D A375 1 Neumann Way Cincinnati, OH 45215</p> <p>(513) 774-6185</p>	<p>Mike Braley General Electric Aircraft Engines 1 Neumann Way 8500 Governor's Hill, 3rd Floor Cincinnati, OH 45215-6301</p> <p>(513) 774-4129 (513) 774-4036 FAX</p>
<p>Patti Allison General Electric Aircraft Engines 1 Neumann Way Cincinnati, OH 45215</p> <p>(513) 243-7281</p>	<p>Jack W. Baldwin General Electric Aircraft Engines M/D M69 1 Neumann Way Cincinnati, OH 45215</p> <p>(513) 786-1412</p>	<p>Guy Nemoz Institute Textile de France Centre Technique Industriel Avenue Guy de Collonque B.P. 60-69132 ECULLY Cedex France</p>
<p>Ying-Jin Chen ITRI Materials Reserch Lab Bldg. 77, 195 Chung Hsing Rd.,Sec.4, Chutung,31015, Hsinchu,Taiwan</p> <p>886-35-820-262 FAX</p>	<p>Dr. Ignaas Verpoest Katholieke Universitiet Leuven Department of Mtlggy. and Mat. Eng. DeCroylaan 2, 3001 Leuven Belgium</p> <p>(011) 32-16-22-09-31 (FAX) 32-16-20-79-95</p>	<p>Jay Shukla Lockheed Aeronautical Systems Marietta, Georgia 30063-0150</p> <p>(404) 494-8165 (404) 494-8345 FAX</p>

<p>Matthias Nohr Center for Composite Materials Daimler-Benz Germany</p>	<p>Chien-Chieh Chao China Textile Institute Fl. 5, No. 12, Ln. 126 Sec. 3 Chun-Yang Road Tu-Chen, Taipei, TAIWAN ROC</p> <p>886-2-260-5101 (phone) 886-2-260-5243 (fax)</p>	<p>Yu-Wei Lin China Textile Institute Fl. 5, No. 12, Ln. 126 Sec. 3 Chun-Yang Road Tu-Chen, Taipei, TAIWAN ROC</p> <p>886-2-260-5101 (phone) 886-2-260-5243 (fax)</p>
<p>Bhuvanesh C. Goswami Clemson University 161 Shrine Hall Clemson, S.C. 29634-1307</p> <p>OFFICE:(803) 656-5957 FAX: (803) 656-5973</p>	<p>S. Rose Matic-Leigh Clemson University 161 Shrine Hall Clemson, S.C. 29634-1307</p> <p>OFFICE:(803) 656-3176 FAX: (803) 656-5973</p>	<p>Mark Condon Draper Labs MS 6D 555 Technology Square Cambridge, MA 02140</p> <p>617-258-4284</p>
<p>Thomas Lee Draper Labs MS 6D 555 Technology Square Cambridge, MA 02140</p> <p>617-258-4284</p>	<p>Moishe Garfinkle Drexel University 1733 Wallace Street Philadelphia, PA 19130</p> <p>(215) 895-1974</p>	<p>Amotz Geshury Drexel University Department of Materials Engineering Fibrous Materials Research Center Bldg. 27-439 Philadelphia, PA 19104</p> <p>(215) 895-6618 FAX:(215) 895-6684</p>
<p>Anisur Rahman Drexel University Department of Materials Engineering Fibrous Materials Research Center Bldg. 27-439 Philadelphia, PA 19104</p> <p>(215) 895-2382 FAX:(215) 895-6684</p>	<p>Charles Lei Drexel University Department of Materials Engineering Fibrous Materials Research Center Bldg. 27-439 Philadelphia, PA 19104</p> <p>(215) 895-2382 FAX:(215) 895-6684</p>	<p>Dominique Ponsolle Drexel University Department of Materials Engineering Fibrous Materials Research Center Bldg. 27-439 Philadelphia, PA 19104</p> <p>(215) 895-6612 FAX:(215) 895-6684</p>
<p>Eric Staudt Drexel University Department of Materials Engineering Fibrous Materials Research Center Bldg. 27-439 Philadelphia, PA 19104</p> <p>(215) 895-1642 FAX:(215) 895-6684</p>	<p>Erin Ross Drexel University Department of Materials Engineering Fibrous Materials Research Center Bldg. 27-439 Philadelphia, PA 19104</p> <p>(215) 895-1642 FAX:(215) 895-6684</p>	<p>Frank Ko Drexel University Department of Materials Engineering Fibrous Materials Research Center Bldg. 27-439 Philadelphia, PA 19104</p> <p>(215) 895-1640 FAX:(215) 895-6684</p>

<p>Tracy Anderson 3M Industrial and Electronic Sector 2465 Lexington Avenue South, M/S 60-N-01 Mendota Heights, MN 55120</p> <p>(612) 736-1842 (612) 736-0431 FAX tlanderson@mmc.mmmg.com</p>	<p>Cam T. Hua Advanced Product Development 2500 Pearl Buck Rd Bristol, PA 19007</p> <p>(215) 785-3230 (215) 785-3123 FAX</p>	<p>David Brookstein Albany International Research Co. 777 West St. P.O. Box 9114 Mansfield, MA 02048-9114</p> <p>(508)339-7300 FAX: (508) 339-4996</p>
<p>R. C. Howard Amatex Corporation</p>	<p>Doug Jacques Atkins & Pearce 3865 Madison Pike Covington, Kentucky 41017</p> <p>(606) 356-2001 (606) 356-2395 FAX</p>	<p>Mark Derstine Atlantic Research Corp. 5945 Wellington Road Gainesville, VA 22065</p> <p>(703)754-5777,5743 FAX (703) 642-4021,4507</p>
<p>Stephen A. Cauffman Atlantic Research Corp. Bldg 300, Room 128 5945 Wellington Road Gainesville, VA 22065</p> <p>(703)754-5777,5743 FAX (703) 642-4021,4507</p>	<p>Richard Brown Atlantic Research Corp. Bldg 300, Room 165 5945 Wellington Road Gainesville, VA 22065</p> <p>(703)754-5777,5743 (703) 368-1553(h) FAX (703) 754-5281</p>	<p>Sabit Adanur Auburn University Textile Engineering Department Auburn University Auburn, AL 36849</p> <p>(205) 844-5497 (205) 844-4068</p>
<p>Yasser Gowayed Auburn University Textile Engineering Department Auburn University Auburn, AL 36849</p> <p>(205) 844-5497 (205) 844-4068</p>	<p>Robert S. Taylor Bentley-Harris Mfg. Co. 241 Welsh Pool Road Lionville, Pennsylvania 19353</p> <p>(215) 363-2600 (215) 524-9086 FAX</p>	<p>Sharad R. Moghe BF Goodrich Aerospace 9921 Brecksville Rd. M/S D/8528 Brecksville, OH 44141</p> <p>(216) 447-5384 (216) 887-5860 FAX</p>
<p>Pierre Minguet Boeing</p>	<p>Dan Kovach Boeing Aerospace P.O. Box 3707 Seattle, WA 98124-2207</p> <p>(206) 393-7058 FAX</p>	<p>Dr. Christian Gunther Boeing Helicopter Company Rt. 291 Stewart Ave. Eddystone, PA 19013</p> <p>(215) 499-9526 FAX (215) 499-9568</p>



REPORT DOCUMENTATION PAGE			Form Approved OMB No. 0704-0188	
Public reporting burden for this collection of information is estimated to average 1 hour per response, including the time for reviewing instructions, searching existing data sources, gathering and maintaining the data needed, and completing and reviewing the collection of information. Send comments regarding this burden estimate or any other aspect of this collection of information, including suggestions for reducing this burden, to Washington Headquarters Services, Directorate for Information Operations and Reports, 1215 Jefferson Davis Highway, Suite 1204, Arlington, VA 22202-4302, and to the Office of Management and Budget, Paperwork Reduction Project (0704-0188), Washington, DC 20503.				
1. AGENCY USE ONLY (Leave blank)	2. REPORT DATE August 1993	3. REPORT TYPE AND DATES COVERED Conference Publication		
4. TITLE AND SUBTITLE FIBER-TEX 1992 The Sixth Conference on Advanced Engineering Fibers and Textile Structures for Composites		5. FUNDING NUMBERS 505-63-50-05		
6. AUTHOR(S) John D. Buckley, Editor				
7. PERFORMING ORGANIZATION NAME(S) AND ADDRESS(ES) NASA Langley Research Center Hampton, VA 23681-0001		8. PERFORMING ORGANIZATION REPORT NUMBER L-17266		
9. SPONSORING/MONITORING AGENCY NAME(S) AND ADDRESS(ES) National Aeronautics and Space Administration Washington, DC 20546-0001		10. SPONSORING/MONITORING AGENCY REPORT NUMBER NASA CP-3211		
11. SUPPLEMENTARY NOTES Co-sponsors: Department of Defense, Washington, DC; Drexel University, Philadelphia, Pennsylvania; Clemson University, Clemson, South Carolina; North Carolina State University, Raleigh, North Carolina.				
12a. DISTRIBUTION/AVAILABILITY STATEMENT Unclassified-Unlimited Subject Category 24		12b. DISTRIBUTION CODE		
13. ABSTRACT (Maximum 200 words) This document is a compilation of papers presented at a joint NASA/Drexel University/Clemson University/North Carolina State University/DoD conference on Fibers, Textile Technology, and Composites Structures held at the Grand Hall, Creese Student Center at Drexel University in Philadelphia, Pennsylvania on October 27-29, 1992. Conference papers presented information on advanced engineering fibers, textile processes and structures, structural fabric production, mechanics and characteristics of woven composites, and the latest requirements for the use of textiles in the production of composite materials and structures as related to global activities focused on textile structural composites.				
14. SUBJECT TERMS Graphite fiber; Ceramic fibers; Fiber testing; 3-D braiding; Stitching; Automation; Towpreg; Thermoplastics; Aircraft		15. NUMBER OF PAGES 367		
		16. PRICE CODE A16		
17. SECURITY CLASSIFICATION OF REPORT Unclassified	18. SECURITY CLASSIFICATION OF THIS PAGE Unclassified	19. SECURITY CLASSIFICATION OF ABSTRACT Unclassified	20. LIMITATION OF ABSTRACT	



National Aeronautics and
Space Administration
Code JTT
Washington DC 20546

Official Business
Penalty for Private Use, \$300

FOURTH CLASS

L4 001 CP-3211 9307123090547A
NASA
CENTER FOR AEROSPACE INFORMATION
ACCESSIONING
800 ELKRIDGE LANDING ROAD
LINTHICUM HEIGHTS MD 210902934

SPECIAL FOURTH-CLASS RATE
POSTAGE & FEES PAID
NASA
PERMIT No. G27

MASTER: If Undeliverable (Section 158
Postal Manual) Do Not Return

